Methods in Molecular Biology™

VOLUME 227

Membrane Transporters

Methods and Protocols

Edited by

Qing Yan, MD, PhD

HUMANA PRESS

1

Pharmacogenomics of Membrane Transporters

An Overview

Qing Yan

1. Introduction

1.1. Membrane Transporters: Essential for Normal Physiological Functions

Membrane transporters play crucial roles in fundamental cellular functioning and normal physiological processes of archaebacteria, prokaryotes, and eukaryotes ***(1)***. Transporters are proteins that span the lipid bilayer and form a transmembrane channel lined with hydrophilic amino acid side chains. Membrane transporters are critical during the formation of electrochemical potentials, uptake of nutrients, removal of wastes, endocytotic internalization of macromolecules, and oxygen transport in respiration ***(2,3)***.

Some transporters are called "uniporters," as they mediate the unidirectional translocation of a single substrate. When two substrates are transported in opposite directions in a firmly coupled process, transporters function as "antiporters." There are also "symporters" that are involved in the connected cotransport of two separate substrates in the same direction. Substrates of transporters move across the lipid bilayer through the transmembrane channels and increase the rate of transmembrane passage. Multiple α-helices constitute transmembrane domains (TMDs), which form the secondary structure of transporters. During the process of solute translocation across the membrane, transporters undergo conformational changes. About one-third of all the proteins of a cell are embedded in biological membranes and about one-third of these proteins function to catalyze the transport of molecules across the membrane ***(4,5)***.

From: *Methods in Molecular Biology, vol. 227: Membrane Transporters: Methods and Protocols*
Edited by: Q. Yan © Humana Press Inc., Totowa, NJ

Based on mechanisms and energetics, membrane transporters can be categorized into two broad classes: passive transporters and active transporters. Passive transporters include ion channels, such as the Na^+ channel, and facilitated diffusion such as glucose transporter. Primary active transporters, such as H^+-ATPase and Na^+K^+ATPase, make use of ATP, light, or substrate oxidation as energy resources. Secondary active transporters, such as Na^+/amino acid symporters and H^+/peptide transporters, use ion gradients as their energy source. In addition to transport mode and energy coupling, phylogenetic grouping reveals structure, function, mechanism, and substrate specificity, providing a reliable secondary basis for classification ***(6)***. The tertiary basis for classification is substrate specificity and polarity of transport, which are more readily altered during the evolutionary history. Details on the classification of membrane transporters will be described in Chapter 2 by Busch and Saier.

Many primary active transporters contain an ATP-binding cassette (*ABC*) and belong to the ABC superfamily that comprises proteins with very diverse functions ***(7)***. More than 50 human transporters have been identified in this superfamily, including the transporter associated with antigen processing (*TAP*) and P-glycoprotein multidrug transporter (*Pgp*). Generally, the ABC superfamily members transport various kinds of substrate, including ions, sugars, amino acids, phospholipids, toxins, and different drugs. The ABC superfamily belongs to an even larger group, the major facilitator superfamily (MFS). This MFS superfamily also includes solute carrier family members such as organic cation transporters.

Transporter malfunction can cause disorders in different systems of the human body, which also demonstrates their important roles in normal physiological processes. For example, glucose-galactose malabsorption characterized by severe diarrhea is associated with defects in the Na^+-dependent glucose transporter (*SGLT1*) ***(8)***. Loss of transporters for Lys, Arg, and Cys from intestinal and renal brush borders can cause cystinuria and kidney stones. Mutations in transporter protein *SLC3A1* (also known as *rBAT*) have been determined to be the cause of type I cystinuria ***(9)***. The genetic disease cystic fibrosis is caused by the dysfunction of cystic fibrosis transmembrane conductance regulator (*CFTR*) ***(10)***.

Genetic polymorphisms can also cause physiological disorders. Polymorphisms are allelic variants in genes that exist stably in the population, typically with an allele frequency above 1%. Polymorphism within the promoter region of the serotonin transporter gene (*5-HTT*) is considered as a potential genetic risk factor for Alzheimer's disease (AD) ***(11)***. Polymorphisms of the dopamine transporter (*DAT*) and *N*-acetyltransferase 2 (*NAT2*) have been found to be significantly associated with Parkinson's disease ***(12–14)***.

With the completion of sequencing of the entire human genome and the annotation of the sequences, it will be possible to catalog all transporter genes. Other features of transporters, including tissue distribution and functions, as well as sequence variants, can also be analyzed systematically. These can be achieved with the assistance of various new technologies such as the microarray technology and bioinformatics, which may help deal with the large number of genes, the tremendous structural and functional heterogeneity of transporters, and complex associations between them.

1.2. Pharmaceutical Relevance of Transporters

Another key role of membrane transporters is their effects on drug therapeutics. Transporters are important in the absorption of oral medications across the gastrointestinal tract. For example, dipeptide transporters are H^+-coupled, energy-dependent transporters. These transporters are crucial in the oral absorption of β-lactam antibiotics, angiotensin-converting enzyme (*ACE*) inhibitors, renin inhibitors, and an antitumor drug, bestatin ***(15)***. Active drug transporter *Pgp* has been found to be involved in apafant and digoxin absorption ***(16)***.

Drug distribution can also be influenced by membrane transporters. Nucleosides and their analogs including antivirals and antineoplastics depend on specific transporters to reach their target sites. Transporters for amino acids, monocarboxylic acids, organic cations, hexoses, nucleosides, and peptides are involved in drug transformation across the blood–brain barrier ***(17)***. Without these transporters, hydrophilic compounds cannot cross the barriers. Recently, regulating the activity of efflux transporters has been suggested to improve the brain entry of certain substrates ***(18)***. In addition to drug entrance, membrane transporters are also crucial for drug exit from the body. For example, diverse secretary and absorptive transporters in the renal tubule enable renal disposition of drugs ***(19)***.

The development of drugs that target transporters may improve drug therapeutic effects such as oral absorption. The bioavailability of poorly absorbed drugs can be improved by transporters that are responsible for the intestinal absorption of various solutes and/or by inhibiting the transporters involved in the efflux system. For instance, the intestinal peptide transporter can be used to increase the bioavailability of several classes of peptidomimetic drugs, especially *ACE* inhibitors and β-lactam antibiotics ***(20)***.

The development of the biology of transporters is of particular pharmaceutical relevance ***(21)***. Structural modification and specific transporter targeting are considered promising strategies for drug design with increased bioavailability and tissue distribution. For example, an approach has been

explored to enhance therapeutic efficacy, by pharmacological modulation of P-glycoprotein (*Pgp*) functions to improve drug bioavailability to the body and drug targets ***(22)***. The strategy of using the breast cancer resistance protein (*BCRP*) and Pgp inhibitor GF120918 has been found to significantly increase the bioavailability of topotecan ***(23)***.

The study of membrane transporters may even result in breakthroughs in the discovery of new drugs. The antiepileptic drug tiagabine, a γ-aminobutyric acid (GABA) uptake inhibitor, came from the research on amino acid transporters ***(24)***. Neurotransmitter transporters are suggested to be the "fruitful targets" for central nervous system (CNS) drug discovery. In addition, multiple drug resistance (*MDR*) genes, which are implicated in native and acquired resistance to antineoplastic agents, have drawn intensive interest ***(25–27)***. The use of transporters in designing drugs is not limited to humans but can be extended to all kinds of therapeutics. The world's three best-selling veterinary antiparasitic drugs (i.e., parasiticides) act on ligand-gated ion channels ***(28)***.

Although the role of membrane transporters in drug effects has attracted much recent interest, the relevant transporters are still unknown for most drugs. In some cases, a transporter is known to interact with a drug. However, it is uncertain whether there are still other transporters that recognize the same drug with unknown interactions. Therefore, a primary goal of current research in drug discovery and development is to fully understand the interactions between transporters and drugs; that is, which transporters recognize a drug candidate and which transporters can be utilized for targeting the drug to its site of action.

2. Pharmacogenomics of Membrane Transporters

2.1. Definition of Pharmacogenomics

Molecular biology is moving from the structural phase toward the functional phase, with the impending identification of most human genes ***(29)***. As an emerging scientific discipline, pharmacogenomics is translating functional genomics into clinical medicine ***(30)***. Pharmacogenomics studies the genetic basis of the individual variations in response to drug therapy ***(31)***. It involves the analysis of gene expression variations related to drug response. The goal of pharmacogenomics is to achieve optimal therapy for the individual patient, using genetic and genomic principles to facilitate drug discovery and development, and to improve drug therapy ***(32)***.

The word "pharmacogenomics" has been used interchangeably with "pharmacogenetics." The history of pharmacogenetics can be traced back to Pythagoras in Croton, southern Italy 510 B.C. He recognized the danger to "some, but not other, individuals who eat the fava bean." This danger was hemolytic anemia in people lacking glucose 6-phosphate dehydrogenase

(*G6PD*). In the 1950s, a series of clinical observations of inherited differences in drug effects gave rise to the area of "pharmacogenetics," a term first introduced by Friedrich Vogel in 1959 ***(33)***. These observations include hemolysis after antimalarial therapy and the inherited level of erythrocyte *G6PD* activity. At that time, this field was primarily concentrated on genetic polymorphisms in drug-metabolizing enzymes and how the differences affect drug effects ***(34)***. Today, people use the term "pharmacogenomics" to represent the entire spectrum of genes that determine drug behavior and sensitivity, although the two words are used with similar meanings in most occasions.

Pharmacogenomics can establish the correlation between specific genotypes and certain phenotypes in the therapeutic context. Such analysis may be useful in diagnosis and predicting drug response at any stage in the clinic ***(35)***. The development of pharmacogenomics can have great impact on every phase of biomedicine, from clinical laboratory tests to personalized (or individually tailored) medicine ***(35–38)***.

2.2. Key Issues in Pharmacogenomics of Transporters

The study of pharmacogenomics in membrane transporters may contribute significantly to our understanding of interindividual variability in response to numerous therapeutic agents. For example, polymorphisms of the dopamine transporter gene (*DAT1*) have been found to play a role in response to methylphenidate, which was used to treat attention-deficit hyperactivity disorder in children ***(39)***.

P-Glycoprotein (also called *MDR*) functions as an efflux pump that translocates substrates from the inner side of the membrane to the outer side. Sequence variations in a Pgp transporter may have functional importance for drug absorption and elimination, as well as clinical relevance to drug resistance response. A significant correlation has been observed between a polymorphism in exon 26 (C3435T) of *MDR-1* and the expression levels and function of *MDR-1* ***(40)***. Individuals homozygous for this polymorphism have been found to have significantly reduced duodenal *MDR-1* expression and increased digoxin plasma levels. This polymorphism has been suggested to influence the absorption and tissue concentrations of other substrates of *MDR-1*.

Serotonin transporter (*5-HTT*) is another example of polymorphisms with impact on drug efficacy. Serotonin (5-HT) is a neurotransmitter that plays important roles in many physiological processes. The malfunction of serotonin may cause severe depression. *5-HTT* is critical in the termination of serotonin neurotransmission. This transporter is the target for selective serotonin-reuptake inhibitors. A functional polymorphism in the transcriptional control region upstream of the coding sequence of *5-HTT* has been

reported ***(41)***. It has been observed that this polymorphism influences responses to the antidepressants fluvoxamine and paroxetine ***(42–45)***. Polymorphisms in the promoter of serotonin transporter have been found to affect responses to a *5-HT(3)* antagonist that relieves symptoms in women with diarrhea-predominant irritable bowel syndrome (D-IBS) ***(46)***.

In the following subsections, we will discuss some key issues that have triggered great interest and have to be solved before we can achieve the ultimate goal of pharmacogenomics.

2.2.1. Structure–Function Association

The objective of studying transporter genetic structures is to find out how they affect functional consequences, which may be used later in therapeutics. One of the most important issues in pharmacogenomics of membrane transporters is to elucidate the relationship between the structural and functional properties of transporter molecules. For example, the function of nucleotide-binding domains (NBDs) of *CFTR* is hydrolyzing ATP to regulate channel gating ***(47)***. The *CFTR* regulatory (R) domain phosphorylation controls the functional channel activity ***(48)***. Sequence structural variation may also cause clinical consequences. For example, studies have shown that allelic variants in the promoter region of the serotonin transporter have an association with the risk for alcohol dependence ***(49)***.

The complexity of the structure–function relationships may be clarified through molecular cloning of transporter subtypes. Transporter subtypes can have a similar function but different tissue distribution, regulation, and specificity toward a drug. For example, the multiple drug resistance-associated protein *MRP1* has highest levels in tissues of the testes, skeletal muscle, heart, kidney, and lung, but low levels in the liver and intestine ***(50–52)***. However, another protein in the same subfamily, *MRP2* (also called *cMOAT* [canalicular multiple organic anion transporter]), is abundant in the liver, kidney, and intestine ***(51)***. The genetic analysis may also provide perception into gene regulation and evolution, such as the example that vesicular choline transporter is contained entirely in the first intron of the choline acetyltransferase gene ***(53,54)***.

The correlation between transporter structure and function will enable a better description of transport mechanisms. Through the insight of transport mechanisms, we can better understand how the transporter proteins may be altered in diseases and regulated by therapeutic agents. The identification of structural elements is necessary to explain the direction of translocation and subcellular localization. In this volume, some approaches to studying the struc-

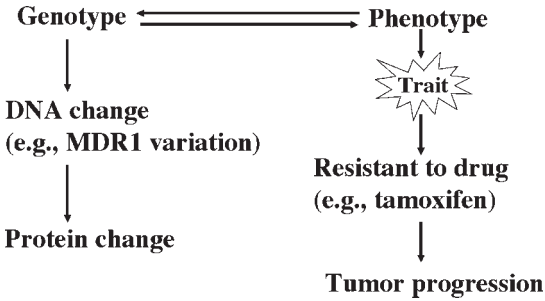

Fig. 1. The correlation between genotype and phenotype.

ture–function relationship in transporters will be described, such as site-directed mutagenesis and fluorescence methods.

The structure–function correlations will also be useful in the design of more specific transporter reagents with high-quality therapeutic effects. To elucidate such correlations, a more complete understanding of transporter structure, including the three-dimensional topology and tertiary structure, is required. Methods to detect transporter structures, including small-angle X-ray scattering, solution nuclear magnetic resonance (NMR), and molecular modeling, will be discussed in this volume.

Another approach in structure–function studies is to elucidate the role of a transporter in the whole genome and the relationship of a transporter gene to other genes nearby on the chromosome. **Table 1** is a sample list of chromosome locations of transporters in the ABC superfamily ***(55)***. Such information indicates where the transporters (and maybe the whole family) are in the whole genome, how they are related spatially in the genome, and what the nearby transporters are. This information may also give us some hints about potential interactions between transporter genes.

2.2.2. Genotype–Phenotype Correlation

The correlation between genotype and phenotype plays a crucial role in the translation of pharmacogenomics into clinical medicine. **Figure 1** illustrates the correlation between genotype and phenotype, using the role of a transporter gene in breast cancer therapy as an example. In classical genetics, the "phenotype" is usually defined as a visible trait, such as black hair or blue eyes. Clinical features, such as drug responses, can also be defined as "phenotypes." The description of the correlation includes two aspects. One is the definition of a clinical phenotype such as resistance to the drug tamoxifen in breast cancer

Table 1
Chromosome Locations of Some Transporters in the ABC Superfamily

Chromosome location	Transporter
1p22	ABCA4
1q21–q23	ATP1A2
1q25–q32	PMCA4; ATP2B4
2q24	BSEP
3q13.3–q21	PEPT2
3p26–p25	ATP2B2; PMCA2
3q22–q23	ATP1B3
3q27	MRP5
4q22	ABCP
5q31–q34	DTD
6p21.3	TAP1; TAP2; NPT3; NPT4
7pter–7qter	ZNT3
7q21.1	MDR1; MDR2; ABCB4
7q31	CFTR
9q22–q31	ABC1
10q23–q24	MRP2
12q11–q12	ABCD2; ALDR
12q12	ALD1; hBNaC2
12q21–q23	ATP2B1; PMCA1
13q12.1–q12.3	ATP1AL1
13q14.3	ATP7B
13q32	MRP4
13q33–q34	PEPT1
14q24.3	ABCD4; PMP69
16p12	SERCA1
16p13.1	MRP6
16p13.12–13	MRP1
16p13.3	ABCA3
17p	ATP1B2
17q21–q23	MRP3
18q21	FIC1
19q12–q13.2	ATP1A3
19q13.1	CSNU3; SLC7A10; ATPGG
20q11.2	ZNT4
Xq12–q13	ATP7A
Xq13.1–q13.3	ABCB7
Xq28	CRTR; ABCD1; PMCA3g

Table 2
Transporters in Tissues of the Liver, Kidney, Intestines, and Brain

Liver	Kidney	Intestines	Brain
AE1	AE2	4F2HC	ALDR
ANT2	ASNA1	ACATN	ASCT1
BGT-1	CNT1	ATP2A3	ATP1AL1
BSEP	ENT1	CAT1	CAT4
CAT1	FATP4	CNT1	CNT1
CAT2	GLUT2	CNT2	CNT2
CNT1	GLUT5	CTR-1	DAT1
CNT2	GLUT6	CTR-2	EAAT1
CTR-1	KCC1	EAAT3	EAAT2
CTR-2	KCC3	ENT1	EAAT3
EAAT2	KCC4	GLUT2	ENT1
EAAT5	LAT-2	GLUT5	ENT2
ENT1	LAT-3	GLUT6	GAT-1
FATP4	MCT4	KCC1	GAT-3
G6PT	MCT5	LAT-2	GLCR2
GLCR2	MDR1	MCT7	GLUT1
GLUT2	MRP1	MDR1	GLUT3
GLUT6	MRP3	MRP1	GLUT6
LAT-2	NCX1	MRP3	GLYT1
LST-1	NHE1	NBC	GLYT2
MCT7	NHE2	NCCT	HTT
MDR1	NHE3	NHE1	KCC1
MDR2	NHE6	NHE2	KCC3
MNK	NKCC1	NHE3	KCC4
MRP1	NKCC2	NHE6	LAT-1
MRP2	NPT1	NTCP2	LAT-2
MRP3	NPT2	OCT1	MCT2
NHE1	NTCP1	OCTN2	MCT6
NHE6	NTCP2	ORCTL2	MCT7
OAT2	OAT1	PEPT1	MRP1
OATP1	OAT2	PGT	NAT1
OCT1	OAT3	PMCA1	NHE1
OCTN1	OATP1	rBAT	NHE5
OCTN2	OCT1	RFC	NHE6
PEPT1	OCT2	SATT	OAT1
PGT	OCTN1	SBC2	OATP1
PMCA4	OCTN2	SDCT1	PROT
PMP34	ORCTL2	SGLT1	WHITE1
PMP70	ORCTL3	SGLT2	ZNT-1
TAUT	ORCTL4	TSC	ZNT-3
UGT1	TAUT	ZNT-1	ZNT-4

Table 3
Transporter Variations and Associations with Diseases:
Examples for the Genotype–Phenotype Correlation

Transporter	Nucleotide change	Nucleotide position	Amino acid change	Variation-related malfunction/ disease	Ref.
ABC1/ABCA1	A→G; A→G	1730; 2744	Arginine → glutamine; asparagine → serine	Tangier disease and familial high-density lipoprotein deficiency	***(57,58)***
ABCR/ABCA4	G→C; T→C	2588; 1622	gly863 → ala; leu541 → pro	Stargardt disease and age-related macular degeneration	***(59,60)***
ABCB4/MDR3	C→A		Alanine 546 → aspartic acid	Intrahepatic cholestasis of pregnancy	***(61)***
ABCD1/ALD	G→A; C→G	1258; 1551	Glutamic acid → lysine; arg389→gly	Adrenoleuko-dystrophy/ adrenomyelo-neuropathy	***(62,63)***
ATP7A	A→G	2462	Exon skipping and activation of a cryptic splice acceptor site	Occipital horn syndrome	***(64)***
ATP7B	GAC→AAC; CGG→CTG		asp765 → arg778 → leu	Wilson disease asn;	***(65,66)***
SLC4A1/AE1	CCC→CGC		pro327 → arginine	Spherocytic hemolytic anemia because of Band 3 Tuscaloosa	***(67)***
SLC22A5	G→A	1196	Arginine →glutamine	Primary carnitine deficiency	***(68)***

(Continued)

Table 3 (*Continued*)
Transporter Variations and Associations with Diseases:
Examples for the Genotype–Phenotype Correlation

Transporter	Nucleotide change	Nucleotide position	Amino acid change	Variation-related malfunction/ disease	Ref.
SLC26A4	T→C; G→T	707; 626	leu236 → pro; gly → val	Pendred syndrome; enlarged vestibular aqueduct	***(69,70)***
TAP1	A→G; A→G	1069; 1982	Isoleucine-333 → valine; asp-637 → glycine	Involved in antigen processing	***(71)***

therapy and the result of tumor progression. The other aspect is the genotype such as an altered *MDR1* gene, which may perform a causal role in the protein alteration and then the phenotypic change.

When we study a transporter gene, one of the first things we need to know is where the transporter is located in tissues. Tissue distribution is one of the most critical phenotypic information about transporters. Such information may be especially important in pharmacogenomics studies. The information about the abundance of transporters in different tissues can be used in designing new drugs that need to target on certain tissues. To determine which drug transporters are candidates for genotyping, this information may also be helpful. In addition, such information may assist in guiding drug therapy in individual patients on the basis of the drug transporter genotype and phenotype. **Table 2** presents some examples of transporters expressed in the liver, kidney, intestines, and brain ***(55)***.

Another key part of phenotype is disease. When the data of human genome sequence and genetic variability become available, whatever is buried in these data contains the entire range of phenotypic variation. For example, at least five distinct disease phenotypes, including retinitis pigmentosa, cone-rod dystrophy, and Stargardt macular dystrophy, have been related to mutations of a photoreceptor-specific ATP-binding cassette transporter *ABCR* ***(56)***. Such correlations between the sequence variation genotype and disease phenotype might also affect drug targets and the correlated drug-response phenotype. The Human Membrane Transporter Database contains a list of known transporter-related diseases ***(55)***. **Table 3** presents examples of genetic variations, includ-

ing nucleotide variations, positions, and resulting amino acid changes in membrane transporter genes and their correlations with malfunctions or diseases. Some methods for studying the transporter genotype–phenotype correlation will be introduced in this volume, such as using laser capture microdissection to examine transporter expression.

2.2.3. Gene–Drug Interaction

The essential gene-drug interaction has been considered "extremely important" in drug development and clinical medicine ***(72,73)***. This interaction composes the central part of pharmacogenomics. Pharmacogenomics represents studies on the essential gene–drug interactions through genetic mechanisms and the functional pharmacological context, in cooperation with clinical studies. When drugs enter the human body, their fate is affected by uptake, binding, distribution, biotransformation, and excretion.

On a molecular basis, the efficacy of a drug is influenced by the alterations in receptor affinity, transporters, or protein binding. An example of transporter gene–drug interaction is that the functional polymorphism in *5-HTT* affects antidepressant responses to fluvoxamine and paroxetine ***(42–45)***. **Table 4** lists some examples of transporter variations and their impact on certain drug/substrate effects.

The gene–drug interactions can be illustrated from several aspects. These may include the responding genes to specific drugs, the expression level of these genes, the sensitivity of a cell to a drug, as well as pharmacological characteristics of drug action. For example, the polymorphism of *MDR-1* could significantly increase digoxin plasma levels in patients and affect the absorption and tissue concentrations of other substrates of *MDR-1* ***(40)***.

3. Conclusion

In this chapter, we have briefly reviewed the definition, history, current status, and key issues in pharmacogenomics of transporters. Here, the three key issues are identified to help us clarify this complex field. However, a comprehensive understanding of these issues will be needed. Some subtopics are also included in these three points, such as the protein–protein interaction between transporters and between transporters and other proteins. The key issues discussed in this chapter cannot be separated but are tightly connected and interlinked, as shown in **Fig. 2**. The correlation between genetic structure and observable normal functions can be represented as normal phenotypes. On the other hand, altered genetic structure may lead to malfunction and be expressed as disease phenotypes. In addition, varied genetic structures may lead to altered functions that can affect the drug-response phenotype, as examples in this chapter illustrated. The drug-response phenotype is also the result of the gene–drug

Table 4
Effect of Transporter Variations on Drugs/Substrates: Examples for the Gene–Drug Interaction

Transporter gene with variations	Drug/substrates	Effects	Ref.
Plasmodium falciparum chloroquine resistance transporter gene (pfcrt)	Chloroquine(CQ)	Resistance	***(74,75)***
Serotonin transporter (5-HTT)	Fluvoxamine; paroxetine	Poor response	***(42–45)***
MDR1 (P-glycoprotein)	Digoxin; fexofenadine	Enhanced efflux of digoxin; enhanced in vivo activity	***(40,76)***
Organic anion transporting polypeptide-C (OATP-C) (gene SLC21A6)	Estrone sulfate and estradiol 17β-D-glucuronide	Reduced uptake	***(77)***
Dopamine transporter (DAT1)	Methylphenidate	Nonresponse	***(78)***

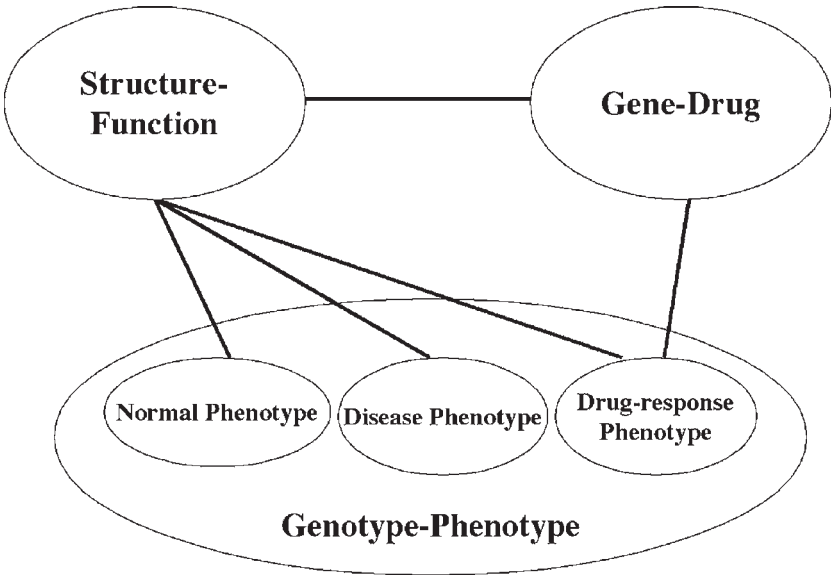

Fig. 2. The comprehensive diagram of the three correlations: structure–function, gene–drug, genotype–phenotype.

interactions. Moreover, varied genetic structures and functions can affect the gene–drug interactions. In these three correlations, genotype–phenotype is the broadest concept that covers the whole biomedical process of drug therapy. However, identification of the other two correlations is also important to provide detailed cause–effect relations in this process.

Here, "pharmacogenomics" is not limited to studies in structural genomics, but really requires insights into functional genomics, proteomics (the study of gene expression at the protein level), disease pathogenesis, as well as pharmacology and toxicology. Pharmacogenomics is, in fact, a multidisciplinary field with interlinking and overlapping of various knowledge domains ***(79)***.

The newly developed microarray technology enables the analysis of gene expression patterns for thousands of genes simultaneously and may expedite the application of pharmacogenomics in clinical practice ***(29,31,38,79)***. Using the microarray technology for the analysis of membrane transporters may help to establish a systematic view of the interactions between transporters and drugs. For example, microarray technology can be used to examine transporter gene expressions in compound-treated cell lines. In the pharmacogenomics studies of membrane transporters, the systematic application of microarray technology may help detect tissue expression and allelic distributions on an individual basis ***(80)***. Such technology may also facilitate the identification of putative defective alleles and the exclusion of affected patients from therapy with a given drug. In this volume, we will introduce the application of some microarray methodologies in transporter studies.

The correlations between allelic variants in transporters and functional consequences will elucidate the impact of genetic variations on therapeutic susceptibility and safety. Studies on functional interactions between different transporters and between transporter and drugs will improve our perception of complex diseases and drug effects. These may ultimately contribute to the development of personalized medicine with high efficacy but less toxicity. This is also the overall goal of pharmacogenomics.

References

1. Clayton, R. A., White, O., Ketchum, K. A., et al. (1997) The first genome from the third domain of life. *Nature* **29,** 459–462.
2. Lehninger, A. L. (1993) *Principles of Biochemistry*, Worth Publishing, New York.
3. Lodish, H., Baltimore, D., Berk, A., et al. (1995) *Molecular Cell Biology*, Scientific American Books, New York.
4. Paulsen, I. T., Sliwinski, M. K., and Saier, M. H., Jr. (1998) Microbial genome analyses: global comparisons of transport capabilities based on phylogenies, bioenergetics and substrate specificities. *J. Mol. Biol.* **277,** 573–592.

5. Paulsen, I. T., Sliwinski, M. K., Nelissen, B., et al. (1998) Unified inventory of established and putative transporters encoded within the complete genome of Saccharomyces cerevisiae. *FEBS Lett.* **430,** 116–125.
6. Saier, M. H., Jr. (2000) A functional-phylogenetic classification system for transmembrane solute transporters. *Microbiol. Mol. Biol. Rev.* **64,** 354–411.
7. Higgins, C. F. (1992) ABC transporters: from microorganisms to man. *Curr. Opin. Cell Biol.* **8,** 67–113.
8. Martin, M. G., Lostao, M. P., Turk, E., et al. (1997) Compound missense mutations in the sodium/D-glucose cotransporter result in trafficking defects. *Gastroenterology* **112,** 1206–1212.
9. Palacin, M., Bertran, J., and Zorzano, A. (2000) Heteromeric amino acid transporters explain inherited aminoacidurias. *Curr. Opin. Nephrol. Hypertens.* **9,** 547–553.
10. Sheppard, D. N. and Welsh, M. J. (1999) Structure and function of the CFTR chloride channel. *Physiol. Rev.* **79,** S23–S45.
11. Hu, M., Retz, W., Baader, M., et al. (2000) Promoter polymorphism of the 5-HT transporter and Alzheimer's disease. *Neurosci. Lett.* **294,** 63–65.
12. Le Couteur, D. G., Leighton, P. W., McCann, S. J., et al. (1997) Association of a polymorphism in the dopamine-transporter gene with Parkinson's disease. *Mov. Disord.* **12,** 760–763.
13. Kim, J. W., Kim, D. H., Kim, S. H., et al. (2000) Association of the dopamine transporter gene with Parkinson's disease in Korean patients. *J. Korean Med. Sci.* **15,** 449–451.
14. Tan, E. K., Khajavi, M., Thornby, J. I., et al. (2000) Variability and validity of polymorphism association studies in Parkinson's disease. *Neurology* **55,** 533–538.
15. Lee, V. H. (2000) Membrane transporters. *Eur. J. Pharm. Sci.* **11,** S41–S50.
16. Leusch, A., Volz, A., Muller, G., et al. (2002) Altered drug disposition of the platelet activating factor antagonist apafant in mdr1a knockout mice. *Eur. J. Pharm. Sci.* **16,** 119–128.
17. Tamai, I. and Tsuji, A. (2000) Transporter-mediated permeation of drugs across the blood–brain barrier. *J. Pharm. Sci.* **89,** 1371–1388.
18. Sugiyama, Y., Kusuhara, H., and Suzuki, H. (1999) Kinetic and biochemical analysis of carrier-mediated efflux of drugs through the blood–brain and blood–cerebrospinal fluid barriers: importance in the drug delivery to the brain. *J. Control Release* **62,** 179–186.
19. Inui, K. I., Masuda, S., and Saito, H. (2000) Cellular and molecular aspects of drug transport in the kidney. *Kidney Int.* **58,** 944–958.
20. Oh, D. M., Han, H. K., and Amidon, G. L. (1999) Drug transport and targeting. Intestinal transport. *Pharm. Biotechnol.* **12,** 59–88.
21. Sadee, W., Drubbisch, V., and Amidon, G. L. (1995) Biology of membrane transport proteins. *Pharm. Res.* **12,** 1823–1837.
22. Silverman, J. A. (1999) Multidrug-resistance transporters. *Pharm. Biotechnol.* **12,** 353–386.

23. Kruijtzer, C. M., Beijnen, J. H., Rosing, H., et al. (2002) Increased oral bioavailability of topotecan in combination with the breast cancer resistance protein and P-glycoprotein inhibitor GF120918. *J. Clin. Oncol.* **1,** 2943–2950.
24. Iversen, L. (2000) Neurotransmitter transporters: fruitful targets for CNS drug discovery. *Mol. Psychiatry* **5,** 357–362.
25. Rund, D., Azar, I., and Shperling, O. (1999) A mutation in the promoter of the multidrug resistance gene (MDR1) in human hematological malignancies may contribute to the pathogenesis of resistant disease. *Adv. Exp. Med. Biol.* **457,** 71–75.
26. Gerlach, J. H., Kartner, N., Bell, D. R., et al. (1986) Multidrug resistance. *Cancer Surv.* **5,** 25–46.
27. Dalton, W. S. and Miller, T. P. (1991) Multidrug resistance, in Cancer: Principles and Practice of Oncology (DeVita, V. T., Jr., Hellman, S., and Rosenberg, S. A., eds.), Lippincott Williams & Wilkins, Philadelphia, pp. 1–13.
28. Raymond, V. and Sattelle, D. B. (2002) Novel animal-health drug targets from ligand-gated chloride channels. *Nat. Rev. Drug Discov.* **1,** 427–436.
29. Kennedy, G. C. (2000) The impact of genomics on therapeutic drug development. *EXS* **89,** 1–10.
30. Evans, W. E. and Relling, M. V. (1999) Pharmacogenomics: translating functional genomics into rational therapeutics. *Science* **286,** 487–491.
31. Shi, M. M., Bleavins, M. R., and de la Iglesia, F. A. (1999) Technologies for detecting genetic polymorphisms in pharmacogenomics. *Mol. Diagn.* **4,** 343–351.
32. Sadee, W. (2002) Pharmacogenomics: the implementation phase. *AAPS PharmSci* **4,** E5.
33. Vogel, F. (1959) Moderne probleme der Humangenetik. *Ergeb. Inn. Med. Kinderheilkd.* **12,** 52–125.
34. Nebert, D. W. (1997) Polymorphisms in drug-metabolizing enzymes: what is their clinical relevance and why do they exist? *Am. J. Hum. Genet.* **60,** 265–271.
35. Emilien, G., Ponchon, M., Caldas, C., et al. (2000) Impact of genomics on drug discovery and clinical medicine. *Q. J. Med.* **93,** 391–423.
36. Hess, P. and Cooper, D. (1999) Impact of pharmacogenomics on the clinical laboratory. *Mol. Diagn.* **4,** 289–298.
37. Roses, A. D. (2000) Pharmacogenetics and pharmacogenomics in the discovery and development of medicines. *Novartis Found. Symp.* **229,** 63–66.
38. March, R. (2000) Pharmacogenomics: the genomics of drug response. *Yeast* **17,** 16–21.
39. Winsberg, B. G. and Comings, D. E. (1999) Association of the dopamine transporter gene (DAT1) with poor methylphenidate response. *J. Am. Acad. Child Adolesc. Psychiatry* **38,** 1474–1477.
40. Hoffmeyer, S., Burk, O., von Richter, O., et al. (2000) Functional polymorphisms of the human multidrug-resistance gene: multiple sequence variations and correlation of one allele with P-glycoprotein expression and activity in vivo. *Proc. Natl. Acad. Sci. USA* **97,** 3473–3478.
41. Lesch, K. P., Bengel, D., Heils, A., et al. (1996) Association of anxiety-related traits with a polymorphism in the serotonin transporter gene regulatory region. *Science* **274,** 1527–1531.

42. Smeraldi, E., Zanardi, R., Benedetti, F., et al. (1998) Polymorphism within the promoter of the serotonin transporter gene and antidepressant efficacy of fluvoxamine. *Mol. Psychiatry* **3,** 508–511.
43. Kim, D. K., Lim, S. W., Lee, S., et al. (2000) Serotonin transporter gene polymorphism and antidepressant response. *Neuroreport* **11,** 215–219.
44. Pollock, B. G., Ferrell, R. E., Mulsant, B. H., et al. (2000) Allelic variation in the serotonin transporter promoter affects onset of paroxetine treatment response in late-life depression. *Neuropsychopharmacology* **23,** 587–590.
45. Zanardi, R., Benedetti, F., Di Bella, D., et al. (2000) Efficacy of paroxetine in depression is influenced by a functional polymorphism within the promoter of the serotonin transporter gene. *J. Clin. Psychopharmacol.* **20,** 105–107.
46. Camilleri, M., Atanasova, E., Carlson, P. J., et al. (2002) Serotonin-transporter polymorphism pharmacogenetics in diarrhea-predominant irritable bowel syndrome. *Gastroenterology* **123,** 425–432.
47. Anderson, M. P., Berger, H. A., Rich, D. P., et al. (1991) Nucleoside triphosphates are required to open the CFTR chloride channel. *Cell* **67,** 775–784.
48. Berger, H. A., Anderson, M. P., Gregory, R. J., et al. (1991) Identification and regulation of the cystic fibrosis transmembrane conductance regulator-generated chloride channel. *J. Clin. Invest.* **88,** 1422–1431.
49. Lichtermann, D., Hranilovic, D., Trixler, M., et al. (2000) Support for allelic association of a polymorphic site in the promoter region of the serotonin transporter gene with risk for alcohol dependence. *Am. J. Psychiatry.* **157,** 2045–2047.
50. Hipfner, D. R., Deeley, R. G., and Cole, S. P. (1999) Structural, mechanistic and clinical aspects of MRP1. *Biochim. Biophys. Acta* **1461,** 359–376.
51. Borst, P., Evers, R., Kool, M., et al. (1999) The multidrug resistance protein family. *Biochim. Biophys. Acta* **1461,** 347–357.
52. Konig, J., Nies, A. T., Cui, Y., et al. (1999) Conjugate export pumps of the multidrug resistance protein (MRP) family: localization, substrate specificity, and MRP2-mediated drug resistance. *Biochim. Biophys. Acta* **1461,** 377–394.
53. Bejanin, S., Cervini, R., Mallet, J., et al. (1994) A unique gene organization for two cholinergic markers, choline acetyltransferase and a putative vesicular transporter of acetylcholine. *J. Biol. Chem.* **269,** 21,944–21,947.
54. Erickson, J. D., Varoqui, H., Schafer, M. K., et al. (1994) Functional identification of a vesicular acetylcholine transporter and its expression from a "cholinergic" gene locus. *J. Biol. Chem.* **269,** 21,929–21,932.
55. http://lab.digibench.net/transporter
56. Lewis, R. A., Shroyer, N. F., Singh, N., et al. (1999) Genotype/Phenotype analysis of a photoreceptor-specific ATP-binding cassette transporter gene, ABCR, in Stargardt disease. *Am. J. Hum. Genet.* **64,** 422–434.
57. Brooks-Wilson, A., Marcil, M., Clee, S. M., et al. (1999) Mutations in ABC1 in Tangier disease and familial high-density lipoprotein deficiency. *Nature Genet.* **22,** 336–345.
58. Bodzioch, M., Orso, E., Klucken, J., et al. (1999) The gene encoding ATP-binding cassette transporter 1 is mutated in Tangier disease. *Nature Genet.* **22,** 347–351.

59. Allikmets, R., Shroyer, N. F., Singh, N., et al. (1997) Mutation of the Stargardt disease gene (ABCR) in age-related macular degeneration. *Science* **277,** 1805–1807.
60. Rivera, A., White, K., Stohr, H., et al. (2000) A comprehensive survey of sequence variation in the ABCA4 (ABCR) gene in Stargardt disease and age-related macular degeneration. *Am. J. Hum. Genet.* **67,** 800–813.
61. Dixon, P. H., Weerasekera, N., Linton, K. J., et al. (2000) Heterozygous MDR3 missense mutation associated with intrahepatic cholestasis of pregnancy: evidence for a defect in protein trafficking. *Hum. Mol. Genet.* **9,** 1209–1217.
62. Cartier, N., Sarde, C.-O., Douar, A.-M., et al. (1993) Abnormal messenger RNA expression and a missense mutation in patients with X-linked adrenoleukodystrophy. *Hum. Mol. Genet.* **2,** 1949–1951.
63. Krasemann, E. W., Meier, V., Korenke, G. C., et al. (1996) Identification of mutations in the ALD-gene of 20 families with adrenoleukodystrophy/adrenomyeloneuropathy. *Hum. Genet.* **97,** 194–197.
64. Kaler, S. G., Gallo, L. K., Proud, V. K., et al. (1994) Occipital horn syndrome and a mild Menkes phenotype associated with splice site mutations at the MNK locus. *Nature Genet.* **8,** 195–202.
65. Figus, A., Angius, A., Loudianos, G., et al. (1995) Molecular pathology and haplotype analysis of Wilson disease in Mediterranean populations. *Am. J. Hum. Genet.* **57**, 1318–1324.
66. Kim, E. K., Yoo, O. J., Song, K. Y., et al. (1998) Identification of three novel mutations and a high frequency of the arg778-to-leu mutation in Korean patients with Wilson disease. *Hum. Mutat.* **11,** 275–278.
67. Jarolim, P., Palek, J., Rubin, H. L., et al. (1991) Band 3 Tuscaloosa: pro327-to-arg327 substitution in the cytoplasmic domain of erythrocyte band 3 protein associated with spherocytic hemolytic anemia and partial deficiency of protein 4.2. *Blood* **78(Suppl.)**: 252a (abstract).
68. Wang, Y., Korman, S. H., Ye, J., et al. (2001) Phenotype and genotype variation in primary carnitine deficiency. *Genet. Med.* **3,** 387–392.
69. Van Hauwe, P., Everett, L. A., Coucke, P., et al. (1998) Two frequent missense mutations in Pendred syndrome. *Hum. Mol. Genet.* **7,** 1099–1104.
70. Usami, S., Abe, S., Weston, M. D., et al. (1999) Non-syndromic hearing loss associated with enlarged vestibular aqueduct is caused by PDS mutations. *Hum. Genet.* **104,** 188–192.
71. Colonna, M., Bresnahan, M., Bahram, S., et al. (1992) Allelic variants of the human putative peptide transporter involved in antigen processing. *Proc. Nat. Acad. Sci. USA* **89,** 3932–3936.
72. Nebert, D. W. (1999) Pharmacogenetics and pharmacogenomics: why is this relevant to the clinical geneticist? *Clin. Genet.* **56,** 247–258.
73. Dirckx, C., Donati, M. B., and Iacoviello, L. (2000) Pharmacogenetics: a molecular sophistication or a new clinical tool for cardiologists? *Ital. Heart J.* **1,** 662–666.
74. Mockenhaupt, F. P., Eggelte, T. A., Till, H., et al. (2001) Plasmodium falciparum pfcrt and pfmdr1 polymorphisms are associated with the pfdhfr N108

pyrimethamine-resistance mutation in isolates from Ghana. *Trop. Med. Int. Health* **6,** 749–755.
75. Basco, L. K. and Ringwald, P. (2001) Analysis of the key pfcrt point mutation and in vitro and in vivo response to chloroquine in Yaounde, Cameroon. *J. Infect. Dis.* **183,** 1828–1831.
76. Kim, R. B., Leake, B. F., Choo, E. F., et al. (2001) Identification of functionally variant MDR1 alleles among European Americans and African Americans. *Clin. Pharmacol. Ther.* **70,** 189–199.
77. Tirona, R. G., Leake, B. F., Merino, G., et al. (2001) Polymorphisms in OATP-C: identification of multiple allelic variants associated with altered transport activity among European- and African-Americans. *J. Biol. Chem.* **276,** 35,669–35,675.
78. Winsberg, B. G. and Comings, D. E. (1999) Association of the dopamine transporter gene (DAT1) with poor methylphenidate response. *J. Am. Acad. Child Adolesc. Psychiatry* **38,** 1474–1477.
79. Sadee, W. (1998) Genomics and drugs: finding the optimal drug for the right patient. *Pharm. Res.* **15,** 959–963.
80. Yan, Q. and Sadee, W. (2000) Human membrane transporter database: a Web-accessible relational database for drug transport studies and pharmacogenomics. *AAPS PharmSci* **2,** E20.

2

The IUBMB-Endorsed Transporter Classification System

Wolfgang Busch and Milton H. Saier, Jr.

1. Introduction

Transport systems are essential to every living cell. They (1) allow the entry of all essential nutrients into the cell and its compartments, (2) regulate the cytoplasmic concentrations of metabolites by excretion mechanisms, (3) provide physiological cellular concentrations of ions that can differ by several orders of magnitude from those in the external medium, (4) export macromolecules such as complex carbohydrates, proteins, lipids, and DNA, (5) catalyze export and uptake of signaling molecules that mediate intercellular communications, (6) prevent toxic effects of drugs and toxins by mediating active efflux, and (7) participate in biological warfare by exporting biological active agents that insert into or permeate the membranes of target cells. Transport is an essential aspect of all life-endowing processes: metabolism, communication, biosynthesis, reproduction, and both cooperative and antagonistic interorganismal behaviors.

This chapter provides a summary of the recently developed transporter classification (TC) system ***(1–3)*** formally adopted by the International Union of Biochemistry and Molecular Biology (IUBMB) in June 2001. The development of a classification system for transport proteins has allowed us to comprehensively view transport systems from structural, functional, and evolutionary standpoints ***(2,4,5)***. This development has been strongly influenced by recent progress in computational biology and genome sequencing. Since our last description of the TC system ***(3)***, we have expanded the transporter classification system by (1) introducing new families and classes of transporters, (2) expanding the memberships of pre-existing families, (3) pro-

From: *Methods in Molecular Biology, vol. 227: Membrane Transporters: Methods and Protocols*
Edited by: Q. Yan © Humana Press Inc., Totowa, NJ

Table 1
TC System Overview

1. Channels/Pores
- A. α-Helical protein channels
- B. β-Barrel protein porins
- C. Toxin channels
- D. Nonribosomally synthesized channels
- E. Holins

2. Electrochemical Potential-Driven Transporters
- A. Porters
- B. Nonribosomally synthesized porters
- C. Ion-gradient-driven energizers

3. Primary Active Transporters
- A. P–P-bond hydrolysis-driven systems
- B. Decarboxylation-driven systems
- C. Methyltransfer-driven systems
- D. Oxidoreduction-driven systems
- E. Light-absorption-driven systems

4. Group Translocators
- A. Phosphotransfer-driven systems

5. Transmembrane Electron Carriers
- A. Two-electron transfer carriers
- B. One-electron transfer carriers

8. Accessory Factors Involved in Transport
- A. Auxiliary transport proteins

9. Incompletely Characterized Transport Systems
- A. Recognized transporters of unknown biochemical mechanism
- B. Putative uncharacterized transport proteins
- C. Functionally characterized transporters lacking identified sequences

Note: The hierarchical system for classifying families of transporters in the TC system is presented. Classes are presented in bold and subclasses are presented below the class designations.

viding more detailed annotation of these families and proteins, (4) updating reference citations relevant to proteins described in the TC system, and (5) creating an interactive database, which we have named TCDB. The results of our analyses, made possible by these updates, are summarized here. For a more detailed account of these studies, *see* **ref. *6***.

2. Classes of Transporters

The properties of the different hierarchical units that comprise the TC system are described briefly in this section and illustrated in **Table 1**. For more extensive descriptions, visit the websites and database (http://tcdb.ucsd.edu).

2.1. Class 1. Channels/Pores

Class 1 consists of channel-type facilitators. Transmembrane channel proteins span the lipid bilayer as either α-helices or β-strands. The transport mode of these systems usually involves the unencumbered passage of molecules across membranes in a process related to passive diffusion. Thus, channel-mediated transport occurs by facilitated diffusion, an energy-independent process in which the substrate passes through the transmembrane aqueous pore or channel without the coupling of the translocation process to another chemical or vectorial process.

2.1.1. 1.A. α-Type Channels

Channel proteins of subclass 1.A usually consist of bundles of transmembrane α-helices that form α-helical aqueous pores or channels. Rarely, β-strands contribute to the channel. These channels are found ubiquitously in the membranes of all types of organism.

2.1.2. 1.B. β-Barrel Porins

The transmembrane pores of subclass 1.C proteins consist exclusively of β-strands that form β-barrels. These channels are found in the outer membranes of bacteria, mitochondria, and plastids.

2.1.3. 1.C. Pore-Forming Toxins

Polypeptides of subclass 1.C attack target cells other than the producer cell by inserting into the target cell membrane, usually forming oligomeric transmembrane pores. The toxic effects are caused by allowing the free flow of electrolytes and other small molecules across the membrane. Polypeptides of this subclass are probably synthesized universally by all types of living cell.

2.1.4. 1.D. Nonribosomally Synthesized Channels

Subclass 1.D systems usually consist of small molecular building blocks such as L- and D-amino acids and hydroxy acids. Assembly of the molecular building blocks allows construction of oligomeric transmembrane ion channels. "Depsipeptides" and amino acid-free substances of this class usually provide a function related to biological warfare. Most of these substances are synthesized by bacteria and fungi.

2.1.5. 1.E. Holins

The many families of channel-forming holins comprise subclass 1.E. They do not exhibit significant sequence similarity between families, but all holins display common structural and functional characteristics. The primary func-

tion of holins is to export murein hydrolases across the cytoplasmic membranes of bacteria where they hydrolyze the cell wall polymer as a prelude to cell lysis. Holins may also facilitate leakage of electrolytes and nutrients from the cell cytoplasm, thereby promoting cell death. They are encoded within the genomes of Gram-positive and Gram-negative bacteria as well as the bacteriophage of these organisms.

2.2. Class 2. Electrochemical Potential-Driven Transporters

Class 2 transport systems, also called secondary carrier-type facilitators, usually exhibit strict stereospecifity and are energy coupled to the proton motive force (pmf) or the sodium motive force (smf).

2.2.1. 2.A. Porters

Subclass 2.A consists of transport systems that utilize carrier-mediated processes to catalyze uniport (a single species is transported either by facilitated diffusion or in a membrane potential-dependent process if the solute is charged), antiport (two or more species are transported in opposite directions in a tightly coupled process, not coupled to a direct form of energy other than chemiosmotic energy), and/or symport (two or more species are transported together in the same direction in a tightly coupled process, not coupled to a direct form of energy other than chemiosmotic energy). These systems are ubiquitous, being found in all living organisms.

2.2.2. 2.B. Nonribosomally Synthesized Porters

Like class 1.D, nonribosomally synthesized channels, molecules of subclass 2.B may be depsipeptides or non-peptide-like substances. They usually facilitate translocation by complexing an ion in their hydrophilic interior, exposing their hydrophobic exterior and moving from one side of the bilayer to the other. Transport can be electrophoretic if the free porter can cross the membrane in the uncomplexed form, or it can be electroneutral if only the complex can cross the membrane. Most of these molecules are products of bacteria and fungi.

2.2.3. 2.C. Ion-Gradient-Driven Energizers

Class 2.C energizers use the proton or sodium motive force across the cytoplasmic membrane. The mechanism is poorly understood, but they undoubtedly couple proton (H^+) or sodium (Na^+) fluxes to the energized process. Currently recognized energizers can drive bacterial flagellar rotation or active transport across the outer membranes of Gram-negative bacteria. They belong to a single family.

2.3. Class 3. Primary Active Transporters

Class 3 transporters use a primary source of energy as compared with a secondary (chemiosmotic) source of energy to drive active transport of solutes against concentration gradients.

2.3.1. 3.A. P–P-bond Hydrolysis-Driven Transporters

Transport systems of subclass 3.A hydrolyze the diphosphate bond of inorganic pyrophosphate or a nucleoside triphosphate to drive the active uptake and/or extrusion of a solute or solutes. The transport protein may or may not be transiently phosphorylated, but the substrate is not chemically modified. Members of this subclass are found in all domains of the living world.

2.3.2. 3.B. Decarboxylation-Driven Transporters

Transport systems that drive solute uptake or extrusion by decarboxylation of a cytoplasmic substrate comprise subclass 3.B. These multisubunit transporters are currently thought to be restricted to prokaryotes and belong to a single family.

2.3.3. 3.C. Methyltransfer-Driven Transporters

A single characterized multisubunit protein family currently falls into subclass 3.C, the Na^+-transporting methyltetrahydromethanopterin: coenzyme M methyltransferases. These transporter complexes have been found only in archaea.

2.3.4. 3.D. Oxidoreduction-Driven Transporters

Subclass 3.D is comprised of transport systems that drive transport of a solute (H^+ or Na^+) energized by the exothermic flow of electrons from a reduced substrate to an oxidized substrate. These multisubunit systems are distributed in all domains of the living world.

2.3.5. 3.E. Light-Absorption-Driven Transporters

Transport systems that utilize light energy to drive transport of an ion are included in subclass 3.E. These systems and their homologs are distributed in all three domains of life.

2.4. Class 4. Group Translocators

Class 4 systems include transporters that chemically alter the substrate during transport across a membrane so that the species released into the cytoplasm differs from the one that was taken up.

2.4.1. 4.A. Phosphotransfer-Driven Group Translocators

Transport systems of the bacterial phosphoenolpyruvate:sugar phosphotransferase system are the only recognized group translocators of subclass 4.A. The product of the transport reaction, derived from extracellular sugar, is a cytoplasmic sugar-phosphate. The enzymatic constituents, which catalyze sugar phosphorylation, are superimposed on transport in a tightly coupled process.

2.5. Class 5. Transmembrane Electron Carriers

Class 5 proteins include systems that catalyze electron flow from one side of a biological membrane to the other. Thus, the electrons are transferred from donors localized to one side of the membrane to acceptors found on the other side. These systems contribute to or subtract from the membrane potential, depending on the direction of electron flow.

2.5.1. 5.A. Transmembrane Two-Electron Transfer Carriers

Subclass 5.A is restricted to systems that catalyze transfer of a pair of electrons across the membrane in one or more discrete steps without splitting the paired electrons.

2.5.2. 5.B. Transmembrane One-Electron Transfer Carriers

Subclass 5.B includes systems that catalyze the sequential transfer of single electrons across the membrane in a free-radical-type process.

2.6. Class 8. Accessory Factors Involved in Transport

Proteins that function with or are complexed to known transport proteins are included in category 8. In some cases, auxiliary proteins are considered to be an integral part of the transport system, and in such cases, the proteins are classified with the transporter. In this case, no distinct entry in category 8 is provided.

2.6.1. 8.A. Auxiliary Transport Proteins

Subclass 8.A consists of proteins that facilitate transport across one or more biological membranes but do not themselves participate directly in transport. These proteins always function in conjunction with one or more established transport system(s). They may provide a function connected with energy coupling to transport, play a structural role in complex formation, serve a biogenic or stability function, or play a regulatory role.

2.7. Class 9. Incompletely Characterized Transport Systems

Transport protein families for which insufficient information is available to allow classification in a defined class (e.g., TC classes 1–5) belong to category 9.

2.7.1. 9.A. Recognized Transporters of Unknown Biochemical Mechanism

Recognized families of transport proteins of unknown classification are grouped in subclass 9.A. These families include at least one member for which a transport function has been established, but either the mode of transport or the energy coupling mechanism is not known. They will be classified elsewhere when the transport mode and/or energy coupling mechanisms are characterized.

2.7.2. 9.B. Putative Uncharacterized Transport Proteins

Putative transport protein families are grouped into subclass 9.B if a transport function has been suggested for one or more members of the family, but evidence for such a function is not yet compelling. They will either be classified elsewhere when the transport function of a member becomes established or will be eliminated from the TC system if the proposed transport function is disproven.

2.7.3. 9.C. Functionally Characterized Transporters Lacking Identified Sequences

Transporters of particular physiological significance are included in category 9.C even though a family assignment cannot be made. When their sequences are identified, they will be assigned to an established family. This is the only TC subclass that includes individual proteins rather than protein families.

3. Practical Applications of Transporter Family Association

About 350 protein families were included in the TC system as of February 2002 (*see* TCDB). Affiliation with a family requires satisfying rigorous statistical criteria of homology *(7)*. Briefly, a protein must exhibit a region of at least 60 residues in comparable portions of the protein that exhibit a comparison score in excess of 9 standard deviations (SD) with at least one established member of that family using any one of a number of programs such as GAP, RDF2, Los Alamos, or ALIGN (*see* **ref. 7**). Whereas the classes and subclasses distinguish functionally distinct types of transporters, the families and subfamilies provide a phylogenetic basis for classification. The TC system is thus a functional/phylogenetic system of classification. Families very rarely cross class or subclass lines.

Recognition of a phylogenetic relationship based on sequence similarity allows certain conclusions to be drawn regarding three-dimensional structural features. Any two proteins that can be shown to be homologous (i.e., that

exhibit sufficient primary and/or secondary structural similarity to establish that they arose from a common evolutionary ancestor) can be expected to exhibit strikingly similar three-dimensional structures, although a few exception have been noted *(8)*. Therefore, extrapolation from one member of a family of known structure to all other members becomes justifiable. Extrapolation of structural data to other proteins should never be made if homology has not been established. Similar arguments apply to mechanistic considerations. Thus, the mechanism of solute transport is likely to be similar for all members of a permease family, and variations on a specific mechanistic theme will be greatest when the sequence divergence is greatest. By contrast, for members of any two independently evolving permease families, the transport mechanism may be strikingly different. Extensive experimental work has established that phylogenetic data can also be used to predict substrate specificity, polarity of transport, and even intracellular localization depending on the family and the degree of sequence divergence observed within that family *(3,9)*.

Transport system families included in the current TC system are described in database format on the World Wide Web (http://tcdb.ucsd.edu). TCDB provides detailed descriptions of and reference citations for (1) TC classes, (2) subclasses, (3) families (4) subfamilies and, (5) individual proteins. Additionally, relevant research tools can be found on our website, facilitating examination of the world of transport proteins. TCDB is equipped with a search tool that allows the user to search by key word, gene name, family, or protein sequence. Any protein demonstrably homologous to a TC family member can be identified using TC-BLAST. TCDB is interconnected with other useful databases and websites.

4. Family Characteristics

Key features of the transporter families currently recognized in TCDB are summarized in Table 2 of **ref.** *(6)*. The TC number of the family, the substrates transported, and the size ranges of the individual protein members within each family are presented. Additionally, the probable numbers of transmembrane segments in the integral membrane constituents of the family are predicted and the organismal groups in which members of each family have been identified are presented. The major conclusions summarized in this chapter are based on the data presented in **ref.** *(6)*.

Several TC family entries are actually superfamilies. In such cases, TCDB indicates the numbers of subfamilies currently recognized within that superfamily. The VIC (1.A.1), MF (2.A.1.), and ABC (3.A.1) superfamilies are the largest and most diverse transporter superfamilies currently recognized, but several other TC families have achieved superfamily status. The interested

reader is referred to TCDB for further explanation. Some of these superfamilies are discussed in the following sections.

5. Transport Protein Topological Types

The topologies of proteins within the different families of the TC system have been predicted using topological prediction programs such as WHAT ***(10)*** and TOPPRED ***(11)***. In relatively few instances have protein topologies been experimentally established.

We previously proposed that channels and carriers are fundamentally different at both structural and functional levels, but that the former may have been the evolutionary precursors of the latter ***(4)***. In **Fig. 1**, the predicted topologies of α-type channels (subclasses 1.A+1.C+1.E) and carrier proteins (subclass 2.A) are shown. The numbers of families represented are plotted versus the numbers of transmembrane segments (TMSs) found in the protein constituent types.

As seen in **Fig. 1**, the topological types that comprise α-type channels differ fundamentally from secondary carriers. Most families of α-helical channels include proteins with one to six TMSs, whereas the vast majority of carrier-type families display 10–14 TMSs. Almost all proteins in subclasses 1.C and 1.E display just one or two TMSs (data not shown), but channel proteins of subclass 1.A can exhibit up to 24 TMSs per polypeptide.

The small numbers of TMSs in most channel-forming proteins reflect their oligomeric structures, whereas the larger numbers of TMSs in the carriers reflect their basically monomeric constructions. The average numbers of TMSs for subclasses 9.A and 9.B are more representative of channellike proteins than carriers, suggesting that the majority of the proteins in these categories that are transporters will prove to be channels. However, some will undoubtedly prove to be carriers, and a few may be found to function by novel mechanisms. The data presented in **Fig. 1** allow one to predict which class 9.A families are likely to be members of TC class 1 or 2.

It has been proposed that large complex transport systems arose progressively from smaller simpler ones ***(4)***. Subclass 1.A channels could have developed from toxinlike peptide channels of subclass 1.C or holinlike channels of subclass 1.E, and subclass 1.A channels may have been the evolutionary precursors of porters. The latter proteins have more TMSs, and by virtue of their increased structural and functional complexity, it is reasonable to propose that carriers arose from channels in processes that involved internal gene duplication events ***(7)***. In fact, sequence analyses have revealed the presence of internal repeat sequences in many of the proteins that comprise families of secondary and primary active transporters as well as some channel proteins

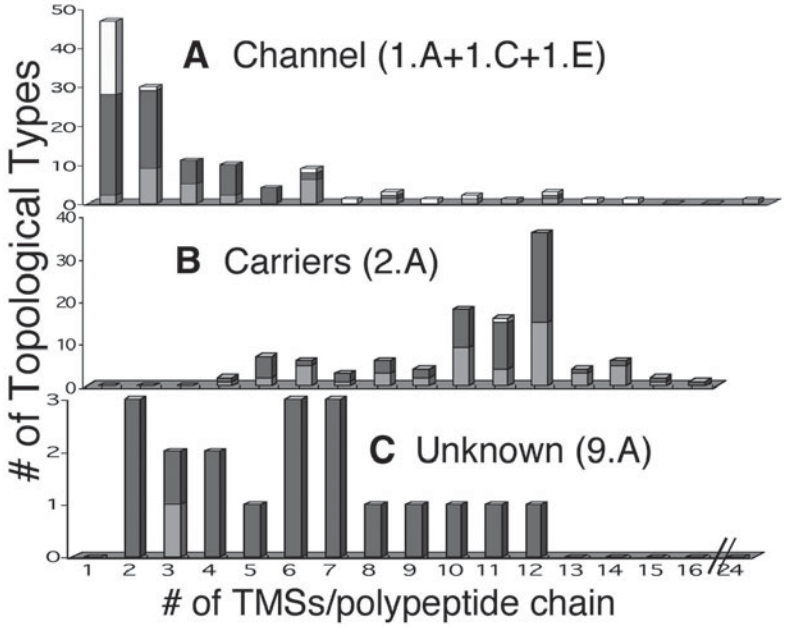

Fig. 1. Distribution of the various topological types of transporters in three subgroups of the TC system: **(A)** channels (TC classes 1.A plus 1.C plus 1.E); **(B)** porters (2.A); **(C)** transporter types of unknown mechanism (9.A). Grey, established; black, putative; white, uncertain.

(1,5,7). The repeat units of these complex transporters resemble the full-length sequences of the simpler channels ***(9)***. It is important to note that very few families of transporters include homologs that function in a capacity other than transport ***(5)***. Arguments that primary active transporters and group translocators resulted from superimposing catalytic proteins such as enzymes onto channels and carriers have been presented ***(4)***.

6. Size Variations in Transporters

We have evaluated the size ranges observed for the families that comprise the different subclasses of the TC system ***(6)***. Most families in TC subclass 1.A are intermediate in size (100–1000 residues per polypeptide chain), but a few are less than 100 or more than 1000 residues. By contrast, most transporter types in TC subclasses 1.C and 1.E are much smaller, and all of subclass 1.E proteins are small. Proteins of subclass 2.A are never smaller than 100 residues in length and most exceed 400 residues. Those of subclass 9.A more closely resemble the channels of subclass 1.A. These size differences reflect the topo-

logical differences noted earlier. Size variability is minimal for channel-forming subclasses 1.C and 1.E but substantially greater for subclass 1.A. The variance for proteins of subclass 2.A is comparable to that of the channels of subclass 1.A. Interestingly, that in subclass 9.A is minimal.

7. Transporter Family Sizes

Recognized transporter families differ over three orders of magnitude with respect to the numbers of currently sequenced proteins which comprise them. The vast majority of the TC families are of intermediate size, having between 6 and 500 currently sequenced members. As of February 2002, only 66 families have 5 members or less, and only 15 families include more than 500 sequenced protein members. Most of these large families are ubiquitous, having membership from all major domains of living organisms. They are probably ancient families dating back before the time that archaea and eukaryotes split apart from bacteria. Of the channels, the five largest families are the ubiquitous VIC, MIP, and HSP70 families (TC 1.A.1, 1.A.8, and 1.A.33, respectively) as well as the eukaryotic-specific TRP-CC and LIC families (TC 1.A.4 and 1.A.9, respectively). Of the secondary active carriers, the MF (2.A.1), RND (2.A.8), DMT (2.A.7), NSS (2.A.22), MC (2.A.29), and MATE (2.A.68) superfamilies have the largest membership. Among the primary active carriers, the ABC (3.A.1), P-type ATPase (3.A.3), and COX (3.D.4) families have the greater family membership with decreasing numbers of members in this order. One putative transporter family (FAT [9.B.17]), the acyl-CoA synthase family, includes thousands of sequenced proteins, but a role of these proteins in transport is not well established ***(12)***. If these enzymes couple fatty acid uptake to coenzyme A thio-esterification, such a process would provide an example of group translocation in which the substrate is modified during transport ***(13)***. These systems may, therefore, be group translocators, which, in addition to the families of the bacterial phosphotransferase system, would fall into TC class 4.

8. Family Representation in Bacteria, Archaea, and Eukaryotes

The occurrence of transporter types in the three domains of life was evaluated by creating a plot that shows the representation of the members of a family in the three domains of living organisms ***(6)***. Most ubiquitous families are found within subclass 2.A (*see* **Subheading 2.2.1.**).

We suggest that this fact in part reflects the larger polypeptide sizes of these usually monomeric proteins. The smaller oligomeric channel-forming proteins may have undergone more extensive sequence divergence, leading to the appearance of multiple families exhibiting insufficient degrees of sequence similarity to allow the establishment of homology. The large protein size

facilitates distant phylogenetic relationship detection, and requirements for retention of specific functional properties restrict the natural process of sequence divergence that occurs over evolutionary time.

Most of the channel families in class 1 are restricted to a single organismal type. This fact may in part reflect the ease with which simple channellike functions can be generated *de novo* from small peptides, but it may also reflect the absence of strict constraints preventing sequence divergence. It is also possible that most of these families arose late, after the three domains separated. If so, lateral transfer of genes encoding these channel proteins occurred very seldom.

Bacterial transport protein families are more prevalent than are those found only in eukaryotes (47% vs 26%). This could be a reflection of evolutionary pressure forcing bacteria to maintain diversity in order to remain adaptive in response to a wide range of environmental stress conditions. Multicellular eukaryotes generally create internal homeostatic environments that obviate the need for extensive cellular stress-response mechanisms. The greater diversity of prokaryotic transporters may also reflect the greater period of evolutionary time that these organisms have been on Earth. Eukaryotes may have evolved from a limited subgroup of primordial bacteria, and these bacteria may not have possessed the full complement of prokaryotic transporter families. Alternatively, eukaryotes may have lost families that were present in the eukaryotic progenitor. Although eukaryotes exhibit fewer families than prokaryotes, they have proliferated tremendous numbers of paralogs within certain families ***(6)***, probably for very specific purposes involving tissue-specific and organelle-specific functions. Some animals, for example, encode within their genomes hundreds of paralogs of a single family ***(14)***.

There are very few archaeal-specific transporter families. This observation may in part reflect the fact that functional data are sparse for archaeal proteins. Molecular biological research over the past six decades has focused almost exclusively on bacterial and eukaryotic systems. However, if archaea, like eukaryotes, arose from primordial bacteria, they may have acquired a restricted subset of proteins from the ancestral bacterium and they then would have had less time to diversify. This interesting postulate should be subject to empirical research. It is noteworthy that the recognition of a transporter family is facilitated by the availability of genomic sequence data only if functional data are available.

Ubiquitous families represent only 14% of the total found in the TC system, and those represented in two of the three domains of life are still less numerous. Those shared by bacteria and eukaryotes (8%) exceed those shared by archaea and bacteria (4%) by about twofold. Only one family is found in the archaeal and eukaryotic domains but not in the bacterial domain. Some of the families found in two but not three domains will undoubtedly prove to

be ubiquitous when more sequence data and more sensitive search tools become available.

9. Three-Dimensional Structural Data for Transporters

Detailed structural data for transport proteins will be necessary in order to gain an ultimate understanding of transport processes. Unfortunately, very few membrane proteins have yielded to the techniques of the X-ray crystallographer. Despite the fact that integral membrane proteins comprise about one-third of all proteins, less than 2% of the available three-dimensional structures reported in the PDB database are for such proteins. The 40 transporters for which high-resolution structural data are available are tabulated in **ref.** ***(6)***.

10. Conclusions and Perspectives

The TC system displayed in TCDB allows any researcher to easily gain access to the extensive body of knowledge available for transport systems. With the tools we provide on our websites, one can convincingly view the relationships between the established transporters in the TC system and novel proteins that have recently been or will soon be sequenced. A valuable tool for this purpose is TC-BLAST which performs a BLAST search against TCDB, revealing the nearest homologs and the families in the TC system to which the query sequences belong. There are also a number of other programs available on our website that help to bring to light the features of newly discovered transporters (e.g., WHAT, AveHAS, BBF, TV, etc.). The interested reader is invited to view our website for in-depth exposure to these tools.

Because of the nature of transporters as integral membrane proteins, we believe that computational approaches will prove particularly useful for their structural elucidation. Phylogenetic analyses should reveal structure–function relationships that greatly facilitate empirical research. With the availability of better tools, it will be easier to track phylogenetic relationships and to uncover the pathways by which transporters have evolved. Tracking the evolutionary pathways taken for the appearance of topologically dissimilar proteins within a family, and for families of transporters exhibiting dissimilar mechanisms of action, will prove to be a daunting but highly worthwhile endeavor. For this purpose, it will be important to create new and more reliable topological prediction programs as well as programs that allow detection of very distant phylogenetic relationships ***(15)***.

Another crucial aspect of analyzing relationships between families and classes of families will involve designing a dataset of proteins within each family in an accurate but automated way. We are currently designing such

software for the TC system. If the datasets for the different families are sufficiently extensive and reliable, we will be able to derive accurate sequence motifs and patterns that characterize the families and have structural–functional significance. New approaches for characterizing families will undoubtedly come to light.

Research into the molecular basis of transport processes will be greatly facilitated by the use of *in silico* approaches. Such approaches are likely to reveal characteristics dictated by primary protein sequences that are currently masked because of, first, our limited understanding of membrane proteins and, second, the inadequacies of currently available computational technologies. Bioinformatic advances should facilitate, for example, the development of transport protein-specific drugs that may comprise new classes of antibiotic, antiprotozoan, and antifungal substances. Many other unforeseen advances can be anticipated.

11. Summary

Over the past several years, we have designed and expanded the TC system. This system is a functional/phylogenetic system designed for the classification of all transmembrane transport proteins found in living organisms on Earth. It parallels but differs from the strictly functional EC system, developed decades ago by the Enzyme Commission of the IUBMB for the classification of enzymes.

The TC system has recently been adopted by the IUBMB as the internationally acclaimed system for the classification of transporters. Here, we described the classes and subclasses of the TC system. Based on the characteristics of the nearly 400 families of transport systems included in the TC system, we summarized statistical analyses of these families and their constituent proteins. Specifically, we reported analyses of various transporter types for size and topological differences and analyzed the families for their protein memberships as well as the numbers and organismal sources of their constituent proteins. We showed that channels and carriers exhibit distinctive structural and topological features. Bacterial-specific families outnumber eukaryotic-specific families about two to one, whereas ubiquitous families, found in all three domains of life, are about half as numerous as eukaryotic-specific families. We propose that the ubiquitous families are the ancient families that arose before archaea and eukaryotes segregated from bacteria. The results argue against appreciable horizontal transfer of genes encoding transporters between the three domains of life over the past two billion years.

Acknowledgments

We wish to thank Arnost Kotyk, Ian Paulsen, Can Tran, Nelson Yang, and YuFeng Zhai for useful discussions. We are particularly grateful to YuFeng Zhai for designing software that facilitated the analyses summarized in this chapter. Work in our laboratory is supported by grants from the National Institutes of Health.

References

1. Saier, M. H., Jr. (1998) Molecular phylogeny as a basis for the classification of transport proteins from bacteria, archaea and eukarya, in *Advances in Microbial Physiology* (Poole, R. K., ed.), Academic, San Diego, CA, pp. 81–136.
2. Saier, M. H., Jr. (1999) Genome archeology leading to the characterization and classification of transport proteins. *Curr. Opin. Microbiol.* **2,** 555–561.
3. Saier, M. H., Jr. (2000) A functional–phylogenetic classification system for transmembrane solute transporters. *Microbiol. Mol. Biol. Rev.* **64,** 354–411.
4. Saier, M. H., Jr. (2000) Vectorial metabolism and the evolution of transport systems. *J. Bacteriol.* **182,** 5029–5035.
5. Saier, M. H., Jr. (2001) Evolution of transport proteins, in *Genetic Engineering. Principles and Methods, Vol. 23* (J. K. Setlow, ed.), Kluwer Academic/Plenum, New York, pp. 1–10.
6. Busch, W. and Saier, M. H., Jr. (2002) The Transporter Classification (TC) System, **2002,** *Crit. Rev. Biochem. Mol. Biol.* **37,** 287–337.
7. Saier, M. H., Jr. (1994) Computer-aided analyses of transport protein sequences: gleaning evidence concerning function, structure, biogenesis, and evolution. *Microbiol. Rev.* **58,** 71–93.
8. Saier, M. H., Jr. and T.-T. Tseng (1999) Evolutionary origins of transmembrane transport systems, in *Transport of Molecules Across Microbial Membranes, Symposium 58, Society for General Microbiology* (Broome-Smith, J. K., Baumberg, S., Stirling, C. J., et al., eds.), Cambridge University Press, Cambridge, UK, pp. 252–274.
9. Saier, M. H., Jr. (2000) Families of proteins forming transmembrane channels. *J. Membr. Biol.* **175,** 165–180.
10. Zhai, Y. and Saier, M. H., Jr. (2001) A web-based program (WHAT) for the simultaneous prediction of hydropathy, amphipathicity, secondary structure and transmembrane topology for a single protein sequence. *J. Mol. Microbiol. Biotechnol.* **4,** 501–502.
11. Claros, M. G. and von Heijne, G. (1994) TopPred II: An improved software for membrane protein structure predictions. *CABIOS* **10,** 685–686.
12. Saier, M. H., Jr. and Kollman J. (1999) Is FatP a long chain fatty acid transporter? *Mol. Microbiol.* **33,** 670–672.

13. Faergeman, N. J., Black, P. N., Zhao, X. D., et al. (2001) The acyl-CoA synthetases encoded within FAA1 and FAA4 in Saccharomyces cerevisiae function as components of the fatty acid transport system linking import, activation, and intracellular utilization. *J. Biol. Chem.* **276,** 37,051–37,059.
14. *C. elegans* Sequencing Consortium. (1998) Genome sequence of the nematode *C. elegans*: a platform for investigating biology. *Science* **282,** 2012–2017.
15. Pei, J. and Grishin, N. V. (2001) AL2CO: calculation of positional conservation in a protein sequence alignment. *Bioinformatics* **17,** 700–712.

3

Bioinformatics and Data Integration in Membrane Transporter Studies

Qing Yan

1. Introduction

With a history of less than 30 years, bioinformatics is a rapidly growing area that applies computational approaches to solve biological problems. Similar to the composition of the word itself, "bioinformatics" is an independent field developed from the union of computer science and molecular biology. This merge was started in 1970s, when it was found that RNA secondary structure might be predicted with computational techniques ***(1,2)***. At that time, people began to build databases of nucleic acids ***(3)*** and proteins ***(4)***. Algorithms and programs were developed to translate DNA sequences into protein sequences ***(5,6)*** and to detect patterns including restriction enzyme recognition sites ***(7,8)***. With years of efforts, sequence analysis methodologies are maturing and have become the most important part of bioinformatics.

As we enter the transition era from structural to functional genomics and proteomics, especially with the overwhelming variety and volume of data, bioinformatics becomes increasingly important and indispensable for other biomedical sciences. Different from most traditional biomedical sciences that are grounded in the observation of the physical world, bioinformatics is the rational study at an abstract level that can influence the way we think in biomedicine, the way we understand biomedical facts, and the way we apply the biomedical knowledge. At this stage, bioinformatics is facing challenges in helping with gene discovery, locating coding regions, molecular modeling, analyzing gene expression patterns, and finding the relationship between genetic structures and functions.

One of the most important issues in bioinformatics is data integration. This includes the integration of data from heterogeneous resources and from vari-

From: *Methods in Molecular Biology, vol. 227: Membrane Transporters: Methods and Protocols*
Edited by: Q. Yan © Humana Press Inc., Totowa, NJ

ous data types, and enterprisewide data integration among different groups and departments. There can be valuable knowledge buried in various unorganized data and the process of data integration can help "unveil" the hidden knowledge. In this chapter, we will briefly introduce methodologies on how to extract useful information from various data so that the information can be applied directly in research and development projects. We will also describe the organization of membrane transporter data, such as how to understand terminologies and the classification of membrane transporters.

Various bioinformatics approaches have been used in transporter studies. For example, the sequence similarity searching tool BLAST (Basic Local Alignment Search Tool) has been used extensively in the analysis of transport systems in different organisms ***(9)*** and in the identification of transporter genes ***(10)***. The database PROSITE has been used for functional analysis in transporter genes ***(11,12)***.

In this chapter, we will provide methodologies and protocols on when and how to use bioinformatics databases and tools in the membrane transporter research. To make the practice of these tools more convenient for any researchers from anywhere, most of the tools are chosen from on-line freely available ones. We will not discuss in detail the algorithms, but will rather focus on practical parts of applying these methods and tools. We will give real examples showing how to use these tools. Each method is described in a structured format as "When to use," "The database or the tool," and "Input and output." These are hands-on guides for analyzing sequence structures and functions and for annotating new sequences that researchers obtain from their experiments. We will address some most frequently encountered problems in the analysis to make the laboratory research faster and easier. The tools we list here are sample tools that are popularly used in academic environments, so that the readers can also use their experience learned here on other available tools, tool packages, and new tools.

2. Data Integration Methods in Membrane Transporter Studies

2.1. From Data to Information: The Processes of Data Integration

Data integration is not just for simple data access but also for knowledge discovery and decision support. The two words "data" and "information" are often used interchangeably. In fact, they are quite different. The term "data" implies a collection of discrete elements, such as a file. Data are rarely clean and may have different formats. Some data are from multiple competing sources. Some data have missing and incomplete fields. In addition, data formats and contents may change over time. When data are cleaned, structured, merged, aggregated, derived, sorted, and displayed, they become "informa-

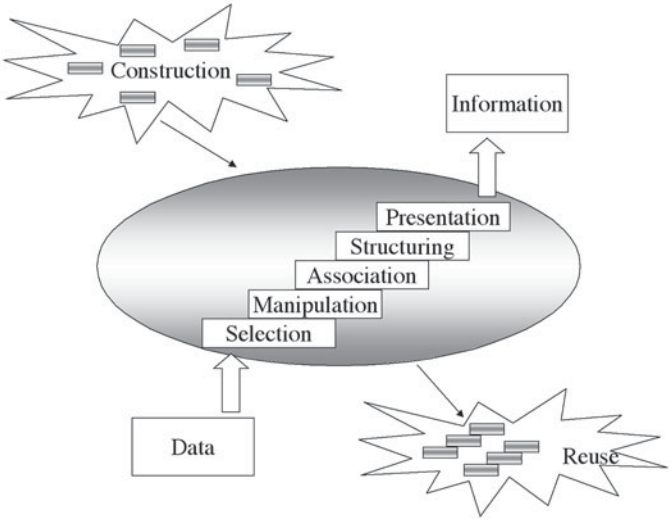

Fig. 1. Data integration: the process from data to information.

tion." Usually a database system provides an area to collect, integrate, and store data to perform the actions to enrich and enhance the value of the data. A database system offers a platform to transform data into information and is often useful for decision support purposes. The data integration methods introduced here can be used when researchers try to organize and integrate their own experimental data or to integrate both public and in-house data. This kind of work has become crucial in routine lab work, in order to organize and even publish one's research results.

Figure 1 shows the data transformation and integration process. This is also a process that standardizes names and values, resolves inconsistencies in representation of data, and integrates common values. The "equal" values of data from disparate sources that represent the same biomedical facts are also resolved in this process. This transformation process is repeated over and over again, during the original development of the target database, when adding new sources to the existing database, and when distributing data from the system to users. Once it has been constructed, this process can be reused in other projects.

Here, we focus on introducing the data consolidation approach in data integration, although other approaches can be used, such as the method of federation. The consolidation approach is based on constructing a database with a single large data model (e.g., when we need to extract data from various data sources and centralize these extracted data at one place). The major ben-

efits of this approach include enforcement of the standardization of heterogeneous data. However, it may have difficulties in case there is a need to evolve the database, because consolidation uses a single model that may be hard to change.

The data integration and transformation process begins with the selection of data sources, as shown in **Fig. 1**. Data are selected through the screening of all available sources and choosing the ones that can best fulfill the requirements. The selected data are then manipulated and transformed. Data consolidation is a procedure that analyzes and merges data from disparate sources or systems into a single, integrated data structure. This is achieved through identifying data that are common across the various source files and investigating the rules that manage the usage of the data. For example, polymorphism data about transporter genes can be retrieved from several sources, such as the databases dbSNP, OMIM (Online Mendelian Inheritance in Man), and GDB (Genome Database). It is necessary to integrate data from these different sources into a common data structure, which includes variation types such as deletion or point mutation.

The process of data consolidation also includes identifying data elements that have common biomedical meaning even though the names are different (synonyms) or those that have the same name but represent different biomedical facts (homonyms). Failing to properly identify these in the source files may result in disparate data that fail to provide the true integration points. If so, a falsely cohesive view of the data that delivers the wrong information can be created. For example, failure to identify the synonyms of one transporter gene may cause these different names to be regarded as different genes, which may lead to unclean data and serious data redundancy, even repeated experiments. This is actually a complicated issue in biomedical science that involves terminology and knowledge representation studies. Specific issues involved in the transporter domain will be discussed in detail in the following sections.

During the data manipulation process, data are also cleaned. In this step, redundant data are removed and outdated data are updated. Data cleaning can be done together with data consolidation and conversion. For example, sometimes the synonyms of a transporter gene are recorded as different records with redundant gene sequences. These redundancies can be removed with the identification of the synonyms. Sometimes, the chromosome location of a gene from one source is not provided in detail (such as only with a number 11). When the detail (e.g., 11p15.5) can be found in other sources, the more detailed data can be used. When the data are manipulated through consolidation, conversion, and cleaning, the result can be presented with a structuring of the information. Such data presentation may include tables and graphs, which can also be used in the decision support process.

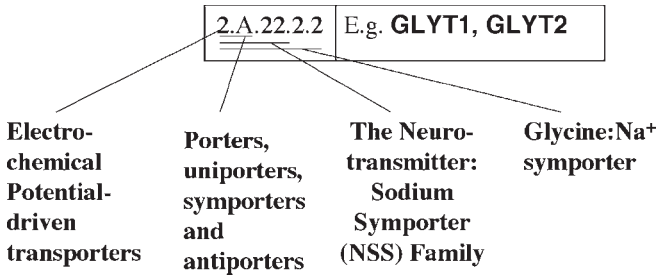

Fig. 2. Understanding the transporter family classification.

2.2. Understanding the Classification of Membrane Transporters

The classification of transporter genes can provide a comprehensive view of all transporters and help elucidate the directions of transporter research. Transporter gene classification is also one of the most important parts involved in data consolidation. Chapter 2 in this volume describes a comprehensive classification system for membrane transport proteins known as the Transport Commission (TC) system. According to Saier's classification ***(13)***, a TC number normally has five components as follows: V.W.X.Y.Z; they are defined as follows:

1. *V* (a number): the transporter class (i.e., channel, carrier [porter], primary active transporter, or group translocator)
2. *W* (a letter): the transporter subclass, which in the case of primary active transporters refers to the energy source used to drive the transport
3. *X* (a number): the transporter family (sometimes actually a superfamily)
4. *Y* (a number): the subfamily in which a transporter is found
5. *Z*: the substrate or range of substrates transported

Figure 2 shows an example of the TC number 2.A.22.2.2 and how to interpret each digit. A list of transporter families and their members in humans using the TC system can be found in the Human Membrane Transporter Database ***(14)***.

2.3. Transporter Nomenclature and Terminology

Because different names are often used for the same gene, terminology regarding genes often causes confusion. Studies of gene nomenclature are crucial in the identification of "synonyms" and in the data integration process. The full name of a gene can be very long, such as "Homo sapiens cellular retinoic acid-binding protein 1." Genes are usually represented by symbols, usually no longer than six characters in length, such as "*CRABP1*" for this

transporter gene. As defined by the Human Genome Organization (HUGO) Gene Nomenclature Committee, gene symbols are designated by uppercase Latin letters or by a combination of uppercase letters and Arabic numbers ***(15)***. Where gene products of a similar function are encoded by different genes, the corresponding loci are labeled by Arabic numerals placed immediately after the gene symbol, without any space between the letters and numbers used. For example, sodium-coupled nucleoside transporters *CNT1* and *CNT2*.

The "many names-to-one gene" situation may cause serious problems because if *4F2*, *4F2HC*, *MDU1*, *NACAE*, *4T2HC*, and *SLC3A2* (activator of dibasic and neutral amino acid transport) are treated as different genes, we will have six duplicated sets of records. Such redundancy may even add the total number of the transporters and cause confusion in further analysis. For example, to look up information on neutral amino acid transporters, should one use "*SATT*" or "*ASCT1*"? If one searches these two gene symbols from the nomenclature database ***(16)***, they are also termed "*SLC1A4*." **Table 1** shows a sample list of transporter genes with at least five symbols for one gene ***(14)***. Each cell in the left column lists the "synonym" symbols of a gene. The right column of the table shows the corresponding GenBank accession number of this gene in the same row.

In the following sections, we will introduce bioinformatics databases and tools, some of which are designed specifically for transporter studies and some are for general usage but are often applied in transporter studies (also *see* **Notes 1** and **2**).

3. Bioinformatics Databases for Membrane Transporter Studies

3.1. Membrane Transporter Database for Pharmacogenomics Studies and Drug Discovery

3.1.1. When to Use

1. To look for the information about membrane transporter genes and their characteristics; for example, membrane transporters' nucleotide and protein sequences, functions, the classification such as family and subfamily, chromosome locations, topology (e.g., transmembrane domains), translocation mechanisms, and tissue distribution
2. To look for the information on pharmacogenomics studies in membrane transporters, such as sequence variations including SNPs (single nucleotide polymorphism)
3. To support drug discovery, such as search for transporter-related diseases, substrates, and drugs
4. To look for the information on transporter nomenclature and terminology

Table 1
Transporters with at Least Five Symbols for One Gene

Transporter symbol	GenBank accession number
4F2, 4F2HC, MDU1, NACAE, 4T2HC, SLC3A2	AH001404
ABC1, ABC-1, ABCA1, TGD, CERP, HDLDT1	AJ012376
ABCA4, ABCR, STGD1, FFM, STGD, ARMD2	NM_000350
ABCB2, TAP1, D6S114E, PSF1, RING4	NM_000593
ABCC2, CMOAT, MRP2, cMRP, DJS	NM_000392
ABCD1, ALD, X-ALD, AMN, ALDP	NM_000033
ABCD4, PXMP1L, P70R, PMP69, EST352188	NM_005050
ABCP, BCRP, ABCG2, MXR, ABC15, EST157481	NM_004827
ANT1, T1, PEO2, PEO3, SLC25A4	NM_001151
ANT2, SLC25A5, 2F1, T2, SLC25A5	L78810
ATBo, SLC1A5, RDRC, hATBo, ASCT2, AAAT, M7V1, RDRC	U53347
BWR1B, SLC22A1LS, BWSCR1B, ORCTL2S, P27bwr1b	NM_007105
CAT1, HCAT1, ERR, REC1L, SLC7A1, ATRC1, CAT-1	AF078107
CAT2, SLC7A2, CAT-2a, CAT-2b, ATRC2, HCAT2	D29990
CNT1, SLC28A1, cit, N2, HCNT1	NM_004213
CNT2, SLC28A2, cif, N1, SPNT1, HCNT2	NM_004212
E16, LAT1, LAT-1, D16S469E, MPE16, SLC7A5	AF077866
E3KARP, NHERF-2, TKA-1, SIP-1, SLC9A3R2	NM_004785
FOLT, SLC19A1, RFC1, REFC, CHMD	NM_003056
GLVR2, GLCR1, MLVAR, GLVR-2, SLC20A2, PiT-2	NM_006749
HGT, SLC25A16, GDC, D10S105E, GDA, ML7	M31659
IMPT1, ORCTL2, BWR1A, BWSCR1A, ITM, TSSC5, SLC22A1L	AF028738
MDR2, MDR3, ABCB4, PGY3, PFIC-3	M23234
MOAT-C, ABCC5, MRP5, SMRP, ABC33, EST277145	AF104942
MRP3, ABCC3, MLP2, ABC31, MOAT-D, CMOAT2, EST90757	AF085692
NBC1, NBC2, pNBC, HNBC1, hhNMC, SLC4A4	NM_003759
rBAT, SLC3A1, D2, D2H, CSNU1, SLC3A1	U60819
SUR1, ABCC8, HI, PHHI, SUR, MRP8, HRINS	U63421
TAP2, ABCB3, D6S217E, PSF2, RING11	X87344/2

Table 2
Data Sources Incorporated in the Human Membrane Transporter Database

Incorporated data sources	Links
Entrez	http://www.ncbi.nlm.nih.gov/Entrez/
dbEST	http://www.ncbi.nlm.nih.gov/dbEST/index.html
dbSNP	http://www.ncbi.nlm.nih.gov/SNP/index.html
GDB (Genome Database)	http://www.gdb.org/
PDB	http://www.rcsb.org/pdb/
OMIM	http://www.ncbi.nlm.nih.gov/omim/
HGMD (Human Gene Mutation Database)	http://www.uwcm.ac.uk/uwcm/mg/hgmd0.html
Genes and Disease Map	http://www.ncbi.nlm.nih.gov/disease/Transporters.html
Gene nomenclature	http://www.gene.ucl.ac.uk/cgi-bin/nomenclature/searchgenes.pl
PubMed	http://www.ncbi.nlm.nih.gov/PubMed/
ABC transporter page	http://nutrigene.4t.com/humanabc.htm
Transporter classification	http://www-biology.ucsd.edu/~msaier/transport/toc.html#1A
Human Enterocyte Transporters	http://bigfoot.med.unc.edu/watkinsLab/hEnt.htm
Human Hepatocyte Transporters	http://bigfoot.med.unc.edu/watkinsLab/hHep.htm

3.1.2. The Database

An integrated and comprehensive database about human membrane transporters is Human Membrane Transporter Database (HMTD), available at http://lab.digibench.net/transporter/.

3.1.3. Input and Output

The Web-accessible relational database supports both browsing and query functions. A user can browse the database by clicking the relevant links that one is interested in and browsing the result forms. Users can also query the database by entering keywords and selecting relevant categories. The database provides integrated information and supports queries in all the above areas, including sequence structural, functional, pathological, and pharmacological information ***(17)***. The database incorporates and provides links to other databases with relevant information, such as dbSNP (a NCBI database of SNPs), OMIM (Online Mendelian Inheritance in Man, a database of human genes, genetic variants, and genetic disorders), and HGMD (Human Gene Mutation Database). The database also includes information from other available transporter databases such as ABC Transporter Database (accessible at http://nutrigene.4t.com/humanabc.htm). **Table 2** lists some data sources incorporated

in HMTD. HMTD provides an inclusive collection and organization of nomenclatures and synonyms of transporter symbols and names. The comprehensiveness of this database can help make the transporter studies more convenient.To facilitate usages, the searching part of the database can be queried with all related symbols as transporter names. For example, to search for information about neutral amino acid transporters, users can type in "*SATT*" or "*ASCT1*" or "*SLC1A4*" as the keyword.

3.2. General Bioinformatics Databases

Table 3 summarizes some general bioinformatics databases and tools that are frequently used in membrane transporter studies. We will describe the details of using some of these databases and tools in the following subsections.

3.2.1. The Entrez Searching System for the GenBank Database

3.2.1.1. When to Use

This system is used to search for nucleic acid and protein sequences, and relevant information, including structures and publications.

3.2.1.2. Databases and Tools

A data retrieval system called Entrez is frequently used to search the GenBank databases. It is available at http://www.ncbi.nlm.nih.gov/Entrez/. This retrieval system can be searched for several linked databases, including the GenBank nucleotide sequence database, protein sequence database, literature database (PUBMED), and the database OMIM.

3.2.1.3. Input and Output

Users can query the linked databases through a keyword search; for example, to look for the nucleotide sequence of the transporter gene *TAP1*, one can use the gene symbol as the keyword. Users can also add some more words to limit their search. The full gene definition, accession number, GI number (GenIn), source, organism, and references are listed on the Entrez pages for nucleotides or proteins. Some features of the gene, such as coding sequences (CDs), are also listed on nucleotide pages. The gene sequence can be displayed in different formats. Hyperlinks to relevant databases, such as the corresponding protein sequence, are also provided.

3.2.2. OMIM Database

3.2.2.1. When to Use

This database can be used to search for genetic disorders, allelic variants, and relevant information.

Table 3
General Bioinformatics Databases and Tools That Can Be Used in Membrane Transporter Studies

Category	SubCategory	Database/ tool example	URL
Sequence Structure and Function	Nucleotide and protein	Entrez	http://www.ncbi.nlm.nih.gov/Entrez/
	DNA	dbEST	http://www.ncbi.nlm.nih.gov/dbEST/index.html
	Gene-oriented	UniGene cluster	http://www.ncbi.nlm.nih.gov/UniGene/index.html
	Sequence variation	dbSNP	http://www.ncbi.nlm.nih.gov/SNP/index.html
	Structure (3D) database	PDB	http://www.rcsb.org/pdb/
	Pathway and cellular regulation	KEGG	http://www.genome.ad.jp/kegg/kegg2.html
	Regulatory structure	TRANSFAC	http://transfac.gbf.de/TRANSFAC/index.html
	Motif database and analysis	Pfam ProfileScan	http://pfam.wustl.edu/hmmsearch.shtml http://hits.isb-sib.ch/cgi-bin/PFSCAN
	Sequence format conversion	fmtseq	http://members.aol.com/_ht_a/lucatoldo/myhomepage/JaMBW/1/2/
	Sequence translation	Translation machine	http://www2.ebi.ac.uk/translate/
	Homology search	BLAST	http://www.ncbi.nlm.nih.gov/BLAST/
	Multiple alignment	Clustal W	http://www.ebi.ac.uk/clustalw/
	Exon finding and gene annotation	GenScan	http://genes.mit.edu/GENSCAN.html
	Transmembrane region detection detection	TMPred	http://www.ch.embnet.org/software/TMPRED_form.html
	Secondary structure prediction	PredicProtein	http://cubic.bioc.columbia.edu/predictprotein/submit_def.html
	3D structure prediction	Geno3D	http://geno3d-pbil.ibcp.fr/
Phenotype	Disorder	OMIM	http://www.ncbi.nlm.nih.gov/omim/

3.2.2.2. Database

The OMIM database is available at http://www.ncbi.nlm.nih.gov/Omim/searchomim.html.

3.2.2.3. Input and Output

The database has a keyword query interface so that users can just type in the keyword in which they are interested. The database contains textual information about genetic disorders, allelic variants, and relevant information such as genotype and phenotype, biochemical and clinical features, clinical diagnosis, population genetics, and references. It also provides links to the MEDLINE database, DNA and protein databases, LocusLink (a query interface to DNA and protein sequences and related information about genetic loci), Gen Map (lists the cytogenetic map location of disease genes and other genes described in OMIM), GDB (Genome Database), and the Human Gene Nomenclature Database.

3.2.3. The EST and Gene Cluster Database

3.2.3.1. When to Use

Expressed sequence tags (ESTs) are short DNA sequences usually around 200–500 bases derived by sequencing an end of a random cDNA clone from a library of interest. Corresponding to fragments of genes, ESTs provide a rapid way of identifying cDNAs of interest and contain information about the cell of origin. ESTs are useful in a wide range of studies, for gene discovery, gene mapping, gene expression studies, microarray studies, polymorphism analysis, and gene prediction.

3.2.3.2. Databases

The database called dbEST is available at http://www.ncbi.nlm.nih.gov/dbEST/index.html. The NCBI database dbEST contains ESTs from more than 250 organisms. The gene cluster database UniGene is accessible at http://www.ncbi.nlm.nih.gov/UniGene/.

3.2.3.3. Input and Output

The databases can be queried by entering keywords. The contents of the databases are also downloadable from their FTP (file transfer protocol) sites. UniGene is a database that contains subsets of related sequences that represent

a unique gene through clustering mRNA sequences, ESTs, and CDs annotated on genomic DNA. It also provides relevant information, including tissue types in which the gene has been expressed, map location, and protein identity in various organisms. Thus, it is especially helpful for gene mapping and large-scale gene expression analysis such as microarray analysis.

3.2.4. SNP Database

3.2.4.1. When to Use

This database is used to search for genetic variation information, especially SNPs, which occur about once every 100–300 bases. The identification of associations between a disease and specific differences (SNPs) in a population plays an important role in pharmacogenomics.

3.2.4.2. Database

The database is available at http://www.ncbi.nlm.nih.gov/SNP/index.html.

3.2.4.3. Input and Output

The database can be searched by keywords and IDs (such as GenBank Accession numbers). In addtion to SNPs, the database also contains information about microsatellite repeats and small insertion/deletion polymorphisms. The query result pages contain a section about SNP data submitter records, the FASTA sequence, LocusLink, integrated maps, including chromosome maps, and variation and validation summaries.

3.2.5. Protein Structure Database

3.2.5.1. When to Use

Three-dimensional (3D) structures of transporter proteins may be useful for analyzing and understanding protein functions. Proteins with known 3D structures detected through methods such as X-ray crystallography and nuclear magnetic resonance (NMR) are stored in structure databases. These known structures can also help predict unknown structures of other proteins.

3.2.5.2. Database

A popularly used public database is Protein Data Bank (PDB), accessible at http://www.rcsb.org/pdb/.

3.2.5.3. Input and Output

The PDB supports keyword search. The search result page provides a summary of the structure information and links to other sources and analysis engines. Some display options can be chosen to view the structure of the pro-

tein, such as using the visualization tool Rasmol (available at http://www.umass.edu/microbio/rasmol/index2.htm). Users can download the structure files onto their desktops. Geometry, such as bond angles, and sequence details, such as secondary structures, are also available on this page.

4. Bioinformatics Tools for Membrane Transporter Studies

4.1. Genomics Analysis

4.1.1. Sequence Format Conversion

4.1.1.1. When to Use

In many cases, a researcher has sequences in different formats that need to be converted to one specific format to standardize or facilitate the research. Many bioinformatics tools require certain sequence input formats, and researchers need to convert their raw sequence data into the format requested before they can use the program. Usually, a sequence can be in a plain-text format, the FASTA format, the GenBank format, or the Swiss-Prot format. An example for the use of the conversion would be a researcher who has sequenced out a new transporter gene and needs to convert it to certain formats to do some analysis or to submit it to some public databanks.

4.1.1.2. Tool

Some on-line tools can be used to do such conversion; a useful tool is at http://members.aol.com/_ht_a/lucatoldo/myhomepage/JaMBW/1/2/.

4.1.1.3. Input and Output

Users can simply paste their original sequences in the upper window, select the target case and format of output sequences, click the "Perform Conversion" button, and see the results in the lower window. Users can then save the results to their own computers.

4.1.2. Similarity/Homology Searching

4.1.2.1. When to Use

Sequence similarity search is usually one of the first steps in analyzing a newly discovered gene product with unknown function. This is used when researchers obtain a sequence from their experiments and want to know if it is new or has been found already, or what the similar sequences are so that they can have an idea of how to classify this new gene. Sequence similarity search can also help to get a clue of the function of the gene, because its function might also be similar to those of related sequences. When researchers have designed a probe and want to know if the probe sequence is unique and will not

bind to genes other than targeted, they may also need to use similarity searching tools.

4.1.2.2. Tool

Basic Local Alignment Search Tool (BLAST) is a set of programs frequently used for sequence similarity searching, including both nucleotide and protein sequences. Because BLAST identifies relationships among sequences that share isolated regions of similarity ***(18)***, it is not only a tool to find homology but also a program to locate regions of sequence similarity with a view to comparing structure and function. BLAST programs are freely available at http://www.ncbi.nlm.nih.gov/BLAST/.

4.1.2.3. Input and Output

Users can paste their sequences into the BLAST program window and submit the request. **Table 4** is a practical guide that shows when to select which program for sequence analysis ***(19)***. The result of BLAST can be presented in different formats.

4.1.3. Multiple Sequence Alignment and Phylogenetic Analysis

4.1.3.1. When to Use

Multiple sequence alignment is a very useful method for comparing two or more sequences. This method can be used to find the conserved regions among a set of sequences, to find the variances among the sequences, to track the sequence alteration, or to trace the evolutionary relationship. This method can also be used to check unique regions in a group of sequences and to determine if the designed hybridization probe is appropriate.

4.1.3.2. Tool

A convenient tool for performing multiple sequence alignment and constructing phylogenetic trees is the Clustal W (available at http://www.ebi.ac.uk/clustalw/).

4.1.3.3. Input and Output

Users can paste or upload a set of sequences in which they are interested; for example, to compare the following sequences and see how they are possibly related to each other in a phylogenetic tree. A phylogenetic tree is an estimation of evolutionary relationships expressed in a tree diagram.

>gi|36061|emb|CAA40741.1| peptide transporter [*Homo sapiens*]
>gi|1200201|gb|AAA91199.1| ABC-transporter [*Gorilla gorilla*]
>gi|6093550|gb|AAB58723.2| TAP1 [*Mesocricetus auratus*]

Table 4
Different BLAST Programs for Sequence Analysis

The sequence you have	You can use this program	What this program does
Amino acid	blastp	Compares an amino acid query sequence against a protein sequence database
Nucleotide	blastn	Compares a nucleotide query sequence against a nucleotide sequence database
Nucleotide	blastx	Compares a nucleotide query sequence translated in all reading frames against a protein sequence database; use this option to find potential translation products of an unknown nucleotide sequence
Amino acid	tblastn	Compares a protein query sequence against a nucleotide sequence database dynamically translated in all reading frames
Nucleotide	tblastx	Compares the six-frame translations of a nucleotide query sequence against the six-frame translations of a nucleotide sequence database (Please note that the tblastx program cannot be used with the nr database on the BLAST Web page because it is computationally intensive)

>gi|1399907|gb|AAB41965.1| TAP1-f
>gi|1771570|emb|CAA71282.1| Tap1 protein [*Rattus norvegicus*]

Figure 3 shows the result page of the alignment; the regions with consensus or different sequences can be highlighted in colors. The phylogenetic tree for this set of sequence is also shown at the bottom of the page.

4.1.4. Exon Finding and Gene Annotation

4.1.4.1. When to Use

This would be used when one has genomic DNA sequences and needs to do some analysis such as identifying exons and polyA signals.

4.1.4.2. Tool

There are several tools for gene finding and annotation. One of the popularly used tools is GenScan, which is available at http://genes.mit.edu/GENSCAN.html.

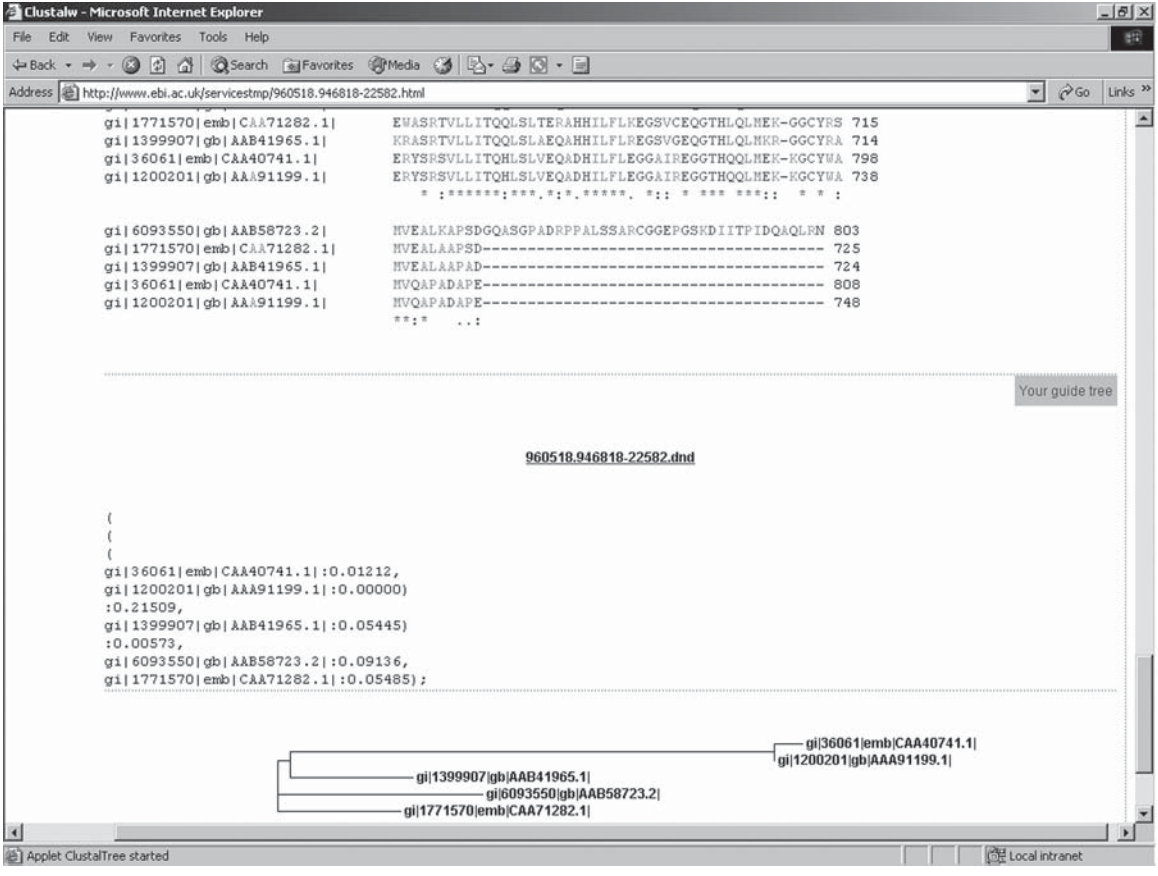

Fig. 3. Multiple alignment and phylogenetic tree analysis using Clustal W.

4.1.4.3. Input and Output

The input for GenScan can be a DNA sequence or a sequence file. It will predict information, including exons and polyA signals. The program also shows the annotation in a diagrammatic PDF format. In addition, it will predict the peptide sequence.

4.1.5. Contig Assembly

4.1.5.1. When to Use

"Contig" is a short version of "contiguous." A contig is a contiguous sequence assembled from a set of shorter overlapping DNA sequences. Contig assembly programs are used to assemble DNA fragments.

4.1.5.2. Tool

A contig assembly program (CAP) with a Web interface is at http://bio.ifom-firc.it/ASSEMBLY/assemble.html.

4.1.5.3. Input and Output

Like other programs, users can paste their sequences for assembling into the window or upload their sequence files. For example, we can input the following EST clusters retrieved from the database UniGene:

>BI918327 603182834F1 HOMO SAPIENS CDNA, 5' END
>H23432 ym52e10.r1 Homo sapiens cDNA, 5' end
>H23433 YM52E10.S1 HOMO SAPIENS CDNA, 3' END

Figure 4 Shows the assembled contig resulting from running the program. By checking the contig sequence using BLAST, we find that it is closest to "Homo sapiens transporter 1, ATP-binding cassette, sub-family B (MDR/TAP) (TAP1)."

4.2. Proteomics Analysis

4.2.1. Sequence Translation

4.2.1.1. When to Use

This is used to translate a DNA sequence into protein sequence for further analysis, or vise versa.

4.2.1.2. Tools

An on-line program to do the translation is at http://www2.ebi.ac.uk/translate/.

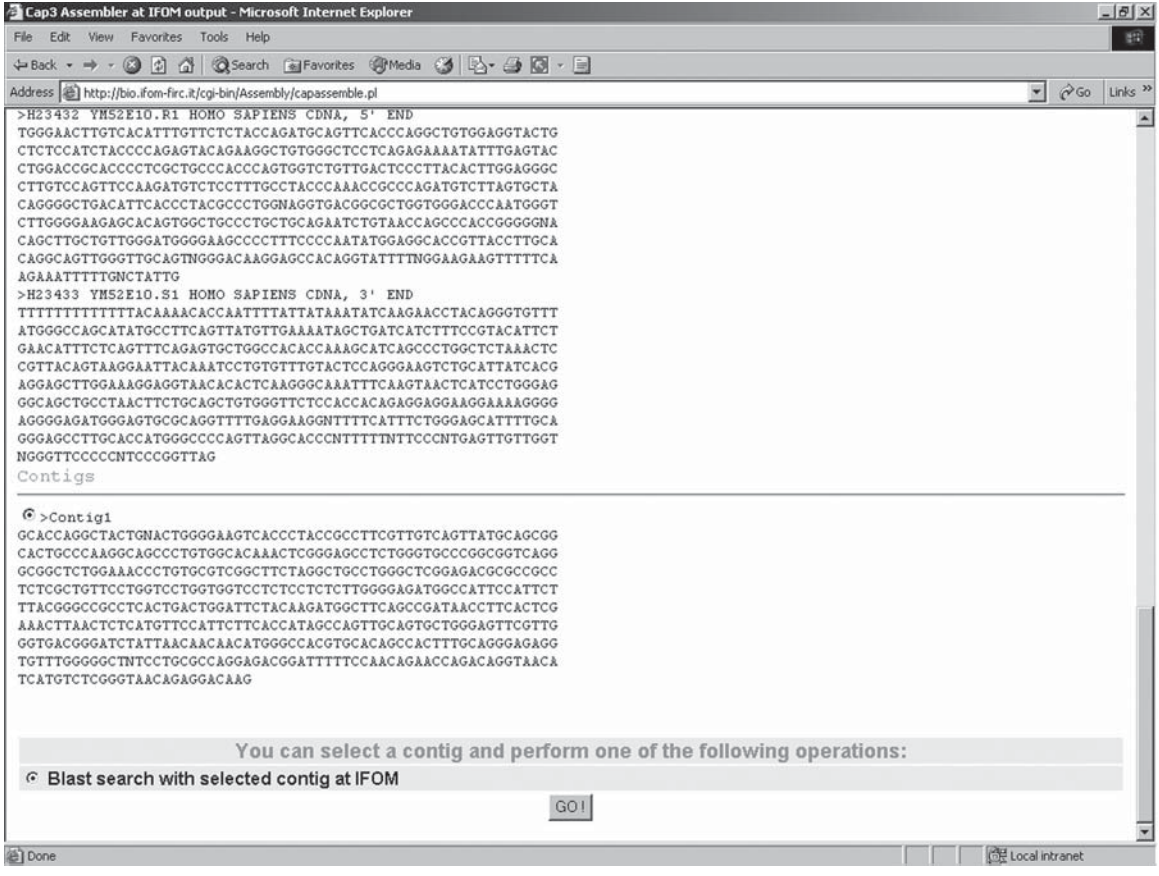

Fig. 4. Assembled contig using the contig assembly program (CAP).

4.2.1.3. Input and Output

This is a fairly straight forward program. Users can paste the sequence to be translated in the window and submit the translation request, the protein sequence is then shown on the next page.

4.2.2. Patterns and Motif Analysis

4.2.2.1. When to Use

Sometimes, direct sequence comparison using BLAST may not generate any interesting results, or researchers may want more detailed comparison. For example, some genes have little or no identical sequences, but share common characteristics and can be related in a protein family. If it is necessary to identify new and distantly related members of the same protein family, *patterns* can be searched in a protein sequence. A *pattern* represents common characteristics of a protein family. A pattern constitutes a usually short but characteristic motif within a protein sequence (i.e., a description of what residues may be present at what positions). For example, the pattern [AV]-x-G-x(3)-{ED} is interpreted as [Ala or Val]-any-Gly-any-any-any-{any but Glu or Asp}.

4.2.2.2. Tool

A popularly used tool for pattern and motif analysis is ProfileScan (at http://hits.isb-sib.ch/cgi-bin/PFSCAN). The program searches for similarities between the submitted protein and some profile databases, including PROSITE and Pfam. PROSITE is a protein family and domain database that contains biologically significant sites, patterns, and profiles. Searching within this database helps identify a new sequence that belongs to a known protein family. Pfam is another database consisting of protein domain families with initial alignment of the domains done manually (but not through automated methods).

4.2.2.3. Input and Output

The input of searching can be a protein sequence. Users can choose the database they want to search against and other flavors and views to format their search results. **Figure 5** shows a sample searching result using a *TAP1* protein sequence. For example, Protein kinase C (*PKC*) phosphorylation sites and their positions are shown.

4.2.3. Transmembrane Regions Detection

4.2.3.1. When to Use

Detecting transmembrane regions can be especially useful in membrane transporters.

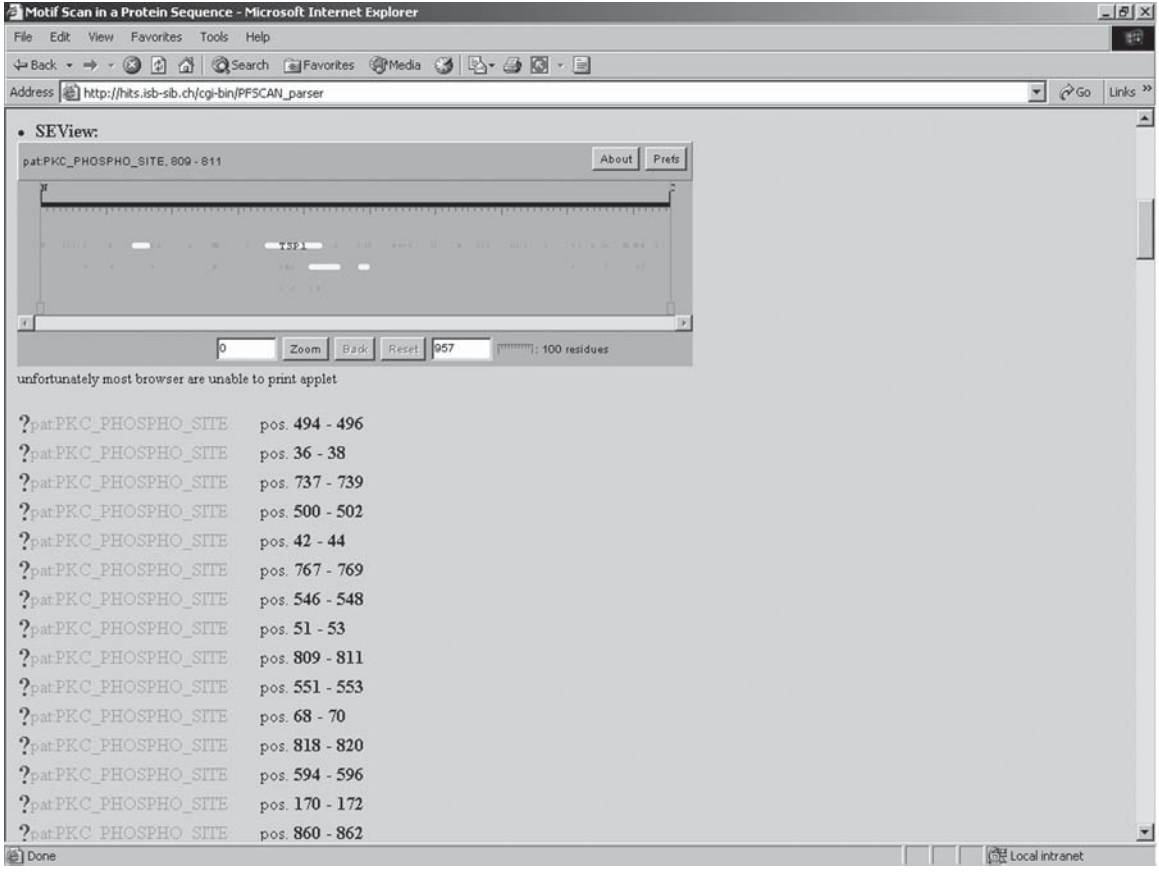

Fig. 5. Motif analysis of the TAP gene using ProfileScan.

4.2.3.2. Tool

A popular tool is TMpred (at http://www.ch.embnet.org/software/TMPRED_form.html). This program predicts membrane-spanning regions and their orientation.

4.2.3.3. Input and Output

The input of the program can be a protein sequence. The output includes possible transmembrane helices, with helices direction and sequence position listed, and a table of correspondences that shows "which of the inside → outside helices correspond to which of the outside → inside helices." The output pages also provide suggested models for transmembrane topology, with segment positions and orientations listed, and a prediction diagram. TMpred is based on the TMbase, a database containing information about transmembrane proteins including the number of transmembrane domains, locations, and features of the flanking sequences ***(20)***.

4.2.4. Secondary and Tertiary Structure Prediction

4.2.4.1. When to Use

This is used to predict the secondary structure such as α-helices or β-strands, and/or 3D structure of a protein sequence. The detailed methods of structure prediction or modeling are described in Chapter 18 by Dwyer.

4.2.4.2. Tools

There are many tools available now. For the secondary structure prediction, one tool called PredictProtein is at http://cubic.bioc.columbia.edu/predictprotein/submit_def.html. For the 3D structure prediction, an on-line tool with Web-based form Geno3D is available at http://geno3d-pbil.ibcp.fr/. Another tool, CPHmodels, is at http://www.cbs.dtu.dk/services/CPHmodels/.

4.2.4.3. Input and Output

Similar to many other programs, users can submit their requests through the Web-based submission forms or through sending e-mails to the program servers. From some programs, the results can be viewed through the Web. Some programs send the results to users' e-mail addresses. PredictProtein uses sequence similarity search, multiple alignment, and neural network algorithms. The program not only predicts the secondary structure type of each residue but also provides statistics showing the confidence of the prediction. The accuracy for the best-case prediction by PredictProtein is reported to be over 90%. Programs for 3D prediction may use different available protein domains in PDB as

templates and therefore, can have apparently different results but they really are models for different domains of the protein.

5. Notes

1. In addition to programs for individual purposes, there are also some bioinformatics packages that contain or combine various programs together. A software package can provide many sequence analysis tools via one user interface, such as for both multiple alignment and sequence translation. For example, a commercial product, the GCG Wisconsin Package (belonging to Accelrys now), contains various tools for sequence comparison, database searching, pattern recognition, primer selection, and protein analysis (http://www.accelrys.com/products/gcg_wisconsin_package/). The sequence retrieval system (SRS) is an integrated database browser of European Bioinformatics Institute (EBI) (http://srs.ebi.ac.uk/). The interface provides access and searching systems to various databanks, including MEDLINE and different kinds of sequence databases. There are also some open-source packages, such as The European Molecular Biology Open Software Suite (EMBOSS) (http://emboss.org/).
2. This chapter introduces some bioinformatics databases and tools that are most frequently used in the membrane transporter study. There are also other databases and tools available for various purposes. Researchers interested in different kinds of tool or new tools can check several major public database websites for their updates, such as the NCBI website (http://www.ncbi.nlm.nih.gov/) and the European Molecular Biology Laboratory (EMBL) at EBI (http://www.embl-heidelberg.de/, http://www.ebi.ac.uk/).

References

1. Pipas, J. M. and McMahon, J. E. (1975) Method for predicting RNA secondary structure. *Proc. Natl. Acad. Sci. USA* **72,** 2017–2021.
2. Studnicka, G. M., Rahn, G. M., Cummings, I. W., et al. (1978) Computer method for predicting the secondary structure of single-stranded RNA. *Nucleic Acids Res.* **5,** 3365–3387.
3. Erdmann, V. A. (1978) Collection of published 5S and 5.8S ribosomal RNA sequences. *Nucleic Acids Res.* **5,** r1–r13.
4. Dayhoff, M. O., Schwartz, R. M., Chen, H. R., et al. (1980) Nucleic acid sequence bank. *Science* **209,** 1182.
5. Korn, L. J., Queen, C. L., and Wegman, M. N. (1977) Computer analysis of nucleic acid regulatory sequences. *Proc. Natl. Acad. Sci. USA* **74,** 4401–4405.
6. McCallum, D. and Smith, M. (1977) Computer processing of DNA sequence data. *J. Mol. Biol.* **116,** 29–30.
7. Fuchs, C., Rosenvold, E. C., Honigman, A., et al. (1978) A simple method for identifying the palindromic sequences recognized by restriction endonucleases: the nucleotide sequence of the AvaII site. *Gene* **4,** 1–23.

8. Gingeras, T. R., Milazzo, J. P., and Roberts, R. J. (1978) A computer assisted method for the determination of restriction enzyme recognition sites. *Nucleic Acids Res.* **5,** 4105–4127.
9. Paulsen I. T., Nguyen L., Sliwinski M. K., et al. (2000) Microbial genome analyses: comparative transport capabilities in eighteen prokaryotes. *J. Mol. Biol.* **4,** 75–100.
10. Chen, L., Ortiz-Lopez A., Jung A., et al. (2001) ANT1, an aromatic and neutral amino acid transporter in Arabidopsis. *Plant Physiol.* **125,** 1813–1820.
11. Dawson, P. A., Mychaleckyj, J. C., Fossey, S. C., et al. (2001) Sequence and functional analysis of GLUT10: a glucose transporter in the Type 2 diabetes-linked region of chromosome 20q12-13.1. *Mol. Genet. Metab.* **74,** 186–199.
12. Kihara, D. and Kanehisa, M. (2000) Tandem clusters of membrane proteins in complete genome sequences. *Genome Res.* **10,** 731–743.
13. http://www-biology.ucsd.edu/~msaier/transport/toc.html#1A
14. http://lab.digibench.net/transporter
15. White, J. A., McAlpine, P. J., Antonarakis, S., et al. (1997) Guidelines for human gene nomenclature. HUGO Nomenclature Committee. *Genomics* **45,** 468–471.
16. http://www.gene.ucl.ac.uk/cgi-bin/nomenclature/searchgenes.pl
17. Yan, Q. and Sadée, W. (2002) Human membrane transporter database: a Web-accessible relational database for drug transport studies and pharmacogenomics. *AAPS PharmSci* **2,** E20.
18. Altschul, S. F., Gish, W., Miller, W., et al. (1990) Basic local alignment search tool. *J. Mol. Biol.* **5,** 403–410.
19. http://www.ncbi.nlm.nih.gov/BLAST/.
20. Hofmann, K. and Stoffel, W. (1993) TMbase—a database of membrane spanning proteins segments. *Biol. Chem.* **374,** 166.

4

DNA Microarrays to Analyze Gene Expression in Animals with Altered Transporter Expression

Gary W. Miller

1. Introduction

Neurotransmitter transporters play a critical role in numerous biological functions. Disruption of transporter function can lead to perturbations in many of these physiological processes. An example of this is the plasma membrane dopamine transporter (DAT). Genetic deletion of this transporter leads to hyperactivity, learning deficits, altered responses to drugs of abuse, and alterations in the hypothalamic pituitary axis ***(1–5)***. DAT may also participate in the etiology of Parkinson's disease (PD) by increasing the cellular content of dopaminergic toxins ***(6)***. Although certain individuals may be genetically predisposed to PD, it seems likely that environmental factors are also a strong contributing factor to the disease. Our lab has been especially interested in the effects of environmental toxicants on DAT function ***(7)***. Because altered DAT function can have widespread effects on an organism, we decided to use DNA microarray technology to examine the expression of thousands of genes from the brains of animals treated with various pesticides known to alter transporter function.

The advent of DNA microarray technology has revolutionized the way we view gene expression. Rather than looking at a handful of genes at one time, now multiple families of genes can be examined. One of the limitations of DNA microarrays is the expense. Commercially available arrays are very expensive. Through a collaborative venture with Dr. Vishy Iyer and Dr. Adron Harris at the University of Texas in Austin, we generated a mouse brain DNA microarray. The array contains the entire Brain Mouse Anatomy Project (BMAP) clone set as well as the sequence verified mouse clone set, both from

From: *Methods in Molecular Biology, vol. 227: Membrane Transporters: Methods and Protocols*
Edited by: Q. Yan © Humana Press Inc., Totowa, NJ

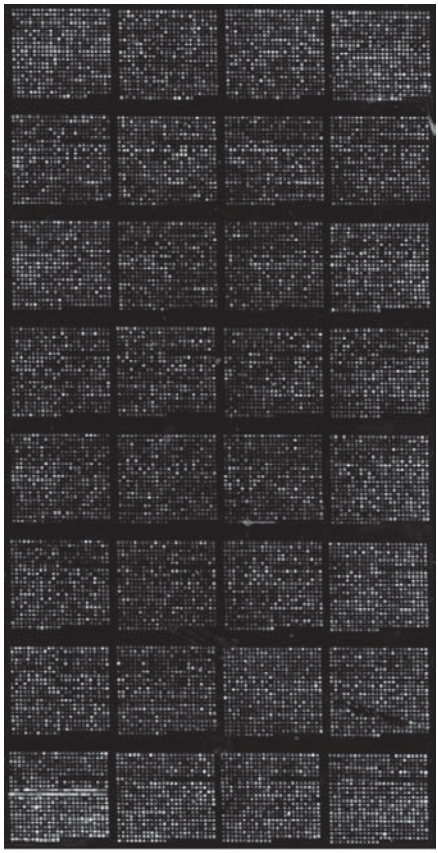

Fig. 1. Texas mouse chip; sixteen thousand elements, including BMAP collection and ResGen Sequence Verified Mouse Set. Samples from control and heptachlor-treated mouse midbrain were labeled and hybridized. Approximately a dozen genes exhibited greater than a twofold change in gene expression.

Research Genetics. The arrays were printed onto glass slides according to the protocols developed by the laboratory of Dr. Pat Brown at Stanford *(8)*.

This chapter focuses on the hybridization protocols adopted in our laboratory and includes many of the problems we encountered along the way. **Figure 1** shows a representative hybridization with mice treated with the organochlorine insecticide heptachlor. Elevated levels of several genes, including chloride channels, microtubule-associated proteins, and monoamine enzymes were found. Heptachlor is known to increase the expression of the dopamine transporter. We have also examined the expression of genes from mice with genetic reduction of various monoamine transporters.

2. Materials

2.1. RNA Isolation

1. RNAseZAP (Ambion, Austin, TX).
2. Dry-ice pellets.
3. Trizol reagent (Invitrogen, Carlsbad, CA) (*see* **Note 1**).
4. Motor-driven tissue homogenizer (e.g., Tissue Tearor by Biospec Products, Inc., Bartlesville, OK).
5. 18-G Needle attached to a 10-mL syringe (Fisher Scientific, Plano, TX).
6. Chloroform: isoamyl alcohol (CI), 24:1, molecular biology grade (VWR, Sugarland, TX) (*see* **Note 1**).
7. Variable-speed centrifuge or microcentrifuge.
8. Acid phenol: chloroform (acid PC), 5:1, molecular biology grade (Ambion, Austin, TX) (*see* **Note 1**).
9. Eppendorf Phase Lock Gel Heavy tubes, optional (Brinkmann Instruments, Westbury, NY).
10. Isopropanol, molecular biology grade (Sigma, St. Louis, MO) (*see* **Note 2**).
11. 75% Ethanol, molecular biology grade, in diethylpyrocarbonate (DEPC)–water (Sigma, St. Louis, MO) (*see* **Note 2**).
12. DEPC–water (Ambion, Austin, TX) (*see* **Note 2**).
13. RNAse-free microfuge tubes (Ambion, Austin, TX).
14. Ultraviolet (UV) spectrophotometer; preferably one that requires 50 μL or less of sample volume.
15. Horizontal, mini-electrophoresis unit.
16. Agarose, molecular biology grade, RNAse-free (Fisher Scientific, Plano, TX).
17. 10X TBE running buffer, RNAse-free: 90 m*M* Tris-borate, 2 m*M* EDTA, pH 8.0 (Ambion, Austin, TX).
18. 10X Native agarose loading buffer, RNAse-free: 40% sucrose, 0.17% xylene cyanol, 0.17% bromophenol blue (Ambion, Austin, TX).
19. Ethidium bromide, 10 mg/mL in DEPC–water (Sigma, St. Louis, MO) (*see* **Note 1**).
20. Ultraviolet (UV)-transilluminator or other UV imaging device.
21. Milli-Q water.

2.2. Preparation of cDNA Probes

1. RNAseZAP.
2. Oligo dT 20mer, nuclease-free, 5 μg/μL (Integrated DNA Technologies, Coralville, IA) (*see* **Note 3**).
3. DEPC–water.
4. Heat block and/or water bath.
5. 50X 2:3 amino-allyl-dUTP/dNTPs (*see* **Note 4**).
6. SuperaseIN RNAse inhibitor, 20 U/μL (Ambion, Austin, TX).
7. Superscript II RNAse H^- reverse transcriptase, 200 U/μL (Invitrogen, Carlsbad, CA). (The enzyme is supplied with its required 5X reaction buffer and 0.1 *M* dithiothreitol [DTT]).

8. 1 *N* NaOH.
9. 0.5 *M* EDTA, pH 8.0.
10. 1 *M* HEPES, pH 7.5.
11. Microcon 30 columns (Millipore, Bradford, MA).
12. 1 *M* Sodium bicarbonate buffer, pH 9.0 (*see* **Note 5**).
13. Cy3 and Cy5 monofunctional dyes (Amersham Pharmacia Biotech, Piscataway, NJ) (*see* **Note 6**).
14. QIAquick PCR purification columns (QIAGEN, Chatsworth, CA).

2.3. Microarray Hybridization

1. Yeast tRNA, 5 μg/μL (Roche Molecular Biochemicals, Indianapolis, IN).
2. Poly dA, 10 μg/μL (Sigma, St. Louis, MO).
3. Mouse COT-1 DNA, 1 μg/μL (Invitrogen, Carlsbad, CA).
4. Filtered Milli-Q water (*see* **Note 7**).
5. 20X SSC, filtered: 3 *M* NaCl, 0.3 *M* sodium citrate, pH 7.0.
6. 10% Sodium dodecyl sulfate (SDS), filtered.
7. 3X SSC (20X SSC diluted with filtered Milli-Q water).
8. cDNA microarray, postprocessed.
9. Microarray hybridization cassette (TeleChem International, Inc., Sunnyvale, CA).
10. Lifter slip (Erie Scientific, Portsmouth, NH). Size will depend on the size of the microarray.
11. Heat block.
12. Water bath.
13. Slide-staining assemblies (stainless steel, 30-slide rack, glass dish and cover) (Brain Research Laboratories, Newton, MA).
14. Coplin jar (Fisher Scientific, Plano, TX).
15. Tabletop centrifuge.
16. High-resolution microarray scanner (e.g., GenePix 4000 microarray scanner, Axon Instruments, Inc., Union City, CA).
17. A lot of patience and perseverance.

3. Methods

3.1. RNA Isolation

1. Clean work area, pipettors, racks, and so forth with RNAseZAP and rinse with nuclease-free water. (Milli-Q water is sufficient.) Use only tips and tubes certified to be free of nucleases.
2. Remove frozen tissue from ultracold freezer and store on dry ice until ready to process.
3. Drop frozen tissue into 10–12 volumes Trizol and immediately homogenize until tissue is completely liquefied (*see* **Note 8**).
4. Pass the homogenate through an 18-G needle three times (*see* **Note 9**).
5. Centrifuge the sample at 12,000*g* for 10 min at 4°C (*see* **Note 10**).
6. Transfer the supernatant to a fresh tube. Incubate at room temperature for 5 min.

7. Add 0.2 mL CI for each milliliter of Trizol used. Shake vigorously for 1 min (*see* **Note 11**).
8. Incubate at room temperature for 3 min.
9. Centrifuge 15 min at 12,000*g*, 4°C.
10. Transfer the top two-thirds of the aqueous phase to a new tube.
11. Extract once with an equal volume of acid PC (*see* **Note 12**).
12. Transfer the top two-thirds of the aqueous phase to a new tube.
13. Extract twice with an equal volume of CI in a Phase Lock Gel Heavy tube (*see* **Note 13**).
14. Transfer the aqueous phase to a new tube and add an equal volume of isopropanol. Mix by inversion and incubate 10 min on ice to precipitate the RNA.
15. Centrifuge at 12,000*g* for 15 min at 4°C.
16. Remove isopropanol and wash the pellet with 1 mL of 75% ethanol. Pipet the sample up and down repeatedly in order to fractionate the pellet.
17. Repellet the RNA by centrifuging at 12,000*g* for 10 min at 4°C (*see* **Note 14**).
18. Remove ethanol and air-dry the pellet (*see* **Note 15**).
19. Re-suspend the pellet in a small volume of DEPC–water (*see* **Note 16**).
20. Determine RNA concentration using standard spectrophotometry.
21. Assess RNA integrity by electrophoresing 1–1.5 μg on 1% native agarose (*see* **Note 17**).
22. Use a standard (genomic DNA) polymerase chain reaction (PCR) assay to verify that RNA is free of contaminating DNA (*see* **Note 18**).
23. Store RNA at –70 to –80°C.

3.2. Preparation of cDNA Probes

1. Clean work area, pipettors, racks, and so forth with RNAseZAP and rinse with nuclease-free water. (Milli-Q water is sufficient.) Use only tips and tubes certified to be free of nucleases for **steps 2–5**.
2. Perform a separate cDNA synthesis reaction for each RNA: Combine total RNA (DNA-free, 20 μg) and oligo dT (5 μg) and adjust the volume to 15 μL with DEPC–water.
3. Incubate at 70°C for 10 min. Chill on ice for 10 min.
4. Prepare a reverse transcription (RT) master mix for all reactions: For each reaction, combine 6 μL Superscript 5X reaction buffer, 0.6 μL 50X 2:3 aa-dUTP/dNTP, 3.0 μL 0.1 *M* DTT, 1.5 μL SuperaseIN RNAse inhibitor, 1.9 μL Superscript II reverse transcriptase, 2 μL DEPC–water.
5. Add 15 μL of RT master mix to each RNA/oligo dT sample. Mix and incubate at 42°C for 2 h.
6. Incubate the RT reaction at 95°C, 5 min, then chill on ice.
7. Add 13 μL of 1 *N* NaOH and 1 μL of 0.5 *M* EDTA. Incubate at 70°C for 15 min to hydrolyze the RNA.
8. Neutralize by adding 50 μL of 1 *M* HEPES.
9. Follow the manufacturer's instructions to clean up each RT reaction with three to four passes through a microcon 30 column (*see* **Notes 19** and **20**). Adjust the final

Table 1
Microarray Hybridization

Total volume required	35 μL	45 μL	50 μL	60 μL
cDNAs and water	25.0 μL	33.0 μL	37.0 μL	45 μL
blocker DNAs	3.0 μL	3.0 μL	3.0 μL	3.0 μL
20X SSC	6.1 μL	7.8 μL	8.7μL	10.4 μL
10% SDS	0.9 μL	1.2 μL	1.3 μL	1.6 μL

volume of the eluted cDNA to 9 μL. (Either add Milli-Q water or vacuum concentrate. The latter is usually necessary.)

10. Add 1 μL sodium bicarbonate buffer to each cDNA.
11. Add the cDNA to the appropriate aliquot of cy dye (cy3 or cy5). Incubate 1 h at room temperature, protected from light.
12. Remove unincorporated dye molecules with a QIAquick PCR purification column (*see* **Note 21**).
13. Combine the purified, cy3- and cy5-labeled cDNAs. Concentrate the pooled cDNA to approx 20 μL with a single pass through a microcon 30 column.

3.3. Microarray Hybridization

1. Add 1 μL each of yeast tRNA, poly dA, and mouse COT-1 (blocker DNAs) to the pooled cDNA.
2. Use **Table 1** to determine the correct volumes of SDS and SSC to add to your probe. Adjust to the appropriate final volume with filtered Milli-Q water.
3. Boil microarray probe for 5 min. Tap spin (*see* **Note 22**).
4. Use compressed air to remove any dust from the lifter slip and microarray surfaces. Place 7 μL of 3X SSC in each groove of the hybridization cassette. Place the array in the cassette and place a clean lifter slip on top of the array (*see* **Note 23**).
5. Pipet the probe solution under the lifter slip using a P20 pipettor (*see* **Note 24**).
6. Seal the cassette and place in a 60°C water bath in the dark. Hybridize 16 h.
7. Prepare wash solutions. Wash 1: 340 mL filtered water, 10 mL 20X SSC, 1 mL 10% SDS. Wash 2: 350 mL filtered water, 1 mL of 20X SSC.
8. Remove the cassette from the water bath and dry it off with a paper towel.
9. Remove the array and submerge it in Wash 1, keeping the array level while it is being submerged. Once submerged, tilt the array to dump off the lifter slip (*see* **Note 25**).
10. Put the array in the slide rack and remove any additional arrays from the water bath. When all microarrays are in Wash 1, plunge rack up and down 20 times.
11. Transfer arrays to a new slide carrier to prevent excess carryover of SDS. Plunge arrays up and down 20 times in Wash 2.

12. Transfer arrays to a new slide carrier and plunge up and down three to five times in filtered water.
13. Place the slide in a 50-mL conical tube containing a wadded-up sheet of Kimwipe at the bottom. If the array is off-center on the slide, the array end should be at the top of the tube. Centrifuge at 500*g* at room temperature for 10 min to dry the slide. Wrap the tube in foil to protect the array from light. Scan as soon as possible.

4. Notes

1. Trizol, phenol, and chloroform are volatile and toxic and should only be used in a chemical fume hood. Ethidium bromide is a known mutagen. Wear gloves when using any of these reagents.
2. Bulk reagents and buffers used for RNA manipulations should be aliquoted into small volumes for storage. This minimizes the potential for RNAse contamination and minimizes losses resulting from contamination when it occurs.-
3. Oligos are supplied lyophilized and should be resuspended in DEPC–water at the desired concentration.
4. Nuclease-free dNTPs and amino-allyl-dUTP (aa-dUTP) can be purchased from Sigma. To prepare 100 m*M* aa-dUTP, spin container at 1000*g* for 10 min at 4°C to bring contents to the bottom of the jar. Resuspend in 18 μL DEPC–water for each milligram of nucleotide. Centrifuge as above and transfer material to an RNAse-free microfuge tube. Verify concentration by spectrophotometry: Dilute 1 *M* potassium phosphate buffer, pH 7.5, 1:10 in water and use to make two, 1:5000 dilutions of aa-dUTP. Measure absorbance at 238 nm and 289 nm. Calculate the concentration for both dilutions at both wavelengths and average the results to obtain an estimate of the true concentration. (Stock concentration [mM] = OD × dilution factor/m*M* extinction coefficient. Extinction coefficients at both wavelengths are lot-specific and are provided with the aa-dUTP.) Adjust the final concentration to 100 m*M* with DEPC–water. Prepare 50X 2:3 aa-dUTP/dNTPs by combining 10 μL each of 100 m*M* dATP, dCTP, and dGTP, 6 μL 100 m*M* dTTP, and 4 μL 100 m*M* aa-dUTP. Store at –20°C.
5. This buffer should be made fresh every 2–4 wk, as the pH changes over time. Proper pH is critical for coupling cy dye esters to the amino-modified cDNAs.
6. Cy dye esters are sensitive to moisture and light. Resuspended one tube of cy-dye ester in 12 μL dimethyl sulfoxide (DMSO). Aliquot 1.4 μL into each of eight tubes, dry by vacuum concentration, and store at 4°C, in the dark, in a desiccator. Once opened, DMSO should be stored at room temperature in a desiccator to prevent it from absorbing moisture.
7. It is extremely important to minimize the amount of dust/particulate matter in microarray reagents. Small bits of dust can create large, obstructive blobs on cDNA microarrays. Reagents should be purified through 0.22-μm cellulose acetate filters before use.
8. For up to 200 mg of tissue, 2.5 mL of Trizol in a 50-mL Falcon tube works well. Smaller Falcon tubes cannot be used, as the top of the tissue homogenizer's probe

is wider than the tube diameter and this prevents the blade from reaching the bottom of the tube.

9. In our experience, RNA isolated from brain tissue is often contaminated with a significant level of DNA. Passing the tissue homogenate through a small-bore needle helps shear the DNA, which facilitates its separation from RNA.
10. This "clarifying" spin is used to remove lipids, which are abundant in brain tissue and impede clean removal of the aqueous phase because of their flocculent nature. Transfer the homogenate to an appropriate tube before centrifugation. If a microcentrifuge is used, the sample must be split between two tubes in order to accommodate the entire sample volume.
11. Take care to add the appropriate amount of CI, as the addition of excess chloroform will promote movement of DNA into the aqueous phase.
12. The acid PC extraction is an additional measure to remove DNA from the aqueous phase. We have found it better to minimize DNA carryover during the purification process, rather than to remove contaminating DNA from the purified RNA.
13. Phase lock gel tubes are not essential, but they are extremely helpful in avoiding carryover of organic contaminants while enabling recovery of the entire aqueous phase. We do not recommend using phase lock gel tubes for extractions with Trizol or acid phenol because additional chloroform must be added to obtain proper phase separation and the additional chloroform compromises RNA purity (*see* **Note 6**). Use phase lock gel tubes according to the manufacturer's instructions.
14. If the pellet appears unusually large or salty, the wash should be repeated. Also, if the sample was split into two tubes at **step 5**, it can be recombined before the final centrifugation step.
15. The RNA pellet will air-dry quickly, usually within 10 min if the ethanol has been completely removed with a pipet tip. Drying the pellet in a vacuum concentrator (SpeedVac) is not recommended for two reasons. First, it tends to overdry the sample, making it difficult to resuspend. Second, it makes the pellet prone to dislodging from, and actually popping out of, the tube because of static electricity.
16. On average, we recover 75–80 μg of total RNA from a single, adult mouse midbrain. Because the final RNA concentration should be at least 1.5 μg/μL for cDNA synthesis, we resuspend each RNA pellet in 45 μL and make adjustments to this as necessary (e.g., if the pellet will not resuspend). If the RNA is too dilute, it can be reprecipitated and resuspended in a smaller volume, or concentrated with a microcon column according to the manufacturer's instructions. However, we try to avoid this situation, as further manipulation of the RNA increases the potential for degradation problems.
17. When analyzed on native agarose, total mouse RNA should exhibit two sharp bands running at about 1.6 and 1.0 kb (28S and 18S ribosomal RNAs, respectively), and a smaller, more diffuse band running at about 200 bp (tRNA, 5S RNA). The ratio of 28S:18S RNA should be 2:1 for high quality, intact total RNA, which produces consistent and reliable microarray data.

18. We use the S15 ribosomal protein PCR assay detailed in many of Ambion's RNA isolation kits. Two dilutions of RNA are assayed to minimize the number of false negatives. If PCR analysis indicates significant DNA contamination, the RNA samples can be DNAse treated. However, we try to avoid this situation because DNAse treatment generally causes RNA degradation in our hands.
19. We have found a considerable number of microcon columns to be damaged and unusable. We recommend performing a "trial" 2-min run with each column immediately before it is used. If all the liquid flows through the column during this spin, discard the column and get a new one.
20. All Tris-HCl and residual aa-dUTP must be removed from the cDNA prior to the dye conjugation, as these also will couple with the cy dye esters and thus diminish labeling of the cDNA.
21. Follow the manufacturer's instructions, with the following modifications. Add 70 μL Milli-Q water and 500 μL PB buffer to each cDNA before loading on the column. Perform two washes with Buffer PE (supplied with kit). Perform two, sequential, 60-μL elutions, incubating the column for 5 min each time.
22. Do not put the denatured probe on ice, as this will cause the SDS to precipitate.
23. The particular lifter slip used will dictate hybridization volume. We have found considerable variability in the volumes accommodated by individual lifter slips, even when they are the same size. We recommend a "trial run" with each lifter slip (using water or hybridization buffer) immediately before use to determine the volume it can accommodate. Used lifter slips can be washed and stored according to accommodated volume in 95% ethanol. (Do not use absolute ethanol, as it often contains contaminants that fluoresce and can interfere with microarray scans.)
24. The probe will need to be added in stages because the P20 cannot hold the entire volume. However, we find this to be a better alternative than using a larger pipettor, the larger tips of which seem to promote more bubble formation.
25. The lifter slip should be completely dislodged from the array before trying to slide it off the array. Otherwise, it may scratch the array surface or cause the poly-l-lysine, along with the spotted DNA, to separate from the glass slide.

Acknowledgments

The author would like to express his appreciation to Elizabeth Osterndorff-Kahanek, who performed all of the studies. In addition, I am indebted to Dr. Vishy Iyer from the University of Texas for taking the time to train our laboratory with the procedures. I would also like to thank Mark Eshoo, formerly of the Buck Institute for helping with the RNA isolation protocols. This work was funded in part by a microarray supplement to NIH grant ES09248 and by the Texas Commission on Alcohol and Drug Abuse.

References

1. Bosse, R., Fumagalli, F., Jaber, M., et al. (1997) Anterior pituitary hypoplasia and dwarfism in mice lacking the dopamine transporter. *Neuron* **19,** 127–138.

2. Fumagalli, F., Gainetdinov, R. R., Valenzano, K. J., et al. (1998) Role of dopamine transporter in methamphetamine-induced neurotoxicity: evidence from mice lacking the transporter. *J. Neurosci.* **18,** 4861–4869.
3. Gainetdinov, R. R., Wetsel, W. C., Jones, S. R., et al. (1999) Role of serotonin in the paradoxical calming effect of psychostimulants on hyperactivity. *Science* **283,** 397–401.
4. Giros, B., Jaber, M., Jones, S. R., et al. (1996) Hyperlocomotion and indifference to cocaine and amphetamine in mice lacking the dopamine transporter. *Nature* **379,** 606–612.
5. Rocha, B. A., Fumagalli, F., Gainetdinov, R. R., et al. (1998) Cocaine self-administration in dopamine-transporter knockout mice. *Nat. Neurosci.* **1,** 132–137.
6. Miller, G. W., Gainetdinov, R. R., Levey, A. I., et al. (1999) Dopamine transporters and neuronal injury. *Trends Pharmacol. Sci.* **20,** 424–429.
7. Miller, G. W., Kirby, M. L., Levey, A. I., et al. (1999) Heptachlor alters expression and function of dopamine transporters. *Neurotoxicology* **20,** 631–637.
8. Iyer VR, Eisen MB, Ross DT, et al. (1999) The transcriptional program in the response of human fibroblasts to serum. *Science* **283,** 83–87.

5

Microarray Data Analysis in Studies of Membrane Transporters

Donglei Hu

1. Introduction

The newly developed microarray technology has made it possible to simultaneously monitor the expression of thousands of genes under specific physiological and pathological conditions. An array contains thousands of nucleic acid probes with known sequences. When the labeled target nucleic acid is applied to the array, it hybridizes to the probe if their sequences are complimentary to each other. The hybridization can be measured and the gene expression level estimated.

In studies of the membrane transporter, microarray technology is a powerful tool for monitoring expression profiles of genes at different conditions. Genes that are differentially expressed in certain conditions can be detected and may reveal mechanisms for specific biological phenomena. Genes with similar expression patterns can be grouped together and may provide insights of signal transduction pathways.

Because it is widely applied in many areas of biomedical research, microarray technology has provided opportunities as well as challenges for laboratory scientists and bioinformaticists. This chapter gives a brief description of commonly used computational methods in microarray data analysis. It summarizes analysis features of current major software packages and other tools. It also reviews a few examples of applications of data analysis methods in studies of membrane transporters.

From: *Methods in Molecular Biology, vol. 227: Membrane Transporters: Methods and Protocols*
Edited by: Q. Yan © Humana Press Inc., Totowa, NJ

2. Review of Microarray Technology

2.1. Spotted Array

Each spotted array is a solid surface (e.g., a glass slide) spotted with drops of probe DNA solution. In a comparative hybridization experiment, two samples are used. Usually, one sample is prepared in the experimental condition and the other one in the control condition. mRNAs are extracted from these two samples and then reverse transcribed to cDNAs. cDNAs of two samples are labeled by different fluorescent dyes and then used to hybridize the array. An array image has spots with measured intensities from two fluorescent dyes. If two fluorescent dyes are colored as red and green, spots with approximately equal amounts of cDNA from each sample show yellow and spots with predominant amounts of cDNA from one sample show red or green. The ratio of fluorescent intensities of a given spot represents the ratio of concentration of mRNA from two samples ***(1,2)***.

2.2. Oligonucleotide Array

This technology synthesizes oligonucleotides on the array surface. The array with oligonucleotide probes is hybridized with labeled sample DNA. A scanned-array image contains thousands of spots with different light intensities which represent expression levels of different probes. The oligonucleotide microarray developed by Affymetrix, Inc. (Santa Clara, CA) uses "Perfect Match (PM)–Miss Match (MM)" probe pairs to measure gene expression. Because the MM probe is used as a reference for background hybridization, the expression of a gene is represented by the difference of intensities between PM and MM probe pairs. A probe set that contains 10–20 PM–MM probe pairs is used to measure the expression of one gene.

3. Data Analysis Methods

After an array is scanned, there are unique procedures to process the array image and to control array image quality. Discussion of these issues is beyond the scope of this chapter. The data analysis procedure described in this chapter starts with the intensity of each probe that is calculated after array image analysis and processing. The intensity value of each probe represents the expression level of a specific gene. After intensities are normalized, they can be used in comparison analysis and clustering analysis.

3.1. Data Normalization

The overall intensity of an array is influenced by nonbiological factors. Expression data of multiple arrays are comparable only if the influence of nonbiological factors is minimized and the overall intensities of multiple arrays

are equivalent to each other. Two basic strategies are used to normalize the intensities of multiple arrays: (1) total intensity scaling or normalization and (2) methods based on regression ***(3,4)***.

3.1.1. Total-Intensity Scaling or Normalization

The total intensity of an array is calculated as the summation of intensity values of all probes on the array. Usually, total intensities of multiple arrays are different from each other. They should be adjusted to the same value (assigned intensity). The total intensity of an array is adjusted to the assigned intensity by multiplying intensities of all probes on one array by the normalization factor. The normalization factor is calculated as

$$\text{Normalization factor} = \frac{\text{Assigned intensity}}{\text{Total intensity}} \quad (1)$$

The assigned intensity can be a predetermined value or the average of all total-intensity values of multiple arrays that are involved in the analysis ***(5)***.

3.1.2. Methods Based on Regression

The relationship between intensities of one array and those of another array is analyzed by linear regression with the *y*-intercept as zero ***(4,6)***. This method adjusts the slope of linear regression to 1 if it is not 1. This is done by multiplying intensity values of all probes of the array on *x*-axis by the slope of linear regression (*see* **Fig. 1**). In many cases, the relationship of intensities between two arrays is not linear. Nonlinear regression should be used in this case. In spotted arrays, intensities of Cy3 and Cy5 channels of the same array can be normalized using total-intensity normalization or regression method ***(3)***.

3.2. Comparison Analysis

A common application of microarray technology in research of membrane transporters is detecting genes that are differentially expressed under certain conditions. The discovery of differentially expressed genes is based on the comparison of expression data of different arrays. Comparison analysis of microarray data can be conducted using various statistical methods.

3.2.1. Sample-to-Sample or Array-to-Array Comparison

Differentially expressed genes can be discovered by simply comparing expression data of one array with those of another array. In the spotted array, a single array is hybridized by cDNAs of two samples. Log ratios of fluorescence intensities in two channels indicate relative changes of gene expression in these two samples. The expression of a gene can be determined to be dif-

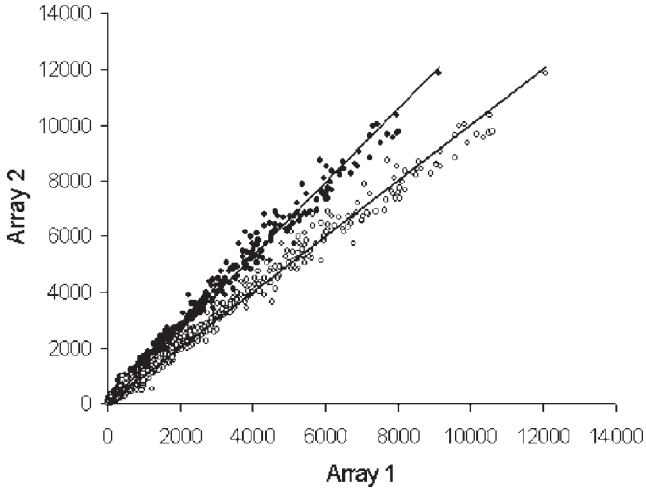

Fig. 1. Normalization of expression intensities of two arrays using the regression method. The linear regression of original data has the slope of 1.32. After normalization, the slope becomes 1. Closed circles, original data; open circles, normalized data.

ferent between two samples if the log ratio of that gene exceeds the cutoff value ***(7–9)***.

A similar method can be applied to compare expression data generated by an oligonucleotide microarray. Affymetrix GeneChip probe array technology adopts a statistical strategy to conduct comparison expression analysis. Differences between PM and MM probe pairs of a specific probe set of one array are compared with those of corresponding PM and MM probe pairs of the same probe set of another array. The comparison is conducted with the signed rank analysis. Change calls of "increasing (I)," "marginally increasing (MI)," "no change (NC)," "marginally decreasing (MD)," and "decreasing (D)" are made based on the resulting *p*-values. The signal log ratio is also calculated to indicate the relative change of intensities in two arrays ***(10)***.

3.2.2. Comparison with Replicates

Methods described in **Subheading 3.2.1.** are designed to compare the expression data of two arrays. When there are biological replicates, conventional statistical tests can be used to compare intensities between different groups.

3.2.2.1. Conventional Statistical Tests

The intensities of each gene in different sample groups can be compared using various conventional statistical tests. **Table 1** lists commonly used para-

Table 1
Parametric and Nonparametric Tests Commonly Used in Microarray Data Analysis

	Parametric test	Nonparametric test
Comparison of two sample groups	*t*-Test with equal variance *t*-Test with unequal variance	Mann–Whitney test
	Paired-sample *t*-Test	Wilcoxon paired-sample test
Comparison of multiple sample groups	ANOVA[a] (equal variance)	Kruskal–Wallis test
	Welch ANOVA (unequal variance)	

[a]Analysis of variance

metric and nonparametric tests that compare intensities in two sample groups or multiple sample groups. In the comparison of two sample groups, the relative change of gene expression between these two groups is usually indicated by the fold change which is the average of intensities of experiment group divided by that of the control group. A cutoff for fold change can also be set to determine differentially expressed genes. In some microarray experiments, a differentially expressed gene is identified if its *p*-value of the statistical test and fold change both reach significant levels. For example, if the cutoff is 0.05 for the *p*-value and 2.5 for fold change, the expression of a gene is significantly different between the two sample groups if the *p*-value of the *t*-test is 0.02 and the fold change is 3.4.

3.2.2.2. Adjustment of *p*-Value

Methods described in the previous section have been successfully adopted in many studies ***(11–14)***. However, they have also raised concerns. The major concern of this strategy is multiple testing. Usually, a microarray experiment provides expression data of a few thousand genes. When statistical tests are performed to examine the expression difference of so many genes between different sample groups, the *p*-values of some genes can become significant by chance. The control of a false positive result or family-wise Type I error rate (FWE) becomes an important issue. Some conventional methods have been designed to adjust *p*-values in multiple testing ***(15)***.

3.2.2.2.1. Bonferroni Single-Step Adjusted p-Value

The adjusted *p*-value is calculated as

$$p_{adj} = \min(kp_{org}, 1),$$

where k is the number of genes being tested. This adjustment simply multiplies the original *p*-value (p_{org}) by the number of genes being tested (k). The adjusted *p*-value (p_{adj}) is this product if it is less than 1. The adjusted *p*-value is set to 1 if the product is greater than 1 (*see* **Note 1**).

3.2.2.2.2. Step-Down Bonferroni Adjusted p-Value

This procedure starts with sorting *p*-values of all genes so that $p_{org}(1) \le p_{org}(2) \le p_{org}(3) \le \cdots \le p_{org}(k)$. Similar to the Bonferroni single-step adjusted *p*-value, the step-down Bonferroni adjusted *p*-value is calculated as

$$p_{adj}(1) = kp_{org}(1),$$

$$p_{adj}(n) = \max\left(p_{adj}(n-1), (k-n+1)\, p_{org}(n)\right) \text{ for } 2 \le n \le k,$$

where k is the number of genes being tested (*see* **Note 1**).

3.2.2.2.3. Westfall and Young Step-Down Adjusted p-Value

The above two methods provide strong control of the FWE. However, they are not designed for the analysis of datasets with a dependence structure between variables. In a biological system, the expression levels of groups of genes may correlate with each other for various reasons. A method developed by Westfall and Young takes into account the dependency between expression profiles of different genes (*see* **Note 1**).

Microarray data are usually organized in a matrix in which each row represents the expression of one gene of all arrays and each column represents the expression of all genes on one array. In the following step-by-step description of the resampling algorithm for the Westfall and Young step-down adjusted *p*-value, it is assumed that there are eight arrays in the control group and seven arrays in the experiment group. It is also assumed that each array measures the expression of k genes. These steps are based on previous descriptions of the same algorithm ***(15,16)***.

1. Compute the *t*-statistic for each gene of the original dataset.
2. Order these *t*-statistics so that $|t_1| \ge |t_2| \ge |t_3| \ge \cdots \ge |t_k|$.
3. Permute the 15 columns of the data matrix. The first eight columns now represent the pseudocontrol group and the remaining seven columns represent the pseudoexperiment group.
4. Compute the *t*-statistics for all genes for the permuted dataset:

$$t_1^{(b)}, t_2^{(b)}, \ldots, t_k^{(b)} \quad (2)$$

5. Compute

$$u_k^{(b)} = \left| t_{rk}^{(b)} \right|,$$
$$u_j^{(b)} = \max\left(u_{j+1}^{(b)}, \left| t_{rj}^{(b)} \right|\right), \text{ for } 1 \le j \le k-1, \tag{3}$$

where $| t_{rk} |$ is the t-statistic of the gene that has the minimum t-statistic for the original dataset, $| t_{rk} - 1 |$ is the one for the gene with the second minimum t-statistic for the original dataset, and so on.

Steps 3–5 are repeated N times and the adjusted p-values are calculated as

$$\tilde{p}_{rj}^{*} = \frac{\sum_{b=1}^{N} I\left(u_j^{(b)} \ge \left| t_{rj} \right|\right)}{N} \tag{4}$$

where $I(\cdot)$ is the indicator function setting to 1 if the condition in the parentheses is true and 0 if it is false.

$$\tilde{p}_{r1}^{*} = \tilde{p}_{r1}^{*},$$
$$\tilde{p}_{rj}^{*} = \max\left(\tilde{p}_{rj}^{*}, \tilde{p}_{r(j-1)}^{*}\right), \text{ for } 2 \le j \le k. \tag{5}$$

3.2.2.3. Significance Analysis of Microarray

The significance analysis of microarray (SAM) is designed to evaluate the significance of changes in gene expression between different biological conditions ***(17)***. For each gene, it assigns a score as an index of relative difference between groups. A gene is labeled as significant if its score surpasses a threshold. SAM does not directly control the FWE. It estimates the false discovery rate (FDR) for each threshold. SAM is an available software tool and easy to be used. Users are encouraged to understand the basic procedure of SAM so they may have a better interpretation of results generated by SAM.

The procedure of SAM is as follows:

1. The relative difference $d(i)$ in the expression of each gene is defined as

$$d(i) = \frac{\overline{x_1(i)} - \overline{x_2(i)}}{s(i) + s_0}, \quad i = 1, 2, \ldots, k, \tag{6}$$

where $\overline{x_1(i)}$ and $\overline{x_2(i)}$ are means of expression intensities of gene i in two groups, respectively, and s_0 is a factor that minimizes the coefficient of variation of $d(i)$.

$$s(i) = \left[\left(\frac{1}{n_1} + \frac{1}{n_2}\right)\left(\frac{1}{n_1 + n_2 - 2}\right)\left\{\sum_{n1}\left[x_{n1}(i) - \overline{x_1(i)}\right]^2 + \sum_{n2}\left[x_{n2}(i) - \overline{x_2(i)}\right]^2\right\}\right]^{\frac{1}{2}}, \tag{7}$$

where n_1 and n_2 are the numbers of arrays in group 1 and group 2, respectively and $x_{n1}(i)$ and $x_{n2}(i)$ are the intensities of gene i in each array in group 1 and group 2, respectively.

2. Genes are ranked by their $d(i)$ values so that $d(1) \geq d(2) \geq d(3) \geq \cdots \geq d(k)$.
3. Permute the data matrix N times.
4. For each permutation, calculate relative difference $d_p(i)$.
5. Rank $d_p(i)$ so that $d_p(1) \geq d_p(2) \geq d_p(3) \geq \cdots \geq d_p(k)$.
6. Calculate the expected relative difference as $d_E(i) = \Sigma_p\, d_p(i)/N$.
7. Plot $d(i)$ versus $d_E(i)$ and detect and count those beyond the set threshold.

The FDR is calculated by the following procedure:

1. For each permutation, count the number of genes whose $d_p(i)$ values are beyond the threshold.
2. Calculate the median and 90th percentile of the number of falsely discovered genes of all permutations.
3. Calculate the FDR as

$$\text{Median (or 90th percentile) FDR} = \frac{\text{Median (or 90th percentile) of falsely discovered genes}}{\text{Number of significant genes}}.$$

3.3. Clustering Analysis

Clustering techniques are widely used in microarray data analysis. With specific measures of similarity, they group together genes, arrays, or both with similar expression patterns. The most commonly used clustering algorithms are hierarchical clustering, *k*-means clustering, and self-organizing maps (SOM). It is beneficial for users to know basic procedures of these algorithms so that they understand the meanings of parameters and are able to select appropriate ones for specific purposes when using clustering software (*see* **Note 2**).

3.3.1. Measure of Similarity

The most common similarity measure is Euclidean distance. It is the distance between two data vectors $x = [x_1, x_2, ..., x_n]$ and $y = [y_1, y_2, ..., y_n]$, where n is the total number of elements in each vector. Elements in vectors x and y can be the intensities of two genes of all arrays or intensities of all genes of two arrays. The Euclidean distance between vectors x and y is

$$d(x, y) = \left[(x_1 - y_1)^2 + (x_2 - y_2)^2 + \cdots + (x_n - y_n)^2\right]^{\frac{1}{2}}, \quad (11)$$

Variations of Euclidean distance are also used in clustering analysis of microarray data ***(18)***.

3.3.2. Hierarchical Clustering

There are two basic methods in hierarchical clustering: the agglomerative hierarchical method and the divisive hierarchical method ***(18)***. The agglomerative method initially treats each individual data vector (e.g., intensities of each gene of all arrays or intensities of all genes of each array) as a single cluster. It then groups the most similar data vectors and merges them based on their similarities. At the end, all data vectors are merged into one single cluster. The divisive hierarchical method starts in the opposite direction. It takes all data vectors as one single cluster at the beginning. This single cluster is then divided into subgroups based on how dissimilar they are until each data vector becomes a single cluster. This section focuses on the agglomerative method. In the following procedure, it is assumed that there are n arrays and each array measures the expression of k genes.

1. Take each gene as a single cluster.
2. Calculate the distance between each pair of clusters.
3. Find two clusters with the closest distance.
4. Merge these two clusters into a new cluster.
5. Repeat **steps 2–4** until all genes are grouped into one cluster.

During the process of hierarchical clustering, a single cluster may contain more than one gene. There are three algorithms to calculate the distance between clusters that contain a few genes ***(18)***.

1. **Single linkage**. The distance between each gene in cluster 1 and each gene in cluster 2 is calculated. The minimum distance among all pairwise distance measures is found and used as the distance between clusters 1 and 2.
2. **Complete linkage**. The distance between each gene in cluster 1 and each gene in cluster 2 is calculated. The maximal distance among all pairwise distance measures is found and used as the distance between clusters 1 and 2.
3. **Average linkage**. The distance between each gene in cluster 1 and each gene in cluster 2 is calculated. The average of all pairwise distance measures is used as the distance between clusters 1 and 2.

3.3.3. k*-Means Clustering*

k-Means clustering starts with a predetermined number of clusters (*k* clusters). There are two ways to initiate these *k* clusters. All genes can be randomly assigned to *k* clusters or a set of seed genes can be assigned to *k* clusters. Basic steps of *k*-means clustering are as follows ***(18)***:

1. Assign genes (random genes or seed genes) into k clusters.
2. Calculate the mean of expression intensities of all genes in each cluster.

3. Take each gene and calculate the distance between the gene and the mean of each cluster. Assign the gene to the cluster whose mean is the closest to the expression vector of that gene.
4. Recalculate the mean of the cluster that received the gene and the mean of the cluster that lost the gene.
5. Repeat **steps 3–4** until no more genes can be assigned to new clusters.

3.3.4. Self-Organizing Maps

Self-organizing maps were originally designed to study neural networks. This unsupervised clustering algorithm places genes with similar expression patterns in neighboring clusters. It provides easy visualization of gene expression data. The following procedure describes basic steps to build SOM ***(18,19)***:

1. A two-dimensional grid is defined by the user.
2. A random vector is assigned to each node of the grid and used as the reference vector of the node.
3. A gene is assigned to a node whose reference vector is the closest to the expression vector of that gene.
4. The reference vector of the node where the gene is assigned is adjusted to be closer to the expression vector of that gene. Reference vectors of all neighboring nodes are also adjusted to be closer to the expression vector of that gene. Reference vectors of neighboring nodes are adjusted so that the more distant the nodes are, the less their reference vectors are adjusted.
5. **Steps 3–4** are repeated for all other genes (*see* **Note 3**).

3.4. Principal Component Analysis

Principal component analysis (PCA) reduces the dimensionality of microarray data by examining the variance of the dataset. It uses a few linear combinations of the original variables to represent the original dataset. By describing the original data on a new set of orthogonal linear coordinates, PCA may be used to identify outliers in microarray data. The mathematics of PCA is complicated. The following steps try to provide basic ideas of this algorithm ***(18)***.

1. A matrix X is built for the microarray dataset so that each row vector x_i contains intensities of each gene in all arrays, and each column vector x_j contains intensities of all genes in one array. Assume that there are n rows and m columns.
2. Find the covariance matrix of the original data matrix.
3. Find eigenvalues and eigenvectors of the covariance matrix.
4. For eigenvalues $\lambda_1 \geq \lambda_2 \geq \lambda_3 \geq \cdots \geq \lambda_m \geq 0$, the kth principal component is

$$z_k = \sum_{j=1}^{m} \alpha_{k,j} x_j , \tag{12}$$

where $\alpha_{k,1}$, $\alpha_{k,2}$, $\alpha_{k,3}$, $\cdots$, $\alpha_{k,m}$ are components of the eigenvector corresponding to the kth largest eigenvalue λ_k.

5. Usually, the first p components ($p \leq m$) are used to represent the original dataset.

3.5. Applications of Analysis Methods in Studies of Membrane Transporters

Methods described in the previous sections have been applied to analyze microarray data in research of membrane transporter. In a study that examined the neurotoxic effects of methamphetamine (METH) on brain dopamine neurons, the fold change was used to identify differentially expressed genes in the mouse ventral midbrain after the treatment of METH alone and METH combined with dopamine-transporter blocker ***(20)***. Liu et al. found with the *t*-test that in the rat liver epithelial cell, long-term exposure to low levels of arsenite induced overexpression of genes encoding for the efflux transporter Mrp1/Mrp2, for the efflux transporter P-glycoprotein, and for glutathione-*S*-transferase II ***(13)***. By comparing data of multiple groups of array with one-way ANOVA and examining gene expression patterns with *k*-means clustering, Richer et al. have shown that two isoforms of progesterone receptor (PR-A and PR-B) regulate different subsets of genes ***(14)***.

3.6. Software Packages and Other Tools for Microarray Data Analysis

Various software packages provide the convenience of analyzing large-scale microarray data. This section briefly reviews statistical tests, clustering algorithms, and other important features of major software packages and other tools for microarray data analysis. All descriptions are based on the current versions of these software packages and tools.

1. Microarray Suite (Affymetrix Inc, Santa Clara, CA)
   Website: www.affymetrix.com
   Statistical tests: Comparison expression analysis of two microarray experiments
2. Data Mining Tool (Affymetrix Inc, Santa Clara, CA)
   Website: www.affymetrix.com
   Statistical tests: *t*-Test with unequal variance, Mann–Whitney test
   Clustering algorithms: SOM and correlation coefficient clustering
   Other computational functions: Average, median, standard deviation, and fold change
   Other analysis function: Matrix analysis (comparing two lists of probe sets and calculating the significance of the overlap between them)
   Graphic features: Scatter graph, fold-change graph, series graph, and histogram
3. GeneSpring (Silicon Genetics, Redwood City, CA)
   Website: www.silicongenetics.com/cgi/SiG.cgi/index.smf
   Statistical tests: *t*-Test (with equal or unequal variance), ANOVA (with equal or unequal variance), Mann–Witney test, Kruskal–Wallis test
   p-Value adjustment: Bonferroni single-step adjustment, step-down Bonferroni adjustment, Westfall and Young's correction

Clustering algorithms: Hierarchical clustering, *k*-means clustering, SOM
Other analysis: Principal component analysis
Other feature: Gene expression shown on a prebuilt map of signal transduction pathway

4. Spotfire (Spotfire, Somerville, MA)
   Website: www.spotfire.com
   Statistical tests: *t*-Test, ANOVA
   Clustering algorithms: *k*-means and hierarchical clustering
   Other analysis: Principal component analysis
5. Cyber T (University of California at Irvine, Irvine, CA)
   Website: genomics.biochem.uci.edu/genex/cybert, Web interface
   Statistical tests: Paired and unpaired *t*-Tests
   p-Value adjustment: Bonferroni single-step adjustment
   Other feature: Bayesian estimate of variance
6. J-express (Molmine AS, Bergen, Norway)
   Website: www.molmine.com, free for academic users
   Clustering algorithms: Hierarchical clustering, *k*-means clustering, SOM
   Other analysis: Principal component analysis
7. Significance analysis of microarray (SAM) (Stanford University, Stanford, CA)
   Website: www-stat.stanford.edu/~tibs/SAM, free for academic users
   Features: Multiple group comparison, paired or unpaired data, estimation of false discovery rate.
8. Cluster and TreeView (University of California at Berkeley, Berkeley, CA)
   Website: rana.lbl.gov/EisenSoftware.htm, free for academic users
   Clustering algorithms: Hierarchical clustering, *k*-means clustering, SOM
   Other analysis: Principal component analysis
9. dChip (Harvard University, Cambridge, MA) ***(21,22)***
   Website: www.biostat.harvard.edu/complab/dchip, free for academic users
   Major function: Calculate model-based expression values for PM–MM data
   Statistical test: *t*-Test
   Clustering algorithm: Hierarchical clustering
   Other analysis: Principal component analysis
   Other features: Viewing PM–MM data and detecting array outliers
10. GenMapp (University of California at San Francisco, San Francisco, CA)
    Website: http://www.genmapp.org/, freeware
    Major features: Visualization of expression data on maps of biological pathways that involve various types of membrane transporter
11. R Project ***(23)***
    Website: www.r-project.org, free software under the terms of the Free Software Foundation's GNU General Public License in source code form
    Feature: A system with a language and environment for statistical computing and graphics; provides various statistical analysis tools, including linear and nonlinear modeling, classical statistical tests, time-series analysis, clustering, and so forth.

12. NetAffx (Affymetrix Inc, Santa Clara, CA)
    Website: www.affymetrix.com
    Function: On-line resource that provides sequences and annotations of probe sets of Affymetrix GeneChip Probe Arrays

4. Notes

1. When the Bonferroni single-step correction is employed to control the FWE in multiple testing, an original *p*-value is multiplied by the number of genes being tested. Because most of the current arrays measure the expression of at least a few thousand genes on each array, very few *p*-values can become significant after this adjustment. The Bonferroni step-down correction does not improve much the power of test. The Westfall and Young step-down adjustment is less conservative than Bonferroni corrections. However, in many cases of microarray data analysis, it might still be too stringent.
2. Usually, one array contains several thousand probes. When the expression data of all these probes are used in clustering analysis, the result may not show clear expression patterns. This is probably because only a limited number of genes are important or relevant to the biological process being studied. Unique expression patterns of those important genes might be masked by the expression data of irrelevant genes, especially when the number of clusters is small. A filtering process can be used to exclude irrelevant genes prior to clustering analysis.
3. Some clustering algorithms (e.g., SOM) involve random processes. It is, therefore, not surprising to see slightly different clustering results each time the clustering analysis is performed.

References

1. Shi, L. (2002) DNA Microarray (Genome Chip)—Monitoring the Genome on a Chip, http://www.gene-chips.com.
2. Buhler, J. (2001) Anatomy of a comparative gene expression study, http://www.cs.wustl.edu/~jbuhler//research/array/.
3. Quackenbush, J. (2001) Computational analysis of microarray data. *Nature Rev. Genet.* **2,** 418–427.
4. Wu, T. D. (2001) Analysing gene expression data from DNA microarrays to identify candidate genes. *J. Pathol.* **195,** 53–65.
5. Tong, L., Shen, H., Perreau, V. M., et al. (2001) Effects of exercise on gene-expression profile in the rat hippocampus. *Neurobiol. Dis.* **8,** 1046–1056.
6. Schadt, E. E., Li, C., Ellis, B., and Wong, W. H. (2001) Feature extraction and normalization algorithms for high-density oligonucleotide gene expression array data. *J. Cell. Biochem.* **37(Suppl.),** 120–125.
7. DeRisi, J., Penland, L., Brown, P. O., et al. (1996) Use of a cDNA microarray to analyse gene expression patterns in human cancer. *Nature Genet.* **14,** 457–460.
8. Schena, M., Shalon, D., Davis, R. W., et al. (1995) Quantitative monitoring of gene expression patterns with a complementary DNA microarray. *Science* **270,** 467–470.

9. Schena, M., Shalon, D., Heller, R., et al. (1996) Parallel human genome analysis: microarray-based expression monitoring of 1000 genes. *Proc. Natl. Acad. Sci. USA* **93**, 10,614–10,619.
10. Affymetrix (2001) *Statistical Algorithms Reference Guide*, Technical Report, Affymetrix, Santa Clara, CA.
11. Hakak, Y., Walker, J. R., Li, C., et al. (2001) Genome-wide expression analysis reveals dysregulation of myelination-related genes in chronic schizophrenia. *Proc. Natl. Acad. Sci. USA* **98,** 4746–4751.
12. Bouton, C. M. L. S., Hossain, M. A., Frelin, L. P., et al. (2001) Microarray analysis of differential gene expression in lead-exposed astrocytes. *Toxicol. Appl. Pharmacol.* **176,** 34–53.
13. Liu, J., Chen, H., Miller, D. S., et al. (2001) Overexpression of glutathione *S*-transferase II and multidrug resistance transport proteins is associated with acquired tolerance to inorganic arsenic. *Mol. Pharmacol.* **60,** 302–309.
14. Richer, J. K., Jacobsen, B. M., Manning, N. G., et al. (2002) Differential gene regulation by the two progesterone receptor isoforms in human breast cancer cells. *J. Biol. Chem.* **277,** 5209–5218.
15. Westfall, P. H. and Young, S. S. (1993) *Resampling-Based Multiple Testing: Examples and Methods for* p-*Value Adjustment*, Wiley, New York.
16. Dudoit, S., Yang, Y. H., Callow, M. J., et al. (2000) Statistical methods for identifying differentially expressed genes in replicated cDNA microarray experiments, http://www.stat.berkeley.edu/users/terry/zarray/TechReport/578.pdf.
17. Tusher, V. G., Tibshirani, R., and Chu, G. (2001) Significance analysis of microarrays applied to the ionizing radiation response. *Proc. Natl. Acad. Sci. USA* **98,** 5116–5121.
18. Johnson, R. and Wichern, D. W. (1988) *Applied Multivariate Statistical Analysis*, Prentice-Hall, Englewood Cliffs, NJ.
19. Kohonen, T. (1995) *Self-Organizing Maps*, Springer-Verlag, Berlin.
20. Xie, T., Tong, L., Barrett, T., et al. (2002) Changes in gene expression linked to methamphetamine-induced dopaminergic neurotoxicity. *J. Neurosci.* **22,** 274–283.
21. Li, C. and Wong, W. H. (2001) Model-based analysis of oligonucleotide arrays: expression index computation and outlier detection. *Proc. Natl. Acad. Sci. USA* **98,** 31–36.
22. Li, C. and Wong, W. H. (2001) Model-based analysis of oligonucleotide arrays: model validation, design issues and standard error application. *Genome Biol.* **2,** 1–11.
23. Hornik, K. (2002) The R FAQ, http://www.r-project.org.

6

Laser Capture Microdissection to Examine Transporter Expression in Specific Cell Regions

Okkyung Rho and Gary W. Miller

1. Introduction

Parkinson's disease (PD) is a progressive neurodegenerative disease as a result of a selective degeneration of dopamine neurons in the substantia nigra. The selective loss of dopamine neurons in Parkinson's disease is thought to involve altered expression or function of the plasma membrane and vesicular transporters for dopamine ***(1)***. The dopamine transporter (DAT) is exclusively found in dopaminergic neurons ***(2)*** and renders the dopamine neuron susceptible to neurotoxins, such as 1-methyl-4-phenyl-1,2,3,6-tetrahydropyridine (MPTP) that can be transported by DAT into the neuron ***(1)***.

The dopamine neurons that are lost in PD are found in a very distinct region of the midbrain called the substantia nigra pars compacta. However, dissection of the midbrain yields a heterogeneous cell population with numerous cell types. To focus on the specific cells that are affected in PD, it would be highly desirable to be able to isolate and purify the substantia nigra pars compacta and more specifically the dopamine neurons within this region. Recent technology has provided an opportunity to selectively isolate these neurons for analysis of gene expression. We have been using the PixCell II Laser Capture Microdissection System (Arcturus, Mountain View, CA) (*see* **Fig. 1**) to isolate dopamine neurons from mouse brain (*see* **Figs. 2** and **3**). Frozen sections of the midbrain can be Nissl-stained with Toluidine Blue O (Sigma, St Louis, MO) to identify the neurons in midbrain and then substantia nigra pars compacta neurons can be isolated. However, the precise microdissection is frequently limited by the difficulty of identifying the specific cell types by morphology only. The immunostaining of adjacent sections with tyrosine hydroxylase (TH) allows us to isolate the defined cell populations. There are two primary ways to

From: *Methods in Molecular Biology, vol. 227: Membrane Transporters: Methods and Protocols*
Edited by: Q. Yan © Humana Press Inc., Totowa, NJ

Fig. 1. Arcturus PixCell II Laser Capture Microdissection System. The Arcturus system uses an infrared laser to melt a polymer into the tissue sample. When the laser pulse is completed, the polymer solidifies and will lift out the captured cylinder of tissue.

isolate brain regions using laser capture. The first is the focused capturing of individual neurons, as shown in **Fig. 2**. The second is to use a sweeping motion of the laser to isolate distinct areas. **Figure 3** shows isolation of the substantia nigra pars compacta.

Figure 2 shows the section of tissue before capture and the captured cells. RNA was then extracted from the captured cells. Reverse transcriptase–polymerase chain reaction (RT-PCR) performed on the entire midbrain reproduced strong bands for both DAT and the housekeeping gene, hypoxanthine phosphoribosyltransfersae (HPRT) (*see* **Fig. 2**). After laser capture, the ratio of DAT to HPRT is greatly increased, indicating a significant purification of dopamine neurons, as DAT is the phenotypic markers of these cells. Furthermore, the expression of DAT from substantia nigra pars compacta was compared to that of the adjacent ventral tegmental area (VTA) using real-time PCR (data not shown). The dopamine neurons in the VTA are less vulnerable

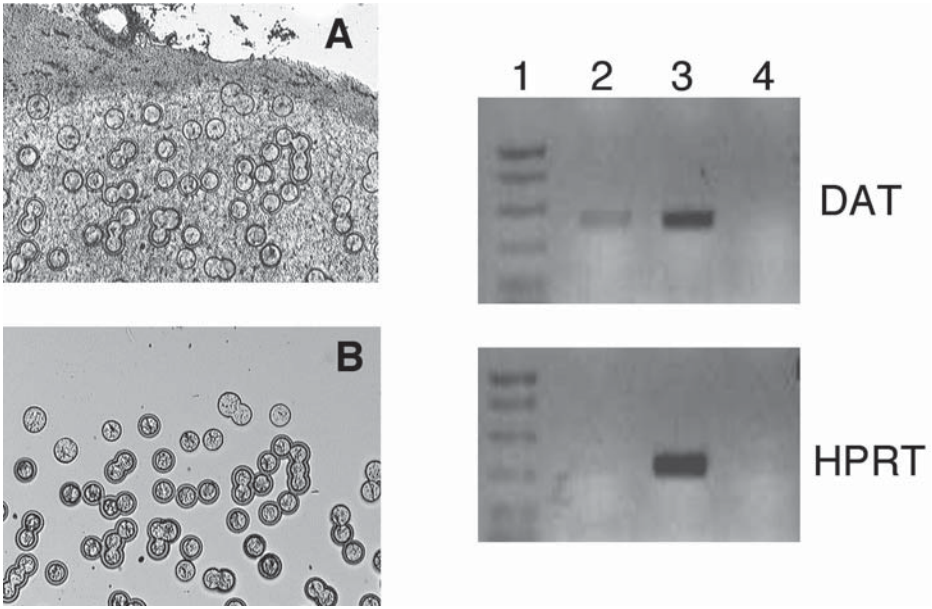

Fig. 2. Laser capture microdissection from Nissl-stained sections (7 μm). **(A)** Individual neurons are targeted with individual laser shots. **(B)** Captured neurons are transferred from each spot to the transfer film. The right panel shows the results of RT-PCR, for the DAT and the housekeeping gene HPRT. Lane 1, ladder; lane 2, cells captured in **(B)**; lane 3, the entire cryostat section from **(A)**; lane 4, control lane with no template. Note the increased amount of DAT compared to HPRT from the captured cells. (Reduced from original magnification.)

to the damage in PD than those in the substantia nigra. DAT levels were found to be five times higher in the substantia nigra than in VTA, which may explain the increased susceptibility in the nigral neurons.

2. Materials

2.1. Tissue Preparation

1. OCT Tissue-Tek frozen tissue embedding medium (Sakura, Torrance, CA).
2. Peel-A-Way disposable embedding molds (22 mm square) (Polysciences Inc, Warrington, PA).
3. Cryostat.
4. RNaseZap (Ambion, Austin, TX).
5. Microscopic slides and cover slips. Wipe with RNaseZap, wash with autoclaved water and 100% ethanol several times, and then dry in a clean hood.

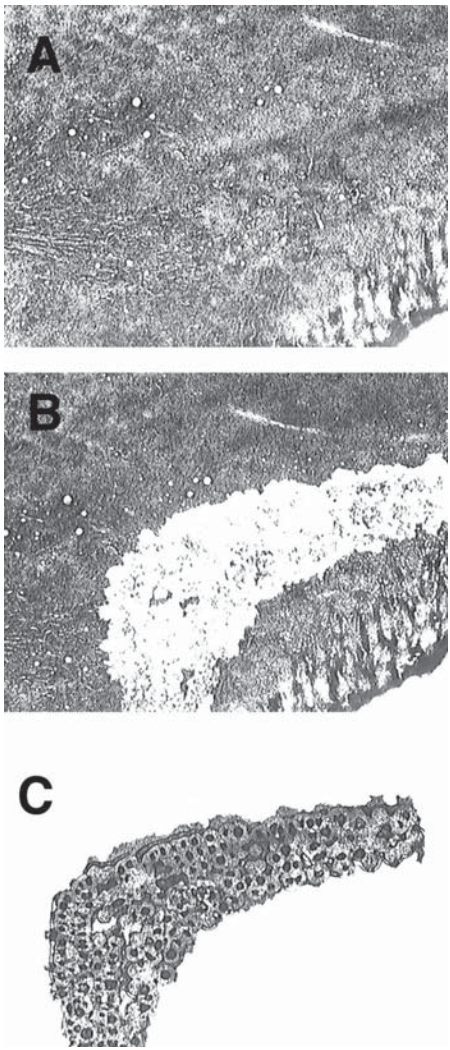

Fig. 3. Laser capture microdissection of substantia nigra pars compacta using sweeping motion. **(A)** midbrain cryostat section; **(B)** midbrain cryostat section after removal of substantia nigra pars compacta; **(C)** isolated substantia nigra pars compacta. When DAT levels were analyzed by real-time PCR, DAT was found to be five times higher in substantia nigra than in the adjacent ventral tegmental area. (Reduced from original magnification.)

2.2. Immunohistochemistry

1. Humidified chamber.
2. Staining dish with tray for holding slides or Coplin staining jar.
3. 1X Tris-buffered saline (TBS): 135 m*M* NaCl, 2.5 m*M* KCl, 25 m*M* Tris-HCl, pH 7.4.
4. 4% Paraformaldehyde solution (*see* **Note 1**), pH 7.4. Dissolve paraformaldehyde powder (Sigma, St. Louis, MO) in deionized water by heating to 60°C and stirring in a fume hood. Add a few drops of 1 *N* NaOH to help dissolve paraformaldehyde. Let the solution cool to room temperature and then add 2X TBS to make 1X TBS.
5. 10% Triton X-100 in H_2O. Store at 4°C.
6. 30% Hydrogen peroxide. Store at 4°C.
7. Normal goat serum. Store at –20°C. Once thawed, store at 4°C (*see* **Note 2**).
8. Biotin/avidin blocking kit (Vector Laboratories, Burlingame, CA). Store at 4°C.
9. Affinity-purified TH polyclonal antibody (1:500, Chemicon, Temecula, CA). Store at –20°C.
10. Vectastain Elite ABC kit containing biotinylated secondary antibody (rabbit) and horseradish peroxidase reagents (Vector Laboratories, Burlingame, CA). Store at 4°C.
11. 3, 3'-Diaminobenzidine (DAB) substrate kit for peroxidase (Vector Laboratories, Burlingame, CA). Store at 4°C (*see* **Note 3**).
12. Toluidine Blue O staining solution (*see* **Subheading 2.3.**).
13. Deionized water and ethanol solutions (50%, 70%, 95%, 100%).
14. Xylene ACS grade (Sigma, St. Louis, MO) (*see* **Note 4**).
15. Cytoseal 60 mounting medium (Richard-Allan Scientific, Kalamazoo, MI) (*see* **Note 5**).
16. Light microscope.

2.3. Toluidine Blue O Staining

1. Toluidine Blue O (TBO) solution: 0.1% w/v ***(3)***. For 500 mL of solution, dissolve 10.32 g $Na_2HPO_4 \cdot 7H_20$ and 6.45 g citric acid in deionized water. Adjust pH to 4.0 with NaOH. Add 500 µL of diethylpyrocarbonate (DEPC) and mix thoroughly. Incubate overnight at room temperature and autoclave. Add 0.5 g Toluidine Blue O (Sigma T0394).
2. Ethanol solutions (50%, 70%, 95%, 100%) (*see* **Note 6**).
3. Xylene ACS grade (Sigma, St. Louis, MO).
4. DEPC-treated water (*see* **Note 7**).
5. Tight slide box.
6. Drierite (anhydrous calcium sulfate).

2.4. Laser Capture Microdissection of Neurons

1. PixCell II LCM system (Arcturus, Mountain View, CA; www.arctur.com).
2. CapSure LCM Caps (Arcturus, Mountain View, CA). Store at room temperature.
3. Prep Strip (Arcturus, Mountain View, CA). Store at room temperature.
4. CapSure Pad (Arcturus, Mountain View, CA). Store at room temperature.
5. 500-μL Eppendorf tube.

2.5. Total RNA Isolation

1. StrataPrep Total RNA Microprep kit (Stratagene, La Jolla, CA).
2. DEPC-treated water.
3. Microcentrifuge.
4. RNase-free microfuge tubes and tips.
5. RiboGreen RNA quantification reagent kit (Molecular Probes, Eugene, OR). Store at –20°C and protect from light for RiboGreen RNA quantification reagent.
6. Spectrofluorometer.

2.6. RT-PCR

1. Thermal Cycler.
2. DEPC-water.
3. Heat block or water bath.
4. SuperScript First Strand Synthesis System for RT-PCR (Invitrogen, Carlsbad, CA).
5. PCR sense and antisense primers.

3. Methods

3.1. Tissue Harvesting and Preparation

It is very critical to maintain an RNase-free environment from tissue preparation to RNA analysis.

1. Dissect midbrain from freshly sacrificed mouse under RNase-free conditions using sterile forceps and scalpel.
2. Place midbrain tissue in a disposable embedding mold and then cover the tissue with OCT Tissue-Tek frozen tissue embedding medium and quickly freeze in liquid nitrogen for 1 min. The block can be wrapped in foil and stored at –80°C until slicing.
3. Place the midbrain block in the cryostat for 20 min in order to equilibrate to the cryostat temperature (–15°C or – 20°C) (*see* **Note 8**).
4. Cut embedded tissue blocks of 7–10 μm onto plain uncoated RNase free-slides (*see* **Note 9**) using the cryostat (Leica CM 1800). A new blade should be used for each block. Freeze slides immediately on dry ice. The slides may be stored at –80°C until needed.

3.2. Immunohistochemistry

The precise microdissection is frequently limited by the identification of the specific cell types by morphology only. The immunostaining of adjacent sec-

tions with TH allows us to isolate the defined dopaminergic cell populations. After the tissue has been fixed, it should not be allowed to dry during the immunohistochemistry procedure.

1. Allow the section (on slide) to air-dry. Fix the section with freshly prepared 4% paraformaldehyde for 4 min at room temperature.
2. Rinse slides twice with TBS at room temperature.
3. Incubate tissue slides in 3% H_2O_2, 1% Triton X-100, and 4% goat serum in TBS for 20 min (*see* **Note 10**).
4. Rinse slides thoroughly in TBS (5 × 10 min).
5. Block sections in a solution containing 4% serum, 0.1% Triton X-100, and avidin (1 drop/mL) in TBS for 30 min (*see* **Note 11**).
6. Rinse 3 times in TBS for 10 min each.
7. Incubate sections in TH primary antibody solution overnight at 4°C (4% goat serum, 0.1% Triton X-100, biotin (1 drop/mL), and TH affinity-purified antibody in TBS) (*see* **Note 12**).
8. Rinse sections in TBS for 3 × 10 min.
9. Incubate sections in secondary antibody solution containing 0.1% Triton X-100 and 1 drop/20 mL of rabbit secondary antibody from the Vectastain Elite ABC kit in TBS for 1 h at room temperature (*see* **Note 13**).
10. Make up the tertiary complex by adding 1 drop of solution A into 20 mL of 1X TBS with 0.1% Triton X-100, mixing well. Then, add 1 drop of solution B and mix well.
11. Rinse sections in TBS for 3 × 10 min.
12. Incubate sections in tertiary complex for 1 h at room temperature in humidified chamber.
13. Rinse sections in TBS for 3 × 10 min.
14. Make the DAB solution by adding 2 drops of buffer solution, 4 drops of DAB, and 2 drops of H_2O_2 solution (*see* **Note 3**). Mix well after each addition.
15. Incubate in DAB solution for 1–5 min under the microscope until staining can be visualized.
16. Rinse sections in tap water.
17. Counterstain with toluidine blue O solution for 5 min and rinse with water.
18. Dehydrate slides in alcohols and clear two times with xylenes.
19. Cover slip with Cytoseal 60 mounting medium.

3.3. Toluidine Blue O Stainining (see Note 14)

Nissl-staining with Toluidine Blue O (Sigma, St. Louis, MO) was used to identify the neurons in midbrain. Nissl bodies are found in the cell body and dendrites of neurons, which are stained by Toluidine Blue O. All the solutions should be prepare with DEPC-treated water and be replaced regularly. During this staining procedure, sections should not be dry at any time.

1. Fix the frozen sections in 70% ethanol for 30 s ***(4)***.
2. Briefly rinse in DEPC-treated water for 30 s.

3. Stain slides with TBO solution for 1 min (*see* **Note 15**).
4. Rinse in DEPC–water two times.
5. Dehydrate sections with 50% ethanol, 70% ethanol, 95% ethanol, and 2 × 100% ethanol for 30 s each (*see* **Note 16**).
6. Dip in xylene 2 × 5 min (*see* **Note 4**).
7. Air-dry in a hood for 20 min. Do not cover slip the slides. Slides are now ready for laser capture microdissection (LCM) or store slides in a desiccator or in a tight slide box with Drierite at room temperature (*see* **Note 17**).

3.4. Laser Capture Microdissection of Neurons

The PixCell II LCM system (Arcturus, Mountain View, CA; www.arctur.com) was used for laser capture of neurons. This system allows the user to identify the cell type under a light microscope. Using a joystick, the user positions the icon over the cell of interest. A simple push of a button activates the infrared laser, which melts and bonds the tissue to the polymer that is found in a microfuge tube lid. This aim-and-shoot method permits multiple microdissections in minutes. In the course of an afternoon, up to thousands of cells can be collected, which is sufficient for mRNA analysis. As suggested by the manufacturer, we used sections less than 10 μm thick. We believe that 8 μm is optimal, as it prevents the cylinder removed by the laser from having more than one cell type. Cryostat sections must be free of folds of the tissue, otherwise sections may not make direct contact with the CapSure surface.

1. Move the joystick to the center.
2. Apply Prep Strip on to a slide surface to make the sections flat on the slide.
3. Position the sample slide on the translation stage and hold the slide using a vacuum chuck.
4. Adjust magnification and illumination controls.
5. Apply the CapSure properly to the surface of slide (*see* **Note 18**).
6. Aim the laser beam on the cell of interest using a joystick.
7. Focus the laser beam using spot size adjust and fine-focus the adjust knob (*see* **Note 19**).
8. Aim the laser beam on the selected region and press the fire button.
9. Move to other areas on the section using the joystick.
10. Repeat **steps 6–9** to capture other cells.
11. Lift the CapSure placement arm to remove the captured cells.
12. Place the cap onto a CapSure pad to remove contaminated cells or tissues.
13. Transfer the cap to a 500 μL Eppendorf tube containing 200 μL of lysis buffer and 14 μL of 2-mercaptoethanol (*see* **Note 20**).
14. Lyse the captured cells on the cap by inverting and tapping tubes and briefly centrifuge tubes to collect samples.

3.5. Total RNA Isolation from Captured Cells

1. Add 200 μL of 70 % ethanol and mix thoroughly by vortexing.
2. Centrifuge briefly and transfer contents to a RNA-binding spin cup within a 2-mL collection tube.
3. Spin the tube for 60 s at maximum speed in a microcentrifuge.
4. Discard the flowthrough and reuse the collection tubes for the next steps.
5. Wash the spin cup with 600 μL low-salt wash buffer and microcentrifuge for 60 s.
6. Discard the flowthrough and spin the cup for 2 min.
7. Mix 5 μL RNase-free DNase I with 25 μL DNase digestion buffer (*see* **Note 21**).
8. Add the above DNase I solution onto inside the spin cup and close the cap.
9. Incubate for 15 min at 37°C.
10. Wash the spin cup with 500 μL high-salt wash buffer. Spin and discard the flowthrough.
11. Repeat wash with 600 μL low-salt wash buffer and microcentrifuge for 60 s.
12. Perform a final wash with 300 μL low-salt buffer and microcentrifuge for 60 s.
13. Centrifuge for 2 min to remove the wash solution.
14. Transfer the spin cup to a fresh 1.5-mL collection tube. Add 30 μL of prewarmed (60°C) elution buffer directly onto the center of the fiber matrix.
15. Incubate the spin cup at room temperature for 2 min.
16. Recover the eluate by spinning the spin cup for 1 min. Repeat the elution step (*see* **step 14**) to increase recovery of RNA in the same tube. Store RNA at –80°C.
17. To quantify the RNA, perform the low-range assay of the RiboGreen RNA quantitation kit and measure the fluorescence using a spectrofluorometer (excitation: approx 480 nm; emission: approx 520 nm).

3.6. RT-PCR or Real-Time RT-PCR

1. Prepare first-strand synthesis mixtures in RNase-free 0.5-mL tubes by adding 20 ng RNA , 1 μL of oligo (dT), 1 μL of 10 m*M* dNTP mix, and DEPC–water to make 10 μL.
2. Incubate tubes at 65°C for 5 min and chill them on ice. Collect samples by spinning down in a microcentrifuge.
3. Add 2 μL RT buffer, 4 μL of 25 m*M* $MgCl_2$, 2 μL of 0.1 *M* dithiothreitol (DTT), and 1 μL RNase inhibitor to the RNA mixture.
4. Mix and incubate at 42°C for 2 min.
5. Add 1 μL (50 units) of SuperScript II reverse transcriptase, mix, and incubate at 42°C for 50 min.
6. Terminate the reaction at 95°C for 15 min; then, chill on ice.
7. Add 1 μL RNase and incubate at 37°C for 20 min.
8. For the conventional RT-PCR, prepare the PCR reaction mixture in thin-wall PCR tubes by adding 2 μL RT reaction, 5 μL of 10X PCR buffer, 1 μL of 10 m*M* dNTP, 1 μL of 10 μ*M* sense primer, 1 μL of 10 μ*M* antisense primer, 2 U *Taq* DNA polymerase, and 40 μL of DEPC–H_2O.

9. Mix the contents and spin briefly.
10. Run the PCR in thermal cycler:
    94°C for 2 min
    40 Cycles with 94°C for 20 s, 58°C for 30 s, and 72°C for 1 min
    72°C for 5 min.
11. Analyze 10–20 μL PCR reactions using agarose gel electrophoresis.
12. For a more quantitative analysis, real-time quantitative PCR using the ABI 7700 (Applied Biosystems, Fostercity, CA) may be performed with a Taqman probe and primers using established procedures and the manufacture's instructions.

4. Notes

1. Buffer should be made fresh daily.
2. The serum used for blocking should be the same from host species of the secondary. The secondary antibody from Vector Vectastain Elite ABC kit makes antibody in goat; therefore, we use goat serum.
3. 3,3'-Diaminobenzidine (DAB) is a suspected carcinogen. Wear gloves and lab coats when using this agent.
4. Perform all xylene washes in a fume hood.
5. Cytoseal 60 mounting medium contains toluene and it should be handled in a fume hood.
6. Dilute ethanol with DEPC–water.
7. DEPC is toxic. Use DEPC in a chemical fume hood. Add 1/1000 volume of DEPC to deionized water (0.1% DEPC) and mix thoroughly by shaking. Leave in a hood overnight and autoclave before use.
8. If the block temperature is not equilibrated with the cryostat, the block will crack during sectioning. The larger blocks need a longer time to equilibrate in cryostat.
9. Wear gloves at all times during the procedure. Wipe glass slides with RNaseZap, wash thoroughly with autoclaved water and 100% ethanol, and then dry in a clean hood. For cutting sections, the thinner, the better.
10. This step is for quenching endogeneous H_2O_2 enzyme activity.
11. Incubation of sections was conducted in humidified chamber to prevent the evaporation of solutions. This step is to prevent binding to endogeneous biotin, biotin-binding proteins, or lectins.
12. The addition of biotin in this step is to block the remaining biotin sites on the avidin and this will reduce a high backround. Incubation was conducted in humidified chamber to prevent the evaporation of solutions.
13. The Vector Vectastain Elite ABC kit contains the biotinylated rabbit secondary antibody (A) and the avidin–peroxidase complex (B and C) for immunostaining. Incubation was conducted in humidified chamber to prevent evaporation of solutions.
14. Staining procedure should be scheduled within 3 days of LCM transfer.
15. Filter TBO solution regularly.
16. Replace 100% ethanol and xylene frequently because hydrated ethanol or xylene may cause poor transfer in LCM. Dehydration of the section is the most impor-

tant factor for LCM transfer! If needed, a repeated or a longer xylene treatment may help an efficient LCM transfer.

17. It is very critical for LCM transfer to store slides in a dry place. Use one slide at a time.
18. Avoid letting the sections fold. Folds may prevent the cap from making direct contact on the surface of tissue sections and cause a poor transfer.
19. Focus a laser beam with a small spot size (<7.5 μm) and fire the laser at outside of sections on slides. A well-focused laser beam has a single bright spot with a well-defined edge. Adjust laser power and duration according to a selected spot size. Once settings are selected, there is no need to adjust for different spot sizes. The corresponding setting is automatically calibrated.
20. The lysis buffer contains guanidine thiocyanate. Add 2-mercaptoethanol to the lysis buffer before use. Perform this procedure in fume hood.
21. DNase I is very sensitive to denaturation and should be handled with caution.

References

1. Miller, G. W., Gainetdinov, R. R., Levey, A. I., et al.(1999) Dopamine transporters and neuronal injury. *Trends Pharmacol. Sci.* **20,** 424–429.
2. Giros, B., Jaber, M., Jones, S. R., et al. (1996) Hyperlocomotion and indifference to cocaine and amphetamine in mice lacking the dopamine transporter. *Nature* **379,** 606–612.
3. Noraberg, J., Kristensen, B. W., and Zimmer, J. (1999) Markers for neuronal degeneration in organotypic slice cultures. *Brain Res. Protocols* **3,** 278–290.
4. Goldsworthy, S. M., Stockton, P. S., Trempus, C. S., et al. (1999) Effects of fixation on RNA extraction and amplification from laser capture microdissected tissue. *Mol. Carcinog.* **25,** 86–91.

7

Site-Directed Mutagenesis in the Study of Membrane Transporters

Renae M. Ryan, Ann D. Mitrovic, and Robert J. Vandenberg

1. Introduction

One of the major goals in membrane transporter research is to understand how transporter proteins work at the molecular level. Ideally, this research would be carried out with a detailed knowledge of the three-dimensional structure of the protein. However, in the absence of protein crystals of transporters suitable for X-ray diffraction analysis other molecular tools need to be employed. In vitro site-directed mutagenesis is one method that has the capacity to provide both structural information and identification of the role of individual residues and/or regions of a protein that are involved in function.

Site-directed mutagenesis involves changing the genetic code for a protein sequence and generating a mutant protein with a subtly different structure. When this is combined with functional assays of the mutant, this method has the capacity to provide very useful information about the structural basis for transporter function. The utility of this approach derives from the fact that, in general, most point mutations do not dramatically alter function. The small number of mutations that do alter or destroy function of the transporter do so because specific contacts between the solute, ion, or substrate and the transporter are disrupted, or conformational changes required for the transport process are prevented ***(1)***. This raises a very important cautionary note in interpreting the significance of loss of function mutants. In addition to disruption of specific contacts between the solute and the transporter, loss of function can arise through misfolding of the protein or altered insertion of the protein into the membrane. Therefore, mutants that lose function are only useful if the cause of loss of function can be accurately ascertained. Even so, if a loss of function is the result of the lack of expression at the cell surface, no conclu-

From: *Methods in Molecular Biology, vol. 227: Membrane Transporters: Methods and Protocols*
Edited by: Q. Yan

sions about the role of particular amino acid residues in the functional properties of the transporter can be made.

A number of site-directed mutagenesis strategies to study structure–function relationships have been used and include the following: construction of chimeric transporters to identify functional domains (e.g., *see* **refs. *2*** and ***3***); mutating consecutive residues to alanine to scan through the amino acid sequence to identify residues involved in important functional properties; cysteine scanning mutagenesis in combination with chemical modifications of the introduced cysteine residues to probe accessibility of various regions to aqueous environments, and their roles in determining functional properties of the transporter (e.g., *see* **refs. *4*** and ***5***); tryptophan scanning to identify regions that may be associated with or interact with lipids within the membrane (e.g., *see* **ref. *6***). In addition, conservative substitutions are very commonly used to address more directed questions concerning the structural basis for functional properties. In general, the methods used to construct the mutations are the same irrespective of the overall goal of the experiment. In the next sections, we describe the methods used in our laboratory to construct mutant transporters and how the functional properties of the transporters are assessed (*see* **Note 1**).

2. Materials

2.1. Reagents

1. Bacterial growth medium (NZYM) broth (Integrated Sciences, Sydney, Australia; but there are many other suppliers). NZYM$^+$: Filter-sterilize 2 mL of 1 *M* D-glucose, 625 µL of 2 *M* $MgCl_2$, and 450 µL of 1 *M* $MgSO_4$ using a 0.2-µm filter (Millipore) and add to 100 mL of autoclaved NZYM.
2. Ampicillin (Sigma Chemical Co.): Make up to 100-mg/mL stock solution in water and store at –20°C. Then, use at a concentration of 100 µg/mL in the broth or agar.
3. LB agar from Sigma.
4. Agarose (Sigma) for gel electrophoresis. DNA fragments in the range of 0.5–5 kb are well separated on a 0.8% (w/v) gel.
5. Ethidium bromide (Sigma) made up as a 5-mg/mL stock solution in water. Add 2 µL to 50 mL of melted agarose prior to pouring the gel to visualize DNA with a transilluminator.
6. Phenol : chloroform : isoamyl alcohol (25:24:1) from Sigma.
7. Chloroform (analytical reagent [AR] grade).
8. Molecular biology grade ethanol from Sigma.
9. 3 *M* Sodium acetate: 40.8 g sodium acetate–H_2O, adjust to pH 5.3 with glacial acetic acid, and add H_2O to 100 mL.
10. 0.1% Diethylpyrocarbonate (DEPC) (Sigma)-treated H_2O (*see* **Note 2**).
11. Tris-acetate (TAE) electrophoresis buffer, use at 1X. 50X: 242 g Tris base, 57.1 mL glacial acetic acid, 100 mL 0.5 *M* EDTA, pH 8.0.

2.2. Kits

2.2.1. Site-Directed Mutagenesis Kit

Many companies sell site-directed mutagenesis kits (e.g., Stratagene, Promega, Clonetech). We routinely use the Quikchange(tm) Site Directed Mutagenesis kit from Stratagene and found that it is easy to use, relatively fast, and reliable. The kit components are as follows:

1. 10X Reaction buffer; 100 m*M* KCl, 100 m*M* $(NH_4)_2SO_4$, 200 m*M* Tris-HCl, pH 8.8, 20 m*M* $MgSO_4$, 1% Triton® X-100, 1 mg/mL nuclease-free bovine serum albumin (BSA).
2. dNTP mix.
3. PfuTurbo(tm) DNA polymerase (2.5 U/μL).
4. DpnI restriction enzyme (10 U/μL).
5. Epicurian Coli® XL1-Blue supercompetent cells.

2.2.2. Plasmid Mini-Prep Kit

Most of the commercially available miniprep kits have similar protocols and similar buffer components. This protocol is based on the Wizard® Plus Minipreps DNA Purification System (Promega). The buffer components are as follows:

1. Cell resuspension buffer: 50 m*M* Tris-HCl, pH 7.5, 10 m*M* EDTA, and 100 μg/mL RNaseA.
2. Cell lysis solution: 0.2 *M* NaOH, 1% sodium (SDS).
3. Neutralization solution: 1.32 *M* potassium acetate.
4. Wash solution: 80 m*M* potassium acetate, 8.3 m*M* Tris-HCl, pH 7.5, 40 μ*M* EDTA, and 55% ethanol (95%).
5. Sterile H_2O for elution of DNA.

2.2.3. RNA Transcription Kit

A number of companies sell kits for in vitro synthesis of RNA that are suitable for use in *Xenopus* oocytes, and in our experience, the mMessage mMachine™ High Yield Capped RNA Transcritpion Kit (Ambion) works very well. The kit components are as follows:

1. Enzyme mix (may be SP7, T7, or T3 RNA polymerase).
2. 10X Reation buffer (specific for each RNA polymerase).
3. 2X NTP/CAP mix.
4. Ammonium acetate stop mix.
5. Nuclease free water.
6. Gel loading buffer.

3. Methods

3.1. Overview of Site-Directed Mutagenesis Method Using the Quikchange Kit

This method uses a double-stranded DNA vector containing the insert to be mutated and two synthetic complementary oligonucleotides with the desired mutation. Some of the advantages of this method are that it does not require the use of specialized vectors, any subcloning steps, or single-strand rescue and can be completed in 3 d. After denaturation of the double-stranded DNA (**step 1**, **Fig. 1**), the oligonucleotides are allowed to anneal to the insert DNA (**step 2**, **Fig. 1**) and *PfuTurbo*™ DNA polymerase is used to synthesize the complementary strands generating the mutated plasmid with staggered nicks (**step 3**, **Fig. 1**). The parental (wild type) plasmid is digested with *Dpn*I endonuclease, which digests only methylated DNA, leaving the in vitro synthesized mutant plasmid intact (**step 4**, **Fig. 1**). The plasmid is then transformed into Epicurian Coli XL1 Blue supercompentant cells (**step 5**, **Fig. 1**). In our experience, this results in approx 80% of colonies containing plasmids with the desired mutation, which can be screened either by restriction digestion or by DNA sequencing.

3.2. Primer Design

1. Both of the mutagenic primers must contain the desired mutation and anneal to the same sequence on opposite strands. Primers should be 20–35 bases in length, and the melting temperature (T_m) of the primers should be ≥78°C. The following formula can be used to estimate the T_m:

$$T_m = 81.5 + 0.41(\%\ \mathrm{GC}) - 675/\mathrm{N} - \%\ \text{mismatch},$$

   where N is the primer length in bases.
2. The mutation should be in the middle of the primer with 10–15 correct bases on either side. Ideally, the GC content of the primer should be 50%, but 40–80% is an acceptable range. The primers should start and end with one or more G or C bases to promote annealing to ensure efficient elongation with the DNA polymerase.
3. Restriction enzymes can be used to confirm that a mutant has been generated. Ideally, a unique restriction site can be engineered into the mutation site and the presence of the restriction site is confirmation that the mutation has been successful. If a restriction site cannot be engineered into the mutation site, it can be engineered into the primer surrounding the mutation without changing the amino acid sequence. The assumption is that if the primer is incorporated into plasmid to generate the restriction site, then the desired mutation has also been generated. Sequencing should always be performed to confirm any mutation and the lack of any extraneous mutations that may arise in the polymerase chain reaction (PCR) steps (*see* **Note 3**).

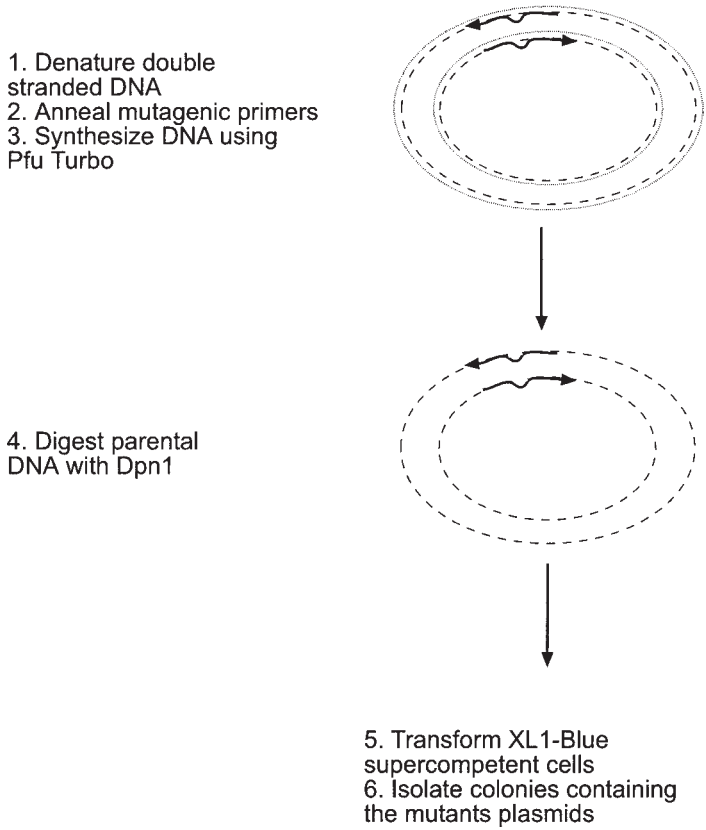

Fig. 1. Flow diagram for generating site-directed mutants using the Quikchange Site Directed Mutagenesis Kit.

4. Make a 100 m*M* stock of primers with autoclaved H_2O or Tris-HCl, pH 8.0. Use a 1 : 10 dilution of this stock in the PCR reaction. Make up a mixed sense and antisense stock.

3.3. Detailed Site-Directed Mutagenesis Method

The cDNA to be mutated can be subcloned into any plasmid and, ideally, one that may also be used for expression in the cell type that best suits the functional analysis of the transporter. In our case, we use pOTV (Oocyte Transcription Vector) because it is designed for efficient production of cRNA and generates high expression levels in Xenopus laevis oocytes.

To maximize temperature-cycling performance, thin-wall polymerase chain reaction (PCR) tubes (Perkin-Elmer) should be used. It is best to keep primer concentrations constant and in excess while varying the DNA template con-

Table 1
Cycling Parameters for PCR Reaction

No. of cycles	Temp (°C)	Time
1	95	30 s
14–18 (*see* **Note 4**)	95	30 s
	55 (*see* **Note 5**)	1 min
	68	2 min/kb of plasmid length
1	72	5 min

centration until the optimal DNA concentration (between 5 and 50 ng) for a particular plasmid is determined.

3.3.1. Setup of PCR Reaction

1. Thaw all of the following components on ice and prepare the sample reaction on ice:
   5 µL of 10X reaction buffer;
   X µL (5–50 ng) of dsDNA template;
   X µL (125 ng) of sense and antisense primer mix;
   1 µL of dNTP mix;
   Sterile H_2O to a final volume of 50 µL.
2. Immediately before starting the PCR cycle, add 1 µL of *PfuTurbo* DNA polymerase (2.5 U/µL).
3. If mineral oil is required in the PCR machine, then it should be overlayed on top of the reaction solution.

3.3.2. PCR Cycling

1. **Table 1** lists the suggested cycling parameters for the PCR reaction.
2. Make sure the reaction tube is cooled to at least 37°C before continuing.
3. Add 1 µL *Dpn*I restriction enzyme (10 U/µL) directly to each amplification reaction (*see* **Note 6**). Thoroughly mix the contents of the tube by gently pipetting up and down. Incubate the tubes at 37°C for 2 h to digest parental (nonmutated) DNA.

3.3.3. Transformation of Competent Cells

1. The Epicurian Coli XL1-Blue supercompetent cells should be stored at –80°C. Allow them to gently thaw on ice immediately before use. For each sample reaction, add 50 µL of competent cells to prechilled 15-mL Falcon® 2059 polypropylene tubes.
2. After *Dpn*I digestion of the plasmid DNA, place tubes on ice to cool for 2 min. Add 1 µL of the sample reaction to 50 µL of competent cells, swirl to mix, and leave on ice for 30 min.

3. Heat shock each tube for 45 s at 42°C by placing the tubes in a heated water bath (*see* **Note 7**), followed by 2 min on ice.
4. Add 500 mL of NZYM$^+$ broth and shake at 37°C for 1 h at 225–250 oscillations per min.
5. Plate the entire transformation reaction of each sample reaction on LB agar plates (*see* **Note 8**) containing the appropriate antibiotic for the plasmid vector used (in our case we use ampicillin at 100 μg/mL). Incubate the plates at 37°C for >16 h.
6. The number of colonies should roughly correspond to the amount of double-stranded DNA (dsDNA) that was used in the initial reaction. The efficiency should be about 80%, so it is best to pick six to eight colonies from each plate to ensure that a mutant is selected.
7. Scrape a single colony with a sterile tip and place into 5 mL of NZYM$^+$ broth (*see* **Note 9**) containing the appropriate antibiotic. Shake at 37°C at 225–250 oscillations per min for >16 h.

3.4. Purification of Plasmid DNA

A number of plasmid purification kits are available and individual researchers may have preferences of one over another. In our lab, we use the Wizard Plus Minipreps DNA purification system from Promega (Sydney, Australia). The first five steps are common to most commercially available kits, but the final step varies with the different kits.

1. Pellet 1.5 mL of bacterial culture by centrifugation at room temperature at 14,000*g*. Discard and carefully remove all of the supernatant (*see* **Note 10**).
2. Resuspend the pellet in 200 μL of cell resuspension solution by gently pipetting the solution up and down.
3. Add 200 μL of cell lysis solution directly into the resuspended cells and wait until the solution is clear (approx 20 s).
4. Add 200 μL of neutralization solution and invert six times.
5. Spin for 5 min at room temperature and 10,000*g* and collect supernatant (*see* **Note 11**).
6. Add 1 mL of purification resin to a 3-mL syringe barrel connected to a minicolumn for each sample.
7. Pour supernatant from **step 5** into the syringe barrel and turn on the vacuum pump.
8. After all of the liquid has been sucked through, add 1 mL of column wash solution. Wait for this to be sucked through and repeat.
9. Place each minicolumn in a 1.5-mL tube and centrifuge at 10,000*g* for 2 min to remove any excess liquid.
10. Place each minicolumn in a fresh 1.5-mL tube.
11. Elute with 50 μL of sterile H_2O, heated to 80°C (for better elution).
12. Run 5 μL of the plasmid sample on a 0.8% (w/v) agarose gel to check the yield and quality of the DNA. Two bands should be present, corresponding to the supercoiled and relaxed plasmid DNA.

3.5. Restriction Digest to Check for Mutation

To check if the purified DNA samples contain the mutation, digest each sample with the appropriate restriction enzyme (engineered into the DNA with the mutation). Also, digest the wild-type plasmid template DNA as a control.

1. Mix 5 μL of miniprep plasmid DNA with 1 μL of restriction enzyme, 2 μL of 10X restriction enzyme buffer (supplied with the restriction enzyme), and 12 μL of H_2O. Incubate at 37°C for 60 min.
2. Check the restriction digest by electrophoresis of 10 μL of the sample on a 0.8% (w/v) agarose gel made up in TAE buffer and containing 0.1 mg/mL ethidium bromide. Visualize DNA in the gel using an ultraviolet (UV) transilluminator
3. The DNA should also be sequenced for confirmation of the desired mutation and that no other mutations have been introduced.
4. Make a glycerol stock of the bacterial culture that contains the mutant plasmid. Mix 700 μL of bacteria and 300 μL of 50% glycerol and store at –70°C.

3.6. In Vitro Transcription of RNA for Expression *in* Xenopus laevis Oocytes

Although a number of kits are available for production of RNA for injection into *Xenopus laevis* oocytes, we have found that the mMessage mMachine kit from Ambion works very well.

3.6.1. pOTV Vector

Linearized plasmid DNA and PCR products that contain an RNA polymerase promoter site can be used as templates for in vitro transcription with the mMessage mMachine kit. We use pOTV *(7)*, which is derived from the pBluescript II SK +/– vector (Stratgene) and contains a number of useful features. First, it contains the *Xenopus laevis* β-globin 5' and 3' untranslated sequences flanking several unique restriction sites for insertion of the cDNA *(8)*. After the 3' untranslated β-globin sequence, there are a number of additional unique restriction sites to be used for linearization of the plasmid (*see* **Subheading 3.6.2.**). Immediately upstream of the 5' untranslated β-globin sequence is a T7 promotor used for RNA synthesis using the T7 RNA polymerase. Other plasmids containing an insert under the control of an RNA polymerase promoter can be used and will give varying levels of expression, depending on the nature of the 5' and 3' untranslated sequences.

3.6.2. Preparation of DNA for Transcription Reaction

1. Linearize the plasmid DNA by mixing 45 μL of the purified miniprep plasmid DNA with 2 μL of restriction endonuclease, 6 μL of 10X reaction buffer, and 7 μL double-distilled H_2O (ddH_2O). The restriction enzyme used should not cut

the 5' untranslated sequence, the cDNA, or the 3' untranslated sequence and ideally cut the plasmid once after the 3' untranslated sequence.
2. Incubate for 1.5–2 h in a 37°C water bath.
3. Purify the linear DNA using a phenol : chloroform extraction procedure. Make up each sample to 200 µL with sterile H_2O and add 200 µL of phenol : chloroform : isoamyl alcohol (25 : 2 : 1). Vortex for 20 s and centrifuge at room temperature at 10,000*g* for 5 min.
4. Transfer the upper aqueous phase to a new 1.6-mL Eppendorf tube. Add an equal volume of chloroform : isoamyl alcohol (24 : 1), vortex for 20 s and centrifuge as in **step 3** for 1 min.
5. Transfer the upper phase to a new tube. Add 1/10 the volume of 3 *M* sodium acetate and three times the total volume of 100% molecular-biology-grade ethanol (*see* **Note 12**). Precipitate the DNA by placing at –20°C for 20 min. Centrifuge at 4°C at 10,000*g* for 20 min.
6. Carefully remove the supernatant and wash the pellet with 200 µL of 70% ethanol (*see* **Note 12**). Centrifuge as in **step 5** min. Carefully remove all liquid with a pipet tip and air-dry the pellet.
7. Dissolve the pellet in 7 µL of DEPC-treated H_2O (use DEPC-treated H_2O from now on). Run 1 µL on a 0.8% agarose gel to confirm linearization and estimate yield.

3.6.3. In Vitro Transcription of RNA

Most eukaryotic mRNA molecules have a 5' 7-methyl guanosine residue or cap structure that functions in the protein synthesis initiation process and protects the mRNA from degradation by intracellular nucleases. This can be achieved in vitro by substituting the cap analog ([m^7G(5')ppp(5')G]) for a portion of the GTP in the reaction. Any in vitro transcripts that are to be microinjected into oocytes, used for transfection experiments or for in vitro splicing reactions, should be capped.

The following protocol is adapted from the mMessage mMachine kit™ instruction manual (Ambion). Linearized DNA concentration should be approx 0.5 µg/µL in DEPC-treated H_2O.

1. Prepare the transcription reaction on ice as follows:

   6 µL Linearized DNA;
   10 µL 2X dNTP mix;
   2 µL 10X Reaction buffer;
   2 µL 10X Enzyme mix (add last).

   The final volume of the reaction is 20 µL (*see* **Note 13).**
2. Incubate the reaction at 37°C for 1.5–2 h in a 37°C oven (do not use a water bath, as condensation may develop and reduce the yield).
3. Purify RNA using the phenol : chloroform extraction procedure as described in **Subheading 3.6.2.**, **steps 3–6**. We find that the RNA is most efficiently precipitated with 1/3 volume ammonium acetate (stop solution provided with the kit).

3.7. Determination of Functional Properties

In all of the experiments investigating the effects of particular mutations of a transporter, it is desirable to compare the results to those obtained with the wild-type transporter measured under the same experimental conditions. In our laboratory, we routinely use the *Xenopus laevis* oocyte expression system to study the functional properties of transporters. This expression system is particularly useful for studying transporters, because oocytes are sufficiently large cells to conduct both electrophysiology and radiolabeled flux measurements on single cells. This is particularly useful when studying the relationships between electrical properties of the transporters and their ability to translocate solutes across the membrane, which allows a detailed exploration of the functional states of transporter proteins. Further details concerning the functional analysis of transporters can be found in Chapters 9–11 and 13.

4. Notes

1. The methods described in this chapter are largely based on commercially available kits, and although we generally follow the manufacturer's instructions we have also introduced a number of modifications that in our experience provide more reliable results.
2. To prepare RNase-free water, add 0.1% (v/v) DEPC to sterile water and incubate for several hours or overnight at 37°C and then autoclave for 45 min. The scent of the DEPC should not be detectable.
3. Extraneous mutations can occur in the PCR reaction because of the innate error rate of the DNA polymerase used. *Pfu Turbo*™ has a very low error rate and, as such, is very suitable for site-directed mutagenesis. The commonly used Taq polymerase has a significantly higher error rate and should be avoided in this type of experiment.
4. Fourteen cycles should be used for point mutations, 16 cycles for single amino acid changes, and 18 cycles for multiple amino acid deletions or insertions.
5. Reduce annealing temp in the PCR cycle if no colonies are obtained.
6. One can use 1.5 μL of *Dpn*I, as it is provided in the kit in excess, which may help to reduce the number of wild-type plasmids obtained.
7. The heat pulse has been designed for Falcon 2059 tubes and the use of other tubes may give different results.
8. Make sure that the plates are dry before you plate and before you put them in the incubator, which may take 30–60 min. However, if the plates are preheated to 37°C, they dry quicker.
9. LB broth can also be used, but we find that you get better yields with NZYM$^+$.
10. **Optional**: This step can be repeated to collect more bacteria and increase yield.
11. This step may be repeated to ensure that no insoluble material is added to the filtration step.
12. The 100% ethanol and 70% ethanol solutions should be stored at –20°C.

13. The linear DNA concentration can be reduced and the volume of water added adjusted accordingly to obtain a final volume of 20 μL.

References

1. Kaback, H. R., Sahin-Toth, M., and Weinglass, A. B. (2001) The kamikaze approach to membrane transport. *Nature Rev./Mol. Cell. Biol.* **2,** 610–620.
2. Buck, K. and Amara, S. G. (1994) Chimeric dopamine–norepinephrine transporters delineate structural domains influencing selectivity for catecholamines and 1-methyl-4-phenylpyridinium. *Proc. Natl. Acad. Sci. USA* **91,** 12,584–12,588.
3. Mitrovic, A. D., Amara, S. G., Johnston, G. A. R., et al. (1998) Identification of functional domains of glutamate transporters *J. Biol. Chem.* **273,** 14,698–14,706.
4. Seal, R. P. and Amara, S. G. (1998) A reentrant loop domain in the glutamate carrier EAAT1 participates in substrate binding and translocation. *Neuron* **21,** 1487–1498.
5. Grunewald, M., Bendahan, A., and Kanner, B. I. (1998) Biotinylation of single cysteine mutants of the glutamate transporter GLT-1 from rat brain reveals its unusual topology. *Neuron* **21,** 623–632.
6. Monks, S. A., Needleman, D. J., and Miller, C. (1999) Helical structure and packing orientation of the S2 segment in the Skaker K+ channel. *J. Gen. Physiol.* **113,** 415–423.
7. Arriza, J. L., Fairman, W. A., Wadiche, J. I., et al. (1994) Functional comparisons of three glutamate transporter subtypes cloned from human motor cortex. *J. Neurosci.* **14,** 5559–5569.
8. Kreig, P. A. and Melton, D. A. (1984) Functional messenger RNAs are produced by SP6 in vitro transcription of cloned cDNAs. *Nucleic Acids Res.* **12,** 7057–7070.

8

Fluorescence Techniques for Studying Membrane Transport Proteins

The P-Glycoprotein Multidrug Transporter

Frances J. Sharom, Paula L. Russell, Qin Qu, and Peihua Lu

1. Introduction

1.1. Fluorescence Spectroscopy

Fluorescence spectroscopic techniques have been widely applied to the study of soluble proteins over the past 20 yr, and they are being increasingly applied to membrane proteins, including membrane transporters. Some advantages of fluorescence approaches include high sensitivity (so that relatively small amounts of protein are required), commonly available and affordable instrumentation, and the ability to explore several different (but complementary) aspects of membrane protein structure and function. For comprehensive coverage of the principles and practice of modern fluorescence approaches for studying proteins, the reader is referred to the excellent book authored by Lakowicz ***(1)***.

1.2. The ABC Superfamily and the P-Glycoprotein Multidrug Transporter

The ABC (ATP-binding cassette) superfamily of proteins is one of the largest and most important group of proteins found in both prokaryotes and eukaryotes, as indicated by the number of sequences found in the growing genome databases. Its members are identified based on the presence of one or two nucleotide-binding (NB) folds with a characteristic ABC signature sequence (or C motif), in addition to the Walker A and Walker B motifs commonly found in other ATP- or GTP-hydrolyzing proteins ***(2)***. Most ABC

From: *Methods in Molecular Biology, vol. 227: Membrane Transporters: Methods and Protocols*
Edited by: Q. Yan © Humana Press Inc., Totowa, NJ

proteins are membrane transporters, and as a group, they are responsible for moving an astonishing array of compounds across membranes; their substrates range from chloride ions, drugs, amino acids, and small peptides, to large proteins ***(3)***. Bacterial ABC proteins include both exporters and importers, whereas mammalian ABC proteins are largely exporters.

The most intensively studied ABC protein is the P-glycoprotein multidrug transporter (Pgp), which carries out the ATP-driven export of hundreds of hydrophobic compounds, including chemotherapeutic drugs, natural products, and peptides (for reviews of Pgp biochemistry and physiology, *see* **refs. *4*** and ***5***). Pgp has been implicated as a major cause of resistance to multiple chemotherapeutic drugs in many human tumors. It is expressed at the apical surface of epithelial cells in the gut and in the endothelial cells of the brain, where it plays an important physiological role in preventing drug absorption from the gut and restricting entry of drugs into the brain. Compounds known as modulators or reversers can inhibit the transport function of Pgp ***(6)***. Modulators such as verapamil and cyclosporin A appear to interact directly with the transporter and likely behave as alternative substrates, engaging Pgp in a futile cycle of transport and ATP hydrolysis.

The 170-kDa Pgp protein is proposed to consist of two symmetrical halves, each made up of six membrane-spanning α-helical segments and a cytosolic NB domain (*see* **Fig. 1A**). The fact that most of its substrates are hydrophobic has presented major challenges in studying the biochemical mechanism of drug transport via Pgp. Drugs are believed to first partition into the membrane bilayer and then interact with the transporter, which subsequently effluxes them into the extracellular environment, the so-called "vacuum cleaner" model ***(7)***. Active transport of drugs is driven by ATP hydrolysis, and the ATPase properties of the purified protein have been well characterized ***(8,9)***. The K_m for ATP hydrolysis is relatively high (0.2–0.8 m*M*), indicating that the transporter has a low affinity for nucleotides compared to other ATP-driven transporters. Pgp has been functionally reconstituted into proteoliposomes, where it retains its ability to transport a variety of substrates, including colchicine ***(10)***, vinblastine ***(10)***, a linear tripeptide ***(11)***, and a rhodamine dye ***(12)***.

The lipophilic nature of its substrates has made it difficult to study drug binding to membrane-bound Pgp by classical biochemical methods. The application of fluorescence spectroscopic approaches has proved valuable in both showing that drugs interact directly with the transporter and quantitatively estimating the affinity of such an interaction ***(13–15)***. Pgp also binds its nucleotide substrates with relatively low affinity, which has made it difficult to directly measure nucleotide binding to the purified protein. Fluorescence techniques have again proved very useful in quantitating the interaction of ATP and its derivatives with Pgp ***(13–15)***.

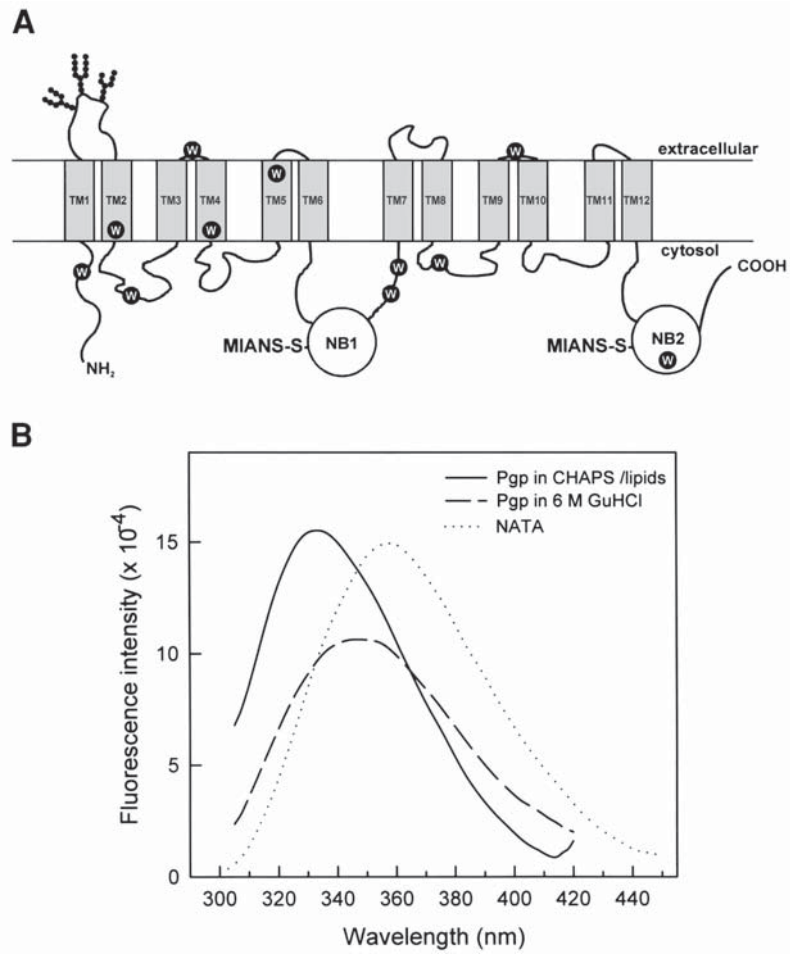

Fig. 1. **(A)** Proposed topology of the hamster MDR1 Pgp, location of Trp residues, and sites of MIANS labeling. The N-terminal half of the transporter contains eight Trp residues; Trp44 in the N-terminal tail, Trp133, Trp229 and Trp312 in TM2, TM4, and TM5, respectively, Trp159 in the first cytoplasmic loop, Trp209 in the second extracellular loop, and Trp695 and Trp705 in the linker region immediately following the first nucleotide-binding domain. The C-half of Pgp contains three Trp residues: Trp800 in cytoplasmic loop 3, Trp852 in extracellular loop 5, and Trp1105 between the Walker A and B motifs of the second nucleotide-binding domain. MIANS covalently labels the Cys residue within the Walker A motif of each NB domain. **(B)** Corrected fluorescence emission spectra for purified Pgp (100 µg/mL) in buffer A containing 2 m*M* CHAPS and 0.5 mg/mL PMPC (—), and following denaturation/unfolding with 6 *M* guanidine hydrochloride (GuHCl; ---), compared with 30 µg/mL of the soluble Trp analogue NATA (···). Fluorescence emission was recorded at 22°C following excitation at 290 nm.

1.3. Intrinsic Tryptophan Fluorescence of Transport Proteins

Most membrane transporters contain several Trp residues, and these can be very useful spectroscopic probes. Trp residues are typically selectively excited at 290–295 nm, to avoid interference from Tyr fluorescence. The wavelength observed for Trp fluorescence emission (λ_{em}) can be quite variable, depending on the polarity of the environment in which they are located. Low values for λ_{em} (e.g., 335 nm) indicate a blue shift, typically seen for Trp residues in a hydrophobic environment, such as within a membrane-spanning segment ***(16,17)***. Higher values of λ_{em} around 355 nm indicate an aqueous environment, as seen for the water-soluble Trp analog *N*-acetyltryptophan amide (NATA). The existence of many Trp residues in different regions of the protein is not a barrier to their usefulness as probes. It is often observed that only a few residues are actually responsible for the fluorescence emission. For example, in the case of Pgp, which has 11 Trp residues, the λ_{em} of the intrinsic Trp fluorescence is 333 nm (*see* **Fig. 1B**), indicating that the emitting Trp residues are likely those located within the membrane-spanning regions, whereas the remaining residues are probably internally quenched by nearby functional groups ***(16)***.

1.4. Labeling of Transport Proteins with Extrinsic Fluorophores

An alternative approach to the application of fluorescence spectroscopy to membrane transporters is to covalently link an extrinsic fluorophore to a known site on the protein, usually a Cys residue. Such fluorophores often have the advantage of emission in the visible region, where there is little interference from protein components. In addition, Cys residues at a defined location can often be engineered into expressed Cys-less transport protein constructs [*see*, e.g., lactose permease ***(18)***]. In the case of Pgp, only two of the seven Cys residues are reactive with sulfhydryl reagents. These two residues, Cys428 and Cys1071 (hamster MDR1), are located within the Walker A motifs of the NB domains, close to the site of ATP binding, and can be labeled with MIANS (2-[4'-maleimidylanilino]-naphthalene-6 sulfonic acid) ***(19)*** (*see* **Fig. 1A**).

1.5. Fluorescence Quenching

Trp residues in proteins are highly sensitive to the local environment, so that binding of substrates and inhibitors often leads to a decrease in the fluorescence intensity, known as quenching. Titration of the protein with the compound in question usually produces concentration-dependent saturable quenching (*see* **Fig. 2**). The quenching data can be fitted to an equation describing binding to a single site (*see* **Fig. 2**) or multiple sites with differing affinities ***(16)***. The existence of a single binding site is likely to be the case for many membrane transporters. However, multidrug transporters such as Pgp

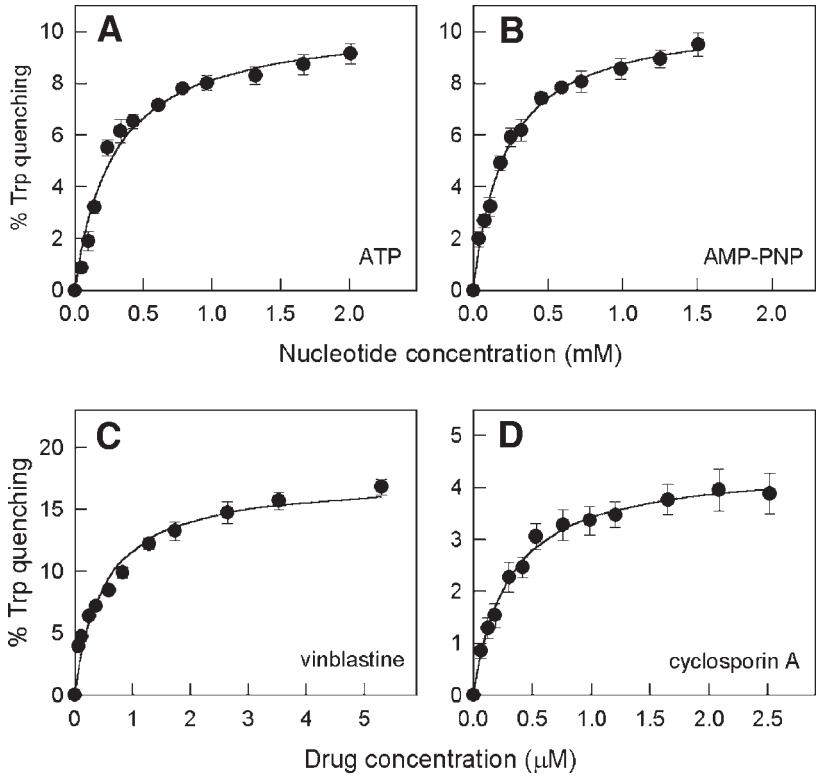

Fig. 2. Determination of substrate-binding affinity by quenching of intrinsic Trp fluorescence. Purified Pgp in buffer A with 2 m*M* CHAPS and 0.5 mg/mL PMPC is titrated at 22°C with increasing concentrations of the nucleotides ATP **(A)** and AMP–PNP **(B)** and the drugs vinblastine **(C)** and cyclosporin A **(D)**. Fluorescence emission is recorded at 330 nm following Trp excitation at 290 nm.

appear to have a flexible binding region that can accommodate many different compounds, rather than a single well-defined binding site, and two substrate molecules can bind simultaneously. Fitting of the quenching data can be carried out using standard graphics/fitting programs such as SigmaPlot (SPSS Inc, Chicago, IL), which allows an estimate for the value of the dissociation constant, K_d for binding, of the substrate to the transporter ***(14)***, which can range from n*M* to m*M* (*see* **Table 1**). The other ΔF_{max} parameter that is obtained from the fitting is the maximum fluorescence quenching at saturating levels of substrate, (*see* **Table 1**), which can be useful in determining the mechanism of Trp quenching by substrate. In the case of Pgp, the value of ΔF_{max} for Trp quenching by a substrate was highly correlated with the spectral overlap inte-

Table 1
Parameters for Binding of Nucleotides and Drugs to Pgp Determined by Quenching of Pgp Intrinsic Trp Fluorescence

Substrate	K_d (μM)	ΔF_{max} (%)
Nucleotides		
ATP	280	10.4
ADP	330	9.46
AMP–PNP	210	10.6
TNP–ATP	50.6	79.6
Nonpeptide drugs		
Colchicine	74.9	102
Quinine	12.5	33.5
Quinidine	7.76	18.5
Vinblastine	0.50	17.5
Peptides and peptide-based drugs		
Pepstatin A	9.53	4.46
Valinomycin	0.72	4.14
Cyclosporin A	0.30	4.44
Reversin 201	0.081	4.02

Note: Values for the dissociation constant for binding, K_d, and the maximum quenching, ΔF_{max}, were estimated by fitting of corrected Trp quenching data (*see* **Fig. 2**) to an equation for a single binding site.

gral, *J*, indicating that quenching of the Trp residues likely took place by energy transfer from Trp to the substrate ***(16)***.

The fluorescence emission of covalently linked extrinsic fluorophores, if located close to the substrate binding site, or in a region of the protein that undergoes a conformational change on substrate-binding, is often either quenched or enhanced on substrate binding in a concentration-dependent saturable fashion (*see* **Fig. 3**). Fitting of the quenching data to a binding curve (as described for Trp fluorescence) can give the K_d for substrate binding (*see* **Table 2**). In the case of Pgp, the binding affinity has been estimated for nucleotides, drugs, peptides, and modulators ***(13–15)***.

The use of collisional quenchers, small soluble molecules that reduce fluorescence emission by colliding with a fluorophore and dissipating the energy of the excited state, can also give very useful information on the accessibility of the fluorophore to the surrounding medium. Changes in accessibility can be

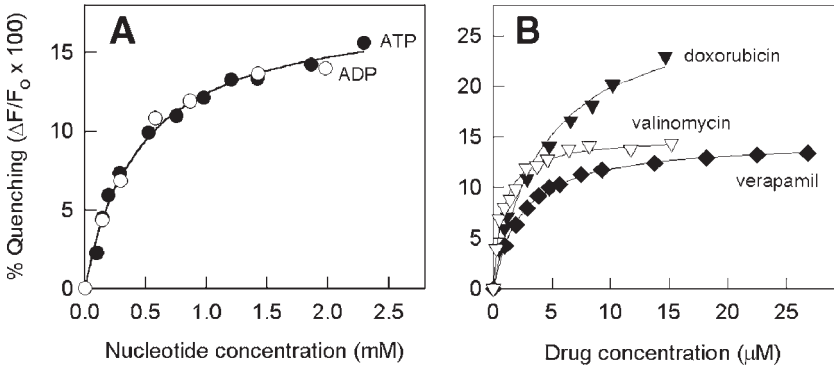

Fig. 3. Determination of substrate-binding affinity by quenching of MIANS–Pgp fluorescence. Purified MIANS–Pgp in buffer A with 2 m*M* CHAPS and 0.5 mg/mL asolectin is titrated at 22°C with increasing concentrations of the nucleotides ATP (●) and ADP (○) **(A)** and the drugs doxorubicin (▼), valinomycin (∇) and verapamil (◆) **(B)**. Fluorescence emission is recorded at 420 nm following MIANS excitation at 322 nm.

Table 2
Parameters for Binding of Nucleotides and Drugs to Pgp Determined by Quenching of MIANS–Pgp Fluorescence

Substrate	K_d (μ*M*)	ΔF_{max} (%)
Nucleotides		
ATP	460	18.1
ADP	410	17.4
AMP–PNP	360	22.2
Nonpeptide drugs		
Nifedipine	48.2	60.1
Rhodamine 123	12.8	92.6
Ritonavir	0.78	9.8
Paclitaxel	0.038	8.1
Peptides and peptide-based drugs		
ALLN	138	7.0
Leupeptin	77.6	12.8
Beauvericin	0.36	8.0
Reversin 205	0.14	8.1

Note: Values for the dissociation constant for binding, K_d, and the maximum quenching, ΔF_{max}, were estimated by fitting of corrected MIANS quenching data (*see* **Fig. 3**) to an equation for a single binding site.

used as an indicator of conformational changes that take place following binding of substrates and inhibitors to the protein. Two collisional quenchers that are commonly used to study proteins are acrylamide and iodide ion. Acrylamide is an excellent neutral quencher, with a small but finite tendency to penetrate into the interior of proteins and lipid bilayers, so that it may quench internal fluorophores to some extent. I^-, on the other hand, cannot penetrate the nonpolar interior of proteins or membranes and can only quench fluorophores on the transporter surface. In addition, I^- is repelled from negatively charged regions of the protein and will quench them very poorly.

A transport protein (in either a membrane or detergent micelles) is titrated with increasing concentrations of quencher, and the loss of fluorescence emission from intrinsic Trp residues (or a covalently linked extrinsic fluorophore) is measured. Quenching data are then analyzed using the Stern–Volmer equation, $F_0/F = 1 + K_{SV}[Q]$, where F_0 and F are the fluorescence intensities in the absence and presence of quencher, respectively, $[Q]$ is the quencher concentration, and K_{SV} is the Stern–Volmer quenching constant. Plotting of the quenching data as a Stern–Volmer plot (F_0/F vs. [quencher]) (*see* **Fig. 4**) allows the estimation of K_{SV} (the slope) (*see* **Table 3**), which is an indicator of the accessibility of the fluorophore to quencher, which, in turn, depends on protein conformation and folding. Changes in K_{SV} can result from changes in protein conformation as a result of substrate binding and so forth. For example, a 10% decrease in K_{SV} is noted following the addition of ATP to MIANS–Pgp (*see* **Table 3**), indicating that nucleotide binding makes the MIANS bound within the catalytic site less accessible to the external aqueous solution. When the NB domain is occupied by ATP, I^- is much less effective as a quencher (lower K_{SV} value; *see* **Table 3**), probably because it shields the positive charge of the Lys residue in the Walker A motif. Linear Stern–Volmer plots are also a good indication that all of the fluorophores within the protein are behaving similarly and have a comparable environment. Curved Stern–Volmer plots suggest that there are two or more classes of fluorophore, with different accessibility.

1.6. Fluorescence Assays for Transport Activity

Fluorescence approaches can also be valuable alternatives to traditional assays for membrane transport. In the case of Pgp, fixed-time-point rapid filtration assays have been used to measure the uptake of radioactive drug substrates (such as [^{3}H]-colchicine, [^{3}H]-vinblastine, or [^{125}I]-peptide) into either inside-out plasma membrane vesicles from multidrug-resistant mammalian cells overexpressing Pgp, or proteoliposomes containing reconstituted transport protein (*see*, e.g., **refs. *10***, ***11***, and ***20***). This methodology does not have the time resolution to measure the initial rate of transport, which is quite

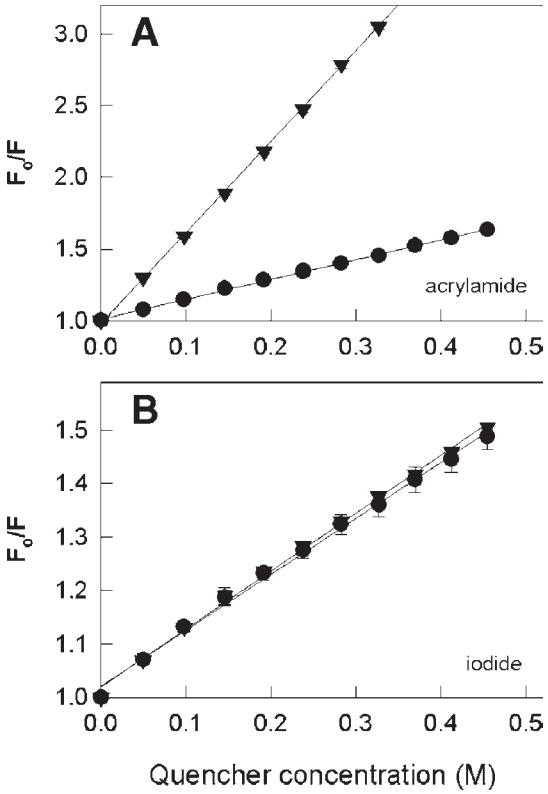

Fig. 4. Stern–Volmer plots for quenching at 22°C of MIANS–Pgp (●) and MIANS-DTE (▼) by **(A)** acrylamide and **(B)** iodide. The value of the Stern–Volmer constant, K_{SV}, is determined from the slope of the plot. DTE = dithioerythritol.

Table 3
Stern–Volmer Constants for Collisional Quenching of MIANS–Pgp and MIANS–DTE Fluorescence

	K_{SV} (M^{-1})	
	Acrylamide	I^-
MIANS–Pgp	1.42	1.11
MIANS–Pgp + 2 m*M* ATP	1.29	0.75
MIANS–DTE	6.29	1.14

Note: For both MIANS–Pgp and MIANS–DTE, K_{SV} values are determined from the slopes of Stern–Volmer plots of the type shown in **Fig. 5**. DTE = dithioerythritol.

fast (transport becomes nonlinear after <1 min), is time-consuming, and uses relatively large amounts of transport protein and radiolabeled substrate. Fluorescence-based assays allow continuous monitoring of the transport process in real time. Because the initial rate of transport can be measured using a single sample of membrane vesicles or proteoliposomes, much smaller amounts of transport protein are needed.

Several fluorescent compounds are transport substrates for Pgp, including various rhodamine dyes, acetoxymethyl esters of Ca^{2+}- and pH-sensitive dyes (calcein-AM, Fura-2-AM), and the dyes Hoechst 33342 and LDS-751. Rhodamine dyes have the interesting property of losing their fluorescence following active transport into the interior of a vesicle or proteoliposome, perhaps as a result of self-quenching at higher concentrations, so that the resultant rate of loss of fluorescence intensity is a direct measure of the rate of transport of the dye into the vesicle lumen. This approach has been used to measure the initial rate of transport of rhodamine G by the yeast multidrug transporter Pdr5p ***(21)*** and the transport of TMR (tetramethylrosamine) by Pgp ***(12)***. The characteristics of transport by many multidrug transport proteins differ from that of transporters with highly water-soluble substrates, because their hydrophobic substrates have a relatively high rate of passive diffusion across membranes and lipid bilayers. Consequently, net uptake of drug into the vesicle lumen increases rapidly after the addition of ATP to the system, generating a substrate concentration gradient across the membrane, then levels off and reaches a plateau. At this point, a steady state is reached ***(12)***, at which inward transport of drug into the vesicle lumen by Pgp, up a gradient, is balanced by outward passive diffusion through the bilayer, down a gradient (*see* **Fig. 5A**). The substrate concentration gradient can be collapsed by the addition of an ATPase inhibitor, such as vanadate, leading to release of substrate into the external solution (*see* **Fig. 5B**) and recovery of the fluorescence intensity back to its former levels.

2. Materials and Instrumentation

2.1. Preparation of Purified Pgp

1. Plasma membrane vesicles prepared from the multidrug-resistant Chinese hamster ovary cell line CH^RB30, which overexpresses Pgp ***(22)***. These vesicles may be stored frozen at –70°C for up to 3 mo.
2. Buffer A: 50 m*M* Tris-HCl, 0.15 *M* NaCl, 5 m*M* MgCl2, 1 m*M* DTE (dithioerythritol; omit if using Cys-reactive fluorophores such as MIANS to label the protein; *see* **Note 1**), pH 7.5.
3. Buffer A containing 25 m*M* 3-[(3-cholamidopropyl) dimethylammonio]-1-propanesulfonate (CHAPS), 15 m*M* CHAPS, and 2 m*M* CHAPS (omit DTE if using Cys-reactive fluorophores such as MIANS to label the protein).
4. Concanavalin A–Sepharose 4B column with a 7-mL bed volume (Pharmacia).

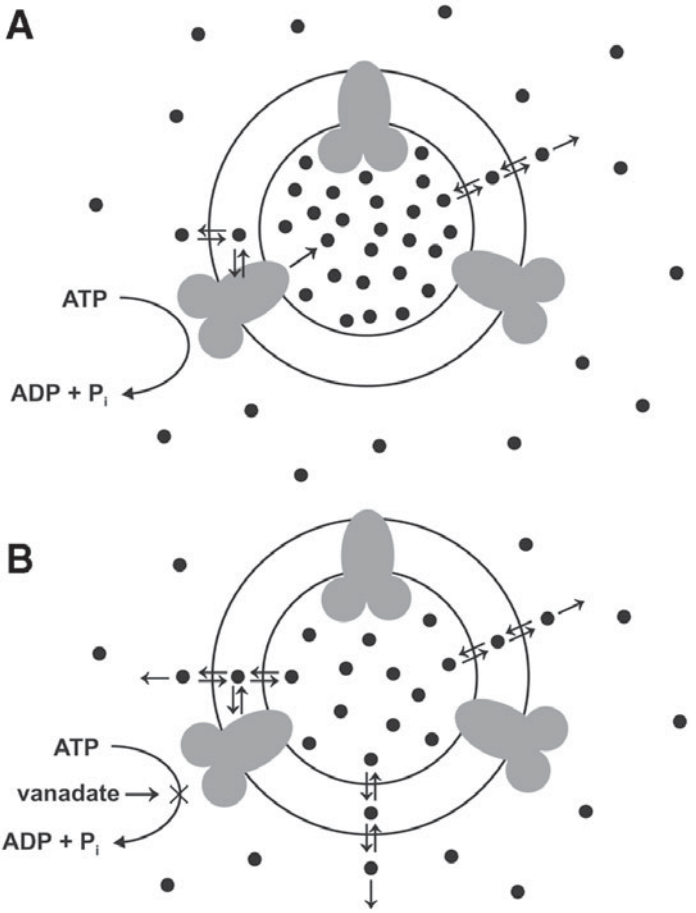

Fig. 5. **(A)** Generation of a substrate concentration gradient by Pgp. Transporters facing inward with their NB domains accessible at the exterior surface of the proteoliposome use the energy of ATP to pump tetramethylrhodamine (TMR) into the vesicle lumen, where it loses its fluorescence, resulting in a time-dependent decrease in the fluorescence intensity (*see* **Fig. 6A**). Uphill pumping of TMR by Pgp generates a TMR concentration gradient. When the steady state is reached, the fluorescence intensity levels off (*see* **Fig. 6A**). At this point, inward transport of TMR by Pgp is balanced by outward passive diffusion down the concentration gradient. Transporters that face outward with their NB domains in the vesicle lumen have no access to ATP and do not contribute to substrate transport or ATP hydrolysis. **(B)** Collapse of the substrate concentration gradient by an inhibitor. Inward pumping of TMR by Pgp is blocked by the inhibitor vanadate (which abolishes Pgp ATPase activity). The concentration gradient built up in **(A)** then collapses by passive diffusion of TMR through the bilayer, resulting in recovery of the fluorescence intensity (*see* **Fig. 6A**).

2.2. Preparation of Proteoliposomes Containing Reconstituted Pgp

1. Partially purified Pgp (S_2 fraction) in buffer A containing 15 m*M* CHAPS.
2. Stock solutions of the desired phospholipids in $CHCl_3$–MeOH 4 : 1 (v/v). Suitable lipids include dimyristoylphosphatidylcholine (DMPC), palmitoylmyristoylphosphatidylcholine (PMPC), egg PC, etc.
3. Sephadex G-50 column (1 × 15 cm), equilibrated in buffer A.

2.3. Preparation of Nucleotides, Drug Substrates and Quenching Agents

1. The presence of phospholipid has been found to greatly improve the extent and reproducibility of quenching by drug substrates and nucleotides. Phospholipids that can be used include asolectin (soybean phospholipids), DMPC, and PMPC. All should be of the highest purity (e.g., Avanti Polar Lipids, Alabaster AL). Lipids are dispensed from a $CHCl_3$–MeOH (4 : 1 v/v) stock solution, dried down as described in **Subheading 3.6.**, **step 1**, and resuspended in buffer A with 2 m*M* CHAPS at 5 mg/mL by vortexing. A solution of unilamellar phospholipid vesicles is then prepared by extrusion through a 100-nm polycarbonate filter using an extrusion device ***(19)*** and used while fresh.
2. Nucleotides for titration with transport protein, such as ATP, AMP–PNP, and ADP, are dissolved in buffer A containing 2 m*M* CHAPS and 0.5 mg/mL phospholipid vesicles (*see* **Subheading 2.3.**, **step 1**) typically at a concentration at least 100-fold higher than the highest concentration required in the titration. For example, if ATP is to be titrated up to a final concentration of 1 m*M*, the stock solution should be made at a concentration of 100 m*M*. Stock solutions may be stored frozen at –20°C for 3–6 mo.
3. Drug substrates for Pgp are usually of limited water solubility, so stock solutions in dimethyl sulfoxide (DMSO) are typically made at a concentration at least 500-fold higher than the highest concentration required in the titration. Just prior to the titration, the stock solution is diluted into buffer A containing 2 m*M* CHAPS and 0.5 mg/mL phospholipid to a concentration 100-fold higher than the highest concentration required in the titration (*see* **Note 2**). (The final concentration of DMSO in the sample solution at the end of the titration should be <1% [v/v].) Stock solutions can be stored frozen at –20°C for approx 12 mo, depending on the stability of the individual drug (follow the supplier's advice).
4. Acrylamide is made up fresh for each experiment, typically as a stock solution of 5 *M* in the required buffer (typically buffer A containing 2 m*M* CHAPS).
5. KI is made up fresh for each experiment, typically as a stock solution of 5 *M* in buffer A with 2 m*M* CHAPS, and 0.1 m*M* $Na_2S_2O_3$ is added to prevent I_3^- formation. A solution of 5 *M* KCl is usually used in a parallel control titration to correct for any ionic strength effects (*see* **Note 3**).

2.4. Real-Time Fluorescence Assay for Monitoring Transport

1. Solution of proteoliposomes containing reconstituted Pgp (*see* **Subheading 2.2.**) in buffer A.

2. Solutions of TMR in buffer A, concentration range-0.1–25 μ*M*.
3. Solutions of ATP (concentration range-0.1–10 m*M*), together with an ATP regenerating system (30 μg/mL creatine kinase, 3.5 m*M* creatine phosphate) in buffer A.

2.5. Fluorescence Instrumentation

An analytical fluorimeter is the best instrument to use when carrying out the types of experiment detailed in this chapter. Inexpensive fluorescent plate readers that use 96-well plates and other formats generally do not have the sensitivity, reproducibility, or time resolution required for collection of data to be used for estimation of K_d values or initial rates of transport. Accurate control of the temperature of the sample compartment (±0.5°C) using a water bath is highly recommended. The use of a quartz microcuvet (0.5 cm path length, 1 mL total volume, 500 μL sample volume) is recommended to reduce the size of the sample and the amount of transport protein required to carry out the experiments. Our laboratory uses a PTI Alphascan-2 spectrofluorimeter (Photon Technology International, South Brunswick, NJ) and an upgraded Spex Fluorolog II spectrofluorimeter (Spectra Research Corporation).

2.6. Corrections to Fluorescence Intensity Data

In general, fluorescence data must be corrected for the inner filter effect that arises when molecules are present in solution that absorb the exciting radiation and the emitted fluorescence radiation. If there are significant numbers of scattering particles in the solution (such as proteoliposomes or detergent micelles), scattering must also be corrected for by subtracting a background fluorescence reading taken on a sample that is identical, but with no fluorescent probe present. In cases in which a titration is carried out during the experiment, the sample becomes progressively diluted, and this must also be taken into account. The most useful equation for simultaneous correction of fluorescence intensities for all these effects is

$$F_{i\mathrm{cor}} = (F_i - B)\left(\frac{V_i}{V_0}\right) \times 10^{0.5b\,(A\,\lambda ex + A\,\lambda ex)} \tag{1}$$

where $F_{i\,\mathrm{cor}}$ is the corrected value of the fluorescence intensity at a given point in the titration, F_i is the experimentally measured fluorescence intensity, B is the background fluorescence intensity (caused mainly by lipid vesicle scattering), V_0 is the initial volume of the sample, V_i is the volume of the sample at a given point in the titration (V_i/V_0 is the dilution factor), b is the path length of the optical cell in cm, and $A_{\lambda ex}$ and $A_{\lambda em}$ are the absorbances of the sample at the excitation and emission wavelengths, respectively. For more details of all of these corrections, the reader is referred to **refs. *1*** and ***23***.

3. Methods

3.1. Purification of Pgp

The P-glycoprotein multidrug transporter may be conveniently purified from CH^RB30 cells using a differential solubilization approach. Plasma membrane vesicles from CH^RB30 cells (Pgp makes up approx 15% of the membrane protein) are first treated with 25 m*M* CHAPS at a relatively high protein concentration (low detergent : protein ratio of approx 1.5 : 1 [w/w]), followed by pelleting of the insoluble material. This procedure extracts many membrane proteins, but leaves the Pgp primarily in the pellet. The pellet is then re-extracted with 15 m*M* CHAPS at a relatively low protein concentration (high detergent : protein ratio of 10–15 : 1 [w/w]), followed by pelleting of the insoluble material. The bulk of the Pgp is now found in the soluble supernatant in 15 m*M* CHAPS solution. Pgp is then further purified by lectin-affinity chromatography to remove contaminant glycoproteins. The resulting protein preparation can be used directly for many fluorescence experiments.

1. Thaw 30 mg of plasma membrane vesicle protein and sediment at 164,000*g* for 30 min at 4°C (70.1 Ti rotor, ultracentrifuge). Resuspend the membrane pellet in 3 mL of buffer A and 25 m*M* CHAPS at a final protein concentration of 10 mg/mL and incubate on ice for 15 min. Collect the insoluble pellet by centrifugation at 164,000*g* for 15 min at 4°C, resuspend in 5–7 mL of buffer A and 15 m*M* CHAPS (final protein concentration: approx 1 mg/mL) by passing repeatedly through a 26-gage needle and incubate on ice for at least 1 h, with periodic passes through the needle. Pellet the sample at 15,000*g* for 15 min (microcentrifuge). The resulting supernatant (designated the S_2 fraction) contains partially purified Pgp.
2. The S_2 fraction is further purified by affinity chromatography on a 7-mL Concanavalin A–Sepharose 4B column equilibrated in buffer A and 2 m*M* CHAPS. Typically, 2.5 mL of the S_2 fraction (2.5–3.0 mg of protein) is loaded onto the column at 4°C at a flow rate of 0.2 mL/min. When the column is washed with the same buffer, the Pgp peak elutes in the run-through fractions and can be detected by absorbance at 280 nm, followed by measurement of its ATPase activity using a colorimetric assay for released P_i, and by Western blotting, if required ***(8)***. Typically, 12 fractions of 0.5 mL volume are collected, and fractions 5–8 are pooled. The final product consists of 90–95% pure Pgp, at a concentration of approx 0.2 mg/mL, in 2 m*M* CHAPS buffer. The Pgp preparation should be kept on ice and used within 24 h. The column is regenerated by washing with ethanol (*see* **Note 4**).

3.2. Nucleotide and Drug-Binding Affinity Determined by Quenching of Intrinsic Trp Fluorescence

1. Quenching experiments are performed by successively adding 5-µL aliquots of nucleotide or drug solution to 500 µL of purified Pgp solution (100 µg/mL) in buffer A containing 2 m*M* CHAPS and 0.5 mg/mL phospholipid (*see* **Note 5**) in

a quartz microcuvet (0.5 cm path length, 1 mL volume) equilibrated at the required temperature (typically 22°C).

2. After each addition, the Pgp sample is excited at 290 nm and the steady-state fluorescence emission is measured at 330 nm (the emission maximum for Pgp Trp residues; *see* **Fig. 1B**).
3. Correct the fluorescence intensities for dilution, scattering, and the inner filter effect. Perform control titrations with 30 μ*M* NATA to assess the nonspecific quenching of Trp fluorescence by nucleotides and drugs. Carry out a control titration with DMSO alone, to confirm that there are no solvent-related effects. Computer-fit the experimental data for nucleotides (*see* **Fig. 2A**,**B**) and drugs that show monophasic quenching behavior (*see* **Fig. 2C**,**D**), to the following equation:

$$\left(\frac{\Delta F}{F_0} \times 100\right) = \frac{\left(\frac{\Delta F_{max}}{F_0} \times 100\right) \times [S]}{K_d + [S]} \quad (2)$$

where $((\Delta F/F_0) \times 100)$ is the percent quenching (percent change in fluorescence relative to the initial value) following addition of substrate at a concentration [S], and K_d is the dissociation constant. Fitting is carried out using nonlinear regression with the Marquardt–Levenberg algorithm (SigmaPlot, SPSS Inc.), and values of K_d and $(\Delta F_{max}/F_0 \times 100)$ are extracted (*see* **Fig. 2** and **Table 1**). For drugs that show biphasic quenching, the experimental data are fitted to the two-site model of Doppenschmitt et al. ***(24)***, and two values of K_d are extracted.

3.3. Covalent Labeling of Pgp with the Extrinsic Fluorophore MIANS

1. To prepare Pgp modified with two MIANS groups (on Cys 428 and Cys 1071 in hamster Pgp, Cys 431 and Cys 1074 in human Pgp; *see* **Fig. 1A**), incubate 0.25 mg of purified protein in 1 mL of buffer A containing 2 m*M* CHAPS and 20 μ*M* MIANS at 4°C for 1 h in the dark. Add 10 μL of 100 m*M* DTE (final concentration of 1 m*M*) to react with the excess MIANS.
2. Separate the MIANS–Pgp by gel filtration on a prefilled 10-mL column of Bio-Gel P-6 (Bio-Rad Laboratories) equilibrated with buffer A containing 2 m*M* CHAPS. The final concentration of MIANS-labeled Pgp is typically approx 50 μg/mL.

3.4. Substrate-Binding Affinity Determined by Quenching of the Fluorescence of the Covalently Bound Extrinsic Fluorophore MIANS

1. Quenching experiments are performed by successively adding 5-μL aliquots of nucleotide or drug solution to 500 μL of MIANS–Pgp solution (50 μg/mL) in buffer A containing 2 m*M* CHAPS and 0.5 mg/mL phospholipid in a 0.5-cm-pathlength quartz microcuvet equilibrated at the required temperature (typically 22°C).

2. After each addition, the MIANS–Pgp sample is excited at 322 nm and the steady-state fluorescence emission is measured at 420 nm.
3. Correct the fluorescence intensities for dilution, scattering, and the inner filter effect. Perform control titrations with MIANS–DTE (*see* **Note 6**) to assess the nonspecific quenching of MIANS fluorescence by nucleotides and drugs. Carry out a control titration with DMSO alone, to confirm that there are no solvent-related effects. Computer-fit the experimental data for nucleotides (**Fig. 3A**) and drugs (**Fig. 3B**) to the equation for single-site binding or two-site binding, as described in **Subheading 3.2., step 3**, and extract values for K_d and ΔF_{max} (*see* **Table 2**).

3.5. Conformational Changes Induced Following Substrate Binding

1. Collisional quenching experiments are performed by successively adding 5-µL aliquots of acrylamide or KI solution to 500 µL of Pgp or MIANS–Pgp solution (50 µg/mL) in buffer A containing 2 m*M* CHAPS in a 0.5-cm-pathlength quartz microcuvet equilibrated at the required temperature (typically 22°C).
2. After each addition, measure the fluorescence emission intensity. For Pgp, the sample is excited at 290 nm and the steady-state fluorescence emission is measured at 330 nm (the emission maximum for Pgp Trp residues; *see* **Fig. 1B**). For MIANS–Pgp, the sample is excited at 322 nm and the steady-state MIANS fluorescence emission is measured at 420 nm.
3. Correct the fluorescence intensities for dilution, scattering, and the inner filter effect. When using KI as a quencher, correct for ionic strength by carrying out a parallel titration with KCl (*see* **Note 3**).
4. When examining intrinsic Trp fluorescence, perform a parallel quenching titration with NATA to assess the quenching of fluorescence by the same agents when Trp is completely accessible in aqueous solution. When examining MIANS–Pgp fluorescence, perform a parallel quenching titration with MIANS–DTE.
5. Analyze acrylamide and I^- quenching data using the Stern–Volmer equation (*see* **Subheading 1.5.**). A Stern–Volmer plot of F_0/F versus [Q] gives a linear plot with a slope of K_{SV} (*see* **Fig. 4***).*

3.6. Reconstitution of Pgp into Large Unilamellar Proteoliposomes

Partially purified Pgp (the S_2 fraction) is reconstituted into the desired phospholipids, or phospholipid mixture, using rapid detergent removal by gel filtration chromatography. For kinetic studies, typically 0.5 mg of S_2 fraction is reconstituted into 5 mg of lipid.

1. Dispense the required amount of lipid stock solution in $CHCl_3$–MeOH into a small glass tube, and evaporate the solvent to dryness under a stream of N_2 gas. Pump the dried lipid under vacuum for 1 h to remove all trace of solvent.
2. Dissolve the dried lipid at a concentration of 20 mg/mL in buffer A containing 100 m*M* CHAPS, with warming to 37°C and occasional vortexing. The final

solution should be optically clear. Then, add Pgp in 15 m*M* CHAPS solution, typically 0.5 mg in a volume of approx 500 µL, mix with a fine-gage syringe, and incubate the mixture on ice for 30 min to mix.

3. Pass the lipid–protein mixture at 4°C through a Sephadex G-50 column (1 × 15 cm, equilibrated with buffer A) and elute with buffer A, collecting eight to nine fractions of approx 1 mL volume. Turbid fractions containing proteoliposomes can be located visually (or the absorbance of the fractions may be read at 280 nm); typically, two to three fractions close to the void volume of the column are pooled.
4. Keep the proteoliposomes on ice until ready for use. Their protein content may be measured using a modified Lowry method ***(25)*** and the ATPase activity using a colorimetric method ***(26)***.

3.7. Real-Time Fluorescence Assay for Monitoring Transport

1. Mix a 440-µL aliquot of reconstituted proteoliposomes containing 10–20 µg of Pgp (dilute with buffer A) with a 10-µL aliquot of TMR in buffer A at the appropriate concentration (for a 1-µ*M* final TMR concentration, add 50 µ*M* TMR). After a 5-min incubation at the desired temperature, transfer the sample to a thermostatted quartz cuvet and allow to equilibrate for about 2 min to allow stabilization of the fluorescence signal (*see* **Fig. 6A**).
2. Initiate transport of TMR by addition of a 50-µL aliquot of buffer containing 10 m*M* ATP (final concentration of 1 m*M*) and an ATP regenerating system, followed by mixing for 10 s. Excitation at 550 nm is carried out with a bandwidth of 1.8 nm to reduce photobleaching. Monitor fluorescence emission continuously at 575 nm (bandwidth, 3.6 nm). Measure the fluorescence intensity at 1-s intervals for about 150 s, until a steady state is approached (*see* **Fig. 6A**).
3. Normalize the traces of fluorescence intensity versus time to the intensity measured immediately after the addition of ATP, which is taken as 100%.
4. Determine the initial rate of TMR transport by carrying out linear regression analysis of the data collected during the first 20 s (*see* **Fig. 6B**), using SigmaPlot (SPSS Inc., Chicago, IL, USA). The initial rate data may be fitted to the Michaelis–Menten equation (*see* **Fig. 6C**,**D**).

4. Notes

1. Many membrane transport proteins may be stabilized by the use of sulfhydryl reagents, such as DTE. However, these compounds should not be used if sulfhydryl-reactive labeling agents, such as MIANS, are to be employed to fluorescently label the transport protein after purification.
2. For highly hydrophobic/water-insoluble drugs, care should be taken to avoid prolonged contact (several hours) of diluted drug solutions with glass or plastic sample tubes, because adsorption of the compound onto the surface may take place. Such drugs are best diluted to the required concentration just prior to use, and used promptly.
3. In the case in which transport protein is titrated with the collisional quencher KI, KCl is usually used in a parallel control titration, and the fluorescence emission

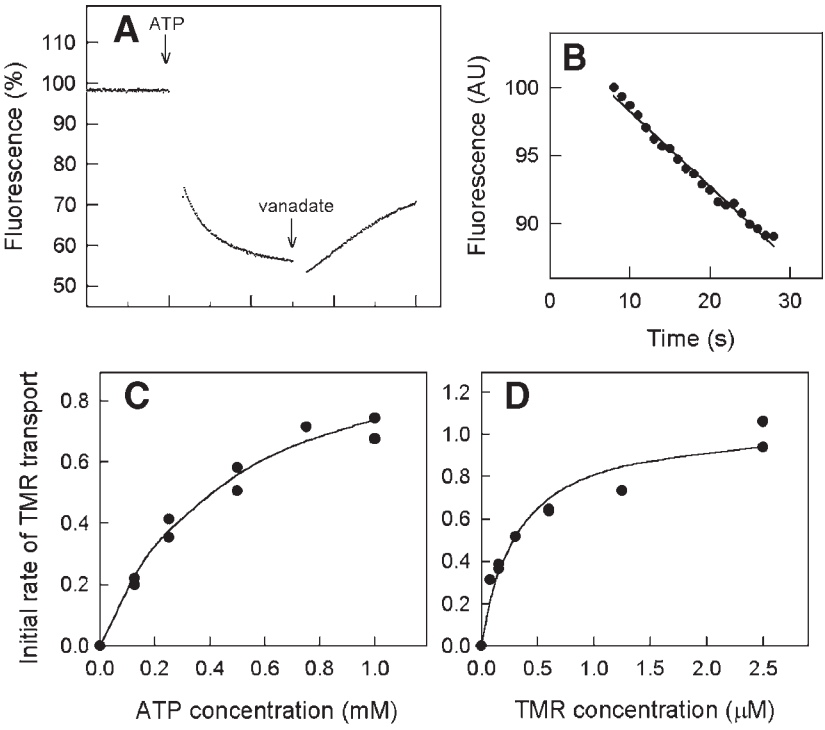

Fig. 6. Real-time fluorescence-based assay for transport of the rhodamine dye TMR into reconstituted proteoliposomes containing Pgp. **(A)** TMR transport is initiated at $t = 0$ by the addition of ATP to a final concentration of 1 m*M*. Following a short mixing period, the intensity of fluorescence emission at 575 nm is measured at 1-s intervals for approx 150 s, until a steady state is approached. The decrease in TMR fluorescence in the early linear time period is used to estimate the initial rate of TMR transport **(B)**. The initial rate of TMR transport is measured at a fixed TMR concentration (1 μ*M*) and varying ATP concentrations **(C)**, or at a fixed ATP concentration (1 m*M*) and varying TMR concentrations **(D)**. Data are fitted to the Michaelis–Menten equation (solid lines) and the values of K_m for ATP and TMR estimated. Once the steady state has been reached, the addition of vanadate (an ATPase inhibitor) abolishes Pgp-mediated transport, and the TMR concentration gradient collapses, with a concomitant increase in fluorescence intensity as TMR flows out of the proteoliposome lumen **(A)**.

at each KI concentration is corrected by subtraction of the corresponding KCl control value.

4. The concanavalin A–Sepharose column is regenerated by washing with 50 mL of 20% ethanol in buffer A, followed by storage in 0.1 *M* sodium acetate, 1 *M* NaCl, 1 m*M* $CaCl_2$, 1 m*M* $MgCl_2$, and 1 m*M* $MnCl_2$, pH 6.0.

5. For Trp quenching experiments, PMPC is the most suitable phospholipid, because it has a lower background fluorescence at the wavelengths used.
6. To prepare MIANS–DTE, react 1 m*M* DTE with 20 µ*M* MIANS at 22°C in the dark for 1 h.

References

1. Lakowicz, J. R. (1999) *Principles of Fluorescence Spectroscopy*, Kluwer Academic, New York.
2. Schneider, E. and Hunke, S. (1998) ATP-binding-cassette (ABC) transport systems: functional and structural aspects of the ATP-hydrolyzing subunits/domains. *FEMS Microbiol. Rev.* **22,** 1–20.
3. Holland, I. B. and Blight, M. A. (1999) ABC-ATPases, adaptable energy generators fuelling transmembrane movement of a variety of molecules in organisms from bacteria to humans. *J. Mol. Biol.* **293,** 381–399.
4. Sharom, F. J. (1997) The P-glycoprotein efflux pump: how does it transport drugs? *J. Membr. Biol.* **160,** 161–175.
5. Ambudkar, S. V., Dey, S., Hrycyna, C. A., et al. (1999) Biochemical, cellular, and pharmacological aspects of the multidrug transporter. *Annu. Rev. Pharmacol. Toxicol.* **39,** 361–398.
6. Ford, J. M. (1996) Experimental reversal of P-glycoprotein-mediated multidrug resistance by pharmacological chemosensitisers. *Eur. J. Cancer* **32A,** 991–1001.
7. Higgins, C. F. and Gottesman, M. M. (1992) Is the multidrug transporter a flippase? *Trends Biochem. Sci.* **17,** 18–21.
8. Sharom, F. J., Yu, X., Chu, J. W. K., et al. (1995) Characterization of the ATPase activity of P-glycoprotein from multidrug-resistant Chinese hamster ovary cells. *Biochem. J.* **308,** 381–390.
9. Urbatsch, I. L., al-Shawi, M. K., and Senior, A. E. (1994) Characterization of the ATPase activity of purified Chinese hamster P-glycoprotein. *Biochemistry* **33,** 7069–7076.
10. Doige, C. A. and Sharom, F. J. (1992) Transport properties of P-glycoprotein in plasma membrane vesicles from multidrug-resistant Chinese hamster ovary cells. *Biochim. Biophys. Acta* **1109,** 161–171.
11. Sharom, F. J., Yu, X., DiDiodato, G., et al. (1996) Synthetic hydrophobic peptides are substrates for P-glycoprotein and stimulate drug transport. *Biochem. J.* **320,** 421–428.
12. Lu, P., Liu, R., and Sharom, F. J. (2001) Drug transport by reconstituted P-glycoprotein in proteoliposomes—effect of substrates and modulators, and dependence on bilayer phase state. *Eur. J. Biochem.* **268,** 1687–1697.
13. Sharom, F. J., Liu, R., and Romsicki, Y. (1998) Spectroscopic and biophysical approaches for studying the structure and function of the P-glycoprotein multidrug transporter. *Biochem. Cell Biol.* **76,** 695–708.
14. Sharom, F. J., Liu, R., Romsicki, Y., et al. (1999) Insights into the structure and substrate interactions of the P-glycoprotein multidrug transporter from spectroscopic studies. *Biochim. Biophys. Acta* **1461,** 327–345.

15. Sharom, F. J., Liu, R., Qu, Q., et al. (2001) Exploring the structure and function of the P-glycoprotein multidrug transporter using fluorescence spectroscopic tools. *Semin. Cell Dev. Biol.* **12,** 257–266.
16. Liu, R., Siemiarczuk, A., and Sharom, F. J. (2000) Intrinsic fluorescence of the P-glycoprotein multidrug transporter: sensitivity of tryptophan residues to binding of drugs and nucleotides. *Biochemistry* **39,** 14,927–14,938.
17. Wu, J. and Kaback, H. R. (1994) Cysteine 148 in the lactose permease of *Escherichia coli* is a component of a substrate binding site. 2. Site-directed fluorescence studies. *Biochemistry* **33,** 12,166–12,171.
18. Kwaw, I., Zen, K. C., Hu, Y. L., et al. (2001) Site-directed sulfhydryl labeling of the lactose permease of *Escherichia coli*: helices IV and V that contain the major determinants for substrate binding. *Biochemistry* **40,** 10,491–10,499.
19. Liu, R. and Sharom, F. J. (1996) Site-directed fluorescence labeling of P-glycoprotein on cysteine residues in the nucleotide binding domains. *Biochemistry* **35,** 11,865–11,873.
20. Sharom, F. J., Yu, X., and Doige, C. A. (1993) Functional reconstitution of drug transport and ATPase activity in proteoliposomes containing partially purified P-glycoprotein. *J. Biol. Chem.* **268,** 24,197–24,202.
21. Kolaczkowski, M., van der Rest, M., Cybularz-Kolaczkowska, A., et al. (1996) Anticancer drugs, ionophoric peptides, and steroids as substrates of the yeast multidrug transporter Pdr5p. *J. Biol. Chem.* **271,** 31,543–31,548.
22. Doige, C. A. and Sharom, F. J. (1991) Strategies for the purification of P-glycoprotein from multidrug-resistant Chinese hamster ovary cells. *Protein Express Purif.* **2,** 256–265.
23. Parker, C. A. (1968) *Photoluminescence of Solutions*, Elsevier, Amsterdam.
24. Doppenschmitt, S., Spahn-Langguth, H., Regardh, C. G., et al. (1998) Radioligand-binding assay employing P-glycoprotein-overexpressing cells: testing drug affinities to the secretory intestinal multidrug transporter. *Pharm. Res.* **15,** 1001–1006.
25. Peterson, G. L. (1977) A simplification of the protein assay method of Lowry et al. which is more generally applicable. *Anal. Biochem.* **83,** 346–356.
26. Doige, C. A., Yu, X., and Sharom, F. J. (1992) ATPase activity of partially purified P-glycoprotein from multidrug-resistant Chinese hamster ovary cells. *Biochim. Biophys. Acta* **1109,** 149–160.

9

Reconstitution of Membrane Transporters

Frances J. Sharom and Paul D. W. Eckford

1. Introduction

1.1. Why Reconstitute?

An important goal for a biochemist studying a membrane transporter is to characterize various aspects of its transport function. Initial studies are often carried out in intact cells, but further work is often directed toward studying the functional properties of the purified protein. Some functions of transport proteins may be studied in detergent solution; for example, if the transporter is driven by ATP hydrolysis, the ATPase catalytic activity may be measured in the absence of actual transport, usually by adding the substrate in the presence of ATP and Mg^{2+}. However, study of the transport process itself can only be carried out in the presence of an impermeable membrane barrier, which necessitates that the transport protein be inserted into a lipid bilayer membrane, a process known as reconstitution. Retention of transport function of the protein is obviously highly desirable, and most reconstitution protocols are designed with this goal in mind. For a detailed discussion of the theory and practice of membrane protein reconstitution, the reader is referred to an excellent review ***(1)***.

Reconstituted systems are extremely useful in the study of membrane transporters. When a purified protein is used, they can demonstrate unambiguously that the component in question transports a particular substrate. Reconstituted systems allow detailed characterization of the transport process, with estimation of initial rates, K_m values, and turnover numbers. Competition experiments can measure the affinity of the transporter for binding various inhibitors, and molecules structurally related to the substrate. Reconstituted systems also allow detailed spectroscopic characterization of the purified transporter, using techniques such as fluorescence spectroscopy ***(2)***. The interaction of membrane

From: *Methods in Molecular Biology, vol. 227: Membrane Transporters: Methods and Protocols*
Edited by: Q. Yan © Humana Press Inc., Totowa, NJ

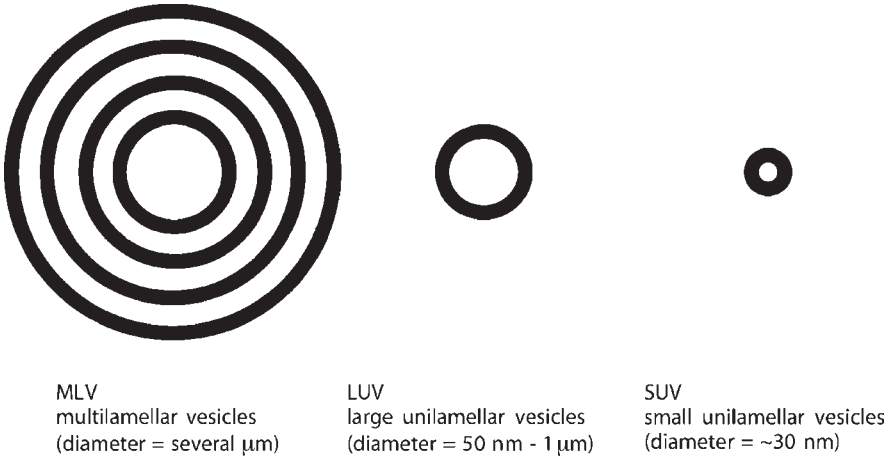

Fig. 1. Different types of bilayer formations formed by membrane phospholipids. Multilamellar vesicles (MLVs) are readily formed by vortexing dried phospholipid films in aqueous buffers. Small unilamellar vesicles (SUV) are generated by prolonged sonication of MLV using a microprobe tip. Large unilamellar vesicles (LUV) are produced by removal of detergent from mixed micelles of protein, lipid, and detergent. LUVs are the systems of choice for reconstitution of membrane transporters.

lipids with the transporter can also be studied in depth using lipid vesicles made up of defined synthetic or natural lipids. The requirement for various types of lipids (e.g., anionic species) for protein function may be delineated and the effects of membrane fluidity on the transport process explored.

1.2. Types of Lipid Bilayer Structures

Several different types of lipid bilayer formations may be formed by membrane phospholipids (*see* **Fig. 1**), and only some of these are useful for reconstitution of membrane transport proteins. Multilamellar vesicles (MLV) are large onionlike structures formed by hydrating phospholipids in aqueous buffers, usually by vortexing vigorously. The phospholipids are usually presented as a thin, dried film following evaporation from a solution of organic solvent (typically $CHCl_3$–MeOH). It is difficult to incorporate membrane transporters into such structures, because their formation does not involve the use of detergent, which is usually essential for solubilization of membrane proteins. MLV structures are usually roughly spherical and are made up of concentric, hollow, lipid bilayer spheres, each bilayer separated from the one beneath it by a thin layer of aqueous solution (*see* **Fig. 1**). Typically, the fraction of phospholipid exposed at the outer surface of the MLV is only 5–10% of the total. This feature of MLV also limits their usefulness for experiments involving the addition

of reagents from the external solution, because only a small fraction of the membrane bilayer will be in contact with the reagent.

Small unilamellar vesicles (SUV) are usually produced by prolonged sonication of MLV structures using a probe sonicator. The input of sound energy results in single-walled lipid bilayer structures of high curvature, with sizes typically around 20–30 nm in diameter (*see* **Fig. 1**). SUV are inherently unstable and fuse to give larger vesicles of lower curvature over periods of 24–48 h. These structures are also unsuitable for reconstitution of membrane transporters, because of the lack of means to incorporate proteins into them and their small size and instability.

The term "liposome" is often used to describe closed, lipid bilayer vesicles of any type, and following the incorporation of membrane proteins into these structures, they are often designated as proteoliposomes. Large unilamellar vesicles (LUV) are the structure of choice for reconstitution of membrane transporters. The use of the term "large" merely indicates that these vesicles have a substantially increased size relative to SUV, which, in practice, covers a wide range of diameters, from 50 to 100 nm at the low end to the low micrometer range at the high end (*see* **Fig. 1**). LUV can be readily formed by the removal of detergent from lipid–detergent solutions, thus allowing the simultaneous incorporation of membrane transport proteins solubilized in detergent solutions. LUV do not have high curvature, are unstrained, and are, thus, quite stable under normal conditions. They also have the added advantage of a relatively high trapped internal volume, which is important for studies involving the transport of solutes from the external solution into the vesicle interior. Collection of the vesicles by filtration or centrifugation, followed by quantitation of accumulated substrate is a very common method for assessing the function of reconstituted transport proteins. Larger vesicle structures with high trapped volumes allow higher levels of accumulation of radioactive substrate, or substrate molecules labeled in other ways, inside the vesicle lumen.

1.3. Choosing a Detergent

There are several factors to consider when choosing a detergent for reconstitution of a membrane transport protein. If transport processes are to be studied, clearly the detergent must be chosen based on its ability to maintain the functional integrity of the membrane transport protein. Mild, nondenaturing detergents are thus most often employed (*see* **Fig. 2**). If the transport protein is to be purified before reconstitution, then the chosen detergent should also be compatible with the separation techniques to be used. One additional criterion relates to the suitability of the detergent for reconstitution procedures. One of the most commonly used techniques for reconstitution relies on removal of the detergent by dialysis (*see* **Subheading 1.5.1.**),

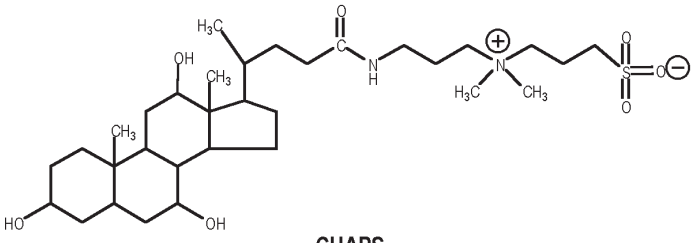

CHAPS

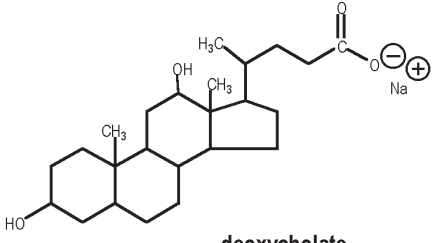

deoxycholate

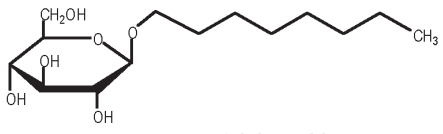

octylglucoside

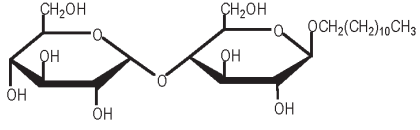

dodecylmaltoside

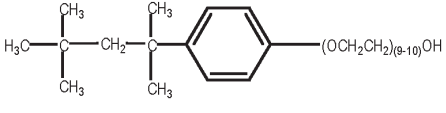

Triton X-100

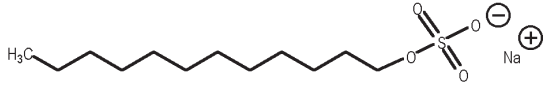

SDS

Fig. 2. Structures of some detergents commonly used to solubilize membrane transport proteins. CHAPS®, deoxycholate (sodium salt), octylglucoside, and dodecylmaltoside are useful for reconstitution into proteoliposomes by detergent removal. Triton X-100, which has a low critical micelle concentration and forms large micelles (*see* **Table 1**), is difficult to remove from mixed protein–lipid–detergent micelles and is, thus, not suitable for reconstitution using this approach. Sodium dodecyl suflate (SDS) is highly denaturing to most membrane proteins and is not used when retention of protein function is desired.

and an overriding factor in this case is that the critical micelle concentration (CMC) of the detergent should be high (see next paragraph). If it is not possible to obtain the membrane transporter directly in a detergent suitable for reconstitution, the protein can often be exchanged into a more appropriate detergent using gel filtration chromatography.

Detergents are amphiphilic and have the property of forming micelles, closed spherical structures in which the polar/charged moiety of the detergent faces the external aqueous solution, with the nonpolar portions sequestered in the middle of the micelle, away from contact with water (*see* **Fig. 3**). The CMC is a very important characteristic of a detergent, and it determines, to a large extent, its usefulness in reconstitution procedures involving dialysis. At concentrations below the CMC, detergent molecules exist as monomers in true solution. Once the CMC is reached, micelles start to form, and any additional detergent molecules contribute to micelle formation, with the monomer concentration remaining constant at a value equal to the CMC (*see* **Fig. 3**). To some extent, the CMC of a detergent depends on the ionic strength of the solution, as well as the temperature, so its value falls in a range, rather than being absolute (*see* **Table 1**). CMC values for detergents range from μ*M* (e.g., Triton X-100) to m*M* (e.g., octylglucoside)(*see* **Fig. 2**). In general, detergents are only effective solubilization agents for lipids and membranes when used at concentrations above their CMC. The size of an average micelle is also an important property of each detergent. Again, a wide range is seen for the commonly used species, from 2 to 4 for the bile salt detergents (such as cholate, deoxycholate, and taurocholate) to 100 to 155 for the nonionic detergent Triton X-100 (*see* **Fig. 2** and **Table 1**). The micelle molecular weight is also highly variable, depending on the molecular weight of the detergent molecule and the number of monomers per micelle, and it ranges from a low of 800–900 for bile salts to 90,000 for Triton X-100 (*see* **Table 1**).

Detergents are usually classified according to their charge. Most detergents commonly used in the study of membranes fall into three classes; charged (anionic), zwitterionic, and nonionic (uncharged) (*see* **Table 1**). In the charged group, sodium dodecyl sulfate (SDS) (*see* **Fig. 2**) is a very harsh detergent, which usually denatures proteins at relatively low concentrations, so it is not used when transport function is to be preserved. The bile salt detergents, cholate, deoxycholate (*see* **Note 1**), and taurocholate, are mild and maintain protein function well, as do the zwitterionic detergents, 3-[3-(cholaminopropyl) dimethylamino]-1-propanesulfonate (CHAPS) and big-CHAPS (*see* **Fig. 2**). Both of these types of detergents have a relatively high CMC value, making them popular for reconstitution studies of membrane transporters. CHAPS is frequently used in the authors' laboratory; it has the additional advantage of forming relatively large LUV upon removal by dialysis or gel filtration chro-

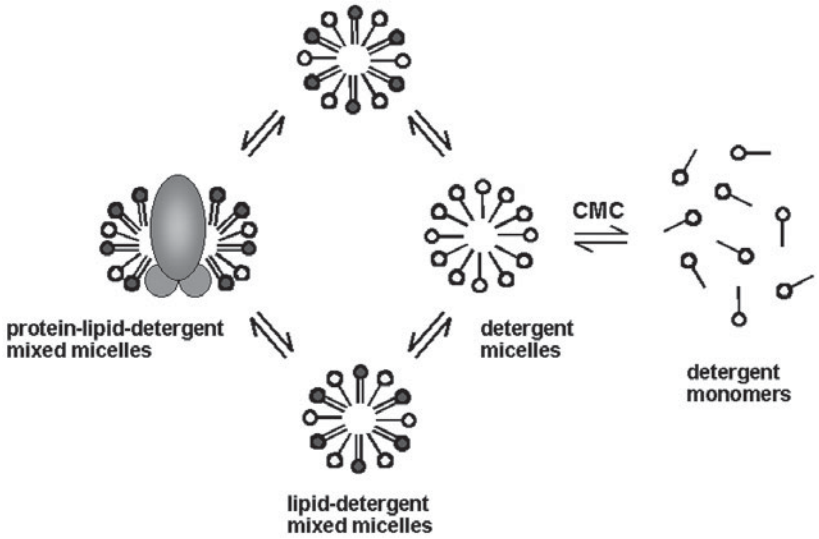

Fig. 3. A major strategy for functional reconstitution of membrane transporters into lipid bilayer vesicles involves detergent removal. The starting point is a solution of protein, lipid, and excess detergent, containing mixed micelles of protein–lipid–detergent, lipid–detergent, and detergent alone. Detergent micelles exist in equilibrium with detergent monomers, at a concentration governed by the CMC of the detergent. Detergent may be removed by dialysis or gel filtration chromatography, or its concentration may be lowered to well below the CMC by dilution.

matography, with trapped volumes suitable for transport studies involving the uptake of substrates into the vesicle lumen ***(3–9)***. In the nonionic group, Triton X-100 has a low CMC value and is very difficult to remove rapidly and completely by either dialysis or gel filtration chromatography, so it is not suitable for membrane protein reconstitution unless additional measures are taken, such as the use of a detergent-binding beaded matrix. Octylglucoside is mild and nondenaturing, with a high CMC value, and is also a popular choice for reconstitution, although it has the drawback of forming quite small vesicles with low trapped volumes upon dialysis.

1.4. Choosing a Lipid

For phospholipid molecules, the variables to be considered include the chemical nature of the head group and the length and degree of unsaturation of the fatty acyl chains. The presence of additional lipid molecules, such as cholesterol, may also be desirable. Several factors influence the choice of the host lipid for reconstitution studies. Some membrane proteins have specific require-

Table 1
Properties of Detergents

Detergent	CMC (m*M*)	Monomer molecular weight (Dalton)	Monomers per micelle	Micelle molecular weight (Dalton)
Charged (anionic)				
Sodium dodecylsulfate	6–8	288.5	62	18,000
Deoxycholate	4–8	416.6	2	800
Cholate	9–15	430.6	2	900
Taurocholate	3–11	537.7	4	2,100
Zwitterionic				
CHAPS	8–10	614.9	10	6,150
Big-CHAPS	3.4	878.1	10	8,800
Nonionic				
Octyl-β-D-glucoside	23–25	292.4	27	8000
n-Dodecylmaltoside	0.18	510.6	0.1–0.6	NA
Triton X-100	0.2	625–650	100–155	90,000

Note: The CMC values and number of monomers per micelle for detergents depend on various properties of the solution, especially ionic strength, temperature, and so forth, so a range is found for commonly used conditions. Typical values are given. Some detergents (e.g., Triton X-100) are mixtures of polymers of various lengths and, thus, do not have a defined molecular weight (an average is given).

ments for certain lipids. For example, the plasma membrane Ca^{2+} (PMCA) pump is activated by binding of anionic (acidic) phospholipids, such as phosphatidylserine (PS) and phosphatidylinositol-4-phosphate, to a specific binding site ***(10,11)***, and the *Rhodobacter sphaeroides* bacterial photosynthetic reaction center has a binding site for cardiolipin, as seen in the 3-dimensional X-ray crystal structure ***(12)***. If it is known *a priori* that a membrane transport protein has such requirements, then the lipids in question should obviously be included in the host bilayer for reconstitution. In the absence of such information, it may be prudent to initially reconstitute the protein into a natural lipid mixture that mimics the membrane from which it was originally extracted, because such mixtures are likely to contain any required lipid species. If it is known or suspected that the transport protein is not particularly fussy about its lipid environment, then a synthetic phospholipid may be employed.

1.4.1. Complex Natural Lipid Mixtures

Complex natural lipid mixtures containing more than one type of lipid, generally extracted from whole cells or tissues, can be very useful for initial reconstitution work, because they will likely contain any lipids specifically required

Table 2
Lipids and Lipid Mixtures Useful for Reconstitution of Membrane Transporters

Lipid	Melting temperature, T_m (°C)	Charge	Preferred phase
Complex natural lipid mixtures			
E. coli lipids	NA		Bilayer
Asolectin (soybean phospholipids)	NA		Bilayer
Natural mixtures of one lipid type			
Egg PC	NA	+–	Bilayer
Egg PE	NA	+–	H_{II} phase
Bovine SM (erythrocyte, brain)	NA	+–	Bilayer
Bovine brain PS	NA	–	Bilayer
Synthetic phospholipids			
DOPC	–20	+–	Bilayer
POPC	–2	+–	Bilayer
SOPC	6	+–	Bilayer
DMPC	23	+–	Bilayer
PMPC	27	+–	Bilayer
DPPC	41	+–	Bilayer
DPPE	63	+–	H_{II} phase

Note: NA, not applicable; only synthetic lipids with defined acyl chains have a sharp melting temperature.

Acronyms are defined in **Subheadings 1.4.2.** and **1.4.3.**

by the transporter for activity. A lipid mixture extracted from *Escherichia coli* (*E. coli* lipids) is available commercially from several sources and has been frequently employed for reconstitution of transporters from Gram-negative bacteria, and asolectin, a complex mixture of phospholipids extracted from soybeans, is a useful choice for many mammalian transporters (*see* **Table 2**). Lipid mixtures of this type will contain species with different head groups, a mixture of acyl chains, and many other nonpolar molecules found in the original membrane, such as hydrophobic peptides. This can present a disadvantage in some situations, because small amounts of many different complex lipid-soluble molecules may be present, and the minor components of such mixtures are often not well characterized. Pigmented and colored compounds commonly found in such extracts may interfere with spectroscopic measurements. Variability from one preparation to the next is also a concern.

1.4.2. Natural Mixtures of One Type of Lipid

Mixtures of phospholipids of a single head-group type can also be useful, because the variability is reduced to only the acyl chains and these preparations tend to be of higher purity than the extracted mixtures discussed earlier. Natural lipid mixtures are generally highly fluid, with the majority of acyl chains being unsaturated. Care must be taken to avoid spontaneous oxidation of the double bonds in the acyl chains, and stock solutions of these lipids are often stored at very cold temperatures, under N_2 or Ar gas. Egg phosphatidylcholine (PC), egg phosphatidylethanolamine (PE), PS, bovine erythrocyte, and bovine brain sphingomyelin (SM) are some examples of commercially available lipids of this type (*see* **Table 2**). Mixtures of these lipids may be used to more closely mimic the makeup of a natural membrane.

1.4.3. Synthetic Lipids

Synthetic phospholipids with defined acyl chains are made chemically and provide the highest purity of any available membrane lipids, as no natural product contaminants are present. They have the added advantage of displaying well-defined melting behavior, and their phase behavior and gel-to-liquid crystalline-phase transition temperature, T_m, are well established (*see* **Table 2**). If a highly fluid lipid mixture with a very low T_m is desired, the lipid of choice is dioleoyl-PC (DOPC; T_m = –20°C). 1-Palmitoyl-2-oleoyl-PC (POPC) and 1-stearoyl-2-oleoyl-PC (SOPC) are also useful host lipids, because their acyl chain pattern mimics that of a typical membrane phospholipid. PC species with two identical saturated acyl chains are often employed; dimyristoyl-PC (DMPC) is one of the most useful, because its T_m is close to room temperature (23°C). This feature allows transport measurements to be made both above and below the melting temperature to explore the effects of membrane fluidity on transport function ***(13)***. 1-Palmitoyl-2-myristoyl-PC (PMPC), which has a T_m of 27°C, can also be used in experiments of this type. Dipalmitoyl-PC (DPPC) has a melting point above the physiological temperature range and is used relatively infrequently as the sole lipid for studies of membrane transport.

Mixtures of synthetic lipids can also be used when it is desirable to more closely mimic a natural membrane. It should be stressed that it is essential to ensure that a bilayer form is maintained when including nonbilayer lipids, such as PE (which prefers to form the hexagonal H_{II} phase), or modified fluorescent lipid derivatives. ^{31}P-NMR (nuclear magnetic resonance) can be useful in establishing that a bilayer structure exists ***(14,15)***, as the characteristics of the phospholipid phosphate peak differ in the H_{II} and bilayer phases.

The choice of lipid can greatly affect the size of the reconstituted proteoliposomes obtained. For example, egg PC generally forms very small LUVs (less than 50 nm) whether reconstitution is carried out by detergent dialysis, gel filtration, or rapid dilution. These vesicles can be difficult to sediment, even at ultracentrifuge speeds, and are also challenging to collect by filtration in transport assays. DMPC, on the other hand, generally forms much larger structures, which are readily collected by sedimentation using a microcentrifuge or by rapid filtration.

1.4.4. Other Membrane Components

Incorporation of other membrane constituents into reconstituted bilayers is relatively straightforward, as long as they can be cosolubilized by detergent along with the other desired lipids and the transport protein. Examples of species that can be coreconstituted include cholesterol, glyco(sphingo)lipids, and molecules designed to provide the membrane with a particular charge density, such as dicetylphosphate (negatively charged) or stearylamine (positively charged) ***(9,16)***. Incorporation of cholesterol or glycosphingolipids is usually limited to less than 30% (w/w) of the total lipid, because they tend to destabilize the bilayer phase at concentrations higher than this.

1.5. Reconstitution Techniques

The most useful procedures for reconstitution of membrane transporters involve the removal of detergent from a solution containing the solubilized transport protein and the chosen lipids. Both lipids and protein are present in the detergent solution as mixed lipid–detergent and lipid–protein–detergent micelles (*see* **Fig. 3**). Progressive removal of detergent results in spontaneous formation of lipid bilayer structures, which are the energetically most favored arrangement for most phospholipids in water. PE species often form the hexagonal H_{II} phase but can be stabilized in bilayer form if they are mixed with >70% (w/w) bilayer-preferring lipids, such as PC. It should be stressed that each membrane transporter will behave differently when subjected to the different reconstitution methods, depending on the detergent used, the rate of detergent removal, the chosen lipids, the molecular behavior of the protein, and the ionic conditions. Thus, the field of membrane transporter reconstitution is still largely empirical.

1.5.1. Detergent Dialysis

Removal of detergent by dialysis is the single most generally applicable technique for reconstituting membrane transporters. Detergents with high CMC values, such as deoxycholate, CHAPS, and octylglucoside (*see* **Table 1**),

are readily removed by dialysis. The mixed micelle sample of detergent, lipid, and membrane transporter is subjected to dialysis against several changes of detergent-free buffer (typically 4 × 500 mL) over a period of at least 24 h. It is essential that the transport protein being reconstituted be stable for 24 h under the conditions used for dialysis. Proteoliposomes form spontaneously, usually during the first few hours, and are harvested by centrifugation. Reconstituted preparations made by detergent dialysis usually consist of LUV with a reasonably unimodal size distribution, although bimodal distributions have been observed ***(7,9,16)***.

1.5.2. Gel Filtration Chromatography

Detergents with small micelle sizes can be effectively removed from mixed micelle solutions of lipid, protein, and detergent using rapid gel filtration chromatography on Sephadex columns. A Sephadex G-50 column works well when CHAPS is used as the solubilizing detergent. Proteoliposomes containing the transport protein form spontaneously on the column and emerge in the void volume. This approach has the advantage of being rapid, thus minimizing the time that the membrane transport protein is in contact with detergent. The resulting preparations often have a less homogenous size distribution than those made by dialysis. Reconstituted preparation made by gel filtration usually consist of LUV, and both unimodal and bimodal distributions are possible ***(8,13,17,18)***. Care must be taken to ensure that no detergent micelles emerge in the tail fractions of the proteoliposome peak. Residual detergent in the proteoliposome preparation may be measured using radiolabeled detergent or a specific chemical assay [e.g., for the bile salt detergents ***(8)***]. If significant residual detergent is present, possible solutions include using a longer gel filtration column, reducing the sample volume, or rejecting the tail fractions from the proteoliposome peak.

1.5.3. Rapid Dilution

Generating reconstituted vesicles using detergent dilution involves starting with a micellar solution containing both the membrane transporter and the chosen lipids or lipid mixture. An aliquot of this solution is then rapidly diluted into a large volume of buffer (typically a 100-fold excess). The purpose of the dilution is to lower the detergent concentration below the CMC, so that proteoliposomes form spontaneously. This technique has the advantage of being rapid, thus minimizing the period of time the transport protein is exposed to detergent. Although detergent dilution has been used with some success for many membrane proteins, there are several shortcomings that must be kept in mind. First, some detergent remains in the preparation and will increase bilayer

leakiness if it is not removed. This is especially critical if the vesicles are to be used for transport experiments. Detergent is typically depleted by removal of the supernatant, and replacement with fresh buffer, or by treatment of the entire preparation with detergent-removing beads (*see* **Subheading 1.5.5.**). Incorporation of the membrane transporter may be lower than for dialysis techniques and the preparation is dilute. Our laboratory has successfully reconstituted two membrane proteins, the P-glycoprotein multidrug transporter ***(19)*** and human placental alkaline phosphatase ***(20)***, using rapid dilution from CHAPS solutions. The resulting vesicles are unilamellar and have a fairly narrow size distribution with a mean diameter of approx 0.3 μm (range: 0.2–0.4 μm).

1.5.4. Other Reconstitution Methods

Several membrane transporters, including bacteriorhodopsin ***(21)***, cytochrome oxidase ***(21)***, human erythrocyte Band 3 anion exchanger AE1 ***(22)***, the sarcoplasmic reticulum Ca^{2+}-ATPase ***(23)***, and a plant plasma membrane H^{+}-ATPase ***(24)***, have been reconstituted by direct incorporation into preformed unilamellar vesicles. Insertion of proteins into the bilayer occurs spontaneously in the presence of destabilizing concentrations of detergent ***(25)***. In some cases, protein insertion into SUVs can occur in the absence of detergent, presumably as a result of packing defects in a strained bilayer. In all cases, reconstitution of the membrane transporter by direct incorporation takes place in an asymmetric fashion, so that the protein is oriented unidirectionally in the membrane, which has advantages for transport studies. However, the technique also has several disadvantages, including the formation of heterogeneous structures with a broad size range and the need for the inclusion of membrane-destabilizing agents. In addition, it also appears to be a "hit or miss" approach, which only seems to work successfully for certain transport proteins. A variation on this theme was reported by Yang and Lundahl ***(26)***, who prepared large immobilized liposomes on a Sephacryl S-1000 column and then mixed detergent-solubilized erythrocyte membrane proteins with the gel beads. Transporters such as the glucose transporter GLUT1 and Band 3 were incorporated into the vesicles.

Incorporation of cytochrome oxidase ***(27)*** and human erythrocyte GLUT1 ***(28)*** into preformed sonicated vesicles following a rapid freeze–thaw was reported several years ago. However, the freeze–thaw sonication procedure has not been systematically investigated, and its application has been infrequent.

A few membrane transporters, such as bacteriorhodopsin ***(29)***, have been successfully reconstituted into lipid bilayer vesicles prepared by reversed phase evaporation, using organic solvents. A "water-in-oil" emulsion of phospholipid, protein, and water is prepared in a solvent such as pentane, hexane, or diethyl-

ether, followed by evaporation of the organic phase under reduced pressure. The reconstituted protein is unidirectionally oriented, in an inside-out topology. This technique is limited in its applicability and only appears to be viable for a few exceptionally hydrophobic membrane proteins that can tolerate apolar solvents.

1.5.5. Other Considerations

The formation of amorphous structures and vesicle aggregates can sometimes be a problem with reconstitution of membrane transporters into lipid bilayers, especially at high protein : lipid ratios. Inclusion in the bilayer of 10–20% (w/w) of a negatively charged phospholipid, such as PS, can greatly improve the homogeneity and reduce aggregation of these structures, likely by a steric repulsion effect ***(3)***. If the reconstituted preparation is too inhomogenous from a size perspective, rapid extrusion through polycarbonate membrane filters of a defined pore size in an extrusion device can be used to make the proteoliposomes into LUV of a uniform size, typically 100 or 200 nm in diameter ***(30)***.

Extracti-Gel D™ and Bio-Beads SM2™ are beaded matrices designed to have a high capacity for binding various detergents and are especially useful in the case of Triton X-100 and related nonionic species, which are very difficult to remove by dialysis because of their low CMC, and by gel filtration because of their large micelle size (*see* **Table 1**). These detergent-binding beads can generally be employed with membrane proteins of molecular weight greater than 10 kDa. They are useful both for removing residual detergent from reconstituted preparations and as the primary means of detergent removal. Systematic studies are usually carried out to vary the rate of detergent removal by the addition of differing amounts of beads at various times, because the rate of detergent removal appears to be the key factor in the final morphology and homogeneity of the resulting proteoliposomes ***(31)***.

Because of their relatively small size and low density (at a protein content typical of that used for transport experiments), LUV can sometimes be difficult to collect directly by centrifugation. Because harvesting these structures is often a prerequisite for quantitative analysis of accumulated substrate in transport experiments, this is an important issue. It has been reported that the inclusion in LUV of brominated phospholipids (which behave very similarly to normal phospholipids) increases their density and makes them much easier to pellet by centrifugation ***(32)***. Alternatively, rapid filtration on fine-pore fiberglass filters can be used to harvest larger reconstituted LUV in transport uptake experiments ***(17)***. For smaller LUV, a short incubation with polyethylene glycol solutions results in rapid aggregation to larger structures that are more highly retained on fiberglass filters ***(3,4)***.

1.6. Characterization of Reconstituted Lipid–Protein Systems

Because of the huge variability possible in reconstituted systems containing membrane transporters, it cannot be stressed enough that thorough characterization of the resulting lipid bilayer structures is very important. A clear understanding of various biophysical and biochemical parameters of the reconstituted system allows optimization of the reconstitution procedure and is often necessary before commencing functional studies of membrane transport.

1.6.1. Lipid and Protein Recovery, Lipid : Protein Ratio, Protein Composition

The lipid : protein ratio of a reconstituted preparation is an important parameter, which may be influential in obtaining data on membrane transport function. Lipid : protein ratios can be varied by the experimenter, and depending on the transporter under study, ratios as low as 6 : 1 (w/w) may be obtained ***(8)***. In general, the higher the protein content in the reconstitution mix, the more likely it is that amorphous and aggregated material (rather than more homogeneous LUV) will be present in the reconstituted preparation. A final lipid:protein ratio of 10–15 : 1 (w/w) will usually give relatively homogeneous proteoliposomes, and the protein content is usually more than sufficient for functional studies of membrane transport ***(13)***. Typically, to obtain the desired ratio, it is necessary to start with higher amounts of protein, because the efficiency of reconstitution of membrane transporters is often in the range 50–70%, whereas the recovery of the lipids is typically substantially higher ***(4,8)***.

An easy way to quantitate lipid recovery is to include tracer amounts of a radioactively labeled phospholipid (such as ^{14}C-DPPC) in the reconstitution mix and then count small aliquots of the supernatant and resuspended pellet following harvesting of the proteoliposomes ***(8,17)***. Alternatively, a chemical assay method for phospholipids may be employed ***(33,34)***. The protein content of proteoliposomes is best measured using a method that is not subject to interference by lipids, such as the modified Lowry assay of Peterson ***(35)***. The protein profile of reconstituted proteoliposomes may be determined by standard sodium dodecyl sulfate–polyacrylamide gel electrophoresis (SDS-PAGE), followed by staining with Coomassie Blue or silver. Unless the lipid : protein ratio is very high, it is not usually necessary to delipidate the sample prior to analysis.

1.6.2. Morphology and Size Distribution

Electron microscopy (EM) in conjunction with negative staining (using, e.g., ammonium molybdate) gives an overview of the types of structure present in the proteoliposome preparation and can indicate the presence of

amorphous material and aggregated structures. The size distribution of the reconstituted proteoliposomes may be determined using dynamic light scattering (DLS), which produces a detailed size profile and indicates the existence of a single vesicle population or more than one population of vesicles ***(8,18)***. It is also possible to visualize larger LUV populations using fluorescence microscopy under high-power magnification by the addition of a fluorescent dye, anilino-naphthalene sulfonate (ANS), to the proteoliposome solution. The fluorescence of ANS is highly quenched in aqueous solution, but it is greatly enhanced upon partitioning into the hydrophobic interior of a lipid bilayer. A final ANS concentration of approx 100 μ*M* in a proteoliposome sample produces an essentially black background, with lipid structures displaying an intense yellow-green fluorescence. This method is very rapid, requires a small amount of sample, and can give a good overview of the size and types of structure present.

1.6.3. Symmetry of Reconstitution

Detergent dialysis, gel filtration, and rapid dilution often produce membrane transport proteins that are approx symmetrically reconstituted. In other words, half of the protein molecules face inward, in the opposite orientation to that found in the native membrane, and half face outward, in the same orientation as that found in the native membrane (*see* **Fig. 4**). There are a few factors that can modify this distribution. If the reconstituted vesicles are small and of relatively high curvature, the outer leaflet will make up a larger fraction of the bilayer than the inner leaflet. For example, for a 33-nm vesicle, 64% of the phospholipids are predicted to be in the outer leaflet and only 36% in the inner leaflet ***(36)***. Transport proteins tend to insert into the bilayer so that their bulkiest portions (such as a large soluble domain) face the vesicle exterior, in order to reduce steric crowding. For example, in a vesicle population with a mean diameter of approx 33 nm, 70–80% of the P-glycoprotein multidrug transporter faces inward, with its two bulky nucleotide-binding domains (normally cytosolic) exposed on the exterior of the vesicles ***(18)***. Even in proteoliposomes with low curvature, membrane transporters tend to insert so that steric hindrance is minimized, and we have observed that a larger fraction of P-glycoprotein faces inward as the protein content of the vesicles increases ***(8)***, again, likely to avoid crowding of the bulky nucleotide-binding domains on the vesicle interior.

The orientation of membrane transporters following reconstitution can be readily estimated if the protein has a measurable enzymatic activity that can be attributed to either a cytoplasmic or extracellular domain of the protein and if the lipid bilayer is impermeant to the substrate. For example, ATP-driven trans-

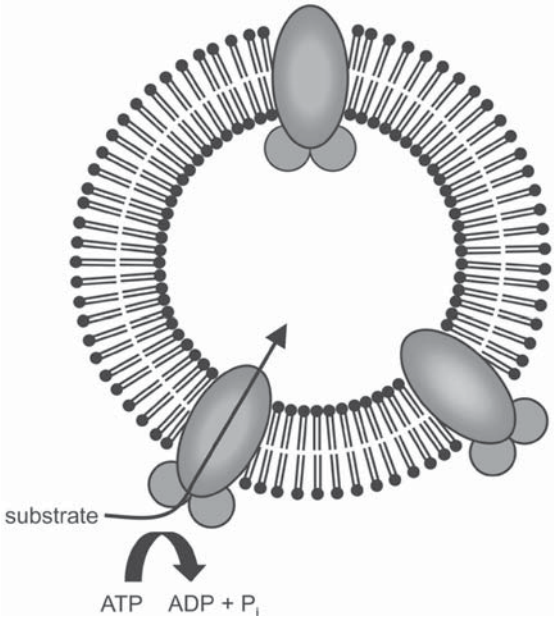

Fig. 4. Orientation of membrane transport proteins following reconstitution. When membrane transporters are reconstituted by removal of detergent, they are often reconstituted in two different orientations. Some of the protein molecules face outward, so their orientation is the same as that of the native membrane, whereas other protein molecules face inward, in the opposite orientation to the native membrane. A transport protein that carries our ATP-dependent export of substrate is illustrated. Inward-facing transporters can hydrolyze ATP and transport substrate into the vesicle lumen. Because the lipid bilayer is impermeable to ATP, outward-facing transporters have no access to ATP and are unable to catalyze ATP hydrolysis or carry out transport. In some instances, the transporter may be reconstituted symmetrically, with approx half the protein in each orientation. If the protein has a large, bulky domain (such as the ATPase catalytic domains) and/or if the vesicle diameter is small, more of the protein may reconstitute in the inward-facing orientation in order to reduce steric hindrance on the lumen side of the membrane.

porters all catalyze ATP hydrolysis and the enzymatic activity arises from a defined cytosolic domain of the protein (*see* **Fig. 4**). To estimate the orientation of reconstitution, ATP is added to the vesicle exterior (often the transport substrate must also be present as well) and the rate of ATP hydrolysis is measured first in the absence and then in the presence of permeabilizing concentrations of detergent (e.g., 2 m*M* CHAPS). In the absence of detergent, outward-facing transporter has no access to ATP and only inward-facing proteins can hydrolyze ATP (*see* **Fig. 4**), whereas in permeabilized proteo-

liposomes, both inward- and outward-facing transporters hydrolyze ATP. Thus, if the transporter is reconstituted symmetrically, the ATPase activity should double after addition of detergent. This approach has been used to estimate the orientation of different membrane proteins following reconstitution ***(8,14,17,18)***. It should be noted that the presence of reconstituted transporters oriented the "wrong way," and therefore inactive in functional assays, is not a barrier to carrying out studies on membrane transport, unless they make up the bulk of the reconstituted preparation. Transporters in the wrong orientation are usually simply ignored, because they do not contribute to transport (*see* **Fig. 4**). Estimated specific activities for the transport process may be corrected for these inactive transporters if the distribution of orientations is known.

1.6.4. Trapped Volume

The trapped volume of reconstituted vesicles can be estimated by inclusion of a "marker" molecule in the buffer during reconstitution, followed by separation of the proteoliposomes from the supernatant and measurement of the amount of the marker associated with them (in the vesicle lumen) ***(37)***. One approach is to add 20 m*M* phosphate to the reconstitution buffer, collect the proteoliposomes by rapid filtration, and measure the trapped inorganic phosphate using a standard colorimetric assay ***(17)***. A typical trapped volume for LUV is 1 μL/mg of lipid. A small trapped volume likely indicates either very small diameter structures, or leaky bilayers (*see* **Subheading 1.6.5.**), and these preparations are usually unsuitable for transport studies.

1.6.5. Sealed Nature of the Vesicles

If the aim of the reconstitution process is to make transport measurements, then it is very important that the vesicles be well sealed. The presence of residual detergent may cause leakiness in the lipid bilayer, so if detergent dilution is employed, it is usually necessary to treat the preparation with detergent-binding beads. This is usually not necessary for proteoliposomes prepared by dialysis or gel filtration.

There are several indicators that reconstituted proteoliposomes may be leaky and, generally, more than one of them should be used before drawing conclusions. If low trapped volumes are obtained using a reconstitution method that is expected to produce high trapped volumes, this can be one indicator of leakiness. Failure to obtain transport activity using either rapid filtration or rapid centrifugation techniques can be another symptom of leaky vesicles, although this can be difficult to distinguish from nonfunctional transport protein. Bilayer permeability may be tested for directly by trapping relatively high concentrations of a fluorescent dye, such as calcein, inside the proteoliposomes during their formation, followed by removal of the

untrapped dye exterior to the lipid vesicles by rapid gel filtration ***(38)***. Calcein is self-quenched at high concentrations (70 m*M*) when trapped within the vesicle lumen, and its fluorescence increases dramatically upon dilution, such as that which occurs when the bilayer is disrupted by detergents. If the reconstituted proteoliposomes are titrated with increasing concentrations of Triton X-100, a large increase in fluorescence will occur when permeabilizing conditions are reached, typically at 0.1–0.4% (v/v) ***(38)***. Failure to observe such a fluorescence increase is a good indicator that the vesicles are leaky and did not retain any trapped dye.

What is the best way to deal with the problem of leaky proteoliposomes? If the protein content is high, reducing it may eliminate the problem, because the presence of large integral proteins produces defects in the packing of bilayer lipids. Another useful strategy is to change the nature of the lipids making up the host bilayer. Certain lipid mixtures, in combination with certain transport proteins, may increase passive permeability, leading to leakiness. Changing to another reconstitution technique is also a strategy worth pursuing.

2. Materials

2.1. Reconstitution by Detergent Dialysis

1. Solution of the membrane transport protein to be reconstituted, in the detergent of choice.
2. Stock solutions of the desired phospholipids in $CHCl_3$–MeOH (4 : 1 [v/v]), typically at a concentration of 5–50 mg/mL. Lipid stock solutions should be stored in tightly stoppered glass containers at –20°C in the dark.
3. Solution of detergent to solubilize phospholipids (usually the same detergent used to solubilize the transport protein); the concentration must be above the detergent CMC. For example, for complete solubilization of PC, a 12.5- to 100-m*M* solution of CHAPS in buffer is used.
4. Dialysis tubing (Spectrapor 4™ tubing, 12- to 14-kDa molecular mass cutoff, is used in the authors' laboratory; *see* **Note 2**) plus clips.
5. Dialysis buffer: Typically, 2 L is needed per sample to be reconstituted. In general, this buffer should be designed to maintain the activity of the transport protein and also be compatible with other assays that may be performed on the reconstituted proteoliposomes. A typical buffer used in the authors' laboratory is 20 m*M* Tris-HCl, pH 7.4. If isotonic NaCl, or other ions, are desirable for maintenance of protein activity, they should be included in the buffer. Sulfhydryl reagents, such as dithiothreitol (DTT) or dithioerythritol (DTE) may also be added. Similarly, the pH of the buffer should reflect the optimum for stability and function of the transport protein. Note that if deoxycholate is used as the solubilizing detergent, the pH should be maintained over 8.0 at all stages of purification and reconstitution (*see* **Note 1**).

2.2. Reconstitution by Gel Filtration Chromatography

1. Detergent solution of the membrane transport protein to be reconstituted.
2. Stock solutions of the desired phospholipids in $CHCl_3$–MeOH (4 : 1 [v/v]), typically at a concentration of 5–50 mg/mL. Lipid stock solutions should be stored in tightly stoppered glass containers at –20°C in the dark.
3. Solution of detergent to solubilize phospholipids (usually the same detergent used to solubilize the protein); the concentration must be above the detergent CMC (*see* **Subheading 2.1., item 3**).
4. Column elution buffer: this buffer should be designed to maintain the activity of the transport protein and be compatible with other assays that may be performed on the reconstituted proteoliposomes (*see* **Subheading 2.1., item 5**).
5. Sephadex G-50 column (1 × 15 cm), equilibrated in the column elution buffer of choice.

2.3. Reconstitution by Rapid Dilution

1. Detergent solution of the membrane transport protein to be reconstituted.
2. Stock solutions of the desired phospholipids in $CHCl_3$–MeOH (4 : 1 [v/v]), typically at a concentration of 5–50 mg/mL. Lipid stock solutions should be stored in tightly stoppered glass containers at –20°C in the dark.
3. Buffer into which to dilute the lipid–protein–detergent mixture (*see* **Subheading 2.1., item 5**).

3. Methods

3.1. Reconstitution by Detergent Dialysis

1. Mix aliquots of stock solution(s) in $CHCl_3$–MeOH (4 : 1 [v/v]) containing the appropriate weight of the desired lipid(s) in a glass tube. Typically, 1–5 mg of lipid is used for each reconstituted sample. Evaporate the solvent to dryness under a gentle stream of N_2 gas and remove any remaining traces of solvent by exhaustive pumping in a vacuum desiccator for at least 1 h.
2. Add detergent solution to solubilize the lipids; usually, the same detergent is utilized as that used to solubilize the membrane transporter. The detergent concentration must be higher than the CMC, otherwise the lipid will not be solubilized into detergent micelles. The final volume desired for the sample dictates the approach that is taken; the following examples give the reader some idea of the various ways that solubilization can be achieved. For example, for complete solubilization of 5 mg of PC in a small volume (*see* **Note 3**), 250 µL of 100 m*M* CHAPS is added to the dried lipid to give a final lipid concentration of 20 mg/mL. If a lower detergent concentration is required (*see* **Note 4**), then a larger volume of detergent solution will be necessary for solubilization, and the final lipid concentration will be lower. For example, to solubilize 5 mg of PC in 12.5 m*M* CHAPS, a volume of 5 mL is needed to give a final lipid concentration

of 1 mg/mL. Typical detergent : lipid ratios used for the lipid solubilization step are 3–8 : 1 (w/w).

3. Incubate the detergent–lipid mixture for up to 30 min to allow complete solubilization. Solubilization of the lipid in the detergent must be complete, to give an optically clear solution. If the lipid has a high T_m, the solution should be warmed over the melting temperature, or solubilization will be slow and incomplete. Commonly used aids for complete solubilization include vortexing the sample with a few small-diameter glass beads (0.5–1 m*M*) or repeated passes of the sample through a syringe with a fine-gage needle (26G). These procedures should be carried out gently, to avoid excessive foaming of the solution. Brief sonication of the sample in a water-bath-type sonicator may also aid in dissolution of the lipid.
4. Add the desired amount of membrane transporter solution in detergent to the detergent–solubilized lipid and incubate the mixture at 4°C for 30 min to promote the formation of mixed lipid–protein–detergent micelles (*see* **Fig. 3**). Periodic passage of the sample through a syringe with a fine-gage needle during this incubation time can be helpful to ensure thorough mixing. For a discussion of the factors that influence the choice of lipid : protein ratio, *see* **Subheading 1.6.1.**
5. Transfer the sample mixture to a piece of "fast" dialysis tubing, with a 12- to 14-kDa molecular weight cutoff (*see* **Note 2**). The sample solution should fill only half the length of the tubing, and the air is then removed from the remaining empty section of tubing to allow for any increase in volume of the sample upon dialysis. Attach the dialysis clips firmly to the tubing, so that there is no risk of detachment.
6. Place the filled dialysis sac in a beaker containing 500 mL of the desired buffer at a temperature of 4°C; then, put the beaker in a cold room at 4°C and stir gently using a magnetic stirrer. Pour off the buffer and replace with fresh solution every 8–12 h, for a total of four changes of 500 mL each. At the first buffer change, noticeable turbidity may be present in the solution inside the dialysis sac, indicating the formation of proteoliposomes.
7. If desired, harvest the proteoliposomes by centrifugation. The ability to pellet the vesicles depends to a certain extent on the host lipid chosen; egg PC vesicles are small and require high speeds to pellet, whereas DMPC vesicles are easily sedimented (*see* **Subheading 1.4.3.**). Each reconstitution procedure also produces vesicles of different sizes and sedimentation properties. Finally, the protein content affects the density of the proteoliposomes and the ease of sedimentation; generally, low lipid : protein ratios produce proteoliposomes of higher density, which can be pelleted at lower speeds. For each combination of transport protein, lipid, and reconstitution technique, it is necessary to empirically determine the centrifugation conditions leading to maximum recovery of the reconstituted structures. The best approach is to first try sedimentation in a microcentrifuge (approx 14,000*g*). If this pellets an insufficient fraction of the vesicles, high-speed centrifugation at up to 40,000*g* should be tried. Finally, for very small vesicles of low density, it may be necessary to pellet the reconstituted structures using an ultracentrifuge or an airfuge. The centrifugation conditions should be adjusted to

recover a large fraction (>90%) of the vesicles (*see* **Subheading 1.6.1.** for a discussion of various methods for measuring lipid and protein recovery). On the other hand, excessively high sedimentation speeds should be avoided, as they will result in a tightly packed pellet that is difficult to resuspend.

8. Resuspend the pellet in the desired buffer at a suitable concentration. Repeated passage of the solution through a syringe with a fine-gage-needle (26G) may help in resuspending the pellet. It is important to obtain a homogeneous suspension at this stage, or further experiments (e.g., of membrane transporter activity) may give unreproducible results.
9. Proteoliposomes are best stored on ice and used immediately for further experiments. Freezing can produce vesicle fusion and aggregation, so if delay is unavoidable, it is recommended that the reconstituted preparation be stored at 4°C. Activity measurements may be made at daily intervals to check the stability of the membrane transport protein under these conditions. Some proteins are remarkably stable once reconstituted and will retain functional activity for days or even weeks at 4°C.

3.2. Reconstitution by Gel Filtration Chromatography

1. Prepare a mixture of dried lipids as in **Subheading 3.1.**, **step 1**.
2. Dissolve the dried lipid in detergent solution (*see* **Subheading 3.1.**, **step 2**). For the gel filtration chromatography technique, the sample volume must be kept reasonably small. For a 1 × 15-cm Sephadex column, a suitable sample volume is less than 1 mL. If a larger sample is being prepared, a proportionately larger column should be used.
3. Mix the lipid–detergent solution with the solution of membrane transporter to be reconstituted, as in **Subheading 3.1.**, **step 3**.
4. Apply the sample to the column, which should be pre-equilibrated in the chosen buffer with no detergent. The column flow rate should be adjusted to approx 0.3 mL/min (about 1 drop every 10 s). Wash the column with buffer and immediately collect approx 10 fractions of about 1 mL volume. The proteoliposomes typically elute in the void volume in two to three fractions. The fractions containing the reconstituted structures can be located visually (they are often turbid) or by measuring the absorbance at 280 nm. Pool the fractions containing proteoliposomes. Detergent micelles will elute just after the proteoliposomes and care should be taken not to include "tail" fractions that might contain detergent, as this will result in leaky vesicles (*see* **Subheading 1.5.2.**).
5. Sediment the proteoliposomes if desired and resuspend in an appropriate buffer (*see* **Subheading 3.1.**, **steps 7** and **8**).

3.3. Reconstitution by Rapid Dilution

1. Prepare a mixture of dried lipids as in **Subheading 3.1.**, **step 1**.
2. Dissolve the dried lipid in detergent solution (*see* **Subheading 3.1.**, **step 2**). For the detergent dilution technique, the sample volume must be kept reasonably small, or the volume of the sample after dilution (*see* **step 4**) may be too large.

3. Mix the lipid–detergent solution with the solution of membrane transporter to be reconstituted, as in **Subheading 3.1.**, **step 3**.
4. Using a syringe with a fine-gage needle (26G), inject the sample into a 50- to 100-fold excess of an appropriate buffer (*see* **Subheading 2.1.**, **item 5**).
5. Collect the reconstituted proteoliposomes by centrifugation and resuspend in an appropriate buffer (*see* **Subheading 3.1.**, **step 7** and **8**). It is highly recommended that this step be carried out if the proteoliposomes are to be used for transport experiments, as it will deplete the preparation of residual detergent that might cause bilayer leakiness. If it is necessary to further reduce the remaining detergent concentration (*see* **Subheading 1.5.5.**), detergent-absorbing beads may also be employed, following the supplier's instructions on their use.

4. Notes

1. Sodium deoxycholate is a commonly used detergent for purification and reconstitution of membrane transporters. It has one drawback: deoxycholate solutions form very viscous gels at pH values less than about 7.8, making chromatography and other experimental manipulations impossible. For this reason, sodium deoxycholate solutions must be carefully buffered to pH values higher than this; it is recommended that the solution pH be at 8.1 and that sufficient buffering capacity be present (e.g., >20 m*M*) to prevent the pH from dropping below 8.0, even transiently.
2. Our laboratory always uses high-quality "fast" dialysis tubing of the same general type as the Spectrapor brand. This tubing allows a relatively rapid rate of detergent removal. Use of lower-quality "regular" dialysis tubing was found to give much more heterogeneous vesicles with some amorphous and aggregated structures.
3. A small sample volume is desirable if the membrane transporter is to be reconstituted by either gel filtration chromatography or dilution, because this keeps the final sample volume in a range that is easy to handle. Sample volume is less important when using the dialysis approach. If the reconstituted proteoliposomes are to be used directly, without concentration by centrifugation and resuspension, then a smaller volume may also be desirable, depending on the experiments to be conducted.
4. If the membrane transporter is known to be sensitive to high concentrations of the chosen detergent, it may be desirable to keep the detergent concentration used to dissolve the lipid as low as is reasonable, because the solubilized membrane transporter solution is added to the lipid–detergent solution, exposing the protein to a high detergent concentration.

References

1. Rigaud, J. L., Pitard, B., and Levy, D. (1995) Reconstitution of membrane proteins into liposomes: application to energy-transducing membrane proteins. *Biochim. Biophys. Acta* **1231,** 223–246.

2. Sharom, F. J., Liu, R., Qu, Q., et al. (2001) Exploring the structure and function of the P-glycoprotein multidrug transporter using fluorescence spectroscopic tools. *Semin. Cell Dev. Biol* **12,** 257–266.
3. Chicken, C. A. and Sharom, F. J. (1983) The concanavalin A receptor from human erythrocytes in lipid bilayer membranes. Interaction with concanavalin A and succinyl-concanavalin A. *Biochim. Biophys. Acta* **729,** 200–208.
4. Campbell, C. D., Ross, T. E., and Sharom, F. J. (1983) Functional reassembly of lymphocyte lentil lectin receptor glycoproteins into lipid bilayer vesicles. *Biochim. Biophys. Acta* **730,** 95–103.
5. Chicken, C.A. and Sharom, F.J. (1984) Lipid-protein interactions of the human erythrocyte concanavalin A receptor in phospholipid bilayers. *Biochim. Biophys. Acta* **774,** 110–118.
6. Sharom, F. J., Head, S., Kupsh, C. C., et al. (1989) Interaction of concanavalin A and a divalent derivative with lymphocytes and reconstituted lymphocyte membrane glycoproteins. *Membr. Biochem.* **8,** 147–163.
7. Chu, J. W. K. and Sharom, F. J. (1992) Glycophorin A interacts with interleukin-2 and inhibits interleukin-2- dependent T-lymphocyte proliferation. *Cell Immunol.* **145,** 223–239.
8. Romsicki, Y. and Sharom, F. J. (1997) Interaction of P-glycoprotein with defined phospholipid bilayers: a differential scanning calorimetric study. *Biochemistry* **36,** 9807–9815.
9. Reid-Taylor, K. L., Chu, J. W. K., and Sharom, F. J. (1999) Reconstitution of the glycosylphosphatidylinositol-anchored protein Thy-1: interaction with membrane phospholipids and galactosylceramide. *Biochem. Cell Biol.* **77,** 189–200.
10. Lehotsky, J., Raeymaekers, L., Missiaen, L., et al. (1992) Stimulation of the catalytic cycle of the Ca^{2+} pump of porcine plasma- membranes by negatively charged phospholipids. *Biochim. Biophys. Acta* **1105,** 118–124.
11. Pinto, F. D. and Adamo, H. P. (2002) Deletions in the acidic lipid-binding region of the plasma membrane Ca^{2+} pump—a mutant with high affinity for Ca^{2+} resembling the acidic lipid-activated enzyme. *J. Biol. Chem.* **277,** 12,784–12,789.
12. McAuley, K. E., Fyfe, P. K., Ridge, J. P., et al. (1999) Structural details of an interaction between cardiolipin and an integral membrane protein. *Proc. Natl. Acad. Sci. USA* **96,** 14,706–14,711.
13. Lu, P., Liu, R., and Sharom, F. J. (2001) Drug transport by reconstituted P-glycoprotein in proteoliposomes—effect of substrates and modulators, and dependence on bilayer phase state. *Eur. J. Biochem.* **268,** 1687–1697.
14. Lehto, M. T. and Sharom, F. J. (1998) Release of the glycosylphosphatidylinositol-anchored enzyme ecto-5'-nucleotidase by phospholipase C: catalytic activation and modulation by the lipid bilayer. *Biochem. J.* **332,** 101–109.
15. Holland, J. W., Cullis, P. R., and Madden, T. D. (1996) Poly(ethylene glycol)-lipid conjugates promote bilayer formation in mixtures of non-bilayer-forming lipids. *Biochemistry* **35,** 2610–2617.
16. Lehto, M. T. and Sharom, F. J. (2002) PI-specific phospholipase C cleavage of a reconstituted GPI-anchored protein: modulation by the lipid bilayer. *Biochemistry* **41,** 1398–1408.

17. Sharom, F. J., Yu, X., and Doige, C. A. (1993) Functional reconstitution of drug transport and ATPase activity in proteoliposomes containing partially purified P-glycoprotein. *J. Biol. Chem.* **268,** 24,197–24,202.
18. Romsicki, Y. and Sharom, F. J. (2001) Phospholipid flippase activity of the reconstituted P-glycoprotein multidrug transporter. *Biochemistry* **40,** 6937–6947.
19. Liu, R. and Sharom, F. J. (1998) Proximity of the nucleotide binding domains of the P-glycoprotein multidrug transporter to the membrane surface: a resonance energy transfer study. *Biochemistry* **37,** 6503–6512.
20. Lehto, M. T. and Sharom, F. J. (2002) Proximity of the protein moiety of a GPI-anchored protein to the membrane surface: a FRET study. *Biochemistry* **4,** 8368–8376.
21. Scotto, A. W. and Zakim, D. (1988) Reconstitution of membrane proteins. Spontaneous incorporation of integral membrane proteins into preformed bilayers of pure phospholipid. *J. Biol. Chem.* **263,** 18,500–18,506.
22. Boulter, J. M., Taylor, A. M., and Watts, A. (1996) Asymmetric and functional reconstitution of band 3 into pre-formed phosphatidylcholine vesicles. *Biochim. Biophys. Acta* **1280,** 265–271.
23. Levy, D., Gulik, A., Bluzat, A., et al. (1992) Reconstitution of the sarcoplasmic reticulum Ca^{2+}-ATPase: mechanisms of membrane protein insertion into liposomes during reconstitution procedures involving the use of detergents. *Biochim. Biophys. Acta* **1107,** 283–298.
24. Simon-Plas, F., Venema, K., Grouzis, J. P., et al. (1991) Spontaneous insertion of plant plasma membrane (H^+)ATPase into a preformed bilayer. *J. Membr. Biol.* **120,** 51–58.
25. Jain, M. K. and Zakim, D. (1987) The spontaneous incorporation of proteins into preformed bilayers. *Biochim. Biophys. Acta* **906,** 33–68.
26. Yang, Q. and Lundahl, P. (1994) Steric immobilization of liposomes in chromatographic gel beads and incorporation of integral membrane proteins into their lipid bilayers. *Anal. Biochem.* **218,** 210–221.
27. Sone, N. and Hinkle, P. C. (1982) Proton transport by cytochrome c oxidase from the thermophilic bacterium PS3 reconstituted in liposomes. *J. Biol. Chem.* **257,** 12,600–12,604.
28. Kasahara, M. and Hinkle, P. C. (1977) Reconstitution and purification of the D-glucose transporter from human erythrocytes. *J. Biol. Chem.* **252,** 7384–7390.
29. Rigaud, J. L., Bluzat, A., and Buschlen, S. (1983) Incorporation of bacteriorhodopsin into large unilamellar liposomes by reverse phase evaporation. *Biochem. Biophys. Res. Commun.* **111,** 373–382.
30. Mayer, L. D., Hope, M. J., and Cullis, P. R. (1986) Vesicles of variable sizes produced by a rapid extrusion procedure. *Biochim. Biophys. Acta* **858,** 161–168.
31. Levy, D., Bluzat, A., Seigneuret, M., et al. (1990) A systematic study of liposome and proteoliposome reconstitution involving Bio-Bead-mediated Triton X-100 removal. *Biochim. Biophys. Acta* **1025,** 179–190.
32. Tortorella, D. and London, E. (1994) Method for efficient pelleting of small unilamellar model membrane vesicles. *Anal. Biochem.* **217,** 176–180.

33. Nanjee, M. N., Gebre, A. K., and Miller, N. E. (1991) Enzymatic fluorometric procedure for phospholipid quantification with an automated microtiter plate fluorometer. *Clin. Chem.* **37,** 868–874.
34. Itoh, Y. H., Itoh, T., and Kaneko, H. (1986) Modified Bartlett assay for microscale lipid phosphorus analysis. *Anal. Biochem.* **154,** 200–204.
35. Peterson, G. L. (1977) A simplification of the protein assay method of Lowry et al. which is more generally applicable. *Anal. Biochem.* **83,** 346–356.
36. Thomas, P. D. and Poznansky, M. J. (1989) Curvature and composition-dependent lipid asymmetry in phosphatidylcholine vesicles containing phosphatidylethanolamine and gangliosides. *Biochim. Biophys. Acta* **978,** 85–90.
37. Chen, C. C. and Wilson, T. H. (1984) The phospholipid requirement for activity of the lactose carrier of *Escherichia coli*. *J. Biol. Chem.* **259,** 10,150–10,158.
38. Sharom, F. J., DiDiodato, G., Yu, X., et al. (1995) Interaction of the P-glycoprotein multidrug transporter with peptides and ionophores. *J. Biol. Chem.* **270,** 10,334–10,341.

10

Equilibrium Binding and Transport Studies

Ana M. Ojeda, Dawn T. Bravo, Terry L. Hart, and Stanley M. Parsons

1. Introduction

One way to characterize structure and function in transporters is chemical. The analysis specifies the three-dimensional structure of the transporter and changes in structure that occur during the transport cycle. It can ignore intermediate steps in the cycle by showing only reactants and products, or it can show intermediates as well. Such analysis is called the *chemical mechanism* of transport.

Another way to characterize structure and function in transporters is mathematical. The analysis quantitates the amount of transporter present and the rate of transport. Like the chemical description, the mathematical description can ignore intermediate steps in the transport cycle or it can provide mathematical relationships for them as well. Such analysis is called the *kinetic mechanism* of transport. Knowledge of the kinetic mechanism is valuable because it, sometimes, can be used to infer chemical mechanism and should be consistent with physiology. An inconsistency would suggest that additional biochemical work on the system remains to be done.

This chapter describes characterization of expressed rat vesicular acetylcholine transporter (rVAChT) by mathematical means. VAChT in cholinergic nerve terminals stores ACh in synaptic vesicles by exchanging vesicular protons for cytoplasmic ACh ***(1)***. Protons are supplied by vacuolar ATPase that acidifies vesicular lumen. Rand and his colleagues ***(2)*** cloned the gene encoding VAChT in 1993. VAChT is a member of the major facilitator superfamily and probably possesses 12 helical transmembrane domains.

The VAChT is a secondary active transporter, which means that an energetically favorable flow of a common ion (in this case, the proton) is coupled to pumping of a specific substrate. Unlike enzymes, primary active transport-

From: *Methods in Molecular Biology, vol. 227: Membrane Transporters: Methods and Protocols*
Edited by: Q. Yan © Humana Press Inc., Totowa, NJ

ers and group translocators, secondary active transporters, do not alter covalent bonding in substrates. The lack of covalent change and current difficulty in determining high-resolution structure decrease the range of tools available to study chemical mechanism. By default, characterization of kinetic mechanism is currently a major avenue to a better understanding of many secondary active transporters. This is true even when combined with site-directed mutagenesis and expression (which are decidedly chemical techniques), as in most cases, the change in kinetic behavior of mutated transporter is all that can be characterized. The study of the effects of mutations on VAChT properties recently began ***(3–5)***.

The chapter presents a schematic diagram of the filter manifold (*see* **Fig. 2**) we use to conduct assays of binding and transport of radiolabeled ligand by VAChT. The free ligand is separated from the tightly bound or transported ligand by rapid filtration and washing. The schematic should allow professional machinists to replicate the device (*see* **Subheading 3.1.**). Although other filter boxes and microtiter-like manifolds are available commercially, this design provides ease of use and superior data at relatively low cost.

Cloned *VAChT* expresses well in $PC12^{A123.7}$ cells, which are a rat pheochromocytoma line. The cells grow rapidly and, unlike the parental PC12 cells, do not express endogenous VAChT ***(6)***. The chapter details the procedure we use to grow a sufficient number of $PC12^{A123.7}$ cells (**Subheading 3.2.**) to characterize one type of VAChT in one type of measurement, such as characterization of wild-type VAChT by saturation of ACh active transport. The chapter also details procedures used to transiently transfect cells with expression vector (**Subheading 3.3.**), harvest expressing cells and prepare postnuclear supernatant (**Subheading 3.4.**), determine amounts of binding at different concentrations of the allosteric, inhibitory compound [^{3}H]vesamicol (**Subheading 3.5.**), determine amounts of transport at different concentrations of [^{3}H]ACh (**Subheading 3.6.**), analyze transport and binding data by regression (**Subheading 3.7.**), and interpret the results (**Subheading 3.8.**).

Three components in total transport (or binding) can be recognized. The first is nonspecific transport (or binding), which is nonsaturable and directly proportional to the concentration of radiolabeled ligand. The second component is apparent transport (or binding) contributed by host cell membranes or introduction of an expression vector. This component may or may not be saturable, but experience has suggested that it is. The third component is specific transport (or binding) carried out by VAChT. This component is saturable. To determine the contributions of the three components, both total and nonspecific transport (or binding) should be determined using postnuclear supernatants prepared from cells transfected with VAChT and from cells transfected with control vector.

2. Materials

2.1. Construction of the 20-Station Filter Manifold and Box

2.1.1. Manifold

1. Polyvinylchloride, 4.5 × 18.5 × 1 in. thick.
2. Teflon fluoropolymer 0.5 in. diameter × 48 in. long.
3. Black Delrin, 0.75 in diameter × 18 in.
4. Nylon 3/16 in. × 24 in.
5. 316 Stainless-steel round stock, 1.5 in. diameter × 40 in.
6. Stainless-steel perforated sheet, 6 × 6 × 0.020 in. thick × 0.030 in. diameter perforations.
7. Stainless-steel tubing 0.25 in. outer diameter × 0.028 in. wall × 24 in.
8. One vacuum gauge.
9. Twenty Viton O-rings (e.g., Parker #2-12).

2.1.2. Acrylic Drain Box and Base

1. Acrylic sheet, 1 × 6.0 × 20 in.
2. Acrylic sheet, 0.5 × 24 × 24 in.
3. Silicon rope, 1/8 in. diameter × 48 in. (approx).

2.2. Growth of $PC12^{A123.7}$ Cells

All of the cell culture media and reagents are obtained from Gibco/Life Technologies. If you are purchasing from other vendors, use tissue-culture-grade reagents. Preparation and use of media should be done under sterile conditions in a laminar flow cabinet.

1. Laminar flow cabinet, CO_2 incubator.
2. Waste trap: Vacuum tubing, one-hole rubber stopper, 4-L vacuum flask, bleach.
3. 2-, 10-, and 25-mL Sterile, cotton-plugged serological pipets.
4. Portable hand-held pipettor (e.g., Drummond; cat. no. 4-000-101).
5. Fine-pointed forceps.
6. Disposable bottle-top filters with 0.22-µm polyethersulfone membrane (e.g., Millipore; cat. no. SCGPT10RE).
7. T-150 flasks: 150-cm^2 Treated polystyrene cell culture flasks with vent cap (0.2-µm filter) and canted neck (e.g., Corning; cat. no. 430825).
8. Complete medium (1 L): 15.6 g DMEM (Dulbecco's modified Eagle's medium)/F-12 Nutrient mixture and 1.2 g $NaHCO_3$ are dissolved in 1 L of distilled water. The pH is adjusted to 7.4 with 1 *M* NaOH, filter-sterilized, and stored at 4°C until used. Before use, 840 mL is mixed with 100 mL fetal bovine serum, 50 mL horse serum, and 10 mL pen/strep (10,000 U penicillin/mL and 10,000 µg streptomycin/mL). Complete medium can be stored at 4°C but should be used within 1 wk.
9. Trypsin–EDTA solution: 2.5 g/L Trypsin, 0.38 g/L EDTA tetrasodium salt in Hanks' balanced salt solution without $CaCl_2$, $MgCl_2$ hexahydrate, and $MgSO_4$ heptahydrate (e.g., Gibco/Life Technologies; cat. no. 25200056). Store at 4°C.

2.3. Transient Expression

1. $PC12^{A123.7}$ cells: sixteen T-150 flasks of cells or 2.4×10^8 cells per type of DNA to be expressed.
2. TE buffer: 10 m*M* Tris-HCl, 1 m*M* EDTA, pH 8.0.
3. pcDNA3.1D/rVAChT and expression control vector (Invitrogen/Life Technologies, cat. no. K49000-01) dissolved in TE buffer at a concentration of 2.5 mg/mL.
4. 2-, 10-, and 25-mL Sterile, cotton-plugged serological pipets.
5. Portable hand-held pipettor.
6. Complete medium (*see* **Subheading 2.2.**, **item 8**).
7. Trypsin–EDTA solution (*see* **Subheading 2.2.**, **item 9**).
8. 50-mL Polypropylene conical tubes, sterile.
9. 200- and 1,000-µL Pipet tips, sterile.
10. Benchtop centrifuge with swing-out rotor, capacity 4×50 mL.
11. Phosphate-buffered saline (PBS), pH 7.4: 1.06 m*M* KH_2PO_4, 155.17 m*M* NaCl, and 2.96 m*M* Na_2HPO_4 (e.g., Gibco Cell Culture; cat. no. 10010). Store at 4°C.
12. 1.5-mL Microcentrifuge tubes.
13. Hemacytometer.
14. Electroporation cuvets with a gap of 0.4 cm (e.g., Bio-Rad; cat. no. 165-2088).
15. Electroporator (e.g., Bio-Rad, Gene Pulser II).
16. 148-cm^2 Treated polystyrene cell culture dishes (e.g., Corning; cat. no. 430599).

2.4. Preparation of Postnuclear Supernatants

1. Protease inhibitor cocktail: Dissolve one tablet (e.g., Roche; cat. no. 1873580) in 2 mL of distilled water. This makes a 25-fold stock solution. Aliquot in 50-µL portions. Store at –20°C.
2. Phenylmethyl sulfonyl fluoride (PMSF): 200 m*M* PMSF (e.g., Sigma; cat. no. P7626) in isopropanol. This makes a 1000-fold stock solution. Store at room temperature.
3. Paraoxon: 100 m*M* Paraoxon (e.g., Sigma; cat. no. D9286) in isopropanol. This makes a 1000-fold stock solution. Store at 4°C.
4. Homogenization buffer (1 mL): One microliter of 200 m*M* PMSF (*see* **Subheading 2.4.**, **item 2**) and 1 µL of 100 m*M* paraoxon (*see* **Subheading 2.4.**, **item 3**) in isopropanol are evaporated to dryness under nitrogen in a microcentrifuge tube shortly before use. One milliliter of 0.32 *M* sucrose and 10 m*M* *N*-2-hydroxyethylpiperazine-*N*'-2-ethanesulfonic acid (HEPES), adjusted to pH 7.4 with 1 *M* KOH), and 40 µL protease inhibitor cocktail (*see* **Subheading 2.4.**, **item 1**) are added and the solution is mixed vigorously. Prepare fresh before use.
5. Motor-driven, 5-mL Potter–Elvejhem (Delrin AF-glass) homogenizer, with a pestle clearance of 0.100–0.115 mm.
6. Disposable transfer pipets (e.g., Fisher; cat. no.13-711-9A).
7. 1.5- and 2-mL Microcentrifuge tubes.
8. 0.4 % Trypan blue solution (e.g., Sigma Cell Culture; cat. no. T8154).
9. Microscope.
10. Liquid nitrogen, tongs.

2.5. Equilibrium Binding of Vesamicol

1. Glass microfiber filter circles, GF/F 1.3-cm diameter (e.g., Whatman; cat. no. 18250134).
2. 0.5% (w/v) Polyethylenimine: Dissolve 5 g of 50% (w/v) polyethylenimine aqueous solution (e.g., Sigma; cat. no. P3143) in 500 mL of distilled water.
3. 186-mm-Diameter Büchner filter funnel (e.g., Fisher; cat. no. 10-356H).
4. Uptake-binding buffer (UBB): 110 m*M* Potassium tartrate, 20 m*M* HEPES adjusted to pH 7.4 with 1.0 *M* KOH, and 1 m*M* ascorbic acid. Store at 4°C.
5. [^{3}H]Vesamicol, 30–60 Ci/mmol in ethanol, 1 mCi/mL (e. g., Perkin-Elmer; cat. no. NET964). Store at –20°C.
6. [^{3}H]Vesamicol solution A (SolA): Pipet 15 µL of [^{3}H]vesamicol (*see* **Subheading 2.5.**, **item 5**) into a 1.5-mL microcentrifuge tube (*see* **Note 1**). Carefully evaporate the ethanol to dryness under a stream of nitrogen in a chemical fume hood. Add 300 µL of UBB (*see* **Subheading 2.5.**, **item 4**) and mix the contents thoroughly. Allow to equilibrate with occasional mixing for 30 min, then transfer the solution to a fresh microcentrifuge tube (*see* **Note 2**). Store at –20°C.
7. [^{3}H]Vesamicol solution B (SolB): Mix 50 µL SolA (*see* **Subheading 2.5.**, **item 6**) with 450 µL of UBB (*see* **Subheading 2.5.**, **item 4**) to dilute 10-fold. Store at –20°C.
8. Scintillation vials and scintillation cocktail.
9. Scintillation counter.
10. Filter manifold (*see* **Fig. 1**).
11. 0.80 m*M* Vesamicol: Dissolve 2.16 mg (–)-vesamicol HCl (e.g., Sigma; cat. no. V-101) in 9.12 mL UBB (*see* **Subheading 2.5.**, **item 4**). Store at –20°C.
12. Twenty 1.5-mL microcentrifuge tubes; 10 labeled T for total binding and 10 labeled NS for nonspecific binding. Label each tube in each set 0, 2, 4, 8, 12, 20, 40, 100, 200, or 400 for the concentrations (in n*M*) of [^{3}H]vesamicol that will be present.
13. P-5000 Gilson pipet and tips.
14. Fine-pointed forceps.

2.6. Transport of ACh

1. Paraoxon-treated UBB (50 mL): Pipet 50 µL of 100 m*M* paraoxon (*see* **Subheading 2.4.**, **item 3**) into a 50-mL conical tube. Evaporate the isopropanol to dryness under a stream of nitrogen. Add 50 mL of UBB (*see* **Subheading 2.5.**, **item 4**). Mix thoroughly and incubate at room temperature for 30 min. Prepare fresh before use and keep on ice.
2. UBB/ATP (10 mL): Transfer 10 mL of paraoxon-treated UBB (*see* **Subheading 2.6.**, **item 1**) to a 50-mL conical tube. Add 50.7 mg of magnesium ATP (e.g., Sigma; cat. no. A9187) and 8 µL of 4.9 *M* magnesium chloride hexahydrate (e.g., Sigma; cat. no. 104-20). Mix thoroughly and adjust to pH 7.4 with 1 *M* KOH. Prepare fresh before use and keep on ice.
3. 80 µ*M* Vesamicol: Pipet 50 µL of 0.80 m*M* vesamicol (*see* **Subheading 2.5.**, **item 11**) into a 1.5-mL microcentrifuge tube. Add 450 µL of paraoxon-treated UBB (*see* **Subheading 2.6.**, **item 1**). Store at –20°C.

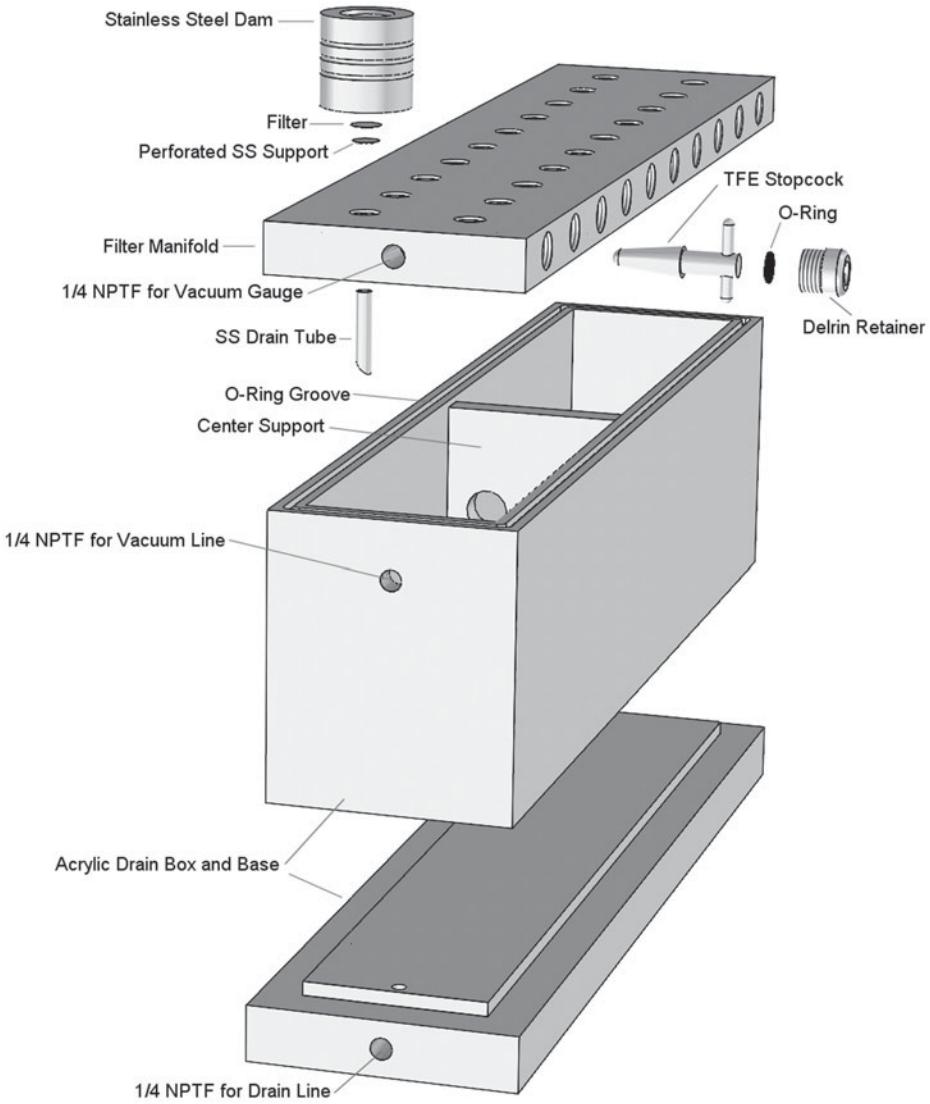

Fig. 1. Overview of filter manifold.

4. [^{3}H]ACh iodide, [acetyl-^{3}H], 50–100 mCi/mmol (e.g., Perkin-Elmer; cat. no. NET113). Store at 4°C.
5. [^{3}H]ACh Solution C (SolC): Dissolve 1 mCi of [^{3}H]ACh iodide in 1 mL of ethanol. Mix thoroughly. Store at –20°C.
6. [^{3}H]ACh Solution D (SolD): Pipet 20 µL of SolC (*see* **Subheading 2.6.**, **item 5**) into a 1.5-mL microcentrifuge tube. Add 180 µL of ethanol. Store at –20°C.

7. Eighty 1.5-mL microcentrifuge tubes; 40 labeled T for total transport and 40 labeled NS for nonspecific transport. Label each tube (in each one of eight sets) 0, 15, 30, 60, 100, 150, 300, 750, 1500, or 3000 for the concentration (in μ*M*) of [^{3}H]ACh that will be present.
8. Filter manifold (*see* **Fig. 1**).
9. Stainless-steel dams (*see* **Fig. 1**).
10. Sodium dodecyl sulfate (SDS) solution: 1% (w/v) SDS in distilled water. Store at room temperature.
11. P-5000 and P-1000 Gilson pipets and tips.
12. Fine-pointed forceps.

2.7. Data Reduction and Model Fitting

Scientist software from Scientific Instrument Services Inc. (http://www.sisweb.com/software/math.htm).

3. Methods

3.1. Construction of the 20-Station Filter Manifold and Box

1. The base for the drain box is machined to 18.75 × 4.75 in. from a 1-in. acrylic sheet.
2. A step 17.25 × 3.25 × 0.25 in. high is then machined to locate the drain box on the base and provide for leak proof gluing of the sidewalls.
3. Drill a 0.25-in. drain hole in the bottom of the base. Drill and tap a 0.25-in. female pipe thread hole from the side edge to meet the drain hole. This will provide for a drain valve in the base.
4. Mill two plates of 0.5-in.-thick acrylic sheet to 18.25 × 5.00 in. and two plates to 3.25 × 5.0 in.
5. Drill and tap a 0.25-in. female pipe thread hole approx 1 in. from the top edge of one of these side wall plates to provide for a vacuum connection. The sidewalls and base of the box are fused using methylene chloride.
6. Mill one plate of 0.5-in.-thick acrylic sheet to 3.25 × 4.625 in.
7. Drill six 0.75-in.-diameter holes in the plate and a step along the bottom edge of the plate to allow passage of fluid in the box.
8. Glue this plate in the center of the box to prevent deformity of the sidewalls because of vacuum pressure.
9. After gluing and testing the box for leaks, mill a 0.140-in.-wide by 0.105-in.-deep O-ring groove into the top edge of the box.
10. From 1/8-in.-diameter silicon rope, cut a length appropriate for groove and splice with Loctite 411 or equivalent adhesive.
11. Machine Delrin-retaining ring and Teflon stopcock (see detail B-B in **Fig. 2**). Assemble and set aside.
12. The filter manifold is machined to 18.375 × 4.375 in. from 1 in. thick polyvinyl-chloride.
13. Bore holes in side edges to 0.625 in. diameter by 0.650 in. deep and tap 11/16-16 thread × 7/16 in. deep in 20 places.

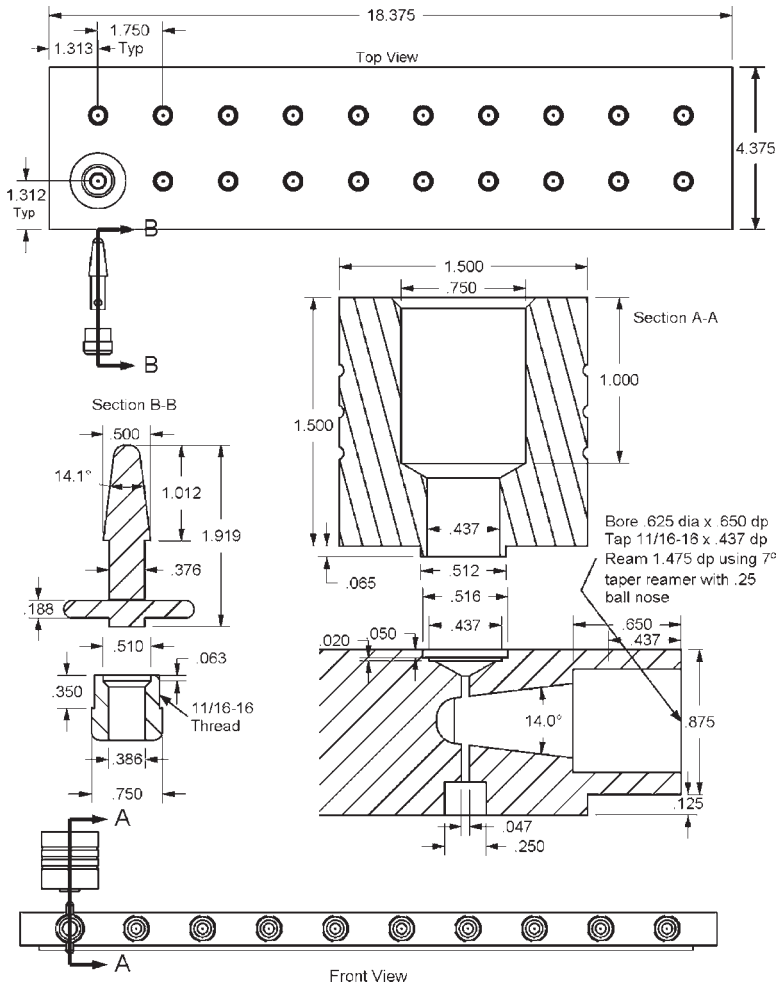

Fig. 2. Detailed schematic of filter manifold components.

14. Ream 1.475 in. deep using 7° taper reamer with 0.25-in. ball end for stopcock (*see* detail A-A in **Fig. 2**). Install stopcock assembly securely into each station.
15. Orient 3/16-in. nylon stopcock handle in upright (open) position and mill detail for stainless-steel dam and filter support into top surface of manifold.
16. Drill 3/64-in. hole through manifold and stopcock. Turn manifold over and drill 0.25-in. hole for stainless-steel drain tube.
17. Remove stopcock assemblies and machine step to fit filter drain box in bottom of manifold. This step is performed last to mitigate possible stress-relief warping of the polyvinyl chloride during previous machining operations.

18. Cut 20 pieces 1.5-in. diameter by 1.62 in. long from 316 stainless-steel round stock. Drill 0.75-in. and 0.437-in. holes (see detail A-A in **Fig. 2**). These holes should be finish bored for smoothness to minimize retention of radioactive materials.
19. Machine 0.512 × 0.065-in. detail in one end. Grooves may be machined into the outside diameter of the dam to afford better grip when pieces are wet.
20. Punch 20 disks, 0.437 in. in diameter from 0.020-in.-thick stainless-steel perforated sheet. Press disks into 0.437 × 0.020 in. deep counter bore in top of manifold (*see* detail A-A in **Fig. 2**).

3.2. Growth of PC12$^{A123.7}$ Cells

Cells are grown on T-150 flasks (*see* **Subheading 2.2.**, **item 7**) and maintained in 10% CO_2 at 37°C in complete medium (*see* **Subheading 2.2.**, **item 8**). Cells are split at confluency every 72–96 h (*see* **Note 3**). All media are at 37°C before cells are exposed to them unless otherwise indicated. Employ rigorous sterile technique throughout the following procedures.

1. Using a 2-mL pipet attached to the vacuum tubing leading to the waste trap (*see* **Subheading 2.2.**, **item 2**), aspirate the medium (*see* **Note 4**). Living cells remain attached to the surface of the flask.
2. Add 4 mL of trypsin/EDTA (*see* **Subheading 2.2.**, **item 9**) per T-150 flask. Gently rock the flask by hand to expose all cells to trypsin. Lay the flask horizontally with the beveled face on the bottom for 5 min at room temperature (*see* **Note 5**).
3. Add 16 mL of complete medium to the flask. Resuspend the cells by pipetting the medium up and down several times onto the surface of the flask to detach cells still adhering to the plastic.
4. Immediately after resuspending the cells before they settle significantly, pipet 10 mL of the suspension into a new T-150 flask. Add 40 mL of complete medium to both flasks. Screw caps on the flasks. Transfer the flasks to the incubator with the beveled face of the flask facing down (*see* **Note 6**).
5. After 48 h, aspirate the medium to waste and add 50 mL of complete medium to each flask. If cells are not confluent, replace the medium again after 72 h (*see* **Note 3**).
6. At confluency, either split the cells again or proceed to **Subheading 3.3** if enough flasks of cells are available. It is desirable always to have multiple flasks of cells growing.

3.3. Transient Expression

1. Trypsinize cells from 16 T-150 flasks as described in **steps 1** and **2** of **Subheading 3.2.**
2. In two steps, transfer the cells from one flask using a 10-mL pipet and the PipetAid to a 50-mL conical tube. Combine cells from the two flasks into one conical tube. Cap the tubes and centrifuge at 800*g* for 10 min at room temperature.

3. Aspirate the medium to waste and add 10 mL of ice-cold PBS (*see* **Subheading 2.3., item 11**) to each cell pellet. Resuspend cells by pipetting up and down several times using a 10-mL pipet that has a 1000-µL disposable tip attached to it (*see* **Note 7**). Combine four of these suspensions into the same conical tube and cap the tube. There should be two tubes at this point.
4. Centrifuge the tubes at 800*g* for 10 min at room temperature.
5. Aspirate the supernatant to waste and add 10 mL of ice-cold PBS to the pellet. Resuspend cells as earlier and combine cells from both tubes into a single tube. Cap the tube. Using water, assemble a tube weighing the same for a counter balance.
6. Centrifuge the tubes at 800*g* for 10 min at room temperature.
7. Aspirate the supernatant to waste and resuspend cells in 8 mL of ice-cold PBS using a 10-mL pipet that has a 1000-µL disposable tip attached to it. Measure the volume of the suspension using the pipet and add more PBS as necessary to a final volume of 10 mL. Immediately after resuspending cells, take a 50-µL sample and transfer it to a 1.5-mL microcentrifuge tube.
8. Centrifuge the cell suspension at 800*g* for 10 min at room temperature. While the cells are centrifuging, place four or five electroporation cuvets (*see* **Subheading 2.3., item 14**) on ice and determine the cell density.
9. Pipet 10 µL of the 50 µL of resuspended cells into another microcentrifuge tube, add 290 µL of PBS to dilute 30-fold, and gently mix well.
10. Immediately load 10 µL of diluted cells into the hemacytometer (*see* **Subheading 2.3., item 13**) by capillarity and place the hemacytometer under a microscope. Count the number of cells on the four squares located at the four corners of the hemacytometer (*see* **Note 8**). Average the counts. This is the number of cells in 0.1 mm^3. To obtain cells/mL, multiply the average by 10^4 and the dilution factor.
11. Aspirate the supernatant to waste and resuspend cells in 3 mL of ice-cold PBS using a 10-mL pipet that has a 1000-µL disposable tip attached to it. Measure the volume of the suspension with the pipet and add more PBS as necessary to achieve a density about 6×10^7 cells/mL (*see* **Note 9**).
12. Pipet 800 µL of cell suspension to each prechilled electroporation cuvet. Add 50 µg of DNA (*see* **Subheading 2.3., item 3**) to each cell suspension, gently mix by pipetting up and down, and incubate the suspensions on ice for 10 min. Place 10 mL complete medium into each of four or five conical tubes at room temperature.
13. Dry the outside of a chilled cuvet, place it in the electroporator (*see* **Subheading 2.3., item 15**), and electroporate the cells (0.2 kV, 1.4 mF). Place the cuvet back in ice. Repeat the procedure with the other cuvets. Using a 2-mL pipet with a 200-µL disposable tip attached to it, take 1 mL of complete medium from a conical tube and transfer it to a cuvet. Carefully mix the contents of the cuvet by pipetting up-and-down and transfer the suspension to the conical tube (*see* **Note 10**). Withdraw 1 mL of complete medium from the conical tube while avoiding cellular debris, add it to the cuvet, pipet up and down several times, and transfer the wash to the conical tube.

14. Using a 10-mL pipet, mix the contents of the conical tube. Immediately transfer 5-mL portions into two polystyrene dishes (*see* **Subheading 2.3.**, **item 16**). Add 45 mL of complete medium to each dish and place the dishes in an incubator. Incubate the dishes for 24 h, after which the medium should be replaced. Replace the medium again after 48 h. At 72 h after electroporation, proceed to **Subheading 3.4.** A total of 8–10 dishes will be available for each DNA type.

3.4. Preparation of Postnuclear Supernatants

1. Trypsinize transfected cells, transfer them to a conical tube, centrifuge them, and wash them twice in ice-cold PBS as outlined in **steps 1–6** in **Subheading 3.3.** Aspirate the supernatant to waste. From this point forward, work should be done in the cold.
2. Using repetitive pipetting, resuspend the cell pellet in the conical tube in 800 µL homogenization buffer (*see* **Subheading 2.4.**, **item 4**).
3. Transfer the cell suspension into a prechilled Potter–Elvejhem homogenizer vessel (*see* **Subheading 2.4.**, **item 5**). Add 250 µL of homogenization buffer to the conical tube, pipet up and down, and transfer the wash to the homogenizer vessel to give a final volume of approx 1.5 mL. With the pestle speed at 800 rpm, homogenize cells using three up-and-down strokes.
4. Using a disposable transfer pipet, transfer the homogenate to a prechilled 2-mL microcentrifuge tube. Pipet 10 µL of the homogenate into a 1.5-mL microcentrifuge tube. Add 90 µL of PBS and 100 µL of 0.4% trypan blue (*see* **Subheading 2.4.**, **item 8**). Mix and wait 5 min. Using the hemacytometer, count the total number of cells and the number of stained cells. Cell viability should be about 5% (*see* **Note 11**).
5. Centrifuge the homogenate in the 2-mL microcentrifuge tube at 800*g* for 10 min at room temperature.
6. Carefully decant postnuclear supernatant into a 1.5-mL microcentrifuge tube. Remove a 10-µL portion and determine the concentration of protein using a standard assay (*see* **Note 12**).
7. Quick-freeze the resulting postnuclear supernatant by immersing the closed microcentrifuge tube in liquid nitrogen using tongs. Store the supernatant at –80°C until use (*see* **Note 13**).

3.5. Equilibrium Binding of Vesamicol

Saturation curves for radiolabeled ligands are obtained by determining two types of binding. The first is total binding, which is obtained in the presence of different concentrations of radiolabeled ligand. It includes specific binding to the site of interest and nonspecific binding to other components in the postnuclear supernatant and the filters used in the assay. The second type of binding is nonspecific, which is determined in the presence of radiolabeled ligand and a 100-fold excess of nonradioactive ligand relative to the highest concentration of radiolabeled ligand that is used. Nonradioactive ligand com-

petes with radiolabeled ligand and reduces binding of radiolabeled ligand to the specific site by 100-fold but does not affect binding of radiolabeled ligand to nonspecific sites. These sites behave as if they are present in very large amount but have very low affinity that is not saturated by the excess nonradioactive ligand. The specific binding component of total binding is obtained by subtracting nonspecific binding from total binding. The following procedure provides the information required to determine the saturation curve for specific binding of [^{3}H]vesamicol to rat vesicular acetylcholine transporter (rVAChT).

1. Filters (*see* **Subheading 2.5.**, **item 1**) are treated several days in advance of need by incubating them in 0.5% (w/v) polyethylenimine (*see* **Subheading 2.5.**, **item 2**) in water for 2 h, after which they are copiously rinsed on a large Büchner filter funnel (*see* **Subheading 2.5.**, **item 3**) with distilled water. They are dried overnight at 80°C and stored in a plastic bag in the dark.
2. Pipet 1 µL of [^{3}H]vesamicol SolA (*see* **Subheading 2.5.**, **item 6**) into a scintillation vial containing 3.5 mL of scintillation cocktail and count radioactivity for 1 min. Calculate the chemical concentration from the specific radioactivity and the efficiency of the scintillation counter (*see* **Note 14**). The concentration of [^{3}H]vesamicol in SolA should be about 1.5 µ*M*.
3. Add 10 µL of 0.80 m*M* nonradioactive vesamicol (V) (*see* **Subheading 2.5.**, **item 11**) to each of 10 microcentrifuge tubes labeled NS (*see* **Subheading 2.5.**, **item 12**).
4. Calculate the volumes of [^{3}H]vesamicol SolA and SolB (*see* **Subheading 2.5.**, **items 6** and **7**) required to yield 200 µL of 0, 2, 4, 8, 12, 20, 40, 100, 200, and 400 n*M* solutions in [^{3}H]vesamicol ([^{3}H]V). For example, assuming that SolA is 1.5 µ*M* in [^{3}H]vesamicol, the top part of **Table 1** gives the volumes required. Add these volumes of SolA and SolB to the 10 microcentrifuge tubes labeled NS. Calculate the volume of UBB required to bring the reaction volume to 200 µL, as shown in the top part of **Table 1** for nonspecific binding. Pipet these volumes into the NS tubes. Calculate the volume of postnuclear supernatant (PS) containing 100 µg of protein. For example, assuming that PS contains 12.5 mg protein/mL (*see* **Subheading 3.4.**, **step 6**), 8 µL of PS will be required, as shown in **Table 1**. Pipet this volume into each NS tube and mix the contents by pipetting up and down. Place the tubes in a 37°C water bath and equilibrate them for 30 min.
5. The top of the filter manifold (*see* **Subheading 2.5.**, **item 10**) should be well washed before each use to avoid contamination from previous experiments. While the samples are incubating, place 20 treated filters (*see* **Subheading 3.5.**, **step 1**) on the filter supports and label the filter positions with the appropriate concentrations of [^{3}H]vesamicol. Apply 500 µL UBB to each filter.
6. Open a stopcock on one of the filters. Apply 90 µL of one sample onto the filter making sure to spread membranes across the filter as the sample is pulled through.

Table 1
Vesamicol Binding

[^{3}H]V (n*M*)	V (µL)	SolA (µL)	SolB (µL)	UBB (µL)	PS (µL)
		Nonspecific binding			
0	10	0	0	182.0	8
2	10	0	2.7	179.3	8
4	10	0	5.3	176.7	8
8	10	0	10.7	171.3	8
12	10	0	16.0	166.0	8
20	10	0	26.7	155.3	8
40	10	5.3	0	176.7	8
100	10	13.3	0	168.7	8
200	10	26.6	0	155.4	8
400	10	53.3	0	128.7	8
		Total binding			
0	0	0	0	192.0	8
2	0	0	2.7	189.3	8
4	0	0	5.3	186.7	8
8	0	0	10.7	181.3	8
12	0	0	16.0	176.0	8
20	0	0	26.7	165.3	8
40	0	5.3	0	186.7	8
100	0	13.3	0	178.7	8
200	0	26.6	0	165.4	8
400	0	53.3	0	138.7	8

Immediately apply 4 mL of ice-cold UBB across the full surface of the filter using a P-5000 Gilson pipet at a rate that keeps the full surface of the filter wet but does not result in overflow.

7. Repeat **step 6** of **Subheading 3.5.** using another 90-µL portion of the same sample and a different filter.
8. Repeat **steps 6** and **7** of **Subheading 3.5.** for every sample.
9. Wait several minutes until all excess buffer has been pulled through before closing the stopcock. Remove filters using fine-pointed forceps and transfer them to appropriately labeled scintillation vials containing 3.5 mL of scintillation cocktail in each. Vortex the vials briefly.
10. Count each vial for 1 min for immediate feedback and for 10 min for accurate measurements.
11. Repeat **steps 4–10** of **Subheading 3.5.** replacing NS by T and using the volumes given in the bottom part of **Table 1** for total binding.

Table 2
ACh Transport

	Set 1			Set 2		
[^{3}H]ACh (μ*M*)	SolC (μL)	SolD (μL)	UBB/ATP (μL)	V (μL)	UBB (μL)	PS (μL)
			Nonspecific Transport			
0	0	0	100	10	70	20
15	0	3	100	10	70	20
30	0	6	100	10	70	20
60	0	12	100	10	70	20
100	0	20	100	10	70	20
150	3	0	100	10	70	20
300	6	0	100	10	70	20
750	15	0	100	10	70	20
1500	30	0	100	10	70	20
3000	60	0	100	10	70	20
			Total Transport			
0	0	0	100	0	80	20
15	0	3	100	0	80	20
30	0	6	100	0	80	20
60	0	12	100	0	80	20
100	0	20	100	0	80	20
150	3	0	100	0	80	20
300	6	0	100	0	80	20
750	15	0	100	0	80	20
1500	30	0	100	0	80	20
3000	60	0	100	0	80	20

3.6. Transport of ACh

1. Pipet 1 μL [^{3}H]ACh SolC (*see* **Subheading 2.6.**, **item 5**) into a scintillation vial containing 3.5 mL of scintillation cocktail and count radioactivity for 1 min. Calculate the chemical concentration (*see* **Note 14**). The concentration of [^{3}H]ACh in SolC should be about 10 m*M*.
2. Calculate the volumes of [^{3}H]ACh SolC and SolD (*see* **Subheading 2.6.**, **items 5** and **6**) required to yield 200 μL of 0, 15, 30, 60, 100, 150, 300, 750, 1500, and 3000 μ*M* solutions in [^{3}H]ACh. For example, assuming that SolC is 10 m*M* in [^{3}H]ACh, **Table 2** gives the volumes required. Pipet SolC into the 150, 300, 750, 1500, and 3000 μ*M* microcentrifuge tubes (Set 1) labeled NS (*see* **Subheading 2.6.**, **item 7).** Pipet SolD into the 15, 30, 60, and 100 μ*M* microcentrifuge tubes

(Set 1) labeled NS. Carefully evaporate the ethanol to dryness under a stream of nitrogen in a chemical fume hood.

3. Add 10 µL of 80 µ*M* nonradioactive vesamicol (V) (*see* **Subheading 2.6.**, **item 3**) to each of 10 microcentrifuge tubes (Set 2) labeled NS (*see* **Subheading 2.6.**, **item 7**).
4. Calculate the volume of paraoxon-treated UBB (*see* **Subheading 2.6.**, **item 1**) required to bring the reaction volume to 100 µL, as shown in the top part of **Table 2** for nonspecific transport. Pipet these volumes into the NS tubes (Set 2). Calculate the volume of PS containing 250 µg of protein. For example, assuming that the PS contains 12.5 mg protein/mL, 20 µL of PS will be required, as shown in **Table 2**. Pipet this volume into each NS tube (Set 2) and mix the contents by pipetting up and down. Place the 10 tubes in a 37°C water bath at the same time and equilibrate them for 15 min. Immediately proceed to next step.
5. Add 100 µL of paraoxon-treated UBB/ATP (*see* **Subheading 2.6.**, **item 2**) to each tube in Set 1. Mix thoroughly.
6. After 15 min incubation of membranes at 37°C, pulse-centrifuge the 10 NS microcentrifuge tubes in Set 2 and pipet the contents of each one into corresponding tubes in Set 1. Mix by pipetting up and down. Place the tubes in a 37°C water bath and equilibrate them for 10 min.
7. While the samples are incubating, place 20 treated filters on the filter supports and label the filter positions with the appropriate concentrations of [^{3}H]ACh. Apply 500 µL UBB to each filter. Wait several minutes. Put the metal dams in place (*see* **Fig. 1**).
8. Place 20 1.5-mL microcentrifuge tubes on ice. They must be labeled according to the [^{3}H]ACh concentration (duplicates). Add 1.0 mL of cold paraoxon-treated UBB to each.
9. Immediately after incubation for 10 min, place the reaction tubes on ice.
10. Pipet 90-µL portions from each tube into the tubes containing 1 mL of ice-cold UBB (*see* **Note 15**). This should be done in the same order as in **step 6** of **Subheading 3.6.**
11. Open a stopcock on one of the filters and pipet all of the diluted sample onto the filter fast enough to cover the entire surface of the filter. Wait for the liquid to be pulled through and pipet 1 mL of ice-cold UBB four times onto the filter using a P-5000 Gilson pipet. Wait for the liquid to be pulled through each time. Remove the dam and apply 1 mL of ice-cold UBB across the full surface of the filter using a P-1000 Gilson pipet at a rate that keeps the full surface of the filter wet but does not result in overflow.
12. Repeat **step 11** of **Subheading 3.6.** with each diluted, ice-cold sample.
13. Close each stopcock before removing the filter and transfer the filter to the appropriately labeled scintillation vial containing 350 µL of 1% SDS solution (*see* **Subheading 2.6.**, **item 10**). Incubate at room temperature for 1 h, gently mixing occasionally (*see* **Note 16**). Add 3.5 mL of scintillation cocktail. Vortex the vials briefly and proceed as in **step 10** of **Subheading 3.5.**

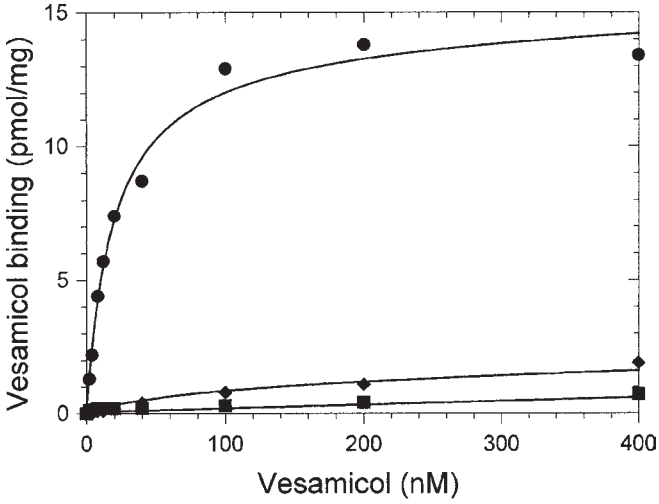

Fig. 3. Binding of [^{3}H]vesamicol. Total binding to postnuclear supernatant from cells expressing rVAChT (●), total binding to postnuclear supernatant from cells expressing control vector (◆), and nonspecific binding to postnuclear supernatants from both types of cells (■) are shown. The regression lines are defined by b = 0.062 ± 0.102 pmol/mg, m = 0.0014 ± 0.0008 pmol/mg/n*M*, Bmaxvec 1.21 ± 0.69 pmol/mg, KDvec = 83.87 ± 114.15 nM, Bmaxrat = 13.16 ± 0.37 pmol/mg, and KDrat = 18.02 ± 1.70 n*M* (*see* **Note 18**).

14. Repeat **steps 4–13** of **Subheading 3.6.** replacing NS by T and using the volumes given in the bottom part of **Table 2** for total transport.

3.7. Data Reduction and Model Fitting

The analysis detailed here uses simultaneous fitting of appropriate equations to the data (*see* **Fig. 3**). This approach yields better-determined values for the adjustable parameters than when nonspecific data are subtracted from total data before the fit or nonspecific data are inferred from the slope of data at high concentrations of radiolabeled ligand.

3.7.1. Equilibrium Binding of Vesamicol

Data are first converted from counts per minute (cpm), which are, in a sense, arbitrary as they depend on specific radioactivities, to more fundamental terms like pmol [^{3}H]vesamicol/mg protein. Three *datasets* are required. The first *dataset* combines two sets of nonspecific binding of [^{3}H]vesamicol to postnuclear supernatants obtained from rVAChT and control vector, the second *dataset* is total binding of [^{3}H]vesamicol to postnuclear supernatant obtained from cells expressing control vector, and the third *dataset* is total binding to postnuclear supernatant obtained from cells expressing rVAChT (*see* **Fig. 3**).

1. In a spreadsheet (e.g., Microsoft Excel), average the cpms for duplicates at each concentration of [^{3}H]vesamicol in each of the datasets for total binding for rVAChT vector and control vector (*see* **Note 17**). Inspect values for the nonspecific binding for both vectors at the same concentration of [^{3}H]vesamicol. They should be the same within errors, and, assuming that they are, average the cpms for the nonspecific quadruplets at each concentration of [^{3}H]vesamicol.
2. In the same spreadsheet, the averaged data in cpm must be transformed into the amounts of bound [^{3}H]vesamicol. Thus, pmol [^{3}H]vesamicol/mg postnuclear supernatant is given by

$$\text{cpm} \times \frac{1\ \text{Ci}}{2.2 \times 10^{12}\ \text{dpm}} \frac{1}{\text{efficiency}} \frac{1}{45\ \mu\text{g}} \frac{10^3\ \mu\text{g}}{\text{mg}} \times (\text{specific radioactivity})^{-1},$$

   where efficiency is in cpm/dpm and specific radioactivity is in Ci/pmol.
3. Open Scientist. Select under the File menu, New, and Model and then press Enter. The file window opens with a model template that you will overwrite with your own model file. Replicate the following model file.

```
IndVars: Ves
DepVars: Bns, Btotvec, Btotrat
Params: b, m, Bmaxvec, KDvec, Bmaxrat, KDrat
Bns = b + m*Ves
Btotvec = Bns + Bmaxvec*Ves/(KDvec + Ves)
Btotrat = Btotvec + Bmaxrat*Ves/(KDrat + Ves)
***
```

   Ves is the concentration of [^{3}H]vesamicol (in n*M*), Bns is the amount of nonspecifically bound [^{3}H]vesamicol, Btotvec is the amount of total [^{3}H]vesamicol bound by postnuclear supernatant of cells expressing control vector, Btotrat is the amount of total [^{3}H]vesamicol bound by postnuclear supernatant of cells expressing rVAChT, b is the intercept at 0 n*M* [^{3}H]vesamicol, m is the slope of nonspecific binding of [^{3}H]vesamicol, Bmaxvec is the maximal "specific binding" for control vector, KDvec is the dissociation constant for specific binding by postnuclear supernatant of cells expressing control vector, Bmaxrat is maximal true specific binding for rVAChT vector, and KDrat is the dissociation constant for specific binding by postnuclear supernatant of cells expressing rVAChT.
4. Select under the Model menu, Compile and then press Enter. A window should appear that says Compilation done. Save the file.
5. Select under the File menu, New, and Spreadsheet and then press Enter. The spreadsheet window opens. The columns should be labeled with the names of the independent and dependent variables. Under the first column, which is labeled Ves, type in the concentrations of [^{3}H]vesamicol (in n*M*), including 0 n*M*. Copy the averaged data for pmol [^{3}H]vesamicol/mg (*see* **step 2**) into the corresponding columns for Bns, Btotvec and Btotrat. Save the file.

6. Select under the File menu, New, and Parameter Set and then press Enter. The parameter spread sheet opens. The rows should be labeled with the names of the parameters. Enter 0 in the Lower Limit cells for all of the parameters. Scan the pmol/mg data visually to estimate values for the parameters. For example, b will be close to the values at 0 n*M* [^{3}H]vesamicol and m will be close to the value for nonspecific binding at 100 n*M* [^{3}H]vesamicol divided by 100. KD for each vector will be about the concentration of [^{3}H]vesamicol one-half way up the curvature region of total binding, and Bmax will be about the difference between the total binding and the nonspecific binding at a high concentration of [^{3}H]vesamicol. Enter these values in the Value column. You can leave the default value infinity in the Upper Limit cells for all of the parameters. Save the file. Some suitable initial values for parameters are listed in **Table 3**.
7. Select under the Calculate menu, Simplex Fit and then press Enter. A new window for Parameter Set containing coarsely adjusted parameters will appear. Select under the Calculate menu, Least Squares Fit and then press Enter. A new window will appear asking whether to use the current parameters instead of the selected parameters. Say yes. The data Spreadsheet will appear containing new columns filled with calculated values for each dependent variable and new columns filled with residuals between observed and calculated values for each dependent variable. Select under the Calculate menu, Statistics and then press Enter. A window containing the Statistics Report will appear. Scroll down the window to find the optimized values for the parameters, their standard errors, and 95% confidence intervals. Save the file.
8. Select under the Plot menu, Plot Template and then press Enter. If you do not want to view residuals, select each "residual" file and click on "Delete Curve." This will leave threes pairs of files active (six files total). Each pair contains a data file for a set of observations and a file for the calculated best-fit line to those observations. The default assignment of Curve Styles to files associates a data file with a Curve Style having an odd number (say, 1) and a best-fit line file with a Curve Style having an even number (say, 2). The default assignment of Curve Styles associates odd-numbered styles with data symbols and even-numbered styles with types of line (say, solid or broken). Click on the Plot tab and change the Plot Title if desired. Click on the X-Axis tab. Change the X-Axis Label to Vesamicol (n*M*). Do not use square brackets, as these are reserved to indicate superscripts and subscripts. Click on the Y-Axis tab. Change the Y-Axis Label to Vesamicol binding (pmol/mg). The Default range and int. should be checked for both X- and Y-Axes. If you do not want grid lines, click on the control buttons labeled Grid lines in the X- and Y-Axis tab pages, and Major Grid Lines. Select under the Plot menu, Save Template, assign a file name, and then save the file.
9. Select under the File menu, New, Plot, and then press Enter. A window with the plot appears. Save the file.

3.7.2. Transport of ACh

The procedure is very similar to that used for binding of [^{3}H]vesamicol. The averaging and reduction of data and regression and plotting are very similar,

Table 3
Initial Parameters for Binding of [^{3}H]Vesamicol

ParamName	Lower limit	Value	Upper limit
b	0	1	5
m	0	0.1	1
Bmaxvect	0	2	100
KDvect	0	100	10,000
Bmaxrat	0	20	Infinity
KDrat	0	20	Infinity

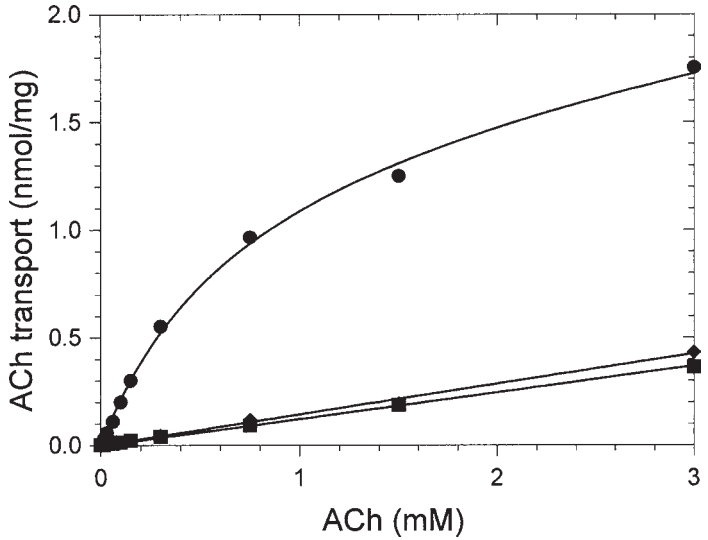

Fig. 4. Transport of [^{3}H]ACh. Total transport by postnuclear supernatant from cells expressing rVAChT (●), total transport by postnuclear supernatant from cells expressing control vector (◆), and nonspecific transport by postnuclear supernatants from both types of cells (■) are shown. The regression lines are defined by b = –0.001 ± 0.004 nmol/mg, m = 0.1234 ± 0.0055 nmol/mg/m*M*, AChmaxvec 0.25 ± 0.79 nmol/mg, KMvec = 10.00 ± 39.93 m*M*, AChmaxrat = 1.60 ± 0.04 nmol/mg, and KMrat = 0.70 ± 0.04 m*M* (*see* **Note 18**).

but the names of independent and dependent variables and parameters differ (*see* **Fig. 4**).

1. Proceed as in **step 1** of **Subheading 3.7.1.** using data for transport of [^{3}H]ACh.
2. The averaged data in cpm must be transformed into the amounts of transported [^{3}H]ACh. Thus, nmol [^{3}H]ACh/mg postnuclear supernatant is given by

$$\text{cpm} \times \frac{1\ \text{Ci}}{2.2 \times 10^{12}\ \text{dpm}} \frac{1}{\text{efficiency}} \frac{1}{112.5\ \mu\text{g}} \frac{10^3\ \mu\text{g}}{\text{mg}} \times (\text{specific radioactivity})^{-1},$$

where efficiency is in cpm/dpm and specific radioactivity is in Ci/nmol.

3. Proceed as in **step 3 of Subheading 3.7.1.** using the following model for the regression.

```
IndVars: S
DepVars: AChns, AChtotvec, AChtotrat
Params: b, m, AChmaxvec, KMvec, AChmaxrat, KMrat
AChns = b + m*S
AChtotvec = AChns + AChmaxvec*S/(KMvec + S)
AChtotrat = AChtotvec + AChmaxrat*S/(KMrat + S)
***
```

S is the concentration of [^{3}H]ACh in m*M*, AChns is the amount of nonspecifically transported [^{3}H]ACh, AChtotvec is the amount of total [^{3}H]ACh transported by postnuclear supernatant of cells expressing control vector, AChtotrat is the amount of total [^{3}H]ACh transported by postnuclear supernatant of cells expressing rVAChT, b is the intercept at 0 m*M* [^{3}H]ACh, m is the slope of nonspecific transport of [^{3}H]ACh, AChmaxvec is the maximal "specific transport" for control vector, KMvec is the Michaelis constant for specific transport by postnuclear supernatant of cells expressing control vector, AChmaxrat is maximal true specific transport for rVAChT vector, and KMrat is the Michaelis constant for specific transport by postnuclear supernatant of cells expressing rVAChT.

4. Proceed as in **step 4** of **Subheading 3.7.1.**
5. Proceed similarly as in **step 5** of **Subheading 3.7.1.** Note the changes in the names of the variables.
6. Proceed similarly as in **step 6** of **Subheading 3.7.1.** Note the changes in the names of the parameters. Save the file. Some suitable initial values for parameters are listed in **Table 4.**
7. Proceed as in **step 7** of **Subheading 3.7.1.**
8. Proceed similarly as in **step 8** of **Subheading 3.7.1.** Change the names of the X- and Y-Axes to ACh (m*M*) and ACh transport (nmol/mg), respectively.
9. Proceed as in **step 9** of **Subheading 3.7.1.**

3.8. Results and Discussion

The important parameters are KDrat and Bmaxrat for specific binding of [^{3}H]vesamicol, and KMrat and AChmaxrat for specific transport of [^{3}H]ACh. These so-called macroscopic parameters ignore the existence of intermediates. They cannot be used for inference regarding intermediates. The value for KMrat is similar to the estimated concentration of ACh in the cytoplasm of cholinergic nerve terminals, as expected for an effective transporter ***(1)***. Also, AChmaxrat (equivalent to Vmax) can be divided by Bmaxrat to obtain the

Table 4
Initial Parameters for Transport of [^{3}H]ACh

ParamName	Lower limit	Value	Upper limit
b	0	0.002	0.1
m	0	2	1
AChmaxvect	0	1	5
KMvect	0	7.5	10
AChmaxrat	0	3	Infinity
KMrat	0	0.750	Infinty

number of molecules of ACh taken up per molecule of transporter at saturating [^{3}H]ACh over the time period of the experiment. This was 179 ACh/VAChT.

The model used to fit specific binding and transport assumed that the Hill coefficient was exactly 1. The possibility that binding or transport is cooperative can be investigated by changing the equations for specific binding and transport to the Hill format by replacing Ves/(KDrat + Ves) with $Ves^n/(KDrat^n + Ves^n)$ and S/(KMrat + S) with $S^n/(KMrat^n + S^n)$ in the models. The exponent n is an additional adjustable parameter that is the Hill coefficient. It must be listed on the Params line of the model. For the current data, optimized n was close to 1 in both cases, and 1 was well within the 95% confidence interval reported by Scientist. Thus, there is no basis to allow n to be different from 1.

4. Notes

1. The appropriate volume of [^{3}H]vesamicol will depend on the chemical concentration in the ethanolic solution. This is because the working solution of [^{3}H]vesamicol that is to be prepared (SolA) should have a concentration at least three times as great as the highest concentration of [^{3}H]vesamicol to be reached in the titration.
2. [^{3}H]Vesamicol in ethanol is in the free-base form. The thin film that remains after evaporation dissolves into UBB slowly because of the heterogeneous phases. It is important to transfer the solution to a fresh tube in case not all of the [^{3}H]vesamicol had dissolved. [^{3}H]Vesamicol is chemically very stable, and it does not adsorb significantly to the surfaces of common containers like microcentrifuge tubes and pipet tips.
3. Cells normally have a round appearance. Only a few cells should appear flat and polygonal because of differentiation. An adherent cell culture is confluent when cells have formed a single layer over the entire area available for growth. Cells must be split before they start to form clusters above the first layer or start to lift up from the surface. Cells are subcultered at confluency every 72 or 96 h.
4. Remove the cotton plug from the pipet to avoid having it sucked into the vacuum line.

5. Most cells will lift from the plastic.
6. Flasks will be upright during pipetting. Up to eight upright flasks can be placed side by side, clamped together with the hands and gently tilted toward the horizontal so that the medium stays away from the neck and the beveled face is on the bottom. Be careful not to wet the filters during transfer to the incubator or when moving them in the incubator.
7. Movement of the cells through the narrow opening of a disposable pipet tip ensures that they are dispersed.
8. The number of cells per square should be between 5 and 35. If it is outside these limits, another dilution should be used.
9. If the number of cells harvested is 2.4×10^8, the final volume will be about 4 mL. This will yield four to five transfections.
10. After electroporation, the cell suspension becomes viscous and debris floats on top. This condition often causes the pipet tip to plug. If this occurs, slowly withdraw the tip from the cuvet, place it below the surface of the complete medium in the conical tube against the wall of the tube, and slowly pull away from the wall while expelling the pipet contents. This usually unplugs the tip.
11. Trypan blue is negatively charged and does not interact with the cell unless the membrane is damaged.
12. The protein concentration should be 10–15 mg/mL.
13. Be careful not to allow liquid nitrogen to reach the top of the tube. There is no difference in the ligand binding and transport properties of fresh and frozen postnuclear extracts.
14. The chemical concentration [*M*] is given by

$$\frac{\text{cpm}}{\mu\text{L}} \times \frac{1\ \text{Ci}}{2.2 \times 10^{12}\ \text{dpm}} \frac{1}{\text{efficiency}} \frac{10^6\ \mu\text{L}}{1\ \text{L}} \times (\text{specific radioactivity})^{-1}, \qquad (3)$$

where efficiency is given in cpm/dpm and specific radioactivity is given in Ci/mol.

15. The transport assay requires more postnuclear supernatant than the binding assay. Two 90-µL portions of the reaction are diluted into 1.0 mL ice-cold UBB in order to avoid clogging the filters.
16. Tritium produces such weak radioactivity that it will not be counted if it is not fully soluble. 1% SDS efficiently solubilizes [^{3}H]ACh bound to the filters. [^{3}H]vesamicol is hydrophobic enough not to require SDS to become fully soluble in scintillation cocktail.
17. Be sure to include 0 n*M* [^{3}H]vesamicol.
18. The large errors in the values of the parameters specifying forms of nonspecific binding and transport are of little significance, as they do not significantly affect confidence intervals for the parameters specifying specific binding and transport.

References

1. Parsons, S. M. (2000) Transport mechanisms in acetylcholine and monoamine storage. *FASEB J.* **14,** 2423–2434.

2. Alfonso, A., Grundahl, K., Duerr, J. S., et al. (1993) The *Caenorhabditis elegans* unc-17 gene: a putative vesicular acetylcholine transporter. *Science* **261,** 617–619.
3. Kim, M. H., Lu, M., Lim, E. J., et al. (1999) Mutational analysis of aspartate residues in the transmembrane regions and cytoplasmic loops of rat vesicular acetylcholine transporter. *J. Biol. Chem.* **274,** 673–680.
4. Kim, M. H., Lu, M., Kelly, M., et al. (2000) Mutational analysis of basic residues in the rat vesicular acetylcholine transporter. Identification of a transmembrane ion pair and evidence that histidine is not involved in proton translocation. *J. Biol. Chem.* **275,** 6175–6180.
5. Zhu, H., Duerr, J. S., Varoqui, H., et al. (2001) Analysis of point mutants in the *Caenorhabditis elegans* vesicular acetylcholine transporter reveals domains involved in substrate translocation. *J. Biol. Chem.* **276,** 41,580–41,587.
6. Inoue, H., Li, Y. P., Wagner, J. A., et al. (1995) Expression of the choline acetyltransferase gene depends on protein kinase A activity. *J. Neurochem.* **64,** 985–990.

11

Electrophysiological Studies of Ion Channels and Therapeutic Potential With Adenovirus-Mediated Gene Transfer

Jihong Qu, Thai V. Pham, and Maria N. Obreztchikova

1. Introduction

Transmembrane ion channels, or, more broadly, membrane transporters, are the subject of electrophysiology that leads us to the understanding of nearly every event of biological activities. Since the introduction of patch clamp concepts and techniques ***(1,2)***, transmembrane ion channels have been extensively studied at tissue and cell levels in terms of biophysical, electrophysiological, and pharmacological properties.

As the knowledge advances in modern molecular biology, now the electrophysiological functionality of ion channels is being correlated to their molecular and genetic traits and explored further with new approaches such as transgenic animals, heterologous gene expression, and mutagenesis. Drugs that target ion channel genes account for about 5% of that are currently marketed ***(3)***, or 50% if ion channels and membrane receptors are included. Electrophysiological studies that probe the expression, function, and regulation of ion channels (or membrane transporters in general) with genetic interventions that are properly designed and delivered could also benefit future drug and therapeutics development.

Although there are various gene transfer methods available ***(4)***, the one with viral vectors is proven the most efficient. Among viral vectors, adenovirus is probably the most attractive as a mammalian gene transfer vehicle. This is because adenovirus has several favorable features, such as high titer that is essential for in vivo studies, capability to infect dividing and nondividing cells, and substantial experience in clinical trials and target screen-

From: *Methods in Molecular Biology, vol. 227: Membrane Transporters: Methods and Protocols*
Edited by: Q. Yan © Humana Press Inc., Totowa, NJ

ings. It can efficiently transduce a high-level gene expression of interest to a variety of cell types. Its modified 36-kb double-stranded DNA genome can be manipulated with relative ease by conventional molecular biology techniques, and it can be readily propagated and purified to yield high-titer stable preparations. Consequently, adenoviruses have been extensively used as vectors for recombinant vaccines, high-level protein production, and gene therapy. It is also very useful for electrophysiological studies to deliver ion channel genes. The adenoviral gene will not integrate into the host genome and will not replicate in the cells that do not have the complementary E1 fragment. Therefore, the expression of the transgene is transient and offers protection of that which is not targeted. Adenovirus is becoming a powerful tool to attack ailments such as neck cancer ***(5)***, hemophilia factor IX ***(6)***, and heart failure ***(7)***. It has also been investigated in electrophysiological studies related to rhythm and arrhythmogenesis ***(8,9)***.

The methods described here provide a paradigm for the electrophysiological studies of ion channels in mammalian myocardium with adenovirus-mediated gene transfer. As a result, the approach, as being introduced, could point to a direction for the development of therapeutics against heart diseases because of disorders of membrane transporters. In this chapter, we will first describe the construction of adenoviral vector for gene delivery. The transient gene transfer and functional expression of HCN2 channels (an isoform of the HCN gene family; *see* **Fig. 1**) via adenoviral vector will then be demonstrated with patch clamp techniques.

Four isoforms of hyperpolarization-activated cyclic nucleotide-gated (HCN) channels have been cloned ***(10,11)*** and underlie the pacemaker current, I_f in the heart, or I_h in the brain, which plays a critical part in maintaining the rhythmic activity. However, the relation between their relative expressions and functional roles has been difficult to determine, especially in homologous system such as the heart, where the cellular regulatory machinery is largely present and complexly modulating HCN channel properties. Thus, adenovirus-mediated gene transfer is uniquely advantageous because it can greatly facilitate delivering a transgene into mammalian cells, which allows characterization of a particular gene of interest (such as the HCN gene family) in a physiological setting. It can also enable the potential correction of genetic defects that are associated with pathogenesis (such as rhythm disorder).

2. Materials

2.1. Construction of Adenoviral Vectors that Carry Genes of Ion Channels

1. Dry and CO_2 humidifier incubators.
2. Water bath.

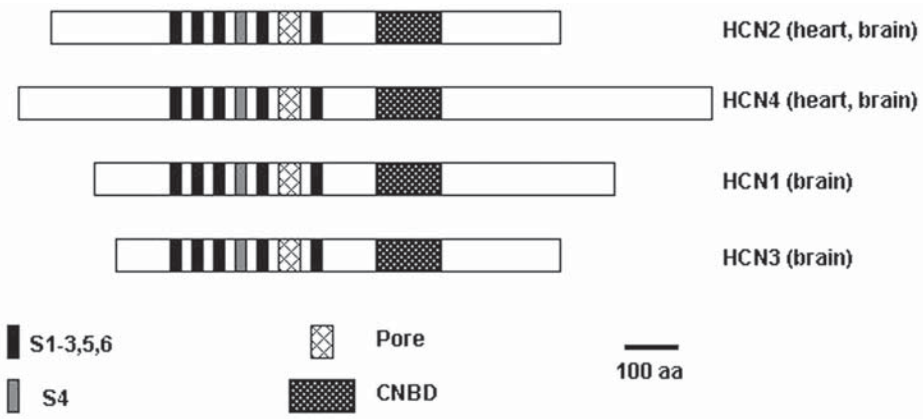

Fig. 1. HCN gene family. Structurally, HCN channels consist of four subunits as a tetramer, and each subunit is made of six transmembrane segments (S1–S6). The channel pore is located in the region between S5 and S6 whereas S4 is considered a voltage sensor. On the cytoplasmic C-terminus of each subunit, there is a cyclic nucleotide-binding domain (CNBD) that is similar to the structure of cyclic nucleotide-gated (CNG) channels. Different isoforms can form multimeric channels that display different gating properties compared with those made of uniform isoforms.

3. Centrifuges.
4. Temperature-controlled shaker.
5. Electrophoresis apparatus.
6. –80°C, –20°C, and 4°C freezers and refrigerator.
7. Liquid N_2.
8. Laminar-flow biological safety hood with ultraviolet (UV) sterilization light.
9. Microscope with xenon light source and fluorescence-light-detection system.
10. Ultracentrifuge and titanium rotor (SW41) (Beckman Coulter [www.beckmancoulter.com]).

2.1.1. Subcloning of Shuttle Vector

Chemical reagents for transformation, bacterial growth, DNA purification, restriction digestion, and ligation are from commercial sources. All of the media and solutions are made and all of the reagents stored under the conditions recommended by the manufacturers.

2.1.2. Recombination and Construction of Adenovirus

Chemical reagents for cell culture, transfection, and infection include Dulbecco's modified Eagle's medium (DMEM) (4.5 g/L glucose), penicillin/streptomycin, fetal bovine serum (FBS), Hanks balanced salt solution (HBSS,

1X), HEPES-buffered saline (8.0 g/L NaCl, 0.37 g/L KCl, 0.125 g/L $Na_2HPO_4 \cdot 2H_2O$, 1.0 g/L dextrose, 5.0 g/L HEPES, pH 7.05), and phosphate-buffered saline (PBS, 1X). All of the media and reagents are prepared and stored under the conditions recommended by the suppliers. The cells for transfection and infection are HEK293 cells (Microbix [www.microbix.com] or American Type Cell Collection [www.atcc.org]).

2.1.3. Adenovirus Amplification

1. Dialysis buffer: 3% Sucrose, 10 m*M* Tris-HCl, pH 7.8, 150 m*M* NaCl, and 10 m*M* $MgCl_2$; sterilize ingredients by 0.22-μm filtering.
2. Spectra/Por dialysis membrane tubing (6000–8000 Dalton molecular weight cut-off (MWCO), flat width 23 mm; Fisher Scientific, [www.fisherscientific.com]).

2.1.3.1. Hirt DNA Purification and Analysis

A mix of 9 parts lysis buffer to 1 part pronase stock. Lysis buffer is made in stock of 11.1 m*M* Tris-HCl, pH 7.4; 11.1 m*M* NaCl; 11.1 m*M* EDTA; 0.555% sodium dodecylsulfate (SDS), kept at room temperature. Pronase stock is made of pronase (Sigma) at 10 mg/mL and incubated at 37°C for at least 30 min to digest any contaminating nucleases. The digested stock is then distributed in 1-mL aliquots and stored at –20°C. Tubes can be frozen and thawed several times and the enzyme will retain activity.

2.1.3.2. CsCl Banding

1. Deoxycholate (Sigma) solution (stock: 5% weight to volume in H_2O). The DOC (deoxycholate stock) is stored frozen at –20°C.
2. DNase (Sigma).

2.1.3.3. The Estimation of Viral Titers

2.1.3.3.1. Fluorescent Focus Assay

1. Mouse anti-adenovirus antiserum (Advanced ImmunoChemical [www.advimmuno.com]).
2. Fluoresceinated goat anti-mouse antiserum (Chemicon International [www.chemicon.com]).

2.1.3.3.2. Plaque Assay

1. 2X LP: Autoclave 2.5 g lactalbumin hydrolysate (Gibco [www.lifetech.com]) and 5 g Bacto-peptone (DIFCO [www.voigtglobal.com/DIFCO]) in 250 mL distilled H_2O in a 500-mL glass bottle. This medium can be made ahead of time and stored indefinitely.
2. To the cooled mix, add 103 mL sterile H_2O, 100 mL sterile 10X Earle's solution (Gibco), 10 mL sterile 50X MEM amino acids (Gibco), 5 mL sterile penicillin/

streptomycin solution, 2 mL sterile 100X vitamin (Gibco), and up to 29.6 mL sterile 7.5% $NaHCO_3$ solution. The final color should be red, not purple. $NaHCO_3$ should be added last, otherwise a precipitate may form.

3. On the day of the assay, warm up enough 2X LP (stored at 4°C) for all dishes (5 mL/dish), and add FBS (stored at –20°C) to 4%, $MgCl_2$ to 2.5 m*M* (essential for obtaining large plaques), and glutamine (stored at –20°C) to 0.025%. Keep 2X LP at 37°C for 15–30 min, but no longer, because precipitation may occur.
4. Agar: Separately make up a solution of purified agar (Agar Noble; Difco) to 1.6% in distilled H_2O (3.2 g agar in 200 mL H_2O). Autoclave and keep it molten at 50°C. Just before overlaying dishes, mix 2X LP and supplements and Agar in a 1 : 1 mix.
5. Neutral red: Make a 1% solution in H_2O (stored at 4°C and shielded from light) and use at a final concentration of 0.01%.

2.2. Expression/Delivery of Adenoviruses That Carry the Ion Channel Genes of Interest

1. Laminar-flow biological safety hood.
2. CO_2 humidifier incubator.
3. Langendoff perfusion apparatus.

2.2.1. Cell Isolation and Culture

1. Media and reagents for cell isolation from rat and dog hearts and those for culture of HEK293 cells and isolated cardiac myocytes are from commercial sources.
2. For dog: Protease (0.35 mg/mL, Type XIV; Sigma) and collagenase (0.47 mg/mL, 389 units/mg, Type II; Worthington).

2.2.2. In Vitro Gene Transfer to Cardiac Myocytes

Media and reagents include DMEM with and without FBS for cardiac myocytes of neonatal rats and ACCTI for those of adult rats and dog (ACCTI of 400 mL contains 400 mL M199, 158 mg carnitine, 264 mg creatine, 250 mg taurine, 0.4 mg insulin, 800 mg salt-free BSA, 4 mL penicillin/streptomycin of 10,000 units/mL, from Sigma, [www.sigmaaldrich.com]). All of the media and reagents are prepared and stored under the conditions recommended by the suppliers.

2.2.3. In Vivo Gene Delivery to the Heart

1. A designated sterile area for survival animal surgery.
2. Surgical instruments for thoracotomy on dog and rat.
3. Solutions for survival animal surgery stored under the conditions recommended by the suppliers.
4. Small respirator (Harvard Apparatus [www.harvardbioscience.com]).

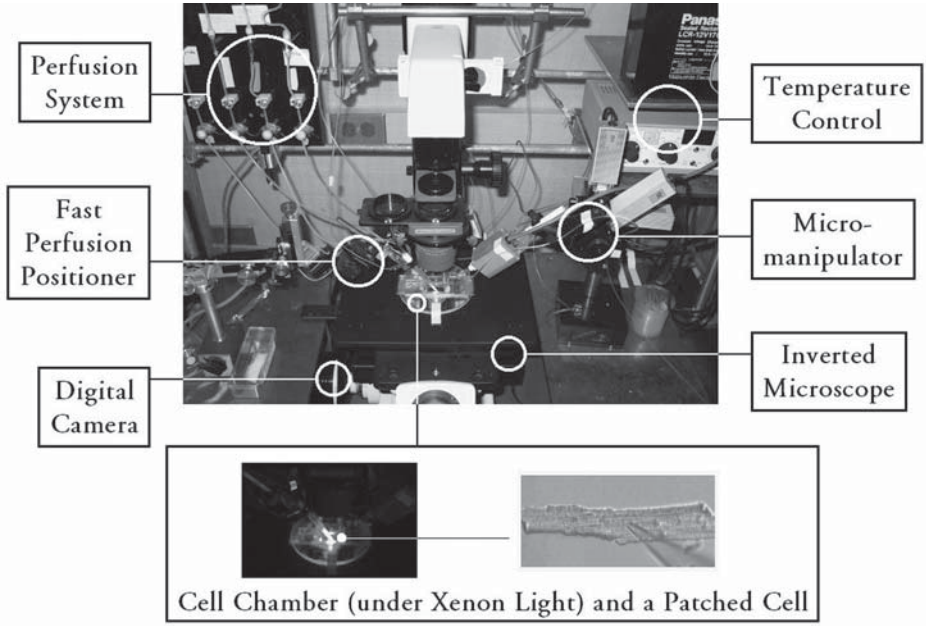

Fig. 2. Patch-clamp setup. Inverted microscope, temperature control, perfusion system, fast perfusion positioner, digital camera, cell chamber, and micromanipulator.

2.3. Electrophysiological Studies of Ion Channels with Adenovirus-Mediated Gene Transfer

2.3.1. Patch Clamping of Single Cultured or Acutely Dissected Cells That Are In Vitro or In Vivo Infected by Adenovirus

Equipment for a typical patch clamp setup (*see* **Fig. 2**) (alternatives for the equipment can be found at http://www.axon.com/notes/lab_setup.htm) are as follows:

1. Vibration isolation table/Faraday cage (Technical Manufacturing Corporation [www.techmfg.com]).
2. Inverted microscope.
3. Digital camera system and video card software to display and store images on the computer.
4. Temperature control system (Cell MicroControls [www.cellmc.com]).
5. Motorized micromanipulator (SD Instruments [www.sd-instruments.com]).
6. Patch pipet puller and Borosilicate patch pipet glass tubing (Sutter Instruments [www.sutter.com]).

7. Narishige microforge (Narishige [www.narishige.co.jp]).
8. Patch-clamp amplifier (Axopatch 200) and data acquisition board (Digidata 1200).
9. Head-stage (CV201) pipet holder, software pClamp8 (Axon Instruments [www.axon.com]).
10. Perfusion system and cell chamber.
11. Computer with sufficient speed/space.

2.3.2. Solutions for Patch-Clamp Recordings

1. Extracellular solution: 140 m*M* NaCl, 2.3 m*M* NaOH, 1 m*M* $MgCl_2$, 5.4 m*M* KCl, 1.0 m*M* $CaCl_2$, 5 m*M* HEPES, and 10 m*M* glucose, pH 7.4, stored at 4°C.
2. Intracellular solution: 130 m*M* Aspartic acid, 146 m*M* KOH, 10 m*M* NaCl, 2 m*M* $CaCl_2$, 5 m*M* EGTA–KOH, 2 m*M* Mg–ATP, 0.1 m*M* Na–GTP, and 10 m*M* HEPES–KOH, pH 7.2. It can be made in a small stock (100–200 mL) and aliquoted depending how much is needed for each experiment and stored at –20°C.

3. Methods

3.1. Construction of Adenoviral Vectors That Carry Genes of Ion Channels

Adenovirus construction consists of two major steps: (1) subcloning of a transgene into the rescuing shuttle vector and (2) recombination of the rescuing shuttle vector with the adenoviral backbone vector.

3.1.1. Subcloning of Shuttle Vector

The transgene, HCN2, as a restriction fragment digested out of the original vector, is ligated as an insert into the shuttle vector pDC516 (Microbix) at the sites of *Eco*RI and *Xba*I. A key consideration for subcloning is to have two ends of the restriction fragment matched with two sites in the cloning region of the shuttle vector, either exactly or compatibly. If there is no readily available match of the sites between insert and vector, one could use DNA polymerase to create blunt end(s) as alternatives. If both ends are blunt, after ligation correct orientation of the transgene in the shuttle vector has to be confirmed simply by properly designed restriction digestions.

The shuttle vector pDC516 is specifically designed for recombination with the adenoviral backbone vector. Several regions (*see* **Fig. 3**) on the shuttle vector are critical for the recombination and, ultimately, production of virus to happen. Make sure that these regions are correctly present.

The protocols for *transformation*, *DNA purification*, *restriction digestion*, and *ligation* are standard and could be found in the commercially available kits. Follow them according to the instructions of the manufacturers or vendors.

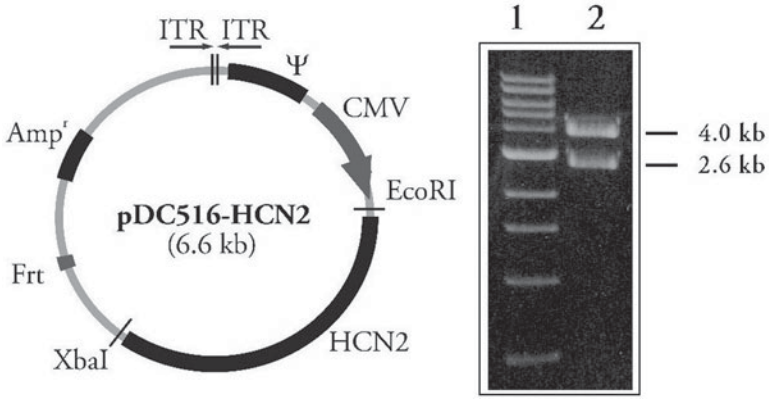

Fig. 3. Map of rescuing shuttle vector pDC516 with the transgene HCN2. **Left panel**: ITR, inverted terminal repeat; Ψ, packaging signal; CMV, cytomegalovirus promoter; Frt, site recognized by FLP recombinase; Amp^r, sequence for the ampicillin resistance; HCN2, gene of interest; *Eco*RI and *Xba*I, restriction sites. **Right panel**: The shuttle vector containing HCN2 is digested with restriction enzymes *Eco*RI and *Xba*I; then, vector and transgene are seen at 4.0- and 2.6-kb positions (lane 2) in a 0.8% agarose gel. *Eco*RI and *Xba*I are the sites where pDC516 and HCN2 are ligated. Lane 1 is loaded with a 1-kb DNA ladder.

3.1.2. Recombination and Construction of Adenovirus

Once the transgene insert is ligated into the shuttle vector and both the shuttle and adenoviral (Ad) backbone vectors are sufficiently stocked, the recombination–construction of an adenovirus carrying the transgene begins.

First-generation human adenoviruses (serotype 5) that have been modified as mammalian gene transfer vectors basically have a foreign DNA inserted in the place of early region 1 (E1) and/or E3. E1-depleted vectors ***(12)*** are replication deficient and propagate only in E1-complementing cells such as the HEK293 cell line. A number of strategies for Ad vector construction have been developed. Typically, foreign DNA is inserted into a small shuttle plasmid containing adenoviral sequences from the left end of the genome with the E1 region deleted. The foreign DNA can be rescued into virus by in vivo homologous recombination after cotransfection of HEK293 cells with the shuttle plasmid and restricted viral DNA ***(13,14)***. The adenoviral genomic plasmid is modified to be noninfectious, thereby virtually eliminating any possibility of generating viruses other than the desired recombinant. This homologous recombination method has been well proven and widely employed, but the vector rescuing is sometimes difficult, perhaps because of the inefficient homologous recombination in cotransfected HEK293 cells.

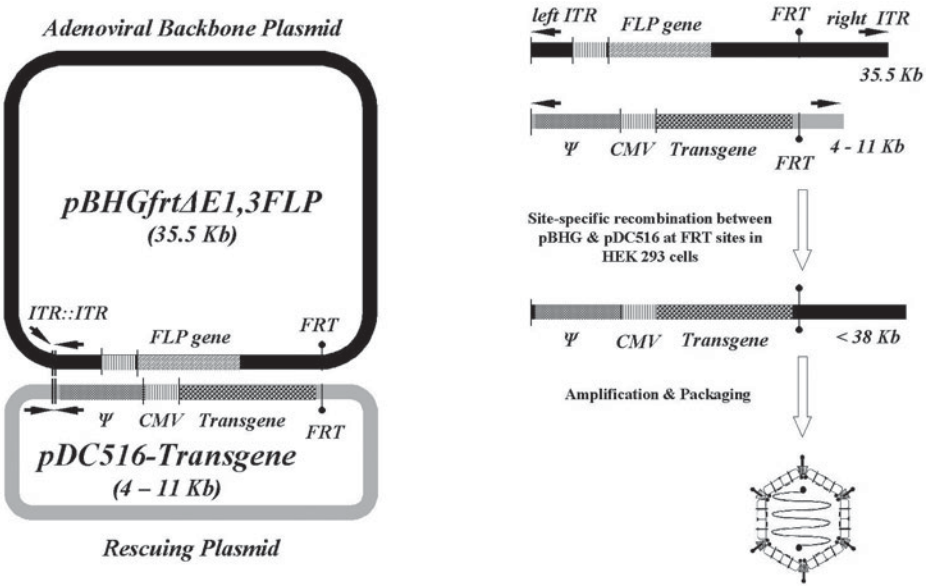

Fig. 4. Recombination of adenoviral backbone and rescuing shuttle vectors. **Left panel**: Ad backbone plasmid pBHGfrtΔE1,3FLP and rescuing plasmid pDC516-Transgene. The Frt site-specific recombination of these two vectors occurs after their cotransfection into HEK293 cells. FLP recombinase is expressed under CMV promoter first in HEK293 cells in accordance with its gene in the Ad backbone plasmid. FLP then recognizes Frt sites on both vectors. **Right panel**: Once Frt sites are recognized by FLP, the left hand from ITR up to Frt of the rescuing plasmid replaces the counterpart in the Ad backbone plasmid. Then, the complete adenoviral genome that includes packaging signal (Ψ), promoter (CMV), and transgene is formed. The viral DNA is enveloped by its capsid based on ψ and then the functional adenovirus is produced and able to replicate in HEK293 cells.

The approach of constructing the adenovirus described here for electrophysiological studies has been demonstrated to be more efficient and simpler compared with the homologous recombination method. It is based on the Frt-site-specific recombination between two plasmids: rescuing plasmid that carries the transgene and adenoviral backbone plasmid, after their cotransfection into HEK293 cells (*see* **Fig. 4**). The Frt site is recognized by recombinase FLP that is first expressed based on its gene in the Ad backbone plasmid after the cotransfection. The flexibility, efficiency, and reliability of this method greatly simplify and expedite construction of Ad vectors for mammalian gene transfer. The efficiency of the two-plasmid rescue method for constructing adenoviral vectors has been enhanced by the replacement of a single

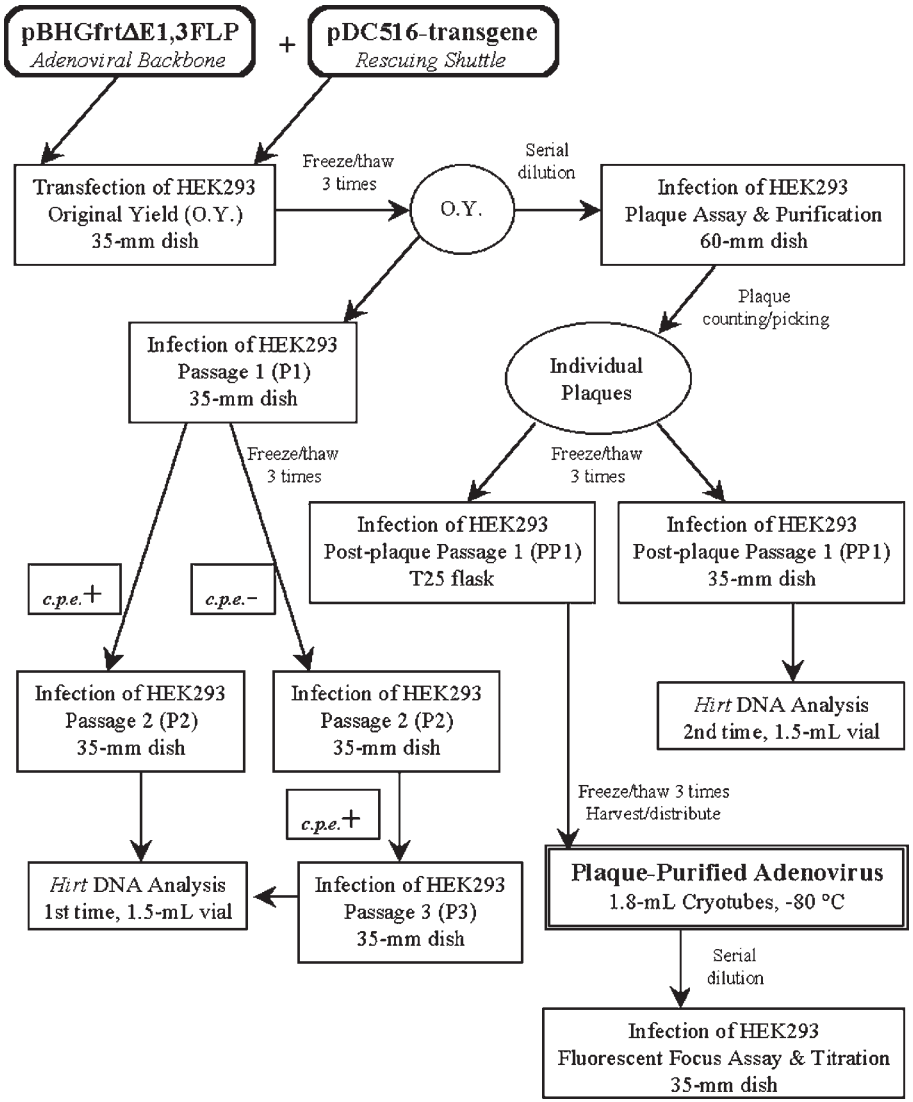

Fig. 5. Scheme of adenovirus construction.

inverted terminal repeat (ITR) in the rescuing plasmid with an ITR junction (two head-to-head ITRs).

The recombination starts with transfecting two plasmids: Ad backbone and rescuing shuttle carrying the transgene, into HEK293 cells (*see* **Fig. 5**). About 1 wk or 10 d after the cotransfection, one should lyse the HEK293 cells by freezing at –80°C and thawing them three times and liberate the virus if any

there has been created at that point. Then, pass the lysate to fresh HEK293 cells via infection. This is passage 1 (P1). Remember, it is important to keep the original yield (O.Y.) at –80°C! Within the following week or 10 d, if indeed there has been a virus created, positive cytopathic effect (c.p.e.$^+$) will occur and become more and more extensive (*see* **Fig. 7**, p. 193) in P1. Pass the cells with c.p.e.$^+$ to fresh HEK293 cells, which is passage 2 (P2), for the virus to sufficiently replicate prior to the *Hirt* viral DNA purification and analysis (refer to the protocol in **Subheading 3.1.3.2.**). *Hirt* DNA analysis is to confirm that the virus created is genetically correct. In the case that no c.p.e.$^+$ is found in P1, another passage from P1 to P2 sometimes is worth pursuing; otherwise one should start another cotransfection. If c.p.e.$^+$ is seen in P2, one should again infect fresh HEK293 cells, which would be passage 3 (P3), for the viral DNA analysis. Once the viral DNA containing the transgene is confirmed correct, one can begin plaque assay and purification by infecting fresh HEK293 cells with 10-fold serial dilution of O.Y. (e.g., $\times10^{-1}$, $\times10^{-2}$, and $\times10^{-3}$). The extent of serial dilution depends on how early and extensively c.p.e.$^+$ has occurred in P1 (or P2). About 12 d or 2 wk later, individual plaques formed and stained with neutral red are ready to be counted and some are picked and resuspended in DMEM, 1 mL/plaque. Then, keep plaques individually at –80°C. Liberate the virus from the plaque in DMEM by freezing/thawing three times and then infect fresh HEK293 cells to grow a plaque-purified virus stock (PP1). The virus collected from PP1 should be stored in cryotubes at –80°C while its titer is measured through titration and fluorescent focus assay (refer to **Subheading 3.1.3.4.**). As a virus stock is being grown from isolated individual plaque(s), the viral genome needs to be confirmed again via *Hirt* DNA analysis. For this purpose, fresh HEK293 cells (PP1) are infected by the same plaque(s) and viral DNA is collected for the analysis. The plaques picked and analyzed should be carefully kept individually at –80°C for the genetic integrity of the virus when it needs to be grown later.

The following protocol is for the transfection of HEK293 cells under sterile conditions for the recombination of the rescuing shuttle vector containing the transgene (pDC516-HCN2, approx 1 μg/μL) and adenoviral backbone vector (pBHGfrtΔE1,3FLP, approx 1 μg/μL).

1. Set up two preparations; one in two 35-mm dishes of HEK293 cells as control and the other in six dishes for the virus to be constructed. All dishes are prepared 2 d in advance and kept in a CO_2 incubator at 37°C. Cells should be 80–90% confluent at the time of transfection.
2. Prepare mixes (*see* **Table 1**) in two 5-mL snap-cap tubes of prewarmed H_2O, HEPES-buffered saline, DNA plasmids, and then $CaCl_2$ (0.125 *M*). HEPES buffer and $CaCl_2$ are separately prepared as 10X stocks (10X HEPES buffer has a pH around 7.25). The stocks are filter-sterilized and stored at 4°C.

Table 1
Preparation of Mixes

	HEPES buffer (×10)	DNA plasmids	$CaCl_2$ (×10)	H_2O	Total volume no. of dishes
Prep. #1 (control)	50 μL	6 μL pDC516 6 μL pBHGfrtΔE1,3FLP	50 μL	388 μL	500 μL, 2 dishes
Prep. #2	150 μL	18 μL pDC516-HCN2 18 μL pBHGfrtΔE1,3FLP	150 μL	1164 μL	1500 μL, 6 dishes

Warm the mixes in the water bath at 37°C for 5 min before finally adding $CaCl_2$. Then, put the tubes in the water bath for 20–30 min. Make sure precipitation is seen. Transfer the mixes, 250 μL each, to the 35-mm dishes that have HEK293 cells plated.

3. Keep the dishes in a 37°C incubator for 4 h and observe precipitation (*see* **Note 1**) on the HEK293 cells. Remove the medium in each dish and add 1 mL of 15% glycerol in PBS and remove it quickly! Then, add 2 mL HBSS and remove it. Add 2 mL HBSS again. It is safe to leave HBSS with the cells until this step is completed for all of the dishes.
4. Remove HBSS and replace with 3 mL DMEM (plus 2% FBS and 1000 U/mL penicillin/streptomycin) to each of the dishes.
5. The c.p.e.$^+$, if any, may occur gradually in the HEK293 cells that have been transfected. An additional set of dishes may be prepared in case the second transfection (*see* **Note 2**) is needed.

3.1.3. Adenovirus Amplification

The possibility of achieving a high tier (up to 10^{12} viral particles/mL) is one of the favorable features of adenovirus and it is essential for in vivo gene transfer and gene therapy. To grow a large stock of adenovirus at high titer, a passage 1 (PP1) of the virus should be produced in a 35-mm dish with an isolated plaque (*see* **Fig. 6**). Then, amplify PP1 through an infection of HEK293 cells in a number of 150-mm dishes with a sufficient amount of the virus. In this way, all cells in the 150-mm dishes are infected at the same time, which means that the virus replication cycle is synchronous and the cells remain fully viable; thus, virus yield per cell is maximized. The cells may be harvested 2–3 d after the infection while the virus is still cell-associated. This is important for the yield of a high-titer virus because as the virus is still contained in the cells, the cells can be centrifuged and the pellet resuspended in small volume to raise the titer (*see* **Note 3**). After extraction of the virus from the resuspended cell pellet, the virus is put on the CsCl distributed in gradients and spun twice at 4°C at 62,500*g* (22.5 krpm with SW41), first for 1.5 h and then overnight. The

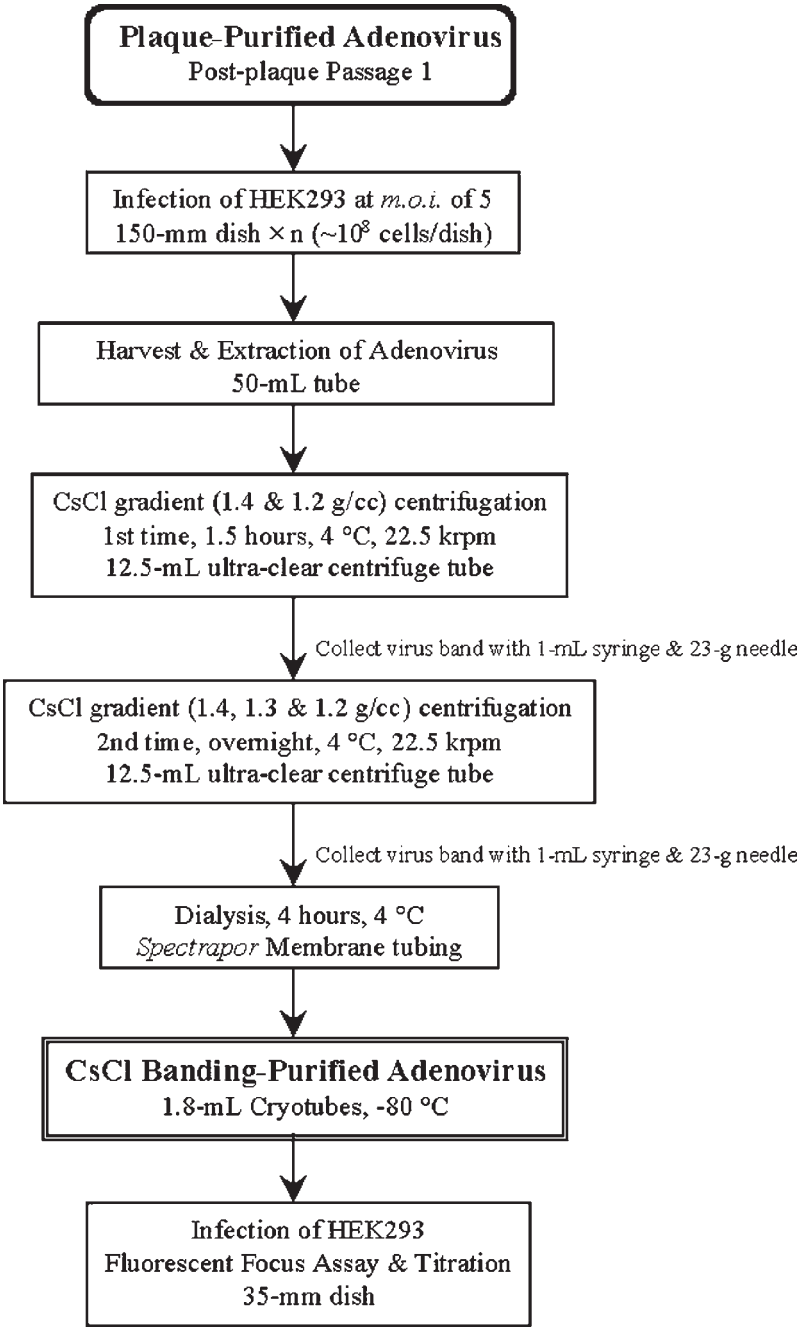

Fig. 6. Scheme of adenovirus amplification.

collected CsCl-banded virus needs to be dialyzed with the membrane tubing for 4 h at 4°C. The CsCl-banding purified virus then should be aliquoted and kept in cryotubes at –80°C as its tier is measured through titration and fluorescent focus assay (refer to **Subheading 3.1.3.4.**).

Figure 7 illustrates how an adenovirus is amplified via infection of HEK293 cells and what c.p.e.$^+$ looks like. In this illustration, AdGFP, an adenovirus that carries the gene of green fluorescent protein (GFP), is used. The c.p.e.$^+$ is a sign of successful recombination of Ad backbone and rescuing shuttle plasmids and production of the virus in HEK293 cells. It is also a sign of replication and propagation of recombinant virus in HEK293 cells.

3.1.3.1. Infection of HEK293 Cells

The following protocol is for the passage of HEK293 cells that may contain viral recombinants or the infection to amplify an adenovirus for a large stock.

1. Prepare culture dishes or flasks with HEK293 cells 2 d in advance, so that the monolayers are confluent on the day of infection.
2. For the growth of a virus stock, it is often necessary to infect cells at a specific multiplicity of infection (MOI, the average number of infectious virus units per cell). This requires two pieces of information: the number of HEK293 cells estimated in a confluent monolayer and the size of culture dishes being used, and the titer of the virus in infectious units/mL. Calculate the total amount of virus needed for the number of cells in the monolayer, using the inoculum volumes shown in **step 3**.
3. When the cells are confluent, remove the growth medium and inoculate with the following volumes of virus sample: 0.3 mL for 25-cm^2 flasks, 2.0 mL for 150-mm dishes, 0.3 mL for 60-mm dishes, and 0.2 mL for 35-mm dishes. These volumes are guides and can be modified to suit specific requirements, but too small a volume can lead to cells drying out during virus adsorption, and too large a volume decreases the efficiency of adsorption. If you have a large number of dishes to inoculate, remove the medium from a few dishes at a time so that the monolayers do not dry out before inoculation.
4. Disperse the inoculum over the monolayer surface every 20 min by shaking/tilting the dishes or flasks that are normally kept at 37°C in a CO_2 incubator during the adsorption period.
5. After 1 or 2 h, overlay the flasks or dishes with prewarmed maintenance medium DMEM plus 2% FBS and 1000 U/mL penicillin/streptomycin, using the same volume of medium as that in which the cells were originally grown.
6. Incubate the infected cells at 37°C for the desired length of time. If the infection is performed in permissive cells, at a high MOI, and the infection proceeds for over 24 h, the cells will show signs of c.p.e.$^+$ and will begin to detach from the surface.

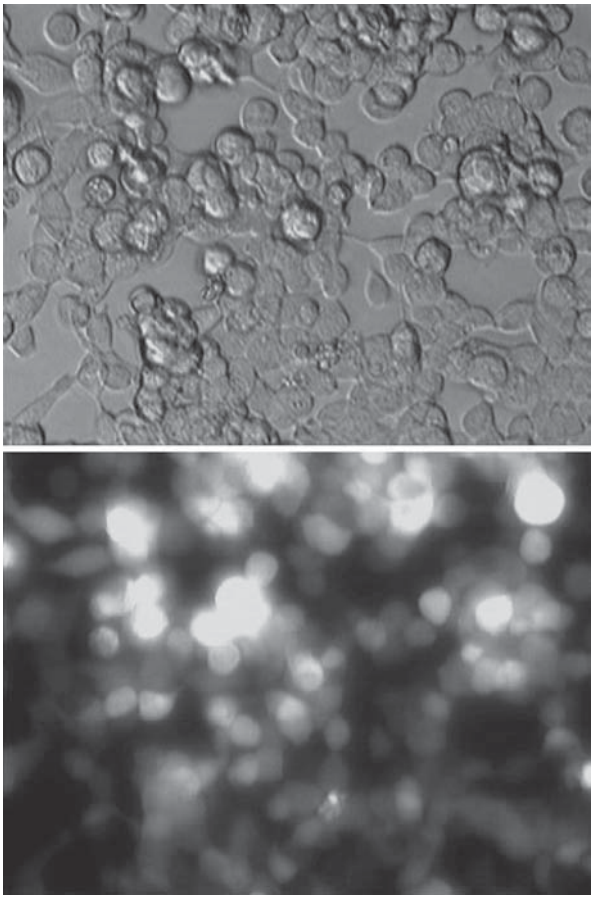

Fig. 7. AdGFP-infected HEK293 cells. Positive cytopathic effect (c.p.e.$^+$) is shown as holes surrounded by rounded HEK293 cells on the dish that have been infected by AdGFP. **Upper panel**: HEK293 cells with c.p.e.$^+$ focus under white microscope light. **Lower panel**: The cells that are infected by AdGFP emit green fluorescence (glowing bright here) in the same view field as the upper panel. (Reduced from original magnification.)

3.1.3.2. *Hirt* DNA Purification and Analysis

The following protocol is for the *Hirt* DNA purification and analysis to confirm the adenoviral genome.

1. Infect HEK293 cells in a 35-mm dish with 0.2–0.3 mL of plaque isolate or of passage 1 after recombination.

2. Wait until extensive c.p.e.$^+$ is observed, usually within 3–4 d. If infection is slow, pass to a second round.
3. Transfer cells to a 5-mL polypropylene snap-cap tube plus cap.
4. Spin at 400*g* at 4°C for 10 min.
5. Resuspend the pellet in 1 mL cold PBS and spin again. At this stage, the pellet can be stored at –20°C.
6. Resuspend the pellet in 1 mL nuclear lysis buffer plus pronase.
7. Incubate the resuspension in water bath at 37°C for 15–30 min.
8. Add 0.25 mL of 5 *M* NaCl. Mix gently and pour the suspension into a 1.5-mL tube.
9. Chill the tube on ice for 30 min or longer; the precipitate can be left indefinitely at 4°C.
10. Spin the tube in a cold room in one orientation (i.e., the tab on the tube points up or down) for 5 min at 12 krpm in a microfuge, then turn the tube 180° and spin for 10 more min.
11. Transfer 500 μL clear supernatant into a 1.5-mL Eppendorf tube and keep the remaining at –20°C. Then, add an equal volume of isopropanol to the tube. Spin the tube at 12 krpm in a microfuge for 15 min. Wash the precipitate well with 70% ethanol.
12. After the DNA precipitate is dry, resuspend it in 50 μL TE (10 m*M* Tris-HCl plus 1 m*M* EDTA). This DNA will digest well, but it is often messy. To preserve the integrity of the DNA, keep the samples frozen at –20°C.

Before use, it is important to purify the virus with CsCl gradient; it is essential especially for in vivo study. The cell debris that contains various proteins together with the harvested virus could impose significant toxicity to the target system (e.g., cardiac myocytes) while the transgene carried by the virus is expressed.

3.1.3.3. CsCl-Banding

The following protocol is for the CsCl-banding to purify the adenovirus produced.

First, prepare HEK293 cells in several (*n*) 150-mm culture dishes (i.e., $n = 5$), 10^8 cells/dish, 2 d before infection. The number of dishes is dependent on how much virus one intends to harvest. Cells are confluent on the day of infection. Infect cells at a MOI of 5 with inoculum of 2 mL for 2 h followed by 25 mL DMEM (refer to **Subheading 3.1.3.1.**) to cover each dish, and check the c.p.e.$^+$ in 2–3 d. Harvest cells when they are ready (cells have come off the dishes) and transfer to several conical 50-mL tubes. Wash dishes with 10 mL PBS to collect the remaining cells as much as possible and transfer them also to the tubes.

1. Pellet $n \times 10^8$ infected cells in the conical tubes (50 mL) at 400*g* for 15 min at 4°C, then resuspend and wash with 40 mL PBS, repellet at 400*g* for 15 min at 4°C, and store the dry pellet frozen at –20°C until ready to extract.

2. Resuspend the pellet in 5–7 mL of 10 m*M* Tris-HCl buffer at pH 7.8 and 20 m*M* $MgCl_2$.
3. Add 1/10 volume of deoxycholate solution. Mix DOC (deoxycholate stock) and cell resuspension. The mix gets very viscous. Incubate it for 15 min in the water bath at 37°C.
4. Add DNase to 20 μg/mL from its stock of 1 mg/mL that is kept frozen at –20°C. Incubate it for 15–30 min at 37°C, or until solution becomes much less viscous.
5. Balance the tubes well before centrifugation. Spin at 1600*g* for 15 min at 4°C to remove larger cellular debris. Transfer the supernatant to a fresh 15-mL snap-cap tube.
6. Prepare the CsCl solution with the density of 1.6 g/mL (made out of 50 g of CsCl in 50 mL of 50 m*M* Tris-HCl at pH 7.8). To have CsCl solutions with densities of 1.4, 1.3, and 1.2 g/mL, mix CsCl of 1.6 g/mL and 50 m*M* Tris-HCl at proper ratios.
7. Set up CsCl gradients 1.4 and 1.2 g/mL in a 12.5-mL ultraclear centrifuge tube that matches the rotor SW41. Lay CsCl gradients carefully in the centrifuge tube, first 3 mL of 1.4 g/mL and second 4 mL of 1.2 g/mL. Then, lay the supernatant from **step 5** on the CsCl cushion. Vary the volumes of CsCl of 1.4 g/mL and CsCl of 1.2 g/mL according to the volume of the supernatant. The final volume in the centrifuge tube should be close to 12 mL, filling the tube all the way to the top (about 2–3 mm below the edge of the tube). This is to prevent the tube from collapsing during the high-speed spinning.
8. Fill another ultracentrifuge tube with CsCl and Tris-HCl as a balance. Balance the two tubes very carefully!
9. Spin an ultracentrifuge rotor SW41 at 62,500*g* (22.5 krpm) for 1.5 h at 4°C.
10. Collect the viral band (1–2 mL) and add an equal volume of 50 m*M* Tris-HCl at pH 7.8 to it and mix. There are likely two bands in the centrifuge tube after the 1.5-h spinning. Take the lower band by slowly twisting and stabbing the needle (23 gage) on a 1-mL syringe through the tube on the side at the level a bit higher than the band.
11. Lay the mix gently onto a preformed CsCl (in 50 m*M* Tris-HCl at pH 7.8 and 10 m*M* $MgCl_2$) gradient (2.5 mL of 1.4 g/mL, 3 mL of 1.3 g/mL, and 3 mL of 1.2 g/mL) in a new ultraclear centrifuge tube. On the top of the virus, add Tris-HCl to fill up the tube.
12. Carefully balance the tubes again and spin an ultracentrifuge SW41 at 62,500*g* (22.5 krpm) overnight at 4°C.
13. Collect the viral band (0.5–1.5 mL) by the same method as in **step 10** (*see* **Fig. 8**).

3.1.3.4. Estimation of Viral Titers

The following protocol is for the estimation of viral titers.

3.1.3.4.1. Fluorescent Focus Assay

1. The virus to be titrated is diluted in medium containing at least 2% FBS. For most stocks, where the titer is in the range of 10^9–10^{10} viral particles/mL, the dilutions are made as serial 10-fold dilutions, to $\times 10^{-6}$. Make sure to change the pipets during the serial dilution!
2. Monolayers of HEK293 cells in 35-mm dishes are prepared and used.

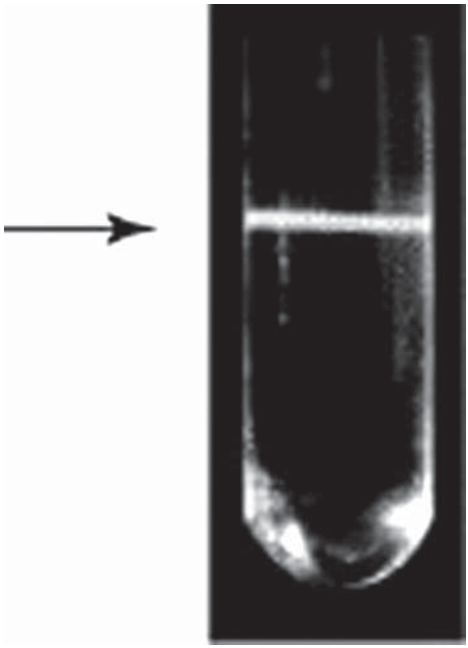

Fig. 8. CsCl-banded virus. Adenovirus forms a white band (pointed by arrow, approx 1.34 g/mL in density) within the CsCl gradient in an ultraclear centrifuge tube after overnight spinning at 62,500*g* with SW41 ultracentrifuge rotor (22.5 krpm) at 4°C.

3. Medium is removed from the 35-mm, dishes, and 0.2 mL of the viral dilution is added. The inoculum is spread across the cells in the dishes by gentle shaking/tilting every 15–20 min. The dishes are incubated at 37°C for 1–2 h and then overlaid with 2.5 mL of DMEM plus 2% FBS.
4. Incubate the infected dishes for 24–28 h. Remove the maintenance medium, wash gently twice with 2.5 mL PBS, and then add 2.5 mL of 90% methanol. Leave at room temperature for at least 4 min. Be careful and gently change the media, as the monolayers become rigid and fragile, especially after being fixed by methanol!
5. Remove the methanol and wash twice with 2.5 mL PBS, letting the PBS remain on the cells for 4 min each time. Dishes can be stored for several days under PBS, if kept at 4°C.
6. Remove PBS and add 0.5 mL of diluted mouse anti-adenovirus antiserum. Incubate at room temperature for 30 min. Wash twice with 2.5 mL PBS.
7. Add 0.5 mL of a solution containing fluoresceinated goat anti-mouse antiserum and incubate for 30 min at room temperature. The solution of the antiserum is kept frozen and in the dark.

8. Remove the stains, wash twice with 2.5 mL PBS, add 0.5 mL PBS to keep the dishes moist, and examine under a UV fluorescence microscope. Dishes can be stored at 4°C, but must be kept in the dark to prevent bleaching of the fluorescein.
9. The titer is calculated on the basis of the number of fluorescing cells per field, and this depends on the optical properties of the microscope. We usually use an objective lens with a graduated eyepiece and multiply the averaged number per grid by 10^4 (a coefficient considering the several factors applied particularly to this titrating procedure and microscope) and the reciprocal of the dilution.
10. The advantage of the fluorescent focus assay is that a titer is derived quickly. The disadvantage is that it requires more hands-on time and specialized materials/equipment.

3.1.3.4.2. Plaque Assay

1. The virus to be titrated is diluted in medium containing at least 2% FBS. For most stocks, where the titer is in the range of 10^9–10^{10} viral particles/mL, the dilutions are made as serial 10-fold dilutions, to $\times 10^{-9}$. Make sure to change pipets during the serial dilution!
2. Monolayers of HEK293 cells in 60-mm dishes for the plaque assay are prepared.
3. Medium is removed from the 60-mm dishes, and 0.3 mL of the viral dilution is added. The inoculum is spread across the cells in the dishes by gentle shaking/tilting every 15–20 min. The dishes are incubated at 37°C for 1–2 h, and then overlaid with 10 mL of 2X LP/agar.
4. After inoculation with the appropriate viral dilution and incubation for 1–2 h, the dishes are overlaid with 10 mL of 2X LP, containing supplements and 0.8% purified agar (*see* **step 6**). After allowing at least 45 min for the dishes to harden, they are incubated at 37°C for 6 d, and 5 mL of 2X LP/supplements/agar is added. At d 9 or 10, 4 mL of 2X LP/supplements/agar containing neutral red is added, and the dishes are incubated in the dark for another 2–3 d. Plaques are readily visible as opaque circles against a deeply stained red background of uninfected cells.
5. The advantage of the plaque assay is that it is easy to perform. The disadvantage is that the titer is not available for almost 2 wk. The titers estimated by the fluorescent focus assay and the plaque assay are comparable.
6. Media preparation for plaque assay–refer to **Subheading 2.1.3.3.2.**

3.1.3.5. Dialysis of CsCl-Banded Virus

The following protocol is for the dialysis of CsCl-banded adenovirus.

1. Dialyze the collected virus after CsCl banding with Spectra/Por dialysis membrane tubing, four times against 1 L dialysis buffer in cold room for 4 h.
2. Soak the membrane in the dialysis buffer before loading the virus into it. Make knots on two ends of the membrane tubing, at least two knots on each end. Leave a bit of air together with the virus that is loaded in the middle of the membrane

tubing. Do not stretch the membrane too much while making knots, although knots have to be made securely so that there will not be any leak of virus.
3. Take a note of the volume of the virus loaded and compare it with the volume of the virus collected at the end of dialysis.
4. Distribute and store dialyzed virus in aliquots (in 1.8-mL cryotubes) at –80°C.

3.2. Expression/Delivery of Adenoviruses That Carry the Ion Channel Genes of Interest

3.2.1. Cell Isolation and Culture

3.2.1.1. HEK293 Cells

HEK293 cells grow in culture dishes in DMEM plus 10% FBS and 1000 U/mL penicillin/streptomycin as a monolayer at 37°C in a CO_2 incubator. They are particularly sensitive to the way they are handled. They should never be allowed to become overconfluent, should not be plated too sparsely, and should have regular medium changes between splits. Usually, they are split twice a week by 0.25% trypsin and 1 m*M* EDTA. HEK293 cells at low passages are suitable for the adenovirus plaque assays and DNA transfections. Higher passages or poorly adherent cells may be usable for virus growth, but the cell quality is critical for plaque assays and transfections. The cells should be 80–90% confluent at the time of transfection or plaque assay.

3.2.1.2. Cardiac Myocytes

3.2.1.2.1. Rat

Adult rats (approx 3 mo old) are anesthetized before being sacrificed, and neonatal rats (1–2 d-old) are just decapitated, in accordance with the Guide for the Care and Use of Laboratory Animal by the US National Institutes of Health (NIH Publication No. 85-23, revised 1985).

To prepare cell cultures of newborn rat ventricular myocytes, a standard trypsin dissociation method is applied ***(15)***. The cells are preplated to reduce fibroblasts, cultured initially in serum-containing medium (DMEM plus 10% FBS) for 24 h, and then switched to a serum-free medium (DMEM). Penicillin/streptomycin is present in the media. The infection with adenovirus can start at any time after this point. On the day of the experiment, the monolayer is resuspended by brief (2–3 min) exposure to 0.25% trypsin and replated onto fibronectin-coated 9 × 22-mm glass cover slips. The cultured cells are ready for electrophysiologic study approx 4 h after the resuspension. For the adult rats, freshly isolated ventricular myocytes are prepared using the procedure described by Kuznetsov et al. ***(16)***. This includes a Langendorff perfusion of the whole heart with a Ca^{2+}-free collagenase solution. The atria are then trimmed away, and the remaining tissue is minced and dissociated in addi-

tional collagenase solution. The isolated myocytes are resuspended in ACCTI and then plated on 9 × 22-mm glass cover slips at $(0.5–1)\times10^3$ cells/mm^2. Two to 3 h later, after the myocytes have adhered to the cover slips, the adenoviral infection procedure could begin (*see* **Subheading 3.2.2.**).

3.2.1.2.2. Dog

To disaggregate myocytes from the sections of epicardial muscle where the virus has been injected in the in vivo gene transfer study, the following procedure is used ***(17)***. The tissue is rinsed in a Ca^{2+}-free trituration solution to remove blood and then immersed in 20 mL trituration solution bubbled with 100% O_2 and maintained at 36.5°C. For the several steps of trituration, 20 mL solution containing both protease and collagenase or collagenase alone is used. After each step, the supernatant containing the dispersed myocytes is collected and a loose pellet is resuspended in the solution containing 50 μ*M* Ca^{2+} and 0.1% bovine serum albumin, pH 7.2. This resuspension solution is changed every 30 min for solutions containing increasing concentrations of Ca^{2+} (100, 200, and 350 μ*M*). Myocytes are kept at room temperature in the final solution (350 μ*M* Ca^{2+}) and then can be used for electrophysiological assay for about 6 h.

3.2.2. In Vitro Gene Transfer to Cardiac Myocytes

Prepare 35- or 60-mm culture dishes of neonatal rat ventricular myocytes, so that the monolayers are evenly formed on the day of infection. Adult rat ventricular myocytes are plated at the density of $(0.5–1)\times10^3$ cells/mm^2 on 9 × 22-mm glass cover slips that are put in either 35- or 60-mm dishes 2–3 h before infection. Remove the culture medium from the dishes and inoculate with 0.4 or 0.6 mL/dish of the adenovirus that is intended to be transferred at a MOI of 10–100. Disperse the inoculum over the monolayer surface or sparsely plated adult rat myocytes every 15–20 min by shaking/tilting the dishes (*see* **Note 4**). The dishes are kept at 37°C in a CO_2 incubator during the adsorption period of 1.5–2 h. Then, the inoculum is discarded, and the dishes of neonatal rat myocytes are filled with 2 or 5 mL DMEM per dish, and those of adult rat myocytes are filled with ACCTI. All of the dishes stay in the CO_2 incubator for 1–2 d or longer before electrophysiological experiment is conducted. **Figure 9** shows an example of in vitro transferring GFP gene to cardiac myocytes.

3.2.3. In Vivo Gene Delivery to the Heart

3.2.3.1. Rat

Before undergoing thoracotomy, adult rats (3–4 mo old) are anesthetized by intraperitoneal injection of ketamine (80 mg/kg) plus xylazine (10 mg/kg). Rats are intubated and ventilated with a small respirator. The skin overlying the

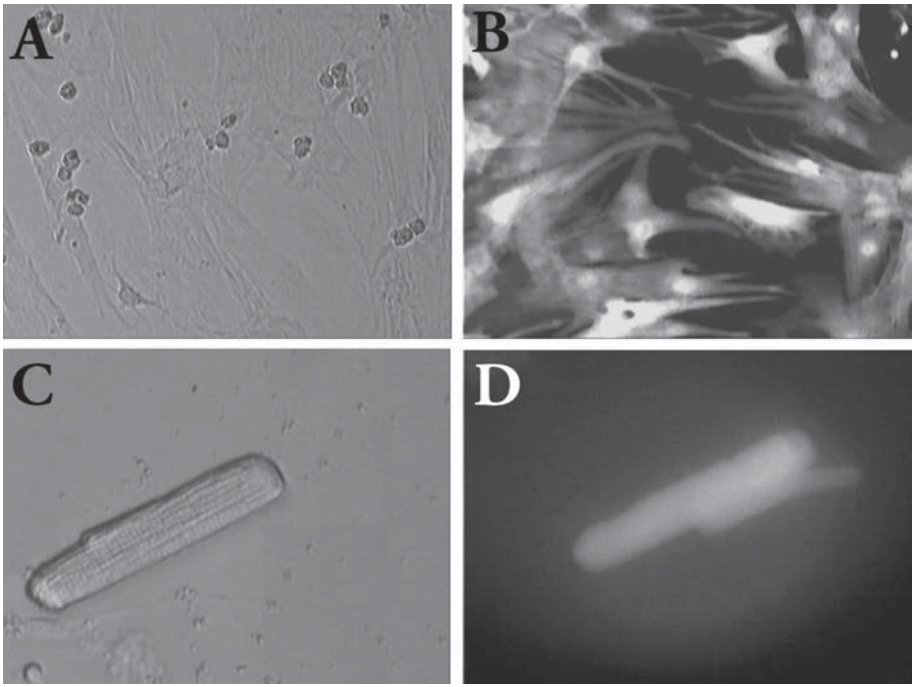

Fig. 9. In vitro adenovirus-mediated gene transfer into cardiac myocytes. Ventricular myocytes dissociated from neonatal and adult rats are infected by AdGFP. **Top panels**: Neonatal cells (flat and spread) under white light of a microscope **(A)** after 3 d in culture, and neonatal cells that have been infected by AdGFP at a MOI of 30 and emit green fluorescence (**B**, glowing bright) after 3 d in culture. The black particles in **(A)** are cell debris. **Bottom panels**: An adult rat cell under white light of a microscope **(C)** after 2 d in culture, and another adult rat cell that has been infected by AdGFP at a MOI of 100 and is green fluorescent (**D**, glowing bright) after 2 d in culture. The majority of cells (at least 90%), from neonatal or adult animals express a foreign gene such as GFP or HCN delivered via adenoviral vector under this condition. (Reduced from original magnification.)

sternum is incised, midline vessels of the sternum cauterized by Bovie forceps, and the sternum divided. The sternum is retracted with 6-0 ligatures, and the heart gently exteriorized with Crile forceps at the apex. Care has to be taken not to damage the lungs or large vessels during the procedure. The heart is briefly held still and receives an injection of 30–50 μL adenoviral vectors of transgenes such as HCN2 and GFP at a concentration of 1×10^{10} ffu/mL (fluorescence focus unit per milliliter) at the apex through a 31-gage needle. The heart then is repositioned back to the thoracic cavity and the sternum closed.

Over the next half an hour, upon returning of spontaneous movement, the rats are released from the ventilator and provided with 100% O_2 through a nose cone. The body temperature is maintained with a heating pad throughout the experiment. The rats that received the injection are usually killed 2–3 d later, and the cells dissociated for experiment. For the examination of gene expression efficiency, persistence, and stability, the rats can be sacrificed at various given times after the injection depending on the experiment design.

3.2.3.2. Dog

Dogs (3–5 yr old, 18–20 kg) are anesthetized with Pentothal (17 mg/kg) through iv followed by Isoflurane (1.5–2.0%) mixed in O_2. A left lateral thoracotomy is performed and the heart suspended in a pericardial cradle. Injection of the adenoviral vectors that carry GFP or GFP+HCN2 genes is made into the epicardium of the left ventricle to a depth of approx 2 mm through a 30-G needle home-made to have a spiral shape (*see* **Note 5**). Two to three injections of 10^{10} ffu viral particles are made using a total volume of 0.6 mL. The area of injections is labeled prior to the closure of the chest in layers, and the dogs are maintained in the Intensive Care Unit. The gene delivery and its electrophysiological functions could be examined 3 d later or longer, depending on the experimental design. **Figure 10** shows an example of in vivo transferring GFP gene to the left ventricle of an adult dog by injection.

3.3. Electrophysiological Studies of Ion Channels with Adenovirus-Mediated Gene Transfer

3.3.1. Patch Clamping of Single Cultured or Acutely Dissociated Cells That Are In Vitro or In Vivo Infected by Adenovirus

The electrical activity of ion channels on the cell membrane, endogenous or exogenous, can be examined with patch-clamp technique, which was invented by Neher and Sakmann ***(18)*** and optimized by Hamill et al. ***(2)***. The basis of the patch-clamp technique is the formation of a high-resistance seal (GΩ) between the cell membrane and the glass wall of a patch pipet tightly placed on the cell. The tight seal makes it possible to register the ionic current with a very low level of background noise, which is especially crucial for the single-channel recording.

There are five patch-clamp configurations: cell attached, inside-out, outside-out, whole cell, and perforated whole cell. The whole-cell enabled by rupture is the configuration for recording ionic current flowing through whole-cell membrane, whereas the other three (2, 3, 5; *see* **Fig. 11**) may be used to register single-channel current through a small patch of cell membrane. The cell-attached patch becomes a perforated whole-cell patch when antibiotics such as

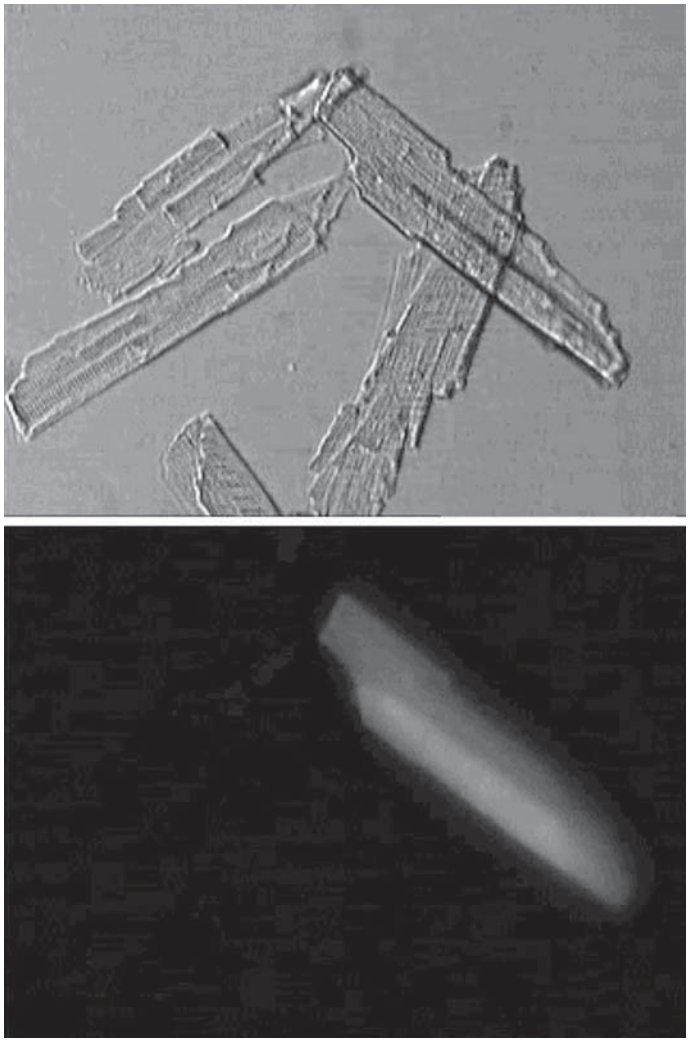

Fig. 10. In vivo adenovirus-mediated gene transfer into the heart of living dog. Cardiac myocytes dissociated from left ventricle of the dog 3 d after injection of AdGFP. **Upper panel**: Several ventricular myocytes under white microscope light. **Lower panel**: The cell expressing GFP (glowing bright), in the same view field as the upper panel. (Reduced from original magnification.)

commonly used Nystatin or Amphotericin B (400 μg/mL final out of the stock of 30 mg/mL in dimethyl sulfoxide [DMSO]) is added to the pipet solution. The antibiotic in the patch pipet acts on the cell membrane under the pipet tip and forms pores; therefore, the access resistance is reduced.

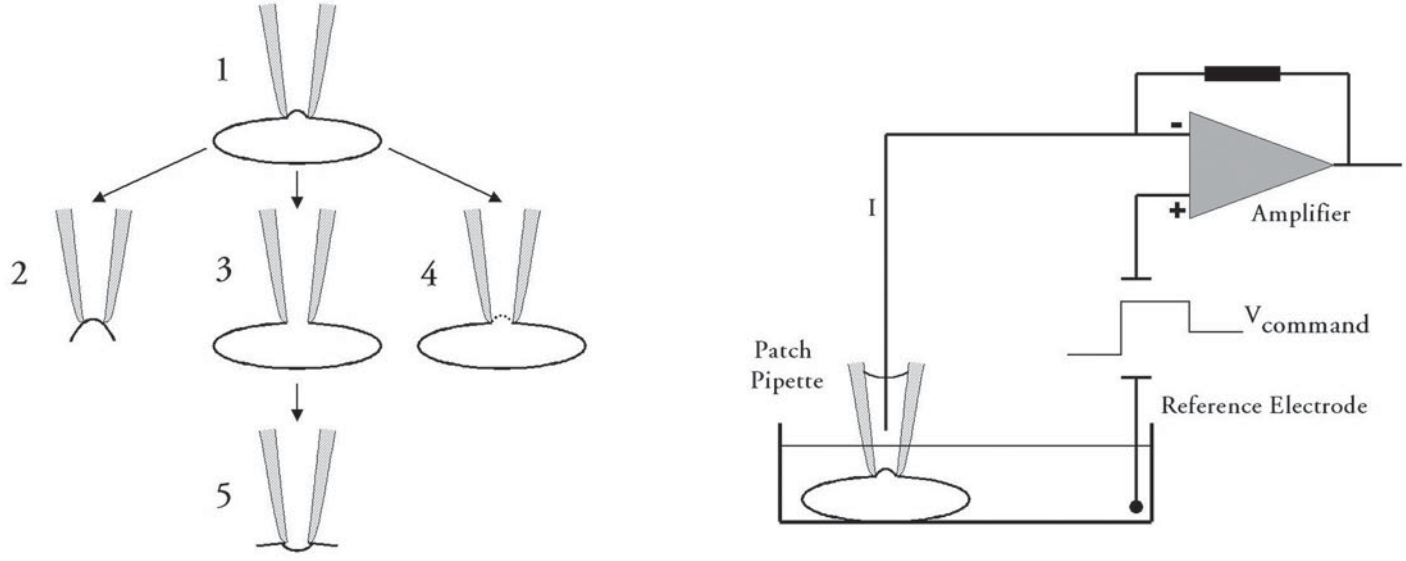

Fig. 11. Patch-clamp configurations and schematic electrical circuit of patch clamping. **Left panel**: The single-cell patch-clamp configurations: (1) cell attached, (2) inside-out, (3) whole cell, (4) perforated whole cell, (5) outside-out. **Right panel**: An illustration of the electrical circuit for single-cell patch clamping.

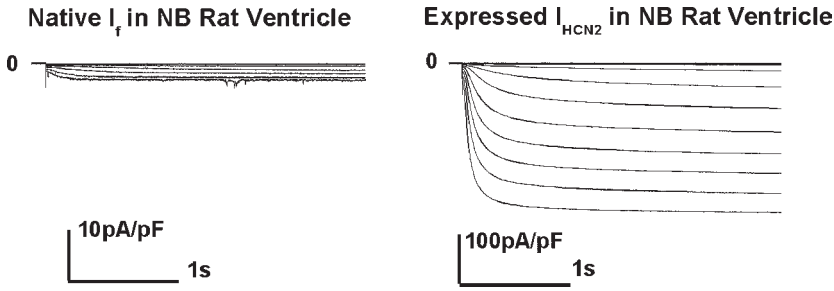

Fig. 12. Pacemaker current recordings from cells infected with adenovirus of HCN2 versus non-infected cells. **Left panel**: The native pacemaker current (I_f) recorded with whole-cell voltage clamp from a ventricular myocyte of neonatal rat in response to hyperpolarization. **Right panel**: The recording of the expressed pacemaker current (I_{HCN2}) whose gene was transferred by adenoviral vector AdHCN2 also in a ventricular cell of neonatal rat. The expressed current is at least 10-fold greater than the native in magnitude. The holding potential is –35 mV.

The whole-cell (ruptured or perforated) configuration is applied to record the pacemaker current, native I_f or expressed I_{HCN2}, in the voltage clamp mode, and the membrane potential, in the current clamp mode (*see* **Fig. 12**). Experiments are carried out on cells superfused at 35–36°C (*see* **Note 6**). $MnCl_2$ (2 m*M*) and $BaCl_2$ (4 m*M*) are added to the superfusate to eliminate I_{Ca}, and I_{K1}, which can obscure I_f or I_{HCN2}. CsCl (1–4 m*M*) is used extracellularly to identify the pacemaker current. A fast solution changing apparatus is in place so that the whole experimental protocol can be done promptly after a patch is formed. The pipet resistance is typically 1–3 MΩ.

Among all of the electrophysiological and biophysical properties of the pacemaker channels (I_f or I_{HCN}), activation kinetics, activation-voltage relation, reversal potential, and maximal channel conductance are the primary ones. I_f or I_{HCN} is defined as a time-dependent ionic current in response to hyperpolarizing voltage steps from –35 mV as the holding potential for neonatal myocytes (–55 mV for the adult) to a range of –55 to –145 mV. The test voltage steps are 6 s and longer in order to reach steady state of activation (*see* **Note 7**) and accurate measurement of biophysical characteristics of I_f or I_{HCN}. The steps should be considerably long, up to 60 s, for the recording of slow-activating members of HCN family such as HCN4. The test pulses are followed by a voltage step to –125 mV (*see* **Note 8**) for 6–8 s where the tail current is measured. After that, a pulse to –5 mV for 0.5 s is applied to deactivate the overexpressed HCN channels (*see* **Note 9**).

Pacemaker current is an inward current activated by hyperpolarization. However, when the channels are open, the current can also flow outwardly in

response to a depolarizing step. The reversal potential is the membrane potential at which the current reverses its direction from inward to outward or vice versa. The current is zero at the reversal potential. Electrochemically, the reversal potential E_{rev} is dependent on the transmembrane gradients of Na^+ and K^+ ions, which are the ionic carriers for this type of channels. It can be experimentally determined by depolarizing the membrane to various levels (e.g., –60 to 0 mV) from the voltage, such as –125 mV, where the channels are sufficiently activated ***(19)***.

The kinetics of activation is determined by a single- or double-exponential fit (with delay) to the time-course of activation at each test voltage (*see* **Fig. 13**). Once E_{rev} is measured, the maximum channel conductance can be calculated with the maximal tail current (refer to **Eq. 7**). The plot of the tail current amplitude versus test voltage after being normalized can be fitted with the Boltzmann function, and then the voltage of half-maximum activation ($V_{1/2}$) and slope factor (K) at $V_{1/2}$ can be decided from the fitting (refer to **Eq. 6**; *see* **Fig. 14**).

The relation of pacemaker current I_f (or I_{HCN2}) and membrane potential V_m can be described by

$$I = g(V_m, t)(V_m - E_{rev}) \tag{1}$$

where $g(V_m, t)$ is the channel conductance, a function of V_m and time t, and E_{rev} is the channel reversal potential.

The tail current I_{tail} can be registered when the channels are activated by a hyperpolarizing step at test voltage V_{test} followed by a second step to tail voltage V_{tail} (*see* **Fig. 14**, left panel). I_{tail} is described by

$$I_{tail} = g(V_{test}, t)(V_{tail} - E_{rev}), \tag{2}$$

where $g(V_{test}, t)$ is the channel conductance in function of V_{test} and t and

$$I_{tail} = g_{max}\, y(V_{test})(V_{tail} - E_{rev}), \tag{3}$$

where g_{max} is the maximum channel conductance at the time when all of the channels are fully activated and $y(V_{test})$ is the available fraction (availability) of the channels that could be activated at V_{tail}. $y(V_{test})$ is also called the activation–voltage relation or activation of the pacemaker channels.

I_{tail} is maximal when all the channels are fully activated, therefore, $y(V_{test}) = y_{max}(V_{test}) = 1$ and

$$I_{tail,max} = g_{max}\, y_{max}(V_{test})(V_{tail} - E_{rev}) = g_{max}(V_{tail} - E_{rev}). \tag{4}$$

By combining **Eqs. 3** and **4**, one obtains

$$\frac{I_{tail}}{I_{tail,\,max}} = y\,(V_{test}) \tag{5}$$

$y(V_{test})$ can be expressed using the Boltzmann function (*see* **Fig. 14**) as

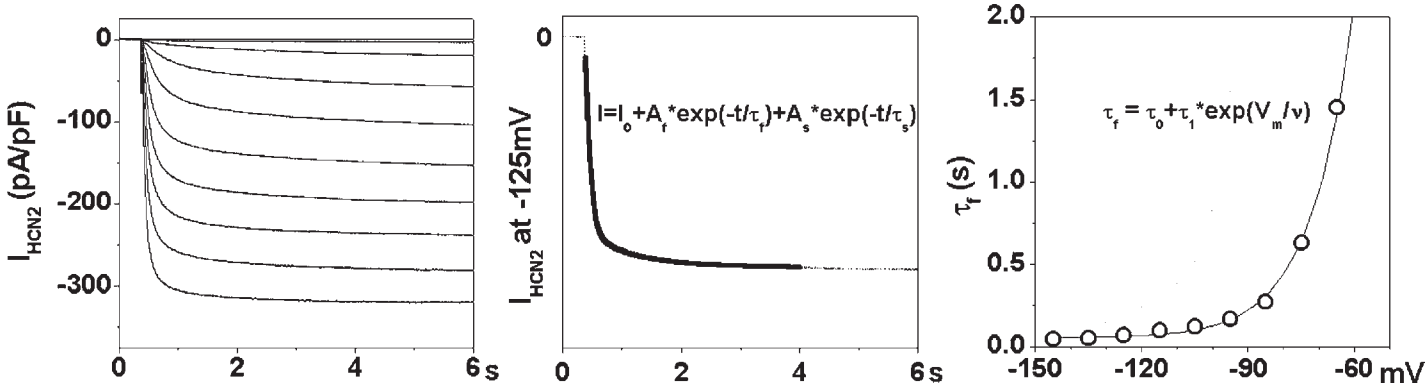

Fig. 13. Gating kinetics during activation of I_{HCN2}. The activation kinetics of pacemaker channels can be described as a single- or double-exponential function depending on the cell type and/or membrane potential and reflecting the nature of multiple states the channels may possess. **Left panel**: A family of I_{HCN2} traces registered in a ventricular myocyte of neonatal rat with test pulses from –55 to –135 mV and HP of –35 mV. **Middle panel**: The I_{HCN2} trace at –125 mV (dashed line, taken from the left panel) fitted with a double-exponential function (thick line) $I = I_0 + A_f \exp(-t/\tau_f) + A_s \exp(-t/\tau_s)$. A_f and A_s represent the amplitudes of fast and slow components of I_{HCN2}, respectively, and whereas τ_f (79.9 ms) and τ_s (832.5 ms) are the activation time-constants. **Right panel**: The relation of τ_f and membrane potential (V_m), and its fitting curve as a function of exponential growth: $\tau_f = \tau_0 + \tau_1 \exp(V_m/v)$.

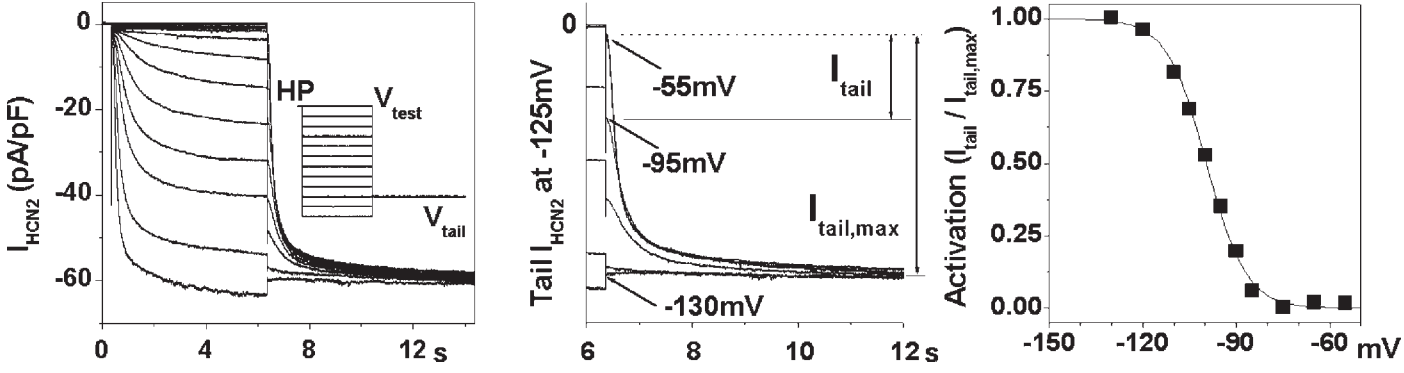

Fig. 14. Activation–voltage relation of I_{HCN2}. **Left panel**: A family of I_{HCN2} traces registered in a ventricular myocyte of an adult rat with a HP of –55 mV, test voltages (V_{test}) from –55 to –130 mV, and tail voltage (V_{tail}) at –125 mV. **Middle panel**: Tail currents elicited as the membrane potential steps from V_{test} to V_{tail}. The tail current (I_{tail}) is zero (dashed line) when the membrane potential steps from V_{test} of –55 mV to V_{tail} and maximal ($I_{tail,max}$) from V_{test} of –130 mV to V_{tail} (short solid line). **Right panel**: The relation of activation of HCN2 channels and membrane potential. Filled squares represent normalized I_{tail}, whereas the solid curve represents the Boltzmann fitting, which gives the $V_{1/2}$ and K values.

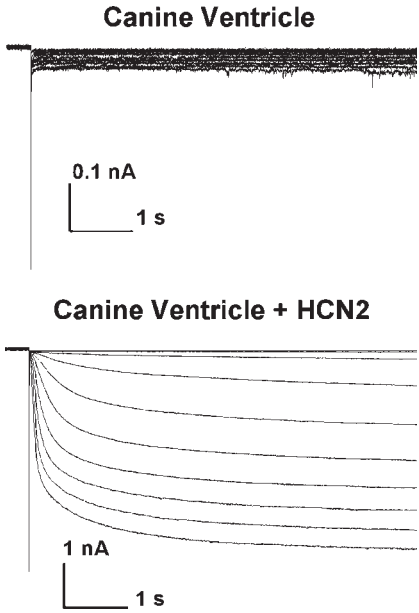

Fig. 15. Pacemaker current (I_{HCN2}) in vivo expressed in dog left ventricle. Ventricular myocytes acutely dissociated from an adult dog whose left ventricle has been injected with AdHCN2 (mixed with AdGFP as a visual marker) are examined with patch clamp. Little native pacemaker current I_f is seen in response to hyperpolarization in a cell that does not fluoresce, whereas a much greater expressed I_{HCN2} is manifested in a cell that fluoresces, indicating a successful in vivo expression of foreign genes HCN2 and GFP. During recording, the HP is –55 mV and the test voltages range from –65 to –145 mV.

$$y(V_{test}) = \frac{1}{(1 + \exp[(V_{test} - V_{1/2})/K])}. \quad (6)$$

where $V_{1/2}$ is the voltage of half maximum activation and K is the slope factor at $V_{1/2}$.

As a result, based on **Eq. 4**, the maximal channel conductance can be determined by

$$g_{max} = \frac{I_{tail,max}}{V_{tail} - E_{rev}} \quad (7)$$

Mediated by adenovirus, GFP and HCN2 genes are able to be efficiently delivered into cardiac myocytes. Such a gene transfer is demonstrated in vitro (*see* **Fig. 12**) and it could also be achieved in vivo. **Figure 15** shows that the HCN2 gene is overexpressed in the left ventricle of an adult dog by injection

through the open-chest operation. After the surgery, the dog lived for 3 d before the ventricular myocytes were dissected for the electrophysiological assay. In vivo gene transfer proves to be achievable and the delivered gene in the target system is significant in terms of physiological functions. There are technical issues, however, including localization and specificity, efficiency and persistence, toxicity and immune response, regulation, and induction, that need to be considered and solved prior to clinical attempts for therapeutic purposes. The therapeutic promise of delivering the gene of pacemaker ion channels is conceptually demonstrated (*see* **Fig. 16**) in the heart where pacemaking physiological function is added through an in vitro adenovirus-mediated HCN2 gene expression.

4. Notes

1. A successful recombination largely depends on whether a sufficient transfection has taken place. With the method described here, as an indication, it is important to see precipitates on HEK293 cells a few hours after cotransfection. The precipitation is largely the result of the addition of $CaCl_2$, which facilitates the absorption of plasmids into HEK293 cells for recombination. Treating cells with glycerol and changing the medium 4–5 h after transfection could remove the precipitates and ease cells from any impact by transfection procedure. Therefore, be sure to see a good precipitation!
2. It is not unusual that two plasmids would not successfully recombine in the first trial after their cotransfection into HEK293 cells. This could happen for various reasons. For instance, some mistakes are made without being noticed during transfection, some media/solutions are not prepared properly, or, basically, a particular transgene in the rescuing plasmid could impose toxic effects to the HEK293 cells, which, in turn, would inhibit recombination from happening. Therefore, it is recommended, for the sake of saving time, to set up a second cotransfection while expecting the recombination from the first cotransfection to occur. Always have a control cotransfection (between the empty rescuing plasmid and the adenoviral backbone plasmid) set in parallel to what is being constructed.
3. The right timing to harvest infected HEK293 cells is crucial to get a high-titer virus. It is obviously too early if a maximal number of HEK293 cells are not infected and thus a maximal amount of virus would not be produced; it is too late if infected cells have ruptured and the virus gets lost in the culture maintenance medium. Usually, when the infected cells are rounded up and detach from the dish at a gentle shake of the dish, it is the time to harvest. Normally, about 2–3 d after infection, one should pay a close attention to the infected cells and decide/catch the right moment to harvest.
4. It is important to use small inoculum for the in vitro infection. This is for the maximal virus adsorption and efficiency. Because of the small inoculum, it is equally important to assure that all of the cells to be evenly exposed to the inoculum by regularly tilting/shaking the culture dishes where the infection takes place.

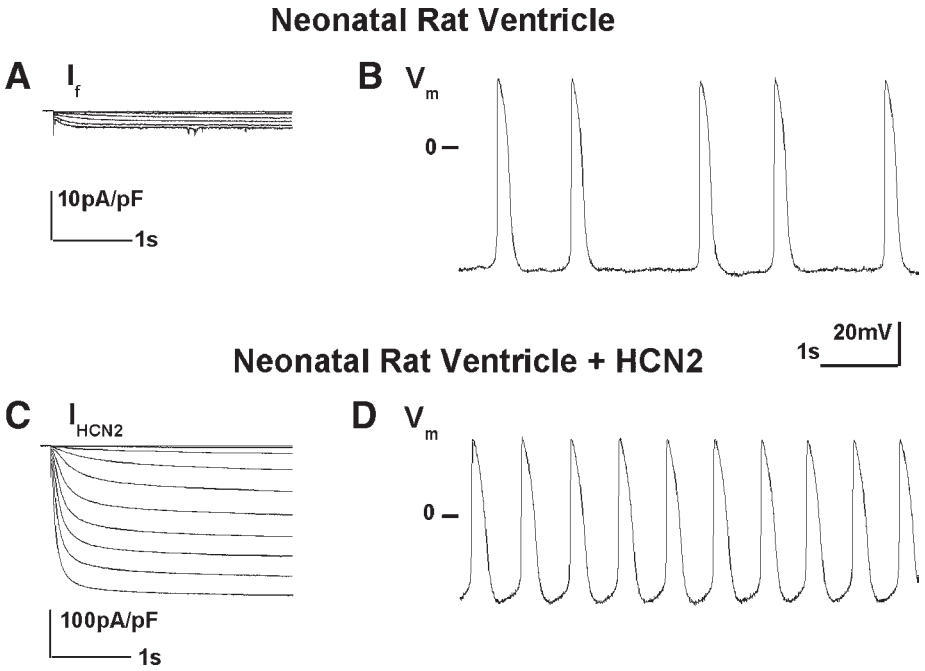

Fig. 16. Cardiac pacemaker activity in ventricle generated by AdHCN2. A monolayer sheet is formed during the culture of ventricular myocytes from neonatal rats. The cells are infected by AdHCN2 at MOI of 10. Spontaneous electrical activity is often observed in this type of cell preparation; however, it is slow and irregular **(B)**. In the monolayer sheet of the cells where the HCN2 gene has been overexpressed, the electrical rhythmic activity becomes much faster and more regular **(D)**. A phase-4 diastolic depolarization—a hallmark of cardiac pacemaker activity—is also manifested. A much greater I_{HCN2} is registered in the cells that are infected by AdHCN2 **(C)** in comparison to the native I_f in the cells that have not undergone HCN2 gene transfer **(A)**.

5. An efficient method to deliver a transgene is the primary step deciding whether the study of the transgene will work or not in in vivo experiments. It is, as a matter of fact, a technical challenge to inject the virus precisely to a targeted location in a contracting heart. A needle made in a spiral shape, as an example, is practically useful for the injection of virus to a working heart because it can grip tissue better for the maximal amount of virus to be injected. Thus, any modification should be explored and pursued in order to optimize the delivery efficiency.
6. It has been proven that the gating of pacemaker channels is sensitive to temperature. Therefore, it is important to be aware of the temperature at which I_f or I_{HCN} is recorded and to compare their gating properties.

7. The pacemaker channels activate slowly in response to less negative hyperpolarizing steps. For instance, the activation time constant of I_{HCN2} is 0.5–1.0 s in rat ventricular myocytes at –90 mV at 35°C. This is especially true with HCN4, which activates very slowly with a time constant of seconds. Therefore, long hyperpolarizing pulses have to be employed to ensure that a steady state of channel activation has been reached! Inadequate duration of hyperpolarizing steps could produce a substantial experimental error in the activation–voltage relation of pacemaker channels ***(20)***.
8. As the voltage (V_{tail}) to register tail HCN2 current, –125 mV is chosen for two major reasons: (1) for a tail current with a reasonable amplitude to build an accurate activation curve and (2) for least contamination of other currents, especially a variety of K^+ currents in adult rat and mouse hearts, at this voltage. This consideration is important especially for working with the cardiac myocytes from adult animals like rats or mice, in which K^+ channels are complex but closed at a negative voltage such as –125 mV.
9. It is advised to deactivate overexpressed HCN channels at a positive voltage once they are activated during voltage clamp for the current–voltage relation. It should be considered for HCN4, in particular, which is slowly activating and deactivating. A positive deactivation step (e.g., to –5 mV for 0.5–1 s) would speed up the recovery of the overexpressed HCN channels from an activated state to a fully closed state so that an accurate measurement of current–voltage relation could be ensured.

Acknowledgments

The authors wish to cordially thank Dr. Hamish Young at the Columbia University Department of Microbiology for his persistent guidance and Mrs. Ming Chen for her technical assistance. J.Q. is supported by a Scientist Development Grant (0130480T) from the American Heart Association Heritage Affiliate.

References

1. Hodgkin, A. L. and Huxley, A. F. (1952) A quantitative description of membrane current and its application to conduction and excitation in nerve. *J. Physiol. (Lond.)* **117,** 500–544.
2. Hamill, O. P., Marty, A., Neher, E., et al. (1981) Improved patch-clamp techniques for high-resolution current recording from cell and cell-free membrane patches. *Pflugers Arch.* **391,** 85–100.
3. Drews, J. (2000) Drug discovery: a historical perspective. *Science* **287,** 1960–1964.
4. Mountain, A. (2000) Gene therapy: the first decade. *Trends Biotechnol.* **18,** 119–128.
5. Khuri, F. R., Nemunaitis, J., Ganly, I., et al. (2000) A controlled trial of intratumoral ONYX-015: a selectively-replicating adenovirus, in combination with cisplatin and 5-fluorouracil in patients with recurrent head and neck cancer. *Nature Med.* **6,** 879–885.

6. High, K. A. (2001) Gene transfer as an approach to treating hemophilia. *Circ. Res.* **88,** 137–144.
7. Isner, J.M. (2002) Myocardial gene therapy. *Nature* **415,** 234–239.
8. Johns, D. C., Marx, R., Mains, R. E., et al. (1999) Inducible genetic suppression of neuronal excitability. *J. Neurosci.* **19,** 1691–1697.
9. Qu, J., Barbuti, A., Protas, L., et al. (2001) HCN2 overexpression in newborn and adult ventricular myocytes: distinct effects on gating and excitability. *Circ. Res.* **89,** e8–e14.
10. Ludwig, A., Zong, X., Jeglitsch, M., et al. (1998) A family of hyperpolarization-activated mammalian cation channels. *Nature* **393,** 587–591.
11. Santoro, B., Liu, D. T., Yao, H., et al. (1998) Identification of a gene encoding a hyperpolarization-activated pacemaker channel of brain. *Cell* **93,** 1–20.
12. Graham, F. L. (2000) Adenovirus vectors for high-efficiency gene transfer into mammalian cells. *Immunol. Today* **21,** 426–428.
13. Ng, P., Parks, R. J., Cummings, D. T., et al. (1999) A high efficiency Cre/loxP based system for construction of adenoviral vectors. *Hum. Gene Ther.* **10,** 2667–2672.
14. Ng, P., Parks, R. J., Cummings, D. T., et al. (2000) An enhanced system for construction of adenovirus vectors by the two-plasmid rescue method. *Hum. Gene Ther.* **11,** 693–699.
15. Ghavami, A., Baruscotti, M., Robinson, R. B., et al. (1997) Adenovirus-mediated expression of 5-HT_{1B} receptors in cardiac ventricle myocytes: coupling to inward rectifying K^+ channels. *Eur. J. Pharmacol.* **340,** 259–266.
16. Kuznetsov, V., Pak, E., Robinson, R. B., et al. (1995) B_2-Adrenergic receptor actions in neonatal and adult rat ventricular myocytes. *Circ. Res.* **76**, 40–52.
17. Lue, W. M. and Boyden, P. A. (1992) Abnormal electrical properties of myocytes from chronically infarcted canine heart: alteration in V_{max} and the transient outward current. *Circulation* **85,** 1175–1188.
18. Neher, E. and Sakmann, B. (1992) The patch clamp technique. *Sci. Am.* **266,** 44–51.
19. Qu, J., Cohen, I. S., and Robinson, R. B. (2000) Sympathetic innervation alters activation of pacemaker current (I_f) in rat ventricles. *J. Physiol. (Lond.)* **526,** 561–569.
20. Santoro, B., Chen, S., Luthi, A., et al. (2000) Molecular and functional heterogeneity of hyperpolarization-activated pacemaker channels in the mouse CNS. *J. Neurosci.* **20,** 5264–5275.

12

Antibody Production and Immunocytochemical Localization of Amino Acid Transporters

David V. Pow, Robert Sullivan, and Heather Scott

1. Introduction

This chapter details the procedural and conceptual issues that underpin the localization of high-affinity amino acid transporters by immunocytochemistry, with particular reference to the mammalian nervous system. Defining a role for transporters in any individual tissue often requires an understanding of the spatial distribution of a specific transport system. Techniques such as *in situ* hybridization provide clear evidence for the potential expression of a transporter by a specific cell type. In many cases however, properties such as targeting to basal or apical surfaces of, for instance, a transport epithelium or targeting to distinct plasmalemmal or cytoplasmic compartments in response to stimulation are most readily determined by the use of antibodies to detect such transporters, in intact tissues, isolated cells, or subcellular fractions of tissues. Methodologies for creating antibodies for the direct immunocytochemical localization of transporters are presented in this chapter. Issues that influence the applicability of methodologies such as postmortem delay, especially in human tissues, are also addressed.

Although selective antibodies are potent tools for investigating transporter biology, antibodies generated without due regard to possible confounding factors such as sequence homologies, or used without appropriate controls, can yield erroneous results. Accordingly, it is imperative that careful choices are made in the method(s) used to create antibodies and in their appropriate usage.

1.1. Strategies for Raising Antibodies

Two distinct approaches have been used in our laboratory to answer distinct questions about transporter localization. Where a transporter has been cloned,

From: *Methods in Molecular Biology, vol. 227: Membrane Transporters: Methods and Protocols*
Edited by: Q. Yan © Humana Press Inc., Totowa, NJ

it is a relatively straightforward task to produce antibodies to that transporter. However, the presence of multiple splice variants and use of alternate promoter regions may be a confounding factor.

This chapter deals with the production of polyclonal antibodies, principally because of the more widespread access to such techniques when compared to the additional steps required to produce monoclonal antibodies. However, the methodologies are not exclusive and readers interested in the subsequent generation of monoclonal antibodies from spleens of mice that have been immunized according to the following protocols should consult standard texts such as that by Harlow and Lane ***(1)***.

Three distinct starting materials are available for use as antigens (substances that induce an immune response) in the production of polyclonal antibodies against transporters. These are the use of a purified native protein, the use of a bacterial fusion protein, and the use of short synthetic peptides.

1.2. Purified Proteins as Immunogens

Purified proteins may appear to be ideal antigens, providing multiple antigens created both by the presence of the correct sequence, and, if purified appropriately, may retain conformational epitopes because of the presence of appropriate tertiary folding structures. This approach also ensures that post-translational modifications such as glycosylation, nitrosylation, and phosphorylation are present in the immunogen and thus likely to be reflected in the antibodies produced. This approach was extremely successful in early studies by Danbolt and coworkers (for review, *see* **ref. *2***). However, it suffers two major disadvantages: (1) the major efforts normally involved in isolating the protein and (2) the potential problem of retention of other protein contaminants in the preparation, against which antibodies may also be generated. Moreover, large proteins may contain regions of protein sequence that are common to many members of a transporter family; thus, such antibodies may not be specific to a single protein but, rather, recognize a related group of proteins.

1.3. Recombinant Proteins as Immunogens

Recombinant fusion proteins produced by bacterial or eukaryotic expression systems may also be effective antigens. Recombinant fusion proteins are commonly considered to be easier to produce than peptide antigens, requiring access only to standard molecular biology techniques and kit-based purification of the protein antigen. Although the recombinant proteins will contain sequence-specific epitopes, these polypeptides are frequently incorrectly folded and may have incorrect disulfide bond pairing. Membrane proteins, which gain their selective conformational organization, in part at least, by virtue of the

environment in which they are located, are likely to be inappropriately folded when generated by bacterial or eukaryotic expression systems. Furthermore, such proteins are likely to lack appropriate posttranslational modifications.

1.4. Synthetic Peptides as Immunogens

Synthetic peptides are often ignored as potential antigens because of concerns such as appropriate choice of sequence and understanding how to couple to an appropriate carrier protein prior to immunization. Although there is undoubtedly a cost associated with the synthesis of high-purity peptides, such synthetic peptides can be synthesized and characterized more quickly and less expensively than a fusion protein.

We have routinely resorted to the use of peptides for several reasons, the most significant of which is the frequent high degree of sequence homology between many members of any given transporter family. Short peptide sequences can be chosen that are specific only to a single member of a family of transporters and, thus, have the potential to be monospecific. Additional structural modifications such as phosphorylation can also be included in the design of the peptide. However, peptides must be chemically coupled to carrier proteins in order to render them immunogenic, and in some cases, individual sequences may not be recognized as foreign by the immune system of the animal that is immunized. The basic rules detailing peptide selection are presented next.

1.4.1. Peptide Length

Most peptide antigens range in length from 12 to 16 residues and are relatively inexpensive and easy to synthesize. Peptides that are 9 residues or shorter may sometimes be effective antigens; conversely, peptides longer than 12–16 amino acids may contain several epitopes. Peptides in excess of 25 residues are much more expensive to synthesize and present few advantages. Most workers will not attempt to perform the synthesis themselves but will use one of the many well-advertised commercial services.

1.5. Defining a Peptide Sequence to Raise Antibodies Against

Standard tools exist for identifying unique and appropriate sequences of transporters and other proteins. These tools enable you to determine features such as uniqueness of the sequence and potential antigenicity.

1.5.1. Repositories for Cloned Sequences

The most commonly accessed source of sequences for known genes is via databases such as the GenBank database run by the National Center for Bio-

technology Information (http://www.ncbi.nlm.nih.gov/). Such databases provide a sensible starting point for comparing the general sequence characteristics of cloned examples of many transporters from a variety of species. The selection of a sequence may be driven by a desire to use any antibodies subsequently created on only a single species such as rat or human or may require selection of a sequence that is common across species to permit wider usage of the final antiserum. Sequence selection usually follows a stepwise process.

Where there is a requirement that an antibody should be usable in studies of multiple species such as rats and humans, the initial step is usually to find sequences that are common across these species. Several programs which are freely available on the World Wide Web permit alignment of amino acid sequences from multiple members of a protein family and thus permit identification of common sequences (e.g., see http://www.ncbi.nlm.nih.gov/BLAST/ for the link for comparing two sequences). Conversely, such tools are invaluable when considering how to discriminate between several closely related proteins in a family of transporter proteins. Programs such as the Conserved Domain and Search Service (http://www.ncbi.nlm.nih.gov/Structure/) permit identification of common structural domains such as PDZ domains, phosphorylation consensus sites, and others, in diverse groups of proteins. The common nature of such sequences will influence your usage of such.

1.5.2. Intracellular, Extracellular and Transmembrane Sequences

It is a routine practice in many laboratories to focus efforts upon producing antibodies against intracellular domains of transporters (*see* **Fig. 1**). This is done because sequences that the host animal considers to be "self" do not normally yield appropriate immune responses, because of prior elimination of those cells which can recognize such "self" proteins (a mechanism to limit autoimmune diseases). Intracellular sequences are not normally exposed to prior surveillance by the immune system and are, thus, usually antigenic. The limitation on use of extracellular portions of proteins can be circumvented if the protein is only expressed in immunologicaly privileged regions of the body such as the brain. Alternatively, if the protein is sufficiently variable between species it may be raised in a remote species (e.g., raising antibodies against a rat sequence in chickens) without encountering this "self" identification barrier.

1.5.3. Defining Transmembrane Domains

In many cases, databases contain suggestions as to the likely membrane topology of a protein. This assignment may be based on a variety of data, including inferences drawn from other members of the same transporter family and experimental techniques such as labeling of specific extracellular residues using membrane-impermeant biotinylation reagents or sulfhydryl-modifying

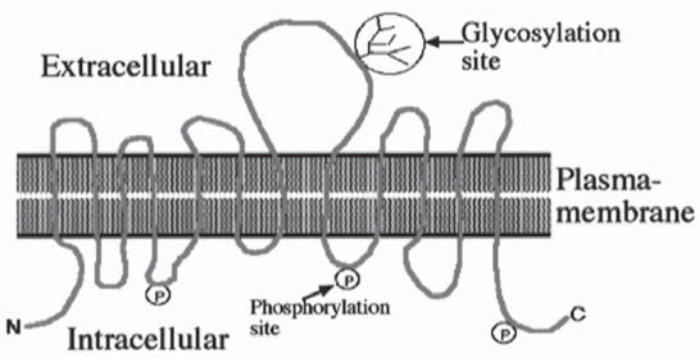

Fig. 1. Diagrammatic representation of a typical generic transporter, represented in this case with multiple transmembrane domains and intracellular carboxyl and amino terminal regions. Features such as notional glycosylation sites and phosphorylation sites are indicated.

reagents. This may be supplemented by the use of computational techniques such as Kyte–Doolittle hydropathicity plots ***(3)***, which try to predict potential transmembrane regions. The Kyte–Doolittle model assigns values of hydrophobicity to each amino acid; thus, a hydrophobic amino acid such as isoleucine is assigned a positive value, whereas a hydrophilic amino acid such as arginine is assigned a negative value. A variety of programs are freely available on the Web (e.g., see http://fasta.bioch .virginia.edu/o_fasta/grease.htm) to calculate the hydrophobicity of any sequence and to potentially identify any regions with a cluster of (typically) 16–20 or more hydrophobic amino acids as possible transmembrane domains. This must be viewed with some caution because a transmembrane domain may, in fact, contain many hydrophilic amino acids if it forms a pore complex that is exposed to a luminal aqueous environment (*see* **Fig. 2**). Conversely, hydrophobic residues may exist in an aqueous environment, especially if any hydrophobic groups are orientated inward away from the aqueous environment. In general, it is unwise to choose a very hydrophobic region as an antigen because if it is normally buried in a membrane, it will not be accessible to antibodies raised against it during normal immunocytochemical studies. Moreover, hydrophobic peptides are difficult to dissolve in an aqueous environment and thus difficult to couple to a carrier protein for the initial immunization.

1.5.4. Tools for Measuring "Antigenicity"

A large number of short (10–20 amino acid) sequences in any single protein may be antigenic. A variety of biocomputational tools are available to calculate the probability that a given portion of a protein sequence may be antigenic.

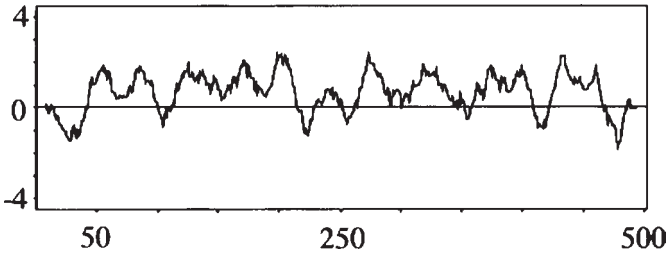

Fig. 2. Typical hydrophobicity plot of a transporter (in this case, the cystine–glutamate antiporter, which plays a role in supplying cystine for use in glutathione synthesis in cells such as astroglial cells), using a window of 18 amino acids (used to create an average weighting for a region sufficient to span a plasmamembrane). The more hydrophobic regions of the protein are indicated by positive values and thus favor the existence in lipid membranes. Negative values are hydrophilic and thus likely to be in cytoplasmic or extracellular domains. The sequence extends from the N-terminus (left) to C-terminus (right). Twelve possible transmembrane sequences were predicted ***(4)*** for this protein, based on the presence of 12 separate highly hydrophobic regions.

These are usually based on the original model by Jameson and Wolf ***(5)*** and utilize a number of weighted parameters to define a probability that a peptide sequence may be antigenic, called the antigenicity index. The antigenicity index is calculated using multiple measures of secondary structure, including hydrophobicity, surface probability, flexibility, and the presence of strong turns or coils. Features such as a high degree of flexibility are often associated with high levels of antigenicity. It is possible to predict the presence of features such as α-helices because Ala, Glu , Leu, and Met are frequently observed in such, whereas Gly, Pro, Tyr and Ser are not normally encountered. The EMBOSS suite of programs (enter via http://www.hg mp.mrc.ac.uk/Registered/Option/emboss.html) and others are freely accessible via the Web and require only that the protein sequence be entered (usually "cut and pasted" from one of the standard databases) in order for the evaluation to occur. Other free tools include "Antheprot," which is downloadable from http://antheprot-pbil. ibcp.fr/ie_sommaire.html. A brief Web search will reveal many more sites from which to access these types of tools.

However, protein folding is not entirely understood and the antigenicity index serves only as a useful guide. A further choice of peptide sequences also needs to be examined in the context of factors such as whether the sequence is intracellular or extracellular or whether it contains one or more potential posttranslational modification sites such as glycosylation site(s).

1.6. Posttranslational Modifications

Posttranslational modifications are a variety of changes that may be induced in a protein. They range from common events such as glycosylation, phosphorylation, and nitrosylation through to unusual events such as replacement of L-aspartate with D-aspartate (in the lens of the eye). Protein cleavage is also an important modification, which has the capacity to eliminate epitopes entirely from the initial protein sequence.

1.6.1. Glycosylation

Sugars are often added to residues of a protein which ultimately exist in extracellular domains. The large bulk of these sugar moieties will block the binding of antibodies to the underlying protein sequence unless the sugar is removed (e.g., enzymatically). For the most common forms of glycosylation, sugars are added to the amino group of an asparagine (N-glycosylation) or to the hydroxyl group of a serine or threonine residue (O-glycosylation). For N-glycosylation, the sequence motif Asn-XXX-Ser/Thr and, more rarely, Asn-XXX-Cys, where XXX is any amino acid other than Pro, are prerequisites for glycosylation. No sequence motif has been defined for O-linked glycosylation.

1.6.2. Phosphorylation Sites

Phosphorylation sites may be important to the functionality of proteins; the activity of many transporters is regulated by phosphorylation. The generic identification of a protein and its presence/absence in a specified tissue or cell type might be most appropriately addressed using antibodies to sequences that do not contain phosphorylation sites. However, antibodies that recognize the phosphorylation status of specific sites can also be potent tools in further functional studies. Phosphorylation sites can potentially be predicted using programs such as Netphos, which are accessible on the Web, at many locations (e.g., http://www.cbs.dtu.dk/service s/NetPhos/).

1.6.3. Cleavage Sites

Many proteins are proteolytically cleaved during processes such as bioactivation or degradation. Accordingly, knowledge of whether a likely cleavage site exists in the middle of the peptide chosen may be important. Again, Web-based tools exist to identify possible cleavage sites in proteins (e.g., see http://au.expasy.org/tools/ peptidecutter/), and some useful data on cleavage sites of signal sequences may be extracted from http://www.cbs.dtu.dk/service s/SignalP/.

1.7. Final Choices of Peptide Characteristics

Technical problems are evident in the solid-phase synthesis of peptides, but these are rapidly being circumvented and, therefore, will not be emphasized here, as most reliable peptide producers can advise as to the current status of their particular chemistries.

1.7.1. Purity of the Peptide

A variety of opinions exist as to the appropriate peptide purity to use for immunization. Peptide impurities are commonly of three sorts. Shortened (truncated) peptides are not necessarily problematic, because they have the correct amino acid sequence but are shorter. Missequences (peptides with missing residues) are a problem because they may ultimately result in production of antibodies that recognize inappropriate proteins. Finally, if amino acids are not fully deprotected, then they tend to be more immunogenic than the native peptide (possibly because they are more resistant to degredation). However, antibodies directed against the modified peptide may not recognize the native peptide.

Some companies offer "immunization grade" peptides that are typically 40–70% pure, whereas other workers only use the highest purity (approx 95%) that is available. If cost is a concern, it may be appropriate to initially immunize an animal with a less expensive grade of peptides. If an immune response is generated, then a small amount of a more expensive pure peptide can be used for further immunization. However, in general, it is recommended that when all costs are taken into account, the use of the purest-quality peptides from the outset may be the most cost-effective and reliable route to take. Mass spectral analysis of the products is essential to verify that the desired peptide has been produced and identify whether there may be lower mass truncation or deletion products. Moreover, it may detect peptides with oxidized sulfhydryl groups or proteins with residual uncleaved side-chain protecting groups. High-performance liquid chromatography (HPLC) analysis can reveal whether significant levels of contaminants are present in the peptide mixture. Both types of analysis are included as standard by all reputable commercial peptide synthesis companies.

1.7.2. Terminal Modifications of Peptides

Peptides are offered with either free amino and carboxyl terminal regions or with these regions modified. Modifications may be needed either because of constraints in the synthesis paradigm (e.g., the carboxyl terminal may be offered with an amide group rather than a free acid) or the terminal regions may be modified to suit experimental needs. A peptide synthesized with free

carboxyl and amino terminals will be more highly charged and, thus, more hydrophilic than a peptide without these characteristics. Thus, it can be solubilized in an aqueous solution prior to coupling to a carrier protein. However, it may be desirable to modify these termini. It is common practice to acetylate the N-terminal, as this may facilitate proper folding of peptide sequences. Other modifications may be included to aid the coupling of the peptide to the carrier protein, including the addition of a terminal -SH-containing amino acid such as cystine.

1.7.3. Phosphopeptides

Phosphopeptides can be readily synthesized in a relatively pure form and may be appropriate when studying the phosphorylation status of proteins. Most commercial suppliers can include a phosphorylated residue in the synthesis of the peptide of interest. Because the phosphate is to be a significant component on the epitope, the length of the peptide should be relatively short (10–14 amino acids) to ensure that it is a part of the epitope that the antibodies will recognize.

1.8. Carrier Protein

Carrier "proteins" are large molecular backbones, which the small peptide antigens must be attached to in order to render them immunogenic (able to render an immune response). These carriers range from natural proteins to synthetic polymers. The most commonly used carrier proteins are keyhole limpet hemocyanin (KLH) and thyroglobulin. Rabbits immunized with peptides coupled to KLH produce antibodies against KLH as well as the peptide. However, because KLH is divergent from any known mammalian protein, this will not manifest itself as any specific immunoreactivity when examining mammalian tissues (**Caution**: This is not, however, the case if examining nonmammalian tissues; invertebrate tissues may contain proteins similar to haemocyanin.) Similarly, thyroglobulin is present only in the thyroid; thus, for most purposes, the presence of additional antibodies against thyroglobulin will be irrelevant unless studying tissues such as the thyroid gland. We generally use thyroglobulin as our carrier protein of choice.

Synthetic polymers such as the multiple antigenic peptide system (MAPS) are also valuable tools. MAPS consist of branched amino acid polymers, which provide an antigenic core. Multiple copies of the peptide of interest can be synthesized directly as an extension to this core, eliminating the need for the peptide to be chemically coupled to the MAP. Some MAPS are also available with modified groups which enable them to be chemically coupled to peptide sulfhydryl groups, for use in circumstances where the peptide was not synthesized as part of the MAP.

2. Materials

2.1. Raising Antisera

The following materials are required for protocols that involve coupling a peptide to a carrier protein via a free amino group, using paraformaldehyde as a coupling agent. In our hands, this is the simplest and most reliable methodology available.

1. Sodium phosphate buffer: 0.1 *M* Sodium phosphate, pH 7.2.
2. Porcine thyroglobulin (Sigma; cat. no. T1126).
3. Sodium phosphate buffer: 0.2 *M* Sodium phosphate, pH 7.2.
4. Sodium hydroxide solution: 5 *M* Sodium hydroxide in distilled water.
5. Paraformaldehyde fixative: 4% (w/v) Paraformaldehyde (extra pure, Merck) in 0.1 *M* phosphate buffer, pH 7.2–7.3. Add 16 g of paraformaldehyde to 100 mL of distilled water and warm to 60°C. Slowly add drops of sodium hydroxide solution until the paraformaldehyde dissolves (depolymerizes) completely. Add distilled water, bringing the volume to 200 mL. To this, add 200 mL of 0.2 *M* phosphate buffer. The fixative must be prepared and used in a fume hood because it is toxic by inhalation and skin contact (*see* **Note 1**).

The following materials are specifically required for coupling a peptide via a carboxyl group:

6. EDAC (1-ethyl-3- (3-dimethylaminopropyl) carbodiimide) (Sigma cat. no. E7750) freshly prepared as a 20-mg/mL solution in distilled water and the pH adjusted to 5.0 with 1 *M* HCl as appropriate.

The following materials are required for coupling a peptide via a sulfhydryl group.

7. 4-(4-Maleimidophenyl)butyric acid-*N*-hyroxysuccinimido ester (SMPB) (Sigma; cat. no. M6286).
8. Dimethyl sulfhoxide (water free; Sigma [cat. no. D8779] or similar).
9. Freund's adjuvant: complete and incomplete (Sigma; cat. nos. F5881 and F5506).
10. Syringes and 23-gage hypodermic needles.
11. Gold chloride solution: 1% (w/v) Gold chloride (Sigma; cat. no. G4022) in double-distilled water.
12. Sodium citrate solution: 1% (w/v) Sodium citrate in double distilled water.
13. Colloidal gold solution: Add 1 mL of gold chloride solution to 80 mL of double-distilled water and warm to 60°C. Quickly add 1 mL of sodium citrate solution while stirring. Boil the solution until the volume has been reduced to approx 10 mL; allow to cool. This will yield approx 50-nm-diameter gold particles. The pH of the colloidal gold solution should be about 6.5. Adjust the pH with small amounts of 1 *M* NaOH or 1 *M* HCl as required.

14. Synthetic peptides: Sourced from commercial or other suppliers. Usually 10–30 mg needed for all purposes, including immunization, dot blots, and preabsorption assays.

2.2. Purification and Immunoblotting

1. For dot blotting, the only specialized material needed is polyvinylidin-difluoride (PVDF) membrane, available from many suppliers such as Amersham (Bucks UK).
2. For Western blotting, a variety of additional materials are needed, which are fully documented by Harlow and Lane ***(1)***.
3. For affinity purification: Affigel 10 or Affigel 15 (Bio-Rad; cat nos. 153-6046 and 153-6052) is required.
4. When coupling at or close to neutral pH, Affigel-10 is better for proteins with p*I* (isoelectric point) of 6.5–11.0, whereas Affigel-15 is better for proteins with p*I* less than 6.5.

2.3. Tissue Fixation

1. Physiological saline: May be 0.9% sodium chloride solution in distilled water or other suitable physiological media such as Ames media (Sigma; cat. no. A1420).
2. 400 mL Paraformaldehyde fixative (*see* **Note 1**).
3. Sodium pentobarbital (Nembutal; Boehringer Ingelheim).
4. Two-Way Luer-lock plastic tap (Sigma; cat. no. S7521).
5. Plastic tubing: Tygon, internal diameter 1/8 in., Sigma; cat no. T2539).
6. Cannula: 12-Gage hypodermic needle (internal bore, 2 mm; length, 50 mm).
7. 60-mL Syringes.

2.4. Immunocytochemistry

1. Phosphate-buffered saline (PBS): 0.9% (w/v) Sodium chloride in 0.1 *M* phosphate buffer, pH 7.2.
2. Blocking solution: 0.5% (w/v) bovine serum albumin (BSA; Sigma; cat. no. A3425) in PBS. Dissolve 0.5 g of BSA in 100 mL PBS.
3. Saponin (Sigma; cat. no. S4521).
4. Primary antibodies used in this laboratory are generated in-house.
5. Fluorescently tagged secondary antibodies (Jackson Immunoresearch Laboratories, West Grove, PA, USA).
6. Biotinylated secondary antibodies and streptavidin–biotin–horseradish peroxidase complex (SABHRP) (Amersham, Bucks, UK).
7. PBS–glycerol mountant: 50% (v/v) Glycerol in PBS.
8. Clear nail varnish (to seal microscope slides after mounting sections in PBS–glycerol).
9. Peroxidase substrate solution: Dissolve 5 mg of DAB (3,3' diaminobenzidine (DAB; Sigma; cat. no. D5637) in 100 µL of distilled water (*see* **Note 2**). Bring

the solution up to 10 mL with PBS, then add 5 µL of hydrogen peroxide just prior to use (analar grade, BDH).

3. Methods

3.1. Raising Antisera

3.1.1. Preparation of Immunogenic Peptide Conjugates

The peptide needs to be conjugated to a suitable carrier in order to render it immunogenic. This step is important because the ratio of peptide to carrier and the choice of coupling method will influence the capacity of the immunized animal to respond to it.

3.1.2. Ratio of Peptide to Carrier Protein

There is a significant amount of debate as to the ideal ratio of peptide that should be coupled to a carrier protein molecule. Some studies have suggested that although too little peptide will result in a poor result, because of the scarcity of the antigen, too high a coupling ratio may also yield poor results for reasons that are not clearly understood. In general, when coupling peptides via their amino groups to thyroglobulin, we couple at the ratio of 1 mg of a 20-amino-acid peptide per 25 mg of thyroglobulin. This ratio is limited by the number of lysine residues and, thus, free-amino groups present on the carrier protein. As cystine residues are less common, the ratio may need to be reduced when coupling via cystine groups to reduce the incidence of unconjugated peptide being present in the immunizing mixture.

The weight of the peptide used should also be changed in a *prorata* fashion as the length of the peptide changes (e.g., use 0.5 mg of a 10-amino-acid peptide).

3.1.3. Choosing the Portion of the Peptide to Couple to the Carrier

When a peptide is bound, the area nearest the coupling site tends to be more conformationally constrained than more distal parts and is not as easily recognized by the immune system. The antibodies tend to be generated against the more mobile portions of the peptide, which are distant from the coupling site. Accordingly, if, for example, one end of a sequence is more unique than the other end, then this should be located distant to the site of coupling. This choice may influence the chemistry of coupling.

Three methods are routinely used to crosslink a peptide to a carrier protein. These procedures chemically link amino groups, carboxyl, or sulfhydryl groups.

3.1.4. Coupling via an Amino Group

Two types of amino group may exist in a peptide: an N-terminal amino group and the free (epsilon) -amino groups of internal lysine residues.

Crosslinking reactions using aldehydes preferentially react with the epsilon-amino group on the lysine residues, causing the peptide to be stably coupled to the carrier at that part of its sequence. This is the method most often used by our group. When a peptide representing the carboxyl terminal region of the native protein is chosen, then it is appropriate to couple that peptide by the amino-terminal region so that the carboxyl terminus of the peptide is comparable to the carboxyl part of the protein. Conversely, if targeting an amino-terminal region of a protein, it is unwise to couple up the amino-terminal region of the peptide, as this will make it structurally distinct from the comparable region of the native protein. When an internal lysine residue is used as the site of coupling, the resultant conformational constraints and steric hindrance in this area will reduce the chances that adjacent amino acids will act as potent antigens. Accordingly, it is generally better to position lysine residues toward the end of the peptide sequence.

1. For a 10-amino-acid peptide which has a free epsilon-amino group or N-terminal amino group, dissolve 1 mg of the peptide in 4.5 mL of ultrapure water. Note: Most hydrophilic peptides will dissolve in ultrapure water. On rare occasions, they may require prior solubilization in mildly acidic or alkaline conditions, depending on their amino acid composition (peptides are least soluble at pH values around their p*I*). Do not try to initially dissolve peptides in buffers such as phosphate buffer because this may sometimes cause problems with solubility.
2. Add 5 mL of a 5-mg/mL thyroglobulin solution dissolved in ultrapure water.
3. Add 0.5 mL of freshly prepared 4% paraformaldehyde fixative.
4. Mix the solution well and allow it to react for 18 h at room temperature.
5. Divide the thyroglobulin-conjugated peptide into 0.5-mL aliquots and store them at –20°C until ready for use.

3.1.5. Coupling via a Carboxyl Group

Only when it is considered inappropriate to couple via an amino group do we then consider coupling via carboxyl groups or cystine residues.

Carboxyl groups can be crosslinked to the epsilon groups of Lys residues on carrier proteins, using reagents such as carbodiimides to produce stable pseudopeptide bonds. However, this strategy is not as routinely useful because glutamate and aspartate residues that contain the requisite free carboxyl groups are common in hydrophilic peptides, leading to the formation of multiple crosslinks. Moreover, this procedure can also form unintended internal crosslinks, which perturb the conformation of the peptide and reduce its value as an immunogen.

Assuming the use of a 10-amino-acid peptide, dissolve 2 mg of peptide in 1 mL ultrapure water.

1. Add 1 mL of 20 mg/mL EDAC at pH 5.
2. Incubate for 5 min at room temperature.

3. Add 50 mg of thyroglobulin dissolved in 4 mL ultrapure water.
4. Incubate at room temperature for 6 h.
5. Stop the reaction by adding 1 mL of 500 m*M* sodium acetate, pH 4.3.
6. Incubate for 1 h and then dialyze against PBS for 12 h at 4°C.
7. Adjust the volume of the conjugate solution to 20 mL and store 0.5-mL aliquots of conjugate at –20°C.

3.1.6. Coupling via a Sulfhydryl Group

If lysine residues are located within the peptide sequence, then this reduces the value of the peptide as an antigen because of the above-mentioned steric constraints mentioned above. It may be beneficial to utilize or insert a cystine residue at one end of the peptide. It must be noted that insertion of a cystine residue may have an impact on the specificity of the peptide as an immunogen. Crosslinking via the sulfhydryl groups of amino acids such as cystine usually produces a biologically stable thioether bond. Again, the cystine residue should not be positioned at a nonterminal region of the peptide, as subsequent steric hindrance will restrict the antigenicity of flanking amino acids. If multiple cystine residues are present, coupling strategies that link cystine residues may lead to the formation of covalently linked peptide aggregates, which are not likely to be effective antigens.

1. Dissolve 25 mg of thyroglobulin in 2.5 mL PBS.
2. Prepare 25 mg/mL SMPB in DMSO.
3. Add 250 µL of SMPB solution dropwise to the thyroglobulin solution.
4. React at room temperature for 4 h.
5. Separate unreacted SMPB from the activated carrier by gel filtration using Sephadex G-25 or G-50.
6. Dissolve 1 mg peptide in 1 mL ultrapure water and add to the activated carrier.
7. React at room temperature for 4 h.
8. Dialyze against PBS for 12 h at 4°C.
9. Adjust the volume of the conjugate solution to 10 mL and prepare 0.5-mL aliquots.
10. Store aliquots of conjugate at –20°C.

3.2. Quantitation of Coupling

Most laboratories, including our own, prepare antipeptide antibodies using standardized procedures without characterizing the final peptide conjugate. We have not identified any practical value in doing so and suggest that it is not vital. However, if required, a number of standard texts give details of procedures such as iodination of the peptide and subsequent assaying of the molar coupling ratio to the carrier protein.

3.3. What Animals Should I Use to Raise Antibodies?

The choice of species is determined by a variety of factors. If it is plausible that monoclonal antibodies might subsequently be generated, then the initial immunization of appropriate strains of mice or (less commonly) rats is indicated. If large quantities of antiserum will be needed, then large species, such as sheep or goats, should be considered. However, for most purposes, we recommend that guinea pigs and rabbits are the species of choice because of the outbred nature of these species. Genetic variability among inbred species such as rats and mice limits the ability of an individual to respond to the peptide. Within outbred animals, such as rabbits, it is a common finding that although the antiserum from one rabbit may work well in immunohistochemical experiments, the antiserum from another rabbit may function better in another technique such as Western blotting. This would indicate that the antibodies generated in each animal may be differentially targeted to different epitopes in the peptide. Accordingly, wherever practicable, multiple animals should be immunized (*see* **Note 3**). Additionally, we commonly find that antibodies raised in different species may have distinct properties that render them optimal for different purposes.

3.4. Preimmune Bleeds

Before immunizing any animal, take a test bleed and utilize the serum in the type of test system in which you will employ it. It is extremely common for some animals, especially those that are not reared in specific pathogen-free conditions, to have many pre-existing antibodies, some of which may give rise to high background levels or nonselective labeling of tissue constituents when used in immunocytochemical studies. Screening and elimination of those animals with unacceptable levels of contaminating antibodies at this point will save considerable work at later time-points. The retained serum sample will serve as a useful immunocytochemical control at a later time.

3.5. Conventional Immunization Paradigm

Note: The following details use of Freund's adjuvant, which may not be permitted by your institution. If so, use one of the other less aggressive adjuvants such as the RIBI adjuvant or TiterMax (available from Sigma).

1. Mix an aliquot (*see* **Note 4**) of the peptide conjugate (0.5 mL) with an equal volume of Freund's adjuvant. Use complete adjuvant for the first injection and incomplete adjuvant for subsequent injections.
2. Emulsify the mixture: Draw up both components into a syringe, cap the syringe tightly, and tape it to a vortex mixer. Vigorously "vortex" the mixture for 10–15 min.

3. Using a 23-gage needle, inject animals subcutaneously at two to four sites, taking care not to enter any blood vessels.
4. Repeat the injections at 3 to 4 wk intervals, and take blood samples 7 d after the second and subsequent injections. For rabbits, collect blood from the rear marginal ear vein.

3.6. Colloidal Gold Immunization Paradigm

This is a more complicated method, but it tends to generate antibodies of a higher titer. Prepare colloidal gold solution as in **Subheading 2.1.**

1. Divide a 0.5-mL aliquot of the peptide conjugate (immunogen) into two.
2. Emulsify 0.25 mL of the immunogen with 0.25 mL Freund's adjuvant as in **Subheading 3.5.**

Absorb the remaining 0.25 mL of immunogen onto colloidal gold particles by *rapidly mixing* the immunogen with an equal volume of colloidal gold solution.

3. Inject this gold-conjugate mixture into the rear marginal ear vein of rabbits.
4. Bleed rabbits 1 wk after immunization, collecting blood from the rear marginal ear vein.

3.7. Bleeding

In most species, the titer of an antibody peaks at around 12–14 d after immunization. We routinely bleed rabbits 7 d after the first and subsequent boosts. Sera harvested at these time-points are then tested within the next 5 d. Where sera have appropriate characteristics, then the options of either a further nonterminal bleed or a terminal bleed can be canvassed.

3.7.1. Taking Test Bleeds

Rabbits are easily bled from the rear marginal ear vein.

1. Wrap the rabbit in a large towel to limit movement. (Do not use the old-fashioned rabbit-restraint boxes, as they often cause injury to animals if they struggle.)
2. Gently warm the ear with a hair dryer to cause vasodilation. Bleeding is induced with a small nick to the rear marginal ear vein using a fresh backed razor blade or by the insertion of an 18-gage butterfly cannula attached to a syringe. Ten milliliters of blood is typically taken in a test bleed. Do not take more, as the rabbit may become anemic, which will be evident as a reduced haematocrit (less than 40% packed cell volume when the blood is centrifuged). Other species such as rats and guinea pigs are much harder to take test bleeds from, usually requiring tail bleeds or cardiac punctures. For ethical reasons, it is suggested that readers consult individuals who are personally competent in these techniques because the procedures cannot be taught well other than by personal demonstration (*see* **Note 5**).

3. Collect blood into heparinized tubes if plasma is required (which is easier to handle); when the presence of heparin is contraindicated, the blood is allowed to clot and the clot subsequently separated from the serum.
4. Centrifuge the blood at low speed (approx 1000*g*) for 10 min to separate the plasma or serum from the residual blood cells and other constituents. Store the plasma or serum at –80°C in small aliquots (to prevent the need for freeze–thawing too often, which may cause aggregation of the antibody solution) until required for testing or other purposes.

3.8. Assaying Antisera

There are multiple ways to assay antibodies. In our laboratory, we utilize standard strategies that evaluate the selectivity of the antibodies for the type of procedures that they will be used, which include immunohistochemistry and Western blotting.

It should be noted at the outset that many antibodies that work well in Western blotting may fail to work in immunohistochemical studies. The converse is a much rarer event.

3.8.1. Dot Blots

We routinely use dot blots as our initial fast and inexpensive screen to determine if there are components of the serum that can recognize the immunizing peptide.

Dot blots are performed by coupling the peptide, using the same chemistry as for the immunization, but linked to a different protein such as bovine serum albumin (because you will also have generated antibodies to the original carrier protein, and these would detect the original carrier protein in your dot blots).

This new conjugate is spotted onto PVDF membranes at varying concentrations. The membranes are then probed using the antiserum at a range of dilutions, to test whether antibodies in the antiserum can recognize the target peptide. This test is very quick, but although it can determine if the target peptide can be recognized, it does not identify any additional nonspecific binding activities in the antiserum.

1. Create a conjugate of the peptide with a new carrier protein, using the same ratio of peptide to carrier as used in the original immunization.
2. Prepare serial dilutions of the peptide conjugate in distilled water, containing from 0.2 µg of peptide per 2 µL (the concentration in aliquots of your conjugate assuming 1 mg of peptide in a final volume of 10 mL) down to a final peptide concentration of 2 ng per 2 µL.
3. Apply 2-µL spots of each diluted conjugate to multiple portions of PVDF membrane (we use strips 3–4 cm long and 4–5 mm wide, which have a range of concentrations of conjugate spotted on each). Control strips have carrier protein or carrier protein coupled to an irrelevant peptide at a similar dilution range.

4. Immerse the membranes in blocking solution (0.5% low-fat-milk powder from the local supermarket, in PBS) for 20 min.
5. Apply a range of diluted antibody solutions (usually prepared by 10-fold dilutions of the original antiserum, from around 1 : 1000 down to a final dilution of about 1 : 1,000,000).
6. Incubate the membranes for 45 min to 2 h in the antibody solution.
7. Wash the membrane thoroughly for 30–60 min in PBS.
8. Apply secondary species-specific antibody coupled to an appropriate tag (e.g., biotinylated goat–anti-rabbit immunoglobulin) for 2 h.
9. Final detection can be performed with probes such as streptavidin–horseradish peroxidase (HRP) complex using diaminobenzedine as a chromagen (*see* **Note 6**) or other approaches such as chemiluminescent detection.

3.8.2. Western Blotting

Western blotting is conceptually similar to dot blotting but requires that a mixture of proteins in target tissues such as brain are separated electrophoretically before being transferred onto PVDF membranes. The membranes are assayed in a similar manner, to determine not only whether the antibody binds to the target protein (as inferred from the predicted molecular weight of the target protein) but also whether other bands of higher or lower molecular weight are detected by the antibody. General instructions on running Western blots are available from a multitude of sources ***(1)***. A few points are directly relevant to running Western blots for the detection of transporter proteins.

3.8.2.1. Conditions for Running Western Blots

The method of sample preparation and the conditions under which the gels are run are of vital importance for membrane-bound transporters. It is possible to separate membrane fractions from cytoplasmic fractions in initial tissue homogenates, but this may bias the outcome of the blot by excluding some possible crossreacting molecular species.

Most gels are run as sodium dodecyl sulfate–polyacrylamide gel electrophoresis (SDS–PAGE) gels (i.e., with the inclusion of the ionic detergent SDS as a denaturing agent that linearizes the protein). This is the most common method of running a gel for separating proteins and is usually applicable when using antibodies created against linear peptide sequence. However, it may not provide appropriate results if using antibodies against, for instance, a fusion protein, where conformational epitopes rather than sequence epitopes are being detected. Under such circumstances, it may be appropriate to consider running gels in the absence of SDS, but this is a more specialized strategy outside the scope of the methodological paradigms presented here.

Standard preparative conditions using SDS allow integral membrane proteins to be solubilized effectively, whereas inclusion of reagents such as β-mercaptoethanol or dithiothreitol (DTT) at all stages ensure that disulfide bonds are broken and remain broken.

3.8.2.2. Why Multiple Bands May be Detected?

There are many reasons why multiple bands may be detected on a Western blot.

Bands may be detected at higher or lower molecular weights than those predicted simply by summation of the molecular weights of the constituent amino acids in the protein.

3.8.2.3. Bands that are Slightly Different to the Predicted Molecular Weight

Increases in molecular weight of around 5–9 kDa may well be attributable to posttranslational modifications such as glycosylation of the protein. This can be verified by prior incubation of the tissue homogenate with enzymes such as *O*-glycosidase (Sigma; cat. no. G1163), which cleave such sugars, whereupon the protein should then have the correct relative mobility. Many proteins exist as multiple splice variants. If you observe multiple bands of slightly different molecular weights or a broad smear instead of one narrow band, you may be detecting several splice variants at slightly different molecular weights.

3.8.2.4. Low Molecular Weight Bands

Many proteins are continually being proteolytically processed by extracellular or intracellular enzymes, which modify the properties of the protein. This cleavage is especially notable in unregulated conditions such as following hypoxia or in response to postmortem delay. Under such conditions it is common to find lower-molecular-weight cleavage products. In some circumstances, all of the immunoreactivity will be present in the lower-molecular-weight band, reflecting cleavage of the majority of the protein.

3.8.2.5. Testing for Effects of Postmortem Delay

Postmortem delay is associated with numerous changes in tissues, resulting from, among other things, the lysis of cells and organelles, rapid changes in ionic homeostasis, and the unregulated proteolysis of proteins by various proteases. Some parts of the transporter molecules may be cleaved more readily than others, yielding different results, depending on the part of the transporter protein that is being studied. Accordingly, whenever examining postmortem

tissue, it is imperative that the effect of postmortem delay AND the conditions of postmortem storage are identified. Studies to date on this effect have been restricted mainly to the glutamate transporters ***(6)***.

3.8.2.6. Higher-Molecular-Weight Bands

It is a common finding that several higher molecular weight bands may be observed following Western blotting of transporter proteins ***(2)***. Several reasons for this exist. Many transporters occur as part of multimolecular complexes, either with distinct co-associated proteins such as specific GTRAP's (glutamate transporter associated proteins) ***(7)*** which may modify transport properties of the transporter, cytoskeleton-interacting proteins such as Ajuba ***(8)*** or form functional heterodimers with ubiquitous proteins such as 4F2hc (also named CD 98) ***(9,10)***. In some cases, transporter proteins, such as the glucose transporter GLUT-1, form a functional transporter complex by the covalent interaction of multiple monomers ***(11)***. A similar possibility has been raised for glutamate transporters ***(12)***. In all cases, the transporter protein has the potential to form covalent linkages either in a biologically relevant manner or as an artifact of preparation. Such associations will inevitably lead to the presence of higher-molecular-weight immunoreactive bands unless the linkages are broken. Disulfide bonds are the most common covalent linkages that may be encountered. These may be cleaved by running gels under reducing conditions, preferably in the presence of β-mercaptoethanol. We routinely perform all our Western blots in the presence of β-mercaptoethanol rather than DTT which we find to be a slightly less effective reagent. In the presence of mercaptoethanol, we rarely encounter multiple bands that are significantly larger than the expected mass of the protein.

3.8.2.7. Is the Antiserum Specifically or Nonspecifically Detecting Other Proteins?

In addition to selective binding to the target protein, it is possible that the antiserum you have created may bind to other proteins. This may be because (1) it specifically detects another protein with a similar (or identical) sequence to that of your immunizing peptide or (2) your antiserum contains additional antibodies that are not a consequence of your immunization process but, instead represent the animals normal response to antigens in its environment. If the result is the result of very high sequence homology, little can be done except to choose a new immunizing sequence. If the result is the result of other contaminating antibodies, those can usually be removed.

3.9. Antibody Purification

In many cases, it is appropriate to initially clean up the serum or plasma to gain a relatively pure immunoglobulin fraction. The standard purification tech-

nique involves sequential purification using ammonium sulfate followed by caprylic (octanoic) acid. Details of these methods can be found in standard texts such as by Harlow and Lane ***(1)***.

3.9.1. Affinity Purification

Whn preabsorption reveals the continued presence of nonspecifically interacting antibodies in a preparation, then it may be appropriate to affinity purify the antibody.

Affinity purification is usually performed using the initial immunizing peptide, which is coupled to an immobile gel matrix (preferably using the same coupling methodology as in the creation of the initial immunizing conjugates). Columns may be prepared using cyanogen bromide-activated Sepharose-type matrices; however, many commercial products such as Affigel (Bio-Rad) exist that link to free-amino groups or other groups such as cystine residues. Affigel is available as two forms (Affigel 10 and Affigel 15), the version to use being dependent on the p*I* of the protein. The p*I* of a protein is a composite of the p*K* of the individual amino acids. This can be calculated using standard Web-based tools (e.g., see http://ca.expasy.org/tools/pi_tool.html). AffiGel 10 is a *N*-hydroxysuccinimide ester at the end of a 10C spacer arm, attached to the gelmatrix. Its primary reactivity is to -NH2. An equivalent alternative is CH-Sepharose 4B-6-aminohexanoic acid *N*-hydroxysuccinimide ester from Sigma (cat. no. A9019). The peptide, when coupled to the gel, acts as a molecular trap for specific antibody molecules. Affigel can be used in a conventional gel separation column, with the fluids being run through a gel column. Alternatively, it can be used in a static manner, mixing gel and antibody in a beaker or similar, which allows the antibody time to bind with the gel in the minimum fluid volume. The gel is then gently centrifuged to separate unbound antibody, which may be retained for analysis of any residual binding activity. In both cases, the bound antibody is subsequently dissociated from the gel by changing the ionic characteristics of the buffer, which reduces the electrostatic interactions that bind the antibody to the peptide. The gel can be reused many times. Such methods result in relatively simple separation of the specific antibody.

The following are methods for Affigel-10 coupling at pH 7.4 with a peptide or protein that has a p*I* greater than 6.5. Ensure that no traces of Tris-HCl (or similar) buffer is present, as this is an amine-containing buffer that will react with the gel.

1. Perform all steps at 4°C.
2. Wash 2 mL of Affigel beads two times in 10 mL cold ultrapure water. Spin down the gel beads between washes at 1000*g* for 15 min.
3. Resuspend beads in 2 mL of binding buffer (100 m*M* (3-N-morpholino)-propane sulfonic acid [MOPS], pH 7.5, plus 70 m*M* $CaCl_2$).

4. Dialyze 2–30 mg antigen protein or peptide (at about 1 mg/mL) against 1 L of 100 m*M* MOPS, pH 7.4, overnight. (**Note**: If coupling a small peptide, use 2–4 mg; if coupling a large protein, use the larger amounts specified).
5. Add the dialyzed peptide or protein to the beads and agitate gently for 4 h at 4°C.
6. Add 1 mL of 0.1 *M* ethanolamine HCl, pH 8.0, or 1 mL of 0.1 *M* glycine methyl ester per milliliter of gel, followed by incubation for 1 h to block free binding sites on the gel. Transfer the gel to an appropriately sized gel column (which can be made from the barrel of a hypodermic syringe, with the bottom plugged with glass wool and a hypodermic needle attached to the bottom to slow the flow rate when required).
7. Wash the column with the following solutions: 10mL of 100 m*M* MOPS, pH 7.5, then 10 mL PBS, then 10 mL of 100 m*M* glycine HCl, pH 2.4, plus 150 m*M* NaCl, and, finally 10 mL PBS.
8. Store the column in PBS containing 0.2% sodium azide at 4°C until ready for use in **Step 9**.
9. Wash column with 10 mL of PBS.
10. Apply serum slowly to the column to which a 23–25-gage needle has been fitted so that the column flows slowly. This allows the specific antibody time to bind to the immobilized peptide. Collect the solution that is eluted and run through the column at least three more times.
11. Remove the needle and wash column with 30 mL PBS.
12. Elute the column with 100 m*M* triethylamine (pH 11.5). Pipet aliquots of elution buffer (roughly equivalent to one-fourth to one-fifth of the column volume) directly onto the top of the column bed and let the aliquot flow through the column, and then advance to another fraction. Collect each fraction into a tube containing sufficient 1 *M* Tris-HCl to neutralize the pH of the elution buffer (check this empirically using a pH meter on separate aliquots of triethylamine that have not been run through the column).
13. Alternatively (instead of **step 12**), elute antibody from the column with 100 m*M* glycine HCl buffer, pH 2.4, containing 150 m*M* NaCl. Collect fractions into 200 µL of 1 *M* Tris-HCl, pH 8, to restore to physiological pH values.
14. Assay the fractions by reading the absorbance at 280 nm and pool all fractions that have an absorbance higher than 0.25. Determine the yield of antibody by reading the absorbance (a 1-mg/mL solution of antibody has an absorbance of 1.35 in a 1-cm light path).
15. Dialyze the antibody into PBS or directly store frozen as a solution. If the yield is low, add 5 mg/mL BSA to maintain protein concentration and prevent aggregation of the antibody during freezing and thawing.

3.9.2. Preabsorption

Preabsorption is a vital step in validating that the antiserum you have generated preferentially recognizes the peptide sequence against which it was generated and that labeling is not attributable to other unrelated antibodies in the

serum, including carrier proteins. Preabsorption is the process of adding an excess of target peptide that is coupled to a carrier protein (as some antibodies may not recognize the target peptide unless it is thus conjugated).

1. Prepare the conjugate using a carrier protein other than that used in the process of immunization (to distinguish between results because of the removal of carrier protein and removal of the target peptide).
2. Add 5–50 µg of the conjugate to each milliliter of diluted antiserum. Incubate for 8 h at 4°C. Specifically interacting antibodies will bind and form large complexes, which are unable to engage in further specific interactions with the target protein. If sufficiently large these, complexes may be removed by high-speed centrifugation, but often this is not the case. However, such complexes do not normally interfere with further immunocytochemical assays.

3.10. Using the Antibodies for Immunocytochemical Studies

Only when you are certain that you have a specific antibody should you embark on immunocytochemical studies. Most transporters require the tissue to be fixed with paraformaldehyde rather than glutaraldehyde. Moreover, in the first instance, fixation may have to be varied from relatively short mild fixation, up to the levels indicated below, which will give optimal cytological preservation but may be too aggressive for some transporters.

3.10.1. Tissue Fixation

Note: Aldehyde fixatives are toxic and should be handled with care in a fume hood and disposed of in accord with local regulations.

3.10.1.1. Perfusion Fixation of Mammalian Tissues

Assuming the animal to be a rat, the following details apply. For mice, reduce the size of the perfusion equipment and volumes of solutions *prorata*.

1. Rapidly anesthetize the animal with a large (120 mg/kg) dose of sodium pentobarbital (Nembutal), given by intraperitoneal injection.
2. As soon as deep anesthesia has been induced, open the thorax and insert the cannula, connected to the 60-mL syringe via the two-way tap, into the heart via the left ventricle. Push the cannula forward until its tip is visible in the ascending aorta.
3. Clamp the cannula in place with a pair of hemostats, sever the right atrium, and begin preperfusion with approx 60 mL of sodium chloride (saline) solution (this is sufficient to flush out all of the blood from a typical 250-g rat) (*see* **Note 7**).
4. Turn the two-way tap to permit perfusion with fixative from a second 60-mL syringe. Administer a total volume of fixative equivalent to about 1.5 mL of fixative per gram of body weight (e.g., approx 400 mL for one rat).

5. After fixation by perfusion, the tissues of interest should be removed and placed into fresh fixative at 4°C overnight.

3.10.1.2. Immersion Fixation of Tissues

1. Remove the tissues from the animal as rapidly as possible, placing the tissues onto a petri dish that is half-full of the fixative.
2. Quickly cut the tissue into pieces 2–10 mm in thickness (*see* **Note 8**).
3. Place the small pieces of tissue into fresh fixative using at least 30 volumes of fixative per volume of tissue.
4. Fix the tissues at room temperature for 1–4 h; larger pieces of tissue require longer times. Continuously agitate the tissues, to maximize the diffusion of fixative into the tissue.
5. Wash the tissues in PBS for 1–2 h and then section the tissue as outlined in **Subheading 3.10.2.** following.

3.10.2. Immunolabeling Vibratome Sections

We prefer free-floating Vibratome sections rather than cryostat sections for the majority of our work because the tissues retain optimal morphology (*see* **Figs. 3** and **4**). Moreover, in our hands, the drying process incurred in affixing cryostat sections to microscope slides may cause denaturation of the transporter such that it is no longer recognized by the antibody.

1. Wash the fixed tissue with PBS for 30 min at 4°C to ensure that the fixative has been thoroughly rinsed away (*see* **Note 9**).
2. Cut sections of fixed tissue at a thickness of 25–40 µm.
3. Incubate the sections in the primary antibody (diluted in PBS containing 0.05% saponin, 0.5% BSA, and 0.05% sodium azide) for 12–48 h (*see* **Note 10**).
4. Wash the sections with three changes of with PBS over 1 h at 4°C to remove unbound primary antibody.
5. Treat the sections with secondary antisera and reveal immunolabeling using an appropriate detection system (*see* **Note 11**).

3.10.3. Immunolabeling Wax-Embedded Sections

For studies that require rapid results, albeit with some compromise of fine structural detail, we use paraffin-wax-embedded sections. Most transporter antisera will, in our hands, produce excellent results when used on conventionally prepared wax sections. This is of significant value, given the extensive archives of wax-embedded tissue that is available in many laboratories. Details of the preparation of wax-embedded blocks can be found in any standard histology textbook.

1. Cut sections of wax-embedded fixed tissue at a thickness of 5–10 µm.
2. Float sections on a water bath set at around 45°C (the actual temperature depends on the brand of wax used) until the sections are stretched.

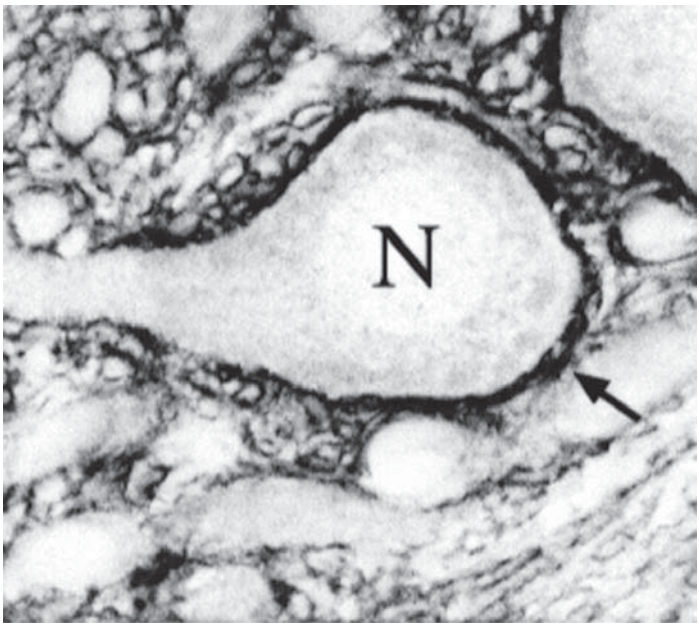

Fig. 3. Example of immunolabeling for a glutamate transporter, GLT1, which is in glial cell membranes (arrow) surrounding a rat spinal cord motor neuron (N). (Reduced from original magnification.)

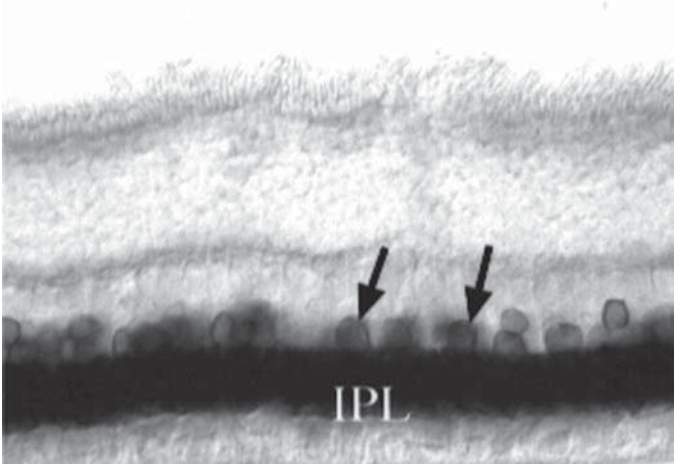

Fig. 4. Example of immunolabeling for a glycine transporter (Glyt-1), which is expressed by the somata (arrows) of glycinergic neurons and their processes in the inner plexiform (synaptic) layer (IPL) of the rabbit retina. (Reduced from original magnification.)

3. Pick up sections onto silane-coated slides and dry down at room temperature.
4. Remove wax by immersing in xylene (toxic) for 10 min. Then, place slides succesively into absolute alcohol, 50% alcohol, and then distilled water (each change takes 20–30 s).
5. Incubate the sections in the primary antibody (diluted in PBS containing 0.05% saponin, 0.5% BSA, and 0.05% sodium azide) for 12 h.
6. Wash the sections with three changes of with PBS over 20 min at 4°C to remove unbound primary antibody.
7. Treat the sections with secondary antisera for 90 min and reveal immunolabeling using an appropriate detection system (*see* **Note 11**).

3.10.4. Immunolabeling Cultured Cells

1. Wash the fixed cells with PBS for 30 min at 4°C to ensure that the fixative has been thoroughly rinsed away.
2. Permeabilize the fixed cells (*see* **Note 12**).
3. Incubate the fixed cells in primary antibody, diluted with PBS–BSA–saponin for 30 min to 24 h.
4. Wash the cells with three changes of PBS over 1 h at 4°C to remove unbound primary antibody.
5. Treat the cells with secondary antisera and reveal immunolabeling using an appropriate detection system (*see* **Note 11**).

3.10.5. Detection Systems

A multitude of appropriate detection systems exist ranging from the use of fluorescently labeled secondary antibodies through to the use of chromogens. Numerous chapters in this series detail such detection methods (*see* **Note 11**).

3.10.6. Immunocytochemical Controls

Despite their essential nature, adequate controls are present in only a small proportion of immunocytochemical studies that are published each year. To ensure the validity of immunocytochemical results, the following controls should be included:

1. Use immunoblotting to confirm the identity of the peptide that the antiserum detects.
2. Use the preimmune serum from each animal that has been used to raise specific antibodies in place of the corresponding primary antiserum. Perform such control experiments using a range of preimmune serum dilutions.
3. Absorb the immune sera with paraformaldehyde conjugates of the appropriate peptide. In general, add 5–50 µg of peptide per milliliter of diluted antibody solution 8 h prior to use and store at 4°C until ready to use.
4. Omit the primary or secondary antibody. This is a poor control but does indicate if a gross abnormality is present in the immunocytochemical method.

3.10.7. Postmortem Delay

Our group routinely works on human materials that are collected postmortem ***(13)***. Because of the possibility of postmortem changes in protein levels because of unregulated proteolysis, we routinely examine the effect of both the length of postmortem delay and temperature of storage on the ability of glutamate transporter antibodies to recognize the glutamate transporter GLAST. In general, most human tissues are cooled to 4°C or similar within 6–10 h of death. Accordingly, we examined the effects of differing lengths of time of initial storage at ambient temperature and the overall postmortem delay for any particular transporter, using rats killed at defined time-points. In general, we find good stability of most proteins up to at least 72 h postmortem IF tissues are cooled within 16 h of death (*see* **Fig. 5**).

Accordingly, subject to the use of similar tests, it is plausible that patterns of expression of many other transporters may be reliably examined in human postmortem tissues.

3.10.8. Negative Results

Despite the use of an antibody that works well in Western blots, it is common to find that many antisera do not recognize proteins in fixed tissues. This inability to detect such cryptic protein epitopes could be the result of the absence of the protein in the area being studied or, more frequently, the result of conformational changes induced in the protein in response to parameters such as extended fixation or storage of the tissues for long periods under suboptimal conditions. Antigen-recovery techniques are available. We routinely use an antigen-recovery solution called Revealit Ag to recover these cryptic epitopes (*see* **Note 13**).

3.11. Colocalization of Transporters, Amino Acid Neurotransmitters, and Other Related Molecules

We frequently utilize immunocytochemistry to localize not only the transporter but also the molecule that the transporter is thought to translocate. This is particularly important when the transporter may have multiple potential substrates and the investigator wishes to determine if the cell type has an enriched content of one specific molecule. We utilize antibodies that have been specifically created against paraformaldehyde conjugates of amino acids and that, thus, recognize these amino acids in paraformaldehyde-fixed tissues. The methods of immunolabeling for amino acids are fully detailed in another chapter in this series ***(14)***, and examples of co-localization of amino acids and transporters can be seen in **ref.** ***15***. Similarly, there are no conceptual constraints to the localization of amino acid transporters and molecules such as receptors to

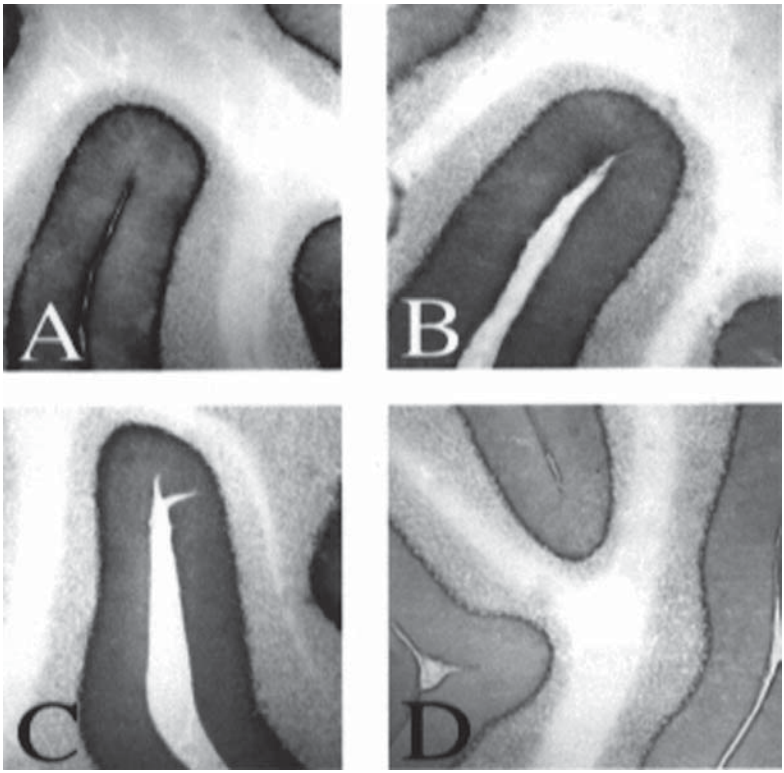

Fig. 5. Series of images of rat cerebellum immunoperoxidase labeled for the glutamate transporter GLAST. The images are from rats at **(A)** 0 h, **(B)** 24 h, **(C)** 48 h and **(D)** 72 h postmortem. Rats were maintained at room temperature (23°C for 16 h prior to cooling to 4°C. Strong labeling persists in comparable structures at all time-points indicated. (Reduced from original magnification.)

amino acid transmitters. By localizing the multiple components of biological systems such as amino acid neurotransmission systems, it is possible to better understand the functioning of the whole system.

4. Notes

1. Extra-pure-grade paraformaldehyde from Merck is preferred, as some other brands do not give adequate fixation, in turn giving rise to poor immunolabeling. It is vital to check the pH of the fixative; a frequent error is to add too much sodium hydroxide during the depolymerization of the paraformaldehyde. If the pH is above 7.4, then fixation is likely to be poor. The fixative should be used within 1 h of preparation. If the tissues will be subsequently embedded in parrafin wax, it is usually possible to add 10% by volume of saturated aqueous picric acid

solution to the paraformaldehyde fixative, because this reduces subsequent tissue shrinkage.

2. The DAB will not dissolve directly in PBS. In our experience, it is not advisable to try to dissolve in other buffers such as Tris-HCl first as this may lead to nonspecific deposition of undissolved DAB particles on the sections.
3. We routinely raise antisera in young adult rabbits, rats, or guinea pigs. For each immunogen, use one rabbit or two rats or two guinea pigs.
4. The quantities of immunogen quoted here are based on the assumption that the animal being immunized is a rabbit. Smaller animals such as rats and guinea pigs need approx half the amount of immunogen as needed for rabbits.
5. It is difficult to take test bleeds from rats and guinea pigs and we routinely choose not to take test bleeds from these animals. Instead, terminally exsanguinate these species under sodium pentobarbitone anesthesia (60 mg/kg, ip) 1 wk after the last of a series of four injections.
6. After incubation in the primary antibody, wash the membranes with PBS and apply a biotinylated secondary antibody (typically diluted 1 : 500) for 2 h. Subsequently, wash the membranes and incubate with streptavidin-biotin-horseradish peroxidase complex (1 : 500) for 2 h. Reveal labeling using DAB as a chromogen, with 5 µL of 30% hydrogen peroxide per 10 mL reaction solution as a catalyst.
7. Preperfusion must be as brief as possible, commensurate with the removal of most of the blood (which will otherwise clot and ruin the perfusion); typically, this is about 15–20 s.
8. Tissues that cannot be fixed by perfusion, such as the rabbit retina (which is avascular and thus fixes poorly by perfusion), invertebrate tissues, cultured cells, brain slices, and so forth, can be fixed by immersion. Although conventional wisdom suggests that the tissue should be only 1–2 mm thick, we have found that blocks of human material up to 10 mm thick and complete mouse brains may be adequately fixed by immersion. However, when large blocks are used, care must be taken to determine if differential labeling occurs between the surface of the block and deeper layers.
9. Even if most of the unbound paraformaldehyde is washed away, it is still possible that residual aldehydes or other reactive groups remain in the tissue. These reactive groups can nonspecifically bind proteins such as antibodies. To prevent this type of nonspecific binding, it is normal practice to block these binding sites by incubating the tissue in an excess of irrelevant protein dissolved in PBS. The most commonly used protein is bovine serum albumin (BSA), which is obtained as a lyophilized powder. BSA works well under most circumstances. However, if high levels of background labeling are observed, then it is advisable to use a 10% (v/v) solution of serum (in PBS) taken from the same species that the secondary antibody is raised in (as the secondary antibody is unlikely to recognize "self" proteins).
10. Longer incubations permit the use of lower dilutions of primary antibody, resulting, usually, in reduced nonspecific background labeling. The optimal dilution of

primary antibody must be ascertained empirically by use of a dilution series. To enhance antibody penetration, add 0.5% (w/v) saponin to the PBS–BSA used as the diluent for the primary and secondary antibodies and the streptavidin-biotin-horseradish peroxidase complex (SAB–HRP). To prevent bacterial contamination, add 0.05% (w/v) sodium azide (Sigma; TOXIC) as a bacteriostat to all antibody solutions. Do not add sodium azide to the SAB–HRP complex (if used), as azide inhibits the HRP enzyme. If a bacteriostat must be added to the SAB–HRP complex, then use 0.05% (v/v) thimerosal (TOXIC).

11. Biotinylated secondary antibodies are used as "bridging" reagents when greater signal intensity is required. Their binding is subsequently detected using streptavidin (a bacterial molecule that binds extremely avidly to biotin), linked either to a fluorophore such as Texas Red or Cy5, or to an enzyme such as horseradish peroxidase. It is usually purchased as a solution, which can be used at a dilution of approx 1 : 200, in PBS–BSA. The solution containing the streptavidin–fluorophore conjugate is applied to the sections for 2–4 h. Thereafter, sections are washed and treated as if they had been labeled with a fluorescently tagged secondary antibody. SAB–HRP is available either as a preformed complex (e.g., from Amersham) or as kits containing two separate components that must be mixed immediately prior to their use (e.g., kits from Vector). We use the preformed complex because in our experience, it is simple to use, gives excellent results, and is considerably cheaper. When diluting the stock solution, make sure that no sodium azide is present in the dilution buffer because azide inhibits the HRP enzyme. Labeling is ultimately revealed using a chromogenic substrate. Labeling is ultimately revealed using a chromogenic substrate (DAB).
12. Penetration of antibodies may be enhanced by a variety of additional techniques. The most common technique is to sequentially dehydrate and rehydrate the specimen by passing through a graded series of alcohols. The alcohol solubilizes some membrane lipids, whereas the shrinkage that also ensues opens up the extracellular spaces, allowing antibodies to permeate between cells. Because isolated cells do not have any cut surfaces, they must be permeabilized. Permeabilize the cells by adding 0.05% saponin to all buffers. Alternatively, permeabilize the cells by immersing cover slips in cold methanol (4°C) for 10 min. Thereafter, rehydrate the cells with PBS. Saponin may still be included in buffers if required. It is important to be conservative in your use of detergents. Excessive concentrations of detergents, especially Triton X-100, which is commonly used instead of saponin, will cause more extensive solubilization of membranes and the proteins that are anchored in them will then be free to diffuse away. In our experience, Triton X-100 concentrations above 0.1% can give rise to diffuse labeling throughout the tissue because of this, especially with GABA transporters.

    The duration of each immunolabeling step is determined by the efficiency of the permeabilization steps and the thickness of the sections. Whereas Vibratome sections may require several d in the primary antibody, wax sections need only 12 h. The duration of the primary antibody incubation step may need to be increased if permeabilization of Vibratome sections is poor. Similar rules apply to the times

for secondary reagents. Typically, apply secondary reagents for 6–8 h on Vibratome sections and 1–2 h on wax sections.

High-background labeling is usually a function of inappropriate dilutions of each reagent. This should be evaluated by modifying first the primary antibody concentration and then the secondary antibody concentration. If you are using an antibody raised against a peptide conjugated to a protein, such as BSA, one potential problem is that this antibody may also recognize BSA. Accordingly, if BSA is used as a blocking agent, high levels of background labeling may arise. This can be cured by using another blocking agent, such as goat or sheep serum.

13. Antigen recovery is performed when the antigen is present in a tissue but is not in a form recognized by the antibody. Several strategies are available, including the use of proteases to cleave open proteins that have folded in a manner that obscures the epitope of interest. Many groups use citrate-buffered recovery solutions. However, in our experience, these are not particularly effective for work with transporters. We use a recovery solution called *Revealit-Ag* (see www.Immuno Solution.com). This solution requires that the tissues be heated in the revealing solution at 85°C for 20 min prior to immunolabeling. Although it might seem surprising, this heating has no negative effects on the general cytology. In our experience, we have been able to reveal strong labeling in situations where no signal was originally obtainable, in both postmortem tissues and in species with some slight differences in sequence of the transporter.

References

1. Harlow, E. and Lane, D. (1988) *Antibodies: A Laboratory Manual* Cold Spring Harbor, NY.
2. Danbolt, N. C. (2002) Glutamate uptake. *Prog. Neurobiol.* **65,** 1–105.
3. Kyte, J. and Doolittle, R. F. (1982) A simple method for displaying the hydropathic character of a protein. *J. Mol. Biol.* **157,** 105–132.
4. Sato, H., Tamba, M., Ishii, T., et al. (1999) Cloning and expression of a plasma membrane cystine/glutamate exchange transporter composed of two distinct proteins. *J. Biol. Chem.* **274,** 11,455–11,458.
5. Jameson, B. A. and Wolf, H. (1988) The antigenic index: a novel algorithm for predicting antigenic determinants. *Comput. Appl. Biosci.* **4,** 181–186.
6. Beckstrom, H., Julsrud, L., Haugeto, O., et al. (1999) Interindividual differences in the levels of the glutamate transporters GLAST and GLT, but no clear correlation with Alzheimer's disease. *J. Neurosci. Res.* **55,** 218–229.
7. Lin, C. I., Orlov, I., Ruggiero, A. M., et al. (2001) Protein Modulation of the neuronal glutamate transporter EAAC1 by the interacting protein GTRAP3-18. *Nature* **410,** 84–88.
8. Marie, H., Billups, D., Bedford, F. K., et al. (2002) The amino terminus of the glial glutamate transporter GLT-1 interacts with the LIM protein Ajuba. *Mol. Cell Neurosci.* **19,** 152–164.
9. Chillaron, J., Roca, R., Valencia, A., et al.(2001). Heteromeric amino acid transporters: biochemistry, genetics, and physiology. *Am. J. Physiol. Renal. Physiol.* **281,** F995–F1018.

10. Wagner, C. A., Lang, F., and Broer, S. (2001) Function and structure of heterodimeric amino acid transporters. *Am. J. Physiol. Cell Physiol.* **281,** C1077–C1093.
11. Zottola, R. J., Cloherty, E. K., Coderre, P. E., et al. (1995) Glucose transporter function is controlled by transporter oligomeric structure. A single, intramolecular disulfide promotes GLUT1 tetramerization. *Biochemistry* **34,** 9734–9747.
12. Haugeto, O., Ullensvang, K., Levy, L. M., et al. (1996) Brain glutamate transporter proteins form homomultimers. *J. Biol. Chem.* **271,** 27,715–27,722.
13. Scott, H., Pow, D. V., Tannenberg, A., et al. (2002) Aberrant expression of the glutamate transporter excitatory amino acid 1 (EAAT 1) in Alzheimer's disease. *J. Neurosci.* **22,** RC206.
14. Pow, D. V. (1997) Immunocytochemical detection of amino acid neurotransmitters in paraformaldehyde-fixed tissues, in: *Neurotransmitter and Neuroreceptor Methods* (Rayne, R. C., ed.) Methods in Molecular Biology, Humana, Totowa, NJ. pp. 103–123.
15. Pow, D. V. and Hendrickson, A. (1999) Distribution of the glycine transporter glyt-1 in mammalian and non-mammalian retinae. *Vis. Neurosci.* **16,** 231–239.

13

Xenopus laevis Oocytes

Stefan Bröer

1. Introduction

During oogenesis, *Xenopus* oocytes accumulate large amounts of storage proteins that—after fertilization—provide the developing embryo with building blocks and energy metabolites. The size of the fully developed oocyte (diameter, 1.2 mm) is largely governed by the stored amounts of egg yolk protein. Thus, the mature oocyte is equipped to initiate protein synthesis, cell growth, and replication after fertilization. The size of the oocyte, the large reserve of storage proteins, and its ability to synthesize protein on demand makes the oocyte an almost ideal single-cell expression system. Some basic physical properties of this expression system are listed in **Table 1**.

The use of *Xenopus* oocytes as an in vitro expression system was initiated in 1971 by the observation of Gurdon that mRNA injected into *Xenopus* oocytes was translated into protein ***(5)***. It was, however, not before 1982 that *Xenopus* oocytes were used to express membrane proteins as pioneered by studies on the acetylcholine receptor in Miledi's and Numa's groups ***(6,7)***. Because of the large amount of stored protein, oocytes do not depend on extracellular resources for nutrition. As a result, only limited numbers of endogenous membrane transporters are expressed. By contrast, large amounts of transporter proteins are synthesized following injection of mRNA. Figures of 10^{10}–10^{11} proteins/oocyte have been reported for the glucose transporter SGLT1 and other membrane proteins ***(8)***. Remarkably, the synthesis of 10^{11} transporters in 4 d translates into the incorporation of roughly 300,000 transporter molecules per second.

In addition to the strength of this expression system in the mechanistic and structural characterization of transport proteins, oocytes are also well equipped

From: *Methods in Molecular Biology, vol. 227: Membrane Transporters: Methods and Protocols*
Edited by: Q. Yan © Humana Press Inc., Totowa, NJ

Table 1
Physicochemical Properties of Oocytes

Property	Value	Ref.
Water-accessible volume	368 ± 21 nL	***(1)***
Water permeability	(1–4) × 10^{-4} cm/s	***(2)***
Surface area	18 mm^2 – 30 mm^2	***(3)***
Membrane potential	–30 to –60 mV	***(3)***
Buffering capacity	20 m*M*/pH unit at pH 7.0	***(4)***
Intracellular pH	7.4 ± 0.1	***(4)***
Na^+ concentration	4–10 m*M*	***(3)***
K^+ concentration	76–120 m*M*	***(3)***
Cl^- concentration	24–50 m*M*	***(3)***
Ca^{2+} concentration	<0.3 μ*M*	***(3)***

with signal transduction pathways that can be exploited to study regulation of transport proteins.

Protein kinase A (PKA) and adenylate cyclase are endogenously expressed in oocytes. Progesterone, which is used to induce maturation in oocytes, drops cAMP levels in minutes by a mechanism that is thought to involve a decrease of PKA activity ***(9)***. By contrast, PKA can be induced by 8-bromo-cAMP, 3-isobutylmethylxanthine (IBMX), or forskolin. Alternatively, β-adrenergic receptors can be expressed in oocytes that couple to G_s-proteins. The α-subunit of the G_s-proteins subsequently activates the adenylate cyclase resulting in the production of cAMP. PKA-coupled pathways have been monitored in oocytes by expression of the cystic fibrosis conductance regulator (CFTR) protein, the chloride conductance of which is activated by PKA ***(10)***.

The α-subunit of oocyte endogenous G_q-proteins activate phospholipase C, Phospholipase C, in turn, splits phopshatidylinostol-4,5-bisphosphate to generate diacylglycerol and inositol-1,4,5-trisphosphate (IP_3). The two molecules activate different pathways. Diacylglycerol activates protein kinase C. Inositol-1,4,5-trisphosphate by contrast binds to the intracellular IP3 receptor channel ($InsP_3$-receptor 1) that resides on the endoplasmic reticulum (ER), resulting in the release of Ca^{2+} from the ER. The elevation of intracellular Ca^{2+} results in the opening of Ca^{2+}-sensitive chloride channels. Similar to monitoring cAMP levels by expression of CFTR, Ca^{2+} levels have been monitored by measuring chloride conductance ***(11)***. The chloride channel can, for example, be activated by lysophosphatidic acid, which binds to an endogenous receptors ***(12)***. The activity of the Ca^{2+}-activated chloride channel may also be modulated by overexpression of foreign proteins in the oocyte membrane.

Pathways that are activated by tyrosine receptor kinases are also endogenous to *Xenopus* oocytes. The oocyte contains a mitogen-activated protein (MAP) kinase pathway that is activated during oocyte maturation (e.g., when treated with progesterone) ***(13)***.

A second pathway related to tyrosine kinases, which has been described in oocytes, is the PI3-kinase-PDK-Akt pathway ***(13)***. Signaling induced by the Akt-related protein kinase Sgk1 is also recognized by the oocyte. Sgk1, when coexpressed with the epithelia Na^+ channel, promotes trafficking of the channel to the plasma membrane ***(14)***.

Thus, it appears possible to simulate signal transduction pathways in oocytes that are occurring in quite different cell types in vivo, such as neurons or epithelial cells of the kidney. However, it has to be kept in mind that regulation in oocytes may not coincide with regulation in every cell type. For example, downregulation of transporters by protein kinase C has been reported frequently in oocytes, but may not occur in all cell types in which the transporter is expressed in vivo ***(15)***.

Acute regulation of transporters occurs by two different mechanisms: (1) changes of mechanistic properties, such as substrate affinity or energetic coupling, and (2) changes of transporter trafficking that alter surface expression.

In this chapter, flux studies and electrophysiological methods are described, on the one hand, that are used to detect changes in the transport mechanism. On the other hand, membrane preparations and immunohistochemical methods are described to evaluate changes in surface expression.

2. Materials

2.1. Oocyte Preparation

1. 3-Aminobenzoic acid ethylester (MS222) (Sigma, St. Louis, MO, USA; cat. no. A5040), 1.5 g/L, prepare fresh.
2. Resorbable suture: Dexon, 1 metric, 5/0 USP, Needle HR13, 45 cm (Braun-Dexon GmbH, Spangenberg, Germany; cat. no. 051007/6).
3. Nonresorbable suture: Dafilon 0.7 metric, 6/0, Needle DSM 11, 45 cm (Braun-Dexon GmbH, Spangenberg, Germany; cat. no. C0936022).
4. Gentamycin sulfate (ICN Biomedicals, Aurora, OH, USA; cat. no. 194530). Stock solution of 50 mg/mL, store at –20°C.
5. Collagenase A from *Clostridium histolyticum* (E.C. 3.4.24.3); 0.3 U/mg (Roche, Mannheim, Germany; cat. no. 154121). Prepare fresh; *see* **Note 1**.
6. Oocyte Ringer 2 without $CaCl_2$ (OR2–): 82.5 m*M* NaCl, 2.5 m*M* KCl, 1 m*M* $MgCl_2$, 1 m*M* Na_2HPO_4, and 5 m*M* *N*-[2-hydroxyethyl]piperazine-*N*'-[2-ethanesulfonic acid] (HEPES). Titrated with NaOH to pH 7.8. A 10X stock can be prepared, stable.
7. Oocyte Ringer 2 with $CaCl_2$ ($OR2^+$) $OR2^-$ supplemented with 1.5 m*M* $CaCl_2$, stable.

8. ND96: 96 m*M* NaCl, 2 m*M* KCl, 1 m*M* $MgCl_2$, 1.8 m*M* $CaCl_2$, and 5 m*M* HEPES. Titrated with NaOH to pH 7.4, stable.

2.2. Flux Measurements

1. Nunc-Immunotubes (NalgeNunc, Naperville, IL, USA; cat. no. 475 477).
2. Plastic Pasteur pipets (Bacto Laboratories, Liverpool, NSW, Australia).

2.3. Electrophysiological Recordings

1. Glass capillaries (GC150F-10) (Harvard Apparatus Ltd., Edenbridge, UK).
2. Tributylchorosilane (Sigma-Fluka, Buchs, Switzerland; cat. no. 90794).
3. Tetrachlorocarbon (CCl_4) (Sigma-Fluka, Buchs, Switzerland; cat. no. 87036).
4. 5% Tributylchorosilane in CCl_4. Store the solution 1–2 d before usage. The solution is stable for 3 mo in the dark.
5. Proton Ionophore Cocktail A (Sigma-Fluka, Buchs, Switzerland; cat. no. 95291).

2.4. Materials for Analysis of Surface Expression

2.4.1. Membrane Preparation

1. Pefabloc [AEBSF 4-(2-aminoethyl)-benzenesulfonyl fluoride hydrochloride] (Roche, Mannheim, Germany; cat. no. 1429868); store at 4°C, unstable in aqueous solutions.
2. Homogenization buffer 1: 50 m*M* Tris 100 m*M* NaCl, 1 m*M* EDTA, and 1 m*M* Pefabloc; titrate with HCl to pH 7.5; prepare fresh each time.

2.4.2. Membrane Fractionation

1. Homogenization buffer 2: 320 m*M* Sucrose, 50 m*M* Tris 1 m*M* EDTA, and 1 m*M* Pefabloc; titrate with HCl to pH 7.5; prepare fresh.
2. Gradient buffers: (i) 2.0 *M* Sucrose, (ii) 1.3 *M* sucrose (iii) 1.0 *M* sucrose, (iv) 0.6 *M* sucrose each in TE buffer; prepare fresh.
3. TE buffer: 50 m*M* Tris, 1 m*M* EDTA, and 5 m*M* $MgCl_2$, titrate with HCl to pH 7.5, stable.

2.4.3. Surface Biotinylation

1. Phosphate-buffered saline (PBS): 137 m*M* NaCl, 2.7 m*M* KCl, and 5 m*M* Na_2HPO_4; titrate with HCl to pH 8.0, stable. pH 8.0 important for reaction.
2. EZ-link Sulfo-NHS-lc-Biotin (0.5 mg/mL dissolved in PBS; use 1 mL/10 oocytes, prepare fresh each time) (Pierce, Rockford, IL, USA; cat. no. 21335).
3. Immunopure, immobilized streptavidin gel (Pierce, Rockford, IL, USA; cat. no. 20347), store at 4°C.
4. Lysis buffer: 150 m*M* NaCl, 20 m*M* Tris, and 1% Triton X-100; titrate with HCl to pH 7.5, stable.

2.4.4. Immunohistochemistry

1. PBS: 137 m*M* NaCl, 2.7 m*M* KCl, 4.3 m*M* Na_2PO_4, and 1.4 m*M* KH_2PO_4 (final pH should be 7.1), stable.
2. Dent's fixant: 80% Methanol and 20% dimethyl sulfoxide (DMSO), stable.
3. 3.7% Paraformaldehyde in PBS, prepare fresh.
4. 90% PBS and 10% normal donkey serum, store frozen at –20°C.
5. Technovit 7100 (Heraeus Kulzer, Wehrheim, Germany), stable.
6. Embedding solution 1: 1 : 1 Mixture of Technovit 7100 and ethanol.
7. Embedding solution 2: Technovit 7100 plus hardener 1 (1 g hardener 1 [dibenzoylperoxide] per 100 mL Technovit 7100; solution stable at 4°C for 1 mo).
8. Embedding solution 3: 15 mL Technovit 7100, 0.15 g hardener 1, plus 1 mL hardener 2; prepare fresh each time.
9. Embedding capsules (BEEM capsules; Proscitech, Turingowa, Queensland; cat. no. RB001).
10. Embedding mold [Tissue-Tek, Cryomold; Miles Inc., Elkhart, IN, USA; cat. no. 4565).
11. Technovit 3040 powder (Heraeus Kulzer, Wehrheim, Germany).
12. Technovit 3040 liquid (Heraeus Kulzer, Wehrheim, Germany).

3. Methods

3.1. Preparation of Oocytes

3.1.1. Anesthesia

1. Submerse frog in 1.5 g/L MS222 for 15–30 s. Anesthesia is complete when the frog can be turned on its back without eliciting any reaction.
2. Place frog on a sheet of wet paper on ice with belly up.
3. Make a small incision (1 cm) slightly off the middle line of the belly. Use a sterile scalpel; first cut through the skin, then through the muscular layer.
4. Remove parts of the ovary with tweezers and scissors.
5. Close incision with one stitch of reabsorbable suture in the muscular layer.
6. Close incision with two stitches of nonabsorbable suture in the skin.
7. Let the frog recover under a moist tissue; when fully awake, submerse in water.

3.1.2. Digestion of Ovary

1. Place ovary in $OR2^-$ buffer.
2. Prepare a collagenase solution (1 mg/mL in $OR2^-$ buffer) in a 100-mL Erlenmeyer flask (*see* **Note 1**). Use tweezers and scissors to cut off very small pieces of ovary (about 20–30 oocytes each) and let them drop into the Erlenmeyer flask.
3. Incubate the ovary at 28°C for 2–4 h under slight agitation (*see* **Note 2**).

4. After digestion is completed, oocytes are thoroughly washed with copious volumes of $OR2^-$ buffer (at least 1 L). Small oocytes can be discarded during the washing procedure.
5. Finally, oocytes are washed three times in $OR2^+$ buffer.
6. On the next day, stage V and VI oocytes are manually selected for injection (*see* **Note 3**).
7. Oocytes are stored at 16–18°C in sterile cell-culture dishes (35 mm) in $OR2^+$ buffer. For long-term storage, gentamycin (10 mg/L) is added. Change buffer daily to increase life expectancy of oocytes. Remove dead or damaged oocytes.

3.2. Determining Kinetic and Mechanistic Properties

The following protocols describe methods of how to perform transport experiments with oocytes. A detailed description of the kinetic analysis itself can be found in Chapter 10 of this volume.

3.2.1. Substrate Uptake

1. Transfer 7–10 oocytes into a Nunc Immunotube (*see* **Note 4**).
2. Flush oocytes two times with 4 mL transport buffer (e.g., ND96).
3. Remove supernatant completely. This is important because, otherwise, the radioactivity may be diluted by an unknown factor. If complete aspiration appears too risky, use an automatic pipet with a yellow tip to remove the last bit.
4. Add 100 µL of transport buffer containing the labeled substrate (*see* **Note 5**).
5. Incubate oocytes for an appropriate time (usually between 5 and 30 min, depending on the expression level of the transporter).
6. Add 4 mL ice-cold transport buffer to terminate transport and remove >95% of the supernatant by aspiration.
7. Flush oocytes three times with 4 mL ice-cold transport buffer and aspirate the supernatant each time.
8. After the third removal, add 1 mL ice-cold transport buffer.
9. Transfer oocytes with a plastic Pasteur pipet to scintillation vials.
10. Dissolve oocytes by addition of 200 µL of 10% sodium dodecyl sulfate (SDS).
11. Vortex briefly to homogenize oocytes; add >1.5 mL scintillation fluid.

3.2.2. Substrate Efflux

3.2.2.1. Preloading Method

1. Transfer 7–10 oocytes into a Nunc Immunotube. If standard deviations are to be shown on the final efflux curve, dispense 3 × 4 oocytes.
2. Flush oocytes two times with 4 mL transport buffer (room temperature).
3. Remove supernatant completely (*see* **Subheading 3.2.1.**, **step 3**).
4. Preloading: Add 100 µL of transport buffer containing the labeled substrate. Incubate oocytes until radioactivity is equilibrated (usually between 30 and 120 min; *see* **Note 6**). Use a low substrate concentration for preloading to maximize the specific activity (e.g., 10 µ*M*).

5. Flush oocytes three times with 4 mL ice-cold transport buffer. Aspirate >95% of the supernatant the first two times. The third time, the supernatant must be removed completely.
6. Add 1 mL of room-temperature transport buffer to the oocytes to initiate efflux. Extracellular substrates should preferably be added at saturating concentrations.
7. Take samples at different times from supernatant for counting.

3.2.2.2. Injection Method

1. Inject oocytes with 10–40 nL radiolabeled substrate. The radiolabeled substrate can be used as delivered by the manufacturer. Incubate 10 min to allow diffusion of the substrate in the oocyte and closure of the injection spot. If the transporter allows net movement of substrates (i.e., it is not an antiporter), injection should be performed in ice-cold transport buffer to avoid loss of substrate.
2. Transfer 7–10 oocytes to a Nunc Immunotube. If standard deviations are to be shown on the final efflux curve, dispense 3 × 4 oocytes.
3. Flush oocytes two times with 4 mL transport buffer (ice cold when transporter mediates net movement).
4. Remove supernatant completely.
5. Add 1 mL of room-temperature transport buffer to the oocytes to initiate efflux. Extracellular substrates should preferably added at saturating concentrations.

3.3. Electrophysiological Techniques

The following protocols only describe how to set up microelectrodes for voltage-clamp recording from oocytes. Electrophysiological analysis is described in more detail in Chapter 11.

3.3.1. Voltage-Clamp Recordings

The two-electrode voltage clamp (TEVC) technique allows the control of the membrane potential (clamping) to measure currents flowing through ion channels, electrogenic transporters, or pumps. For the technicalities of the electrophysiological setup, the reader is referred to reviews in this area (e.g., **ref. *16***). Two glass microelectrodes are impaled into the oocyte, a membrane potential recording electrode and a current-delivering electrode. The membrane potential electrode connects to a feedback amplifier, where the signal is compared to the command voltage given by a generator. A variable current is applied through the current-delivering electrode, across the membrane, and to the bath-grounding electrode that aligns the membrane potential with the command potential. All electrogenic ion or substrate fluxes across the membrane are now measured as a deflection from the baseline current. By convention, upward deflections correspond to the influx of anions (or efflux of cations) and downward deflections correspond to the influx of cations (efflux

of anions). The setup is described for a Geneclamp 500 amplifier (Axon Instruments, Union City, CA, USA).

1. Pull capillaries to form microelectrodes, fire-polish the back end to avoid damage to the $AgCl_2$ coating of the $Ag/AgCl_2$ electrode.
2. Backfill electrodes with 3 *M* KCl and insert into $Ag/AgCl_2$ electrode holder (*see* **Note 7**). Microelectrode 1 is the voltage-recording electrode, Microelectrode 2 is the current-passing electrode in the voltage clamp modus (*see* **Note 8**).
3. Switch amplifier to the setup mode.
4. Submerse electrodes in the bath. Cancel voltage offset to ± 1 mV.
5. Measure resistance of microelectrodes, which should be between 0.5 and 5 MΩ.
6. Impale oocyte with both microelectrodes (*see* **Note 9**).
7. Set command voltage to the resting potential of the oocyte (about –40 mV). Switch amplifier to the voltage-clamp mode and adjust voltage to the resting potential.
8. Apply test pulse (e.g., –10 mV square wave from the resting potential) and increase gain until the output looks like the command pulse. Oscillations can be counteracted by introducing a phase shift (stability setting).
9. Put command voltage to the desired value (e.g., –60 mV) and apply substances.

3.3.2. Ion-Sensitive Electrodes

Ion-sensitive electrodes are particularly useful to investigate H^+-coupled transporters ***(4)***. Movement of Na^+ ions can be followed as well, however, changes of the intracellular Na^+ concentration in oocytes are rather slow even when expressing very fast transporters. Ion-selective electrodes are made out of the same borosilicate glass as membrane potential recording electrode. In order to generate ion selectivity, the inner side of the tip is coated with a hydrophobic ionophor. Because of the hydrophobic nature of the ionophor, the glass capillary has to be pretreated with silane to generate a hydrophobic surface to which the ionophor adheres. As ion-selective electrodes record both the membrane potential and the electrochemical gradient of the respective ion species, a second standard membrane potential recording electrode has to be used to subtract the membrane potential from the combined signal. Double-barreled electrodes can be used to combine both electrodes, but those demand a special pulling device. Because of the large size of the oocyte, two separate electrodes can be used instead. Ion-selective electrodes have a very high resistance (10^{10}–10^{12} Ω); thus head stages or preamplifier with an even higher input resistance have to be used. The preparation of the ion-sensitive electrodes is described in the following:

1. Pull capillaries as for membrane potential recording.
2. Backfill the first 2–3 mm of each capillary with silane CCl_4 solution.
3. Place the capillaries tip to the center on a hot plate at 450°C.

4. Incubate for 5 min to evaporate CCl_4.
5. Backfill ionophor solution (for pH, use Proton Ionophore Cocktail A) into the silanized tip. Use less ionophor than silanizing solution.
6. Layer 0.1 *M* Na-citrate, pH 6.0 (titrated with HCl to add chloride ions), on top and fill capillary to completion.
7. Insert capillary into $Ag/AgCl_2$ electrode holder.

Capillaries should be calibrated with solutions of defined pH. The response of the electrode should be instantaneous and be >50 mV/pH unit.

3.4. Determining Surface Expression

3.4.1. Simple Oocyte Membrane Preparation (Does Not Discriminate Between ER and Plasma Membrane)

1. Twenty-five oocytes are homogenized in 1 mL homogenization buffer 1 by trituration in a blue tip of an automatic pipettor.
2. Spin the homogenate in a microcentrifuge at 2000*g* for 10 min at 4°C (*see* **Note 10**).
3. Transfer the supernatant and spin it at 140,000*g* for 30 min at 4°C.
4. Discard the supernatant.
5 Dissolve pellets in 30–50 µL homogenization buffer 1 supplemented with 4% SDS.
6. Add sample buffer and subject to polyacrylamine gel elecrophoresis (PAGE).

3.4.2. Fractionation of Oocyte Membranes (17)

1. One hundred fifty oocytes are homogenized in 2 mL homogenization buffer 2 by 15 strokes of a tight-fitting pestle in a chilled Dounce homogenizer.
2. The homogenate is centrifuged twice at 1000*g* for 10 min at 4°C (*see* **Note 10**).
3. Transfer the supernatant on top of a discontinuous sucrose gradient: 2.0 *M* (2 mL), 1.3 *M* (3.2 mL), 1.0 *M* (3.2 mL), and 0.6 *M* (2.0 mL); all solution prepared in TE buffer containing 5 m*M* $MgCl_2$.
4. The gradient is centrifuged in a Beckman SW41 swing-out rotor at 275,000*g* (40,000 rpm) for 4 h at 4°C. Fractions (1 mL) are collected starting from the bottom. Each fraction is diluted fourfold with 0.15 *M* sucrose in TE buffer.
5. Pellet membranes from each fraction by centrifugation at 300,000*g* (48,000 rpm) in a Beckmann SW 50.1 rotor for 3 h at 4°C.
6. Resuspend pellet in 80 µL TE buffer or in 15 µL SDS-PAGE sample buffer (*see* **Note 11**).

3.4.3. Biotinylation of Oocyte Surface Proteins

1. Wash 5–10 oocytes three times with 4 mL ice-cold PBS, pH 8.0. The pH is important for the succinimide–ester formation.
2. Incubate 5–10 oocytes in 0.5 mL Sulfo-NHS-lc-Biotin solution for 10 min at room temperature.
3. Wash oocytes four times with 4 mL ice-cold PBS, pH 8.0.
4. Transfer oocytes into a 1.5-mL reaction tube.

5. Lyse oocytes by incubation in 1 mL of lysis buffer for 30 min on ice, invert tube from time to time. Do not vortex!! (*see* **Note 12**).
6. Spin down at top speed in tabletop centrifuge for 15 min at 4°C.
7. Transfer supernatant into fresh 1.5-mL reaction tubes.
8. Add 50 µL streptavidin-coated agarose particles (*see* **Note 13**).
9. Incubate at 4°C for 1 h with slight agitation.
10. Spin down 10 min at maximum speed in a tabletop centrifuge. Carefully remove most of the supernatant. Do not remove any pellet (pellet difficult to see).
11. Wash pellets four times with 1 mL lysis buffer. Each time, repeat **step 10**.
12. Resuspend pellet in 20 µL SDS-PAGE sample buffer, boil for 5 min, and use for gel electrophoresis.

3.4.4. Immunohistochemical Analysis of Transporter Expression

This protocol describes the procedure of how to prepare oocytes for immunohistochemical analysis. More details about immunocytochemical procedures can be found in Chapter 12.

1. Incubate oocytes in a Petri dish in 200 m*M* potassium aspartate for 10–20 min.
2. Defolliculate oocytes in the Petri dish (*see* **Note 14**).
3. Transfer oocytes to high-performance liquid chromatography (HPLC) vials. Solutions can be easily exchanged with Pasteur pipets. All volumes are given as per vial.
4. Fix oocytes in 1 mL Dent's fixant for 2 h at room temperature (or overnight at –20°C).
5. Wash oocytes with 0.5 mL each of solution A (90% methanol in H_2O), solution B (70% methanol in H_2O), solution C (50% methanol in PBS), and solution D (30% methanol in PBS). Apply each solution for 10 min.
6. Wash oocytes three times for 10 min with 1 mL PBS.
7. Incubate oocytes at 4°C overnight (or 3 h at room temperature) with primary antibody in 90% PBS and 10% normal donkey serum (or goat serum). Dilute antibody as appropriate.
8. Wash oocytes with PBS using 2-mL aliquots in each step: three times for 5 min, three times for 15 min, three times for 30 min, and, finally, two times for 1 h.
9. Incubate oocytes with secondary antibody in 90% PBS and 10% normal donkey serum (or goat serum) for 1 h in the dark at room temperature. Use dilution as recommended by the manufacturer, the volume can be kept as small as convenient (e.g., 200 µL).
10. Wash oocytes six times with 2 mL PBS.
11. Wash oocytes overnight with 2 mL PBS.
12. Postfixate oocytes with 3.7% paraformaldehyde in PBS for 30 min.
13. Wash oocytes two times with 2 mL PBS for 15 min.
14. Dehydrate oocytes by incubating in 0.5 mL ethanol solutions of increasing concentrations each for 15 min: solution A2 (30% ethanol in PBS), solution B2 (50% ethanol in PBS), solution C2 (70% ethanol in H_2O), solution D2 (90% ethanol in H2O), and, finally, in 100% ethanol.

15. Embed oocytes in acrylic resin by infiltration for 2 h at room temperature with 0.5 mL embedding solution 1 (Technovit 7100/ethanol mixture [1:1]).
16. Exchange infiltration solution to 0.5 mL embedding solution 2 (Technovit 7100/ hardener 1). Incubate for 2 h at room temperature.
17. Renew embedding solution 2 and incubate overnight at 4°C.
18. Prefill disposable embedding capsules with 100 μL embedding solution 3 (15 mL embedding solution 2 + 1 mL hardener 2).
19. Transfer oocytes on top of the embedding solution.
20. Add more embedding solution until capsules are filled to completion. Close capsules. Polymerization requires about 2 h.
21. To mount the specimen on a microtome, the specimen is supported by a basis of a plastic resin.
22. Mix Technovit 3040 powder (20 g) with Technovit 3040 liquid (10 mL) and pour the mixture into a disposable embedding mold. Press polymerized acryl-resin specimen into mounting resin. Polymerization of the mounting resin is complete after 10 min.
23. Fix complete specimen using the plastic basis on microtome specimen holder. Cut-5 μm slices for microscopy. Straighten out slices on a water surface. Transfer on microscope slides, dry for 15 min at 60°C (or 2 h at 37°C), and embed with Entellan or other appropriate medium.

4. Notes

1. For long-term survival of oocytes (> 5 d), it is critical to use collagenase with low tryptic activity. Companies usually provide information about tryptic activity of batches that are in stock. An excellent lot, for example, has a trypsin activity (BAEE method) as low as 0.05 U/mg lyophilisate.
2. Digestion is complete when (1) most oocytes float around separately, (2) most oocytes are devoid of adhering blood vessels, and (3) the follicular cell layer is removed. Oocytes are still surrounded by the vittelin layer (glycoprotein matrix) at this stage.
3. Stage V/VI oocytes are large in size (diameter >1 mm) and have a brown color on the animal pole. Pigmentation is fine-grained, and poles are separated by a sharp border. Injection may be performed on the 2 d following preparation. Life expectancy of oocytes injected on the second day is slightly shorter than for those injected on the first day. We use custom-made Perspex egg cups for injection. The design is identical to a 100-mm Petri dish but with a thicker bottom plate (5 mm). Holes (0.5 mm deep and 1.1 mm wide) are drilled into the bottom plate (15 × 12; distance, 3 mm).
4. Flux measurements are best carried out in 5 mL Nunc Immunotubes or γ-counter tubes. Oocytes are transferred from the storage culture dishes to the tubes using disposable plastic Pasteur pipets. The transport buffer ND96 can be aspirated using a glass Pasteur pipet with a tilted end attached to a vacuum pump.
5. As a first approximation, the transport buffer should contain 10 kBq of labeled substrate/100 μL. This usually gives a well-detectable result. Unlabeled substrate is added as necessary. For uncharacterized transporters, 10 μ*M* is a good concentration to start with.

6. Preloaded substrates are usually not metabolised quickly by the oocyte. Amino acids such as isoleucine or glutamine are stable for at least 2 h.
7. $Ag/AgCl_2$ electrodes can easily be prepared from silver wire by bathing two-thirds of its length in 12% NaOCl for 20 min.
8. The current passing head stage/microelectrode 2 should be able to pass currents of up to 100 μA. The voltage-recording electrode 1, however, does not need to pass large currents. The head stage with a lower output resistance should thus be chosen for the current-passing electrode; for example, a head stage with $R_0 = 1$ MΩis best suited to serve as microelectrode 2 and a head stage with $R_0 = 10$ MΩ as Microelectrode 1.
9. Penetration can easily be monitored in the current-clamp mode (where both electrodes monitor the membrane potential) by the rapid deflection of the electrical potential, which is usually in the range of about –35 to –45 mV, depending also on the expressed protein. In Ringer's solution, the membrane potential of the oocyte is mainly dominated by a K^+ diffusion potential generated by potassium channels and a contribution of the endogenous NaK-ATPase to the membrane potential. Thus, elevation of KCl in the buffer effectively depolarizes *Xenopus* oocytes.
10. Spinning down homogenized oocytes generates three layers of material: (1) the egg yolk pellet, (2) the homogenization buffer containing cytosolic components, and (3) a top layer of white lipids. It is very difficult to avoid the transfer of lipids to the next step completely. Avoid repetitive pipetting. Use a blue tip, punch through the floating lipids and remove the clear supernatant as completely as possible. The more oocytes are used, the thicker the lipid layer becomes.
11. According to ***(17)***, the rough ER is found in fraction 2–3, the plasma membrane is detected in fraction 5 and the trans-Golgi network is in fraction 9–10.
12. Vortexing results in homogenization of the oocyte generating a layer of lipids after centrifugation that is difficult to remove (*see* **Note 10**).
13. Mix content of bottle well to resuspend agarose particles. Cut the end of a yellow tip to transfer the suspension.
14. Start to remove the follicle cell layer when it becomes apparent as a silvery shining integument that is too large for the oocyte. Use very fine tweezers to tear the layer apart. If necessary, sharpen tweezers. This procedure requires a considerable amount of training before it becomes routine. Defolliculated oocytes are very fragile. Transfer them with plastic Pasteur pipets, the orifice of which has been rounded in a flame.

References

1. Stegen, C., Matskevich, I., Wagner, C. A., et al. (2000) Swelling-induced taurine release without chloride channel activity in *Xenopus laevis* oocytes expressing anion channels and transporters. *Biochim. Biophys. Acta* **1467,** 91–100.
2. Zeuthen, T., Meinild, A. K., Loo, D. D., et al. (2001) Isotonic transport by the Na^+-glucose cotransporter SGLT1 from humans and rabbit. *J. Physiol.* **531,** 631–644.

3. Weber, W. (1999) Ion currents of *Xenopus laevis* oocytes: state of the art. *Biochim. Biophys. Acta* **1421,** 213–233.
4. Broer, S., Schneider, H. P., Broer, A., et al. (1998) Characterization of the monocarboxylate transporter 1 expressed in *Xenopus laevis* oocytes by changes in cytosolic pH. *Biochem. J.* **333,** 167–174.
5. Gurdon, J. B., Lane, C. D., Woodland, H. R., et al. (1971) Use of frog eggs and oocytes for the study of messenger RNA and its translation in living cells. *Nature* **233,** 177–152.
6. Barnard, E. A., Miledi, R., and Sumikawa, K. (1982) Translation of exogenous messenger RNA coding for nicotinic acetylcholine receptors produces functional receptors in Xenopus oocytes. *Proc. R. Soc. Lond. B: Biol. Sci.* **215,** 241–246.
7. Mishina, M., Kurosaki, T., Tobimatsu, T., et al. (1984) Expression of functional acetylcholine receptor from cloned cDNAs. *Nature* **307,** 604–608.
8. Zampighi, G. A., Kreman, M., Boorer, K. et al. (1995) A method for determining the unitary functional capacity of cloned channels and transporters expressed in *Xenopus laevis* oocytes. *J Membr. Biol.* **148,** 65–78.
9. Maller, J. L., Butcher, F. R., and Krebs, E. G. (1979) Early effect of progesterone on levels of cyclic adenosine 3':5'-monophosphate in *Xenopus* oocytes. *J. Biol. Chem.* **254,** 579–582.
10. Uezono, Y., Bradley, J., Min, C., et al. (1993) Receptors that couple to 2 classes of G proteins increase cAMP and activate CFTR expressed in *Xenopus* oocytes. *Receptors Channels* **1,** 233–241.
11. Landau, E. M. and Blitzer, R. D. (1994) Chloride current assay for phospholipase C in *Xenopus* oocytes. *Methods Enzymol.* **238,** 140–154.
12. Guo, Z., Liliom, K., Fischer, D. J., et al. (1996) Molecular cloning of a high-affinity receptor for the growth factor-like lipid mediator lysophosphatidic acid from *Xenopus* oocytes. *Proc. Natl. Acad. Sci. USA* **93,** 14,367–14,372.
13. Ferrell, J. E., Jr. (1999) *Xenopus* oocyte maturation: new lessons from a good egg. *Bioessays* **21,** 833–842.
14. Wagner, C. A., Ott, M., Klingel, K., et al. (2001) Effects of the serine/threonine kinase SGK1 on the epithelial Na(+) channel (ENaC) and CFTR: implications for cystic fibrosis. *Cell Physiol. Biochem.* **11,** 209–218.
15. Trotti, D., Peng, J. B., Dunlop, J, et al. (2001) Inhibition of the glutamate transporter EAAC1 expressed in *Xenopus* oocytes by phorbol esters. *Brain Res.* **914,** 196–203.
16. Levis, R. A. and Rae, J. L. (1992) Constructing a patch clamp setup. *Methods Enzymol.* **207,** 14–66.
17. Corey, J. L., Davidson, N., Lester, H. A., et al. (1994) Protein kinase C modulates the activity of a cloned gamma-aminobutyric acid transporter expressed in *Xenopus* oocytes via regulated subcellular redistribution of the transporter. *J. Biol. Chem.* **269,** 14,759–14,767.

14

Measurement of Intracellular pH

Frederick B. Loiselle and Joseph R. Casey

1. Introduction

Intracellular pH regulation is critical for most cellular processes, including cell volume regulation, vesicle trafficking, cellular metabolism, cell membrane polarity, muscular contraction, and cytoskeletal interactions ***(1–6)***. Changes of intracellular pH (pH_i) affect the concentration of intracellular messengers like Ca^{2+} and cAMP and thus influence cellular signaling ***(7,8)***. In addition, some growth-stimulating signals, including epidermal growth factor, platelet-derived growth factor, insulin, vasopressin, and serum, activate sodium–proton exchange activity to induce cellular alkalinization, which is important in cell activation, growth, and proliferation ***(9–13)***.

Techniques to measure intracellular pH include H^+ permeable microelectrodes, nuclear magnetic resonance (NMR) analysis of metabolites whose resonance frequency is influenced by pH, and emission/excitation of weak acid fluorescent dyes ***(14,15)***. pH microelectrodes are essentially microscopic versions of the pH electrodes in routine laboratory use to measure solution pH. Microelectrode based measurement of intracellular pH involves inserting an electrode small enough so as not to damage the cell, usually 1 μm or less in diameter, through the plasma membrane and into the cytoplasm ***(15)***. The electrode is filled with a solution of low pH, producing a H^+ gradient across the electrode wall that generates a potential proportional to the concentration of H^+ outside and the permeability to H^+. The most popular types of electrodes are the recessed-tip microelectrode and the double-barrel microelectrode ***(16,17)***. The recessed-tip electrode allows for small-bore tips, whereas the double-barreled electrode allows for the independent measurement of membrane potential and pH. This is a major advantage, as single-barreled electrodes measure the sum of the pH response and the membrane potential.

From: *Methods in Molecular Biology, vol. 227: Membrane Transporters: Methods and Protocols*
Edited by: Q. Yan © Humana Press Inc., Totowa, NJ

Nuclear magnetic resonance spectroscopy is potentially the most powerful method for intracellular pH measurement and provides the added advantage of being amenable to tomography, which allows for two- or three-dimensional imaging. In NMR, the behavior of nuclei with nonzero spin in a strong magnetic field is measured. The pH-dependent protonation/deprotonation alters the electronic environment of nuclei, which shifts the position of the NMR peak. For measurement of intracellular pH by NMR, spectroscopy of phosphate groups is most useful, because of the high abundance of phosphate-containing compounds in cells and the pK_a of phosphate groups is in the physiological range ***(15)***. In practice, ^{31}P-NMR is most effective for studying pH_i in whole tissues (e.g., to measure changes of pH_i in isolated hearts during ischemia) ***(18)***. In these experiments, the relative concentrations of protonated and deprotonated forms of a phosphate group can be determined. Because the concentration ratio of the protonated and deprotonated forms is a function of pH, this allows easy calculation of pH_i. However, using NMR to measure intracellular pH requires complex equipment, methodology, and data analysis. The technique also suffers from low sensitivity, which requires high concentrations of cells or long data acquisition times ***(15)***.

Fluorescence spectroscopy is a highly sensitive method of pH_i measurement. The basis for this approach is that cells can be loaded with a fluorescent dye (fluorophore) whose fluorescence varies with pH. Fluorescent molecules will absorb photons of light of the appropriate wavelength (excitation wavelength), causing the molecule to rise to an excited state. Some time later, the energy will be emitted as heat combined with a photon released at a longer wavelength (emission wavelength) than the photon it absorbed. Fluorometers are spectroscopic devices that allow one to illuminate a sample with light at a particular excitation wavelength and to monitor and quantify light at the emission wavelength.

For measurement of pH_i, fluorescence spectroscopy has several technical and practical advantages over other methods. NMR may be the least invasive technique. However, its low sensitivity and technical complexity make it a less desirable choice. Microelectrode techniques offer the advantage of potentially recording both pH changes and total ion flux at the same time, which can be useful when looking at electrogenic H^+ or H^+-equivalent transporters. However, the difficulties encountered in the preparation of microelectrodes, experimental cell size limits, and the invasiveness of the technique make fluorescence spectroscopy the best option for most applications ***(14)***. Fluorescent pH-responsive indicators are also more ion selective, thereby reducing background signal observed with microelectrodes as a result of ions other than H^+. Finally, fluorescence allows either a whole population of cells or several individual cells to be studied at the same time by combining cell-imaging techniques with fluorescence spectroscopy.

Table 1
Intracellular pH Indicators and Their Characteristics

Parent fluorophore	Useful pH range	Typical measurement
SNAFL indicators	7.2–8.2	Excitation ratio 490/540 nm or emission ratio 540/640 nm
SNARF indicators	7.0–8.0	Emission ratio 580/640 nm
HPTS (pyranine)	7.0–8.0	Excitation ratio 450/405 nm
BCECF	6.5–7.5	Excitation ratio 490/440 nm
Oregon green dyes	4.2–5.7	Excitation ratio 510/450 nm or excitation ratio 490/440 nm
Rhodols (including NERF dyes)	4.0–6.0	Excitation ratio 514/488 nm or excitation ratio 500/450 nm
LysoSensor probes	3.5–8.0[a]	Excitation ratio 340/380 nm
pH-sensitive GFP mutants	5.1–8.1	Single measurement: excitation 440 nm or 480 nm; emission 480 nm or 535 nm

[a]Several probes of differing pK_a are available.

Several indicator fluorophores are available that span the physiological organellar and cytosolic pH range (*see* **Table 1**). In general, fluorescent indicator dyes are loaded into the cell as an acetoxymethyl ester (AM), which is readily permeable to cell membranes ***(19)***. Esterification with AM groups converts negatively charged, membrane-impermeant acids into neutral, membrane-permeant ester analogs. Once inside the cell, the AM groups are cleaved by ubiquitous intracellular esterases, which release a charged species that cannot exit the cell (*see* **Fig. 1**) ***(19)***. pH indicators can be delivered to specific cellular compartments either by conjugation to targeting molecules or partitioning into more acidic compartments by protonation (e.g., lysosensor probes) ***(20,21)***. Recently pH-sensitive green fluorescent proteins (GFPs) have been developed that allow for precise compartmental targeting via fusion proteins ***(20,22,23)***.

A gradual loss of fluorescence signal may occur during the course of an experiment to measure pH_i. The pH indicator dye may slowly leak out of the cell, be released from lysed cells, or may be bleached by exposure to light during the experiment. Ratiometric indicator dyes allow for correction of the fluorescence signal for these losses. Some pH indicator dyes display a peculiar spectral property when one examines emitted fluorescent light over a range of pH values. The amount of emitted light is the same at all pH values at one

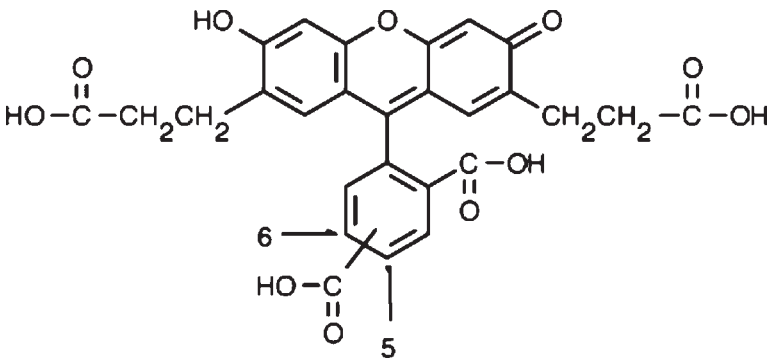

Fig. 1. Molecular structure of the pH-sensitive fluorescent dye, BCECF acid. (Courtesy of Molecular Probes Inc.)

particular excitation wavelength, called the isobestic point. The significance of this pH-independent wavelength is that it can be used to normalize fluorescence data; that is, the dye can be excited at both the pH-sensitive and pH-insensitive wavelengths ***(24,25)***. Dividing the fluorescence signal at the pH-sensitive wavelength by the fluorescence signal at the insensitive wavelength gives a fluorescence ratio that can reduce or eliminate variability as a result of dye loss. BCECF, SNAFL, and SNARF pH indicator dyes all exhibit a spectral isobestic point that is insensitive to pH change.

The pH indicator BCECF is ideally suited to study pH_i because its pK_a of 6.98 allows measurements in the physiological pH 6.0–8.0 range ***(26)***. With four to five negative charges at pH 7–8, BCECF is well retained and not very susceptible to leakage. When excited at 505 nm, the wavelength of peak emission intensity does not change as a function of pH for BCECF. Fluorescence excitation scans at a range of pH values show an isobestic point around 440 nm, which allows this wavelength to be used for ratiometric normalization, as discussed earlier. The maximum pH-sensitive excitation wavelength of 505 nm is well resolved from the pH-insensitive excitation wavelength (440 nm). Typically, intracellular pH measurements are made by determining the ratio of emission intensity, at 535 nm, when BCECF is excited at 440 (pH insensitive) and 505 (pH sensitive) nm (*see* **Fig. 2**).

Changes of pH_i following an acid or alkaline load are a function of both the amount of acid or base added to the cell and the cellular buffering capacity. Buffer capacity is a measure of the ability of a cell to withstand the addition or removal of H^+, without change of pH, in much the same way that buffered solutions resist pH changes. Buffer capacity is the sum of all of the proton

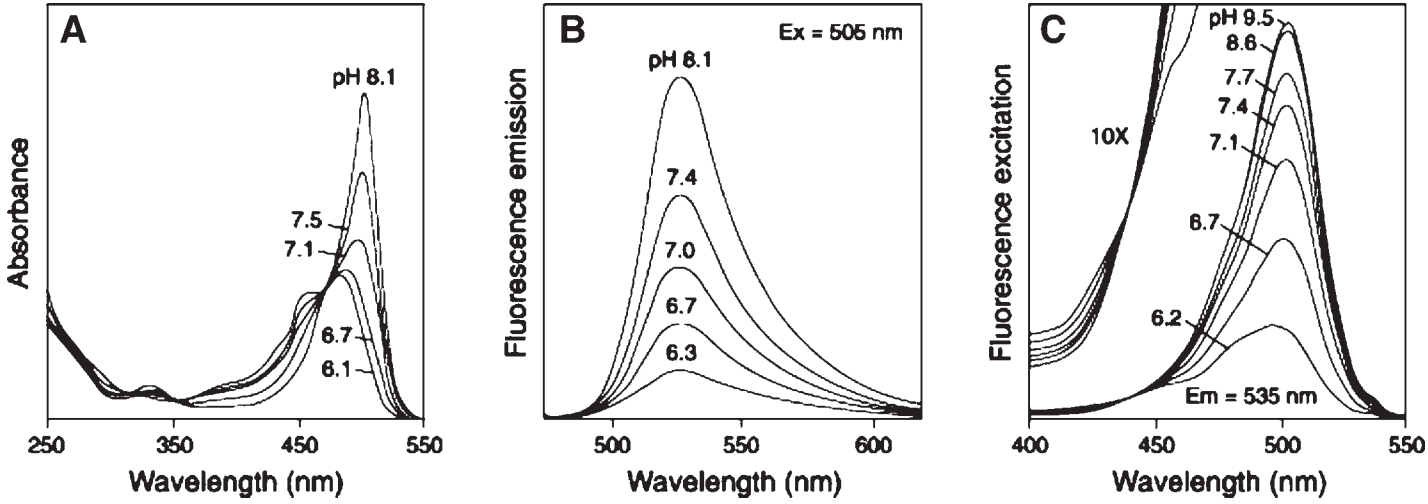

Fig. 2. The pH-dependent spectra of BCECF: **(A)** absorption spectra at a range of pH values; **(B)** emission spectra at a range of pH values; **(C)** excitation spectra at a range of pH values. The excitation spectrum around the isobestic point has been enlarged 10-fold (**C**, left). Ex is excitation wavelength; Em is emission wavelength. (Courtesy of Molecular Probes Inc.)

buffers within a cell and is usually divided into CO_2- and non-CO_2-dependent buffering such that

$$\beta_{total} = \beta_i + \beta CO_2$$

Intrinsic buffer capacity, β_i, is provided by metabolites in acid–base equilibria such as PO_4^{3-} containing molecules and ionizable amino acid side chains *(27)*. βCO_2 depends on PCO_2 and HCO_3^- concentration. Under most in vivo and in vitro experimental conditions, PCO_2 is constant. Thus, βCO_2 depends only on HCO_3^- concentration. For example, in mammalian muscle (pH_i-7.1 and PCO_2 = 37 mm Hg), β_i = 40 m*M* and βCO_2 = 29 m*M* or about 40% of β_{total} *(27)*. Most cells have buffer capacities that are highest below pH 7.0, because of the pK_a's of carbonic acid, amino acid side chains, and phosphate groups. Above pH 7.0, cellular buffer capacities drop off dramatically. Thus, the buffer capacity varies not only with cell type but also with pH. In order to relate changes of pH_i to the amount of acid or base added to a cell, β_{total} must be experimentally determined over the experimental pH range, as described in **Subheading 3.4.**

Measurement of changes of pH_i can report on the transmembrane flux of H^+ equivalents (H^+, HCO_3^-, etc.) because of facilitated transport. Ionic flux is related to the measured pH_i change and the buffer capacity of the cell. The H^+-equivalent flux (J_{H^+}) is related to the buffer capacity by

$$J_{H^+} = \frac{d\text{pH}}{dt}\ \beta_{total}$$

J_{H^+} is the flux of protons in m*M* H^+ per unit time, *d*pH/*dt* is the rate of pH change, and β_{total} is the total buffer capacity.

The following is an overview of the methodology for measurement of pH_i employed by our laboratory (*see* **Subheading 3.3.**). Our system is appropriate for the measurement of pH_i in primary and immortalized cell lines that adhere to glass cover slips. Cells are trypsinized and then plated onto polylysine-coated glass cover slips and allowed to adhere. In the case of transiently transfected cells, transfection is performed after cells are plated. Cells are allowed to grow to a cell density of between 25% and 90% confluency and are then loaded with BCECF–AM dye to facilitate ratiometric pH_i measurement. Cells are transferred to a modified fluorescence cuvet in a fluorometer and perfused with physiological buffer. The perfusion solution can be changed, to achieve acid or alkaline loading or to add pharmacological agents (*see* **Subheadings 3.3.6.** and **3.3.7.**). Some H^+-equivalent transporters can be studied by alternatively adding and removing substrate from the perfusion solution. For example, plasma membrane Cl^-/HCO_3^- anion exchange is studied by switching from Cl^--containing perfusion buffer to Cl^--free buffer, thereby driving HCO_3^- movement coupled to Cl^- movement (*see* **Subheadings 3.3.5.**). BCECF in the

cells is excited at 440 nm and 505 nm and the resulting fluorescence emission at 535 nm is recorded by a photomultiplier.

At the end of each experiment, the fluorescence ratio data are calibrated to reflect pH_i, using the nigericin/high potassium method (*see* **Subheading 3.3.8.**) ***(28)***. Together, the H^+/K^+ ionophore, nigericin, and strongly pH-buffered high-concentration K^+ solutions of known pH values break down the pH gradient across the plasma membrane and equilibrate pH_i with pH_0 (extracellular pH). Measurement of the fluorescence ratio data (i.e., excitation at 505 nm/excitation at 440 nm) at three different pH values for the nigericin solutions allows a standard curve to be plotted, with a linear relationship between fluorescence ratio (*x* axis) and pH (*y* axis). The standard curve, with the form pH = slope × (fluorescence ratio) + *y*-intercept, can be applied to fluorescence data to determine pH_i values that were recorded. In membrane transport experiments, the rate of H^+-equivalent transport is assessed from the initial rate of pH_i change. To determine substrate flux, the cellular buffer capacity (**Subheading 3.4.**) under the experimental conditions must be known.

2. Materials

2.1. Tissue Culture

2.1.1. Cover Slip Preparation

1. #1.5-2 Glass cover slips, 22 × 22 mm (Fisher Scientific).
2. Tungsten-carbide glass scoring rod (or glass-cutting stylus).
3. 5 *M* NaOH.
4. 100% Ethanol.
5. Phosphate-buffered saline (PBS), pH 7.4: 140 m*M* NaCl, 3 m*M* KCl, 6.5 m*M* Na_2HPO_4, and 1.5 m*M* KH_2PO_4, pH 7.5.
6. 1X Polylysine in PBS, pH 7.4. Store aliquots of polylysine as 100X stock (10 mg/mL in water) at –20°C.
7. Sterile PBS, pH 7.4.

2.1.2. Tissue Culture Media and Reagents

1. Cell culture medium (e.g., Dulbecco's Modified Eagle's Medium [DMEM], store in the dark at 4°C).
2. Cell-culture-grade trypsin solution. Store as 10X stock at 4°C.
3. Serum-free medium. Store in the dark at 4°C.
4. Sterile PBS, pH 7.4.
5. Light microscope with 10X and 20X objectives.

2.2. BCECF Loading

BCECF–AM stock solution: 1 m*M* BCECF–AM in dimethyl sulfoxide (DMSO). Aliquots stored in darkness at –20°C are stable for months.

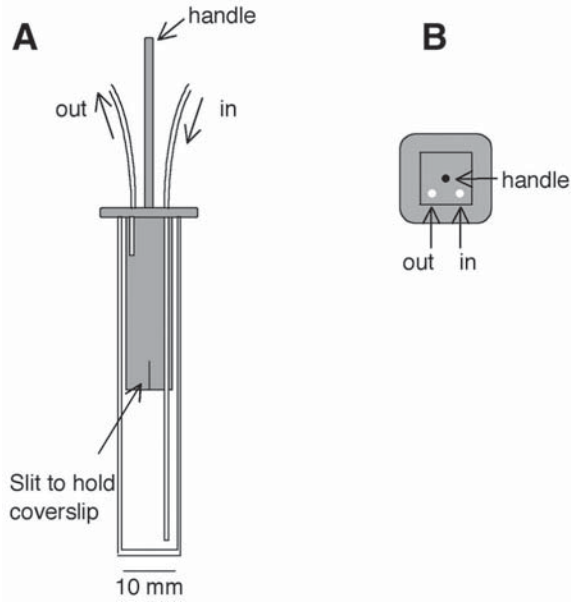

Fig. 3. Schematic diagrams of perfusion cuvet. **(A)** Side view of perfusion cuvet. The inflow line empties into the cuvet near the bottom and is arranged to be distant from the cover slip to reduce turbulence in the light paths. The outflow line draws near the top of the cuvet such that the cover slip is always submerged in perfusion buffer. The cover slip lid slit should be sized to hold the cover slip snugly. Petroleum jelly may be applied to the slit to hold the cover slip in place. **(B)** Top view of cuvet lid.

2.3. Fluorometer Apparatus

2.3.1. Cuvet Design

See **Fig. 3** for construction details and component dimensions.

1. Disposable, plastic fluorometer cuvet, 10 × 10 mm internal dimensions. The height of the cuvet can be adjusted by cutting the cuvet so that the cover slip, attached to the cuvet lid, will be in the middle of the excitation beam path when placed in the fluorometer sample chamber.
2. Tygon microtubing, 0.04–0.06 in. internal diameter.
3. Plexiglas cuvet lid.
4. Petroleum jelly.

2.3.2. Perfusion Pump

1. Peristaltic perfusion pump with at least two lines (inflow and outflow) capable of 3–4 mL/min flow.
2. Waste container to collect perfusion solutions.

2.3.3. Gas System

1. 5% CO_2/95% air gas cylinder.
2. 100% O_2 gas cylinder (for HEPES buffer).
3. Two-stage gas cylinder regulators (appropriate for gas type).
4. 1–5 L/min gas-flow monitor (optional).
5. Tubing (3/8 in. internal diameter) and "T" valves (to divide gas flow among several perfusion solution bottles).
6. Bubble stones (small aquarium type).

2.3.4. Perfusion Solutions

1. Ringer's buffer: 5 m*M* Glucose, 5 m*M* K gluconate, 1 m*M* Ca gluconate, 1 m*M* $MgSO_4$, 10 m*M* HEPES (light sensitive), 140 m*M* transport anions (e.g., NaCl or Na gluconate), and 2.5 m*M* NaH_2PO_4 [add after dilution, to prevent $Ca_3(PO_4)_2$ precipitation], 25 m*M* $NaHCO_3$ (add just before adjusting pH), pH 7.4. Bubble with 95% air/5% CO_2. Solution can be prepared and stored as a 10X stock without transport ions and $NaHCO_3$. pH should be adjusted with HCl or NaOH (or KOH for Na^+-free solutions) just before use.
2. Acid loading solutions: (1) NH_4Cl prepulse technique: Ringer's buffer containing 40 m*M* NH_4Cl. Bubble with 95% air/5% CO_2. (2) HEPES/HCO_3^- prepulse technique: (a) HEPES buffer is Ringer's buffer without $NaHCO_3$. Bubble with 100% O_2 to remove any CO_2. (b) Bicarbonate buffer is Ringer's buffer without HEPES. Bubble with 95% air/5% CO_2.

2.3.5. Fluorometer Hardware and Software

1. Photon Technologies International RCR DeltaScan fluorometer, or equivalent. Fluorometer needs to be able to make dual excitation wavelength measurements either by slewing between wavelengths or with two excitation monochromators and a chopper.
2. FeliX version 1.21 Photon Technology International, or equivalent.

2.4. pH Calibration

1. 10,000X nigericin stock: 10 m*M* nigericin in ethanol. Store separate aliquots at –20°C. During experiment, store on ice.
2. pH Calibration solutions: Ringer's buffer with 140 m*M* KCl substituted for transport ions and made to 30 m*M* HEPES. Store in the dark at room temperature.

3. Methods

3.1. Tissue Culture

3.1.1. Cover Slip Preparation

1. Either by hand or with a graphics program draw a 7 × 11-mm grid to use as a template for cover slip cutting. Tape the template to a table. Place the cover slip on the template and score the surface with tungsten–carbide rod into the grid and

gently break apart into rectangles. Minor imperfections at the edges are acceptable.
2. Place 10–15 cover slips in a 100-mm Petri dish and prepare the cover slips for polylysine coating by sequential washing with 5 *M* NaOH, water, 100% ethanol, and twice with PBS. Perform washes in a Petri dish for 10 min each step.
3. Coat each cover slip with several drops of 1X polylysine solution, leaving a domed droplet on each cover slip.
4. Sterilize overnight in a tissue culture hood, using the overhead ultraviolet (UV) lamps. Place Petri dish lids inside next to the dishes. In the morning, cover slips should look salt-encrusted.
5. In a tissue culture hood, under sterile conditions, wash the cover slips with sterile PBS for 10 min or until salt grains cannot be seen under a light microscope (cells will not be able to grow on salt grains). Rinse with PBS twice before using the cover slips (*see* **Note 1**).

3.1.2. Preparation of Cells

The assay will work for most cell types that can be grown on the polylysine-coated glass surface, including primary and immortalized cell lines, whether transfected or not.

1. Deplate and split apart the cells by trypsinolyis (or the splitting method appropriate for that cell type).
2. Place cover slips in dishes (60-mm dish holds up to 10 cover slips) and plate cells on top. Confluency at the time of assay should be between 25% and 90%. At this density, approx 10^4 cells will be in the beam path of the fluorometer. Stable cell lines can be plated down the night before and transiently transfected cells should be plated and transfected so as to give maximal expression on the day of experimentation (*see* **Note 2**).

3.2. BCECF Loading

This procedure is performed immediately prior to the experiment to measure pH_i. Serum contains esterases that may cleave the acetoxylmethyl-ester (AM) groups on BCECF–AM. Therefore, all steps of the loading procedure should be carried out in serum-free medium.

1. Add 2 mL serum-free culture medium to a 35-mm Petri dish. Add 4 μL of 1 m*M* BCECF–AM and swirl to mix.
2. Remove a cell-covered cover slip from the Petri dish by gently holding the cover slip by one corner with forceps. Pass the cover slip through three sequential 60-mm Petri dishes, containing 8 mL of serum-free media. Then, place the cover slip in the dye-containing dish.
3. Incubate 10–15 min at 37°C and use in pH_i measurement experiment immediately. Also *see* **Notes 3–6** on BCECF loading.

3.3. Fluorometer Assay

3.3.1. Perfusion Preparation

1. Prepare perfusion buffers. Buffers should be stored in foil-covered or opaque flasks, since light-generated breakdown products of HEPES can be cytotoxic (*see* **Note 7**).
2. Perfusion buffers should be bubbled with 5% CO_2 (or 95% O_2 for HEPES buffer acid load method) for at least 15 min prior to experiments to allow an equilibrium to be established (*see* **Note 8**).
3. Monitor perfusion buffer pH constantly during assays and adjust as needed with 1 *M* NaOH (or KOH).
4. Apply a thin layer of petroleum jelly to the underside of the cuvet lid. This will help to hold the cover slip in place.
5. Perfuse the cuvet for at least 5 min with Ringer's buffer before starting a new experiment to ensure that all traces of nigericin have been removed. The perfusion flow rate is usually 3.5 mL/min and should be checked each day. See **Note 9** on leaks and balancing inflow versus outflow rates.

3.3.2. Fluorometer Apparatus Start-Up

1. Ensure that all system components are turned off. Then turn on the lamp power supply and ignite the lamp. A power surge during lamp ignition may damage computer and other electrical components if they are on prior to lamp ignition. The remaining system components may now be turned on (*see* **Note 10** on lamp life).
2. Set up the fluorometer system software so that fluorescence from the pH-sensitive excitation wavelength is divided by fluorescence from the pH-insensitive wavelength. Start fluorometer system software, and under Acquire, select Excitation ratio. Record both excitation and the emission monochromator position settings. Load the appropriate excitation ratio file and acquire new preparation.
3. If your excitation monochromators have slits, ensure that they are set to the same slit width (about 1.5 nm to start).
4. Recalibrate pH meter at the start of each day.

3.3.3. Fluorometer Assay Data Collection

1. Remove coverslip from BCECF–AM solution and insert into cuvet lid holder (*see* **Fig. 3**). Replace the cuvet lid, ensuring that the cells are facing the light source and rotated 45° toward the photomultiplier (*see* **Fig. 4**). Start perfusion with the appropriate buffer.
2. Start fluorescence data collection using fluorometer software. Check absolute fluorescence for pH-sensitive and pH-insensitive wavelengths. Values should be between (4.0–10.0) × 10^5 counts/s and (0.5–2.5) × 10^5 counts/s, respectively. Adjust monocromator slits as necessary. *See* **Note 11** on maximum slit widths.

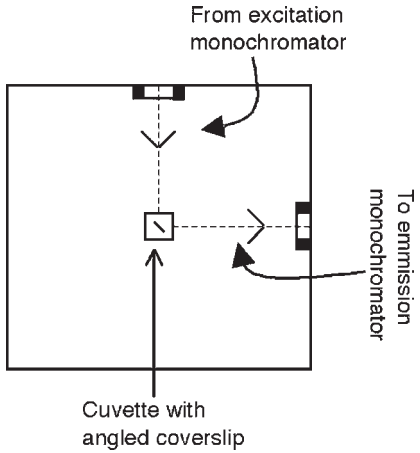

Fig. 4. Schematic diagram of fluorometer sample chamber. The excitation and emission monochromator beam paths are set at right angles to reduce fluorescent noise. The cover slip is rotated 45° to both paths and the angle may be adjusted to increase or decrease the intensity of light received by the photomultiplier.

3. To change perfusion solutions, stop the peristaltic pump and move the intake line to the new flask. Take care not to bump the line so as to avoid introducing bubbles into the line (*see* **Note 12** on bubbles). (Also *see* **Notes 13–16** on other assay considerations.)

3.3.4. Types of Transport Assay

Cells regulate their pH_i using regulatory transport proteins, including the monocarboxylate/H^+ cotransporters (lactate/H^+ cotransporter), Na^+/H^+ exchangers (NHE), Na^+-dependent and independent Cl^-/HCO_3^- exchangers, and Na^+/HCO_3^- cotransporters. Depending on the direction and mechanism of transport being studied, different methods of altering intracellular pH must be employed. For example, Cl^-/HCO_3^- exchange is normally studied by alternately removing or adding Cl^- to establish a Cl^- gradient across the plasma membrane (*see* **Fig. 5A**). The other families of transporters can be studied by loading cells with acid (**Subheadings 3.3.6.** and **3.3.7.**) and monitoring recov-

▶

Fig. 5. Manipulation of cell pH. **(A)** Cl^-/HCO_3^- exchange assay. Cells are equilibrated with Ringer's buffer containing Cl^- (1), then switched to Ringer's buffer without Cl^- (2). This creates an outwardly directed Cl^- gradient. If a Cl^-/HCO_3^- exchanger is expressed in the plasma membrane, then the cell will undergo alkalinization as a result of the uptake of HCO_3^-. Similarly, when the cell is switched back to Ringer's buffer containing Cl^-, the process is reversed and an acid load results. **(B)** Manipulation of cell pH with NH_4Cl. Cells are placed in an NH_4Cl solution. Extracellular NH_3 diffuses passively into the cell (1) and equilibrates with NH_4^+ (2). Extracellular NH_4^+,

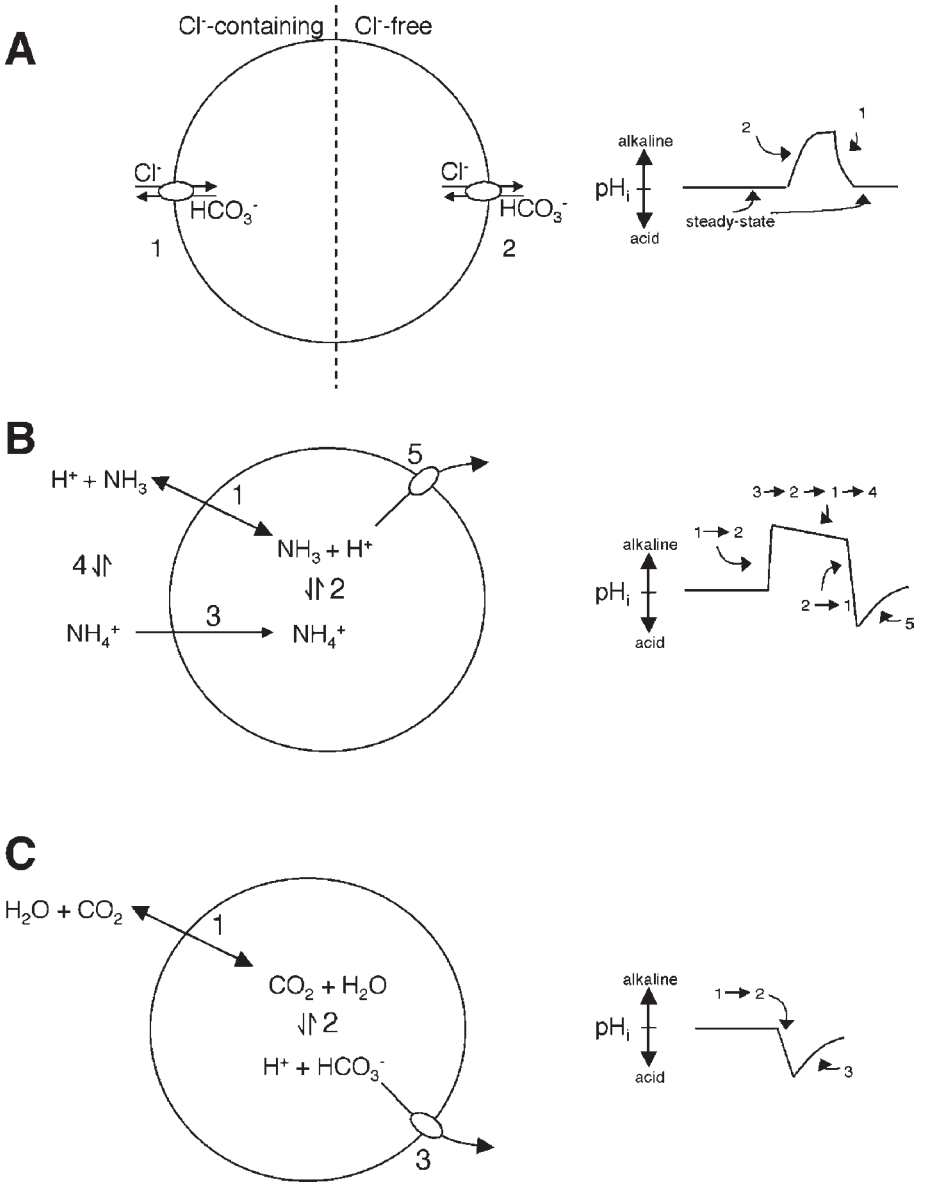

(Fig. 5. *continued*) which is much less permeable, then begins to diffuse into the cell, driving NH_3 plus H^+ out of the cell, thereby effectively setting up a H^+ shuttle (3). When the perfusion solution is switched to Ringer's buffer without NH_4Cl, an acid load results and transport can be assessed as pH recovery (5). **(C)** cell acidification with HEPES/bicarbonate technique. Initially, the cells are made nominally free of CO_2 by perfusion with HEPES buffer bubbled with 95% O_2 to remove dissolved CO_2. The perfusion solution is then switched to CO_2-containing buffer, resulting in an acid load (1 and 2). Transport is then assessed as pH recovery (3).

ery of cell pH. Several techniques are available to acidify the cytosol, including direct microinjection of acid or passing current through microelectrodes. The most common methods are to incubate cells with weak acids or bases. Two acids used in our lab are NH_4Cl and H_2CO_3 (*see* **Fig. 5B**,**5C**). The following methodologies are all employed in our laboratory during studies of pH_i regulatory transporters.

3.3.5. Cl^-/HCO_3^- Exchange Assay

The identification of a Cl^-/HCO_3^- exchanger is based on coupled Cl^-/HCO_3^- exchange. Transport of Cl^- in one direction is coupled to movement of HCO_3^- in the opposite direction across the membrane and concomitant change of pH_i ***(29)***.

1. Perfusion is initiated with Cl^- containing Ringer's buffer until pH_i is stable. Switching to Cl^--free (Na gluconate replaces NaCl) Ringer's buffer stimulates HCO_3^- uptake and alkalosis.
2. After a plateau of fluorescence is reached, the perfusion solution is switched back to Cl^--containing Ringer's, which stimulates HCO_3^- efflux and acidosis.
3. Transport rates are measured by linear regression of the initial rates of change of pH_i.

3.3.6. NH_4Cl Prepulse Technique of Acid Loading

Cytosolic acidification is useful so that the cell's pH recovery mechanisms may be studied ***(30)***. Acidification may be performed by the NH_4Cl prepulse method outlined here or the HEPES/HCO_3^- technique (**Subheading 3.3.7.**).

1. Perfusion is initiated with physiological Ringer's buffer and switched to Ringer's buffer containing 40 m*M* NH_4Cl. Extracellular NH_4^+ is in equilibrium with NH_3, which enters the cell and combines with a H^+ to form NH_4^+, causing the cell to alkalinize (*see* **Fig. 5B**). Eventually, the poorly permeable NH_4^+ will begin to diffuse into the cell, likely driven by the large electrical gradient across the plasma membrane. For each NH_4^+ that enters the cell, an NH_3 then leaves the cell leaving a H^+ behind and causing a slow acidification. In the presence of external NH_4Cl, any NH_4^+ that enters the cell causes a proton to disproportionately accumulate in the cell so that when the extracellular NH_4Cl is removed, the cell will acidify below its starting pH, before NH_4Cl exposure.
2. After 5 min of treatment with NH_4Cl-containing Ringer's buffer, the perfusion solution is switched back to Ringer's buffer. At this point, the intracellular NH_4^+ dissociates into NH_3 plus H^+ and the NH_3 diffuses out of the cell, resulting in an acid load in proportion to the extent of additional NH_4^+ loaded during the incubation. The amount of acid loaded will depend on the permeability of the plasma membrane to NH_4^+, the initial concentration of NH_4^+, and the duration of the prepulse.
3. Following recovery, drugs may be added and a second acid load performed to assay the effect of the drug on the ion transport rate.

3.3.7. HEPES/HCO_3^- Prepulse Technique of Acid Loading

1. Perfusion is initiated with HEPES buffer bubbled with 95% O_2, which drives any CO_2/HCO_3^- from the cells (*see* **Fig. 5C**) ***(31)***.
2. After collecting at least 100 s of fluorescence equilibrium plateau data, switch to bicarbonate buffer. CO_2 will diffuse into the cell, combine with H_2O and establish an equilibrium with HCO_3^- plus H^+, causing the cell to acidify. Proton extrusion by a transporter (e.g., NHE) can then be measured as the rate of pH recovery.
3. Following recovery, drugs may be added and a second acid load performed to assay their effect on transport rate.

3.3.8. pH Calibration

1. Prepare 10 mL of each pH calibration solution per experiment at pH values of approx 6.5, 7.0, and 7.5. The exact pH of each solution should be recorded. Immediately before pH calibration, add nigericin to 10 mL of each pH calibration solution to a final concentration of 1 μM.
2. Turn off the peristaltic pump. Move the inflow line to the calibration solution and turn on the pump. When the calibration solution has all been pumped, stop the pump again and wait for the new fluorescence level to stabilize. Note, some cell lines exhibit a transient alkalosis above the plateau during calibration. Record at least 100 s of stable fluorescence data before switching to the next calibration solution. The general order of calibration is pH 7.5, 6.5, and, finally, 7.0.
3. To calibrate the experiments, plot the calibration solution pH versus the fluorescence ratio value for all three points and perform linear regression on the line. The slope (multiplier) and *y*-intercept (offset) are then used to perform a linear scaling of the fluorescence ratio.

3.4. Determination of Buffer Capacity

Intracellular buffer capacity (β_{total}) is not constant. β_{total} is influenced by pH_i such that a plot of β_{total} versus pH_i appears exponential with little buffer capacity at pH_i greater than 7.2 and progressively higher buffer capacity at pH less than 7.0 ***(32)***. In part, this is seen because the pK_a of most ionizable groups is well below physiological pH values. Because each cell type has a different concentration of buffering components, the buffer capacity of each must be calculated at pH_i values encountered within a given experimental protocol. For example, transiently transfected cells differ in their buffer capacity from untransfected cells. Buffer capacity is determined by adding a known amount of weak acid or base to the experimental system and measuring the change of pH_i observed. The following is a method to determine buffer capacity over the pH 6.5–8.0 range. Note that at acidic pH_i values, it is difficult to measure β_{total} accurately. Thus, during experiments performed at acidic pH_i, care should be taken to ensure that the extent of acid loading in the control and experimental samples is the same. In this way, the β_{total} will be the same for both conditions and H^+-equivalent fluxes can be compared directly.

$[NH_4Cl]_o$ (mM)	Equilibrium pH_i	$[NH_4Cl]_i$ (mM)	$\Delta[NH_4Cl]_i$ (mM)	ΔpH_i	Midpoint pH_i	β_i (mM/pH)
20						
10						
5						
1						
0						

1. Data collection. Prepare Ringer's buffers containing 0, 1, 5, 10, and 20 m*M* NH_4Cl. Mount a cell-covered cover slip in the fluorescence cuvet. Perfused cuvet with Ringer's buffer without NH_4Cl until fluorescence is stable. Sequentially perfuse with Ringer's buffer containing 20, 10, 5, 1, and 0 m*M* NH_4Cl. Perfuse with each solution for enough time to give a fluorescence reading that is stable for 200 s. The perfusion interval should be consistent for each solution. At the end of the experiment, the pH_i should be calibrated by the nigericin high-K^+ method (**Subheading 3.3.4.**). Data should be collected for four to eight cell-covered cover slips.
2. Data analysis. Prepare the table shown above. For each $[NH_4Cl]_0$ determine the equilibrium pH_i value from the average pH_i over the stable fluorescence range (*see* **Fig. 6**). For each equilibrium pH_i value, calculate $[NH_4Cl]_i$ using the equation, $[NH_4Cl]_i = ([NH_4Cl]_0 \times 10^{(9.02 - pH_i)})/(1 + 10^{(9.02 - pH_0)})$. To determine $\Delta[NH_4Cl]$ calculate the difference between sequential NH_4Cl concentration steps (e.g., 20–10 m*M* = 10 m*M*, for the first step). The midpoint pH_i corresponds to the pH_i value halfway between equilibrium pH_i values (*see* **Fig. 6**). The intrinsic buffer capacity (β_i) is calculated from the equation $\beta_i = \Delta[NH_4Cl]_i/\Delta pH_i$. Once the data from the four to eight cell-covered cover slips has been analyzed, calculate the mean and standard error of the midpoint pH_i and buffer capacity for each $\Delta[NH_4Cl]_0$ step. Plot β_i (*y*-axis) against pH_i (*x*-axis). $\beta_{total} = \beta_i + \beta CO_2$ where $\beta CO_2 = 2.3[HCO_3^-]_i$. $[HCO_3^-]_i$ is a function of PCO_2, pH_i, temperature, and the pK_a for CO_2 (6.37). For example, at room temperature, physiological PCO_2 (5%), pH_i 7.4 $[HCO_3]_i$ is 25 m*M* so that βCO_2 equals 57.5 m*M*.

4. Notes

1. Occasionally, variability in polylysine coating is seen because of uneven drying of the solution on cover slips. Some care should be taken to choose cover slips that have an even coating of salt crystals.
2. Cells more than 90% confluent, may be stressed as a result of the accumulation of metabolic waste products and can exhibit unusual transport characteristics.

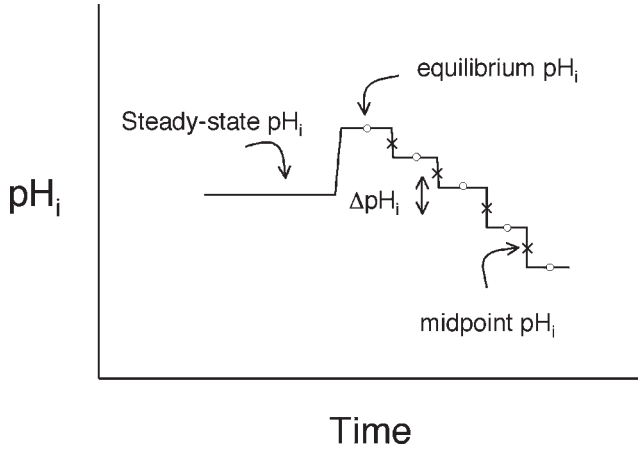

Fig. 6. Determination of cellular buffer capacity. Example data for buffer capacity determination. Cells are perfused with Ringer's buffer until a steady-state pH_i is achieved. Buffer is then changed to Ringer's buffer plus 20 m*M* NH_4Cl and 200 s of steady fluorescence recorded. The equilibrium pH_i is calculated as the average pH_i over the steady interval. The buffer is then changed to the next concentration of NH_4Cl, a new equilibrium pH_i determined, and the midpoint pH_i is identified as the pH_i between two consecutive equilibrium pH_i values. The process is repeated for the remaining NH_4Cl concentration steps and the data analyzed, as in **Subheading 3.4.2.** Circles represent example positions of equilibrium pH_i. × represents the position of midpoint pH_i values.

This effect can be reduced by changing media a few hours before performing transport experiments. Cover slips with too few cells will have a low fluorescence signal, resulting in a decreased signal-to-noise ratio.

3. Preparations of BCECF contain three different molecular species that are all hydrolyzed to BCECF acid by intracellular esterases. A mixture of forms II and III shows better solubility and cell loading characteristics than pure form I. Therefore, commercial preparations are usually of the mixture. Because the forms differ in molecular weight, the effective molecular weight of each lot is reported on the packaging and should be noted for preparing stock solutions.
4. BCECF–AM loading efficiency varies from batch to batch. Therefore, the time of loading and or concentration of BCECF–AM can be varied to achieve effective loading.
5. BCECF–AM is light sensitive and should be stored in a lightproof container when thawed.
6. Hydrolyzed BCECF–AM. Rarely, BCECF–AM can hydrolyze to BCECF acid during storage. If so, cell loading will be inefficient because BCECF is poor mem-

brane permeant. Because BCECF–AM is only weakly fluorescent, cleavage can be assessed by fluorescence before and after exposure to serum or NaOH. If BCECF–AM is hydrolyzed to BCECF, its fluorescence will not rise upon hydrolysis.

7. Rinsing perfusion lines with water or buffer is critical because nigericin contamination can ruin an experiment by causing H^+ leakage. Between experiments, lines should be rinsed with ethanol, water, and then the appropriate experimental buffer. All perfusion tubing should be washed once a week in 10% sodium dodecylsulfate (SDS). Rinse well with water to remove the SDS.
8. Check gas levels before the start of experiments to ensure sufficient supply. All gas components should be checked for leaks by spraying with dilute detergent solution and looking for bubbles, as even small leaks can rapidly consume gas supply. Gas lines for bubble stones should be labeled and not used interchangeably between different buffers. In addition, they should be changed at least once a month.
9. Peristaltic pump failure. The pump should be checked for leaks and the flow rate calibrated at least once a month to ensure constant flow. In the event of pump failure, check the fuse within the unit (have spares available). It is essential that the outflow line pumps slightly faster than the inflow line to ensure that the cuvet does not overflow and buffer leak into the scanning chamber. This can be accomplished by setting the flow rate of both lines to 3.5 mL/min and then relaxing the resistance tensioner slightly on the outflow line.
10. Fluorescence lamp. Fluorometers use a high-intensity light source, which will decline in light output with use. The decline in lamp function can be measured in two ways: (1) As the lamp ages, the voltage across the lamp will rise. If your system provides data on voltage across the lamp, keep a logbook for the fluorometer and record the initial value when the lamp is installed. The lamp manufacturer or fluorometer supplier may be able to tell you the voltage level that represents an aged lamp. (2) The light intensity will drop with time. One way to assess light intensity of the lamp in a reproducible, objective way is to measure the light output in a water Raman assay. Place pure water in a quartz fluorescence cuvet. Use a single excitation wavelength of 350 nm. Perform an emission wavelength scan from 360 to 450 nm. Set the excitation slits to a standard setting (e.g., 5 nm) each time water Raman spectra are collected. Compare the peak light output with a new lamp (in our system this is about 1×10^5 counts/s) to light output from an aged lamp. If the output drops by 30% or more, a new lamp may be needed.
11. Fluorescence signal. The optimal fluorescence level is determined by two factors. First, the amount of fluorescent light measured is determined by a photomultiplier tube (PMT) that counts photons. The PMT will saturate its capacity to count beyond a certain maximum level (check specifications for your system) and can be damaged by a high light level. Second, the amount of light measured must be above a certain level, or the signal-to-noise ratio will be unacceptable. This is determined empirically, as the noise level will be very high at low fluores-

cence levels. Typically, experiments are performed at fluorescence levels that are in the range of 10–100 % of maximum counting level of the PMT. Occasionally the fluorescence signals fall outside of the optimal range. This may be the result of problems with dye loading, cell number, monochromator slit width, or rotation of the cover slip in relation to the excitation or emission monocromator beam path. Several remedies are possible and should be performed in the following order: (1) Adjust excitation and emission monochromator slit width. Most monochromators have a pair of slits for each monochromator. These slits determine the range of wavelengths that the monochromator will allow to pass; that is, slits of 2.0 nm will allow wavelengths of light ± 1 nm of the set wavelength to pass through the monochromator. Wider slits allow more light to pass and a higher fluorescence signal. However, this comes at the cost of potentially collecting light from wavelengths whose fluorescence is pH independent; thus, a slit width of more than 2.5 nm is not recommended. Slits should be adjusted so that pairs are identical. (2) Adjust rotation of cover slip (toward emission monochromator if signal is too high and away if too low). (3) Start a new cover slip with a different cell density or with higher or lower BCECF–AM loading.

12. Bubbles in the fluorescence cuvet. Bubbles can be introduced into the cuvet if the intake line sucks up air (e.g., when a buffer container runs dry or forgetting to turn off the pump while changing buffers). Bubbles in the cuvet cause an extremely noisy fluorescence signal from both the pH-sensitive and pH-insensitive wavelengths. The experiment can usually be salvaged by pausing data collection to allow the bubble to pass through the cuvet; fluorescence signals will likely return to normal.
13. Electrical problems. On rare occasions, changes in electrical demands can cause a small sharp decrease in fluorescence signal at pH-sensitive and pH-insensitive wavelengths. This can be remedied by immediately stopping and restarting data collection. A new trace will begin and the data can be spliced when transferred to a graphing program. Most often, electrical problems arise when turning the peristaltic pump on an off. Try to have fluorometer system components and computer wired on a different circuit then the peripheral electrical components (peristaltic pump).
14. Cover slip falls out of groove in cuvet lid. Start a new assay.
15. Gradual change of pH-insensitive wavelength may indicate photobleaching of the fluorescent dye, dye leakage, or cell death or loss. Photobleaching can be reduced by closing the excitation monochromator slits to reduce light intensities. Dye leakage may indicate a problem with AM hydrolysis, and cell death may indicate a problem with perfusion buffers. Cell loss from the cover slip may occur if solution flow is too turbulent in the cuvet or if cells do not adhere sufficiently strongly to cover slip. Some alternative to polylysine coating may be required.
16. The wavelength calibration of each fluorometer may vary so it is worthwhile to determine the spectral characteristics of pH-sensitive dyes on your system. Using a fixed excitation wavelength (e.g., 505 nm) perform a scan of the emission spectrum (e.g., 510–540 nm). Likewise, once optimal emission wavelength is deter-

mined, use this wavelength to determine optimal excitation wavelength. In experiments, use the wavelengths that provide the highest fluorescence levels. Note that excitation and emission wavelengths must be separated by at least 5 nm to prevent excessive excitation light from spilling over into the emission wavelength, which can damage the PMT.

Acknowledgments

We would like to thank Dr. Bernardo Alvarez and Dr. Deborah Sterling for discussion and critical review of the manuscript and the Academic Press and Molecular Probes, Inc. for permission to reprint figures from previous publications.

References

1. Busa, W. B. and Nuccitelli, R. (1984) Metabolic regulation via intracellular pH. *Am. J. Physiol.* **246,** R409–R438.
2. Ritter, M., Woll, E., Haussinger, D., et al. (1992) Effects of bradykinin on cell volume and intracellular pH in NIH 3T3 fibroblasts expressing the ras oncogene. *FEBS Lett.* **307,** 367–370.
3. Edmonds, B. T., Murray, J., and Condeelis, J. (1995) pH regulation of the F-actin binding properties of Dictyostelium elongation factor 1 alpha. *J. Biol. Chem.* **270,** 15,222–15,230.
4. Nosek, T. M., Fender, K. Y., and Godt, R. E. (1987) It is diprotonated inorganic phosphate that depresses force in skinned skeletal muscle fibers. *Science* **236,** 191–193.
5. Hao, W., Luo, Z., Zheng, L., et al. (1999) AP180 and AP-2 interact directly in a complex that cooperatively assembles clathrin. *J. Biol. Chem.* **274,** 22,785–22,794.
6. Joseph, D., Tirmizi, O., Zhang, X. L., et al. (2002) Polarity of alveolar epithelial cell acid–base permeability. *Am. J. Physiol. (Lung Cell Mol. Physiol.)* **282,** L675–L683.
7. Brokaw, C. J. (1987) Regulation of sperm flagellar motility by calcium and cAMP-dependent phosphorylation. *J. Cell Biochem.* **35,** 175–184.
8. Speake, T. and Elliott, A. C. (1998) Modulation of calcium signals by intracellular pH in isolated rat pancreatic acinar cells. *J. Physiol.* **506 (Pt 2),** 415–430.
9. Li, X., Galli, T., Leu, S., et al. (2001) Na^+–H^+ exchanger 3 (NHE3) is present in lipid rafts in the rabbit ileal brush border: a role for rafts in trafficking and rapid stimulation of NHE3. *J. Physiol.* **537,** 537–552.
10. Yan, W., Nehrke, K., Choi, J., et al. (2001) The Nck-interacting kinase (NIK) phosphorylates the Na^+–H^+ exchanger NHE1 and regulates NHE1 activation by platelet-derived growth factor. *J. Biol. Chem.* **276,** 31,349–31,356.
11. Kaloyianni, M., Bourikas, D., and Koliakos, G. (2001) The effect of insulin on Na^+-H^+ antiport activity of obese and normal subjects erythrocytes. *Cell Physiol. Biochem.* **11,** 253–258.

12. Aharonovitz, O. and Granot, Y. (1996) Stimulation of mitogen-activated protein kinase and Na^+/H^+ exchanger in human platelets. Differential effect of phorbol ester and vasopressin. *J. Biol. Chem.* **271,** 16,494–16,499.
13. Yip, J. W., Ko, W. H., Viberti, G., et al. (1997) Regulation of the epithelial brush border Na^+/H^+ exchanger isoform 3 stably expressed in fibroblasts by fibroblast growth factor and phorbol esters is not through changes in phosphorylation of the exchanger. *J. Biol. Chem.* **272,** 18,473–18,480.
14. Wray, S. (1988) Smooth muscle intracellular pH: measurement, regulation, and function. *Am. J. Physiol.* **254,** C213–C225.
15. Kotyk, A. S. and Slavík, J. (1989) Intracellular pH and its measurement, CRC, Boca Raton, FL.
16. Thomas, R. C. (1981) pH microelectrodes: tips on making the recessed-tip type for intracellular use. *Kroc. Found. Ser.* **15,** 1–6.
17. de Hemptinne, A (1979). A double-barrel pH micro-electrode for intracellular use [proceedings]. *J. Physiol.* **295,** 5P–6P.
18. Kupriyanov, V. V., Xiang, B., Sun, J., et al. (2002) Effects of regional hypoxia and acidosis on Rb^+ uptake and energetics in isolated pig hearts: ^{87}Rb MRI and ^{31}P MR spectroscopic study. *Biochim. Biophys. Acta* **1586,** 57–70.
19. Tsien, R. Y. (1981) A non-disruptive technique for loading calcium buffers and indicators into cells. *Nature* **290,** 527–528.
20. Llopis, J., McCaffery, J. M., Miyawaki, A., et al. (1998) Measurement of cytosolic, mitochondrial, and Golgi pH in single living cells with green fluorescent proteins. *Proc. Natl. Acad. Sci. USA* **95,** 6803–6808.
21. Luby-Phelps, K. (1989) Preparation of fluorescently labeled dextrans and ficolls. *Methods Cell Biol.* **29,** 59–73.
22. Miesenbock, G., De Angelis, D. A., and Rothman, J. E. (1998) Visualizing secretion and synaptic transmission with pH-sensitive green fluorescent proteins. *Nature* **394,** 192–195.
23. Jankowski, A., Kim, J. H., Collins, R. F., et al. (2001). *In situ* measurements of the pH of mammalian peroxisomes using the fluorescent protein pHluorin. *J. Biol. Chem.* **276,** 48,748–48,753.
24. Bright, G. R., Fisher, G. W., Rogowska, J., et al. (1989) Fluorescence ratio imaging microscopy. *Methods Cell Biol.* **30,** 157–192.
25. Silver, R. B. (1998) Ratio imaging: practical considerations for measuring intracellular calcium and pH in living tissue. *Methods Cell Biol.* **56,** 237–251.
26. Paradiso, A. M., Tsien, R. Y., and Machen, T. E. (1984) Na^+–H^+ exchange in gastric glands as measured with a cytoplasmic-trapped, fluorescent pH indicator. *Proc. Natl. Acad. Sci. USA* **81,** 7436–7440.
27. Roos, A. and Boron, W. F. (1981) Intracellular pH. *Physiol. Rev.* **61,** 296–434.
28. Thomas, J. A., Buchsbaum, R. N., Zimniak, A., et al. (1979) Intracellular pH measurements in Ehrlich ascites tumor cells utilizing spectroscopic probes generated *in situ*. *Biochemistry* **18,** 2210–2218.
29. Tang, X. B., Fujinaga, J., Kopito, R., et al. (1998) Topology of the region surrounding Glu681 of human AE1 protein, the erythrocyte anion exchanger. *J. Biol. Chem.* **273,** 22,545–22,553.

30. Burnham, C. E., Amlal, H., Wang, Z., et al. (1997) Cloning and functional expression of a human kidney Na^+:HCO_3^- cotransporter. *J. Biol. Chem.* **272,** 19,111–19,114.
31. Camilion de Hurtado, M. C., Alvarez, B. V., Perez, N. G., et al. (1998) Angiotensin II activates Na^+-independent Cl^-–HCO_3^-exchange in ventricular myocardium. *Circ. Res.* **82,** 473–481.
32. Sterling, D. and Casey, J. R. (1999) Transport activity of AE3 chloride/bicarbonate anion-exchange proteins and their regulation by intracellular pH. *Biochem. J.* **344 (Pt 1),** 221–229.

15

Small-Angle X-Ray Scattering Studies of Membrane Transporter Peripheral Components and Soluble Domains

Brian H. Shilton

1. Introduction

1.1. Structural Analysis of Membrane Transport Systems

Structural data are critical for an understanding of how membrane transport systems function; unfortunately, high-resolution crystal structures for these systems are rare, primarily because of difficulties in crystallization. One alternative approach to the structure problem is to dissect the system into individual components and domains; that is, the integral membrane components of transporters are often multisubunit complexes that interact with soluble, peripheral subunits, or they may contain domains that can be expressed as soluble proteins. Structural information for individual domains and soluble components of the system will help to illuminate the mechanism, and this information can be integrated into models for the structure of the complete system. Small-angle X-ray scattering (SAXS) is a method that can be used to investigate the low-resolution structure and conformational changes of soluble proteins, without the requirement for crystals (for examples, *see* **refs. *1–9***).

1.2. Small-Angle X-Ray Scattering

Small-angle X-ray scattering measurements are, in principle, not more complicated than measuring the ultraviolet absorption of a protein solution. In a SAXS experiment (*see* **Fig. 1**), the protein solution is placed in a cuvet and an X-ray beam is passed through the solution. Molecules in the solution are randomly oriented with respect to the X-ray beam so that the X-ray scattering is radially isotropic; therefore, the scattered radiation is measured solely as a func-

From: *Methods in Molecular Biology, vol. 227: Membrane Transporters: Methods and Protocols*
Edited by: Q. Yan © Humana Press Inc., Totowa, NJ

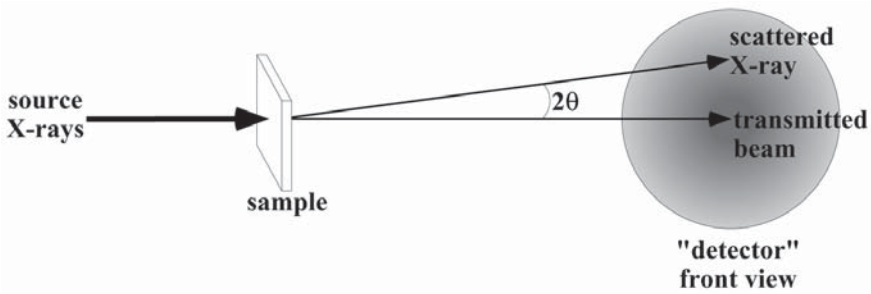

Fig. 1. Measurement of small-angle X-ray scattering. An incident X-ray beam impinges on a sample containing protein at a concentration of approx 5 mg/mL. The scattered X-rays are radially isotropic and, therefore, the scattered radiation is measured simply as a function of the scattering angle, 2θ.

tion of the scattering angle, 2θ. The scattering from the buffer alone must be measured and subtracted from the scattering of the protein solution. After this subtraction, one obtains the scattering curve for the hydrated protein molecule (*see* **Fig. 2B**).

1.3. SAXS: Basic Theory and Capabilities

Before embarking on a SAXS study, it is useful to consider the nature of the information that is obtained. Structural information from SAXS experiments arises from the same physical process—scattering of X-rays by electrons—that yields structural information in crystal diffraction experiments. In a crystal diffraction experiment, the ultimate goal is to use the diffraction intensities and phases to calculate the distribution of electron density within the protein: the information is *vectorial* in nature, because it comprises both magnitude and direction. Thus, from a crystal diffraction experiment, we can derive the position of atoms in the protein relative to a common origin.

The major difference between solution scattering and scattering from crystals is that the scattering particles in SAXS experiments are randomly oriented with respect to the X-ray beam and therefore, all positional information is lost. Nevertheless, embedded in the scattering curve is information that describes the distribution of *scalar* distances between atoms in the protein. This can be most easily understood by consideration of the *distance distribution function*, which is produced from the Fourier transform of the scattering curve.

Fig. 2. (*Opposite page*) Particle shape and its effect on solution scattering. The crystal structure of ligand-bound maltose binding protein ***(10)*** is shown **(A)**, along with its SAXS curve **(B)** and distance distribution function **(C)**. To demonstrate the

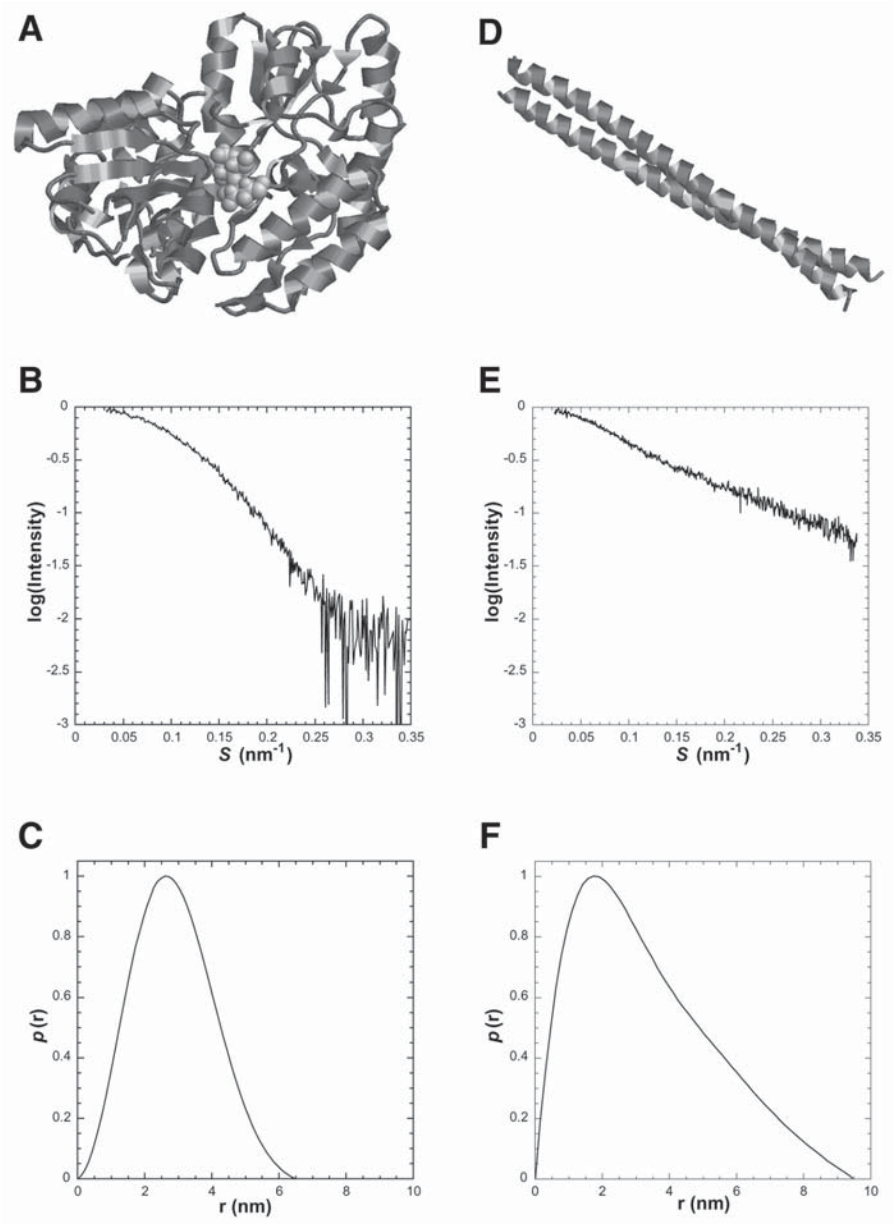

effect of a protein's shape on solution scattering, the model structure for the dimeriza-
(Fig 2. *continued*) tion domain of the *Escherichia coli* ATP synthase *b* subunit ***(2)*** is illustrated **(D)**, along with the experimentally determined SAXS curve **(E)** and derived distance distribution function **(F)**. [**D** and **F** reproduced from **ref. *2*** with permission. Copyright 2002 American Chemical Society.]

The distance distribution function, $p(r)$, can be thought of as a histogram describing the relative frequencies of interatomic distances in the scattering particle. Thus, globular proteins are characterized by a Guassian distance distribution function, whereas extended proteins yield a highly skewed $p(r)$ function (*see* **Fig. 2**).

The information that can be obtained from SAXS experiments includes the radius of gyration, R_g (defined as the root mean square of the distances of all electrons from their common center of mass), the maximal dimension of the particle, r_{max} , and the molecular mass of the scattering particle. These parameters alone offer a description of the overall size, shape, and oligomeric state of the scattering particle. If the presence of ligand or changes in solution conditions, such as pH, are thought to affect the structure of the scattering particles, then structural changes will be reflected by changes in the SAXS profile. Finally, methods have been developed that use solution scattering data for *ab initio* calculation of a molecular envelope. Thus, given that the protein solution is monodisperse, a low-resolution structure for the scattering particle can be derived from SAXS data.

Small-angle X-ray scattering measurements are usually made at a synchrotron radiation source or using a dedicated laboratory system. In either case, the measurements are typically carried out in collaboration with the (expert) operator of these systems. The goal of this chapter is to provide the nonexpert with enough basic knowledge so that he or she is able to design and plan the experiment and then process and interpret the data.

1.4. Terminology

The scattering angle is defined as 2θ. This angle is embedded in the modulus of the scattering vector, S, which is equal to $(2 \sin \theta)/\lambda$, where λ is the wavelength of the incident radiation. If λ is measured in nanometers, the units of S will be nm^{-1}. The "momentum transfer," Q, is defined as $(4 \pi \sin \theta)/\lambda$ and is related to the modulus of the scattering vector by the factor 2π.

The "forward scattering" is the X-ray scattering by the sample that is parallel with the incident X-ray beam; in other words, forward scattering is measured at a 2θ angle of 0°. The intensity of forward scattering, $I(0)$, cannot be measured directly, because it is coincident with the transmitted beam. However, forward scattering can be estimated from the measured scattering curve using a Guinier plot (*see* **Subheading 3.4.1.**) or the indirect transform method (*see* **Subheading 3.4.2.**). For a protein solution, the intensity of the forward scattering is proportional to the protein concentration and the molecular mass of the scattering particle.

2. Materials

2.1. Synchrotron X-Ray Sources

Small-angle X-ray scattering from biological macromolecules can be carried out using conventional X-ray sources (*see*, for example, **ref. 6**). However, synchrotron sources provide a powerful, well-collimated, and finely focused X-ray beam, which allows SAXS to be measured at lower protein concentrations with greater signal-to-noise ratio and fewer required corrections. Beam-time applications can be made at a number of synchrotron sources (*see* **Table 1**). The beamlines have a contact person to whom inquiries can be made regarding the application process.

2.2. Description of SAXS Beamlines

In a typical beamline setup (*see* **Fig. 3A**), the intensity of the X-ray beam is measured before and after the sample. The X-ray intensity can be recorded by ion chambers on either side of the sample, as is the case at EMBL-Hamburg beamline X-33. Alternatively, measurement of incident beam is made using an ion chamber before the sample, and transmitted beam intensity is made from a pin-diode integrated into the beam stop, a system used at the BioCAT beamline at Advanced Photon Source (APS). The sample chamber typically requires 100–150 µL of protein solution and is comprised of either a specialized cuvet or a quartz capillary; in either case, the path length is approx 1 mm. To minimize air scatter, the beam path between the sample and the detector consists of an evacuated tube.

2.2.1. Sample-to-Detector Distance

The sample-to-detector distance, which will be referred to as the "camera setting," determines the angular range that is covered during the recording. For radiation with a wavelength of 1.5 Å, a 3-m camera setting with a 15-cm detector would cover $0 < S < 0.33$ nm^{-1} (*see* **Eq. 1**, **Subheading 3.2.3.**). A shorter camera setting (e.g., 1 m) could be used to collect higher-angle data out to $S = 1$ nm^{-1} at the expense of the lower-angle data.

Changing the camera setting is not a trivial process. The beampath must be disassembled band reassembled, and the detector moved and realigned with the X-ray beam. Depending on the collimation, the X-ray beam may also require refocusing at the new detector position. Therefore, when planning experiments at two different camera settings, low-angle SAXS data from *all* samples should be recorded first using a long camera setting, then the camera may be adjusted to a shorter setting and the higher-angle data measured.

Table 1
SAXS Beamlines at Synchrotron Radiation Facilities

Beamline and location	URL
BioCAT at the Advanced Photon Source (APS), Chicago, IL, USA	www.bio.aps.anl.gov/biocat
Beamline X33 at EMBL-Hamburg, Germany	www.embl-hamburg.de/ExternalInfo/Research/Sax
Beamline 4-2 at Stanford Synchrotron	www-ssrl.slac.stanford.edu/~saxs/
Beamline X12-B at Brookhaven National Laboratory, Stony Brook, NY, USA	www.px.nsls.bnl.gov/x12b_main.html
Stations 2.1, 2.2, 8.2, and 16.1 at Daresbury Laboratory, Manchester, UK	srs.dl.ac.uk/NCD/index.html
Beamline 10C at The Photon Factory, Tsukuba, Japan	pfwww.kek.jp/users_info/users_guide_e/station_spec_e/b l10c.pdf

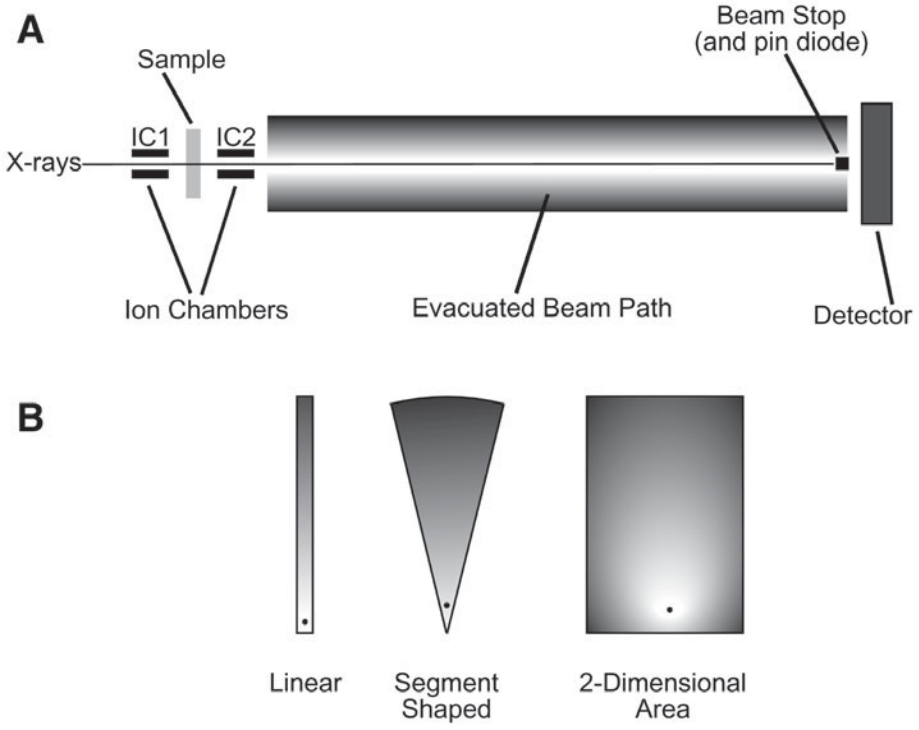

2.2.2. Detectors

Commonly encountered detectors used for SAXS are position-sensitive linear or segment-shaped multiwire detectors (*see* **Fig. 3B**). These systems rely on the ionizing property of X-rays to produce an electric charge that can be quantified and mapped to a specific 2θ angle. Solution scattering is much stronger at lower angles than at higher angles, and the segment-shaped detector is a "one-dimensional" detector optimized to obtain a greater signal at higher angles. Data can also be measured using a two-dimensional area detector, such as the charge-coupled device (CCD) detector at the BioCAT beamline of APS, in which case the image must be radially integrated.

2.3. Standard Protein

A protein standard is required for molecular mass determinations. Cytochrome-*c* (relative molecular mass [M_R] = 12.4 kDa) is used at the APS BioCAT beamline. At EMBL-Hamburg beamline X-33, bovine serum albumin (BSA; M_R = 67 kDa) is used. Other proteins could function as standards, keeping in mind a few important points. The first is that the protein concentration and molecular mass must be accurately known. Second, the protein solution must be absolutely free of aggregates. Finally, the buffer in which the standard protein is dissolved should be similar, in terms of electron density, to the buffer containing the samples. In other words, if the samples are in a high-salt buffer, the protein standard should also be in a high-salt buffer so that the protein–solvent electron density contrast is the same in both cases.

An aggregate-free solution of BSA at a known concentration of approx 6 mg/mL is prepared as follows; note that this solution should be prepared fresh, just prior to making the SAXS measurements. First, make a buffer consisting of 50 m*M* HEPES, pH 7.5, and degas. Resuspend approx 6 mg BSA (Sigma A7906) in 1 mL of the HEPES buffer at 4°C. Centrifuge at 12,000*g* for 15 min at 4°C. Dilute an aliquot of the solution 10-fold and measure the absorbance at 280 nm (where $A_{280,1\%} = 6.14$) to calculate an accurate concentration.

Fig. 3. (*Opposite page*) Beamline components and detector geometries. **(A)** The components in a generic SAXS beamline are illustrated. Ion chambers are located before (IC1) and after (IC2) the sample to measure the intensity of the incident and transmitted beams. The BioCAT beamline at APS also incorporates a pin diode in the beamstop to measure transmitted beam intensity. **(B)** Detector geometries are illustrated with a scattered radiation profile. The black spots represent the shadow cast by the beamstrop. The linear and segment-shaped detectors are one-dimensional, in the sense that they record the scattered radiation solely as a function of distance from the incident beam position. A two-dimensional detector records an image of the scattered radiation that must be radially integrated.

Before measuring X-ray scattering from the sample, add dithioreitol (DTT) from a 1 *M* stock to both the BSA solution and the HEPES buffer to bring the final concentrations to 5 m*M*.

2.4. Software

Programs dedicated for processing and analysis of SAXS data, such as Otoko ***(11)*** and Sapoko ***(12)***, *GNOM* ***(13)***, and Fit2D ***(14–16)***, are described in this chapter. These programs are available free of charge to academic users; the relevant URLs are provided in **Table 2**. Because they come with their own documentation, detailed, command-line descriptions of how to use the programs are not given. Rather, I have provided the relevant command(s) so that the reader is able to navigate his or her way through the software and documentation. SAXS curves typically contain no more than several hundred points so that much of the data processing and manipulation can be carried out using spreadsheet software if desired.

3. Methods

3.1. Preparation of Protein

Apart from the function of the beamline and detector, both of which are largely beyond the user's control, the greatest determinant for a successful SAXS experiment is the quality of the protein. Protein that is pure and absolutely monodisperse will yield clean and interpretable SAXS data. To prepare protein for SAXS experiments, we typically subject it to gel filtration chromatography, concentrate it using ion-exchange chromatography, and then dialyze it; these steps are outlined in more detail in the following subsections.

3.1.1. Requirements and Considerations

Because all of the proteins in a solution will contribute to the scattering of X-rays, it is important that the protein analyzed be pure, as indicated on an overloaded, Coomassie-stained sodium dodecyl sulfate–polyacrylamide gel electrophoresis (SDS–PAGE) gel. Once this level of purity is achieved, it is critical that the protein be free from high-molecular-mass aggregates. SAXS is extremely sensitive to such aggregates, and they are present in most protein preparations. Therefore, to obtain the best results, it is strongly recommended that the purified protein be subjected to gel filtration chromatography prior to SAXS experiments (*see* **Subheading 3.1.2.**).

Approximately 100 µL of sample is required for each SAXS measurement. Because the protein will suffer radiation damage during measurement, the samples are not recovered. When measuring low-angle data using a long camera setting (*see* **Subheading 2.2.1.**), scattering from several protein concentra-

Table 2
Software for SAXS Data Processing and Analysis

Software description	URL
Data processing, analysis, and *ab initio* shape determination (Sapoko, Otoko, *GNOM*, Sasha, Masha)	www.embl-hamburg.de/ExternalInfo/Research/Sax/index.html
Saxs3D (ab initio shape determination) and xlattice (display program)	www.cmpharm.ucsf.edu/~walther/saxs
Dalai_GA (ab initio shape determination)	akilonia.cib.csic.es/DALAI_GA2
Fit2D (processing for two-dimensional detector data)	ccp14.sims.nrc.ca/ccp/web-mirrors/fit2d/computing/scientific/FIT2D/index.html

tions, ranging from 1 to 5–8 mg/mL, should be made, for the reasons discussed in **Subheading 3.4.3.** Ideally, a stock protein solution with a concentration of 5–8 mg/mL is prepared, which can then be diluted at the beamline. For these measurements, the absolute protein concentration must be accurately known so that readings can be normalized with respect to protein concentration (the forward scattering will therefore be proportional to the molecular mass; *see* **Subheading 3.2.4.**). Collection of higher-angle data using short camera settings may require greater protein concentrations—on the order of 20–50 mg/mL—depending on the intensity of the beamline and sensitivity of the detector.

Other components of the protein solution, such as buffer salts, detergents, and so on, will contribute to the scattering. Detergent micelles and vesicles must be avoided, as these particles will scatter very strongly. Salts should be included in the buffer because many proteins will tend to aggregate under low-ionic-strength conditions. However, both ionic and nonionic solutes will likely reduce the electron density contrast between the bulk solution and the protein and thereby decrease the scattering signal from the protein. High concentrations of salts or components such as glycerol should therefore be avoided. Finally, it is advisable to include a reducing agent, such as β-mercaptoethanol or DTT, to ensure that the protein does not form larger complexes via intermolecular disulfide bonds.

3.1.2. Gel Filtration Chromatography

We have used gel filtration through a 2.6 × 65-cm column of Superdex 200 preparative resin (Amersham Biosciences), which will separate all but the largest proteins from aggregates. After gel filtration, the protein will need to be concentrated (*see* **Subheading 3.1.3.**). Alternatively, a smaller gel filtration

column, such as a 1.0 × 30-cm Superdex 200 HR column (Amersham Biosciences) may be used with concentrated protein, approx 15 mg/mL or higher. Collection of the eluted protein into small fractions (200–400 µL) may allow recovery of fractions in which the protein concentration is such that it can be used directly for SAXS measurements.

3.1.3. Concentration of Protein

A typical protein concentration for SAXS experiments is 5 mg/mL, but higher or lower concentrations may be required depending on the beamline and experiment. Concentration by ultrafiltration often results in the formation of aggregates and attendant losses of sample. We have found that concentration using ion-exchange chromatography is far superior to any other method in terms of recovery, ease, and the absence of aggregates.

All operations are conducted at 4°C. The protein should be in a solution of relatively low ionic strength, such that it will bind to an ion-exchange matrix. The ion-exchange columns used for concentration are 1 mL HiTrap Q or HiTrap S (Amersham Biosciences) for anion or cation exchange, respectively. These columns are designed for use with the fast protein liquid chromatography (FPLC) system, but also come with fittings to connect them to Luer-lock syringes or to standard laboratory tubing.

The protein is loaded onto the column with a peristaltic pump, at a rate of 1–2 mL/min. The protein is eluted using a 10-mL syringe to slowly pump a high salt buffer (typically 1 *M* NaCl) through the column. Fractions (approx 250 µL) are manually collected in 1.5-mL microcentrifuge tubes. The protein usually emerges in the third or fourth fraction, in a volume of approx 300 µL. The capacity of these columns is greater than 30 mg; therefore, very high concentrations can be achieved. Approximately 1 µL of each fraction should be assayed for protein concentration using a rapid method such as the Bradford assay ***(17)***. Fractions containing detectable protein are carefully pooled, avoiding the formation of bubbles, using an automatic pipet.

After concentration, the protein must be dialyzed. To minimize handling and sample loss, small-volume dialysis is carried out in a microcentrifuge tube, as shown in **Fig. 4**. A hole is made in the cap of an empty microcentrifuge tube using the heated top of a disposable Pasteur pipet. The tube is then filled (or partially filled) with the solution to be dialyzed. A dialysis membrane is laid across the top of the tube, and the lid is closed to secure the membrane. The microcentrifuge tube is placed in a 50-mL conical culture tube containing a stir bar and filled with dialysis buffer (*see* **Fig. 4**). The conical tube is inverted and placed on a magnetic stir plate, and the solution is left dialyzing for 2 d to reach equilibrium. The system should be inverted occasionally to ensure that the dialysate is adequately mixed. At the end of the dialysis, the microcentrifuge

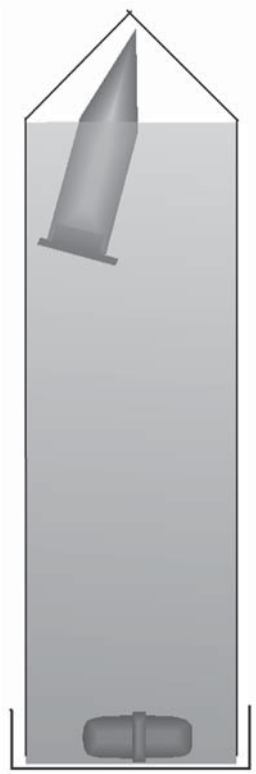

Fig. 4. Small-volume dialysis. A "cut-away" view of a system to dialyze small volumes with high recovery. A microcentrifuge tube with a hole in the top, sealed with a dialysis membrane, contains the sample to be dialyzed (200–1300 μL) and is inverted inside a 50-mL culture tube so that the dialysis membrane remains in contact with the dialysis buffer. A small stir bar is included for mixing the dialysis buffer.

tube is removed, the dialysate spun down, and the modified cap and dialysis tubing replaced with an intact microcentrifuge tube cap. The dialysis buffer must be retained for SAXS measurements.

3.2. Data Collection

For users unfamiliar with SAXS, assistance in data collection and processing will be provided at the beamline. However, it is useful to know what measurements are required to ensure that all the necessary data have been collected before ending experiments or changing the camera settings. An overall outline of data collection, processing, and analysis is presented in **Fig. 5**.

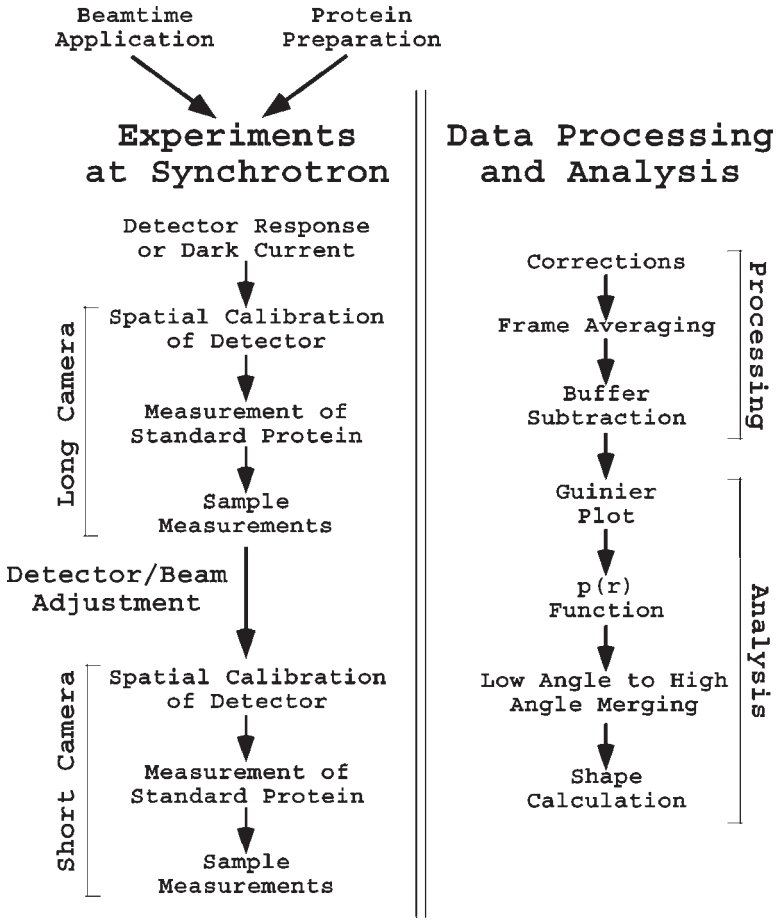

Fig. 5. Flowchart for data collection and processing. The steps involved in a SAXS study are illustrated. The required experiments in the left-hand column are described in detail in **Subheading 3.2.**, whereas data processing and analysis, in the right-hand column, is described in **Subheadings 3.3.** and **3.4.**, respectively.

3.2.1. Data Collection Strategy

The sample-to-detector distance determines the angular range of the data that are collected (*see* **Subheading 2.2.1.**). Given the difficulty in adjusting the sample-to-detector distance and the limited time available at the beamline, it is imperative that all measurements are completed at the long camera setting before moving to a shorter camera (*see* **Fig. 5**).

3.2.2. Detector Response and Dark Current

Linear and segment-shaped position-sensitive detectors do not display a uniform response to radiation; therefore, SAXS curves must be corrected for "detector response." To measure the detector response, the detector is flooded with a uniform field of radiation, typically from an ^{55}Fe source. The resulting detector response curve is used to divide SAXS data collected for samples (*see* **Subheading 3.3.2.**).

The pixels in CCD detectors respond uniformly to X-rays; however, the pixels accumulate charge over time in the absence of radiation—this is called the "dark current." Therefore, for a given exposure time, the dark current of the detector must be measured so that it can be subtracted from the sample data (*see* **Subheading 3.3.3.**). This is done by recording an image with the X-ray shutter closed. It is important to remember that any change in the data collection time requires a new dark current image.

3.2.3. Spatial Calibration

Each position on the detector must be associated with a value for the scattering vector, *S*. This is easily accomplished for a two-dimensional detector system because the exact position where the incident beam strikes the detector is relatively easy to locate. Crystals of silver behanate are placed in the X-ray beam, and exposure produces a series of concentric circles (*see* **Fig. 6A**). From the image and using the program Fit2D ***(14–16)***, the center of the circles and, hence, the position of the incident beam on the detector are located (*see* **Subheading 3.3.3.**). To assign *S* values to given positions on the detector, the sample-to-detector distance must be known; the *S* value for any position on the detector can then be calculated using the formula

$$S = \frac{2 \sin \left[\frac{1}{2} \tan^{-1} (y/x) \right]}{\lambda}, \quad (1)$$

where *x* is the sample-to-detector distance and *y* is the distance from the position of the incident beam to the relevant point on the detector. In practice, the program Fit2D carries out this calculation when it integrates the image.

For position-sensitive one-dimensional detectors, a sample that diffracts with a well-characterized *d*-spacing is measured and used to find the beam center and spatially calibrate the detector. First, diffraction from collagen, for example, is recorded and the baseline is adjusted in Otoko ***(11)*** using the command ".bpk" to yield the pattern in **Fig. 6B**; at this point, there are 512 channels, each corresponding to a different position on the detector. The collagen diffraction peaks of order 2–12 are recorded: the first -order peak is obscured by the beamstop, and the zero-order peak is coincident with the transmitted beam. Note that the strongest peaks correspond to the second, sixth, and ninth

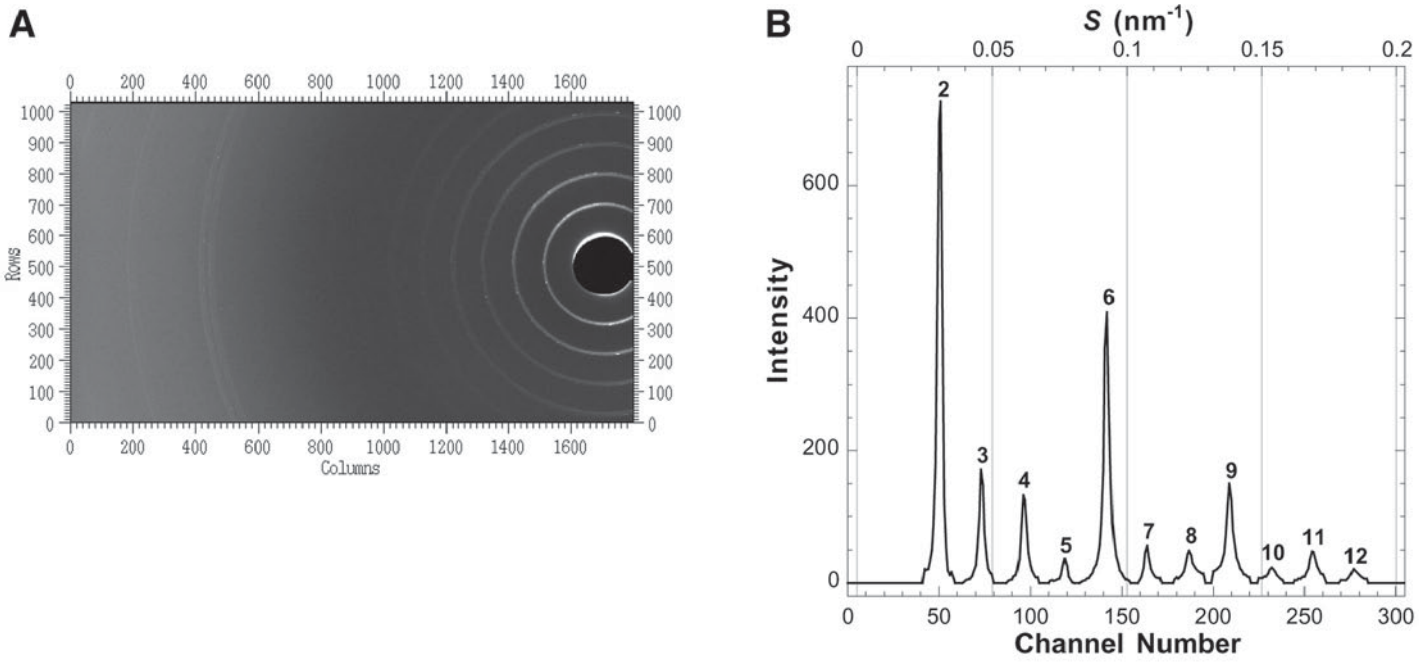

Fig. 6. Spatial calibration of detector. **(A)** Spatial calibration of a two-dimensional detector is carried out by measuring the powder diffraction from silver behanate crystals; the rings produced facilitate the location of the transmitted beam, which is obscured by the beamstop. This image was recorded using a sample-to-detector distance of 25.5 cm; a longer 2.5-m camera would record only the innermost ring. **(B)** A one-dimensional detector is calibrated using a collagen diffraction pattern (in this case, dry turkey tendon collagen with a *d*-spacing (repeat distance in a periodic structure) of 65 nm and recorded using a sample-detector distance of 3 m). The background scatter has been removed using Otoko ***(11)*** as described in the text. The peak order is indicated by the numbers above each peak. Note that the first-order diffraction peak is hidden behind the shadow of the beamstop.

orders. The position of each peak on the detector is located using the baseline-adjusted pattern with the command ".cur" in Otoko. At this point, Otoko can be used to construct an *S* axis by issuing the command ".xax" and then entering the peak order, detector position (i.e., channel number), and *d*-spacing of the sample (65 nm for the collagen used at beamline X33 at EMBL-Hamburg). Note that there is also an excellent description of this process on the EMBL-Hamburg website (www.embl-hamburg.de/ExternalInfo/Research/Sax/s_axis.html)

3.2.4. Measurement of Standard Protein

The intensity of "forward scattering", or $I(0)$, is directly proportional to both the concentration and molecular mass of the protein. To relate $I(0)$ of a sample to its molecular mass, the signal from the detector must be put on an absolute scale using a well-characterized standard, such as BSA (*see* **Subheading 2.3.**; M_R = 67 kDa, R_g = 2.9 nm, and r_{max} = 8.5 nm [r_{max} = maximal dimension of scattering particle]). Scattering from a known concentration of BSA (or another suitable standard) should be measured, preferably before beginning sample measurements. The R_g and r_{max} for the standard should agree with theoretical values, indicating that the protein is monodisperse and the detector properly calibrated. The derived $I(0)$ value can then be used to estimate the solution molecular mass of scattering particles in the samples, provided the protein concentrations of the samples are known.

3.2.5. Protein SAXS Measurements

X-ray scattering from a protein solution is the sum of scattering from the buffer and from the protein; therefore, to obtain the scattering for the protein alone, a measurement of the buffer alone must be subtracted from that of the protein solution. Solutes will affect scattering from the buffer and therefore the buffer and the protein solution must be matched. The best way to achieve this is to dialyze the protein and save the dialysis buffer for SAXS measurements.

Measurement of the protein solution should be bracketed by buffer measurements. The buffer measurements can be inspected for consistency by dividing one by the other: If the divided curve shows systematic deviations from 1, it means that something has compromised the measurements. Possibilities are a failed ion chamber (IC) reading, an improperly cleaned sample cell, the presence of bubbles in the beam path, or a difference in the position of the sample cell. Because the sample was recorded *between* the buffer measurements, the sample measurement becomes suspect and should be repeated.

Proteins are subject to degradation by X-rays, a problem that becomes more serious as the beam intensity is increased. To address the possibility of sample degradation, SAXS data are usually recorded as multiple "frames," which

are then averaged. For example, a 15-min recording will be made as 15, 1-min recordings; decay of the sample during measurement will cause changes in the scattering curves. The individual curves are inspected during data processing and those that show no significant differences are averaged to improve the signal-to-noise ratio.

3.3. Data Processing

The "raw" data for SAXS collected on one-dimensional and two-dimensional detectors is illustrated in **Fig. 7**. The steps required to yield a scattering curve for the hydrated protein, such as those shown in **Fig. 2B**,**E**, are described next.

3.3.1. Correction for Beam Intensity and Sample Absorption

Synchrotron beams vary in intensity and this will affect the magnitude of the scattering. During data collection, the signal from an ion chamber *before* the sample (*see* **Fig. 3A**) is monitored and integrated to obtain a measure of the incident beam intensity during the scattering experiment.

X-rays will be absorbed by the sample and buffer. In other words, the incident beam is attenuated as it passes through the sample, and this will have an effect on the intensity of the scattered X-rays. The relative absorption of samples can be assessed from the ratio of readings from IC1 and IC2 (or the pin diode in lieu of IC2; *see* **Fig. 3A**). In practice, differences in absorption from dilute protein solutions are insignificant; therefore, readings from IC2 are not required for data processing.

3.3.2. One-Dimensional Data Processing

For one-dimensional data, the program Sapoko ***(12)*** can be used in a batch mode to carry out all of the required processing, outputting the final, averaged scattering curves (*see* **Fig. 7A**,**B**). In practice, this data processing can be done using Sapoko in a "black-box" mode at the beamline with the help of beamline personnel. The following is a description of the steps that are carried out by Sapoko during data processing.

During a scattering experiment, one-dimensional position-sensitive counting detectors measure, in real time, the number of X-ray photons impinging at defined positions on the detector, represented by "channels." This signal is integrated for a user-defined time interval, typically 1 min. Thus, the "raw data" consists of channels—usually 512—each of which has an associated magnitude (**Fig. 7A**). A 10-min exposure is typically recorded as 10 individual 1-min "frames" (*see* **Subheading 3.2.5.**), which are averaged during data processing. Sapoko will carry out this frame averaging, automatically rejecting outlying measurements based on user-defined criteria. A very important point here is that Sapoko overwrites the original file with the averaged and corrected file: it

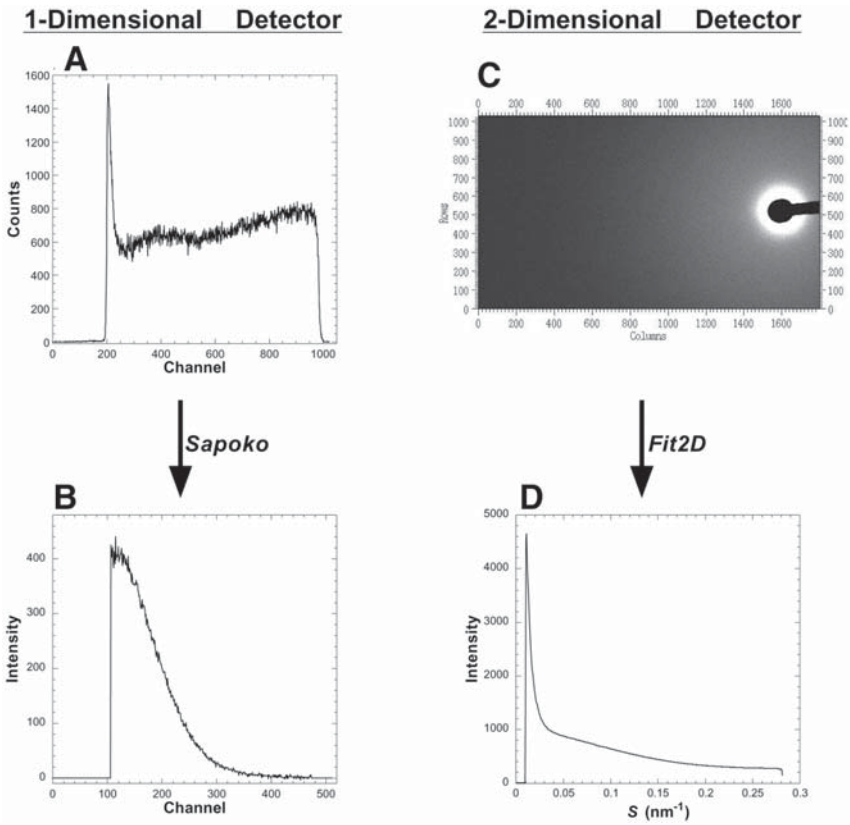

Fig. 7. Processing of one-dimensional and two-dimensional detector data. **(A)** The "raw" signal from a one-dimensional Quadrant detector is illustrated. The program Sapoko ***(12)*** is used to correct for detector response, normalize with respect to ion chamber readings and protein concentration, and subtract buffer scattering, to yield the curve of intensity versus position (channel), illustrated in **(B)**. Channels are assigned a scattering vector value, as outlined in **Subheading 3.2.3. (C)** A two-dimensional SAXS image is illustrated; note that the "keyhole" shape on the right side of the image is the shadow from the beamstop. Given the coordinates of the direct beam and the sample-to-detector distance, the program Fit2D ***(14–16)*** will integrate the pixel intensities to produce the curve in **(D)**. Because the image in **(C)** is of the protein solution, the curve in **(D)** represents SAXS from both the buffer and protein; a separate curve for buffer alone remains to be subtracted.

is therefore essential that the raw data be copied into a separate "working" directory for data processing to ensure that the original dataset is preserved.

After averaging, the data are divided by the detector response curve (*see* **Subheading 3.2.2.**). Normalization for beam intensity is accomplished by

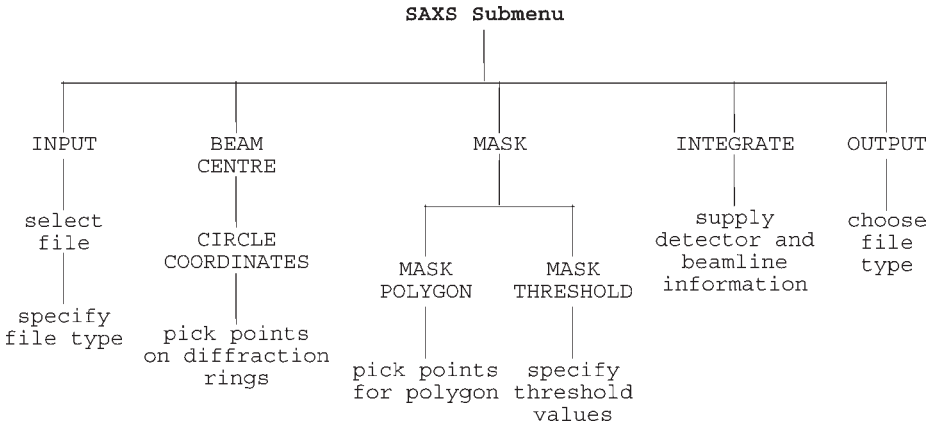

Fig. 8. Data processing with Fit2D. Command sequences commonly used for SAXS two-dimensional image data processing are illustrated. From the Fit2D main menu, the SAXS submenu is chosen, from which "point-and-click" commands and subcommands are written in uppercase.

dividing the entire curve by the integrated reading from IC1. In addition to this basic data reduction, Sapoko will also subtract the background (buffer) scattering curve from the relevant protein scattering curve and divide the protein curves by protein concentration to normalize them so that forward-scattering values are proportional to the molecular mass of the scattering species.

3.3.3. Two-Dimensional Data Processing

Two-dimensional images may require correction prior to data processing, depending on the detector type. For instance, CCD detector images require subtraction of the "dark current" image; this is usually done automatically when data are dumped from the detector at the end of the exposure, resulting in two image files: the original "raw" image and the image with dark current subtracted.

Fit2D ***(14–16)*** can be used to reduce a two-dimensional image to a one-dimensional scattering curve (**Fig. 7C**,**D**). The relevant Fit2D command sequences are illustrated in **Fig. 8**. The image is input into Fit2D and displayed; note that the program recognizes some detector types, but for custom detectors, Fit2D must be supplied with information such as the number of pixels, pixel size, and file structure. Regions of the detector that are not to be used in the integration—primarily the shadow cast by the beamstop—must be specified by creating a "mask." This can be done manually by drawing a polygon around the relevant regions. A faster procedure is to create the mask by specifying that it covers any regions with pixel values below a certain threshold. To carry out the integration, Fit2D requires the coordinates of the incident beam

(*see* **Subheading 3.2.3.**) and the sample-to-detector distance so that integrated intensities can be assigned the correct scattering vector values. After integration, the curve is displayed and the intensities and associated scattering vector values can be saved in a variety of file types.

Additional processing of the data is required: correction for beamline intensity, averaging of images, and buffer subtraction. These relatively simple operations can be carried out using Fit2D or spreadsheet software.

3.4. Data Interpretation and Analysis

3.4.1. Guinier Plot

The Guinier plot is used to calculate the radius of gyration, R_g , and the intensity of forward scattering, $I(0)$. At low angles, the scattering intensity can be approximated using

$$I(S) \cong I(0) \exp\left(-\frac{4\pi^2}{3} S^2 R_g^2\right) \quad (2)$$

Therefore, a plot of $\ln[I(S)]$ versus S^2 should be linear in the low-angle region, with an intercept of $I(0)$ and a slope equal to $-4\pi^2 R_g^2/3$ ***(18)***. Examples of Guinier plots are illustrated in **Fig. 9**. The data in **Fig. 9** have been normalized for protein concentration so that $I(0)$ values are proportional to the molecular mass of the proteins. For monodisperse systems of noninteracting particles, the slopes of Guinier curves should be independent of protein concentration.

Note that only the low-angle region of the Guinier plot approaches a straight line. In fact, an empirical decision must be made as to what part of the plot to use for calculation of the slope and intercept. The first few data points, being very close to the shadow of the beamstop, are often unreliable, and at higher angles, the plot is no longer linear. A stringent rule for delimiting the linear Guinier region is that $2\pi SR_g < 1$ ***(18)***, but, in practice, the linear region often extends up to (or beyond) $2\pi SR_g = 1.3$ ***(19,20)***; in the case of the proteins in **Fig. 9**, data were used up to $2\pi SR_g = 2.0$ to fit the Guinier curve, and the linear region extends even further.

3.4.2. Distance Distribution Function

As described in **Subheading 1.3.**, the distance distribution function, $p(r)$, is calculated from the Fourier transform of the scattering curve, which requires data from $S = 0$ nm^{-1} outward. In practice, a complete scattering curve cannot be obtained because of limitations imposed by the incident beam and beamstop; therefore, missing data between $S = 0$ nm^{-1} and the lowest angle measured must be extrapolated from the measured data. This could be accomplished using the Guinier curve; however, the "indirect transform" method ***(21)***, implemented in the program *GNOM* ***(22,23)***, is less sensitive to statistical and systematic

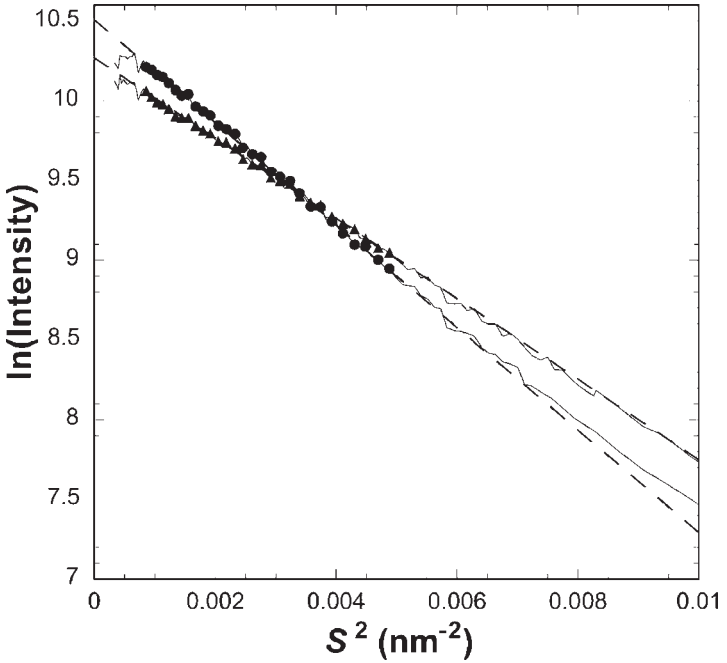

Fig. 9. Guinier plot. Guinier plots from two proteins are illustrated. In both cases, the complete scattering data are represented by solid lines, and points used for calculation of the Guinier curves are indicated by circles (for the 257-kDa protein, R_g = 4.8) or triangles (for the 202-kDa protein, R_g = 4.2). The calculated Guinier curves are indicated by dashed lines. (Reproduced from **ref. *3*** with permission from the publisher.)

errors and makes calculation of the distance distribution function straightforward. The user supplies *GNOM* with a ASCII data file containing scattering vector values and their associated intensities, as outlined in the *GNOM* instructions. The user must supply the program with an estimate of the maximal dimension of the scattering particles, $r_{\max}$, and from this, *GNOM* calculates a $p(r)$ function.

3.4.3. Aggregation, Interparticle Interference, and Self-Association

Large particles will produce very strong scattering at low angles and will therefore have an adverse effect on the most important region of a SAXS curve. Large aggregates, which are often present in protein preparations, will produce misleading results. Fortunately, such aggregates are relatively easy to identify because of their effects on the scattering data. To illustrate these effects, Guinier plots and distance distribution functions of two preparations of the

same protein are compared (*see* **Fig. 10**); one of preparations is monodisperse and the second contains large-molecular-mass aggregates. A Guinier plot with an upward inflection at low angles indicates that a preparation is not monodisperse (compare **Fig. 10A**,**C**). Aggregated protein also has effects on the distance distribution function, $p(r)$. When $p(r)$ is calculated using the program *GNOM (13)*, the user must provide an estimate of r_{max}. The protein used for **Fig. 10** has an r_{max} of 12.5 nm, and it can be seen in **Fig. 10B** that for the monodisperse preparation, the calculated $p(r)$ is independent of the estimate provided to *GNOM*: $p(r)$ always crosses the abscissa at 12.5 nm, even if an estimate of 20 nm is provided to *GNOM*. On the other hand, a protein preparation containing aggregates will yield $p(r)$ functions that are strongly dependent on the value of r_{max} provided to *GNOM* (*see* **Fig. 10D**).

Interparticle interference occurs at high protein concentrations and leads to lower intensities at very low angles and a downward inflection of the Guinier curve (not illustrated). Although the effect is always present to some degree (because the limiting case requires the protein to be present at infinite dilution), interparticle interference typically becomes a concern only when the protein concentration reaches approx 8 mg/mL and above.

Because many protein preparations contain aggregates, and proteins may self-associate to form oligomers, it is essential to collect data for an uncharacterized protein at several different concentrations (e.g., 2, 4, 6, and 8 mg/mL). The forward scattering $I(0)$ should be directly proportional to the protein concentration, and the calculated R_g should be independent of protein concentration. $I(0)$ values that are not directly proportional to protein concentration, along with concentration-dependent changes in R_g, indicate a self-associating system.

3.4.4. Merging of Low- and High-Angle Data

Low-angle data, collected using a long camera setting, are required for Guinier analysis and for calculation of the distance distribution function and are important for describing the overall shape of the scattering particle. Data collected at a short camera setting provide information about the internal structure of the protein. Scattering data from two or more camera settings can be merged to yield a single curve for use in *ab initio* shape calculation (*see* **Subheading 3.4.5.**), to assess structural changes brought about by ligand binding, or to compare the scattering with a structural model using the program Crysol *(24)*.

Merging two SAXS curves together is a matter of multiplying all data in one curve by a constant so that the two curves contain a region of overlap, and then editing the data to remove redundant higher-angle data from the long camera setting and lower-angle data from the short camera setting. This can be done

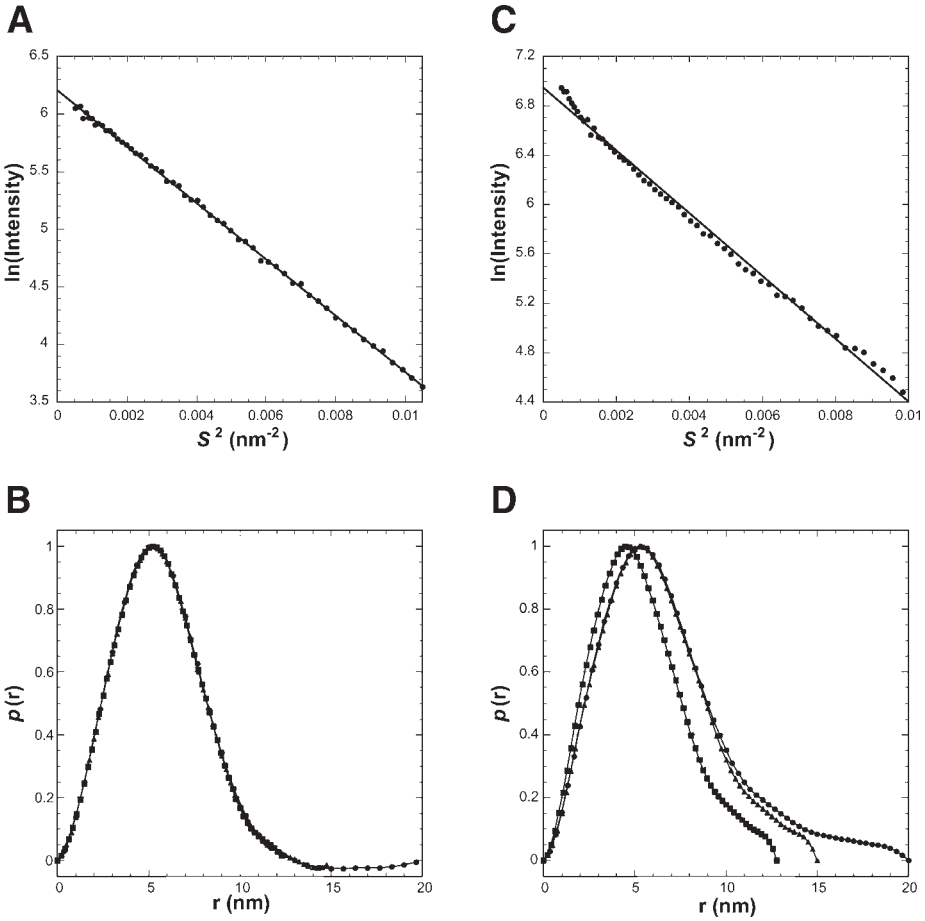

Fig. 10. SAXS data appraisal. X-ray solution scattering from a monodisperse protein preparation **(A**,**B)** is compared to the same protein but from a different preparation that contained high-molecular-mass aggregates **(C**,**D)**. In **(A)** and **(C)**, Guinier plots of the data are illustrated along with least-squares linear fits (*solid lines*). In **(B)** and **(D)**, the program *GNOM (13)* was used to calculate the distance distribution functions from the same SAXS data used in **(A)** and **(C)**. The program *GNOM* must be provided with an estimate of the maximal dimension, r_{max} , and for **(B)** and **(D)**, three different values were used: 20.0 nm (*circles*), 15.0 nm (*triangles*), and 12.5 nm (*squares*).

using a spreadsheet. Alternatively, the program *GNOM (13)* can be used to merge two curves together (*see* **Fig. 11**). The program will also calculate a regularized curve that extends to a scattering vector value of 0 nm^{-1} , which may be required for some shape determination programs.

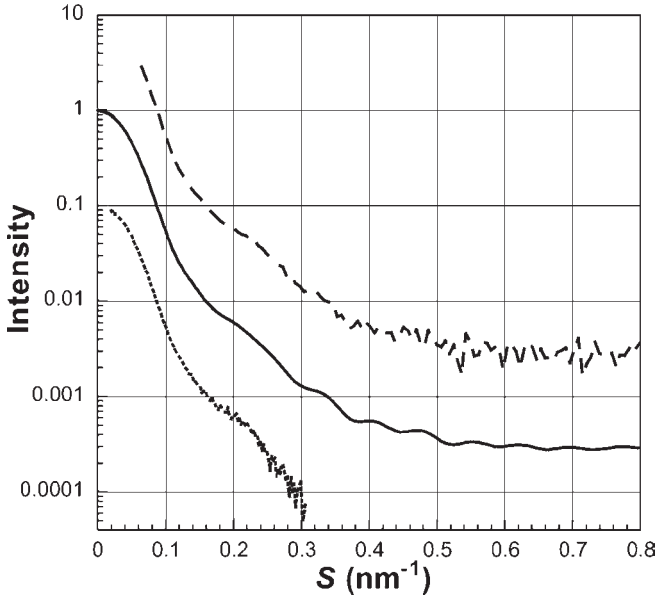

Fig. 11. Merging data from two camera settings. Data were collected at two different camera settings: a 3-m sample to detector distance [short dashes, normalized to an $I(0)$ of 0.1] to measure the low-angle region and a 1-m sample to detector distance [long dashes, normalized to an $I(0)$ of 10] to measure the high-angle region. The program *GNOM* ***(13)*** was used to merge the data and produce a regularized curve spanning the entire region, including the extreme low-angle data that are obscured by the beamstop (solid curve).

3.4.5. Shape Calculation

The high quality of SAXS data collected from synchrotron sources, combined with advances in computational capabilities, have facilitated the *ab initio* determination of a scattering particle's shape. The process can be described as follows: a shape is calculated and the degree to which it agrees with the experimental SAXS data is assessed; the shape is then changed to improve agreement with the SAXS data; and the process is repeated until the agreement between the shape and the SAXS data cannot be improved. There are a number of computational approaches, but they are all subject to the same fundamental problem: the shape that is determined may not represent a unique solution. In other words, for any given SAXS curve, there could be a number of different structures that match the experimental data and there is no way of knowing which one is correct. The problem can be restated as a situation in which there are potentially thousands of parameters (the position of each protein atom), but

far fewer data points. This problem is overcome in two ways: the number of parameters is limited, and constraints, such as smoothness, are imposed on the calculated shape. It appears that reproducible low-resolution protein structures can be determined from SAXS data. The following paragraphs describe the shape determination process as it is implemented in several software packages. Detailed instructions on how to use the individual programs are beyond the scope of this chapter, but they are provided with the software.

There are two approaches being used for shape determination from SAXS data. In the first ***(25)***, which is implemented in the program Sasha ***(26)***, the molecular envelope (the boundary between the relatively high electron density of the protein and the lower electron density of the solvent) is described using a mathematical function. The function contains a number of parameters, typically 10–15, as well as information on the probable symmetry of the structure. A starting envelope is used—often a simple sphere—and then the parameters are refined so that the theoretical "shape scattering" matches the experimental data. This method has the advantage that the number of parameters is small, and, therefore, the solution is more likely to be unique ***(26)***. The weakness of this method is that the mathematical function may not be capable of describing certain irregular shapes, and it may be difficult to arrive at a solution that adequately fits the experimental data.

In the second approach, the shape is determined using models constructed from "dummy atoms" (spheres of electron density) with a single defined radius and fixed positions ***(27–30)***. As their name suggests, these dummy atoms are not meant to represent the real protein atoms that exist in the structure; instead, they simply provide a "scaffold" on which to build the protein's shape. The number of parameters is limited by fixing the atomic positions of the dummy atoms; that is, they are constrained to positions corresponding to a densely packed array, and only their occupancies are refined. The parameters can be further limited by increasing the size of the dummy atoms, hence decreasing the number of atoms used to model the scattering particle. In addition, there are constraints in the algorithms, either explicit or implicit, that select against isolated dummy atoms and very irregular or rough surfaces. A variation on these bead methods has been developed and implemented in the program Gasbor ***(31)***, in which the position of "dummy residues" is refined.

Acknowledgements

The author thanks Michel Koch for his assistance and discussions at beamline X-33. Michel Koch, Tom Irving, Stan Dunn, Eric Ball, and Paul Del Rizzo are gratefully acknowledged for reading this manuscript and providing comments and corrections. Use of the Advanced Photon Source is supported by the US Department of Energy, Basic Energy Sciences, Office of Science,

under contract No. W-31-109-ENG-38. BioCAT is a National Institutes of Health-supported Research Center (grant RR-08630).

References

1. Abele, R., Svergun, D., Keinanen, K., et al. (1999) A molecular envelope of the ligand-binding domain of a glutamate receptor in the presence and absence of agonist. *Biochemistry* **38,** 10,949–10,957.
2. Del Rizzo, P. A., Bi, Y., Dunn, S. D., et al. (2002) The "second stalk" of *Escherichia coli* ATP synthase: structure of the isolated dimerization domain. *Biochemistry* **41,** 6875–6884.
3. Dempsey, B. R., Economou, A., Dunn, S. D., et al. (2002) The ATPase domain of SecA can form a tetramer in solution. *J. Mol. Biol.* **315,** 831–843.
4. Grüber, G., Svergun, D. I., Godovac-Zimmermann, J., et al. (2000) Evidence for major structural changes in the Manduca sexta midgut V1 ATPase due to redox modulation. A small angle X-ray scattering study. *J. Biol. Chem.* **275,** 30,082–30,087.
5. Kataoka, M., Head, J. F., Vorherr, T., et al. (1991) Small-angle X-ray scattering study of calmodulin bound to two peptides corresponding to parts of the calmodulin-binding domain of the plasma membrane Ca^{2+} pump. *Biochemistry* **30,** 6247–6251.
6. Newcomer, M. E., Lewis, B. A., and Quiocho, F. A. (1981) The radius of gyration of L-arabinose- binding protein decreases upon binding of ligand. *J. Biol. Chem.* **256,** 13,218–13,222.
7. Shilton, B. H., Flocco, M. M., Nilsson, M., et al. (1996) Conformational changes of three periplasmic receptors for bacterial chemotaxis and transport: the maltose-, glucose/galactose- and ribose-binding proteins. *J. Mol. Biol.* **264,** 350–363.
8. Shilton, B., Svergun, D. I., Volkov, V. V., et al. (1998) *Escherichia coli* SecA shape and dimensions. *FEBS Lett.* **436,** 277–282.
9. Svergun, D. I., Konrad, S., Huss, M., et al. (1998) Quaternary structure of V1 and F1 ATPase: significance of structural homologies and diversities. *Biochemistry* **37,** 17,659–17,663.
10. Spurlino, J. C., Lu, G.-Y., and Quiocho, F. A. (1991) The 2.3-Å resolution structure of the maltose- or maltodextrin-binding protein, a primary receptor of bacterial active rransport and chemotaxis. *J. Biol. Chem.* **266,** 5202–5219.
11. Boulin, C., Kempf, R., Koch, M. H. J.,et al. (1986) Data appraisal, evaluations and display for synchrotron radiation experiments: hardware and software. *Nucl. Instrum. Methods* **A249,** 399–407.
12. Svergun, D. I. and Koch, M. H., unpublished.
13. Semenyuk, A. V. and Svergun, D. I. (1991) GNOM—a program package for small-angle scattering data processing. *J. Appl. Crystallogr.* **24,** 537–540.
14. Hammersley, A. P., Svensson, S. O., Hanfland, M., et al. (1996) Two-dimensional detector software: from real detector to idealised image or two-theta scan. *High Pressure Res.* **14,** 235–248.

15. Hammersley, A. P. (1997) FIT2D: an introduction and overview. *ESRF Internal Report* ESRF97HA02T.
16. Hammersley, A. P. (1998) FIT2D V9.129 Reference Manual V3.1. *ESRF Internal Report* ESRF97HA02T.
17. Bradford, M. M. (1976) A rapid and sensitive method for the quantitation of microgram quantities of protein utilizing the principle of protein-dye binding. *Anal. Biochem.* **72,** 248– 254.
18. Guinier, A. and Fournet, G. (1955) *Small Angle Scattering of X-rays*, Wiley, New York.
19. Olah, G. A., Trakhanov, S., Trewhella, J., et al. (1993) Leucine/isoleucine/valine-binding protein contracts upon binding of ligand. *J. Biol. Chem.* **268,** 16,241–16,247.
20. Kataoka, M., Nishii, I., Fujisawa, T., et al. (1995) Structural characterization of the molten globule and native states of apomyoglobin by solution X-ray scattering. *J. Mol. Biol.* **249,** 215–228.
21. Glatter, O. (1977) A new method for the evaluation of small-angle scattering data. *J. Appl. Crystallogr.* **10,** 415–421.
22. Svergun, D. I., Semenyuk, A. V., and Feigin, L. A. (1988) Small-angle scattering data treatment by the regularization method. Acta Cryst. A44**,** 244–250.
23. Svergun, D. I. (1993) A direct indirect method of small-angle scattering data treatment. *J. Appl. Crystallogr.* **26,** 258–267.
24. Svergun, D. I., Barberato, C., and Koch, M. H. J. (1995) CRYSOL—a program to evaluate X-ray solution scattering of biological macromolecules from atomic coordinates. *J. Appl. Crystallogr.* **28,** 768–773.
25. Svergun, D. I. and Stuhrmann, H. B. (1991) New developments in direct shape determination from small-angle scattering. 1. Theory and model calculations. *Acta Crystallogr.* **A47,** 736–744.
26. Svergun, D. I., Volkov, V. V., Kozin, M. B., et al. (1996) New developments in direct shape determination from small-angle scattering. 2. Uniqueness. *Acta Crystallogr.* **A52,** 419–426.
27. Chacon, P., Moran, F., Diaz, J. F., et al. (1998) Low-resolution structures of proteins in solution retrieved from X-ray scattering with a genetic algorithm. *Biophys. J.* **74,** 2760–2775.
28. Chacon, P., Diaz, J. F., Moran, F., et al. (2000) Reconstruction of protein form with X-ray solution scattering and a genetic algorithm. *J. Mol. Biol.* **299,** 1289–1302.
29. Svergun, D. I. (1999) Restoring low resolution structure of biological macromolecules from solution scattering using simulated annealing. *Biophys. J.* **76,** 2879–2886.
30. Walther, D., Cohen, F. E., and Doniach, S. (2000) Reconstruction of low-resolution three-dimensional density maps from one-dimensional small-angle X-ray solution scattering data for biomolecules. *J. Appl. Crystallogr.* **33,** 350–363.
31. Svergun, D. I., Petoukhov, M. V., and Koch, M. H. (2001) Determination of domain structure of proteins from X-ray solution scattering. *Biophys. J.* **80**, 2946–2953.

16

Membrane Protein NMR Studies

Stanley J. Opella

1. Introduction

Not only do membrane proteins represent a substantial fraction of the information in a genome, but also they are responsible for many essential biological functions, some of which are unique (e.g., as membrane transporters). As a result, some mutations in genes for membrane proteins cause human diseases. Thus, there are many reasons that the structural biology of membrane proteins is of considerable interest. However, because membrane proteins are not soluble in aqueous solution, only a few examples have been amenable to experimental structural analysis with X-ray crystallography and solution nuclear magnetic resonance (NMR) spectroscopy. The relatively few structures of helical membrane proteins that have been determined provide an initial view of the design principles involved in the use of helices as structural and functional elements, setting the stage for the evaluation of new structures of membrane transporters and other membrane proteins. NMR spectroscopy is an extraordinarily powerful method for describing the structure and dynamics of proteins and other biopolymers. Although there have been some initial successes, further development is needed for it to be generally applicable to membrane proteins.

2. NMR Spectroscopy

The overall rotational correlation time of a protein, the extent of alignment of the protein molecules in the sample, and strategy for assignment of the resonances to sites in the protein are the principal considerations for NMR structural studies of proteins. Each of these considerations needs to be taken into account in the development and application of NMR for determining the structures of membrane proteins ***(1)***. In contrast, for relatively small globular pro-

From: *Methods in Molecular Biology, vol. 227: Membrane Transporters: Methods and Protocols*
Edited by: Q. Yan © Humana Press Inc., Totowa, NJ

teins, the sample conditions, instrumentation, experiments, and calculations that lead to structure determination are well established *(2)*. The chief requirement for the structure determination of globular proteins is that samples can be prepared of isotopically labeled polypeptides that are folded in their native conformation and reorient relatively rapidly in solution. Such samples have been prepared for many hundreds of proteins and it is likely that this can be done for thousands more of the polypeptide sequences found in genomes *(3)*.

The rotational correlation time problem is paramount.If the protein reorients rapidly in solution, then the standard methods of NMR can be applied and the structure determined. However, it is simply not possible to obtain NMR spectra of slowly reorienting or immobile proteins such as membrane proteins in most lipid environments, using conventional solution NMR methods and instruments.From the start, NMR studies of membrane proteins require crucial choices about samples, instrumentation, and experimental methods.It is feasible to apply both solution NMR and solid-state NMR to helical membrane proteins, depending primarily on the choice of lipids as well as other sample conditions.

3. Proteins and Lipids

Figure 1 illustrates the types of lipid assembly used in NMR structural studies of membrane proteins. Membrane proteins require the presence of lipids to maintain their native conformations and functions. Membrane proteins can be reconstituted with lipids that self-assemble into micelles, bicelles, or bilayers. The properties of the lipid–protein complex determine the rotational correlation time of the protein molecules. Micelles can be prepared so that they contain a single polypeptide and reorient rapidly enough for solution NMR spectroscopy. Micelles are spherical aggregates of lipids with the hydrophobic chains on the interior. Samples for solution NMR spectroscopy require the use of relatively high temperatures and high concentration of lipids that form small micelles *(4)*, most commonly sodium dodecyl sulfate (SDS), dodecyl phosphocholine (DPC), or dihexanoyl phosphatidylcholine (DHPC). Bicelles are bilayer disks and their size can be adjusted through the molar ratios of long-chain and short-chain lipids *(5)*. Bilayers are infinitely large in two dimensions, and two molecules thick in the third. In bilayers, nearly all of the residues in the polypeptide are immobile on time-scales longer than milliseconds, and the relevant dipolar coupling and chemical shift interactions in individual backbone sites are not motionally averaged. As a result, bilayer samples of membrane proteins give very broad and poorly resolved spectra when instruments and methods appropriate in solution NMR are used. On the other hand, bilayer samples are suitable for the application of solid-state NMR methods where radio-frequency irradiations replace molecular reorientation as the

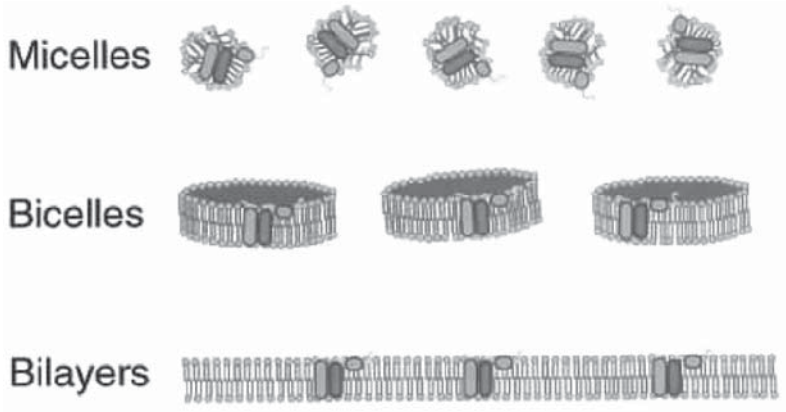

Fig. 1. Representations of proteins in micelles (**top**), bicelles (**middle**), and bilayers (**bottom**).

principal mechanism of averaging the dipolar couplings responsible for the line broadening. The solid-state NMR approach that uses stationary, uniaxially aligned samples ***(6)*** is particularly well suited for membrane proteins in lipid bilayers because the proteins are immobilized and can be highly aligned ***(7)***. Spectroscopically, it is the combination of decoupling the heteronuclear dipolar interactions and sample alignment that results in narrow, single-line resonances and well-resolved, orientationally dependent spectra that provide the input for structure determination.There is a direct mapping of protein structure onto the solid-state NMR spectra of aligned samples, and the determination of complete three-dimensional structures from the spectra is feasible when multiple orientationally dependent frequencies are measured for nuclei at each residue.

Samples can be prepared with no, weak, or complete alignment of the protein molecules. Complete alignment is possible only with immobile proteins. Rapidly reorienting proteins can have either no or weak alignment. The vast majority of NMR studies have been performed on samples without molecular alignment. This is the case for globular proteins, which undergo effectively isotropic reorientation in solution. It is also the case for membrane proteins in micelles and small bicelles. For these samples, structure determination is based on measurements that reflect internal molecular parameters, such as nuclear Overhauser effects (NOEs) that give short-range distance measurements and variations in isotropic chemical shifts associated with secondary structure ***(8)***.

Unoriented, immobile samples, including membrane proteins in bilayers, can be studied using magic-angle, sample-spinning, solid-state NMR spectroscopy ***(9)***, where distances and torsion angles are measured through spectro-

scopic parameters affected by both homonuclear and heteronuclear dipolar interactions. In the past few years, there has been a great deal of interest in weakly aligned samples of proteins, including soluble, globular proteins in the presence of various types of additive and gel-forming medium. Because the proteins are reorienting rapidly, solution NMR methods are used for the measurement of residual dipolar couplings (RDCs). It is possible to weakly align membrane proteins in micelles and small bicelles through lanthanide ion ***(10,11)*** and gel methods ***(12)***. Immobile bilayer samples can be completely aligned to a degree rivaling that observed in single crystals of peptides ***(7)***. Membrane proteins in bilayers can be aligned mechanically between glass plates, and membrane proteins in large bicelles can be aligned magnetically and then "flipped" to the desirable parallel orientation through the addition of lanthanide ions ***(13)***.

The traditional approach to protein structure determination is based on the same overall principles, whether solution NMR or solid-state NMR methods are used and whether the sample is aligned. This involves the resolution of resonances through the use of isotopic labels and multidimensional NMR experiments, the measurement of spectral parameters associated with individual resonances (e.g., NOEs, J couplings, dipolar couplings, or chemical shift frequencies), the assignment of all resonance to specific sites in the protein, and then the calculation of structures. There are examples of the application of this approach to membrane proteins in micelles ***(8)*** and bilayers ***(14)***. The availability of orientational information associated with individual resonances means that it is now possible to make effective use of limited amounts of assignment information (e.g., some residue-type assignments or a few sequential assignments). It may also be feasible to implement an "assignment-free" approach ***(15)***. The use of either limited or no assignment information prior to calculating structures greatly speeds the process of structure determination by NMR spectroscopy, especially in the case of membrane proteins, for which assignments are difficult to make in nearly all situations because of overlap of resonances and unfavorable relaxation parameters.

4. The Local Field

"The interaction between two nuclear spins depends on the magnitude and orientation of their magnetic moments and also the length and orientation of the vector describing their relative positions" ***(16)***. The local field, which results from the interactions of two or more proximate nuclei, provides a particularly direct source of structural information. Other nuclear spin interactions, especially the chemical shift, can also provide essential structural constraints, but their interpretation is generally more complicated and less firmly grounded. Taken together, the restrictions resulting from measurements of spectral

parameters from several spin interactions, where at least one of them is a local field, are sufficient to determine the three-dimensional structures of proteins.

It is possible to study unoriented "powder" samples, including membrane proteins with the use of magic-angle sample spinning. However, there is a second way to obtain high-resolution chemical shift spectra of solid samples, and that entails the use of single crystals, where depending on the space group, the molecules have only one or a few orientations relative to each other and the applied magnetic field. Fortunately, it is not necessary to have a single-crystal sample. One direction of molecular orientation is sufficient, as long as it is parallel to the magnetic field, to give all of the spectroscopic benefits of sample orientation. It is generally easier to prepare uniaxially oriented samples of many materials, including proteins in biological supramolecular structures like membrane bilayers, than single crystals for X-ray diffraction or rapidly reorienting solutions for NMR spectroscopy. In uniaxially oriented samples, each site on one molecule can be transformed into the identical site on another molecule through a combination of translation, inversion, and rotation operations about an axis parallel to the direction of the applied magnetic field. Just as observed for single crystals, the spectra of oriented protein samples are characterized by narrow single-line resonances rather than powder patterns. The resonance frequencies reflect the orientations of the individual groups and, as a result, the solid-state NMR spectra of oriented samples are a rich source of structural information.

Polarization inversion spin exchange at the magic angle (PISEMA) ***(17)*** is a high-resolution version of separated local field spectroscopy ***(18)***. By combining polarization inversion with flip-flop Lee–Goldburg homonuclear decoupling on the abundant I spins following spin-lock cross-polarization to the dilute S spin during the t1 interval of the pulse sequence, very high-resolution two-dimension heteronuclear I–S dipolar spectra of solid samples can be obtained. Linewidths in the dipolar dimension are reduced by more than an order of magnitude compared to a conventional separated local field spectrum obtained without homonuclear decoupling during the t1 interval. The combination of narrow lines and favorable scaling factor has such a dramatic effect on the appearance of the spectra that it is now feasible to formulate solid-state NMR experiments where heteronuclear dipolar coupling frequencies provide a mechanism for resolution among similar chemical sites. Even more interestingly, dipolar coupling and chemical shift frequencies can be used in a number of complementary ways to enhance resolution in reduced or maximum dimensional experiments and to provide qualitative and quantitative indications of molecular structure. Two-dimensional $^{1}H/^{15}N$ and $^{1}H/^{13}C$ PISEMA spectra have narrow linewidths in both the heteronuclear dipolar coupling and chemical shift frequency dimensions, enabling dipolar couplings to complement

chemical shifts for resolution among sites as well as the measurement of readily interpretable orientationally dependent frequencies. PISEMA experiments are being used on a variety of systems, including membrane proteins.

5. Wheels and Waves

The secondary structure and topology of membrane proteins can be determined from the two-dimensional $^{1}H/^{15}N$ PISEMA spectra of uniformly ^{15}N-labeled samples in oriented bilayers. The characteristic "wheellike" patterns of resonances observed in these spectra reflect helical wheel projections of residues in both transmembrane and in-plane helices and, hence, provide direct indices of secondary structure and topology of membrane proteins in phospholipid bilayers.We refer to these patterns as PISA (polarity index slant angle) wheels ***(19,20)***.

The resonance frequencies in both the $^{1}H/^{15}N$ heteronuclear dipolar and ^{15}N chemical shift dimensions in PISEMA spectra of aligned samples of membrane proteins depend on helix orientation, as well as on backbone dihedral angles, the magnitudes and orientations of the principal elements of the amide ^{15}N chemical shift tensor, and the N-H bond length.It is possible to calculate spectra for any protein structure ***(21)***. The principles involved in the PISA wheel analysis of helices ***(22)*** are illustrated in **Fig. 2** In **Fig. 2A** the projection down the axis of a helical wheel shows that the 3.6 residues per turn periodicity characteristic of an α-helix results in an arc of 100° between adjacent residues. The drawing of a peptide plane in **Fig. 2B** shows the orientations of the principal axes of the three operative spin interactions at the ^{15}N labeled amide site. The 17° difference between the N-H bond axis and the σ_{33} principal element of the amide ^{15}N chemical shift tensor is of particular importance because of its impact on the spectral appearance of a PISA wheel.The striking "wheellike" pattern of resonances calculated from a two-dimensional PISEMA spectrum of an ideal helix is shown in **Fig. 2C**. A PISA wheel reflects the slant angle (tilt)of the helix and the assignment of the resonances reflects the polarity index (rotation)of the helix.

When the helix axis is parallel to the bilayer normal, all of the amide sites have an identical orientation relative to the direction of the applied magnetic field and, therefore, all of the resonances overlap with the same dipolar coupling and chemical shift frequencies. Tilting the helix away from the membrane normal results in variations in the orientations of the amide N-H bond vectors relative to the field. This is seen in the spectra as dispersions of both the heteronuclear dipolar coupling and chemical shift frequencies. Nearly all trans-membrane helices are tilted with respect to the bilayer normal, and it is the combination of the tilt and the 17° difference between the tensor orientations in the molecular frame that make it possible to resolve many resonances

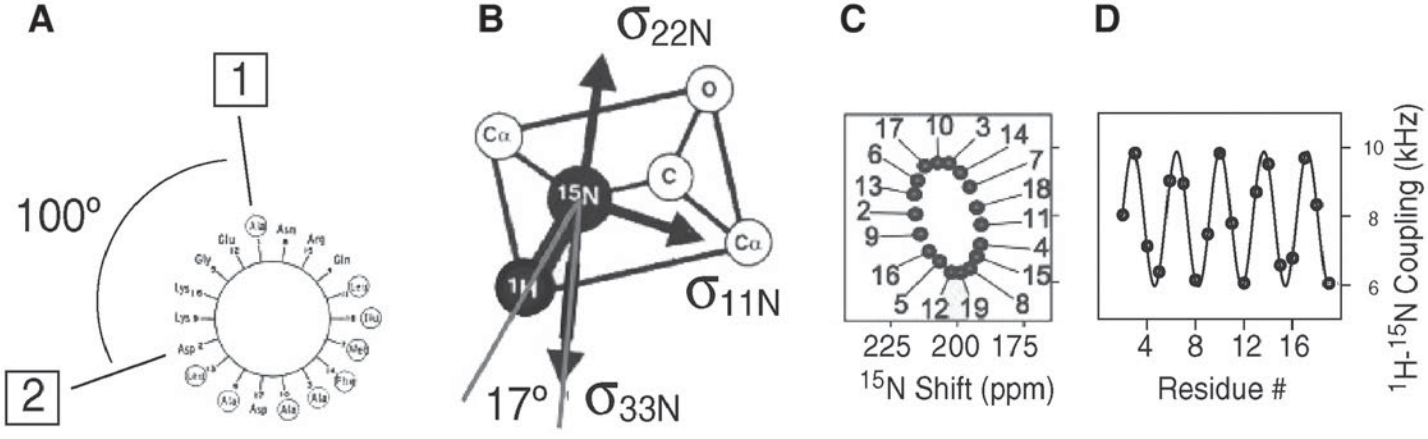

Fig. 2. Principals of PISA wheels. **(A)** Helical wheel showing the 100° arc between adjacent residues that is a consequence of the periodicity of 3.6 residues per turn in an α-helix; **(B)** orientations of the principal elements of the spin-interactions tensors associated with ^{15}N in a peptide bond. **(C)** PISA wheel for an ideal α-helix; **(D)** dipolar wave for an ideal α-helix.

from residues in otherwise uniform helices and is responsible for the "wheellike" pattern in PISEMA spectra, such as that illustrated in **Fig. 2C**.

Dipolar waves can serve as maps of protein structure in NMR spectra of both weakly and completely aligned samples ***(22)***. The periodicity inherent in secondary structure elements is key to the use of both PISA wheels and dipolar waves as indices of secondary structure and topology in membrane proteins. **Figure 2C** displays a classical two-dimensional PISA wheel of an α-helix. **Figure 2D** illustrates the periodic-wavelike variations of the magnitudes of the static heteronuclear dipolar couplings as a function of residue number.Similar patterns are observed in RDCs measured for weakly aligned proteins.

6. Application of NMR to an Ion Channel

We determined the three-dimensional structure of a functional peptide corresponding to the M2 segment from the α-subunit of the acetylcholine receptor (AchR) by both solution NMR and solid-state NMR methods ***(14)***. The relatively large quantities of isotopically labeled M2 peptides required for NMR spectroscopy were prepared by expression of recombinant peptides in *Escherichia coli*. The incorporation of the M2 peptides into lipid bilayers reconstitutes functional, cation-selective channels; the single-channel currents recorded from AchR M2 in lipid bilayers, under voltage-clamp conditions, have heterogeneous conductances and lifetimes, as expected for monomeric peptides that self-assemble into conductive oligomers of discrete, yet variable, size. These results indicate that the recombinant and M2 peptide used in the NMR experiments is functional and forms sequence-specific discrete ion channels in lipid bilayers.

The experimental two-dimensional PISEMA spectrum in **Fig. 3B** of a sampling of the uniformly ^{15}N-labeled M2 peptide in aligned bilayers has excellent resolution, with each amide resonance characterized by ^{15}N chemical shift and ^{1}H–^{15}N dipolar coupling frequencies. The PISA wheel and dipolar wave derived from the experimental data are shown in **Fig. 3C,D**, respectively.The experimental PISEMA spectrum in **Fig. 3B** is similar to that of the PISA wheel in **Fig. 3C**, which was calculated for an ideal trans-membrane α-helix tilted by 12° with 3.6 residues per turn. Differences between the experimental spectrum and the calculated spectrum are the result of deviations between the experimentally determined backbone dihdral angles and those of an ideal α-helix and differences resulting from variations of the chemical shift tensors among the various amide sites. Without making a single resonance assignment, comparison of the experimental and calculated spectra leads to the conclusion that the AchR M2 helix is transmembrane with a tilt angle of approx 12°. A similar tilt angle is determined from the dipolar wave fitted to the experimental data in **Fig. 3D**.

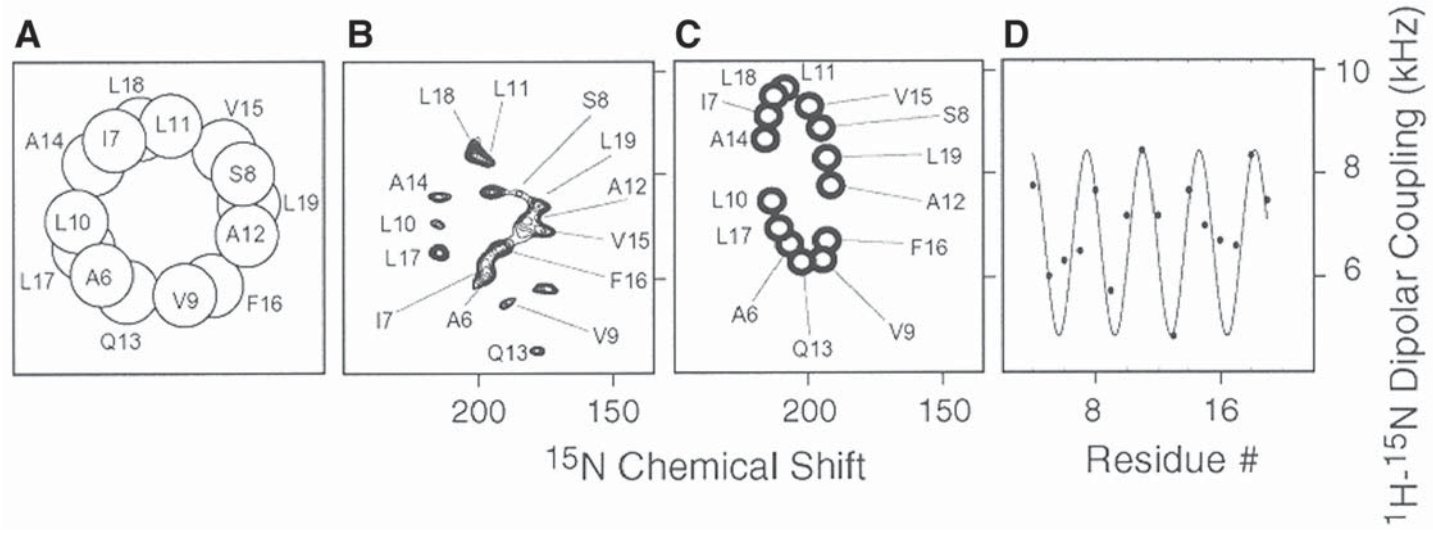

Fig. 3. Experimental data and PISA wheel and dipolar wave for the acetycholine receptor M2 ion-channel peptide: **(A)** helical wheel; **(B)** experimental PISEMA spectrum; **(C)** PISA wheel for and ideal α-helix with a 12° tilt; **(D)** dipolar wave using the experimental dipolar couplings and resonance assignments in **(B)**.

In the experimental PISEMA spectrum of the peptide, the locations of assigned resonances in the wheellike pattern are nearly identical to those in the helical wheel projection of the peptide, also shown in **Fig. 3A**. Thus, the polarity of the resonances observed in the wheellike pattern of a PISEMA spectrum provides a direct measure of the angle of the helix rotation about its long axis within the membrane. In principle, one well-resolved two-dimensional PISEMA spectrum of an aligned sample of a uniformly ^{15}N-labeled protein provides sufficient information for complete structure determination. The orientationally dependent frequencies associated with each resonance depends on the magnitudes and orientations of the principal elements of the spin-interaction tensors in the molecule and on the orientation of the molecular site with respect to the direction of the applied magnetic field. Because the orientation of the bilayer is fixed by the method of sample preparation and the properties of the nuclear spin-interaction tensors are generally well characterized, each frequency reflects the orientation of a specific site in the protein with respect to the bilayer. The backbone structure of a protein is defined by the planes formed by the individual rigid peptide bonds and their directly bonded atoms. This is equivalent to the conventional description by vectors representing bonds between nonhydrogen atoms. A standard planar peptide geometry serves as the building block for the structure assembly process. The orientation of a peptide plane consistent with the measured NMR frequencies is defined in terms of polar angles relative to the magnetic field. The input to the computer program consists of the NMR frequencies measured from a PISEMA spectrum the magnitudes and orientations of the principal elements of the amide ^{15}N and ^{1}H chemical shift tensors, and the N-H bond length. Once the orientations of all the peptide planes in the protein are determined from the experimental data, neighboring planes of fixed orientation are connected through their common α-carbon atom, with the only constraint of a fixed tetrahedral angle of 110°. Another program calculates the ϕ and χ dihedral angles for the two contiguous peptide plane combinations that satisfy tetrahedral angle geometry at the α-carbon. The structure of the AchR peptide determined in this way is incorporated into **Fig. 4**.

The advantage of this direct mathematical analysis is that it is possible to determine the standard deviations in ϕ and μ based on uncertainties in the experimentally determined angles. Another important advantage of the method is that is results in the “piecewise” assembly of structures. Different parts of the protein structure can be determined independently of the rest.This is not possible in methods for which distance constraints between different regions of the protein must be established for three-dimensional structure determination. Because the orientation of individual peptide planes is determined relative to a unique external reference, the corresponding errors are not cumulative.

Fig. 4. Pentameric M2 ion channel in lipid bilayers.

However, it does require complete sequential resonance assignments before the structure can be calculated.

7. Summary

Nuclear magnetic resonance structural studies of membrane proteins yield valuable insights into their structure and topology. For example, the structure of the M2 peptide determined by solid-state NMR spectroscopy in lipid bilayers is tilted by 12° and rotated about its helix axis so that the hydrophilic residues face the N-terminal side of the membrane. This has important consequences for ion-channel pore geometry and conduction, as it leads to the assembly a symmetric, pentameric, and funnellike pore with its wide opening at the N-terminal side of the membrane. All of these conclusions about the structure of the peptide in bilayers are immediately apparent from inspection of the assigned PISEMA spectrum prior to complete structure determination. The three-dimensional structures calculated from NMR data have atomic resolution.

Figure 4 shows a model of the AChR channel pore, constructed from the three-dimensional structure of the AChR M2 helix in lipid bilayers and the known pentameric organization of the channel. The optimized pentameric

bundle has a right-handed, interhelical twist with an orientation angle of 12°. A central narrow pore has a diameter ranging from about 3.0 to 8.6 Å. Nonpolar residues are predominantly on the exterior of the bundle, whereas polar residues line the pore. The residues exposed to the pore lumen are Glu-1, Ser-4, Ser-8, Val-15, Leu-18, and Gln-22, which is in agreement with evidence collected from mutagenesis, affinity labeling, and cysteine accessibility measurements. A side view shows a funnel-shaped bundle, 33 Å in length, with the wide mouth at the N-terminus. A dotted contour depicting the profile of the ion- conduction pore calculated from the structure is shown. The channel lining hydroxyl residues are in agreement with the expectations of a water-filled pore, and the constrictions are compatible with the permeation of both Na and K ions and the model of the pore shown in **Fig. 4**.

The structure of the polypeptide shown in **Fig. 4** was determined using solid-state NMR methods that were direct descendents of the initial observations of doublets resulting from local fields in 1948. The advances required to transform solid-state NMR from a spectroscopic technique to a generally applicable method for determining molecular structures included multiple-pulse sequences, double-resonance methods, and separated local field spectroscopy. It also required improvements in instrumentation, especially the use of high-field magnets, and efficient probes capable of high-power radio-frequency irradiations at high frequencies. The pace of development is accelerating and the local field is being utilized in an increasing number of ways in spectroscopic investigations of molecular structure and dynamics. Applications to many helical membrane proteins are underway and promise to add to our understanding of membrane proteins in health and disease.

Acknowledgments

The research on solid-state NMR of proteins was supported by grants R37GM24266, P01GM64676, RO1GM29754, and PO1GM56538 from the National Institute of General Medical Sciences and utilized the Resource for Solid-State NMR of Proteins supported by grant P41RR09731 from the Biomedical Research Technology Program, National Center for Research Resources.

References

1. Opella, S. J. (1997) NMR and membrane proteins. *Nature Struct. Biol.* **4(suppl.),** 845–848.
2. Cavanagh, J., Fairbrother, W. J., Palmer, A. G., et al. (1996) *Protein NMR Spectroscopy*, Academic, San Diego, CA.
3. Wuthrich, K. (1998) The second decade-into the third millennium. *Nature Struct. Biol.* **5(suppl.),** 492–495.

4. McDonnell, P. A. and Opella, S. J. (1993) Effect of detergent concentration on multidimensional solution NMR spectra of membrane proteins in micelles. *J. Magn. Reson.* **B102,** 1205–1225.
5. Sanders, C. R., Hare, B. J., Howard, K., et al. (1993) Magnetically-oriented phospholipid micelles as a tool for the study of membrane-associated molecules. *Prog. NMR Spectrosc.* **26,** 421–444.
6. Opella, S. J., Stewart, P. L., and Valentine, K. G. (1987) Structural analysis of solid-state NMR measurement of peptides and proteins. *Q. Rev. Biophys.* **19,** 7–49.
7. Marassi, F. M., Ramamoorthy, A., and Opella, S. J. (1997) Complete resolution of the solid- state NMR spectrum of a uniformly ^{15}N-labeled membrane protein in phospholipid bilayers. *Proc. Natl. Acad. Sci. USA* **94,** 8551–8556.
8. Almeida, F. C. L and Opella, S. J. (1997) fd coat protein structure in membrane environments:structural dynamics of a loop connecting a hydrophobic trans-membrane helix and an amphiapathic helix in a membrane protein. *J.Mol.Biol.* **270,** 481–495.
9. Griffin, R. G. (1998) Dipolar recoupling in MAS spectra of biological solids. *Nature Struct. Biol.* **5(suppl.),** 508–512.
10. Ma, C. and Opella, S. J. (2000) Lanthanide ions bind specifically to an added "EF-hand" and orient a membrane protein in micelles for solution NMR Sspectroscopy. *J. Magn. Reson.* **146,** 381–384.
11. Veglia, G. and Opella, S. J. (2000) Lanthanide ion binding to adventitious sites aligns membrane proteins in micelles for solution NMR spectroscopy. *J. Am. Chem. Soc.* **122,** 11,733–11,734.
12. Chou, J. J., Kaufman, J. D., Stahl, S. J., et al. (2002) Micelle-induced curvature in a water-insoluble HIV-1 Env peptide revealed by NMR dipolar coupling measurement in stretched polyacrylamide gel. *J. Am. Chem. Soc.* **124,** 2450–2451.
13. Howard, K. P. and Opella, S. J. (1996) High resolution solid-state NMR spectra of integral membrane proteins reconstituted into magnetically oriented phospholipid bilayers. *Magn. Reson.* **B112,** 91–94.
14. Opella, S. J., Marassi, F. M., Gesell, J. J., et al. (1999) Structures of the M2 channel-lining segments from nicotinic acetylcholine and NMDA receptors by NMR spectroscopy. *Nature Struct. Biol.* **6,** 374–379.
15. Nevzorov, A. and Opella, S. J. (2003) Structural fitting of solid-state NMR spectra of oriented proteins. *J. Magn. Reson.* **160,** 34–40.
16. Abragam, A. (1961) *The Principals of Nuclear Magnetism*. Oxford Univ. Press, Oxford, UK.
17. Wu, C. H., Ramamoorthy, A., and Opella, S. J. (1994) High-resolution heteronuclear dipolae solid-state NMR spectroscopy. *J. Magn. Reson. A* **109,** 270–272.
18. Waugh, J. S. (1976) Uncoupling of local field spectra in nuclear magnetic resonance: Determination of atomic positions in solids. *Proc. Natl. Acad. Sci. USA* **78,** 1894–1897.
19. Marassi, F. M. and Opella, S. J. (2002) A solid-state NMR index of helical membrane protein structure and topology. *J. Magn. Reson.* **144,** 150–155.
20. Wang, J., Denny, J., Tian, C., et al. (2000) Imaging membrane protein helical wheels. *J. Magn. Reson.* **144,** 162–167.

21. Bak, M., Schultz, R., Vosegaard, T., et al. (2002) Specification and visualization of anisotropic interaction tensors in polypeptides and numerical simulations in biological solid-state NMR. *J. Magn. Reson.* **154,** 28–45.
22. Mesleh, M. F., Veglia, G., DeSilva, T. M., et al. (2002) Dipolar waves as NMR maps of protein structure. *J. Am. Chem. Soc.* **124,** 4206–4207.

17

Analysis of Soluble Sugar Permease Domains by Solution NMR

Thomas A. Wilkinson and Yuan Chen

1. Introduction

Knowledge of membrane transporter molecular structures is crucial for obtaining a detailed understanding of the mechanism by which these proteins shuttle their cargo across a biological membrane. Unfortunately, ascertaining complete structures of these transporters currently poses a difficult challenge for the structural biologist, as whole membrane proteins are generally refractory to analyses by X-ray crystallography or nuclear magnetic resonance (NMR) spectroscopy. The hydrophobic nature of these proteins leads to aggregation that represents a barrier to crystallization; similarly, the aggregation properties of these proteins in solution thwart efforts to collect high-quality NMR spectra. Nonetheless, NMR spectroscopy does provide some experimental avenues for characterizing membrane transporter structure and function. Membrane transporters frequently take on a modular structure, being organized into cytoplasmic and integral membrane domains that perform distinct functions. The soluble cytoplasmic domains of a number of sugar permeases have been studied extensively using various solution NMR techniques ***(1–6)***, and NMR methodologies applied toward such studies will be described in this chapter. In addition, solid-state NMR has been employed to examine the conformation of transmembrane segments in lipid environments; descriptions of such studies are provided elsewhere in this volume (*see* Chapter 16).

We describe here NMR methodologies that have been applied toward studies of enzyme IIA and IIB (EIIA and EIIB, respectively), the soluble domains of transmembrane sugar permeases from the bacterial phosphoenolpyruvate-dependent phosphotransferase system (PTS). The PTS directs transport of particular sugars into the cell concurrently with their phosphorylation ***(7)*** and is

From: *Methods in Molecular Biology, vol. 227: Membrane Transporters: Methods and Protocols*
Edited by: Q. Yan © Humana Press Inc., Totowa, NJ

involved in overall regulation of cell metabolism and in chemotaxis of PTS substrates ***(8)***. The system is comprised of three protein components: enzyme I (EI), histidine-containing protein (HPr), and enzyme II (EII). The proteins EI, HPr, and EII, in turn, participate in transferring a phosphoryl group in a cascade of reactions that originates from the donor phosphoenolpyruvate (PEP) and involves key histidine residues in phosphoprotein intermediates, ultimately phosphorylating a sugar molecule acceptor ***(9)***. EI and HPr are phosphoryl-transfer enzymes that are common in the PTS pathway regardless of the sugar substrate, whereas EII is sugar-specific and contains at least three domains: EIIA and EIIB (cytoplasmic domains) and EIIC (a transmembrane domain).

General considerations for undertaking protein NMR studies are first discussed in this review, followed by a description of the following methodologies that have been applied toward the study of the soluble domains of sugar transporters: (1) characterization of the active-site histidines; (2) NMR structure determination; (3) characterization of protein–protein interactions; and (4) characterization of protein conformational flexibility.

2. Materials

1. A diethylaminoethyl (DEAE)–Sephacel column (Amersham-Pharmacia Biotech; 50 mL bed volume), a Sephadex G-50/superfine column (Amersham-Pharmacia Biotech; 2 × 85 cm), and a hydroxylapatite column (Bio-Rad; 50 mL bed volume).
2. *Escherichia coli* MZ1 cells, plasmid RE33 (an expression vector encoding IIA^{glc}), and a French press.
3. TDP buffer (20 m*M* Tris-HCl buffer, pH 7.2, containing 1 m*M* dithioreitol (DTT) and 0.1 m*M* phenylmethylsulfonyl fluoride (PMSF).
4. $^{15}NH_4Cl$ or $(^{15}NH_4)_2SO_4$, and [$^{13}C_6$]-glucose.
5. Modified M9 minimal media ***(10)*** for expressing ^{15}N-,^{13}C-labeled proteins, prepared as follows:
   a. Weigh out 6.7 g Na_2HPO_4, 3.0 g KH_2PO_4, 0.16 g NaCl, and 1.61 g Na_2SO_4; bring up these materials in 1 L of deionized water, autoclave for 20 min, and allow the solution to cool.
   b. Add 1 mL of 0.1 *M* $CaCl_2$, 1 mL of 1.0 *M* $MgCl_2$, appropriate antibiotics, and 10 mL of 100X modified Eagle's medium (MEM) vitamin solution (Gibco-BRL).
   c. Prepare a 1000X trace mineral solution as follows: Bring up 286 mg H_3BO_3, 1.5 g $CaCl_2$•H_2O, 4 mg $CoCl_2$•$6H_2O$, 20 mg $CuSO_4$•$5H_2O$, 28 mg $FeSO_4$•$7H_2O$, 20.8 g $MgCl_2$•$6H_2O$, 18 mg $MnCl_2$•H_2O, 0.2 mg MoO_3, and 20.8 mg $ZnCl_2$ into 100 mL of H_2O. Add 1 mL of 1000X trace mineral solution to the 1 L of autoclaved minimal media.
   d. Add 1 g of $^{15}NH_4Cl$ and 2.0 g of [$^{13}C_6$]-glucose to yield minimal M9 media for expressing ^{15}N-,^{13}C-labeled proteins.
6. Amicon centricons and a lyophilizer.

7. Precision 5-mm NMR tubes.
8. High-field NMR spectrometer (500 MHz or above) equipped with four channels, pulse shaping, and pulsed-field gradient capabilities.
9. A triple-resonance NMR probe.
10. Computers and software for processing and analysis of NMR data and for calculation of protein structures. Both academic and commercial software are available for NMR data analysis and structural calculation.

3. Methods

3.1. General Considerations and Sample Preparation

3.1.1. Protein Size

High-resolution structure determination studies by NMR are typically restricted to proteins or protein complexes <30 kDa in molecular weight, although protein structures larger than 30 kDa have been successfully tackled ***(11)***. The reason behind this size limitation is mainly the increased nuclear spin-relaxation rates for increasingly larger proteins, which significantly reduce the sensitivity in multidimensional heteronuclear NMR experiments. The recent development of transverse relaxation-optimized spectroscopy (TROSY) experiments ***(12–14)*** in combination with deuterium labeling ***(15)*** allows the assignment of backbone resonances of proteins up to 110 kDa, an important step toward solving solution structures of proteins in this molecular-weight range.

3.1.2. Protein Quantity and Solubility

The protein concentration required for NMR structural analysis should be approx 0.5 m*M* or higher using a conventional NMR probe. Recently introduced cryoprobes provide a threefold to fourfold improvement in signal-to-noise ratio during data acquisition, and NMR spectrometers that are equipped with such a probe allow users to run experiments with roughly threefold or fourfold lower sample concentrations. Typical sample volumes needed for an NMR experiment are 600–700 µL when using a standard precision 5-mm NMR tube, or 250–300 µL when using a 5-mm Shigemi NMR tube (a matched set of precision glassware consisting of an outer sleeve and an inner insert; Shigemi, Inc.) (*see* **Note 1**). Thus, a 0.5 m*M* concentration of a 15-kDa protein solution in a Shigemi tube would require that approx 2 mg of protein be expressed and purified for a single NMR sample.

The protein of interest should not aggregate at these concentrations, because (as noted earlier) the increased molecular mass leads to increased relaxation rates that produce low signal-to-noise ratios. Initial ^{1}H–^{15}N heteronuclear single quantum coherence (HSQC) spectra of the protein of interest should be collected to gage the aggregation state of the protein at "NMR concentrations"

(i.e., millimolar). Furthermore, the sample should be stable for extended periods of time at temperatures under which structural studies are being pursued. A two-dimensional (2D) NMR experiments can take several hours, and 3D or 4D NMR experiments typically last half a day to several days. Acquisition of the complete set of 3D and 4D experiments for structure determination of a protein can take weeks of instrument time. Thus, the stability of the protein sample should be monitored as NMR studies progress, and additional protein samples may need to be prepared if aggregation/degradation of the NMR sample occurs over the duration of a structure determination project.

If evidence of protein aggregation is observed in the initial ^{1}H–^{15}N HSQC survey spectrum of the protein of interest, then all is not lost: Various sample conditions can be changed to stabilize the monomeric form of the protein. Temperature and pH can be readily adjusted; also, if the protein of interest contains free cysteines, then a reducing agent such as β-mercaptoethanol or DTT should be included in the NMR sample to prevent aggregation via disulfide formation (*see* **Note 2**). The addition of nondenaturing detergents such as CHAPS can also discourage protein aggregation and significantly improve the appearance of NMR spectra ***(16)***. An excellent review chapter that focuses upon even more aspects of NMR sample preparation in greater detail is available ***(17)***. Despite the seemingly strict experimental requirements described earlier, these issues are overcome fairly routinely in NMR studies of soluble domains of proteins, and investigators are ultimately rewarded with a wealth of atomic-resolution structural information.

3.1.3. Protein Labeling

Proteins smaller than 10 kDa can be studied by routine 2D ^{1}H-NMR methods, and such samples do not require isotopic labeling of ^{15}N and ^{13}C for NMR analysis. Isotopic enrichment of larger proteins (>10 kDa) is necessary for the prerequisite 3D or 4D NMR experiments, as the "NMR-detectable" ^{15}N and ^{13}C nuclei have a natural abundance of only 0.4% and 1.1%, respectively (^{1}H nuclei are nearly 100% abundant). Without such enrichment, even millimolar protein concentrations would produce an "effective concentration" of ^{15}N and ^{13}C isotopes in the sample that is far too low to be useful. NMR studies of larger proteins thus demand that protein expression be performed in isotopically enriched minimal media containing, for example, either $^{15}NH_4Cl$ or $(^{15}NH_4)_2SO_4$ (relatively inexpensive) or both $^{15}NH_4Cl$ and ^{13}C-glucose (more costly).

Once expressed in isotopically enriched media, the purified protein is then uniformly labeled with ^{15}N and ^{13}C nuclei, allowing an analysis using multidimensional NMR techniques. The ensuing spectral simplification from 3D/4D

NMR methods allows structures to be determined for proteins of up to 30 kDa in molecular mass. Still larger proteins can be tackled through deuterium labeling ***(15,18)***, where proteins are grown in media prepared with D_2O instead of H_2O with or without deuterated glucose (*see* **Note 3**). Such proteins have their nonexchangeable hydrogen atoms replaced by deuterons, a situation that dramatically reduces the relaxation rates of ^{13}C spins and increases the sensitivity of the triple-resonance spectra. Finally, although ^{15}N- or ^{15}N-, ^{13}C-labeling of proteins smaller than 10 kDa is not strictly necessary, the resulting spectral simplification can save much time when assigning spectra. In some situations, a particular investigator may decide that this time savings warrants the added expense of labeling a relatively low-MW (molecular weight) protein sample. A protocol (adapted from **refs. *5,19,*** and ***20***) for preparing ^{15}N-, ^{13}C-labelled IIA^{glc} (162 residues, 17.4 kDa) from *Bacillus subtilis* that can be readily modified as needed to prepare other proteins of interest follows:

1. Grow 6 L of *E. coli* MZ1 cells containing plasmid RE33 to mid-logarithmic phase at 30°C in minimal M9 media.
2. Induce cells using a 2-h incubation period at 42°C; harvest cells by centrifugation and wash twice with TDP buffer.
3. Resuspend cells in a minimal volume and rupture with two passages through a French press at 10,000 psi. Remove cellular debris using a 15-min centrifugation at 20,000*g*.
4. Purify the crude cell extracts by ion-exchange chromatography using a DEAE–Sephacel column and a linear salt gradient (0–0.4 *M* NaCl). IIA^{glc} elutes at about 0.130 *M* NaCl.
5. Pool the IIA^{glc}-containing fractions and concentrate to 15 mL. Load this material onto a Sephadex G-50 column equilibrated with TDP buffer with 100 m*M* NaCl and collect fractions containing IIA^{glc} ***(20)***.
6. Concentrate the IIA^{glc}-containing fractions, dialyze against 10 m*M* potassium phosphate (pH 6.6), and load the dialyzed material onto a hydroxylapatite column (Bio-Rad). Elute IIA^{glc} with a linear gradient of 1–150 m*M* potassium phosphate buffer (pH 6.6). IIA^{glc} will elute at about 34 m*M* potassium phosphate.

3.2. Characterization of the Active-Site Histidines

Phosphoryl group transfer is mediated by key histidine residues of the PTS enzymes, and analysis of the active-site histidines in both EII^{glc} and the soluble domain of EII^{mtl} (the mannitol-specific PTS receptor) from *E. coli* has been performed using NMR spectroscopy ***(4,21,22)***. Determination of the histidine protonation state (*see* **Fig. 1**), the hydrogen-bonding states, and phosphorylation sites on the aromatic ring are necessary to understand the mechanism of action of these proteins. The ^{15}N chemical shifts of the histidine aromatic ring are directly correlated to the different states of the residue and can be used to

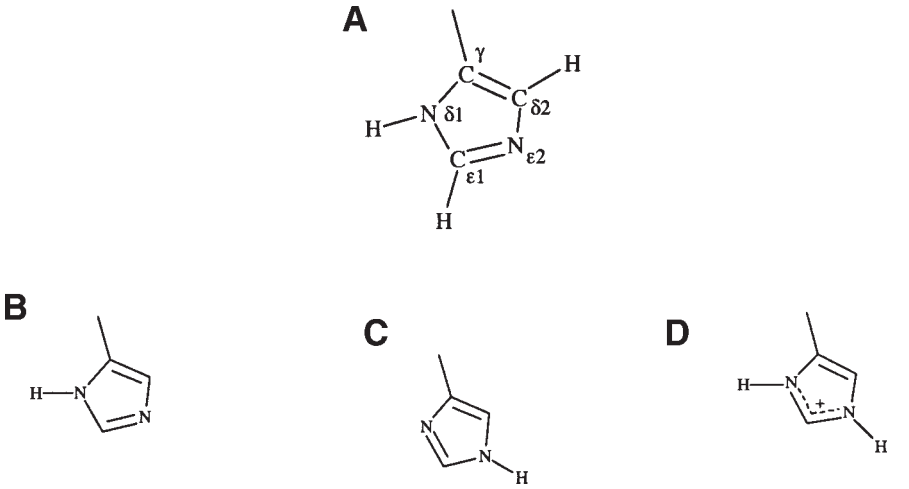

Fig. 1. **(A)** Histidine side-chain labeling and **(B–D)** various histidine protonation states.

determine these states, as summarized in **Tables 1** and **2**. Identification (i.e., assignment) of the histidine aromatic resonances in NMR spectra is necessary for these characterizations.

Historically, the resonances of the histidine residue are identified from the comparison of 1D ^{15}N or proton NMR spectra of wild-type and mutant proteins where the active-site His residue is mutated and its signals disappear ***(21)***. However, this method does not unambiguously identify the tautomeric state of the histidine imidiazole ring (identified as α, α+, and β; *see* **Table 1**) because scalar-coupling correlation to other ^{1}H or ^{13}C spins of the ring is necessary for the identification. More recently, multidimensional NMR methods using uniformly ^{15}N-, ^{13}C-labeled proteins have been employed to both assign the resonances of histidine residues and unambiguously identify the tautomeric state of the histidine imidazole ring ***(4)***.

Whereas general resonance assignment strategies for protein sidechains are summarized in **Subheading 3.3.**, one specific assignment approach for histidine aromatic resonances (employed in **ref. *4***) is described as follows. The histidine aromatic ^{13}C signals can be distinguished from other aromatic carbon atoms via ^{13}C chemical shifts and both $^{1}J_{CH}$ and $^{1}J_{CC}$ coupling constants. ^{13}C NMR studies show that histidine ring $^{1}J_{CH}$ coupling constants are typically much larger ($^{1}J_{C\varepsilon 1H\varepsilon 1} \approx 208–222$ Hz) than those found for the phenylalanine ring ($^{1}J_{CH} \approx 155$ Hz) ***(24)***. Histidine $^{13}C^{\varepsilon 1}$ signals resonate about 10 ppm downfield from aromatic phenylalanine signals, and histidine $^{13}C^{\delta 2}$ signals either near or upfield from these aromatic phenylalanine signals, depending on

Table 1
Histidine Nitrogen Tautomeric States and Associated ^{15}N Chemical Shifts

Structure	Tautomeric state	^{15}N chemical shift (ppm)	Miximum hydrogen-bond effect
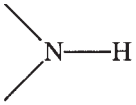	α	167.5	10 ppm downfield
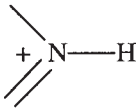	α+	176.5	10 ppm downfield
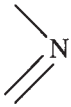	β	149.5	10 ppm upfield

Note: Nomenclature and typical ^{15}N shifts derived from NMR studies of model compounds ^{15}N chemical shifts are referenced relative to liquid NH_3.
Source: Data from **refs. *21*** and ***23***.

Table 2
Phosphohistidine States and Associated ^{15}N Chemical Shifts

Structure	^{15}N chemical shift (ppm)
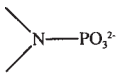	202.1
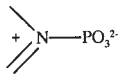	209.6
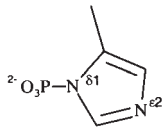	244.4[a]
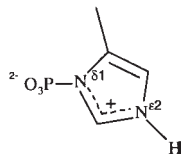	174.4[a]

Note: Expected chemical shifts for *N*-phosphohistidine are taken from **refs. *4*** and ***21***. ^{15}N chemical shifts are referenced relative to liquid NH_3.
[a]Chemical shift for the ε2 nitrogen.

histidine protonation state ***(25)***. Also, the histidine C^{γ}–C^{δ} coupling constant (measured from ^{13}C–^{1}H correlation spectra) is about 70 Hz, much larger than that observed for 1-bond coupling constants for phenylalanine aromatic carbons (about 55 Hz). Thus, the histidine signals can be distinguished from other aromatic signals in the protein, and the tautomeric state of the histidine side chains can be determined by correlation of the ^{15}N to ^{13}C attached protons or by comparison to reference values ***(4,23)***. Hydrogen-bond interactions can also be inferred from ^{15}N chemical shift perturbations from canonical values: Participation in hydrogen-bond formation can shift the chemical shift of an ^{15}N nucleus in the α or α+ state downfield as much as 10 ppm, and the chemical shift of a β ^{15}N nucleus as much as 10 ppm upfield ***(4,23)*** (*see* **Table 1**).

The pK_a values of the active-site histidines are frequently very different from other histidine amino acids (e.g., those located at protein surfaces), and determining histidine pK_a's is important for understanding the pH dependence of PTS enzyme activity. These pK_a values can be determined by tracking ^{1}H and/or ^{15}N chemical shift changes as a function of pH and determining the midpoint of the titration curve. The histidine ε1 ^{1}H chemical shifts are distinct from signals from other aromatic protons in 1D ^{1}H spectra of proteins and, therefore, are commonly used for pH titration experiments to monitor changes in protonation states.

3.3. Protein Structure Determination

The three-dimensional structures of several permease domains in the sugar transport system have been solved by NMR spectroscopy ***(2,5,18,26)***. The experiments and computational methods for the determination of protein structures are described in several publications ***(27–29)*** and are summarized here. The first step in any NMR studies of proteins is to correlate the atoms in a protein to resonances in the NMR spectra. In resonance assignments, the backbone ^{1}H, ^{15}N and ^{13}C resonances are identified first. Typically, the following experiments are performed for the assignments of backbone resonances: 2D ^{1}H-^{15}N HSQC, 3D ^{15}N–resolved-2D nuclear Overhauser effect (NOESY)–HSQC, ^{15}N-resolved– total correlation spectroscopy (TOCSY)–HSQC, HBHA(CBCACO)NH, HNCA, HNCACB, CBCA(CO)NH, CC–(TOCSY–CO)–NH, HCC–(TOCSY–CO)NH, HNCO, and HN(CA)CO ***(30)***. These spectra provide connections among ^{1}H, ^{15}N and, ^{13}C resonances within the same amino acid residue and between sequentially connected residues. The side-chain resonances of a protein can be assigned using CC–(TOCSY–CO)–NH, HCC–(TOCSY–CO)NH, and HCCH–TOCSY ***(30)***. Resonance assignments are the basis for further NMR structural analysis, such as the determination of protonation/tautomeric states of active-site residues, interactions with other proteins, or side-chain phosphorylation states (*see* **Note 4**).

Once resonance assignments are obtained, subsequent NMR experiments can produce a huge collection of site-specific structural information for a given protein, such as distances between protein protons, backbone and side-chain dihedral angles, and orientation of backbone bonds. This collection of individual "structural constraints" is then used to calculate the three-dimensional structures of proteins using computational methods such as distance geometry and simulated annealing ***(28)***. Interproton distances provide the most important information in structure determination and are usually obtained from nuclear Overhauser effects (NOE), which provide information on distances between protons that are less than 5Å apart. ^{13}C-resolved-NOESY and ^{15}N-resolved NOESY spectra are typically used to obtain NOE information. The dihedral angles are related to measured vicinal J-coupling constants by the Karplus equation. These J-coupling constants are generally obtained from experiments such as HNHA, HNHB, and HN(CO)HB ***(29)***. In addition, the chemical shifts of backbone atoms have been found to be directly correlated to the backbone dihedral angles and, therefore, can be used as structural constraints in protein structure calculations. Residual dipolar coupling constants (RDCs) provide information on the orientations of bond vectors ***(31,32)***. RDC information is collected from experiments where a small degree of alignment is induced in the protein through the addition of oriented media (such as phage particles, lipid bicelles, or other liquid-crystal formulations) to the sample ***(31)***. In special cases, such alignment can be achieved spontaneously from the intrinsic anisotropic magnetic susceptibility of the protein sample itself (e.g., heme-containing proteins) ***(33)*** or the protein can be modified to enhance its magnetic susceptibility ***(34,35)***. It has been shown recently that dipolar coupling constants can provide information on sequential connections for resonance assignments and can be used to calculate the global folds of proteins ***(36,37)***.

3.4. Characterization of Protein-Protein Complexes

The permease domains interact with other proteins in the phosphoryl-transfer cascade. Characterization of protein–protein interactions is necessary for understanding the mechanism of these transport systems. The binding interfaces between the proteins can be identified from chemical shift perturbation ***(1,3,6)***. Chemical shift perturbation is extremely sensitive to molecular interactions and has been widely used to map binding surfaces. In this technique, aliquots of an unlabeled protein are titrated into a ^{15}N-labeled protein NMR sample. When the two molecules form a specific complex, changes in the environments of the nuclei at the interface will inevitably cause changes in chemical shifts. ^{15}N–^{1}H HSQC spectra of the resulting complex are acquired, and the ^{15}N and ^{1}H chemical shift changes of protein amide groups (as well as ^{15}N-containing sidechain groups) are monitored. Amide groups with peaks

that show significant changes in chemical shift are then identified in the structural model of the ^{15}N-labeled protein, thus mapping the protein-binding surface. Conformational changes resulting from the interaction will result in additional chemical shift perturbation beyond the direct contacting surface. Distinguishing chemical shift perturbations resulting from either "direct binding effects" or "indirect effects" that stem from conformational change is not always unambiguous.

Chemical shift perturbation is sensitive to specific interactions over a wide range of affinities. ^{15}N–^{1}H HSQC spectra are typically used to monitor the chemical shift changes upon complex formation. If the exchange rate between the free and complexed protein is "fast" on the chemical shift time-scale, a single resonance corresponding to the population-weighted average of the signals from the free and complexed protein will be observed. In this situation, the affinity constant of the interaction can be estimated by monitoring chemical shift changes as a function of unlabeled protein concentration ***(38)***.

To determine the three-dimensional structure of the protein–protein complexes, heteronuclear filtered and edited NMR experiments are employed to obtain intramolecular NOEs within each protein to characterize the conformational changes associated with the complex formation. Specific interactions between the proteins are characterized using intermolecular NOEs ***(39)***. In addition to NOEs, relative orientations between the proteins can be obtained from RDC constants. The orientation measurements, in combination with the identification of binding surfaces via chemical shift perturbations, can provide significant information regarding the structure of the complex. Such an approach has been applied successfully to a protein–protein complex in a phosphoryl-transfer system recently ***(2)***.

3.5. Characterization of Protein Conformational Flexibility

One of the major advantages of NMR is its ability to provide site-specific information on protein conformational flexibility. Conformational flexibility information is obtained through measurement of various nuclear spin relaxation rates (e.g., T_1, T_2, and steady-state NOE measurements). These nuclear spin-relaxation rates are related to the internuclear spectral density function, which is a direct description of the mobility of the internuclear vectors ***(40)***. The conformational flexibility of the IIA^{glc} has been characterized by NMR spectroscopy ***(41)***. IIA^{glc} contains a highly flexible loop, and this conformational flexibility is probably important for IIA^{glc}–HPr recognition in the glucose transport system. The flexibility of this loop is expected to be quenched upon complex formation with HPr. This "folding upon binding" phenomenon is likely to be important for the specificity of molecular recognition, as nonspecific interactions will not induce a specific structure upon complex forma-

tion. In addition, the change in flexibility contributes to free-energy changes and thus modulates IIA^{glc}–HPr binding affinity. It has been shown that phosphorylation induces significant conformational changes in *E. coli* IIA^{glc} ***(42)***, suggesting that IIA^{glc} flexibility is also probably necessary for both IIA^{glc} phosphorylation and for the subsequent transfer of the IIA^{glc} phosphoryl group to other proteins or protein domains in the glucose transport system.

4. Notes

1. A protein NMR sample should contain 5–10% (v/v) D_2O to provide a "reference signal" that is used by the spectrometer hardware to maintain a stable magnetic field.
2. A disadvantage of DTT is its tendency to oxidize above pH 7.5. If care is not taken to purge the sample with nitrogen or argon gas, then any added DTT (usually in 5- to 10-fold molar excess of protein) may be effective in preventing disulfide formation for only about 1 d before oxidation renders the compound useless.
3. *Escherichia coli* cells initially do not grow well in D_2O-containing media, but can be readily "trained" to adapt to the D_2O environment. The "training process" is to grow small amount of cells several times with increasing ratio of D_2O/H_2O until achieving a final ratio that will be used to produce the protein. Large-volume cultures of the trained cells can then be prepared to produce sufficient quantities of protein for structural studies.
4. A protein sample in D_2O is usually necessary for structure studies. Exchanging the protein from the typical H_2O medium into a D_2O buffer is usually achieved by lyophilization of the sample followed by reconstitution into D_2O. However, one should determine that the lyophilization process does not adversely affect the activity of the protein of interest. If a protein cannot be lyophilized, exchange into a D_2O buffer can be achieved using a centricon.

References

1. van Nuland, N. A., Kroon, G. J., Dijkstra, K., et al. (1993) The NMR determination of the IIA^{mtl} binding site on HPr of the *Escherichia coli* phosphoenol pyruvate-dependent phosphotransferase system. *FEBS Lett.* **315,** 11–15.
2. Wang, G., Louis, J. M., Sondej, M., et al. (2000) Solution structure of the phosphoryl transfer complex between the signal transducing proteins HPr and $IIA^{glucose}$ of the *Escherichia coli* phosphoenolpyruvate : sugar phosphotransferase system. *EMBO J.* **19,** 5635–5649.
3. Wang, G., Sondej, M., Garrett, D. S., et al. (2000) A common interface on histidine-containing phosphocarrier protein for interaction with its partner proteins. *J. Biol. Chem.* **275,** 16,401–16,403.
4. Pelton, J. G., Torchia, D. A., Meadow, N. D., et al. (1993) Tautomeric states of the active-site histidines of phosphorylated and unphosphorylated III^{Glc}, a signal-

transducing protein from *Escherichia coli*, using two-dimensional heteronuclear NMR techniques. *Protein Sci.* **2,** 543–558.

5. Chen, Y., Case, D. A., Reizer, J., et al. (1998) High-resolution solution structure of *Bacillus subtilis* IIA^{glc}. *Proteins* **31,** 258–270.
6. Chen, Y., Reizer, J., Saier, M. H., Jr., et al. (1993) Mapping of the binding interfaces of the proteins of the bacterial phosphotransferase system, HPr and IIA^{glc}. *Biochemistry* **32,** 32–37.
7. Meadow, N. D., Fox, D. K., and Roseman, S. (1990) The bacterial phosphoenolpyruvate: glycose phosphotransferase system. *Annu. Rev. Biochem.* **59,** 497–542.
8. McEvoy, M. M. and Dahlquist, F. W. (1997) Phosphohistidines in bacterial signaling. *Curr. Opin. Struct. Biol.* **7,** 793–797.
9. Neidhardt, F. C. (1996) Phosphoenolpyruvate:carbohydrate phosphotransfer systems, in: *Escherichia coli and Salmonella: Cellular and Molecular Biology*, ASM Press, Washington, DC, pp. 1149–1174.
10. Sambrook, J., Fritsch, E. F., and Maniatis, T. (1989) *Molecular Cloning: A Laboratory Manual*, 2nd ed., Cold Spring Harbor Laboratory Press, Cold Spring Harbor, NY, p. A.3.
11. Caffrey, M., Cai, M., Kaufman, J., et al. (1998) Three-dimensional solution structure of the 44 kDa ectodomain of SIV gp41. *EMBO J.* **17,** 4572–4584.
12. Salzmann, M., Pervushin, K., Wider, G., et al. (1998) TROSY in triple-resonance experiments: new perspectives for sequential NMR assignment of large proteins. *Proc. Natl. Acad. Sci. USA* **95,** 13,585–13,590.
13. Riek, R., Wider, G., Pervushin, K., et al. (1999) Polarization transfer by cross-correlated relaxation in solution NMR with very large molecules. *Proc. Natl. Acad. Sci. USA* **96,** 4918–4123.
14. Pervushin, K., Riek, R., Wider, G., et al. (1997) Attenuated T_2 relaxation by mutual cancellation of dipole-dipole coupling and chemical shift anisotropy indicates an avenue to NMR structures of very large biological macromolecules in solution. *Proc. Natl. Acad. Sci. USA* **94,** 12,366–12,371.
15. Venters, R. A., Huang, C. C., Farmer, B. T., 2nd, et al. (1995) High-level $^{2}H/^{13}C/^{15}N$ labeling of proteins for NMR studies. *J. Biomol. NMR* **5,** 339–344.
16. Anglister, J., Grzesiek, S., Ren, H., et al. (1993) Isotope-edited multidimensional NMR of calcineurin B in the presence of the non-deuterated detergent CHAPS. *J. Biomol. NMR* **3,** 121–126.
17. Primrose, W. U. (1993) Sample preparation, in: *NMR of Macromolecules: A Practical Approach* (Roberts, G. C. K., ed.), IRL Oxford University Press, New York, pp. 7–34.
18. Garrett, D. S., Seok, Y. J., Liao, D. I., et al. (1997) Solution structure of the 30 kDa N-terminal domain of enzyme I of the *Escherichia coli* phosphoenolpyruvate : sugar phosphotransferase system by multidimensional NMR. *Biochemistry* **36,** 2517–2530.
19. Fairbrother, W. J., Palmer, A. G., 3rd, Rance, M., et al. (1992) Assignment of the aliphatic ^{1}H and ^{13}C resonances of the *Bacillus subtilis* glucose permease IIA

domain using double- and triple-resonance heteronuclear three-dimensional NMR spectroscopy. *Biochemistry* **31,** 4413–4425.
20. Reizer, J., Sutrina, S. L., Wu, L. F., et al. (1992) Functional interactions between proteins of the phosphoenolpyruvate : sugar phosphotransferase systems of *Bacillus subtilis* and *Escherichia coli*. *J. Biol. Chem.* **267,** 9158–9169.
21. van Dijk, A. A., de Lange, L. C., Bachovchin, W. W., et al. (1990) Effect of phosphorylation on hydrogen-bonding interactions of the active site histidine of the phosphocarrier protein HPr of the phosphoenolpyruvate-dependent phosphotransferase system determined by ^{15}N NMR spectroscopy. *Biochemistry* **29,** 8164–8171.
22. van Dijk, A. A., Scheek, R. M., Dijkstra, K., et al. (1992) Characterization of the protonation and hydrogen bonding state of the histidine residues in IIA^{mtl}, a domain of the phosphoenolpyruvate-dependent mannitol-specific transport protein. *Biochemistry* **31,** 9063–9072.
23. Bachovchin, W. W. (1986) ^{15}N NMR spectroscopy of hydrogen-bonding interactions in the active site of serine proteases: evidence for a moving histidine mechanism. *Biochemistry* **25,** 7751–7759.
24. Bristrov, V. F. (1976) Spin–spin coupling and the conformational states of peptide systems. *Prog. NMR Spectrosc.* **10,** 41–81.
25. Reynolds, W. F., Peat, I. R., Freedman, M. H., et al. (1973) Determination of the tautomeric form of the imidazole ring of L-histidine in basic solution by carbon-13 magnetic resonance spectroscopy. *J. Am. Chem. Soc.* **95,** 338–341.
26. Garrett, D. S., Seok, Y. J., Peterkofsky, A., et al. (1999) Solution structure of the 40,000 Mr phosphoryl transfer complex between the N-terminal domain of enzyme I and HPr. *Nat. Struct. Biol.* **6,** 166–173.
27. Wuthrich, K. (1986). *Protein NMR spectroscopy*, Wiley, New York.
28. Clore, G. M. and Gronenborn, A. M. (1998) Determining the structures of large proteins and protein complexes by NMR. *Trends Biotechnol.* **16,** 22–34.
29. Bax, A., Vuister, G. W., Grzesiek, S., et al. (1994) Measurement of homo- and heteronuclear J couplings from quantitative J correlation. *Methods Enzymol.* **239,** 79–105.
30. Cavanagh, J., Fairbrother, W. J., Palmer, A. G., 3rd, et al. (1996) *Protein NMR Spectroscopy*, Academic, San Diego, CA.
31. Bax, A., Kontaxis, G., and Tjandra, N. (2001) Dipolar couplings in macromolecular structure determination. *Methods Enzymol.* **339,** 127–174.
32. Prestegard, J. H. and Kishore, A. I. (2001) Partial alignment of biomolecules: an aid to NMR characterization. *Curr. Opin. Chem. Biol.* **5,** 584–590.
33. Tolman, J. R., Flanagan, J. M., Kennedy, M. A., et al. (1995) Nuclear magnetic dipole interactions in field-oriented proteins: information for structure determination in solution. *Proc. Natl. Acad. Sci. USA* **92,** 9279–9283.
34. Feeny, J., Birdsall, B., Bradbury, A. F., et al. (2001) Calmodulin tagging provides a general method of using lanthanide induced magnetic field orientation to observe residual dipolar couplings in proteins in solution. *J. Biomol. NMR* **21,** 41–48.

35. Ma, C. and Opella, S. J. (2000) Lanthanide ions bind specifically to an added "EF-hand" and orient a membrane protein in micelles for solution NMR spectroscopy. *J. Magn. Reson.* **146,** 381–384.
36. Tian, F., Valafar, H., and Prestegard, J. H. (2001) A dipolar coupling based strategy for simultaneous resonance assignment and structure determination of protein backbones. *J. Am. Chem. Soc.* **123,** 11,791–11,796.
37. Mueller, G. A., Choy, W. Y., Yang, D., et al. (2000) Global folds of proteins with low densities of NOEs using residual dipolar couplings: application to the 370-residue maltodextrin-binding protein. *J. Mol. Biol.* **300,** 197–212.
38. Sherman, M. A., Chen, Y., and Mas, M. T. (1997) An engineered amino-terminal domain of yeast phosphoglycerate kinase with native-like structure. *Protein Sci.* **6,** 882–891.
39. Clore, G. M. (2000) Accurate and rapid docking of protein-protein complexes on the basis of intermolecular nuclear overhauser enhancement data and dipolar couplings by rigid body minimization. *Proc. Natl. Acad. Sci. USA* **97,** 9021–9025.
40. Abragam, A. (1961) *The Principles of Nuclear Magnetism*, Clarendon, Oxford.
41. Stone, M. J., Fairbrother, W. J., Palmer, A. G., 3rd, et al. (1992) Backbone dynamics of the *Bacillus subtilis* glucose permease IIA domain determined from ^{15}N NMR relaxation measurements. *Biochemistry* **31,** 4394–4406.
42. Pelton, J. G., Torchia, D. A., Meadow, N. D., et al. (1992) Structural comparison of phosphorylated and unphosphorylated forms of III^{Glc}, a signal-transducing protein from *Escherichia coli*, using three-dimensional NMR techniques. *Biochemistry* **31,** 5215–5224.

18

Molecular Modeling and Molecular Dynamics Simulations of Membrane Transporter Proteins

Donard S. Dwyer

1. Introduction

In silico methods are increasingly being used to address problems of biological significance. In the realm of structural biology, computational approaches have been applied to modeling the three-dimensional (3D) conformation of proteins and other molecules whose structures have not been solved, to simulate dynamic functions of proteins (such as catalysis and transport) ***(1–6)***, to study interactions between ligands and their receptors (docking) ***(7–9)***, and to perform initial screens in drug discovery efforts ***(10,11)***. With recent advances that have increased the speed of computations (i.e., "faster chips") and with greater sophistication of software programs, it is now possible to undertake computational projects related to protein structure and folding that would have been virtually impossible 5–10 yr ago. There are two areas where computational methods have provided significant new insights into protein structure, namely molecular modeling and molecular dynamics (MD) simulations. This chapter will describe the theory and methodology related to these procedures.

Generally, there are two major goals for computational studies of transporter proteins: (1) to model the 3D conformation of a protein whose structure has not been solved and (2) to analyze transport at the molecular level with MD simulations. These types of study are necessitated by the fact that X-ray crystal structures of relatively few transporter proteins are available for detailed analysis. Recently, the structures of several transporters have been derived including that of mannose/sucrose porins ***(12,13)***, aquaporin ***(14)***, the glycerol facilitator GlpF ***(15)***, and the MsbA protein from *Escherichia coli* ***(16)***, which is a member of the ATP-binding cassette (ABC) transporter family. In addi-

From: *Methods in Molecular Biology, vol. 227: Membrane Transporters: Methods and Protocols*
Edited by: Q. Yan © Humana Press Inc., Totowa, NJ

tion, X-ray structures of related ion channel proteins—the potassium channel from *Streptomyces lividans* ***(17)***, the mechanosensitive ion channel from *Mycobacterium tuberculosis* ***(18)***, and prokaryotic chloride channels ***(19)***—have been solved. This structural information has enhanced our understanding of the movement of substrates across cell membranes. However, many transporters have a complex topology, with 10–16 transmembrane (TM) segments, and it may be difficult to obtain high-resolution crystal structures of these proteins. Consequently, a number of groups have resorted to molecular modeling to provide structures of transporter and ion channel proteins for further investigation. A partial list of proteins characterized by this approach includes symporters and antiporters ***(4,20)***, glucose transporters (GLUTs) ***(5,21,22)***, the dipeptide transporter PepT1 ***(23)***, ionotropic glutamate receptors ***(3)***, and sodium and potassium channels ***(2,24)***. In some cases, transport of ions or glucose via these proteins has been studied by MD methods ***(2,5,24)***. In one of the most sophisticated studies to date, the movement of water through aquaporin or GlpF embedded in a lipid bilayer has been analyzed in 10-ns MD simulations ***(25)***. These studies approach "real-time" analysis of dynamic protein function *in silico*.

Molecular modeling of transport processes can potentially be accomplished by one of several different strategies: homology modeling, analogy modeling (or threading), or modular blueprints. The first two methods rely on a template structure that is either homologous to the protein of interest or is structurally similar for the assignment of atomic coordinates. The starting point for model building involves identification of the best template (through homology searches and sequence and structure alignments) whose 3D structure is already known. By contrast, the modular blueprint approach involves the assembly of individual structural components (e.g., α-helices) into a complex protein in the absence of a template by relying on information from mutational analyses and/or biochemical studies. This information specifies the global arrangement of secondary structures and the relative positioning of modular domains in the molecule. Although the models derived by these approaches are not high-resolution structures of the protein, they can provide significant insights into structure–function relationships.

There are important theoretical foundations upon which molecular modeling and MD studies are based. A fundamental assumption of molecular modeling is that the rules that govern protein folding are consistent and deterministic. Otherwise, a single protein could conceivably assume multiple native conformations, and structural variability among homologs could be significant. Second, with enough accurate information, it should be possible to predict the structure of a protein on the basis of its amino acid sequence, in other words, the sequence dictates the folding pattern of a pro-

tein. The accuracy of secondary-structure prediction algorithms is approaching 80% and *ab initio* prediction schemes have met with some success ***(26)***. Third, it is assumed that there are a limited number of structural motifs that are used in nature to build domains and entire proteins ***(27,28)***. At the secondary-structure level, there are α-helices, β-strands, and loop or coil conformations. At the protein level, there are β-barrels, helical bundles, trefoils, immunoglobulin folds, and other highly recurring motifs, which support the notion of a limited set of optimum protein structures. Finally, MD calculations are based on the premise that important molecular properties can be reduced to simplified mathematical representations of molecular mechanics principles. Although molecular modeling and dynamics programs will continue to be improved and refined, the current methods have already provided an invaluable tool for research in structural biology.

2. Materials

The computational demands of molecular modeling/MD studies require the use of a powerful workstation in order to handle a large number of atoms in a reasonable time frame. The studies described here were performed with a Silicon Graphics Indigo2 extreme workstation with a R4400 processor. The SGI Octane 2 system (R12000A 400 MHz processor) would be a current example of a preferred platform for such studies. Molecular modeling software is available from a number of different companies and university websites. For the present studies, Insight II software from Molecular Simulations, Inc. (now Accelrys; San Diego, CA) was used. This package included the Homology module for model building, Biopolymer for constructing and modifying peptides/proteins from assorted building blocks and for the selection of force fields, assignment of partial charges, and so forth, and the Discover module for energy minimization and MD simulations. One alternative source of modeling software is Tripos (St. Louis, MO). For 3D visualization of protein structures, a stereoscopic system (CrystalEyes®) from StereoGraphics (San Rafael, CA) was used. This system is invaluable for model building to check side-chain orientations, to inspect for bumps and to select the best-fitting loop.

3. Methods

3.1. Modeling

3.1.1. Homology Modeling versus Modular Blueprint Methods

The choice of starting point for molecular modeling will depend on the availability of 3D structures of protein homologs or analogs. Ideally, one would build a model on the basis of the atomic coordinates of a highly homologous

protein. From a practical standpoint, it may sometimes be necessary to employ a modular *ab initio* approach if a suitable structure is not available. Because this latter approach is highly idiosyncratic, it will not be discussed further here. A recent example of successful application of this strategy to modeling the GLUT1 glucose transporter has recently been published ***(22)***. This chapter will cover homology modeling and threading approaches to model building.

3.1.2. Template Selection and Sequence Alignment

The goal of template selection is to identify a protein from a structural database that most closely resembles the protein of interest to be modeled (*see* **Note 1**). A useful starting point for modeling transporter proteins is to predict the location of the TM segments of the protein (*see* **Note 2**). The Kyte-Doolittle hydropathy plot has commonly been used for this purpose. More sophisticated methods, such as PHDtopology (www.embl-heidelberg.de/predictprotein/predictprotein. html), provide a more detailed analysis of the protein topology. The next step involves selection of the reference protein. In some cases, this choice may be obvious because of the availability of the 3D structure of a close homolog. In other cases, an automated search of structural databases may be necessary. Several automated search programs can be accessed via the Internet at the following sites: EMBL-PredictProtein (embl-heidelberg.de/predictprotein/predictprotein.html), UCLA-DOE Structure Prediction Server (fold.doe-mbi.ucla.edu), and the SCOP server (scop.mrc-lmb.cam.ac.uk/scop/aln.cgi). Threading approaches, based on multiple sequence alignments are available from the EMBL–PredictProtein site, the GenTHREADER program developed by Jones et al. ***(29)***, and commercial sources (Accelrys). From these searches, the template protein is selected and an initial amino-acid-sequence alignment is obtained.

It is important that the overall alignment be optimized according to available biochemical information (*see* **Note 3**). Secondary-structure prediction alogrithms can be used to reveal potential initiation and termination points of structural elements such as α-helices and β-strands. This information can also be used to confirm that homologous regions of proteins have a tendency to adopt similar secondary structures. Older methods, such as Chou–Fasman ***(30)*** and GOR II ***(31)***, are adequate for most analyses of this type; however, newer algorithms offer greater refinement. These include the PHDsec algorithm and the PROF secondary-structure prediction program (www.aber.ac.uk/~phiwww/prof).

Additional biochemical information should be incorporated into the model at this stage (*see* **Note 3**). For example, if it is known that two cysteine residues form a disulfide bond in the model protein, then the reference protein should

be checked to ensure that the corresponding amino acids in the template are close enough in space to allow disulfide formation. If the initial alignment appears inadequate, it may be possible to shift the sequences through the introduction of gaps or by modifying the position of nearby loops to obtain a more favorable alignment. In automated model building (*see* **Subheading 3.1.3.**), this information can be incorporated via distance restraints. Additional information can be used to guide the sequence alignment, including location of glycosylation sites at the surface of the protein, the results of crosslinking studies that reveal the relative location of particular amino acids, and findings from scanning mutagenesis experiments.

3.1.3. Assignment of Atomic Coordinates to the Model Protein

Once the amino acid sequences of the model protein and the template have been aligned, the next step is to assign atomic coordinates to the model (*see* **Note 4**). The model can be constructed in one step with programs such as MODELLER, which is available at Rockefeller University (guitar.rockefeller.edu/modeller/modeller.html). Alternatively, the coordinates of the model can be obtained automatically with a modular approach such as SWISS-MODEL (www.expasy.org). Our model of GLUT3 was constructed with the modular approach of the Homology software of the Insight II package ***(5)***. On the basis of the sequence alignment, structurally conserved regions (SCRs) were defined in the model protein. As a general rule, the SCR should not include more than one element of secondary structure and cannot span gaps in the sequence alignment. The optimum boundaries of the SCRs are determined by calculating root mean square (rms) values and homology scores for segments of varying lengths in comparison to the reference protein(s). Homology can be scored on the basis of the Dayhoff ***(32)*** convention, however, other scoring matrices could also be used. In the Insight II environment, SCRs are then delineated with boxes that surround the desired amino acid sequences (*see* **Fig. 1**). The model is built in piecemeal fashion by transferring the atomic coordinates of the reference protein to the model protein for each of the SCRs. During this process, the amino acids from the model protein are superimposed on those of the template with the major difference being the length and composition of the projecting side chains.

3.1.4. Building Loop Segments

The most variable regions of conserved proteins are the loops or turns that connect elements of regular secondary structure—the α-helices and β-strands. Moreover, the loops or turns from homologous proteins are often variable in length, leading to the introduction of gaps in the aligned sequences. For these

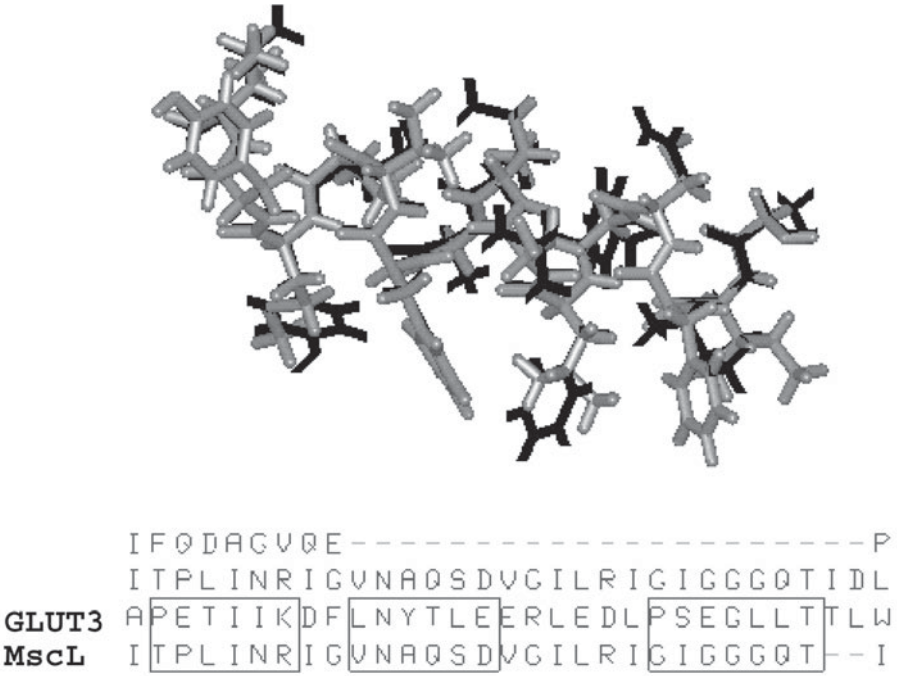

Fig. 1. Assignment of atomic coordinates to SCRs. A partial sequence alignment is shown at the bottom of the figure for the GLUT3 glucose transporter and the MscL ion channel. Sequences surrounded by boxes represent SCRs. Atomic coordinates have been assigned to such an SCR from GLUT3 (light gray) on the basis of the template protein (black). The Cα atoms show good overlap, whereas the side chains differ in their lengths and orientations.

regions, designation as an SCR is not an option. The variable segments must be built by inserting loops of known structure in the gaps between SCRs. Loops are selected automatically via a search algorithm that computes a distance matrix for the flanking SCR segments and compares this with values calculated from a population of source proteins with an intervening peptide and flanking regions of the same length as in the model protein. The search is typically restricted to a database of proteins whose structures are resolved to <2.5 Å. The 10 best loops are identified in terms of rms scores. These loops are then inspected individually to determine which one best fits into the gap (i.e., that connects the SCRs while avoiding steric clash). The selection process is facilitated by 3D visualization of the protein and loop segments with the stereographics system. With the Insight II software, it is also possible to generate loops *de novo* that can be used in the event that no suitable choices are

found in database searches. The best-fitting loop is then selected and atomic coordinates are assigned.

3.1.5. Fixing Bumps and Other Adjustments to the Model

Steric clash (or bumps) can be introduced into the model protein during various stages of the modeling process. Differences in the length or disposition of the side chains relative to the template can create bumps, and loop building is often associated with steric overlap at the junction between the inserted loop and the SCRs. These unfavorable geometries must be corrected before energy minimization and refinement of the model are attempted. A search of interatomic distances reveals any significant steric overlap. Side-chain geometry can be corrected automatically by applying the rotamer command. In other cases, it may be necessary to manually rotate an amino acid side chain that is too close to its neighbor. Sometimes, more extensive adjustments must be made to the model structure. The Insight II software allows rotation about essentially any two atoms in the protein. The application of torsion to a segment allows movement of a defined region relative to the rest of the protein in order to obtain the desired conformation. At this stage, the only parts of the model protein that may require adjustment are the N- and C-terminal ends. An automated approach can be used to repair these segments and manual assignment of structures is also possible.

3.1.6. Force Fields

The force field is a mathematical representation of the potential energy function of a molecule (*see* **Note 1**). Various properties are parameterized, including bond stretching, bond angles, torsions, and van der Waals and electrostatic forces. This information is used for calculations related to energy minimization and MD runs. A number of force fields are suitable for studies of protein conformations, including AMBER ***(33)***, CHARMM ***(34)***, CVFF ***(35)***, and CFF91 ***(36)***, to name a few. The choice will depend on availability in a particular software package, additional improvements in these force fields, and experience with a particular method. We have found AMBER and CVFF to be particularly useful for molecular modeling projects involving a wide variety of proteins.

3.1.7. Energy Minimization

At this stage, the refined structure of the model protein is not in the lowest-energy conformation. The process of energy minimization proceeds through a series of steps, often involving several different algorithms. The initial model at this point typically has a high potential energy as a result of unfavorable

geometries that remain. The steepest-descents algorithm is a robust method of producing an initial lower-energy conformation of the protein. The method relies on a line search along a direction vector that is updated after each iteration. In our experience, 300–1000 iterations with this method are sufficient as an initial step in energy minimization. The conjugate gradients algorithm represents a successive refinement of the direction vector by the addition of an orthogonal gradient term to the computation. This method has the advantage of more efficient convergence as the system approaches the energy minimum. Energy minimization is monitored continuously and can be terminated upon convergence to some cutoff value (e.g., in the range of 0.02–0.5 kcal/mol Å for large proteins). In some cases, further minimization may be needed and switching to another algorithm, such as the Newton–Raphson method, may yield better results. Computational time is much greater with this algorithm and the added degree of refinement may not be required for most large protein structures. The optimum end point for energy minimization is somewhat arbitrary. Ideally, minimization would be terminated when the average derivative approaches a value on the order of 0.005 kcal/mol Å; however, if additional MDs will be performed, it may not be necessary to reach this point.

3.2. Molecular Dynamics

There may be several purposes for undertaking MD studies of a protein. A major use of this method is to further improve a molecular model. This may be necessary if it is suspected that the structure obtained after energy minimization represents a local energy minimum rather than the global energy minimum of the protein. MD may also be used to simulate transport of substrate or to characterize functional regions of transporter proteins and ion channels (*see* **Note 4**). For MD studies, a force field is selected and the potentials and partial charges on the protein are set accordingly. Next, a discrete kinetic energy is imparted on the atoms of the molecule through a velocity term that is related to the temperature of the system. By dividing the applied force by the mass of the atom, the acceleration of each atom can be calculated. The projection of the acceleration of the atoms over time in relation to the initial coordinates describes the MD trajectory. Atomic coordinates are saved periodically during the simulation and the resulting ensemble of structures can be analyzed to determine if a particular conformation represents a more realistic version of the model protein. Additional energy minimization can be performed on structures from the MD trajectory to derive the final structure of the model. The authenticity of the model can be evaluated by assessing various features such as the Ramachandran scores and the number of polar residues buried in the hydrophobic core of the protein. In addition, programs such as Verify3D (doe-

mbi.ucla.edu/ Services/Verify_3D) can be used to judge the quality of the model structure.

For the case study described here, MD simulations were performed to study glucose transport in a molecular model of the GLUT3 protein. An assembly was created that included both halves of the GLUT3 model and a molecule of glucose positioned near the selectivity filter of the pore. Restraints were imposed on the model in order to maintain the relative position of the two halves throughout the simulation. Several pairs of residues at the interface were constrained with a force constant of 50 kcal/mol Å^2. In addition, the Cα atom of residue 321 was fixed in order to provide a constant landmark for the simulation. For the MD run, the CVFF force field was used with a 1-fs time step. The dielectric constant was set to 1 to represent that of the membrane environment. A nonbond cutoff of 20 Å was employed and the final temperature of the system was 310°K. The MD simulation spanned 15 ps, including 3 ps for equilibration. Temperature and energy factors stabilized during this equilibration period. Atomic coordinates from the trajectory were saved every 400 iterations and each frame was inspected to evaluate the movement of glucose through the transporter. During the course of the simulation, glucose traveled over 5 Å in the pore. Two views from the simulation are depicted in **Fig. 2**. The data show movement of glucose in the pore region over approx 5 Å in going from (A) to (B). The overall structure of GLUT3 remains rather constant through the simulation. However, more subtle changes, including a tilt in the TM segments and partial unraveling of the helices, accompany transport of glucose through the pore. In addition, different subsets of amino acids interact with glucose as it moves through the channel and the nature of these contacts provides information about the transport process. A detailed discussion of the findings from this MD simulation has been published previously ***(5)***.

The MD trajectory with GLUT3 represents a minimalist approach to such simulations, which was dictated in part by the large number of atoms in the assembly and the length of the computations. For other MD simulations, we have added solvent in order to more closely model real conditions. In the Insight II environment, water is added to an assembly with the Soak command to create a specified layer of solvent. The movement of solvent can be controlled by tethering with a high-force constant or, preferably, by the use of periodic boundary conditions. The inclusion of solvent may improve the performance of the system, especially if hydrophobic effects are a driving force for rearrangements of the protein conformation.

The last issue for MD simulations concerns the length of the run (*see* **Note 5**). The size of the system (i.e., the more atoms in the assembly, including solvent, lipid, and any heteroatoms) and the power of the computer will determine the

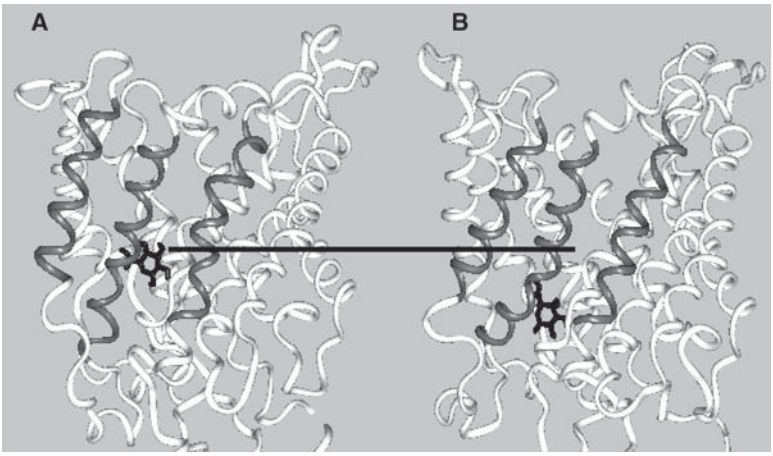

Fig. 2. MD simulation of glucose transport in GLUT3. A ribbon diagram of GLUT3 is shown here together with glucose (in black) near the top of the selectivity filter region of the pore **(A)** and near the exit site **(B)**. For comparison, a line was drawn to serve as a landmark. Several helices have been highlighted with darker shading to illustrate some of the conformational changes that accompany the transport of glucose. The TM segments have a greater degree of tilt (on average) as glucose moves through the pore, and there is some unraveling of the middle helix in the vicinity of the glucose molecule. Reversible conformational changes such as these may allow transport of substrate while providing a restrictive barrier to the passage of other molecules through the pore.

practicality of running long simulations. With moderate-sized assemblies and older computers, it may require 2–3 wk to perform a 50- to 100-ps simulation. The overall goal of most simulations is to reach equilibrium at a given temperature (and perhaps pressure) and to examine protein conformations along the pathway toward this equilibrium. One way to monitor whether a system has achieved equilibration is to determine if various thermodynamic quantities, such as the temperature and energy values, have stabilized over time. Another useful indicator of equilibration is to run several MD simulations with different initial velocities (generated through a random number seed) and to check whether there is convergence to a common final structure. In many cases, MD simulations on the order of 20–100 ps are sufficient to evaluate conformational changes in a protein or to explore the possibility of other lower-energy conformers of the model protein. To model processes that take place over a longer time-scale, such as transport of substrate, it may be necessary to perform simulations that last on the order of 1 ns or more (*see* **Note 6**).

4. Notes

1. A number of points are worth bearing in mind when considering molecular models of proteins. The model is, by definition, a low-resolution counterpart of the real protein structure; overinterpretation of results based on a model should be avoided. Molecular modeling is subject to many unintentional biases. For instance, selection of the reference protein will be biased by the composition of the databases used for searching. Most protein structural databases have relatively few structures of integral membrane proteins with complex topologies because of the inherent difficulties in the expression, purification and crystallization of such proteins. Moreover, structure–prediction algorithms have been trained on a population of proteins that reflect the state of the art today, but not the entirety of possible structures in nature. The force fields used for energy minimization and MD studies may be oversimplified in some respects and the results obtained in a simulation may vary depending on the force field used for the calculations. This means that empirical methods must often be employed to determine the best force field to use for a particular problem in molecular modeling. Despite these various shortcomings, great strides have been made in modeling various protein structures and simulating elaborate processes such as transport and ion flux ***(2,5,24,25)***.
2. Progress in this field has been hampered by the fact that most transporter proteins have a complex topology with multiple TM segments and numerous possible arrangements of these segments to form a pore. Although some common features are beginning to emerge from the structures of the transporters and ion channels solved thus far, it is clear that there is not a single blueprint for the assembly of transport proteins. In general, there appears to be a weak correlation between the size of the substrate that is transported and the number of TM segments in the transporter protein. GLUTs have 12 TM helices, whereas most of the ion channels and transporters whose structures have been solved have 4–6 TM segments. Therefore, we chose to build the model of GLUT3 in two parts, with each half comprised of six TM helices based on the overall arrangement of the MscL ion channel. This choice was rationalized on the grounds that GLUTs appear to have arisen during evolution from a gene duplication event. Biochemical data also supported the choice of an ion channel as the template protein, namely the observation that many calcium channel blockers inhibit glucose transport at the level of the GLUT protein ***(37)*** and the finding of amino acid sequence similarities between calcium channels and other transporter proteins in their TM segments ***(38)***. Although the assumptions that are applied to the choice of templates for molecular modeling may be justified, it is helpful to remain skeptical about these assumptions and to implement an ongoing process of model refinement. Nevertheless, creative insights are an important component of molecular modeling and instinctive judgments about the "reality" of a model structure may provide an additional level of quality control.

3. With homology modeling and threading methods, the molecular model is only as good as the sequence/structure alignment. Therefore, it is critical that the alignment be optimized right from the start. Subsequent adjustments to the model are typically difficult to make without disrupting the overall conformational integrity of the protein. Rapid construction of a partial mock-up of the model can be useful for identifying the major limitations of a particular alignment. Available biochemical data should be factored into the derivation of the best sequence alignment. If the pattern of disulfide bonds is known, this information can be extremely useful in determining the final position of cysteine residues in the model. The corresponding amino acids in the template need to be within about 2–4 Å of each other to approximate a disulfide bond. Another important consideration in deriving the final alignment concerns the orientation of amino acids in the TM segments. In many transporter proteins, these segments are likely to assume an α-helical conformation. Secondary-structure–prediction algorithms can be used to confirm this possibility. Typically, the more polar residues will line the pore of the transporter protein, whereas hydrophobic residues will face away from the solvent or substrate channel and tend to stabilize interhelical contacts. Projection of the amino acids in a TM segment according to a helical wheel can reveal a potential polar face of the helix that might be expected to line the pore. This orientation can be transferred onto the template protein so as to create a more polar environment for the protein pore. Nevertheless, there may be some exceptions to the relative polarity of the pore region. For instance, in our model of GLUT3, a number of aromatic residues were found to project toward the solvent-accessible region of the pore ***(5)***. These residues were suggested to play a role in the transport process by providing a slippery path for glucose to traverse without the formation of stable hydrogen bonds along the way. Finally, chemical crosslinking or other data may guide the positioning of amino acid residues in the pore region.
4. In terms of the general strategy for creating a molecular model, automated single-step methods have the advantage that multiple models can easily be built and evaluated. On the other hand, the modular approach outlined here offers more flexibility in the design of the model and is much simpler to customize in order to meet the special requirements of a particular protein. There are also a number of choices in the design of MD studies. Ideally, solvent and lipids should be included in simulations of transporter function. From our own experience, the presence of solvent may help to drive conformational changes in proteins that are promoted by hydrophobic effects ***(39)***. Solvent can be included as explicit water molecules whose mobility is restricted by tethering forces. Alternatively, motion in the solvent shell can be governed by periodic boundary conditions. Temperature is another variable that affects the results of MD simulations. Although 300 K is used for most studies, we have found that higher temperatures (310–315 K) can sometimes produce better results ***(39)***. Higher temperatures may be useful for studies of protein denaturation or to generate greater variability in the ensemble of structures obtained from a trajectory.

5. As a general rule, longer MD simulations (>50–100 ps) may provide a more accurate picture of the dynamic state of a protein. Simulations of water and glycerol transport that lasted 1 ns and longer have been performed and reveal precise details about mechanisms of transport ***(25,40)***. However, we have found that conformational changes, which mimic real transitions in proteins, can be observed with much shorter simulations (around 20 ps) ***(39,41)***. The length of the MD run may depend on the main objective of the study. Functional processes with a long time-scale, such as transport or unfolding, may require a longer simulation to characterize the underlying mechanisms. For the simulation of ligand-induced conformational changes or catalysis, a shorter run may be sufficient.
6. The last area that merits comment concerns strategies to reduce computing time in MD studies. Obviously, a faster computer is one solution to the problem and distributing the computational task over multiple processors may be an option. Another time-saving method is to minimize the number of atoms in the system. This usually means reducing the number of solvent molecules in the assembly. In some cases, it may be possible to reduce computing time by fixing (constraining) parts of the protein during the MD simulation. This shortcut can be implemented if it is known that certain domains or regions of the protein contribute negligibly to the conformational changes that are under investigation. A valid alternative to performing a single extended simulation of a process is to run several shorter simulations (each with a different initial velocity) and to evaluate the trajectories for evidence of convergence to a consensus conformation. By adjusting variables such as temperature, the force field, and applied restraints, it may be possible to empirically derive conditions that allow optimization of the output from the simulation relative to the time spent. Finally, new approaches to MD simulations, such as the multiple-time-step method ***(42)***, can reduce the time needed to effectively characterize a system under dynamic conditions. With the approaches outlined here (and described in the references and websites), the possibility of modeling transport processes at the molecular level has become a reality. It is now a matter of harnessing the technology to fulfill the imagination of the computational biologist.

References

1. Kumosinski, T. F. and Liebman, M. N. (eds.) (1994) *Molecular Modeling. From Virtual Tools to Real Problems.* American Chemical Society, Washington, DC.
2. Smith, G. R. and Sansom, M. S. P. (1998) Dynamic properties of Na^+ ions in models of ion channels: a molecular dynamics study. *Biophys. J.* **75,** 2767–2782.
3. Sutcliffe, M. J., Smeeton, A. H., Wo, Z. G., et al. (1998) Molecular modeling of ligand-gated ion channels. *Methods Enzymol.* **293,** 589–620.
4. Durell, S. R. and Guy, H. R. (1999) Structural models of the KtrB, TrkH, and Trk1,2 symporters based on the structure of the KcsA K^+ channel. *Biophys. J.* **77,** 789–807.
5. Dwyer, D. S. (2001) Model of the 3D structure of the GLUT3 glucose transporter and molecular dynamics simulation of glucose transport. *Proteins* **42,** 531–541.

6. Bertaccini, E. and Trudell, J. R. (2001) Molecular modeling of ligand-gated ion channels: progress and challenges. *Int. Rev. Neurobiol.* **48,** 141–166.
7. Pattabiraman, N., Levitt, M., Ferrin, T. E., et al. (1985) Computer graphics in real-time docking with energy calculation and minimization. *J. Comput. Chem.* **6,** 432–436.
8. Jones, G., Willett, P., Glen, R. C., et al. (1997) Development and validation of a genetic algorithm for flexible docking. *J. Mol. Biol.* **267,** 727–748.
9. Bissantz, C., Folkers, G., and Rognan, D. (2000) Protein-based virtual screening of chemical databases. 1. Evaluation of different docking/scoring combinations. *J. Med. Chem.* **43,** 4759–4767.
10. Boehm, H. J., Boehringer, M., Bur, D., et al. (2000) Novel inhibitors of DNA gyrase: 3D structure based biased needle screening, hit validation by biophysical methods, and 3D guided optimization. A promising alternative to random screening. *J. Med. Chem.* **43,** 2664–2674.
11. Terstappen, G. C. and Reggiani, A. (2001) In silico research in drug discovery. *Trends Pharmacol. Sci.* **22,** 23–26.
12. Schirmer, T., Keller, T. A., Wang, Y.-F., et al. (1995) Structural basis for sugar translocation through maltoporin channels at 3.1 Å resolution. *Science* **267,** 512–514.
13. Forst, D., Welte, W., Wacker, T., et al. (1998) Structure of the sucrose-specific porin ScrY from *Salmonella typhimurium* and its complex with sucrose. *Nature Struct. Biol.* **5,** 37–46.
14. Murata, K., Mitsuoka, K., Hirai, T., et al. (2000) Structural determinants of water permeation through aquaporin-1. *Nature* **407,** 599–605.
15. Fu, D., Libson, A., Mierke, L. J., et al. (2000) Structure of a glycerol-conducting channel and the basis for its selectivity. *Science* **290,** 481–486.
16. Chang, G. and Roth, C. B. (2001) Structure of MsbA from *E. coli*: a homolog of the multidrug resistance ATP binding cassette (ABC) transporters. *Science* **293,** 1793–1800.
17. Doyle, D. A., Cabral, J. M., Pfuetzner, R. A., et al. (1998) The structure of the potassium channel: molecular basis of K^+ conduction and selectivity. *Science* **280,** 69–77.
18. Chang, G., Spencer, R. H., Lee, A. T., et al. (1998) Structure of the MscL homolog from *Mycobacterium tuberculosis*: a gated mechanosensitive ion channel. *Science* **282,** 2220–2226.
19. Dutzler, R., Campbell, E. B., Cadene, M., et al. (2002) X-ray structure of a ClC chloride channel at 3.0 Å reveals the molecular basis of anion selectivity. *Nature* **415,** 287–294.
20. Varela, M. F., Sansom, C. E., and Griffith, J. K. (1995) Mutational analysis and molecular modelling of an amino acid sequence motif conserved in antiporters but not symporters in a transporter superfamily. *Mol. Membr. Biol.* **12,** 313–319.
21. Zeng, H., Parthasarathy, R., Rampal, A. L., et al. (1996) Proposed structure of a putative glucose channel in GLUT1 facilitative glucose transporter. *Biophys. J.* **70,** 14–21.

22. Zuniga, F. A., Shi, G., Haller, J. F., et al. (2001) A three-dimensional model of the human facilitative glucose transporter Glut1. *J. Biol. Chem.* **276,** 44,970–44,975.
23. Bolger, M. B., Haworth, I. S., Yeung, A. K., et al. (1998) Structure, function and molecular modeling approaches to the study of the intestinal dipeptide transporter PepT1. *J. Pharmaceut. Sci.* **87,** 1286–1291.
24. Capener, C. E., Shrivastava, I. H., Ranatunga, K. M., et al. (2000) Homology modeling and molecular dynamics simulation studies of an inward rectifier potassium channel. *Biophys. J.* **78,** 2929–2942.
25. de Groot, B. L. and Grubmueller, H. (2001) Water permeation across biological membranes: mechanism and dynamics of aquaporin-1 and GlpF. *Science* **294,** 2353–2357.
26. Orengo, C. A., Bray, J. E., Hubbard, T., et al. (1999) Analysis and assessment of ab initio three-dimensional prediction, secondary structure, and contacts prediction. *Proteins* **3(Suppl.),** 149–170.
27. Chothia, C. (1993). One thousand families for the molecular biologist. *Nature* **357,** 543–544.
28. Thornton, J. M., Orengo, C. A., Todd, A. E., et al. (1999) Protein folds, functions and evolution. *J. Mol. Biol.* **293,** 333–342.
29. Jones, D. T., Tress, M., Bryson, K., et al. (1999) Successful recognition of protein folds using threading methods biased by sequence similarity and predicted secondary structure. *Proteins* **3(Suppl.),** 104–111.
30. Chou, P. Y. and Fasman, G. D. (1978) Prediction of the secondary structure of proteins from their amino acid sequence. *Adv. Enzymol.* **47,** 45–148.
31. Garnier, J. and Robson, B. (1989) The GOR method for predicting secondary structures in proteins, in *Prediction of Protein Structure and the Principles of Protein Conformation* (Fasman, G. D., ed.), Plenum, New York, pp. 417–465.
32. Dayhoff, M. O., Schwartz, R. M., and Orcutt, B. C. (1983) Establishing homologies in protein sequences. *Methods Enzymol.* **91,** 524–545.
33. Weiner, S. J., Kollman, P. A., Case, D. A., et al. (1984) A new force field for molecular mechanical simulation of nucleic acids and proteins. *J. Am. Chem. Soc.* **106,** 765–784.
34. Brooks, B. R., Bruccoleri, R. E., Olafson, B. D., et al. (1983) CHARMM: a program for macromolecular energy, minimization, and dynamics calculations. *J. Comp. Chem.* **4,** 187–217.
35. Lifson, S., Hagler, A. T., and Dauber, P. (1979) Consistent force field studies of intermolecular forces in hydrogen-bonded crystals. 1. Carboxylic acids, amides, and the C=O...H hydrogen bonds. *J. Am. Chem. Soc.* **101,** 5111–5121.
36. Maple, J. R., Dinur, U., and Hagler, A. T. (1988) Derivation of force fields for molecular mechanics and dynamics from ab initio energy surfaces. *Proc. Natl. Acad. Sci. USA* **85,** 5350–5354.
37. Ardizzone, T. D., Lu, X.-H., and Dwyer, D. S. (2002) Calcium-independent inhibition of glucose transport in PC12 and L6 cells by calcium channel antagonists. *Am. J. Physiol.* **283,** C579–C586.

38. Dwyer, D. S., Ardizone, T. D., and Bradley, R. J. (2002) Psychoactive drugs affect glucose transport and the regulation of glucose metabolism. *Int. Rev. Neurobiol.* **51,** 501–530.
39. Dwyer, D. S. (2002) Molecular dynamics studies of the conformational change induced by ligand binding in PPAR-gamma. *FASEB J.* **16,** A740.
40. Jensen, M. O., Tajkhorshid, E., and Schulten, K. (2001) The mechanism of glycerol conduction in aquaglyceroporins. *Structure* **9,** 1083–1093.
41. Dwyer, D. S. (1999) Molecular simulation of the effects of alcohols on peptide structure. *Biopolymers* **49,** 635–645.
42. Schlick, T. (2001) Time-trimming tricks for dynamic simulations: splitting force updates to reduce computational work. *Structure* **9,** R45–R53.

19

Imaging Plasma Membrane Proteins by Confocal Microscopy

Stella W. Y. Tsang and Peter M. Haney

1. Introduction

Confocal microscopy has become a widely used method in the study of plasma membrane proteins. A Medline search for the terms "plasma membrane" and "confocal" returns over 1300 references since 1966. Of these, over 1000 references appeared in the past 5 yr, and over 500 in the past 2 yr. The recent widespread adoption of confocal microscopy is the result of the advantages of the method, which eliminates out-of-focus light, producing sharp, high-contrast images of cells and subcellular structures even within thick sections, and the availability of increasingly powerful, sensitive, and user-friendly instruments from several manufacturers. The purpose of this chapter is to provide guidance in the use of confocal microscopy in the study of subcellular localization and trafficking of membrane proteins. Protocols for immunostaining of fixed slides and for studying protein targeting in living cells are included. An outline for the use of confocal microscopy is provided, but readers must rely on the instruction manual provided with their instruments for details.

A full review of the principles of confocal microscopy is beyond the scope of this chapter. The reader is referred to an excellent overview ***(1)*** as well as several chapters of an earlier volume of this series devoted to confocal microscopy ***(2–8)***. Briefly, using a pinhole, a point source of light is focused into a point within the specimen and then the emitted light is focused onto a second pinhole, behind which there is a photodetector. All three planes are mutually in focus. The use of pinholes eliminates out-of-focus light. In modern instruments, laser light is scanned over the plane of the image in a rectangular pattern; the proportional intensity of the signal at each point in the pattern is displayed on a

From: *Methods in Molecular Biology, vol. 227: Membrane Transporters: Methods and Protocols*
Edited by: Q. Yan © Humana Press Inc., Totowa, NJ

video monitor and the data are stored digitally. The major pitfall of confocal microscopy is photobleaching, which can be minimized by using the least laser light for the shortest duration and by preparing specimens using agents that inhibit bleaching.

2. Materials

2.1. Double Immunofluorescent Staining of Fixed Specimens

1. 22 × 22-mm cover slips (baked at 200°C for 2 h).
2. Six-well tissue culture dishes.
3. Cells of interest and appropriate tissue culture media.
4. 4% Paraformaldehyde solution, in Dulbecco's modified Eagle's medium/Ham's nutrient mixture F12 (DMEM–F12) (microwave briefly to dissolve; cool; adjust pH to 7.4).
5. Phosphate-buffered saline (PBS).
6. Glycine, 100 m*M* in PBS.
7. Triton X-100, 0.1% in PBS.
8. Horse serum, 2% in PBS.
9. Horse serum, 0.1% in PBS.
10. Primary antibody.
11. Fluorescently labeled secondary antibody or antibody-binding fragment.
12. Antifade kit (Molecular Probes).
13. Clear fingernail polish.

2.2. Preparation of Living Cells for Confocal Microscopy

1. Custom-designed circular cover slips (baked at 200°C for 2 h).
2. Cells of interest, fluorescently labeled or expressing a fluorescent protein.
3. Bioptechs (Butler, PA) Focht Chamber System (FCS) a live cell chamber system.
4. 1/16-in. Tygon #2275 tubing.
5. Appropriate media.
6. Perfusion pump.

2.3. Confocal Microscopy

1. Confocal microscope.
2. Associated equipment (lasers, controller, computer, storage device).

3. Methods

3.1. Double Immunofluorescent Staining of Fixed Specimens

1. Sterilize forceps by flaming with ethanol and use them to transfer cover slips into the wells of a six-well tissue culture dish.
2. Harvest cells of interest and passage them into the wells. Allow at least several hours for attachment.
3. Change media. Allow growth to take place until cells are subconfluent to nearly confluent. Excessively dense growth of cells should be avoided.

4. Remove media and add 2 mL of 4% paraformaldehyde in DMEM–F12 media to each well to fix the cells on the cover slips. Incubate at room temperature for 20 min on shaker.
5. Remove paraformaldehyde. Replace with 2 mL of 100 m*M* glycine in PBS. Incubate at room temperature for 10 min on shaker.
6. Rinse twice with PBS using shaker at gentle setting to avoid dislodging cells.
7. Semipermeabilize the cells with 0.1% Triton X-100 in PBS. Incubate for 15 min at room temperature on shaker. Rinse twice with PBS.
8. Block nonspecific staining with 2% horse serum in PBS. Incubate for at least 15 min at room temperature. Rinse twice with PBS.
9. Label new six-well dishes for cover slip transfer. Carefully use a disposable scalpel to overcome the surface tension holding cover slips to the six-well dish. Using forceps, transfer cover slips, cell side up, to the clean six-well dish. Label dish and put new plates in the storage box. Prepare the storage box with wet paper towels to maintain humidity.
10. Make up the primary antibody in 0.1% horse serum with PBS. Centrifuge for 2 min in a benchtop minicentrifuge. Add about 150 µL of antibody solution per cover slip. Place dishes in storage box and store in 4°C overnight.
11. Remove primary antibody from the cover slips and rinse three times with PBS at room temperature for 5 min.
12. Make up the secondary antibody fluorescein isothiocyanate (FITC)–IgG or another appropriate fluorescent antibody in 1:100 dilution with 0.1% horse serum in PBS (*see* **Notes 1** and **2**). Centrifuge for 2 min in a benchtop minicentrifuge. Add about 150 µL to each cover slip and incubate for 1 h at room temperature in the dark.
13. Rinse three times with PBS at room temperature for 5 min. Put on the shaker and cover the plates to keep them in the dark. At this time, thaw out the solution from the antifade kit (Molecular Probes) and add 1 mL component B to tube A and mix.
14. Dab a drop (about 50 µL) of the mounting solution onto a clean, labeled slide and place cover slips onto the slide with cells facing down. Avoid bubbles. Do one at a time so that the mounting solution will not dry out.
15. Let the slides dry in the dark for about 15 min and seal them with clear nail polish (*see* **Note 3**).

3.2. Preparation of Living Cells for Confocal Microscopy

1. Sterilize forceps by flaming with ethanol and use them to transfer cover slips into the wells of a six-well tissue culture dish (*see* **Notes 4** and **5**).
2. Harvest cells of interest and passage them into the wells. Allow at least several hours for attachment. Change media.
3. On the following day, cells may be transfected using a variety of methods, including our preferred method, lipofection. This allows expression of constructs consisting of fusions of the protein of interest and fluorescent proteins such as blue, green, or yellow fluorescent protein, or more recently available, structurally unrelated, and less reliable red fluorescent proteins (*see* **Note 6**). Of course,

if cells are to be examined using a small-molecule fluorescent marker, such as BODIPY–Texas red (BODIPY–TR) ceramide, a marker of trans-Golgi, no transfection is required at this point.
4. Allow growth to take place until cells are subconfluent to nearly confluent. Excessively dense growth of cells should be avoided.
5. Release and disengage the chamber top by rotating the large knurled ring in the chamber base as far as possible.
6. Remove the black electrical contact unit by counterclockwise rotation of the two small knurled nuts on each side of the unit.
7. Attach perfusion tubing to inlet and outlet ports of the chamber.
8. Aligning the perfusion clearance holes with the perfusion tubes, place the upper gasket into the chamber.
9. Fit the microaqueduct slide on the upper gasket, aligned with perfusion tubes, groove side up.
10. Fit the lower gasket on the microaqueduct slide and create a seal by pressing along perimeter.
11. Perfuse enough media to clear air from chamber inlet, placing one drop in the chamber.
12. Place the cover slip, cell side down, on the drop of media in the chamber.
13. Place closure assembly on top of this stack, lining up the black electrical connector with oval gap in chamber top. Gently press together, turn over, and turn large knurled ring counterclockwise until tight, sealing the chamber.
14. Place black power/sensor connector back on two threaded posts and tighten knurled nuts, making sure that the wires contact the bus bars on the microaqueduct slide and that flat side of the surface probe is flush to the aqueduct slide.
15. Plug chamber into controller.
16. Mount objective heater (*see* **Note 7**).
17. Mount chamber onto microscope stage.
18. Begin perfusion of closed chamber with appropriate media (*see* **Notes 8–10**).

3.3. Confocal Microscopy

1. Power up the system, including light sources, lasers, controller, and computers and monitors. Start the appropriate software.
2. On the microscope, select the light path for direct observation, focus on the specimen, find an area of interest, and select the confocal light path (*see* **Note 11**).
3. In software, select the dyeing method (*see* **Note 12**).
4. On the scan unit, set the confocal aperture, detection mode, appropriate barrier filters, and neutral-density (ND) filter. Proper settings for the first three parameters should be available from properly configured software; the ND filter setting is varied depending on signal intensity, keeping in mind that the minimizing laser exposure of the sample minimizes its photobleaching. This is particularly important in studies of living cells.
5. In software, set the objective magnification to match the microscope objective, set the zoom to 1×, set the channels from which data will be collected, set the

highest scan speed, select the XY observation mode, and initiate repeated scanning (*see* **Note 13**).

6. In software, photo multiplier-tube (PMT) voltage must be adjusted for each channel. Display each channel using not the appropriate color but rather a high–low false-color scheme. Adjust the PMT voltage so that only a few pixels in the entire field of interest exhibit the highest intensity (*see* **Note 14**). It may be possible to further reduce laser intensity in software. The use of the lowest possible laser intensity is important to minimize photobleaching, particularly in studies of living cells.
7. In software, systematically vary the Z dimension while continuously scanning to define the optimal plane of focus, or, for a Z-series, to define the optimal starting and ending points of the Z-series.
8. Set the area to be observed, using zoom as needed to enlarge the area of interest until it fills the screen. For certain purposes, such as convincingly demonstrating reproducibility of a finding, low-power views including several cells may be needed. For other purposes, such as defining subcellular localization or examining membrane trafficking, very high zooms may be used, so that only a fraction of a cell fills the field. When examining single cells or portions of cells, it is very important to choose representative cells.
9. Stop repeated scanning. Acquire an image by selecting a single acquisition. For a fixed slide, consider using Kallman averaging over four to six scans of the same field, thereby reducing PMT noise and producing scans of much higher quality. Fields with very low signal can be effectively studied by repeated cumulative scanning. Save the image to a storage device (hard disk, CD, Zip disk, etc.). For Z-series, a series of optical sections collected at different levels from a specimen, Kalman averaging should also be considered, but may be time-consuming depending on the number of sections collected (*see* **Note 15**). Z-series may be used to construct three-dimensional representations of the scanned area using software supplied with the confocal microscope or available from third parties (*see* **Note 16**).
10. For living cells exhibiting dynamic changes, neither Kalman averaging nor repeated cumulative scanning may be used, as the result would be blurred data. Rather, select the slowest scan speed to acquire the highest-quality images. To capture very rapid processes, image quality is sacrificed to acquire scans at higher speeds. To demonstrate dynamic changes, a time series must be collected (*see* **Note 17**). The interval selected is a property of the phenomenon under study and can vary from a few seconds to 1 h or more. The number of images that can be collected may be limited by software or by available memory (*see* **Note 18**).
11. To display a Z-series or a time series as a movie, the images must be processed in software that creates QuickTime videos, Motion Picture Experts Group (file type) (MPEGs), or some other format that may be viewed using common software. An alternative is Macromedia Flash, which allows the creation of Flash Players that require no additional software to be viewed. Limitations of format and file size imposed by journals in which publication is considered should be kept in mind.

4. Notes

1. Autofluorescence, usually elicited by excitation wavelengths of 500 nm or less, can significantly increase background signal and decrease the signal-to-noise ratio. Proper selection of excitation wavelength, for example by use of cyanine 5 as a fluorescent probe, minimizes this problem.
2. Fluorescein isothiocyanate is the most commonly used fluorescent probe. It is water soluble and strongly fluorescent with an excitation maximum of 490 nm, very close to the 488 nm available on most confocal microscopes, and it is easily detected using standard filter sets. However, one should be aware that its fluorescence is sensitive to pH, is not useful if autofluorescence is observed, and has a long emission tail that can cause bleedthrough in double-labeling experiments.
3. It is very important to seal cover slips completely with nail polish to preserve the slides for long-term storage. In general, the sooner slides are viewed after preparation, the better. The signal may degrade and the background may increase over time.
4. In studies of living cells, cover slips, gaskets, and the white plastic portion of the chamber should be autoclaved before use.
5. Adherent cells on a cover slip, maintained safely in a temperature-controlled optical environment, may also be observed by low- and high-numerical-aperture (N.A.) objectives, transmitted, bright-field, dark-field, phase contrast, differential interference contrast (DIC), and reflected modes of fluorescence, as well as confocal.
6. Green fluorescent protein (GFP) is a 27kDa protein that is nontoxic, somewhat resistant to bleaching, and usually does not interfere with the targeting of proteins with which it is fused. Expression of GFP chimeras has been a powerful tool in understanding dynamic aspects of protein targeting in living cells. The recent expansion of commercially available similar fluorescent proteins, including blue, cyan, and yellow fluorescent proteins has added even more useful tools. Disappointingly, certain red fluorescent proteins structurally unrelated to GFP, such as DsRed1 and DsRed2, do not reliably reflect targeting of proteins to which they are fused.
7. In studies of living cells, the use of high-N.A. objectives will require the use of an objective heater to prevent the objective from acting as a heat sink.
8. In studies of living cells, a siphoning effect occurs as a result of the downward extension of the drain tubing, causing negative pressure in the chamber and distortion of the cover slip. Placing a “T fitting” at the height of the specimen breaks the siphon and prevents distortion.
9. In studies of living cells, the power/sensor connector cannot be immersed in liquid. A poor seal resulting in liquid coming into contact with the power/sensor connector will destroy it.
10. The perfusion tubing may be modified by placing a stopcock close to the chamber, permitting introduction of media containing agents of interest and the study of their effects.
11. In the choice of field, particularly in transfected cells, it is often wise to avoid the very brightest cells, as there may be saturation of natural targeting pathways and

consequent aberrant targeting. As a corollary, in transfection experiments, the goal is not high-level expression, but expression of the exogenous protein at a level similar to the endogenous level of the protein being studied.

12. The excitation wavelength does not need to match the absorption maximum of the dye, provided the extinction coefficient of the dye at that wavelength is sufficient.
13. Bleedthrough, the detection of fluorescence from the shorter-wavelength probe in the longer-wavelength channel, can cause confusion and false interpretation of images in double-labeling experiments. One can erroneously believe that there is colocalization of a green and a red label, seen as yellow in a merged image, when one is actually seeing bleedthrough. The extent of bleedthrough should be determined for each label pair in each cell type. If bleedthrough is a significant problem, scan with each laser sequentially rather than scanning with two lasers simultaneously.
14. Failure to properly adjust for PMT sensitivity may result in images that contain too much signal, in which signals of different intensities falsely appear equal, or in images that contain too little signal, which do not take advantage of the full range of signal intensity. Do not exceed PMT sensitivity recommendations made by the manufacturer; this would be potentially harmful to the instrument and also produces noisy images.
15. The term "optical section thickness" does not refer to the step size between sections of a Z-series, but rather to the thickness of a single scanned section of the sample. It is a function of the lens and pinhole aperture and is independent of step size. The higher the N.A. of the lens, the thinner the optical sections will be. However, the higher the N.A. of the lens, the smaller the working distance will be. When possible, a higher N.A. lens should be used to obtain the best resolution. The smaller the pinhole aperture, the thinner the optical section will be.
16. An important advantage of the confocal microscope with respect to membrane proteins, which may exhibit polarized targeting in epithelial cells, is that X–Z series can also be acquired, or generated by three-dimensional reconstruction. This allows comparison of targeting to apical membrane and basolateral membrane.
17. Four-dimensional imaging refers to the acquisition of Z-series over time.
18. It is important to develop a disciplined and systematic approach to selecting file names. It is also important to develop a systematic approach to storage of data in a manner that facilitates its retrieval. Make sure that associated information, such as magnification, pixel size, and so forth, is not lost, or else the addition of size bars for publication will be difficult.

Acknowledgments

Support was provided by NIH grant 1R29HD/DK34701. This project of the USDA/ARS Children's Nutrition Research Center, Department of Pediatrics, Baylor College of Medicine and Texas Children's Hospital has been funded in part with federal funds from the USDA/ARS under cooperative agreement number 58-6250-6-001.

The contents of this publication do not necessarily reflect the views or policies of the U.S. Department of Agriculture, nor does mention of trade names, commercial products or organizations imply endorsement by the U.S. government.

References

1. Pawley, J. B. and Centonze, V. E. (1994) Practical laser-scanning confocal light microscopy: obtaining optimal performance from your instrument, in *Cell Biology: A Laboratory Handbook* (Celis, J. E., ed.), Academic, San Diego, CA, Vol. 2, pp. 44–64.
2. Paddock, S. W. (1999) An introduction to confocal imaging, in *Confocal Microscopy: Methods and Protocols*. (Paddock, S. W., ed.), Humana Totowa, NJ, pp. 1–34.
3. Carter, D. (1999) Practical considerations for collecting confocal images, in *Confocal Microscopy: Methods and Protocols*. (Paddock, S. W., ed.) Humana, Totowa, NJ, pp. 35–58.
4. Langeland, J. A. (1999) Imaging immunolabeled *Drosophila* embryos by confocal microscopy, in *Confocal Microscopy: Methods and Protocols*. (Paddock, S. W., ed.) Humana, Totowa, NJ, pp. 167–172.
5. Kulesa, P. M. and Fraser, S. E. (1999) Confocal imaging of living cells in intact embryos, in *Confocal Microscopy: Methods and Protocols*. (Paddock, S. W., ed.) Humana, Totowa, NJ, pp. 205–222.
6. Francis-Lang, H., Minden, J., Sullivan, W., et al. (1999) Live confocal analysis with fluorescently labeled proteins, in *Confocal Microscopy: Methods and Protocols*. (Paddock, S. W., ed.) Humana, Totowa, NJ, pp. 223–240.
7. Haseloff, J., Dormand, E. L., and Brand, A. H. (1999) Live imaging with green fluorescent protein, in *Confocal Microscopy: Methods and Protocols*. (Paddock, S. W., ed.) Humana, Totowa, NJ, pp. 241–260.
8. Hazen, J. (1999) Morphing confocal images and digital movie production, in *Confocal Microscopy: Methods and Protocols*. (Paddock, S. W., ed.) Humana, Totowa, NJ, pp. 421–442.